



HAL
open science

Mechanistic insights in the decarboxylation and CO insertion into novel copper (I) complexes

Kieu Phung

► **To cite this version:**

Kieu Phung. Mechanistic insights in the decarboxylation and CO insertion into novel copper (I) complexes. Catalysis. Université Paris-Saclay, 2023. English. NNT : 2023UPASF082 . tel-04511563

HAL Id: tel-04511563

<https://theses.hal.science/tel-04511563>

Submitted on 19 Mar 2024

HAL is a multi-disciplinary open access archive for the deposit and dissemination of scientific research documents, whether they are published or not. The documents may come from teaching and research institutions in France or abroad, or from public or private research centers.

L'archive ouverte pluridisciplinaire **HAL**, est destinée au dépôt et à la diffusion de documents scientifiques de niveau recherche, publiés ou non, émanant des établissements d'enseignement et de recherche français ou étrangers, des laboratoires publics ou privés.

Mechanistic insights in the decarboxylation and CO₂ insertion into novel copper (I) complexes

*Aperçus mécanistiques de la décarboxylation et de l'insertion de CO₂ dans
de nouveaux complexes de cuivre (I)*

Thèse de doctorat de l'université Paris-Saclay

École doctorale n°571 : sciences chimiques : molécules, matériaux, instrumentation et
biosystèmes (2MIB)

Spécialité de doctorat : Chimie

Graduate School : Chimie. Référent : Faculté des sciences d'Orsay

Thèse préparée dans l'unité de recherche **NIMBE** (Université Paris-Saclay, CEA, CNRS),
sous la direction de **Jean-Claude BERTHET**, Ingénieur de recherche, et le co-
encadrement de **Thibault CANTAT**, Ingénieur de recherche

Thèse soutenue à Paris-Saclay, le 05 décembre 2023, par

Kieu PHUNG

Composition du Jury

Membres du jury avec voix délibérative

Laurence GRIMAUD

Directrice de Recherche,
CNRS, ENS,
Université Paris Sciences & Lettres

Présidente

Guillaume LEFEVRE

Directeur de Recherche,
CNRS, Chimie ParisTech,
Université Paris Sciences & Lettres

Rapporteur & Examineur

Nicolas MEZAILLES

Directeur de Recherche,
Université Toulouse III Paul Sabatier

Rapporteur & Examineur

Jerôme HANNEDOUCHE

Directeur de Recherche,
Université Paris-Saclay

Examineur

Titre : Aperçus mécanistiques de la décarboxylation et de l'insertion de CO₂ dans de nouveaux complexes de cuivre (I)

Mots clés : catalyse, cuivre, phenanthroline, décarboxylation, insertion de CO₂, déshydrogénation, acide formique, mécanisme, calculs DFT.

Résumé : La décarboxylation des acides carboxyliques en composés biarylés, catalysée par les complexes de cuivre, est depuis des décennies un sujet majeur dans le domaine du couplage croisé. Alors que de nombreuses études se concentrent sur l'optimisation des conditions de réaction et de l'étendue des substrats, les espèces actives de cuivre sont mal connues. Par ailleurs, la déshydrogénation de l'acide formique catalysée par des complexes de cuivre a été peu étudiée et les activités rapportées sont faibles. Ainsi, des études offrant une meilleure compréhension des mécanismes et des espèces impliquées dans ces transformations catalytiques sont capitales. Cela passe par l'isolement de complexes de cuivre, l'étude de leur réactivité et l'identification des intermédiaires réactionnels. Bien que les ligands azotés bidentes, telle que la phenanthroline, soient connus pour favoriser les

réactions de décarboxylation catalysées au cuivre, ceux-ci n'offrent pas toujours la solubilité et la stabilité requises pour des études en solution organiques.

Dans cette thèse, j'ai synthétisé de nouveaux composés carboxylates et aryles de cuivre(I), *eg* [(phen*)Cu(O₂CAr)] et [(phen*)Cu-Ar] (Ar= aryle), avec un ligand ancillaire azoté volumineux (phen*). Les structures cristallines de ces espèces sont présentées. Ce travail rapporte également mes essais de décarboxylation des complexes [(phen*)Cu(O₂CAr)] ainsi que la réaction inverse d'insertion de CO₂ dans les dérivés aryles. La déshydrogénation de l'acide formique catalysée par le formiate de cuivre [(phen*)Cu(O₂CH)] est également décrite. Différents mécanismes sont proposés pour ces transformations.

Title : Mechanistic insights in the decarboxylation and CO₂ insertion into novel copper (I) complexes

Keywords : catalysis, copper, phenanthroline, decarboxylation, CO₂ insertion, dehydrogenation, formic acid, mechanism, DFT calculation.

Abstract : Decarboxylation of carboxylic acids to biaryl compounds catalyzed by copper complexes is of tremendous interest in cross-coupling. While many studies focused on the optimising reaction conditions and the substrates range, little is known about the active Cu species. Furthermore, the dehydrogenation of formic acid catalysed by copper complexes has been poorly studied and the reported activities are low. Studies offering a better understanding of the mechanisms and of the species involved in these catalytic transformations are vital. This requires to isolate copper complexes, studying their reactivity and identifying the reaction intermediates. Although bidentate nitrogen ligands

such as phenanthroline are known to favor copper-catalysed decarboxylation reactions, they do not always offer the solubility and stability required for studies in solution. In this thesis, I synthesised novel carboxylate and aryl Cu(I) compounds, *eg* [(phen*)Cu(O₂CAr)] and [(phen*)Cu-Ar] (Ar=aryl), with a bulky nitrogen ancillary ligand. Their crystal structures are presented. This work reports on my experiments to decarboxylate the carboxylate complexes [(phen*)Cu(O₂CAr)] and to insert CO₂ into the aryl derivatives. Dehydrogenation of formic acid catalysed by copper formate [(phen*)Cu(O₂CH)] is also described. Different mechanisms are proposed for these transformations.

Acknowledgement

Foremost, I would like express my deep and sincere gratitude to the jury members: Dr. Nicolas Mézailles, Dr. Laurence Grimaud, Dr. Guillaume Lefèvre, Dr. Jérôme Hannedouche for agreeing to revise and judge my work. Each of you has inspired me greatly during the time I have worked or studied with you. I am where I am thanks in part to you, and your presence as a jury to finally evaluate my years of research is a great honor. For me, you are not only the best among the best in your field, but also someone who had a great influence on my decision to pursue this PhD.

Thibault Cantat: Merci de m'avoir accepté dans ce laboratoire rempli de personnes exceptionnelles. Et je te remercie également pour tous tes conseils durant ces trois années.

Jean-Claude Berthet (Mon directeur de thèse/ Grand fan de vache mais ne supporte pas le fromage): J'ai tellement de chance d'être ton étudiante. Merci pour ta dynamique, ta passion pour la chimie, pour ton accompagnement continu lors de ma thèse. Merci m'avoir encouragé. J'ai tellement appris grâce à toi, non seulement en chimie mais aussi la culture française et beaucoup de conneries. Ce sont des souvenirs for me, **Formidable !**

Pierre Thuéry (Cristallographe légendaire et fantôme du LCMCE): Tant qu'il y a de la vie...il y a des cristaux ! Merci de prendre soin de tous mes cristaux, même si tu dois conduire l'engin comme une voiture à 3 roues (par contre, je trouve que ce type de voiture te va très bien). Non seulement pour le temps que vous avez pris pour la diffraction, mais aussi pour le temps de nos petites discussions (ou je dirais parfois de bavarder sur JC étant trop JC, il se reste jamais !) Merci pour les rappels pour les vacances, ton sage des conseils quand je suis déprimé avec mes cristaux défaillants.

Emmanuel Nicolas: Thank you for all your valuable advice on the DFT calculations, but also in all other areas in which you also have vast knowledge, from which I have learned a lot.

Marie-Hélène Pietraru (Ma jumelle/ My tatwin): I call you my twin, but I hope I can be half as excellent as you. During our master, I had my eyes on you, thinking this girl is so cool, speaks her mind, fights for her beliefs and hoped to become your friend one day. And guess who was so happy to find out that you will be in the same lab with me in the same year! Thank you for your presence, your support and for sharing these three years with me in the same lab¹⁵ (where both the heat and the cold are unbearable). Thank you for all the cigarette/coffee breaks, for listening to my worries and taking some of the burden off my shoulders. All these beautiful memories, I remember them **All too well !**

Marie Kobylarski (Ma motivatrice/ Girl boss/ Team JCB): Merci pour ces moments très joyeux partagés dans le même bureau avec toi. Ton caractère incroyable et attentionné m'a aidé à traverser des moments difficiles et m'a inspiré à devenir une personne aussi positive et énergique que toi. C'est la vie, on dit toujours, mais pour moi c'est les gens. Et ta présence rend la vie plus belle ! Thank you for always making me **Feel good!**

Marianne Kjellberg (Mon inspiratrice de mode): I truly appreciate your presence, from your beautiful figure to your sweet heart. Thank you for sharing your love of fashion and great cocktails. C'est toujours mon verre de vin!

Kajetan Bijourd: J'ai rien à te dire que Fous ta cagoule et merci d'avoir transformé les journées de travail en pures soirées.

Guilhem Zwart: Merci pour ta gentillesse et pour toutes tes délicieuses recettes. Merci pour tous les moments de course où tu ne m'as jamais laissé seul.

Étienne Crochet: Thank you for helping me paying my tax and moving out. Thank you for your big laugh and sweet personality.

Alexandre Touron et Félix Mandelaire (Tic and Tac): Merci pour vos gentillesse, pour avoir apporté de la joie au labo et pour avoir soutenu mon caractère méchant.

Nathan de Riggi: Merci pour ton caractère tranquille et le partage de l'amour de la nourriture avec moi.

Neethu Thyagarajan: Thank you for sharing your delicious Indian foods and for the time we had at Charmmat.

Uros Todorovic: Thank for your funny comments and for sharing our sassy personality.

Xin Liu: Merci beaucoup pour toutes tes suggestions pour apprendre la langue française et découvrir la culture française tout en restant dans la délicieuse cuisine asiatique.

Cyril Theulier: Merci d'être si cool et d'avoir autant de petits talents. Merci pour ton street style et tes connaissances académiques, que j'apprécie beaucoup.

Laurent Severy: It was both a pain and a pleasure to share the lab with you for your silly and serious character! Thank you for your talent with words and your expertise in copper chemistry.

Kirk Smith: Thank you for your positive and joyful character and for bringing a whole new horizon to our laboratory.

Alexis Mifleur: Thank you for 10 hours of Pink fluffy unicorn, your advices and your time to correct my manuscript.

Lucile Anthore-Dalion: Merci pour tes conseils en chimie organique et ton caractère chaleureux.

Caroline Genre: Thank you for all your comedic and sassy comments while being cool about almost everything.

Merci à mes camarades de cours de français et à notre professeur Henriette, j'ai eu tellement de plaisir à apprendre le français avec vous tous.

Je tiens également à exprimer ma gratitude aux personnes du LISSEN que j'ai rencontrées lors de ma thèse, notamment Stephane Campidelli, Daniel Medina-Lopez, Cynthia Banga-Kpako, pour votre gentillesse et le temps que j'ai passé avec vous.

Thank to my friends: Machoud Amoussa, Stelina (Στελλίνα Γιαννοπούλου), Chrisa Theodorakidou, Phung Ngoc Tram, Huynh Quoc Thai, Pham My Hang, Aurélien Bailly, Cam Huong. Thank you for being my friends, for your presence and support when I needed it the most.

Je souhaite remercier tout particulièrement Philippe Rigot, Martine Rigot, pour l'accueil chaleureux qu'ils m'ont réservé chez eux pendant mon master et la première année de mon doctorat. D'eux, j'ai appris la gentillesse des Français, sans conditions et avec beaucoup de compréhension. La barrière de la langue n'a jamais été un obstacle lorsqu'elle est évoquée avec le cœur.

My family: Thanks to my family, my parents for letting me go to France to study, for the support from afar. Thank to my brother and his wife for taking care of my parents for the time I was away. A big thank you to my sister and her family in Italy, for the support and the care they bring to me. Thank you to my aunts in the USA, for their financial support, for loving and caring for me.

My love: Merci d'apporter de la chaleur à mon cœur. Je sais ce que je vais faire au **Paradis** ! You are the cider of my eye.

Résumé substantiel

L'objectif principal des processus de décarboxylation et de carboxylation est de rompre et de former de nouvelles liaisons C-C fortes afin de fabriquer des composés utiles à des fins pharmaceutiques et industrielles. Le problème est que la plupart de ces processus nécessitent une activation à haute énergie avec une température opérationnelle supérieure à 150 °C dans la chimie des solutions. Une compréhension mécanique claire de ces transformations peut aider à rationaliser et à optimiser les conditions de réaction. Cependant, dans le cas présent, les conditions difficiles rendent difficile le contrôle des intermédiaires réactionnels. Par conséquent, l'objectif d'amélioration d'un processus donné est semé d'embûches, en particulier pour la conception de systèmes catalytiques complexes impliquant des ions métalliques, des ligands et un solvant.

Depuis le premier rapport de Gooßen sur la réaction de couplage croisé décarboxylatif catalysée par Pd/Cu, le domaine de l'activation décarboxylative s'est considérablement développé. De nombreux chercheurs ont largement contribué au développement de plusieurs voies pour la construction de liaisons C-C décarboxylatives à partir d'une large gamme d'acides carboxyliques et de partenaires de couplage (hétéro)aromatiques. Grâce à leurs travaux, les acides benzoïques, qui sont des réactifs peu coûteux, stables et facilement accessibles ou naturels, ont été reconnus comme des alternatives économiques aux partenaires de couplage croisé traditionnels. Par exemple, en 2007, le groupe de Gooßen a présenté un système catalytique dimétallique Pd^{II}/Cu^I pour la réaction de couplage entre des acides benzoïques ortho-substitués et une série d'arènes halogénées. Ils ont souligné l'importance des substituants en position ortho des substrats d'acides benzoïques qui améliorent généralement l'efficacité de la réaction. Ce point crucial a été observé, à quelques exceptions près, dans de nombreux rapports traitant du couplage décarboxylatif avec des haloarènes ou des composés aromatiques non fonctionnalisés. Bien que plusieurs méthodes aient été proposées pour accommoder une large gamme de dérivés de l'acide benzoïque et de partenaires de couplage, beaucoup de ces développements partagent le même inconvénient de températures de réaction élevées (environ 150 °C), avec dans certains cas la nécessité d'une quantité stœchiométrique d'agent oxydant tel que les sels d'argent ou de cuivre(II).

En raison de ses performances élevées dans les processus décarboxylatifs, le cuivre a été le métal de transition le plus étudié. Les réactions de couplage croisé décarboxylatif promues par le cuivre ont été adaptées avec succès à une large gamme d'acides carboxyliques fonctionnalisés, y compris des dérivés méta- et para-substitués, et utilisées à la fois en quantité stœchiométrique et catalytique. L'inconvénient le plus cité de ces réactions est la température opérationnelle élevée (environ 170 °C). Les études théoriques sur le mécanisme de décarboxylation catalysé par le cuivre ont suggéré que le carboxylate de cuivre(I) et les espèces aryl-cuivre sont des intermédiaires clés. L'étape de décarboxylation est thermodynamiquement défavorable et se produit généralement à des températures élevées. Le consensus sur le mécanisme est basé sur une décarboxylation en une étape d'un carboxylate de cuivre(I) en un dérivé aryle de cuivre(I).

En collaboration avec notre laboratoire, Destro et al. du CEA ont développé une réaction dynamique d'échange d'isotopes du carbone pour marquer une gamme d'acides carboxyliques avec du $^{14}\text{CO}_2$. Un tel enrichissement a été possible avec un catalyseur cuivre(I) supporté par des ligands présentant un échafaudage bisoxazoline dans du DMSO à 150 °C. Cette méthode permet l'incorporation de $^{14}\text{CO}_2$ marqué dans une large série d'acides carboxyliques et fournit une voie de synthèse très efficace pour des produits marqués au carbone d'intérêt pour des applications pharmaceutiques. Ils ont proposé un mécanisme de réaction dans lequel l'extrusion du CO_2 du carboxylate de cuivre(I) et l'incorporation du $^{14}\text{CO}_2$ dans l'intermédiaire aryle de cuivre(I) ont lieu de manière réversible. Cependant, leurs tentatives d'isoler les intermédiaires de cuivre ont échoué et aucune conclusion définitive n'a été tirée concernant les espèces de cuivre actives et leurs états d'oxydation.

Le but de cette thèse était donc d'étudier et de comprendre le mécanisme du processus de décarboxylation catalysé par le cuivre avec un ligand simple dérivé de la 1,10-phénanthroline.

Chapitre 1 - Introduction générale : Réactions de couplage croisé décarboxylatif catalysées par des métaux de transition

Ces dernières années, les réactions de couplage croisé décarboxylatif catalysées par des métaux de transition sont apparues comme une nouvelle catégorie importante de transformation organique qui trouve une grande variété d'applications dans l'établissement de liaisons carbone-carbone et carbone-hétéroatome. Dans ces réactions, les acides carboxyliques sont utilisés comme matériau de départ pour former de nouvelles liaisons C-C avec les partenaires de couplage et libérer du CO_2 comme produits secondaires. Les partenaires de couplage peuvent être des alcynes, des hétéroarènes ou des haloarènes, tandis que les acides carboxyliques (hétéro)aromatiques, les acides alcaniques et les acides carboxyliques insaturés peuvent être utilisés. Le couplage croisé de la décarboxylation avec des produits biaryliques a fait l'objet d'une grande attention, car il s'agit de motifs structuraux importants dans de nombreux composés biologiquement actifs.

Dans ce chapitre, différents types de réactions de couplage croisé décarboxylatif pour la synthèse de composés biaryliques catalysés par différents complexes de métaux de transition seront passés en revue. La portée et les applications de ces réactions seront discutées, ainsi que les défis et les limites dans ce domaine. Le processus de décarboxylation catalysé par le cuivre sera au centre de l'attention, car il se prête à des conditions de réaction plus générales. Des aperçus mécanistiques concernant les intermédiaires actifs du cuivre feront l'objet d'une discussion, au cours de laquelle des études expérimentales et computationnelles seront présentées.

Depuis les travaux pionniers de Shepard en 1930, d'énormes progrès ont été réalisés dans la chimie décarboxylative de construction de liaisons C-C médiée par le cuivre en utilisant des acides carboxyliques et des partenaires de couplage aryles. L'intérêt de cette transformation décarboxylative provient de son avantage par rapport aux réactions de couplage croisé traditionnelles, car les acides benzoïques sont peu coûteux, stables et faciles à préparer par rapport à certains partenaires de couplage organométalliques pré-fonctionnalisés. L'un des principaux inconvénients du processus de décarboxylation qui n'a pas été résolu est la température élevée requise pour l'extrusion du CO_2 , car ce clivage de la liaison C-C nécessite une énergie d'activation élevée.

De nombreux esprits brillants ont rassemblé des éléments importants pour créer diverses voies de synthèse de biaryles par décarboxylation d'acides carboxyliques aromatiques, soit par un processus redox-neutre, soit par un processus oxydatif. Le groupe de Gooßen a grandement contribué à la réalisation d'un couplage croisé direct entre les acides benzoïques et les halogénures d'aryle, en particulier dans des conditions catalytiques. Une limitation commune observée est la nécessité de substituants coordinatifs en position ortho du groupe carboxylique. L'état de transition pour les $C_{Ar}-C_{COO}$ est généralement élevé, mais leur présence diminue l'énergie nécessaire pour atteindre l'état de transition, ce qui favorise le processus de décarboxylation. Des études approfondies ont permis de concevoir de nouvelles conditions catalytiques afin d'élargir la gamme de substrats des acides carboxyliques aromatiques, y compris les groupes supports non *ortho*-substitués.

En quelques années, leurs observations et études fructueuses ont finalement permis d'élargir le champ des substrats aux acides carboxyliques aromatiques *para*- et *mé*ta-substitués.

Dans le domaine du couplage oxydatif décarboxylatif d'un acide benzoïque avec un arène, il s'agit d'une approche plus économique que les couplages décarboxylatifs avec des haloarènes, où aucun sel d'halogénure n'est produit comme sous-produit. Cependant, ce domaine est encore pauvre en transformations efficaces, dans lesquelles des quantités stœchiométriques de métaux de transition sont nécessaires, et manque d'aperçus mécanistiques. À ce jour, seuls deux exemples rapportés par les groupes de Maiti et Su nécessitent une quantité catalytique d'un métal de transition, bien qu'avec des limitations en termes de gamme de substrats ou de régiosélectivité sur le partenaire de couplage de l'arène. En outre, les deux domaines de l'homocouplage décarboxylatif et du couplage croisé entre les acides arylcarboxyliques sont sous-développés. L'homocouplage d'acides carboxyliques via une double décarboxylation est possible avec une charge catalytique élevée en cuivre, mais il nécessite un groupe fonctionnel en position orthogonale sur les acides benzoïques. Alors que des molécules biaryles asymétriques peuvent être obtenues à partir d'une large gamme d'acides carboxyliques (hétéro)aromatiques, le protocole rapporté souffre d'une faible chimiosélectivité et nécessite une quantité stœchiométrique d'oxydant.

Initialement considérée comme une réaction indésirable au cours du couplage décarboxylatif redox-neutre et oxydatif, la réaction de protodécarboxylation a été incluse ultérieurement dans une stratégie synthétique élégante afin d'éliminer les fonctions d'acide carboxylique utilisées comme groupes directeurs. Parmi les métaux à transition d, le cuivre et l'argent sont les plus efficaces pour promouvoir cette réaction. Alors que la protodécarboxylation médiée par le cuivre est indépendante de l'acide benzoïque *ortho*-substitué, la protodécarboxylation catalysée par l'argent fonctionne à des températures plus basses mais nécessite un groupe *ortho*.

En raison de leur rôle essentiel dans le processus de décarboxylation, les espèces métalliques de cuivre ont fait l'objet d'une attention particulière. Les premières études mécanistiques réalisées par Nilsson, Cohen et Sheppard se sont principalement concentrées sur le mécanisme de décarboxylation et la génération d'intermédiaires organocuvrés. Quelques décennies plus tard, l'observation d'espèces aryles de cuivre a été confirmée par des calculs modernes effectués par le groupe de Gooßen et Su. Ils ont proposé un mécanisme général dans lequel la décarboxylation se produit via la libération de CO_2 du complexe carboxylate de cuivre (I) et génère ensuite une espèce aryle de cuivre. En outre, l'importance positive des substituants ortho dans les acides carboxyliques a été expliquée par deux

aspects différents et l'influence du ligand sur l'activité du cuivre a été soigneusement calculée. Le cuivre (II), crucial dans certaines décarboxylations médiées, manque cependant d'une étude mécanistique pour déchiffrer son rôle.

Des études expérimentales et théoriques ont mis en lumière l'ensemble du processus de décarboxylation, particulièrement centré sur le système médié par le cuivre. La recherche a montré que non seulement le cuivre métallique peut favoriser la rupture d'une liaison C-C forte par décarboxylation, mais qu'il peut également favoriser la création de liaisons C-C par l'insertion de CO₂ dans une liaison Cu-C. Depuis le premier rapport de DePasquale et al. sur l'insertion de CO₂ dans [Cu-(C₆F₅)] dans du DMA à 70 °C, la fixation du gaz CO₂ et son utilisation comme source de C1 dans les composés aromatiques pour générer des dérivés de l'acide benzoïque catalysés par des métaux de transition ont attiré une attention considérable. Les années 2000 et 2010 ont vu l'évolution des méthodologies de synthèse vers la carboxylation, ajoutant ainsi de nouvelles dimensions aux réactions d'addition de nucléophiles carbonés au CO₂ catalysées par le cuivre. Inspirés par les travaux de Takaya et al., Hou et ses collaborateurs ont introduit une méthode d'addition du CO₂ catalysée par le cuivre. Hou et ses collaborateurs ont introduit un système catalytique à base de cuivre avec des ligands N-hétérocycles (NHC) pour préparer des composés d'acide carboxylique via la fixation du CO₂ dans des réactifs organoboroniques. Les chercheurs ont proposé un cycle catalytique soutenu par des réactions de contrôle stœchiométriques. Les chercheurs ont proposé un cycle catalytique soutenu par des réactions de contrôle stœchiométriques. Ils ont montré que l'aryle de cuivre et le carboxylate de cuivre sont des intermédiaires. Une autre stratégie a été développée par Daugulis et al. en 2013, où le système catalytique CuI/TMEDA combiné à Et₂Zn comme agent réducteur est utilisé pour une carboxylation réductrice des iodures d'aryle. Sans aller plus loin dans la chimie de la fixation du CO₂, nous laisserons ce sujet aux origines et aux développements, et nous renverrons le lecteur aux études dans le domaine en évolution de l'insertion du CO₂.

Comme nous l'avons vu plus haut, le cuivre métal s'est avéré efficace pour les réactions de décarboxylation et de carboxylation. Les similitudes notables entre les processus de décarboxylation et de carboxylation catalysés par le cuivre sont les ligands contenant de l'azote et les intermédiaires de cuivre. Dans ce contexte, certains groupes ont conçu des conditions permettant de procéder simultanément à la décarboxylation et à la carboxylation. Ces conditions créent un échange dynamique favorable à l'incorporation en une seule étape de dioxyde de carbone marqué au ¹¹C, ¹³C ou ¹⁴C dans des molécules d'acide carboxylique natif au ¹²C. Cet échange d'isotopes de carbone (CIE) a été optimisé pour réaliser le marquage au carbone de nombreux arènes, hétéroarènes avec un pourcentage d'enrichissement isotopique relativement élevé. Une telle réactivité est fortement demandée pour les applications pharmaceutiques. Néanmoins, aucune information mécanistique n'est rapportée en dehors d'un cycle catalytique général proposé.

Nous nous sommes donc fixé pour objectif de clarifier le mécanisme et les espèces impliquées dans le processus CIE, en commençant par étudier le comportement des complexes de cuivre(I) carboxylate et de cuivre(I) aryle dans l'activation réversible de la liaison C-C. L'état actuel de l'art est basé sur un ligand bisoxazoline coûteux et peu courant. Nous avons donc prévu d'isoler et de caractériser divers complexes de cuivre(I) en utilisant un ligand azoté phénanthroline (phen) plus conventionnel et bien

développé dans la chimie du cuivre. En cas de succès, il s'agira du premier aperçu direct du processus réversible de décarboxylation/carboxylation par l'intermédiaire de complexes isolés de cuivre(I).

Chapitre 2 - Synthèses, structures et réactivité des complexes [(2,9-(^tBu)₂-phen)Cu(O₂CAryl)] et [(2,9-(^tBu)₂-phen)Cu(Aryl)] : Étude expérimentale et théorique de l'extrusion ou de l'insertion du CO₂

Le développement du couplage décarboxylatif catalysé par le cuivre a été entièrement décrit, dans lequel il est proposé que le mécanisme de perte de CO₂ passe par des espèces de carboxylate de cuivre(I) et des intermédiaires aryliques de cuivre(I). Entre-temps, quelques exemples de ces complexes de cuivre(I) ont été décrits, avec un nombre limité d'acides carboxyliques.

En 2019, Destro et al. ont démontré une réaction dynamique d'échange isotopique de carbone (CIE) catalysée par un système cuivre-bisoxazoline, où une variété d'acides carboxyliques ont été enrichis avec succès en fragment ¹³CO₂ ou ¹⁴CO₂. On suggère que cette réaction se déroule via un événement initial de décarboxylation des espèces carboxylates de cuivre(I) transformées en intermédiaires aryliques de cuivre(I), qui réagissent ensuite avec le CO₂ marqué pour donner les complexes carboxylates de cuivre(I) enrichis en ¹³C ou en ¹⁴C. Néanmoins, le mécanisme n'est pas clairement établi et les efforts pour isoler une espèce de cuivre(I) bisoxazoline se sont avérés infructueux.

Ce défi nous a conduits à essayer de clarifier le mécanisme de la réaction CIE, en isolant des carboxylates de cuivre(I) et leurs dérivés aryliques de cuivre(I). Pour éviter l'utilisation de ligands bisoxazoline qui sont coûteux et difficiles à préparer, nous avons porté notre attention sur des espèces de phénanthrolines de cuivre(I) plus accessibles, qui sont beaucoup plus courantes et bien décrites dans la chimie du cuivre.

Nous avons choisi le ligand 2,9-di-*tert*butyl-1,10-phénanthroline et [Cu(O^tBu)] comme précurseur pour synthétiser des carboxylates de cuivre(I) et des espèces aryliques.

La préparation des complexes [(phen*)Cu(O₂CR)] (**2–7**) a été réalisée par réaction de [Cu(O^tBu)] et de phen* avec les acides correspondants. Les complexes [(phen*)Cu(O₂CR)] (R = *o*-F-C₆H₄ (**2**), *p*-F-C₆H₄ (**3**), C₆F₅ (**4**), *o*-NO₂-C₆H₄ (**5**), *p*-NO₂-C₆H₄ (**6**), CF₃ (**7**)) ont été facilement obtenus en traitant une solution de THF jaune pâle de [Cu(O^tBu)] avec 1 équiv. de 2,9-di-*tert*butyl-1,10-phénanthroline (phen*) puis 1 équiv. de l'acide correspondant (Figure 1).

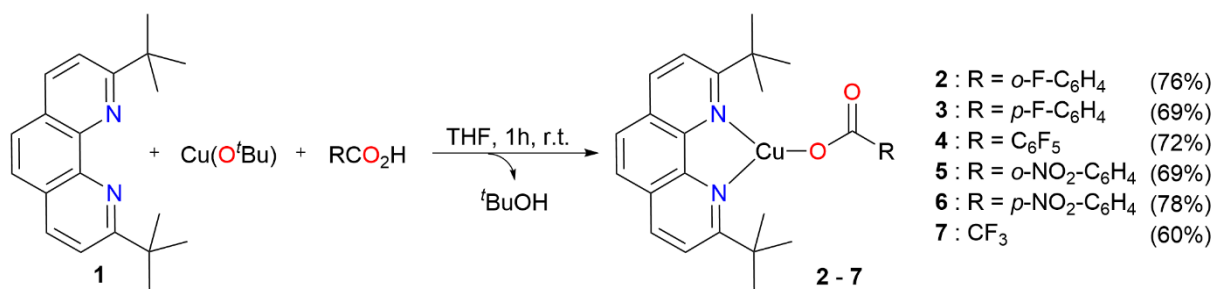


Figure 1. Synthèse des complexes [(phen*)Cu(O₂CR)] **2-7**

Le complexe $[(\text{phen}^*)\text{Cu}-\text{C}_6\text{F}_5]$ (**8**) a été synthétisé à partir du précurseur $[\text{Cu}(\text{C}_6\text{F}_5)_4]$, qui a été préparé selon une procédure de la littérature par la réaction métathétique de Grignard $\text{C}_6\text{F}_5\text{MgBr}$ avec un halogénure de CuCl dans l'éther (Figure 2). En suivant cette procédure, l'ajout de 1 équivalent de phen^* à 0,25 équivalent de $[\text{Cu}(\text{C}_6\text{F}_5)_4]$ a conduit à une suspension orange immédiate. Une simple filtration du solide a donné du **8** pur avec un rendement non optimisé de 72 % et de gros cristaux orange de **8** ont pu être obtenus en refroidissant lentement une solution de toluène chaude.

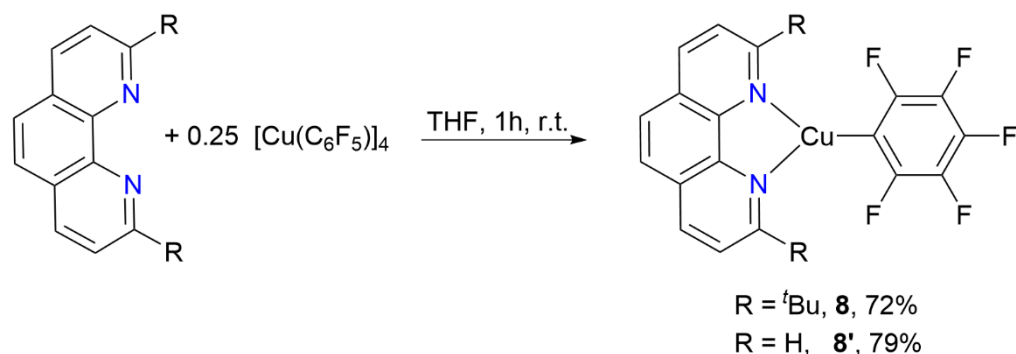


Figure 2. Synthèse des complexes $[(\text{phen}^*)\text{Cu}-\text{C}_6\text{F}_5]$ (**8**) and $[(\text{phen})\text{Cu}-\text{C}_6\text{F}_5]$ (**8'**).

L'espèce cuivre (I) $[(\text{phen}^*)\text{Cu}(\text{C}_6\text{H}_4\text{-o-NO}_2)]$ (**9**) a été synthétisée de manière différente car le précurseur aryle $[\text{Cu}(\text{C}_6\text{H}_4\text{-o-NO}_2)]_n$ n'est pas signalé. Nous avons utilisé la méthode publiée par le groupe Hoover pour la préparation de l'espèce cuivre(I) $[(\text{phen})\text{Cu}(\text{C}_6\text{H}_4\text{-o-NO}_2)]$. Après purification habituelle, le composé **9** a été obtenu pur avec un rendement de 57 % à partir du ajout du 5,5-diméthyl-2-(2-nitrophényl)-[1,3,2]-dioxaborinane à un mélange de phen^* et du $[\text{Cu}(\text{O}^t\text{Bu})]$ fraîchement sublimé dans le THF (Figure 3).

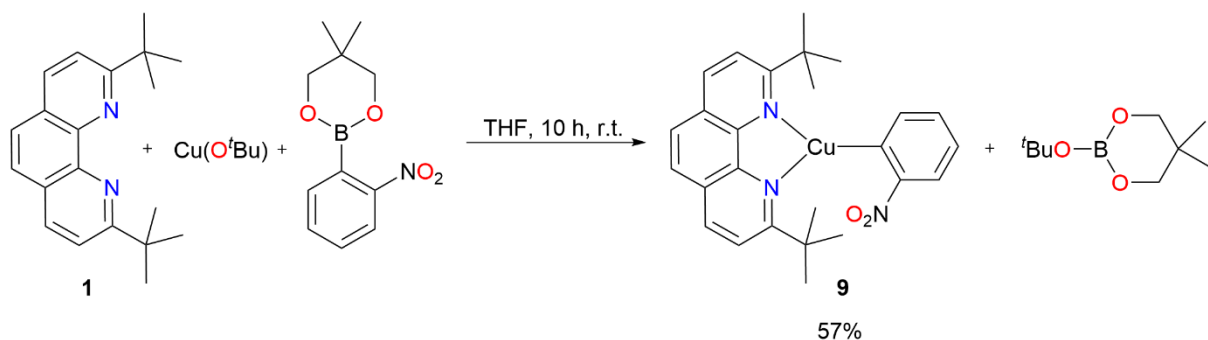


Figure 3. Synthèse du complexe $[(\text{phen}^*)\text{Cu}(\text{C}_6\text{H}_4\text{-o-NO}_2)]$ (**9**).

Le complexe $[(\text{phen}^*)\text{Cu}(\text{CF}_3)]$ (**11**) a été synthétisé de manière légèrement différente de la procédure rapportée par le groupe de Hartwig en 2011. Le traitement du complexe **10** généré in situ à température ambiante pendant 1 h avec un excès de TMSCF_3 (3 équiv.) a donné le composé **11** pur sous la forme d'un solide jaune (60,3 mg, 60 %) après le traitement habituel (Figure 4).

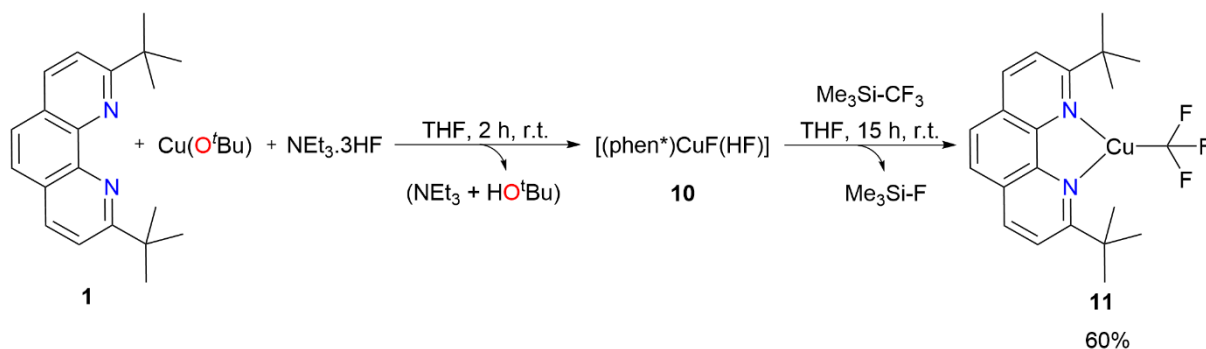


Figure 4. Synthèse du complexe [(phen)Cu(CF₃)] (**11**) à partir de la préparation « in situ » de [(phen*)CuF(HF)] (**10**).

En résumé, la structure cristalline de la phénanthroline volumineuse 2,9-^tBu₂phen (phen*) a été déterminée et une série de complexes de cuivre(I) impliquant ce ligand ont été synthétisés, isolés et caractérisés structurellement. Les espèces [(phen*)Cu(O₂CR)] (R = *o*-F-C₆H₄ (**2**), *p*-F-C₆H₄ (**3**), C₆F₅ (**4**), *o*-NO₂-C₆H₄ (**5**), *p*-NO₂-C₆H₄ (**6**), CF₃ (**7**)) (Figure 5 et Figure 6) et les contreparties aryl/alkyl [(phen*)CuR] (R = C₆F₅ (**8**), *o*-NO₂-C₆H₄ (**9**), CF₃ (**11**)) (Figure 7) font partie des rares complexes isolés de cuivre(I) présentant une stabilité thermique et une solubilité supérieures à celles des complexes de cuivre existants. Ces améliorations nous permettent de réaliser des études mécanistiques dans des solvants courants tels que le THF ou dans des conditions thermiques.

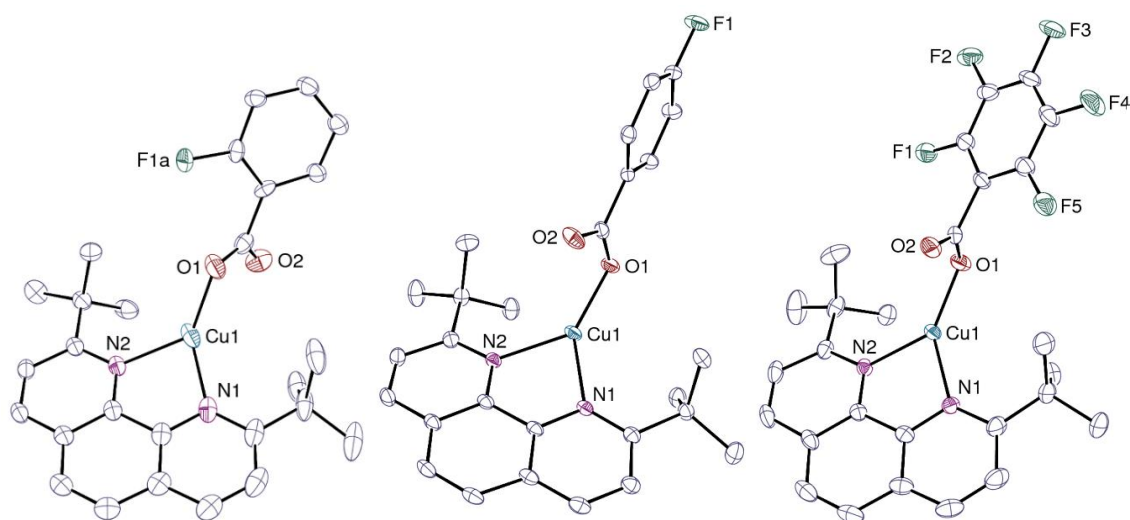


Figure 5. De gauche à droite : vue du complexe **2**, **3**, **4** avec la molécule de solvant et les atomes d'hydrogène omis. Une seule position du groupe désordonné est représentée. Les ellipsoïdes de déplacement sont dessinés à un niveau de probabilité de 50 %.

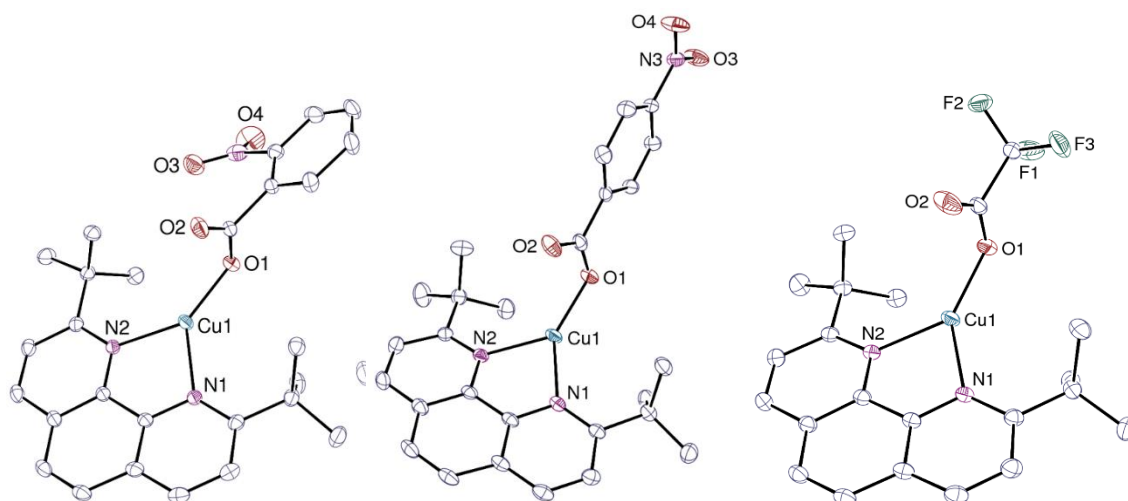


Figure 6. De gauche à droite : vue du complexe **5**, **6**, **7** avec la molécule de solvant et les atomes d'hydrogène omis. Une seule position du groupe désordonné est représentée. Les ellipsoïdes de déplacement sont dessinés à un niveau de probabilité de 50 %.

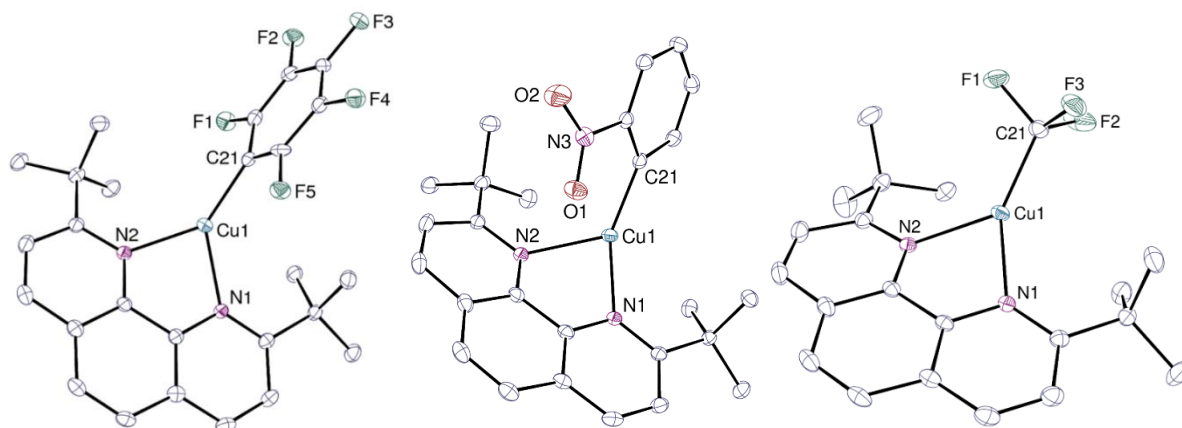


Figure 7. De gauche à droite : vue du complexe **8**, **9**, **11** avec la molécule de solvant et les atomes d'hydrogène omis. Une seule position du groupe désordonné est représentée. Les ellipsoïdes de déplacement sont dessinés à un niveau de probabilité de 50 %.

En utilisant ces composés, nous avons étudié la réaction de décarboxylation des complexes $[(\text{phen}^*)\text{Cu}(\text{O}_2\text{CR})]$ et le processus de carboxylation inverse avec les dérivés organométalliques. La perte de CO_2 dans les complexes $[(\text{phen}^*)\text{Cu}(\text{O}_2\text{CR})]$ ($\text{R} = o\text{-F-C}_6\text{H}_4$ (**2**), C_6F_5 (**4**), $o\text{-NO}_2\text{-C}_6\text{H}_4$ (**5**), CF_3 (**7**)) a été réussie, sauf pour le complexe **7**, en particulier dans la quinoléine. Cependant, la carboxylation des complexes $[(\text{phen}^*)\text{CuR}]$ d'alkyle et d'aryle n'a pas eu lieu comme prévu. Ceci peut être expliqué par différents facteurs, tels que la stabilité des complexes et la réaction compétitive de protodécarboxylation. La rationalisation de ces données à l'aide de la DFT corrobore les résultats expérimentaux.

Nous pouvons proposer pour $[(\text{phen}^*)\text{Cu}(\text{O}_2\text{CC}_6\text{F}_5)]$ (**4**) un processus de décarboxylation via l'intermédiaire $[(\text{phen}^*)\text{Cu}(\text{C}_6\text{F}_5)]$ (**8**) en utilisant la quinoléine comme solvant. Cependant, la perte de CO_2 des complexes $[(\text{phen}^*)\text{Cu}(\text{O}_2\text{CC}_6\text{H}_4\text{-}o\text{-F})]$ (**2**) et $[(\text{phen}^*)\text{Cu}(\text{O}_2\text{CC}_6\text{H}_4\text{-}o\text{-NO}_2)]$ (**5**) dans la quinoléine n'a pas permis d'obtenir les espèces décarboxylées souhaitées $[(\text{phen}^*)\text{Cu}(\text{C}_6\text{H}_4\text{-}o\text{-F})]$ et $[(\text{phen}^*)\text{Cu}(\text{C}_6\text{H}_4\text{-}o\text{-NO}_2)]$ (**9**), mais seulement les produits de protodécarboxylation fluorobenzène et

nitrobenzène, respectivement. Néanmoins, dans le THF, seul $[(\text{phen}^*)\text{Cu}(\text{O}_2\text{C}_6\text{F}_5)]$ (**4**) a subi une protodécarboxylation.

Les calculs DFT incluant les effets de solvant ont donné des résultats similaires concernant la thermodynamique des réactions avec la quinoléine et le THF. D'autre part, les résultats expérimentaux ont montré que les complexes de carboxylate de cuivre se décarboxylent plus facilement dans la quinoléine que dans le THF. Par exemple, la protodécarboxylation n'a été observée que pour le complexe **4** à 100 °C (1 h) dans le THF, alors que le processus s'est produit à 35 °C (1 h) dans la quinoléine. En outre, les complexes **2** et **5** ont subi une protodécarboxylation dans la quinoléine (120 °C après 72 h et 150 °C après 17 h, respectivement), alors que les réactions n'ont pas été observées dans le THF. La quinoléine n'a pas déplacé le phen* mais s'est avérée être un meilleur solvant que le THF pour la décarboxylation des complexes carboxyliques $[(\text{phen}^*)\text{Cu}(\text{O}_2\text{C}\text{Ar})]$. Ceci pourrait favoriser, par une coordination supplémentaire au niveau du centre métallique, la formation d'intermédiaires plus stabilisés contre la dégradation et donc plus enclins à la décarboxylation. On pense également que la protodécarboxylation prédomine sur la décarboxylation parce que la quinoléine agit comme une source de protons. Ainsi, le solvant quinoléine est essentiel pour l'extrusion du CO₂, tandis que le ligand phen* a la capacité de stabiliser les intermédiaires qui capturent la partie aryle. Ces deux éléments sont essentiels à la décarboxylation.

En ce qui concerne le mécanisme, trois voies différentes ont été proposées, consacrées aux processus de décarboxylation et de protodécarboxylation des complexes **4** et **5**, en particulier dans les solvants de quinoléine (*Figure 8*) et de THF (*Figure 9*). Nous avons considéré le mécanisme de décarboxylation concertée proposé par les groupes de Gooßen et de Lin, où le CO₂ est extrudé du complexe carboxylate de cuivre vers les aryles de cuivre en une seule étape. Cependant, ce mécanisme n'explique pas la formation du protodécarboxylate C₆F₅ avant la génération des espèces aryles de cuivre. Par conséquent, nous avons proposé une deuxième voie, dans laquelle le rôle de la quinoléine est mis en évidence : la quinoléine se coordonne d'abord au complexe carboxylate de cuivre, suivi par l'extrusion concertée de CO₂ et l'abstraction de protons pour produire C₆F₅H et un ion $[(\text{phen}^*)\text{Cu}]^+[\text{Q}]^-$ species (Q = quinoléine). Alternativement, dans le THF, un mécanisme distinct est apparu dans lequel le phen* est d'abord déplacé par le solvant pour former $[\text{Cu}(\text{O}_2\text{CR})(\text{THF})_n]$ (R = C₆F₅ (**4**), *o*-NO₂-C₆H₄ (**5**)). Cette dernière espèce, non stabilisée par le ligand phen*, se disproportionne rapidement pour former le cuivre(0) et le carboxylate de cuivre(II) $[\text{Cu}(\text{O}_2\text{CR})_2(\text{THF})_n]$ (dans le cas du complexe **5**). En revanche, la protodécarboxylation est principalement observée pour le complexe **4**.

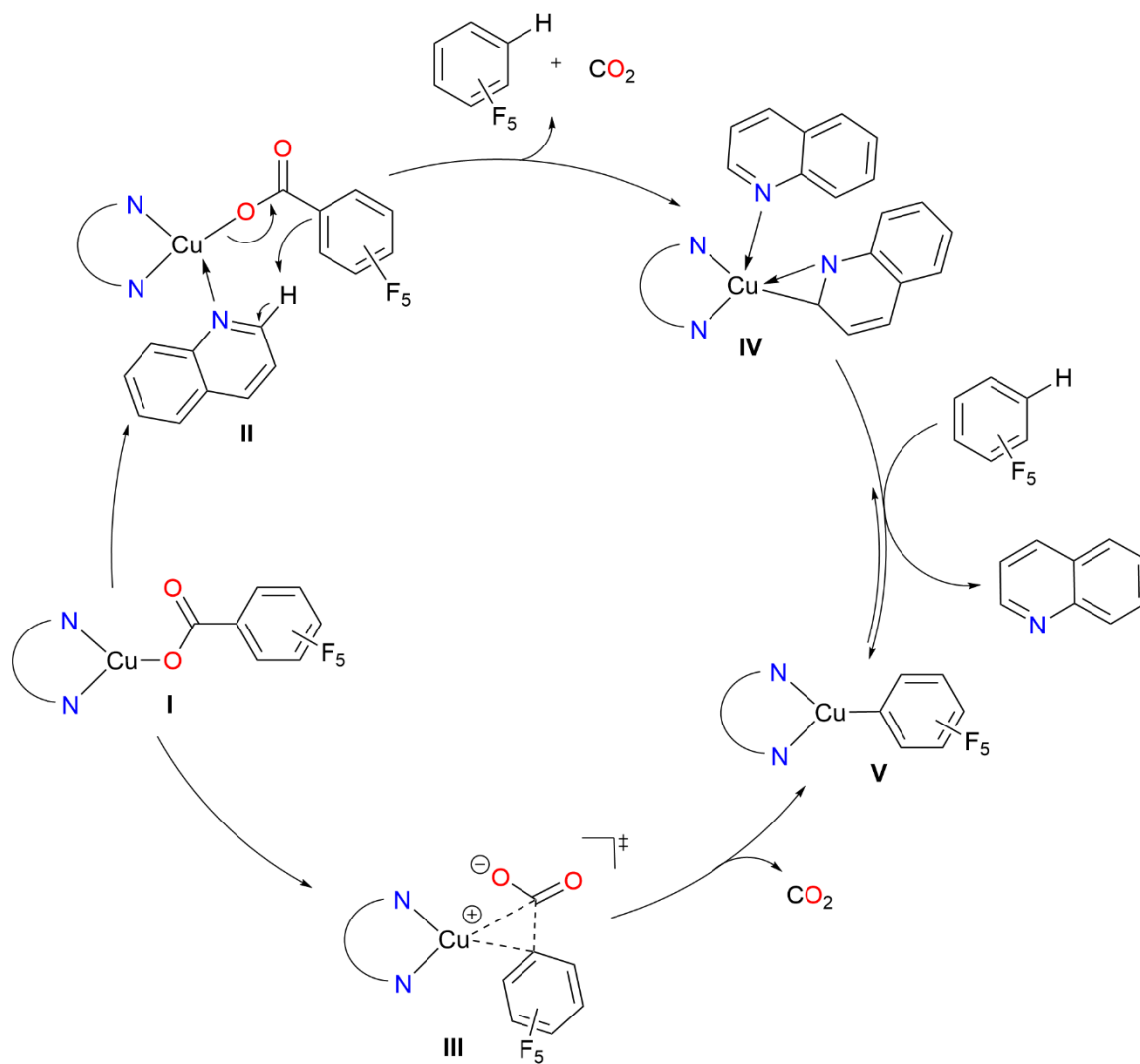


Figure 8. Mécanisme proposé pour la décarboxylation de $[(phen^*)Cu(O_2CC_6F_5)]$ (4) dans la quinoléine.

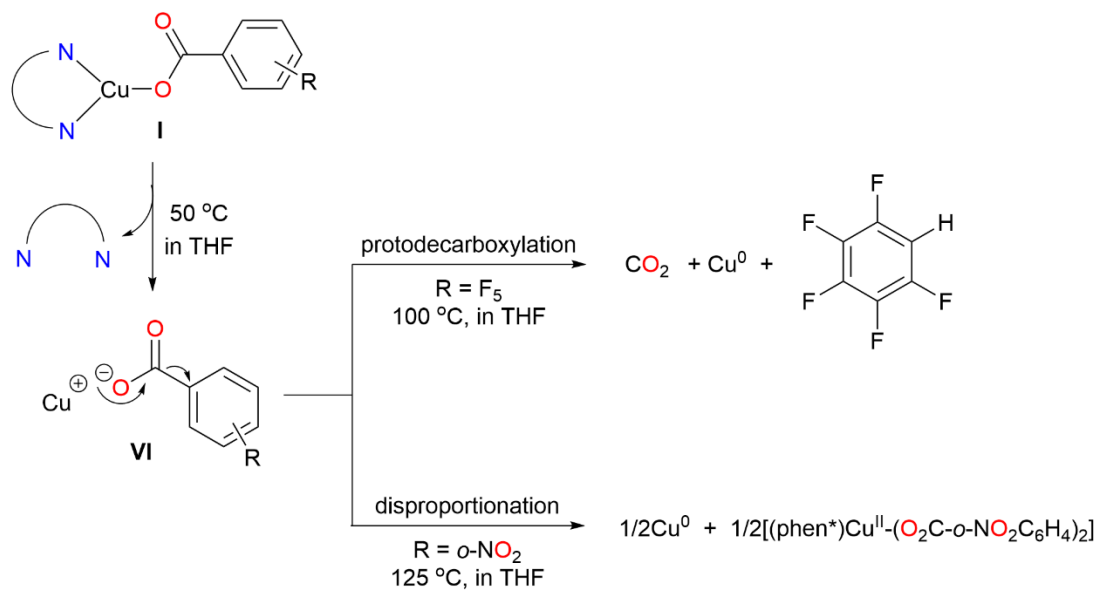


Figure 9. Proposition de décarboxylation de $[(phen^*)Cu(O_2CC_6F_5)]$ (4) et $[(phen^*)Cu(O_2CC_6H_4-o-NO_2)]$ (5) dans le THF.

Chapitre 3 - L'isolement d'un complexe de formiate de cuivre (I) et sa réactivité dans l'échange isotopique dynamique et la déshydrogénation de l'acide formique

L'acide formique (AF) est considéré comme un candidat prometteur pour le stockage de l'hydrogène liquide, qui a un grand potentiel dans les applications du carburant hydrogène. De nombreuses recherches ont été consacrées au développement de systèmes catalytiques efficaces pour la conversion sélective de l'AF en H₂ et CO₂, les catalyseurs à base de métaux précieux, tels que Ir, Ru, étant les plus performants. Contrairement à d'autres catalyseurs à base de métaux, les complexes de cuivre ont reçu peu d'attention et on ne connaît que trois exemples qui présentent une faible activité catalytique. Des études mécanistes sur les espèces de cuivre pour l'hydrogénation catalytique de l'alcool furfurylique ont suggéré la formation d'espèces transitoires d'hydrure de cuivre et de formiate de cuivre. Néanmoins, seule une poignée de complexes cuivre-formate a été isolée avec succès. Si l'insertion de CO₂ dans l'hydrure de cuivre est bien documentée, la réaction inverse de décarboxylation du formiate de cuivre n'est pas courante.

Comme nous avons réussi à isoler des complexes de carboxylate de cuivre(I) monoligaturés en utilisant le ligand volumineux 2,9-di-*tert*butyl-1,10-phénanthroline (phen*), nous avons ciblé le formate de cuivre(I) ligaturé par le phen*, par exemple [(phen*)Cu(O₂CH)], pour voir son activité potentielle dans la déshydrogénation de l'acide formique. En tant que catalyseur, la formation de l'espèce transitoire cuivre-hydrure [(phen*)Cu-H] issue de la décarboxylation de [(phen*)Cu(O₂CH)] a été suivie par différentes méthodes, y compris l'échange isotopique dynamique avec ¹³CO₂.

Nous avons synthétisé un complexe monomère de formiate de cuivre(I) impliquant une phénanthroline substituée volumineuse comme ligand auxiliaire (phen*) qui assure la solubilité et la stabilité. Le complexe [(phen*)Cu(O₂CH)] (**12**) a été facilement obtenu par l'ajout de 1 équiv. de phen* à une solution THF du tétramère jaune [Cu(O^{*t*}Bu)]₄ (1 équiv.) puis par traitement à l'acide formique (1 équiv.) à température ambiante (*Figure 10*). Le changement de couleur (jaune à orange) a été immédiat. Après agitation pendant 1 heure à température ambiante puis évaporation des substances volatiles et lavage du résidu avec du pentane, le complexe **12** a été facilement isolé avec un bon rendement (89 %) sous la forme d'un solide orange foncé qui conservait encore des traces de FA malgré un séchage prolongé. Il a été caractérisé en solution par les spectres RMN ¹H et RMN ¹³C{¹H} et à l'état solide par son spectre infrarouge et par analyse élémentaire.

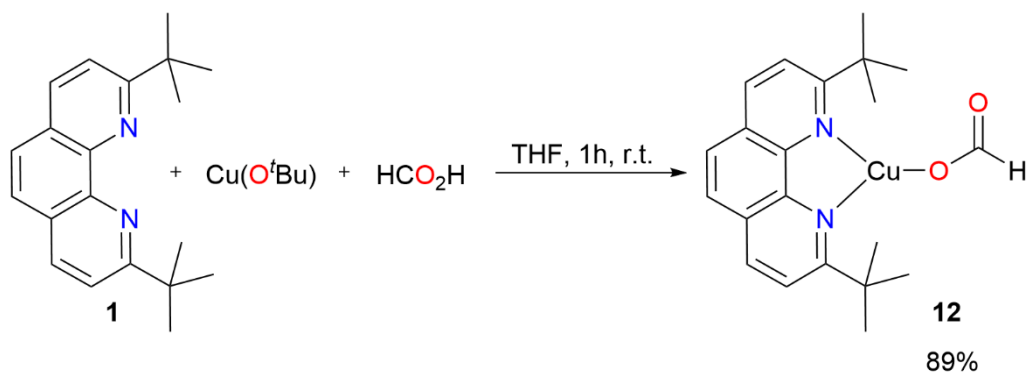


Figure 10. Synthèse de [(phen*)Cu(O₂CH)] (**12**).

De telles espèces $\text{Cu}^{\text{I}}(\text{O}_2\text{CH})$ avec des ligands azotés simples sont rares. Le complexe $[(\text{phen}^*)\text{Cu}(\text{O}_2\text{CH})]$ (**12**) a montré une activité catalytique dans la décomposition de l'acide formique en H_2 et CO_2 sans nécessiter d'agents supplémentaires. L'intermédiaire hydrure $[(\text{phen}^*)\text{Cu}-\text{H}]$, qui devrait être généré lors de la décarboxylation de **12**, n'a pas pu être détecté ou piégé par des piègeurs organiques. Cependant, l'augmentation régulière du signal RMN $^{13}\text{C}\{^1\text{H}\}$ NMR de l'anion formate lorsque **12** est placé sous 1 atm. La réaction d'échange isotopique du carbone avec $^{13}\text{CO}_2$ apporte des preuves solides de la décarboxylation de **12** en hydrure de cuivre(I) supposé. En revanche, l'analogie du dioxyde de carbone CS_2 ne s'est pas inséré dans le $[\text{Cu}-\text{H}]$ pour produire le dithioformate de cuivre attendu $[(\text{phen}^*)\text{Cu}(\text{S}_2\text{CH})]$. La réaction de CS_2 avec l'hydrure est probablement inhibée pour des considérations thermodynamiques ou peut-être en raison de sa stabilité thermique inférieure à celle de **12**.

Des cristaux uniques de $[(\text{phen}^*)\text{Cu}^{\text{I}}(\kappa^1\text{-O}_2\text{CH})_{0.8}\text{I}_{0.2}]\cdot(\text{THF})_{0.5}$ (**12'**) ont pu être cultivés dans un tube RMN par diffusion lente de pentane dans un mélange THF brut de **12** préparé in situ. La présence d'atomes d'iode dans le cristal résulte probablement d'une impureté résiduelle de KI contenue dans $[\text{Cu}(\text{O}^t\text{Bu})]$, ce dernier étant synthétisé par traitement de CuI avec du KO^tBu . Des vues de la structure du **12'** déterminée par diffraction des rayons X sont présentées dans la *Figure 11* avec des longueurs de liaison et des angles sélectionnés.

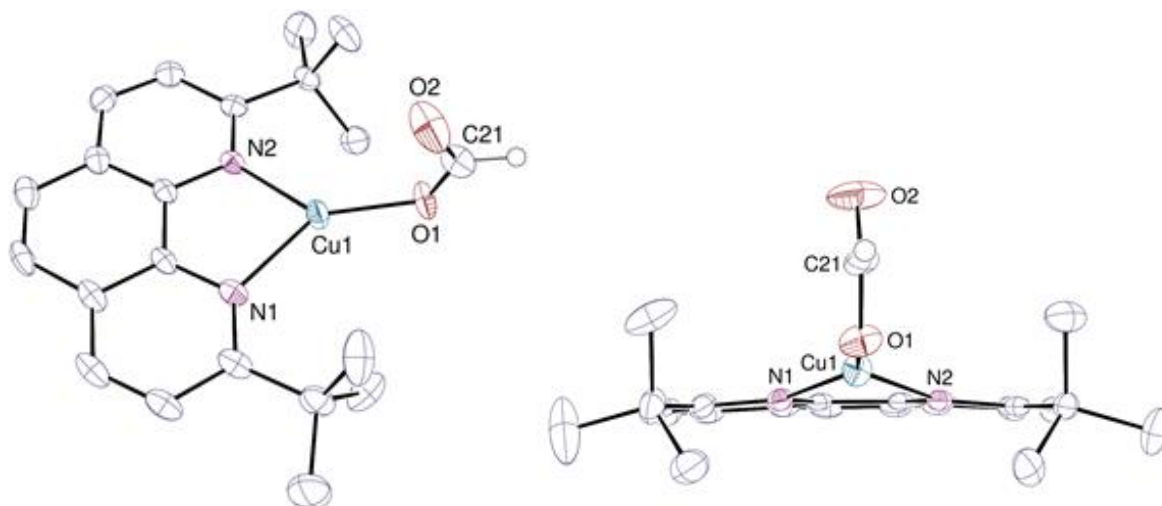


Figure 11. Deux vues de la structure cristalline du complexe 12'. Les ellipsoïdes de déplacement sont dessinés au niveau de probabilité de 50 % et les atomes d'hydrogène sont omis, à l'exception de celui du formiate. La composante mineure d'iode n'est pas représentée. Distances (Å) et angles (deg) des liaisons sélectionnées : Cu1-O1 1.883(3), Cu1-N1 2.029(3), Cu1-N2 2.080(3), O1-C21 1.248(5), O2-C21 1.242(4) ; N1-Cu1-N2 83.44(10), N1-Cu1-O1 140.69(13) ; N2-Cu1-O1 135.23(12).

Le complexe **12** n'est pas très actif dans la décomposition de FA en H_2 puisqu'il présente un TOF de 4 h^{-1} à 100°C pour une charge de catalyseur de 10 % en moles. Cette activité est cependant supérieure à celle rapportée pour certains précurseurs simples Cu(0), Cu(I) et Cu(II) en présence de NEt_3 et qui présentaient des TOF inférieurs à 1 h^{-1} à 95°C . L'espèce $[\text{Cu}(\text{NCMe})_4][\text{PF}_6]$ avec la présence de divers ligands et additifs phosphine ($^t\text{BuNC-NEt}_3$) à 70°C dans l'acétonitrile, a montré de plus grandes activités dans la décomposition du HCO_2H avec des TOF rapportés compris entre 10 et 240 h^{-1} . Cependant, tous ces catalyseurs au cuivre présentent des activités nettement inférieures aux valeurs TOF de 5 000 à $10\,000 \text{ h}^{-1}$ requises pour un procédé économiquement viable. Les systèmes catalytiques au fer ont des TOF d'environ $10\,000 \text{ h}^{-1}$ et des TON de 10^5 , et les complexes les plus efficaces sont actuellement basés

sur des métaux nobles (Ru et Ir), avec des valeurs TON supérieures à 10^6 . Par exemple, Williams et ses collègues en 2016 et Li et al. en 2015, ont rapporté un catalyseur binucléaire iridium(III) et deux organométalliques mononucléaires $(C_5Me_5)Ir(III)$ présentant, à $90^\circ C$, un TOF de $2,28 \times 10^5 h^{-1}$ (TON = $2,16 \cdot 10^6$) et $4,88 \times 10^5 h^{-1}$ (TON = $2,4 \cdot 10^6$ à $80^\circ C$), respectivement.

Un cycle catalytique peut alors être proposé (Schéma 1) : Dans un premier temps, une molécule de FA se coordonne ou interagit avec le complexe **12** pour donner soit l'adduit **I**, soit l'espèce **I'**. Ces deux composés se décarboxylent sous chauffage pour former l'hydrure de cuivre (**II**) qui réagit immédiatement avec l'acide voisin pour libérer du dihydrogène avec régénération de **12**.

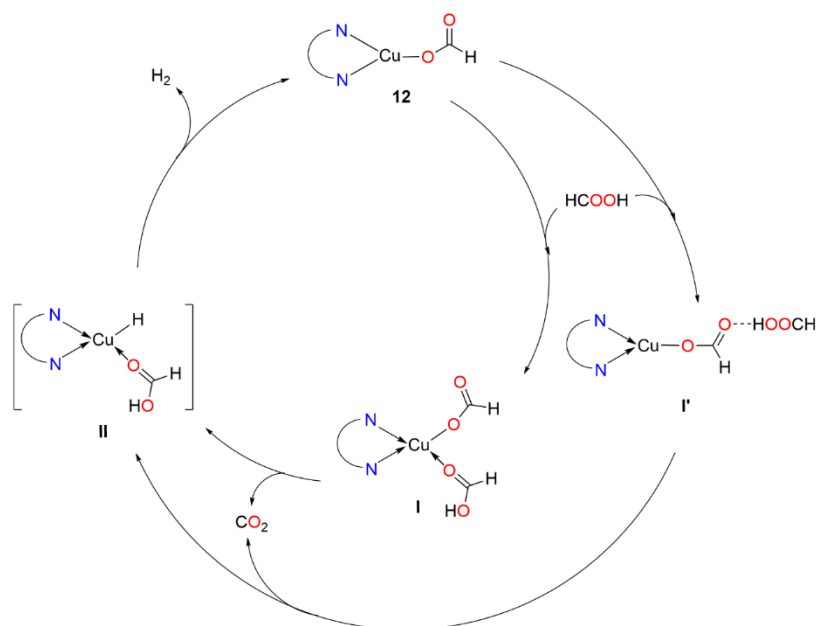


Schéma 1. Cycle catalytique proposé pour la déshydrogénation de l'acide formique par $[(phen^*)Cu(\kappa^1-O_2CH)]$ **12** comme pré-catalyseur.

Comme indiqué précédemment, le cuivre s'est avéré moins réactif que d'autres catalyseurs métalliques dans la déshydrogénation de l'alcool furfurylique pour produire de l' H_2/CO_2 . Cependant, le cuivre étant bon marché et abondant, le développement de la chimie du cuivre, avec des applications en catalyse, se poursuivra et s'étendra fortement.

En ce qui concerne notre système actuel, le rôle du ligand phen* est indéniablement important pour maintenir le centre de cuivre pendant le processus de transformation. Cependant, il y a des indications selon lesquelles l'encombrement et la labilité du phen* pourraient ne pas être efficaces pour fournir une stabilité adéquate au centre de cuivre sans compromettre sa réactivité. Par conséquent, une autre génération de dérivés phen peut être envisagée, comme la néocuproïne ou un ligand 2,9-di-néopentyl-1,10-phénanthroline. Avec une rigidité similaire mais moins d'encombrement stérique dans la sphère de coordination, ces ligands à base de phen pourraient améliorer l'activité catalytique du métal cuivre tout en évitant la décoordination du centre du cuivre qui conduit à la dégradation du complexe. Les ligands à pince NNO, NNN sont également une option, comme le (E)-N'-(phényl(pyridin-2-yl)méthylène)isonicotinohydrazide (Figure 12, a) (type NNO), bis(imidazolin-2-imine) à pont pyridinique (type NNN) (Figure 12, b), et (2,6-bis(diisopropylaminométhyl)-pyridine (type NNN) (Figure 12, c). Ce type de ligand possède trois sites de coordination via des atomes N et/ou O qui sont

hémilabiles. Ces ligands offrent une plus grande flexibilité dans la sphère de coordination, ce qui permet d'ajouter ou de supprimer des liaisons supplémentaires en fonction des besoins du centre de cuivre. Par conséquent, une nouvelle génération de catalyseurs à base de cuivre peut être développée sur la base des ligands à pince de type azote.

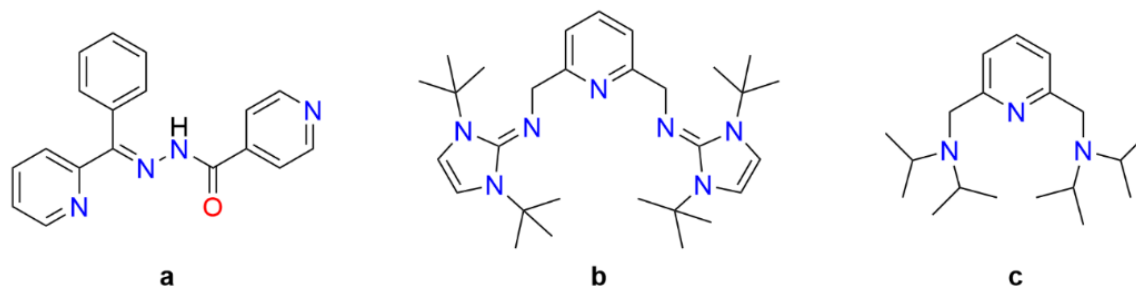


Figure 12. Exemples de ligands de type pince proposés.

Conclusion

Dans le chapitre 2, j'ai rapporté la synthèse d'une variété de complexes de (phen*)cuivre(I) carboxylate et de cuivre(I) aryle, en particulier des paires de composés avec le même fragment aryle. La plupart d'entre eux ont été caractérisés par leur structure cristalline.

Cette série de complexes a permis d'étudier le processus de décarboxylation des carboxylates de cuivre [(phen*)Cu(O₂CAr)] ainsi que l'insertion de CO₂ dans les dérivés aryliques de cuivre [(phen*)Cu-Ar]. J'ai démontré que certaines espèces de carboxylates de cuivre [(phen*)Cu(O₂CAr)] (Ar = *o*-F-C₅H₄ (**2**), C₆F₅ (**4**), *o*-NO₂-C₅H₄ (**5**)) pouvaient se décarboxyler dans un solvant de quinoléine à différentes températures, et que la réaction secondaire de protodécarboxylation (formation de Ar-H) se produisait inévitablement. La décarboxylation des complexes *ortho*-substitués **2** et **5** a été mise en évidence par le dégagement de gaz CO₂ par analyse GC et la formation des composés arènes correspondants, le fluorobenzène et le nitrobenzène, respectivement. Grâce à l'extrusion de CO₂ dans le complexe **4**, le complexe aryle de cuivre correspondant (**8**) a été détecté, ainsi que le produit secondaire de protodécarboxylation C₆F₅H. L'influence du solvant est cruciale et, par rapport au THF, la quinoléine favorise considérablement les processus de décarboxylation et de protodécarboxylation. Cependant, je n'ai jamais observé l'insertion de CO₂ dans les autres aryles de cuivre(I), un point qui reflète probablement la plus faible stabilité de ces composés aryliques qui sont rapidement dégradés sous l'effet de la chaleur et/ou à cause d'une thermodynamique défavorable.

Sur la base des expériences, deux voies plausibles sont proposées pour la décarboxylation de **4**. La première est en accord avec la littérature et procéderait par une extrusion concertée de CO₂ où le centre de cuivre interagit à la fois avec le carbone ipso de l'aryle et le fragment de CO₂. La seconde possibilité implique la coordination de la quinoléine au centre de cuivre qui favorise la première réaction latérale de protodécarboxylation. L'anion quinoléine dans [(phen*)Cu(quin)] réagit alors avec C₆F₅-H pour générer [(phen*)Cu(C₆F₅)] et la quinoléine.

Il reste donc des questions non résolues sur la réversibilité de la réaction et sur le fait de savoir si la voie de décarboxylation concertée passe par un intermédiaire de cuivre (III).

Je rapporte la synthèse du complexe de formate de cuivre $[(\text{phen}^*)\text{Cu}(\text{O}_2\text{CH})]$ (**12**) et sa structure à l'état solide obtenue par diffraction des rayons X sur un seul cristal. Il s'agit d'un complexe de formate monométallique très rare soutenu par un ligand azoté. Nous émettons l'hypothèse qu'une espèce de formate, comparée à un véritable dérivé de carboxylate, serait plus sensible et réactive à la décarboxylation. L'échange isotopique dynamique de **12** avec $^{13}\text{CO}_2$ a produit un mélange de **12** et de son dérivé marqué $[(\text{phen}^*)\text{Cu}(\text{O}_2^{13}\text{CH})]$ (**12***). Ce résultat a clairement mis en évidence la décarboxylation de **12** et, en raison de la réversibilité du processus sous CO_2 , la formation transitoire de l'hydrure de cuivre intermédiaire $[(\text{phen}^*)\text{Cu}-\text{H}]$. Ce dernier hydrure réactif insère immédiatement $^{13}\text{CO}_2$ pour donner $[(\text{phen}^*)\text{Cu}(\text{O}_2^{13}\text{CH})]$ (**12***). Susceptible d'être monomère, j'ai essayé d'isoler ou de détecter l'hydrure $[(\text{phen}^*)\text{Cu}-\text{H}]$ car les espèces $[\text{Cu}]-\text{H}$ monométalliques réactives sont activement recherchées depuis des années. Cependant, cette espèce instable est restée inaccessible et n'a pas pu être obtenue même par d'autres voies synthétiques qui ont toutes donné du cuivre élémentaire.

J'ai également montré que le complexe **12** est un catalyseur actif dans la déshydrogénation de l'acide formique. Il est intéressant de noter que la réaction ne nécessite aucun additif pour se dérouler. Cependant, ce catalyseur se dégrade à la fin de la réaction avec la libération du ligand phen^* . A partir des rapports de la littérature et de nos résultats, nous avons proposé un cycle catalytique pour la déshydrogénation de l'AF catalysée par **12**. Il implique soit la coordination de l'AF à l'ion cuivre, soit l'espèce solvate $[(\text{phen}^*)\text{Cu}(\text{O}_2\text{CH})] \cdot n(\text{HCO}_2\text{H})$ où le ligand formate interagit avec le proton de l'acide par liaison hydrogène. Une telle interaction des espèces de cuivre et de métaux de transition d avec l'acide fluorhydrique est bien documentée. Après l'extrusion du CO_2 , l'hydrure de cuivre généré est immédiatement piégé par l'acide pour produire du H_2 avec une régénération de **12**.

Introduction

The main goal of the decarboxylation and carboxylation processes, is to break and form new strong C–C bonds to make useful compounds for pharmaceutical and industrial purposes. The problem is that most of these processes require high energy activation with operational temperature exceeding 150 °C in solution chemistry. A clear mechanistic understanding of these transformations can help to rationalize and optimize the reaction conditions. However, in the current case, the harsh conditions make it difficult to monitor the reaction intermediates. As a result, the goal of improving a given process is fraught with pitfalls, particularly for the design of complex catalytic systems involving metal ions, ligands and solvent.

Since Gooßen first report on the Pd/Cu catalyzed decarboxylative cross-coupling reaction, the field of decarboxylative activation has grown tremendously. Many researchers have greatly contributed to the development of several pathways for the decarboxylative C–C bond construction starting with a wide range of carboxylic acids and (hetero)aromatic coupling partners.^{1–4} Thanks to their work, benzoic acids, which are inexpensive, stable, and easily accessible or natural reagents, became recognized as atom-economic alternatives to traditional cross-coupling partners. For instance, in 2007, the group of Gooßen introduced a Pd^{II}/Cu^I dimetallic catalyst system for the coupling reaction between *ortho*-substituted benzoic acids and a series of halogenated arenes.⁵ They highlighted the significance of substituents in *ortho*-position of benzoic acid substrates which generally improve the efficiency of the reaction. This crucial point was observed, with few exceptions, in many reports dealing with decarboxylative coupling with haloarenes or non-functionalized aromatic compounds. Although several methods have been proposed to accommodate a wide range of benzoic acid derivatives and coupling partners, many of these developments share the similar drawback of high reaction temperatures (*ca.* 150 °C), with in some cases the requirement of a stoichiometric amount of oxidizing agent such as silver or copper(II) salts.^{3,4}

Because of its high performance in decarboxylative processes, copper has been the most studied transition metal. Copper-promoted decarboxylative cross-coupling reactions have been successfully adapted to a wide range of functionalized carboxylic acids, including *meta*- and *para*-substituted derivatives, and employed in both stoichiometric and catalytic amount. The most cited drawback of these reactions is the elevated operational temperatures (*ca.* 170 °C). Theoretical investigations on the copper-catalyzed decarboxylation mechanism have suggested that copper(I) carboxylate and aryl-copper species are key intermediates. The decarboxylation step is thermodynamically unfavorable and generally occurs at high temperatures. The consensus on the mechanism is based on a one-step decarboxylation of a copper(I) carboxylate to a copper(I) aryl derivative.

In collaboration with our laboratory, Destro *et al.* at the CEA have developed a dynamic carbon isotope exchange reaction for labelling a range of carboxylic acids with ¹⁴CO₂. Such enrichment was possible with a copper(I) catalyst supported by ligands featuring a bisoxazoline scaffold in DMSO at 150 °C.⁶ This method allows the incorporation of labeled ¹⁴CO₂ into a wide series of carboxylic acids and provides a highly efficient synthetic pathway for carbon labeled products of interest for pharmaceutical applications. They proposed a reaction mechanism in which the extrusion of CO₂ from

copper(I) carboxylate and the incorporation of $^{14}\text{CO}_2$ into the copper(I) aryl intermediate take place reversibly. However, their attempts to isolate the copper intermediates were unsuccessful and no definitive conclusions were reached regarding the active copper species and their oxidation states.

The aim of this thesis was therefore to study and understand the mechanism of the decarboxylation process catalyzed by copper with simple ligand derived from 1,10-phenanthroline.

I propose in the first chapter of this manuscript a state of the art concerning the decarboxylative coupling reactions. Assessment of the advantages and drawbacks of the different metal complexes catalysts that promote these transformations will be presented. While copper catalysts are the most powerful, a part of the discussion will focus on the mechanistic studies carried out to explain the reactivity, and on the challenging tasks to isolate key intermediates.

In the second chapter, I present my synthetic work and the full characterization of a variety of copper(I) substituted benzoate complexes and their aryl derivatives with the goal to study their behavior in decarboxylation or carboxylation. We have first chosen 1,10-phenanthroline as a classical and common ancillary ligand. Due to problems of solubility and ligand redistribution, we then switched toward a bulkier derivative, *e.g.* 2,9-di-*tert*-butyl-1,10-phenanthroline (phen*), which offered solubility and greater stability of the complexes. With these novel complexes in hands, I studied by NMR the decarboxylation of copper(I) benzoate complexes as well as insertion of carbon dioxide into the aryl-copper(I) species. DFT calculations were carried out to rationalize the results.

Along my work on copper carboxylates, I also synthesis the copper (I) formate $[(\text{phen}^*)\text{Cu}(\kappa^1\text{-O}_2\text{CH})]$ that was expected to be more reactive than the above $[(\text{phen}^*)\text{Cu}(\text{O}_2\text{CR})]$ complexes. Monometallic copper formates are barely reported and those involving nitrogenated ancillary ligands are uncommon. In this third chapter, I present the synthesis and characterization of $[(\text{phen}^*)\text{Cu}(\kappa^1\text{-O}_2\text{CH})]$. Attempts at decarboxylation have been carried out to access or detect a monomeric hydride, *e.g.* $[(\text{phen}^*)\text{CuH}]$, which are generally instable species and attract interest for years. Even though the monohydride complex could not be observed or detected, its transient formation was indirectly evidenced by the dynamic carbon isotope exchange reaction which enabled the ^{13}C enrichment of $[(\text{phen}^*)\text{Cu}(\kappa^1\text{-O}_2\text{CH})]$ when placed under 1 bar of $^{13}\text{CO}_2$. This behavior suggested that $[(\text{phen}^*)\text{Cu}(\kappa^1\text{-O}_2\text{CH})]$ could be a catalyst in the formic acid dehydrogenation and I detailed the results.

I will finish by a general conclusion and some possible perspectives for this work. In particular, inspired by a recent work in our group regarding the copper(I)-catalyzed sulfonylative Hiyama cross-coupling, I have considered the SO_2 insertion into aryl-copper species and the reverse reaction (desulfonylation) from the isolated copper(I) sulfinate intermediate $[\text{Cu}(\text{O}_2\text{S-R})]$. Some results will be discussed.

References:

- (1) Perry, G. J. P.; Larrosa, I. Recent Progress in Decarboxylative Oxidative Cross-Coupling for Biaryl Synthesis: Recent Progress in Decarboxylative Oxidative Cross-Coupling for Biaryl Synthesis. *Eur. J. Org. Chem.* **2017**, 2017 (25), 3517–3527.
- (2) Rodríguez, N.; Goossen, L. J. Decarboxylative Coupling Reactions: A Modern Strategy for C–C Bond Formation. *Chem. Soc. Rev.* **2011**, 40 (10), 5030.
- (3) Wei, Y.; Hu, P.; Zhang, M.; Su, W. Metal-Catalyzed Decarboxylative C–H Functionalization. *Chem. Rev.* **2017**, 117 (13), 8864–8907.
- (4) Zhang, T.; Wang, N.-X.; Xing, Y. Advances in Decarboxylative Oxidative Coupling Reaction. *J. Org. Chem.* **2018**, 83 (15), 7559–7565.
- (5) Gooßen, L. J.; Thiel, W. R.; Rodríguez, N.; Linder, C.; Melzer, B. Copper-Catalyzed Protodecarboxylation of Aromatic Carboxylic Acids. *Adv. Synth. Catal.* **2007**, 349 (14–15), 2241–2246.
- (6) Destro, G.; Loreau, O.; Marcon, E.; Taran, F.; Cantat, T.; Audisio, D. Dynamic Carbon Isotope Exchange of Pharmaceuticals with Labeled CO₂. *J. Am. Chem. Soc.* **2019**, 141 (2), 780–784.

Abbreviation

acac	acetylacetonate	FLP	Frustrated Lewis Pair
BINAP	(2,2'-bis(diphenylphosphino)-1,1'-binaphthyl)	GC	gas chromatography
bipy	2,2'-bipyridine	GC-MS	gas chromatography-mass spectrometry
CIE	carbon isotopic exchange	<i>i</i> Pr	isopropyl
cod	1,5-Cyclooctadiene	LOHC	liquid organic hydrogen carriers
Cp	Cyclopentadienyl	Me	methyl
Cp*	pentamethylcyclopentadienide	Mes	1,3,5-trimethylbenzene
Cy	cyclohexyl	MOF	metal organic framework
DBU	1,8-diazabicyclo[5.4.0]undec-7-ene	MS	molecular sieve
dcpe	1,2-Bis(dicyclohexylphosphino)ethane	napy	1,8-naphthyridine
DFT	Density-functional theory	NHC	N-heterocyclic carbene ligands
DMA	Dimethylacetamide	NMP	<i>N</i> -methyl-2-pyrrolidone
DME	Dimethoxyethane	OTf	triflate (CF ₃ SO ₃ ⁻)
DMF	Dimethylformamide	OTs	Tosylate
DMSO	Dimethyl sulfoxide	P(<i>o</i> -Tol) ₃	Tri(<i>o</i> -tolyl)phosphine
dppp	1,3-Bis(diphenylphosphino)propane	Ph	phenyl
equiv.	equivalent	phen	1,10-phenanthroline
ESI-MS	Electrospray ionization	phen*	2,9-di- <i>tert</i> butyl-1,10-phenanthroline
ESR	Electron paramagnetic resonance	^t Bu	terbutyl
Et	ethyl	^t Bu-Li	tertbutyl lithium
FA	formic acid	TEMPO	(2,2,6,6-Tetramethylpiperidin-1-yl)oxyl
		TFA	Trifluoroacetic acid
		TFE	tetrafluoroethylene
		THF	tetrahydrofuran

TMEDA	Tetramethylethylenedia mine	TS	transition state
TOF	turnover frequency	XRD	X-Ray analysis diffraction
TON	turnover number		

Table of contents

Résumé substantiel	6
Introduction	21
Abbreviation	24
Chapter 1 – General introduction: Transition metal-catalyzed decarboxylative cross-coupling reactions	
Abstract :.....	31
I. Introduction	33
I. 1. Transition metal-catalyzed cross-coupling reactions	34
II. Transition metal-catalyzed decarboxylative process	35
II. 1. Carboxylic acid	35
II. 2. The origins of the decarboxylative processes	39
II. 3. Redox-neutral decarboxylative coupling reaction	42
II. 3. 1. Bimetallic system (Pd/Cu).....	42
II. 3. 2. Bimetallic system (Pd/Ag).....	47
II. 3. 3. Monometallic system	50
II. 4. Decarboxylative oxidative coupling.....	51
II. 4. 1. Decarboxylative C–H functionalization.....	51
II. 4. 2. Decarboxylative C–CO ₂ H functionalization (homo-coupling and cross-coupling).....	54
II. 5. Protodecarboxylation	56
III. Mechanistic study of copper catalyzed decarboxylation step in catalysis	59
III. 1. Experimental study.....	59
III. 2. DFT studies carried out for determining the mechanism of the copper catalyzed decarboxylation step in catalysis.....	61
III. 2. 1. Ortho effect	65
III. 2. 2. Effect of the nitrogen ligand:.....	68
IV. Conclusion	71
V. Objectives	73
VI. References	75
Chapter 2 – Syntheses, structures and reactivity of complexes [(2,9-(^tBu)₂-phen)Cu(O₂CAryl)] and [(2,9-(^tBu)₂-phen)Cu(Aryl)]: Experimental and Theoretical Investigation of the CO₂ Extrusion or Insertion	
Abstract :.....	86

I. State-of-the-art of the synthesis of copper(I) complexes supported by phenanthroline ligand.	88
II. Choice for the nitrogened ligand	90
III. Results and discussion	93
III. 1. Syntheses and crystal structures of the phen* (1) ligand	93
III. 2. Synthesis of the carboxylic complexes [(phen*)Cu(O ₂ CR)] (R = <i>o</i> -F-C ₆ H ₄ (2), <i>p</i> -F-C ₆ H ₄ (3), C ₆ F ₅ (4), <i>o</i> -NO ₂ -C ₆ H ₄ (5), <i>p</i> -NO ₂ -C ₆ H ₄ (6), CF ₃ (7)) and characterization.....	94
III. 3. Synthesis and structure of the aryl and alkyl [(phen*)Cu-R] complexes, R = C ₆ F ₅ (8), <i>o</i> -NO ₂ -C ₆ H ₄ (9), CF ₃ (11) & structure of the fluoride solvate [(phen*)CuF(HF)]·C ₆ H ₆ (10).....	100
III. 4. Study of the decarboxylation of the [(phen*)Cu(O ₂ CR)] complexes (R = C ₆ H ₄ - <i>o</i> -F (2), C ₆ H ₄ - <i>o</i> -NO ₂ (5), C ₆ F ₅ (4), CF ₃ (7))......	107
III. 4. 1. Decarboxylation in THF.....	107
III. 4. 2. Decarboxylation in other solvents.....	109
III. 5. Study of the carboxylation of the [(phen*)Cu-R] complexes 8 , 9 , and 11	115
III. 6. DFT calculation	118
III. 7. Proposed mechanism	121
IV. Conclusion	124
V. References	126
Chapter 3 – The isolation of a copper (I) formate complex and its reactivity in dynamic isotopic exchange and formic acid dehydrogenation	
Abstract	131
I. Introduction	133
I. 1. Physical and chemical methods to store dihydrogen.....	133
I. 2. State-of-the-art on the dehydrogenation of formic acid (FA).....	135
I. 2. 1. Formic acid as liquid hydrogen carrier	135
I. 2. 2. Transition metal-catalyzed dehydrogenation of formic acid	137
I. 2. 3. Copper-catalyzed dehydrogenation of formic acid and hydrogenation of CO ₂	140
I. 2. 4. Synthesis of monomeric copper(I) formate complexes	142
II. Results and discussions	147
II. 1. Synthesis and characterization of [(phen*)Cu(κ ¹ -O ₂ CH)] (12)	147
II. 2. Attempts to the copper monohydride [(phen*)Cu-H].....	149
II. 3. Stoichiometric reaction with ¹³ CO ₂	150
II. 4. Catalytic dehydrogenation of formic acid (FA).....	158
III. Conclusion and perspectives	164
III. 1. Conclusion	164
III. 2. Perspectives.....	164

IV. References.....165

Conclusion and Perspectives

I. Conclusion177

- I. 1. The synthesis of copper(I) carboxylate and copper(I) aryl complex supported by 2,9-^tBu₂phen (phen*) ligand and their reactivity toward decarboxylation and CO₂ insertion (Chapter 2) 177
- I. 2. The synthesis of phen* ligated copper formate complex (**12**) and its reactivity in dynamic isotopic exchange and formic acid dehydrogenation (Chapter 3) 178

II. Perspectives.....179

- II. 1. Decarboxylation of copper carboxylate complexes supported by quinoline ligand. 179
- II. 2. Insertion SO₂ into copper complexes 180

III. References.....182

Experimental part

I. General information186

II. Experimental part of chapter 2.....186

- II. 1. Synthese of phen* (**1**) ligand and [Cu(O^tBu)] 186
 - II. 1. 1. Spectra of 2,9-di-*tert*butyl-1,10-phenanthroline (**1**), (Formula: C₂₀H₂₄N₂, M= 292.19 g/mol) 186
 - II. 1. 2. Synthesis of [Cu(O^tBu)]₄..... 188
 - II. 1. 3. Data of complex [(phen*)Cu-O^tBu]: 189
- II. 2. General synthesis procedure for the formation of carboxylate complexes (phen*)Cu^I(O₂CR) (R = C₆H₄-*o*-F (**2**), C₆H₄-*p*-F (**3**), C₆F₅ (**4**), C₆H₄-*o*-NO₂ (**5**), C₆H₄-*p*-NO₂ (**6**), CF₃ (**7**)). 190
 - II. 2. 1. Data for complex [(phen*)Cu-(O₂CC₆H₄-*o*-F)] (**2**):..... 190
 - II. 2. 2. Data for complex [(phen*)Cu-(O₂CC₆H₄-*p*-F)] (**3**):..... 193
 - II. 2. 3. Data for complex [(phen*)Cu(O₂CC₆F₅)] (**4**):..... 195
 - II. 2. 4. Data for complex [(phen*)Cu(O₂CC₆H₄-*o*-NO₂)] (**5**): 198
 - II. 2. 5 Data for complex [(phen*)Cu(O₂CC₆H₄-*p*-NO₂)] (**6**): 200
 - II. 2. 6. Data for complex [(phen*)Cu(O₂CCF₃)] (**7**): 202
- II. 3. Synthesis of the [(phen*)Cu-R] complexes..... 205
 - II. 3. 1. Data for complex [(phen*)Cu-C₆F₅] (**8**): 205
 - II. 3. 2. Data for complex [(phen)Cu-C₆F₅] (**8'**): 208
 - II. 3. 3. Data for complex [(phen*)Cu(C₆H₄-*o*-NO₂)] (**9**): 209
 - II. 3. 4. Data for complex [(phen*)Cu-CF₃] (**11**): 213
 - II. 3. 5. Crystal structure of [(phen*)Cu-F(HF)]•C₆H₆ and NMR of [(phen*)Cu-F(HF)] (**10**)..... 216
- II. 4. Decarboxylation of the [(phen*)Cu(O₂CR)] complexes (R = C₆H₄-*o*-F, C₆F₅, C₆H₄-*o*-NO₂, CF₃) . 218
 - II. 4. 1. Decarboxylation in THF:..... 218

a. Thermal decarboxylation of [(phen*)Cu(O ₂ CC ₆ H ₄ -o-F)] (2)	218
b. Thermal decarboxylation of [(phen*)Cu(O ₂ CC ₆ F ₅)] (4):	220
c. Thermal decarboxylation of [(phen*)Cu(O ₂ CC ₆ H ₄ -o-NO ₂)] (5)	222
d. Thermal decarboxylation of [(phen*)Cu(O ₂ CCF ₃)] (7).....	223
II. 4. 2. Decarboxylation in quinoline:.....	225
a. Control experiment:.....	225
b. [Cu(C ₆ F ₅)(quinoline) _n].....	226
c. Reaction of [Cu(C ₆ F ₅)(quinoline) _n] and 1 equiv. phen*.....	227
d. Thermal decarboxylation of [(phen*)Cu(O ₂ CC ₆ H ₄ -o-F)] (2) in quinoline.....	230
e. Thermal decarboxylation of [(phen*)Cu(O ₂ CC ₆ F ₅)] (4) in quinoline.....	230
g. Thermal decarboxylation of [(phen*)Cu(O ₂ CCF ₃)] (11) in quinoline.....	233
h. Thermal decarboxylation of [(phen*)Cu(O ₂ CCF ₃)] (11) in DMF-d ₇	234
II. 5. Carboxylation of the [(phen*)Cu-R] complexes 8 , 9 , and 11	234
II. 5. 1. Carboxylation of [(phen*)Cu(C ₆ F ₅)] (8).....	234
a. Carboxylation of [(phen*)Cu(C ₆ F ₅)] (8) in DMA.....	235
b. Carboxylation of [(phen*)Cu(C ₆ F ₅)] (8) in quinoline.....	235
c. Carboxylation of [(phen*)Cu(C ₆ F ₅)] (8) in THF-d ₈	236
II. 5. 2. Carboxylation of [(phen*)Cu(C ₆ H ₄ -o-NO ₂)] (9).....	237
a. Carboxylation of [(phen*)Cu(C ₆ H ₄ -o-NO ₂)] (9) in C ₆ H ₆ -d ₆	238
b. Carboxylation of [(phen*)Cu(o-NO ₂ -C ₆ H ₄)] (9) in Tol-d ₈	239
II. 5. 3. Carboxylation of [(phen*)Cu(CF ₃)] (11) in DMA.....	240
II. 5. 4. Carboxylation of [(phen*)Cu(CF ₃)] (11) in THF-d ₈	241
III. Experimental part of Chapter 3	243
III. 1. Synthesis of [(phen*)Cu(κ ¹ -O ₂ CH)] (12) (Formula : C ₂₁ H ₂₅ CuN ₂ O ₂ , M= 400.99 g/mol).....	243
III. 2. [(phen*)Cu-(O ₂ CH)] in THF-d ₈ at low temperatures.....	245
III. 2. 1. Solution of [(phen*)Cu(O ₂ CH)] in THF-d ₈ at 210 K (-63 °C).....	247
III. 3. Thermal decomposition of [(phen*)Cu(O ₂ CH)] (12).....	248
III. 4. Attempts to isolate/detect copper hydride	249
III. 4. 1. Reaction of Cu(O ^t Bu) + Phen* with dihydrogen:.....	249
III. 4. 2. Reaction of Cu(O ^t Bu) + Phen* with HBpin:.....	249
III. 4. 3. Reaction of Phen* with Stryker reagent [Cu(PPh ₃)H] ₆ :	250
III. 4. 4. Reaction of [(phen*)CuI] with hydride reagents:	251
III. 4. 5. Thermal reaction of 12 in presence of EtN=C=O:.....	251
III. 4. 6. Thermal behavior of 12 in presence of BEt ₃ :.....	252
III. 4. 7. Synthesis of [{(phen*)Cu} ₂ (μ-O ₂ CH)][(HCO ₂ -κ ¹)B(C ₆ F ₅) ₃] (13) by reaction of 12 with B(C ₆ F ₅) ₃ :	252

III. 4. 8. Synthesis of $[\text{HNEt}_3][(\text{HCO}_2-\kappa^1\text{B}(\text{C}_6\text{F}_5)_3)]$:	255
III. 4. 9. Thermal behavior of 12 in presence of with phenylacetylene:	257
III. 4. 10. Stoichiometric reaction of 12 with $^{13}\text{CO}_2$:	257
III. 4. 11. Stoichiometric reaction with CS_2	262
III. 5. Procedure for the catalytic dehydrogenation of formic acid	262
III. 5. 1. General catalysis experiment	262
III. 5. 2. Representative procedure for the catalytic dehydrogenation	262
III. 5. 3. GC analysis for catalytic dehydrogenation of formic acid	266
III. 5. 4. Proof for the decomposition of complex 12 after catalysis	267
VI. Experimental part of Perspectives	269
VI. 1. Formation of $[\text{Cu}(\mu\text{-O}_2\text{C-C}_6\text{H}_4\{\text{o-NO}_2\})(\text{quin})]_2$ (14) and $[\text{Cu}(\mu\text{-O}_2\text{C-C}_6\text{H}_4\{\text{o-F}\})(\text{quin})]_2$ (15) ...	269
IV. 1. 1. Data for $[\text{Cu}(\mu\text{-O}_2\text{C-C}_6\text{H}_4\{\text{o-NO}_2\})(\text{quin})]_2$ (14):	269
IV. 1. 2. Data for $[\text{Cu}(\mu\text{-O}_2\text{C-C}_6\text{H}_4\{\text{o-F}\})(\text{quin})]_2$ (15):	270
IV. 2. Synthesis of $[(\text{phen}^*)\text{Cu}(\kappa^1\text{-O}_2\text{SCF}_3)]$ complex (16)	271
IV. 3. SO_2 insertion into $[(\text{phen}^*)\text{Cu-CF}_3]$ (11) for the formation of $[(\text{phen}^*\text{-Cu})_2\text{-O}_2\text{S-CF}_3]$ (17). ...	273
V. Computational details	275
VI. Crystallography	275

Chapter 1 – General introduction: Transition metal-catalyzed decarboxylative cross-coupling reactions

Abstract:

In recent years, transition metal-catalyzed decarboxylative cross-coupling reactions have emerged as a new and important category of organic transformation that find a wide variety of applications in building carbon-carbon and carbon-heteroatom bonds. In these reactions, carboxylic acids are used as starting material to form new C-C bonds with the coupling partners and releases CO₂ as side products. The coupling partners can be varied from alkynes, heteroarenes to haloarenes, while (hetero)aromatic carboxylic acids, alkanolic acids and unsaturated carboxylic acids can be used. Decarboxylation cross-coupling to biaryl products has received much attention as these are important structural motifs in many biologically active compounds.

In this chapter, various types of decarboxylative cross-coupling reactions for the synthesis of biaryl compounds catalyzed by different transition metal complexes will be reviewed. The scope and applications of these reactions will be discussed together with the challenges and limitations in this field. The copper-catalyzed decarboxylation process will be the focus of attention, as it is amenable to more general reaction conditions. Mechanistic insights with respect to the active copper intermediates will be the subject of discussion, where both experimental and computational investigations will be presented.

Table of contents

Abstract:	31
I. Introduction	33
I. 1. Transition metal-catalyzed cross-coupling reactions	34
II. Transition metal-catalyzed decarboxylative process	35
II. 1. Carboxylic acid	35
II. 2. The origins of the decarboxylative processes	39
II. 3. Redox-neutral decarboxylative coupling reaction	42
II. 3. 1. Bimetallic system (Pd/Cu).....	42
II. 3. 2. Bimetallic system (Pd/Ag).....	47
II. 3. 3. Monometallic system	50
II. 4. Decarboxylative oxidative coupling.....	51
II. 4. 1. Decarboxylative C–H functionalization.....	51
II. 4. 2. Decarboxylative C–CO ₂ H functionalization (homo-coupling and cross-coupling).....	54
II. 5. Protodecarboxylation	56
III. Mechanistic study of copper catalyzed decarboxylation step in catalysis	59
III. 1. Experimental study.....	59
III. 2. DFT studies carried out for determining the mechanism of the copper catalyzed decarboxylation step in catalysis.....	61
III. 2. 1. Ortho effect	65
III. 2. 2. Effect of the nitrogen ligand:.....	68
IV. Conclusion	71
V. Objectives	73
VI. References	75

I. Introduction

The creation of carbon-carbon (C-C) bonds is at the heart of organic synthesis, to build organic molecules with increasing complexity. Among these man-made chemicals, biaryl units are relevant molecules in organic chemistry. They are convenient building blocks in many biologically active and functional molecules, from pharmaceuticals and functional materials to agrochemicals (*Figure 13*).¹⁻⁶ While traditional syntheses of biaryl derivatives developed by Scholl,⁷ Gomberg-Bachmann⁸ and Ullmann^{9,10} in the XIXth century are limited by harsh reaction conditions and low efficiency, the developments of catalytic synthetic procedures in milder conditions have favored their use and their rise. Numerous catalytic synthetic strategies have been designed and explored, with transition metal-catalyzed cross-coupling reaction being especially prominent and superbly applicable (*Scheme 2*).

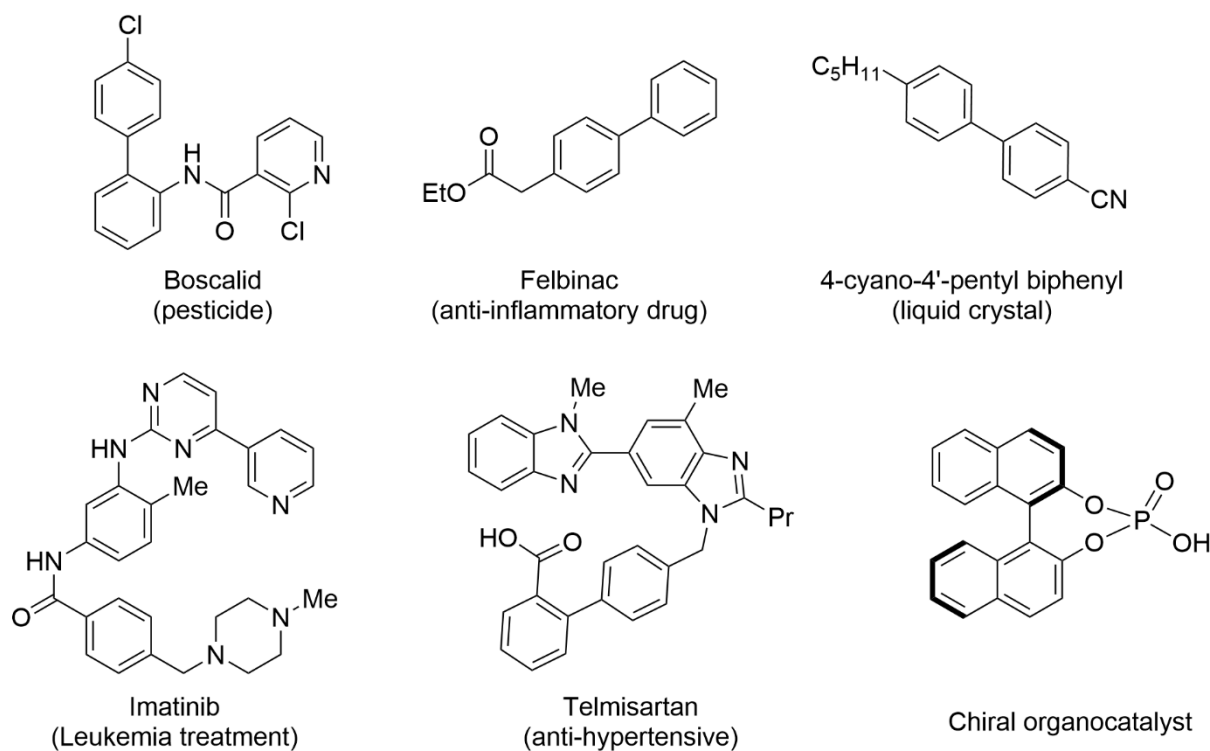
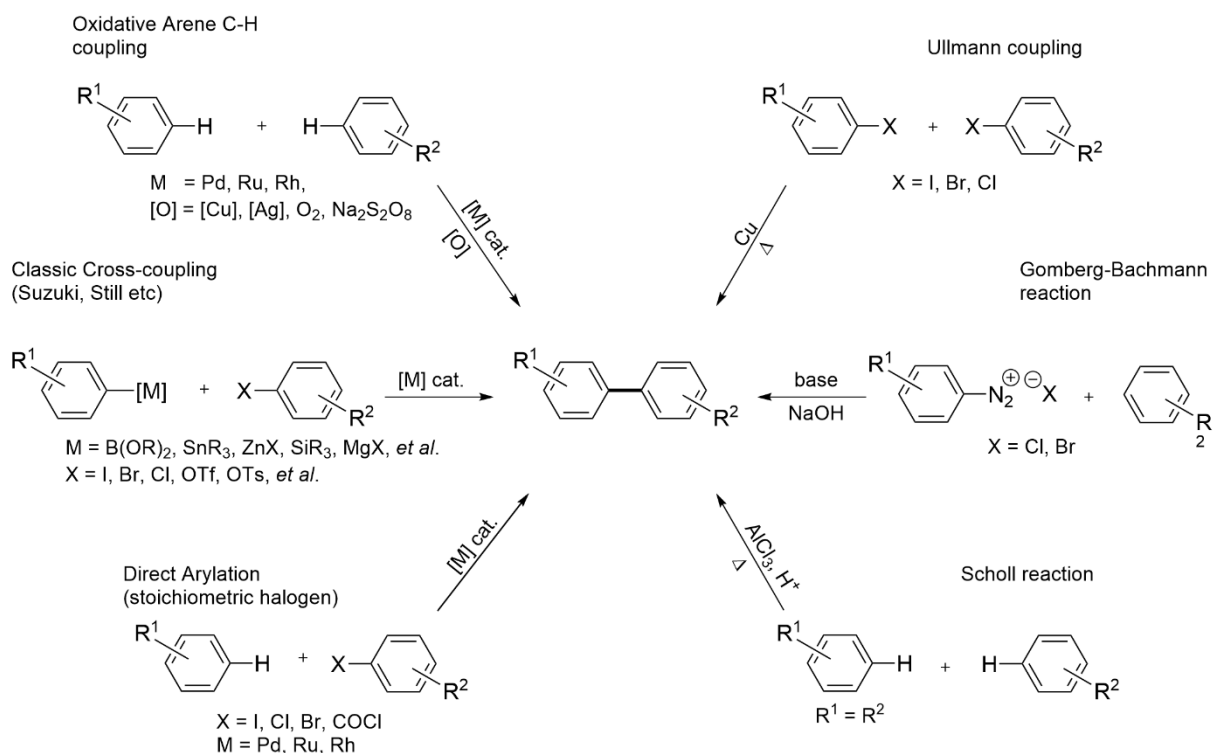
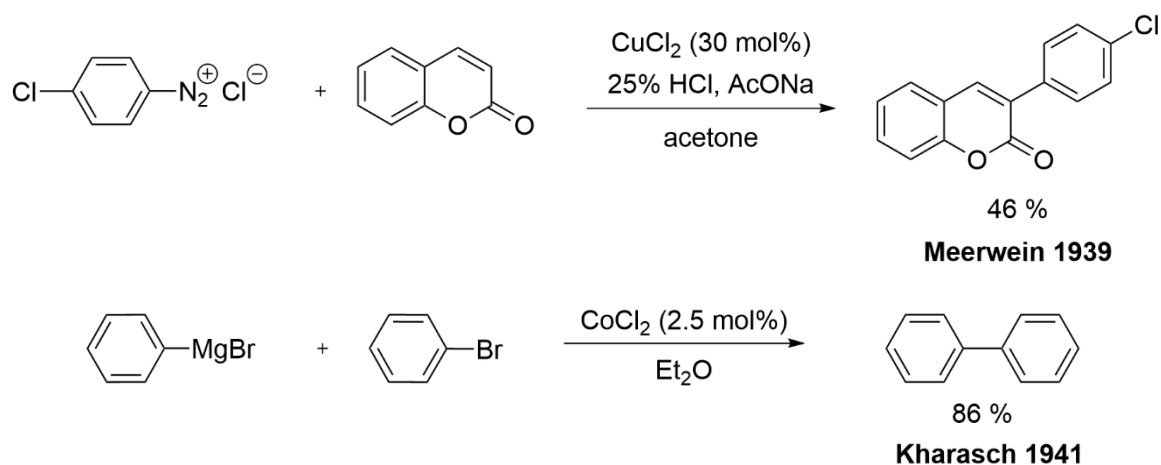


Figure 13. Some examples of functional biaryls in medicinally, functional material, and agriculturally important compounds.^{11,12}

Scheme 2. Selected traditional biaryl syntheses.¹¹⁻¹³

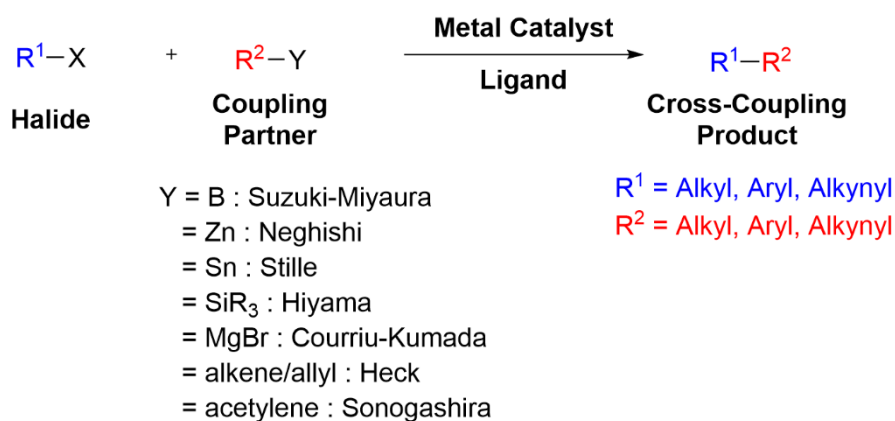
1.1. Transition metal-catalyzed cross-coupling reactions

The fundamental premise of the cross-coupling catalysis was first demonstrated by Meerwein¹⁴ for the coupling of aryl diazonium salts with substituted alkenes by copper(II) salt in 1939 and later in 1941 by Kharasch¹⁵ in the cross-coupling of phenyl bromide with Grignard reagents using cobalt chloride (Scheme 3). In subsequent study in 1943, Kharasch extended this reaction to vinyl bromide as coupling partner with higher loading of cobalt chloride salt. Although these two types of coupling are limited in substrates scope and chemical selectivity, these discoveries serve as the foundation of the formation of carbon–carbon bonds catalyzed by transition metals.



Scheme 3. The first catalytic cross coupling syntheses of aryl towards biaryls and bicycles: Meerwein and Kharasch reactions.

The main developments in the coupling process have taken an innovative turn in the 1970's. In 1972, Kumada and Corriu independently reported the nickel- and palladium-catalyzed coupling reaction of aryl and alkenyl halides with Grignard reagents.^{16,17} Their discoveries were a major breakthrough to solve the selectivity problem of Kharasch coupling reaction, in which homodimerization byproducts prevailed, and to introduce the beneficial role of phosphine ligand. Alongside the discoveries of Kumada and Corriu, several innovative cross-coupling protocols employing aryl or vinyl halides with much less nucleophilic coupling partners have been designed, namely Mizoroki-Heck, Sonogashira-Hagihara, Negishi, Stille and Suzuki-Miyaura cross-coupling reactions. These reactions provide a synthetic method for the formation of a C-C bond between a sp²-hybridized aryl halide electrophile and a nucleophilic partner, which can be an organometallic reagent or an activated alkene, allylic, or acetyl. In these classical cross-coupling reactions, it is well known that the key roles are played by the palladium catalyst and the ligands, especially those of the phosphine type (*Scheme 4*).^{18,19} These highly convenient methodologies for building C-C bonds between an electrophilic substrate and a nucleophilic coupling partner have become powerful in organic synthesis with applications in industry.²⁰⁻²³



Scheme 4. General transition metal-catalyzed cross-coupling reaction.

The interest of these discoveries was highlighted by the attribution of the Chemistry Nobel Prize (2010) to the groups of Heck, Negishi and Suzuki.²⁴ Despite the significance of these transition-metal-catalyzed C-C bond formations, there are still some drawbacks. One of them is the requirement of specific organo-coupling reagent. Since the functionalization of both coupling partners are essential for a successful C-C formation, readily available coupling partners would be of high interest. Among the most common functionalities, carboxylic acids are strong candidates to serve as building blocks in the construction of biaryl frameworks without the need of additional activation.

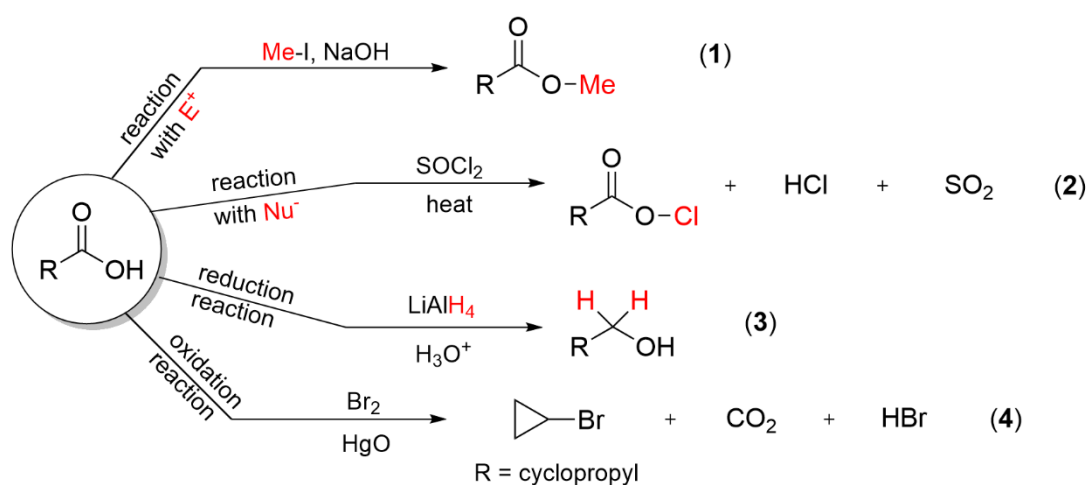
II. Transition metal-catalyzed decarboxylative process

II. 1. Carboxylic acid

Carboxylic acids are naturally abundant, with a structural diversity, they are thus highly important in chemical feedstocks for the industrial production of polymers (polyester and polyamides),²⁵ pharmaceuticals,²⁶⁻²⁸ food additives,²⁹ etc. They can be easily and largely accessible from industrial or laboratory via various synthetic methods.³⁰ In general, industrial routes to carboxylic acids includes

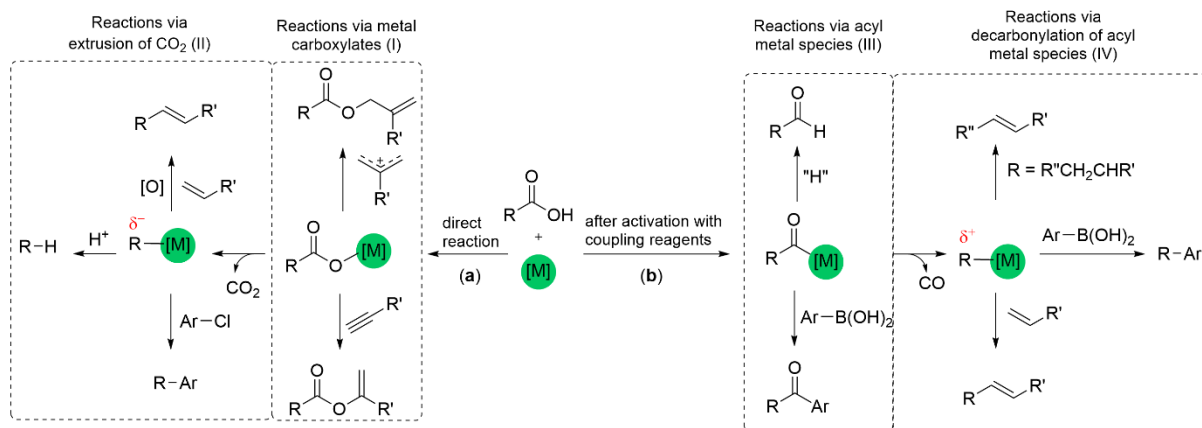
petroleum-based production,³¹ fermentation,^{32,33} oxidation of aldehydes³⁴ and natural sources extraction and/or synthesis.^{35,36} Small-scale preparative methods for carboxylic acids on the other hand often employ oxidants or reagents. For instance, aromatic carboxylic acids can be obtained by oxidizing the alkyl chains on the aromatic rings with a strong oxidizing reagent such as potassium permanganate or chromic acid.³⁰ This method can be applied for any side chains notwithstanding its length; however, it is most convenient for methyl group. Another possible approach is the employment of aryl Grignard reagents that add to one C=O bond of CO₂ to give magnesium carboxylate salts.³⁰ Subsequent treatment of this salt by a strong aqueous acid affords the carboxylic acid product.

With two oxygen active sites, carboxylic acids can react distinctly depending on the reaction conditions and the reagents (*Scheme 5*). For instance, under basic condition, carboxylic acid can undergo substitution of the hydroxyl hydrogen by an electrophilic substrate (*Scheme 5, 1*). On the other hand, the hydroxyl group of a carboxylic acid can be replaced by another nucleophilic group for the production of functional derivatives of carboxylic acids. For example, acyl chloride can be prepared by hydroxyl substitution reaction of carboxylic acid with thionyl chloride (SOCl₂) (*Scheme 5, 2*). Moreover, carboxylic acids undergo Fischer esterification with alcohol, in the presence of an acid as catalyst. In addition, due to the high oxidation state of the carbon atom of a carboxyl group, the powerful metal hydride reagent such as lithium aluminum hydride (LiAlH₄) can reduce carboxylic acids to alcohol rapidly (*Scheme 5, 3*). In the contrary, further oxidation of carboxylic acids results in the generation of carbon dioxide, so called decarboxylation, by oxidizing agent such as Br₂ or Pb(OCOCH₃)₄ (*Scheme 5, 4*).³⁷



Scheme 5. Examples of reactions of carboxylic acids.

In homogeneous catalysis, carboxylic acid can be used as convenient substrates towards carboxylate and acyl entities for the preparation of different product classes, using metal catalysts. The activation of carboxylic acid by metal catalyst follows two main pathways, either to generate a metal carboxylate, (RCO₂)[M], via a direct reaction (*Scheme 6a*) or the formation of metal acyl species, (RCO)[M], through activating reagents (*Scheme 6b*).

Scheme 6. Carboxylic acids in catalytic transformations.³⁸

For the first pathway, after the direct deprotonation of the hydroxyl group O-H bond, the resulted metal carboxylates can undergo addition with alkene, alkyne or allene to produce ester derivatives, namely hydroacyloxylation reaction or oxidative acyloxylation reaction in the presence of oxidant (Scheme 6, I).^{39,40} Here, a wide range of carboxylic acids, from saturated carboxylic acids to (hetero)aromatic, can be used. In hydroacyloxylation process, predominant transition metal catalysts are Ru,^{41–44} Rh,⁴⁵ Au,^{46–48} Pd.^{49,50} The reaction conditions varies from room temperature to 110 °C, depending on the catalyst systems, with the presence of common bases such as DMAP, NEt₃ or Na₂CO₃.^{49–52} Alternatively, under oxidative conditions, an addition of carboxylic acids with alkenes to form enol esters takes place. Such oxidative acyloxylation reactions are mostly promote by Pd or Pd/Cu catalysts with oxygen or other oxidizing agents such as MnO₂ or PhI(OAc)₂.⁵³

At higher temperatures (110 °C–170 °C), these metal carboxylates can further undergo CO₂ extrusion to generate a nucleophilic [R-M] complexes (Scheme 6, II). [R-M] intermediates are reported with aromatic derivatives (for R) and various transition metals such as Pd, Cu, Ag, etc. (for M). The reaction temperature varies depending on the metals, and the generation of metal aryl complexes are not often observed but rather react with electrophilic substrates. For example, copper or silver metals can mediate catalytically the decarboxylation of aromatic carboxylic acids to produce arene compounds in the presence of proton sources at high temperature (*ca.* 170 °C).^{54–56} This reaction is known as protodecarboxylation. As an alternative, the use of a palladium catalyst reduces the reaction temperature to 70 °C, but the system only works with electron-rich 2,6-disubstituted benzoic acids.⁵⁷ [R-M] intermediates are also known to enable coupling reaction with haloarene to afford biaryl products. This C-C bond formation between aromatic carboxylic acids and the aryl coupling partners can be catalyzed by Pd/Cu, Pd/Ag bimetallic systems; Pd, Cu single catalysts are also used but require higher temperatures (*ca.* 170 °C).^{58–61} This transformation becomes well-known and widely used under different variations which are generally known as decarboxylative coupling reaction. A Heck-type reaction is also introduced, in which the aromatic or heteroaryl carboxylic acids are treated with alkenes in the presence of oxidizing agents to form vinyl arene via the metal aryl [R-M] species upon release of CO₂. The reaction carried out at around 100 °C with most often employed mediators are palladium metal in catalytic amount and oxidant such as Ag₂CO₃ or Me₃NO.^{62,63}

The second pathway involves a cleavage of C(O)-O bond by a oxidative addition of the metal assisted by the activating reagent such as anhydrides ((^tBuCO)₂O, (MeCO)₂O), or acid chloride to generate a

metal acyl species $RC(O)[M]$ (Scheme 6, b). These metal acyl species can be employed for the preparation of aldehydes via direct hydrogenation (Scheme 6, III). The reaction proceeds under relatively mild condition (ca. 80 °C) using Pd catalyst to transform a wide range of carboxylic acids into aldehydes in moderate to good yields (30% - 99%).⁶⁴

The acyl metal species can also be transferred to carbon nucleophiles, such as organozinc, organotin, organoboron, and nitriles (Scheme 6, III),⁶⁵ for the synthesis of aryl ketones. The classic methods often promote by Pd-catalyst with anhydride activate agent at low temperature (ca. 60 °C).^{66–68}

Alternatively, another type of reactivity has been observed, the $RC(O)M$ may undergo a decarbonylative process and loose a CO molecule to afford a R-M intermediate (Scheme 6, IV). Most reactions takes place at high temperature (ca. 120 °C) in the presence of Pd catalysts and anhydride as activating agent for the carboxylic acids.^{69,70} This R-M species can react in different ways with alkenes to produce vinyl arene via Heck-type reaction or with organoboron reagent to form Suzuki-coupling product. This Heck-type reaction is generally catalyzed by Rh or Pd catalysts and proceeds under elevated reaction temperature (ca. 140 °C).^{71–73} This Suzuki-coupling reaction is achieved by the use of Rh catalyst with a catalytic amount of KF as a base for the formation of biaryl products.⁷⁴ Hetero aromatic carboxylic acids can also react with boronic acids to afford heterobiaryls compounds.⁷⁵ The reaction employs Pd as catalyst, in presence of a base (NEt_3) and pivalic anhydride to activate the carboxylic acids. Alternatively, when R contains β -hydrogen atoms, β -hydride elimination can occur, producing the corresponding 1-alkene derivatives.

From the 2000's and the pioneer works of different research groups, decarboxylative coupling for biaryl synthesis has been the source of a renewed interest. Depending on the substrate as well as the reaction condition, metal-catalyzed decarboxylation of carboxylic acid have been sorted into three categories:

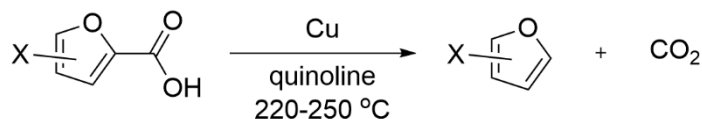
- Redox-neutral decarboxylative cross-coupling
- Decarboxylative oxidative coupling
- Protodecarboxylation

The challenging step of these three reactions is the extrusion of CO_2 to generate an organometallic species that reacts with the coupling partner or undergoes fast protonation. One main drawback of these reaction is the requirement of high temperature to extrude CO_2 .

The aliphatic or aromatic carboxylic acids (RCO_2H) is activated by anhydride ($(R'CO)_2O$) to form a mixture of new carboxylic acid ($R'CO_2H$) and homo- and heteroanhydrides ($(RCO)_2O$, RCO_2CO). Although this reaction is in equilibrium, the formation of sterically less demanding new anhydride is preferred. Recently, another strategy for ketones synthesis via direct coupling between aromatic carboxylic acids and organohalides were developed.^{28,76} This method is enabled by visible-light Ir photoredox catalysis with or without Ni catalysts, and triphenylphosphine as an activating agent for carboxylic acids and a base (e.g. K_3PO_4).

II. 2. The origins of the decarboxylative processes

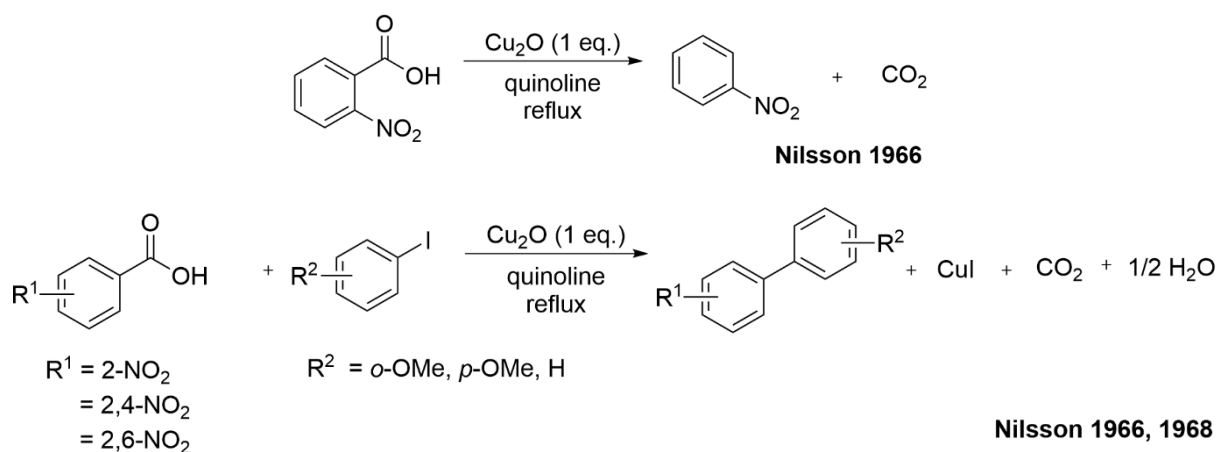
Historically, the discovery of transition metal-promoted decarboxylation dates from 1930 when Shepard *et al.* reported a synthesis of halogenated furans from the corresponding furoic acids (Scheme 7).⁷⁷ In their study, they observed that copper bronze (metal alloys consisting copper as principal component) promoted the protodecarboxylation of halogenated furancarboxylic acids at high temperatures (*ca.* 250 °C) in good yields (75–97 %).



Shepard 1930

Scheme 7. First example of copper-promoted decarboxylation of halogenated furoic acids.

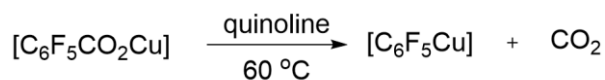
Forty years after this pioneering work, the copper-mediated protodecarboxylation protocol was extended to larger scope of activated aromatic and vinylic acids by the groups of Nilsson,^{78,79} Sheppard,⁸⁰ and Cohen⁸¹ during the 1970's. Studies on the ability of cuprous salts to promote carbon dioxide extrusion by Nilsson revealed the intermediacy of aryl-copper complexes, which are able to couple with iodobenzene to give a biaryl derivative (Scheme 8).^{78,79}



Nilsson 1966, 1968

Scheme 8. Copper-mediated decarboxylation processes by Nilsson.

Meanwhile, Sheppard *et al.* described the direct decarboxylation of cuprous carboxylates into copper(I) aryl complex.⁸⁰ They demonstrated a synthetic method for carboxylate cuprous complexes by the reaction of *m*-(trifluoromethyl)phenyl copper octamer and carboxylic acids with nearly quantitative yields (*ca.* 99 % for benzoic acids derivatives). Most significantly, the discovery that pentafluorophenylcopper complex [Cu(C₆F₅)] can be produced and isolated by decarboxylation of cuprous pentafluorobenzoate [Cu(O₂CC₆F₅)] (Scheme 9). This is the first example of the production of a copper aryl compound by the decarboxylation of a copper carboxylate. They also observed that basic solvents promote the decarboxylation event, in which quinoline gave the fastest reaction rate compared to other solvents, such as tetraglyme, nitrobenzene, and tri-*n*-butylamine.⁸⁰



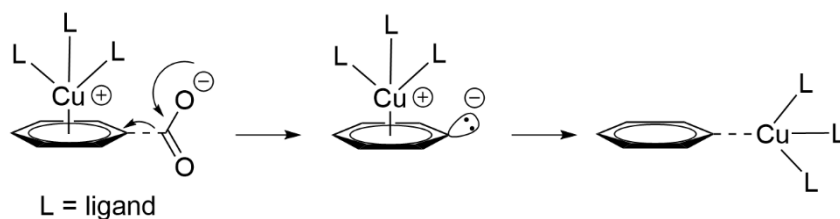
Sheppard 1970

Scheme 9. Decarboxylation of copper carboxylate to copper aryl complex by Sheppard.

In his kinetic study for the decarboxylation promoted by cupric or cuprous salts,⁸² Cohen *et al.* disclosed several important observations:

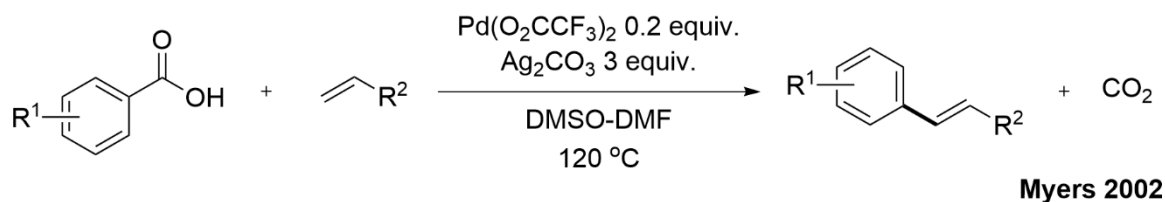
- The loss of CO₂ is first order in both cuprous and cupric carboxylates;
- Copper(I) and copper(II) salts react in identical fashion and nearly at the same rate;
- Chelating ligands such as 1,10-phenanthroline enhance the rate of decarboxylation of both types of salt;
- The reduction of cupric benzoate by quinoline is prior to the loss of CO₂.

Overall, they proposed a mechanism via the transient formation of a π -bonded copper(I) complex that would stabilize the negative charge on the aromatic ring thus favoring the loss of carbon dioxide (Scheme 10). Subsequent formation of σ -bond between the Cu⁺ ion and a carbon atom of the aromatic ring was proposed from Nilsson's investigation.⁷⁸

Scheme 10. Proposed decarboxylation mechanism by Cohen *et al.*⁸¹

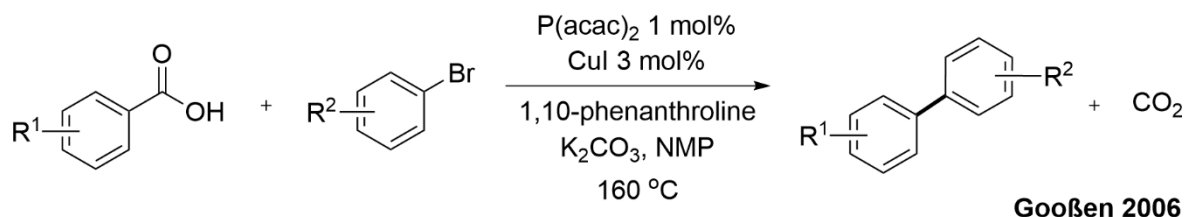
Although the early decarboxylation protocols by Shepard, Nilsson, Sheppard, and Cohen were extremely limited in substrate scope and required copper reagents in stoichiometric amount, their insightful works were of paramount significance to the current understanding of the transition metal-mediated decarboxylation reaction.

The 2000's and 2010's saw a wealth of innovations in the field of transition metal catalysis with major contributions from the groups of Myers, Gooßen, Crabtree, Larrosa, Greaney, Cahiez and Su. These contributions demonstrated that not only copper but other transition metal ions such as Ag⁺, Pd²⁺, Au⁺ and Rh³⁺ can promote C(sp²)-C(sp²) bond formation via decarboxylation process of aromatic carboxylic acids. Myers *et al.* arose again the interest in decarboxylative functionalization, after 3 decades of silence, when they reported in 2002 the first palladium-catalyzed decarboxylative coupling reaction of arene carboxylates with olefinic substrates (Scheme 11).⁶² However, a stoichiometric amount of silver additives is mandatory for the reaction to occur.



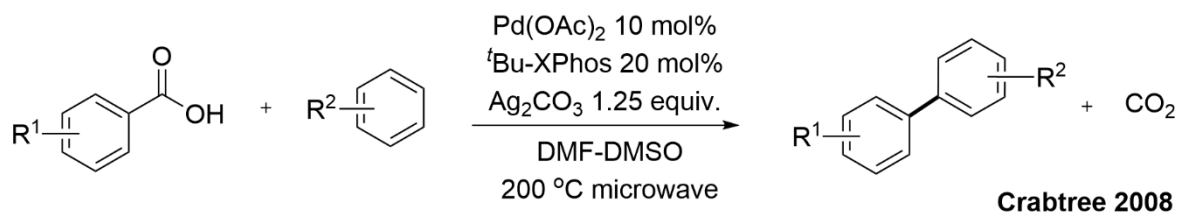
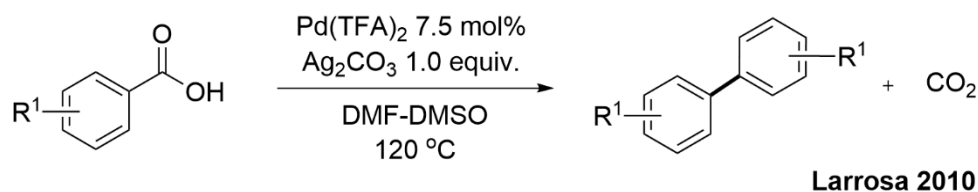
Scheme 11. First example of palladium catalyzed Heck-type decarboxylative cross-coupling reaction.

A few years later, the group of Gooßen reported a novel strategy for the direct decarboxylative arylation of benzoic acid derivatives and their coupling with bromoarenes to form biaryls (*Scheme 12*).⁸³ This study highlighted the unusual employment of two different metals (palladium and copper) in catalytic amounts used in tandem to perform the catalysis. This remarkable achievement ushered in a new era of carboxylic acid transformation as alternative aryl sources in cross-coupling procedures, which stimulated efforts to broaden the scope of such type of reaction. Consequently, a number of research groups have focused their efforts on the development of more efficient and more general catalytic systems. Their goal was the design of new complexes with various metals and ligands with different steric and electronic properties. Furthermore, the influence of solvents and the technique for applying to various activated or deactivated carboxylic acids were also investigated. Cross-coupling of benzoic acid derivatives with a variety of arenes or with other benzoic acid derivatives subsequently derived.



Scheme 12. First truly catalytic decarboxylative cross-coupling reaction

In 2008, the group of Crabtree reported the first arylation of iodo-anisole and arenes with the disubstituted benzoic acid 2,6(MeO)₂PhCO₂H in the presence of a palladium catalyst with a ^tBu-XPhos ligand and excess of silver salts under microwaves irradiation (*Scheme 13*).⁸⁴ Microwave heating greatly enhances yields and shortens reaction time in these decarboxylative coupling reactions. Moreover, decarboxylative homo-coupling of (hetero)aromatic compounds was first revealed by Larrosa and co-workers using Pd/Ag catalytic system (*Scheme 14*).⁸⁵ Although these new concepts for preparing useful biaryl from arene carboxylate precursors display elegant procedures, they however still remain limited regarding the functionalities and also require stoichiometric amounts of metallic additives such as Ag₂CO₃.

Scheme 13. First C-CO₂H/C-H decarboxylative cross-coupling.Scheme 14. First C-CO₂H/C-CO₂H decarboxylative homo-coupling reaction.

Notwithstanding the practical issues, these pioneering works represented a significant advancement in the direct utilization of carboxylic acid for the C–C bond construction. For the first time, a low cost, less halogenated alternative of nucleophilic coupling partner to the traditional cross-coupling reactions has been found.

At this stage of discovery, a set of requirements is necessary for successful decarboxylation of aromatic acids:

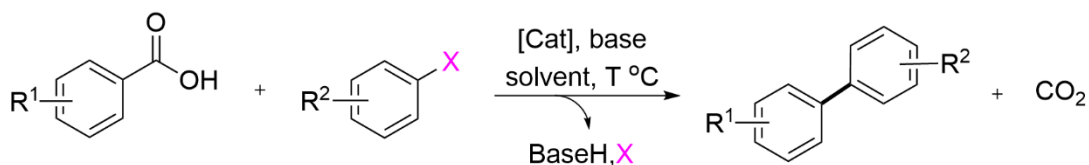
- The presence of electron attracting groups in *ortho*-position of the carboxylic moiety (*cf.* C₆F₅[−]);
- The use of forcing conditions (*ca.* 170 °C);
- The fitting transition-metal catalysts (Pd, Cu, Ag, Rh, Au) to facilitate the loss of CO₂.

In a broad sense, the advances in the chemistry of C–C coupling via a decarboxylation process using transition metals lie on three strategies: redox-neutral decarboxylative coupling, decarboxylative oxidative coupling, and protodecarboxylation. In the next parts, we will detail these areas, with mentions of the different transition metals used for each of them.

II. 3. Redox-neutral decarboxylative coupling reaction

II. 3. 1. Bimetallic system (Pd/Cu)

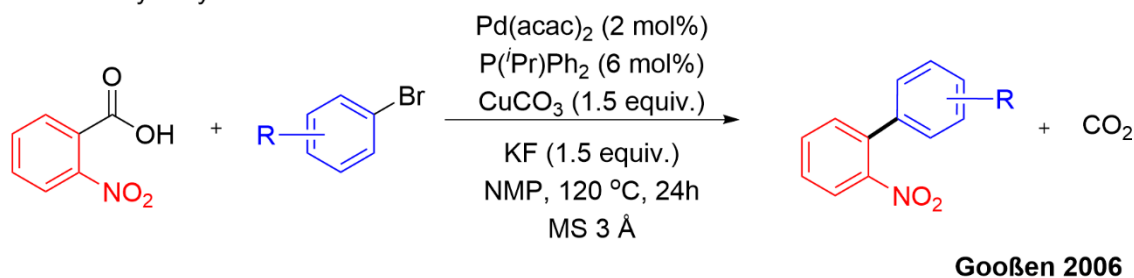
Decarboxylative cross-coupling is a pathway involving an organometallic species formed via the extrusion of CO₂ from a metal carboxylate RCO₂[M] species. This metal-aryl intermediate then reacts with an aryl substrate Ar-X to give a coupling product R-Ar (*Scheme 15*).



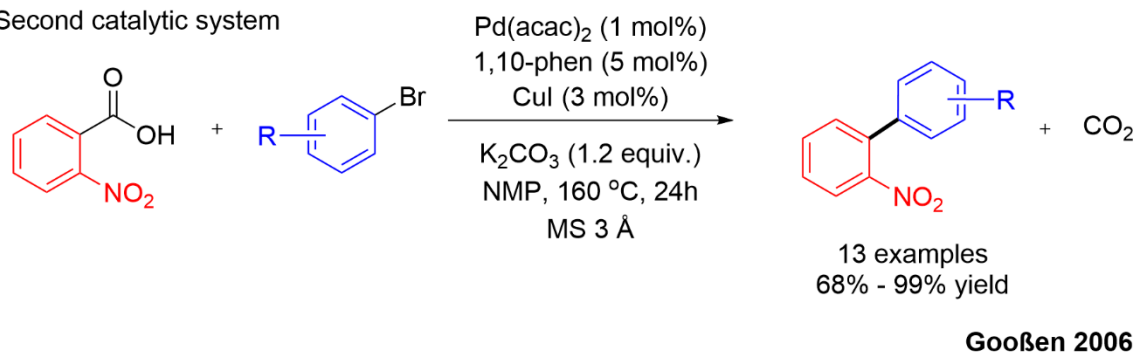
Scheme 15. A biaryl synthesis via a metal-catalyzed decarboxylative cross-coupling reaction of carboxylic acid and aryl halide.

This modern strategy towards biaryls through catalytic decarboxylative coupling, was first evidenced by Gooßen *et al.* in 2006.⁸³ They used bimetallic Pd(II)/Cu(II) or Pd(II)/Cu(I) systems to catalyze the reaction between substituted aryls bromide and substituted aryl carboxylic salts, mainly *ortho*-nitro benzoic acid (Scheme 16). Highly effective for the biaryl synthesis at relatively low temperature (120 °C), this Pd(II)/Cu(II) process was catalytic in Pd(acac)₂ (acac = acetylacetonate) supported by the phosphine ligand P(*i*Pr)Ph₂ but not in Cu^{II}(CO₃). Moreover, it required the presence of stoichiometric amount of KF additives (Scheme 16a). The second Pd(II)/Cu(I) system presented in their article used both Pd(II) and copper(I) salt in catalytic quantities (Scheme 16b).⁸³

a. First catalytic system



b. Second catalytic system



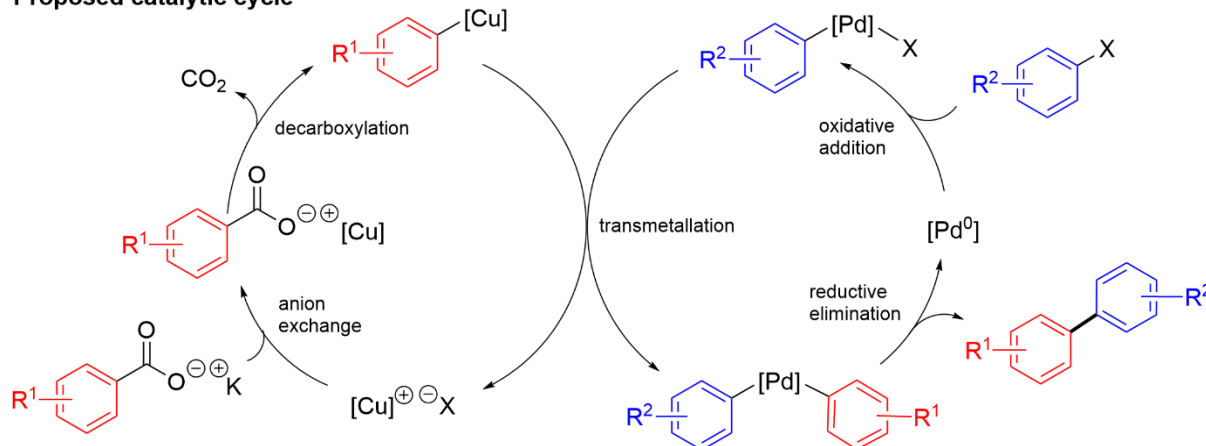
Scheme 16. Synthesis of biaryls via catalytic decarboxylative cross-coupling.

It was a major improvement and, in that case, the Pd and the Cu(I) catalysts were coordinated by phenanthroline ligand. This nitrogen ligand favored the reactivity of the copper(I) center, and this result initiated a powerful trend in redox-neutral decarboxylative cross-coupling reaction.⁸³

The proposed mechanism to this co-catalytic Pd(II)/Cu(I) system is consisting of two catalytic cycles where the palladium catalyst cycle shares similarities with traditional cross-coupling one (Scheme 17). The decarboxylation step was assumed to occur at the carboxylate Cu(I) complex generated after reaction of the acid with K₂CO₃/CuI. The subsequent arylcopper species undergoes a transmetalation with arylpalladium(II) complex generated by oxidative addition of an aryl halide to a palladium catalyst.

The following reductive elimination of resulted biaryl palladium species affords biaryl product and regenerating the initial palladium(0) precursor, thus closes the catalytic cycle.

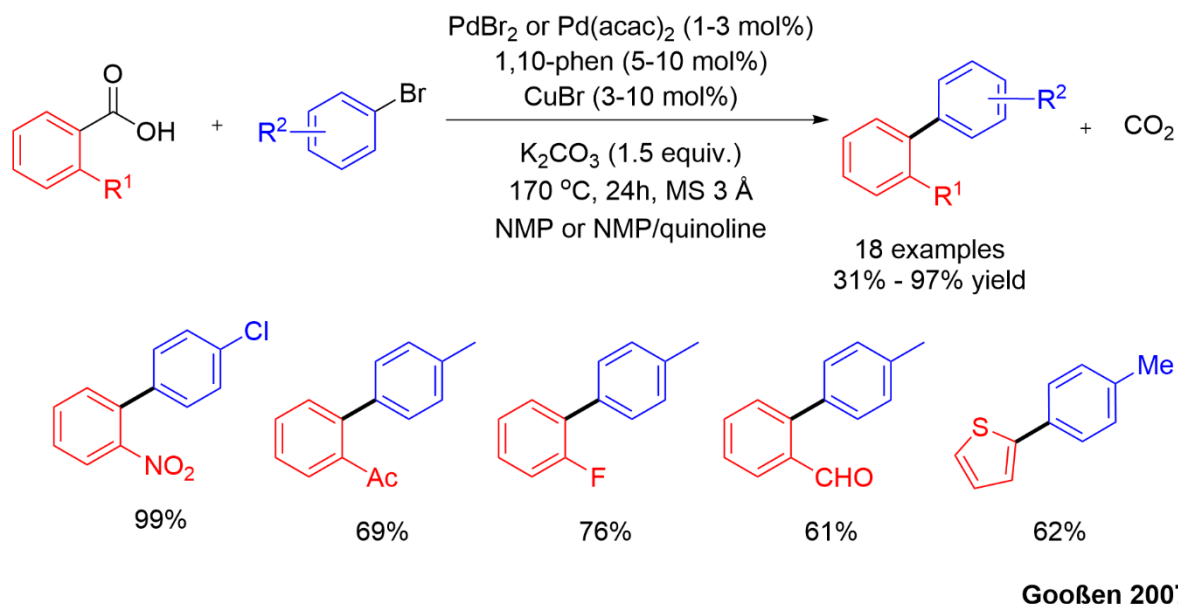
Proposed catalytic cycle



Scheme 17. Proposed catalytic cycles for the copper decarboxylation and palladium cross-coupling catalysis.

Based on the proposed mechanism, the cupric salt should be as well regenerated after the transmetalation step and a catalytic amount should be sufficient. However, CuCO_3 is not able to promote the reaction catalytically. The authors discussed about the probable reduction of CuCO_3 into Cu(I) species in the NMP solvent, whereas Cu(I) is inactive under the given reaction conditions (*i.e.* 120 °C with phosphine ligand, Scheme 17). In addition, the generation of copper halide salt after the transmetalation step could retard the decarboxylation. This is due to the strong affinity between copper and halides, causing a less favorable binding of carboxylates to the copper center in the anion exchange step. Therefore, the choice of copper salt precursor and a ligand environment that enhance the copper reactivity and promote the anion exchange are desired.

One year later in 2007, Gooßen *et al.* revisited and carefully investigated the conditions for the decarboxylative cross-coupling reactions with the Pd(II)/Cu(I) system.⁸⁶ The catalyst system consists of a copper phenanthroline complex that mediated the extrusion of CO_2 from aromatic carboxylates to generate aryl copper species, and a Pd(II) precursor supported by phenanthroline ligand that catalyzed the cross-coupling of these intermediates with aryl halides. This Pd/Cu system allowed the direct coupling of various aryl, heteroaryl, or vinyl carboxylic acids with aryl or heteroaryl iodides, bromides, or chlorides at 170 °C in the presence of a mild base such as K_2CO_3 (Scheme 18).



Scheme 18. Gooßen's decarboxylative cross-coupling of *ortho*-substituted benzoic acids.

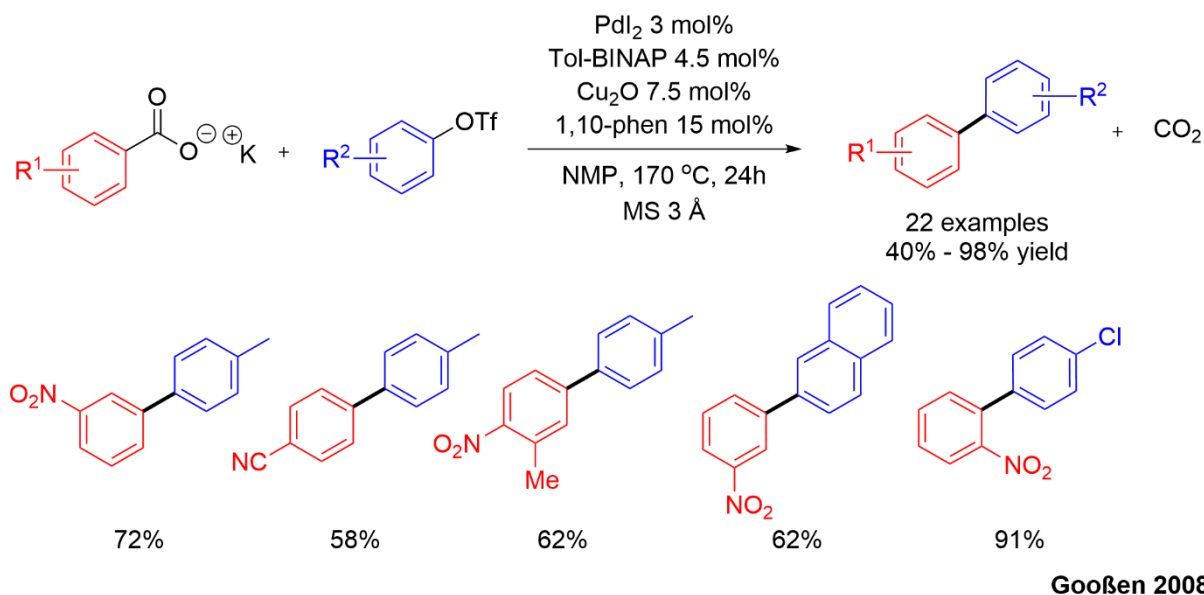
The authors revealed the importance of the reagents for an optimized Pd/Cu catalytic system and provided new elements to rationalize the different activities between cuprous and cupric salts. They observed that CuCO_3 was readily reduced by NMP solvent into Cu(I) at 160 °C in less than 1 h. While a more stable copper (I) salt is less effective and gave only very low conversion even at forcing condition and at stoichiometric loading. However, by using a nitrogen chelating ligand (bipyridine or phenanthroline), the decarboxylation activity of the cuprous salt improved dramatically, with phenanthroline proved to be the best ligand: 98% yield for the biaryl (0.5 mol% $\text{Pd}(\text{acac})_2$, 1 mol% CuI, 3 mol% phenanthroline). In the meantime, reaction with stoichiometric amount of CuCO_3 and catalytic amount of $\text{Pd}(\text{acac})_2$ supporting by bipyridine ligand leads to low yield of coupling product (e.g. 35 %).

At this stage, a pattern for a catalytic decarboxylation process became apparent. It would require two crucial components to achieve the catalytic decarboxylative coupling event:

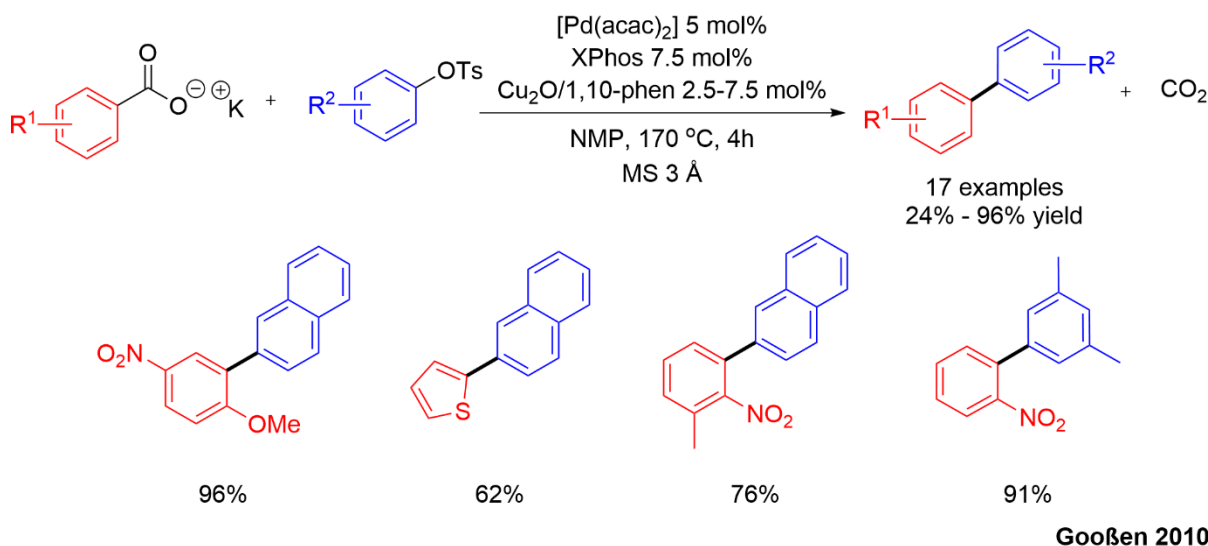
- cuprous salt precursor
- a fitted chelating ligand for the Cu^+ ion

These components would appear to be the guiding principle behind the redox-neutral decarboxylation coupling throughout the years. A common limitation for these decarboxylation methods was the inherent dependence to the *ortho*-substituted heterocyclic carboxylic acids.

Taking advantage of their previous studies, Gooßen and co-workers unlocked the substrates constraints with a novel catalyst system efficient with *meta*- and *para*-substituted benzoic acids.^{87,88} By replacing aryl halides with aryl triflates⁸⁷ or aryl tosylates⁸⁸ as coupling partners, and with a halide-free Cu(I) source (Cu_2O), the decarboxylation step was then favored (Scheme 19 and Scheme 20).



Scheme 19. Pd/Cu catalyzed decarboxylative cross-coupling of aryl triflates and aromatic carboxylic acids.



Scheme 20. Pd/Cu catalyzed decarboxylative cross-coupling of aryl tosylates and aromatic carboxylic acids.

Simplified versions of these catalytic procedures for industrial applications have been designed using a microwave reactor.⁸⁸⁻⁹⁰ This carboxylative cross-couplings of carboxylic acid salts with aryl bromide, using the $\text{Pd}(\text{acac})_2/\text{CuI}$ catalysts and phenanthroline ligands, allowed fast (*ca.* 5 min.) and convenient synthesis of biaryls and aryl ketones in high yields from a broad range of aromatic carboxylic acids. The decarboxylative coupling with less reactive chloro-arenes was also explored with focus on the efficiency of palladium catalyst. It was found that phosphine ligands bearing bulky and electron-rich substituents such as (bis(^tbutyl)biphenylphosphine),⁹¹ Tol-BINAP,⁸⁷ or Beller's ImiPrAd⁸⁸ helped to improve the coupling activity of palladium metal while maintaining the highest level of performance of copper in the decarboxylation process (Figure 14).

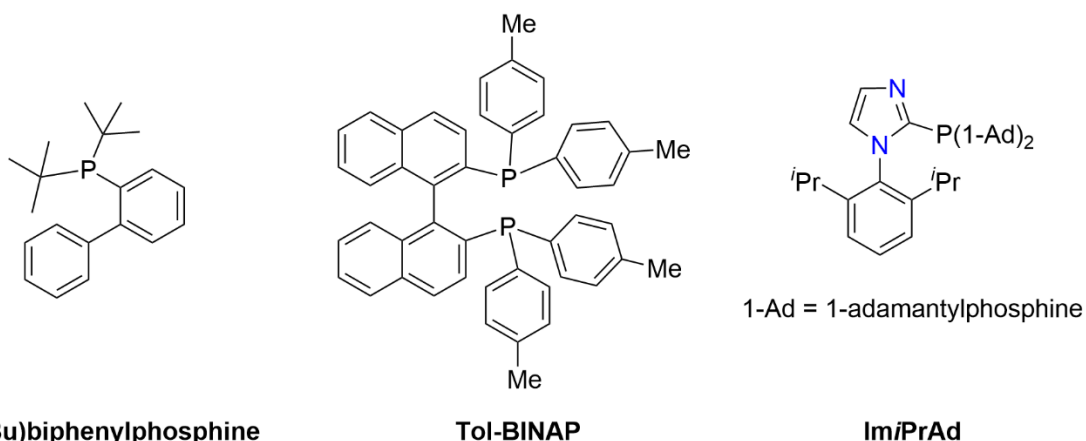


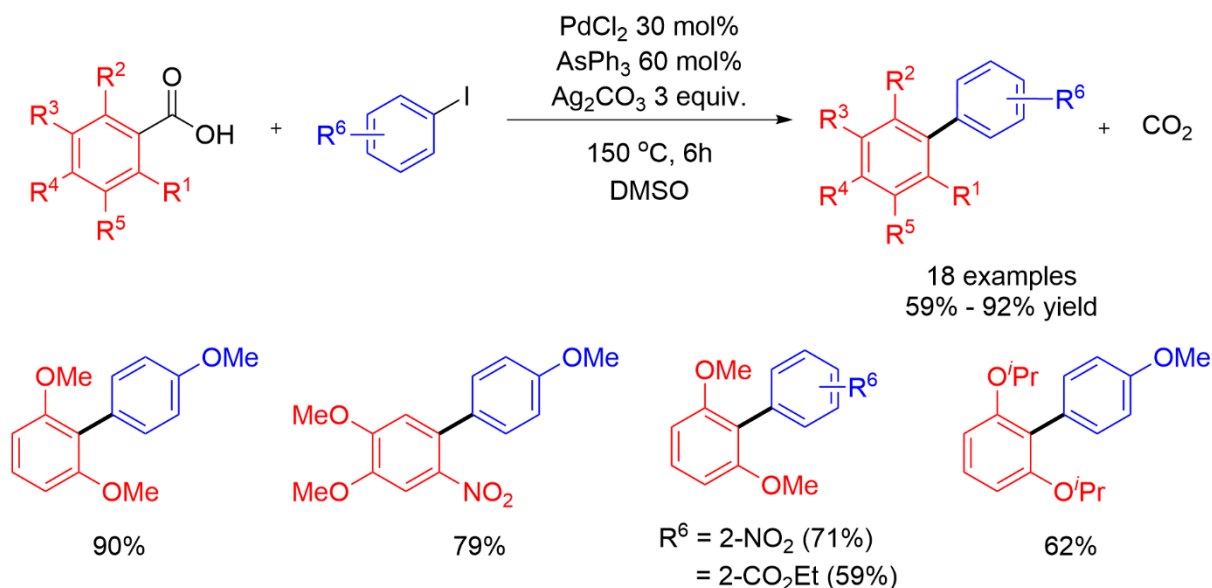
Figure 14. Examples of electron-rich phosphine ligands that applied in the Pd/Cu catalyst system for decarboxylative cross-coupling.

Thus, in just four years, Gooßen's insightful work has led to major advances to these reactions and to the development of a more versatile methodology for a wider range of applications.

Mechanistic investigations dedicated to the decarboxylation step have been carried out in order to identify why *ortho*-substitution is so important. In the earliest work by Gooßen *et al.*, the use of *non-ortho*-substituted benzoic acid derivatives in copper-catalyzed protodecarboxylation highlighted the influence of the substitution position.⁵⁷ Of importance was the role of the halide anion released in the cross-coupling step. Having a strong affinity for the copper ions, coordinated halide can stall or impede the decarboxylation event. The presence of *ortho*-substituents on the aromatic benzoate, by favoring displacement of the halide ligand, would prevent the deactivation process.

II. 3. 2. Bimetallic system (Pd/Ag)

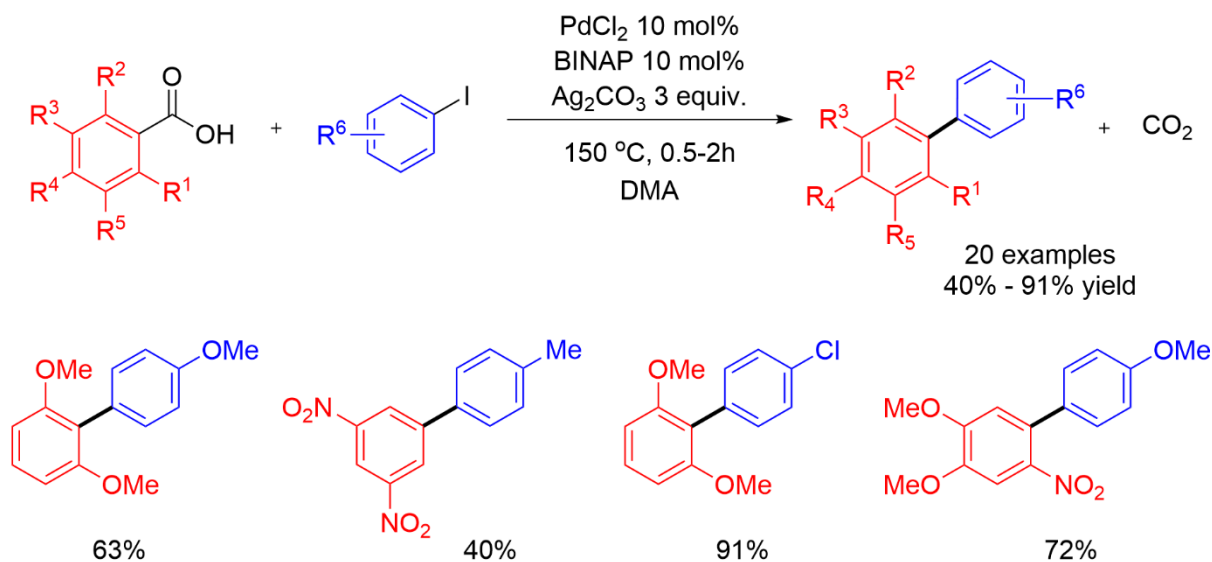
Besides copper, the role of silver in decarboxylation process was also considered in Pd(II)/Ag(I) catalyzed decarboxylative cross-coupling. Several reports showed that the transformation of *ortho*-benzoic acid with iodoarene, thiazole and oxazole into biaryl compound is accessible in the presence of stoichiometric amount of Ag₂CO₃.^{60,83,86,92–94} The first proof of concept was evidenced by Gooßen *et al.* from their Pd(II)/Cu(II) catalyst system, where they replaced CuCO₃ with Ag₂CO₃.^{83,86} They obtained moderate yield in the formation of 4-chloro-2'-nitrobiphenyl (47 %), which is lower than that obtained with CuCO₃ in the same conditions. The yields were optimized by Becht *et al.* when they introduced a Pd/Ag bimetallic system for a coupling reaction between *ortho*-substituted benzoic acid and iodoarenes or diaryliodonium salts.^{60,92} However, if the yields are improved, a high loading in Pd and stoichiometric amount of Ag are required (*Scheme 21*).



Becht 2007

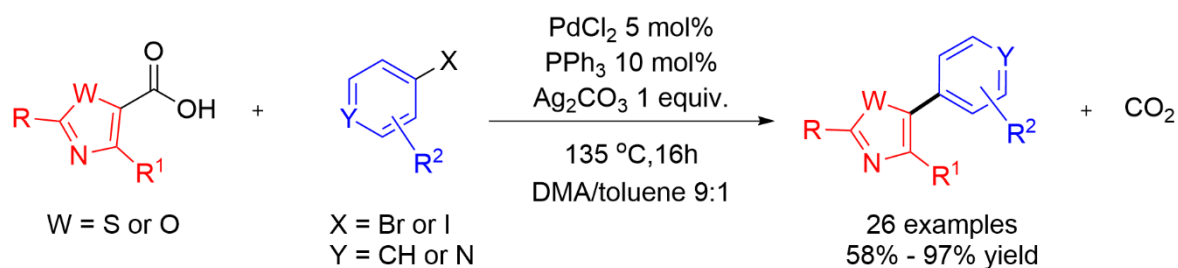
Scheme 21. Becht's Pd/Ag catalyzed decarboxylative cross-coupling of *ortho*-substituted benzoic acids and iodoarenes

In 2009, Wu *et al.* introduced another protocol for the cross-coupling of *ortho*-substituted benzoic acid with aryl iodide catalyzed with the system combining PdCl_2 and BINAP in the presence of Ag_2CO_3 (Scheme 22).⁹³ Although their catalytic system required a lower charge in Pd(II) and is faster, the yields are in general lower when compared to the results obtained by Becht's group.^{60,92} Later on 2010, Greaney and Zhang expanded the scope to thiazole and oxazole carboxylic acids for a decarboxylative coupling reaction with a wide range of aryl bromide and iodide with the $\text{PdCl}_2/\text{Ag}_2\text{CO}_3$ catalytic system (Scheme 23).⁹⁴



Wu 2009

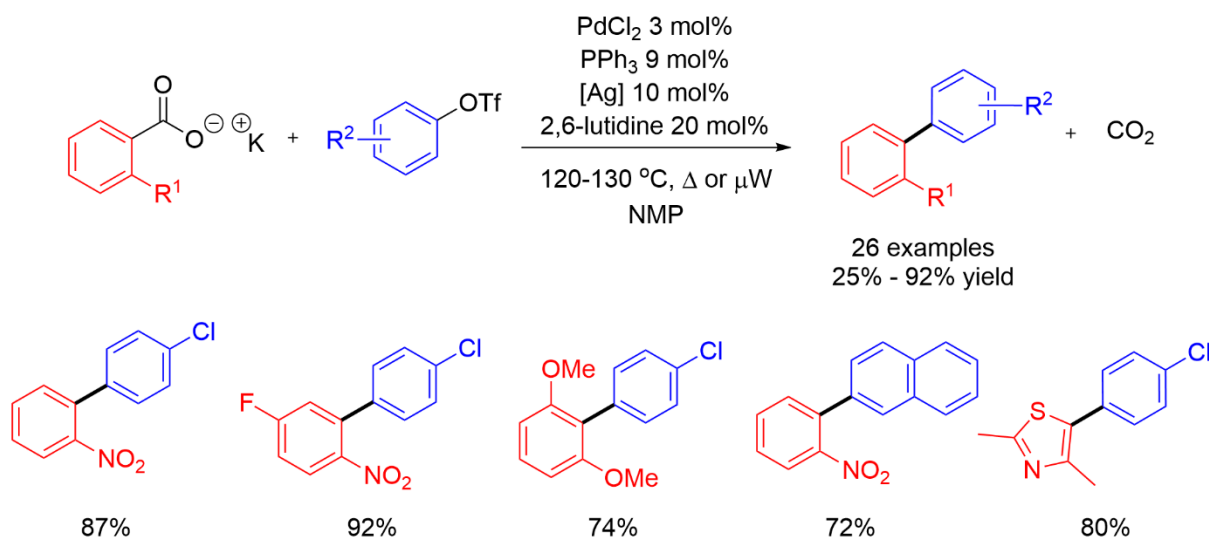
Scheme 22. Wu's Pd/Ag catalyzed decarboxylative cross-coupling of *ortho*-substituted benzoic acids and iodoarenes.



Zhang and Greaney 2010

Scheme 23. Synthesis of biaryl via Pd/Ag catalyzed decarboxylative cross-coupling of thiazole and oxazole carboxylic acids.

The stoichiometric requirement of silver-based has been an obstacle which was solved by Gooßen and coworkers in their mechanistic investigation of the decarboxylation step.⁵⁴ Here again, the high loading in silver salt was explained by the formation of the stable and inactive AgX ($X = \text{halide}$) species by the release of halide anion during the coupling. As previously mentioned with copper, a solution to address this problem was the use of arene sulfonates to prevent the formation of inactive silver halide entity, and in that case, catalytic amount of silver salt were sufficient (Scheme 24).⁹⁵ In contrast to copper catalysts, silver catalyzed decarboxylative coupling of arene carboxylates with aryl triflates proceeded at 120 °C in the presence of Pd(II), but the scope was limited to *ortho*-substituted or heterogenated carboxylic acids.⁹⁵



Gooßen 2010

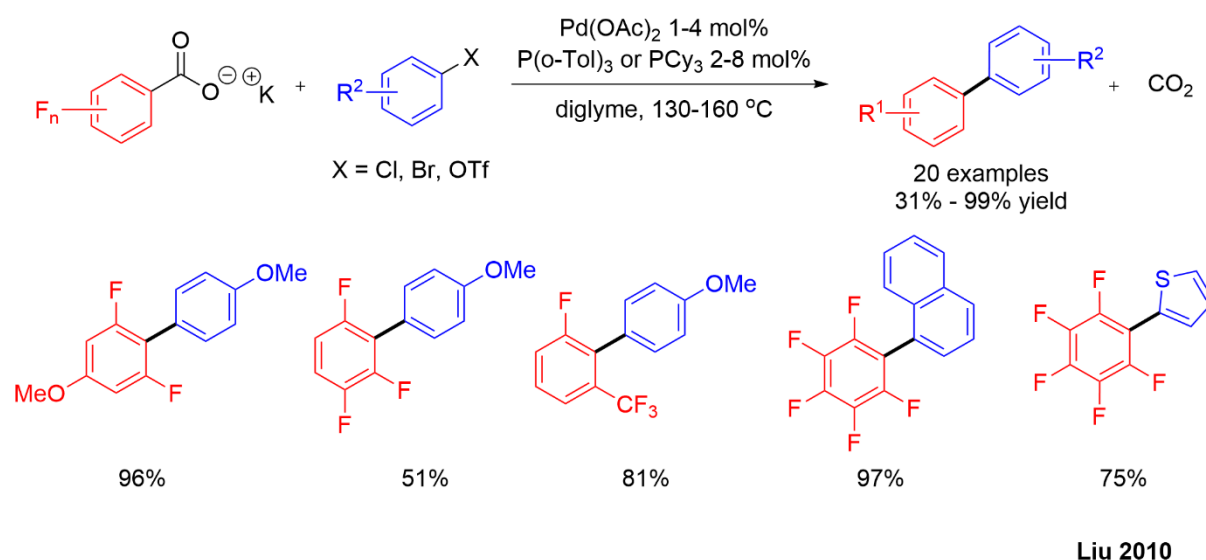
Scheme 24. Pd/Ag catalyzed decarboxylative coupling of arenecarboxylates and aryl triflates.

From Gooßen and co-workers, formation of C–C bond via decarboxylation of carboxylic acids (as sources of aryl nucleophiles) instead of organometallic compounds has evolved into a well-constructed catalytic reaction with a diverse range of substrates. By highlighting the efficiency of the bimetallic Pd/Cu catalytic system, Gooßen and co-workers have significantly broadened the concept of the redox-neutral decarboxylative cross-coupling approach and paved the way for the discovery of milder

reaction conditions and wider application. The use of the decarboxylative cross-coupling reaction has been recognized as offering a versatile route for the synthesis of biaryl compounds from an available and inexpensive carboxylic acids. However, most often cited drawback of this method is the demand of elevated temperature.

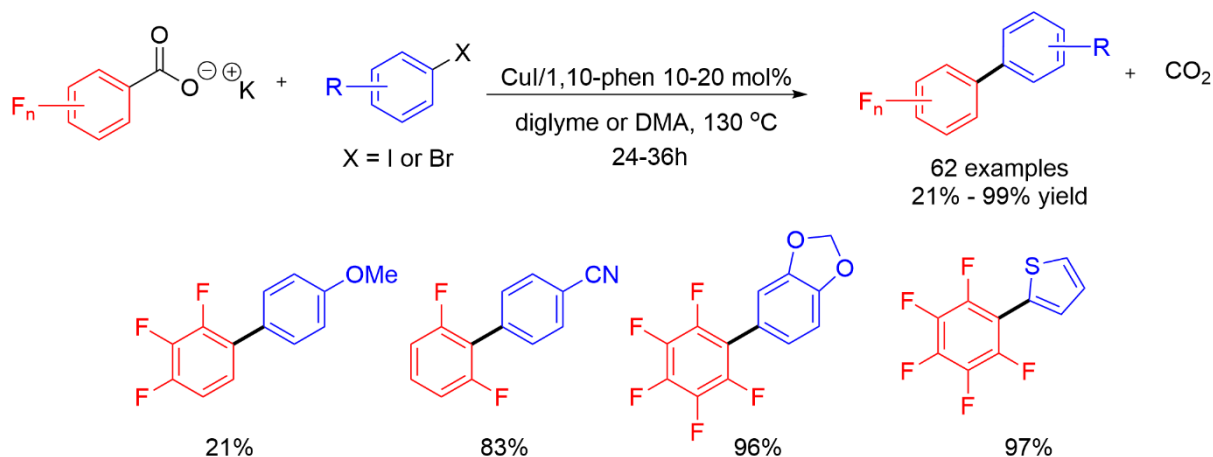
II. 3. 3. Monometallic system

A number of palladium complexes are capable of promoting decarboxylative cross-coupling reaction between activated carboxylate substrates and iodo- or bromo-arenes without the need for co-catalyst. For example, Steglich *et al.*, in a pioneering work, reported that Pd(OAc)₂ (in stoichiometric amount) mediated intramolecular reaction of pyrrole carboxylic acid and phenyl moiety to form indolizine motif.⁹⁶ Later on, different strategies have been developed to prepare a variety of heterocyclic compounds useful for the synthesis of natural products or drugs.^{59,97–100} In 2006, Bilodeau and Forgione reported an intermolecular decarboxylative cross-coupling of 5-membered heteroaromatic carboxylic acids and aryl bromide, in the presence of Pd[P(^tBu)₃]₂ as catalyst and excess of Cs₂CO₃ additive.⁹⁷ Miura *et al.* developed the synthesis of 2,3-diarylbenzo[b]thiophenes by combining Suzuki-Miyaura cross-coupling with a Pd catalyzed decarboxylative arylation of 3-chloro-2-methoxycarbonylbenzo[b]thiophenes.¹⁰¹ Recently, a more general procedure was demonstrated by Liu and co-workers where activated polyfluorobenzoates could undergo coupling with aryl halides (X = Br, Cl) or aryl triflate (Scheme 25).⁵⁹



Scheme 25. Pd catalyzed cross-coupling between polyfluorobenzoates and aryl halides or aryl triflates.

Unlike palladium catalyst, only one example of copper catalyzed cross-coupling reaction was reported for monometallic system by Liu and co-workers (Scheme 26).⁵⁸ The coupling of polyfluorobenzoic acids and aryl iodides or aryl bromides was successful. The oxidative addition appeared to be the rate-determining step from DFT calculations, while for palladium, it is the decarboxylation step.⁵⁹



Liu 2009

Scheme 26. Cu-catalyzed cross-coupling between polyfluorinated benzoic acids and aryl halides.

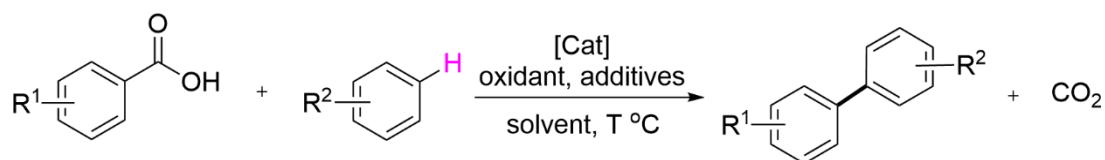
From the above results, Pd or Cu complexes were found to be alone capable of catalyzing C–C bond formation via the decarboxylation process. Even though they needed lower operational temperatures in comparison to the bimetallic Pd/Cu systems, the scope is limited to activated carboxylic acids involving electron-attracting *ortho*-substituents. To date, this type of reaction has remained underdeveloped.

Overall, the decarboxylative cross-coupling reaction offers an inexpensive method for a C–C bond construction a readily available carboxylic acid and a haloarene. This process can be promoted by bimetallic or monometallic catalyst systems. Unfortunately, the forcing conditions to remove CO₂ decrease the chemoselectivity and favor side reactions such as the protodecarboxylation. This latter reaction will be a subject of discussion later in this chapter.

II. 4. Decarboxylative oxidative coupling

II. 4. 1. Decarboxylative C–H functionalization

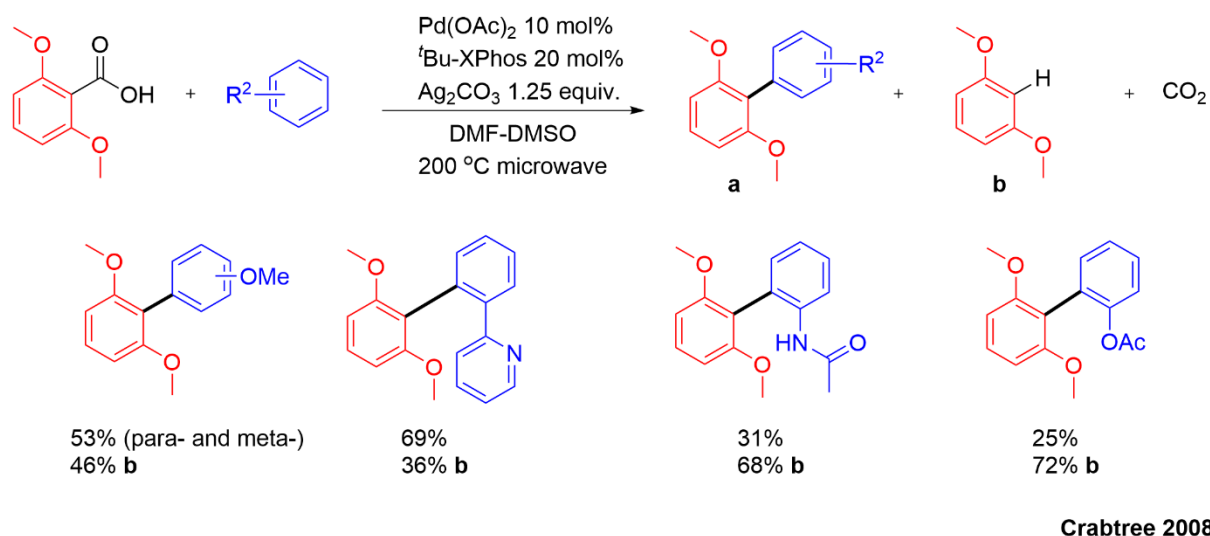
The decarboxylative oxidative coupling reaction concerns the formation of biaryl compounds by decarboxylation of a carboxylic acid and its reaction with a C–H bond of an aromatic molecule (Scheme 27).



Scheme 27. A biaryl synthesis via a metal-catalyzed decarboxylative C–H functionalization of carboxylic acid and aryl compound.

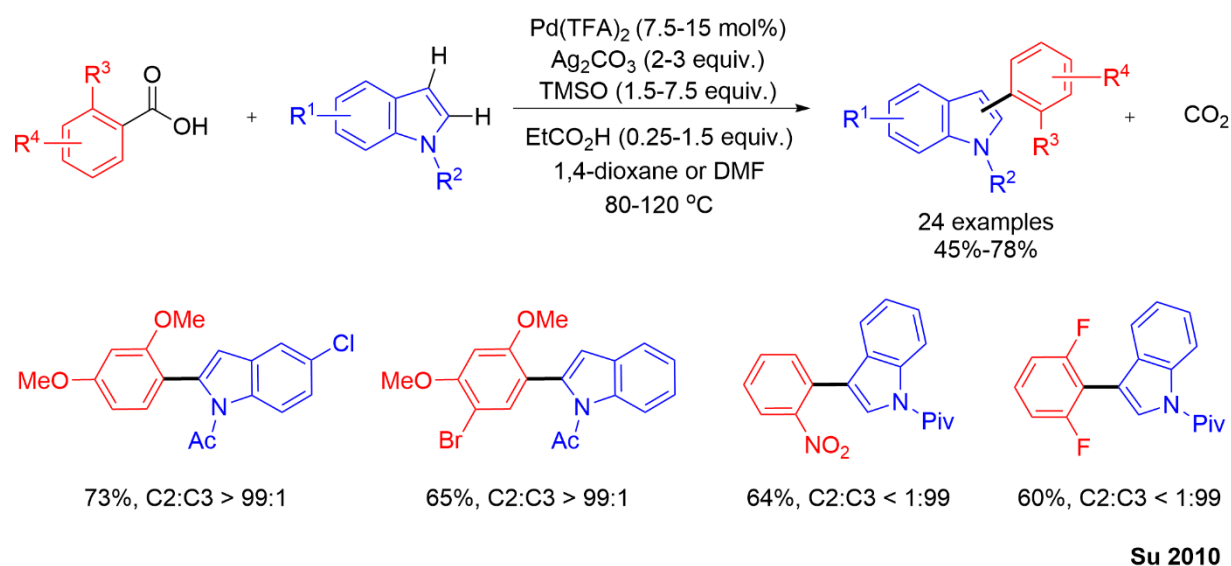
Such coupling between benzoic acid derivatives and simple arenes is appealing, due to the availability of each type of substrates. Generally, these systems use Pd(II) catalysts and stoichiometric silver or Cu(II) salts as oxidants for the oxidation of Pd(0). These Ag and Cu species are also involved in the decarboxylation step and transfer of the aryl fragment to palladium(II).

An initial strategy for the decarboxylative coupling of aromatic acids with non-activated arenes was established by Crabtree in 2008 with Pd(OAc)₂ as catalyst supported by ^tBu-XPhos ligand and where an excess of Ag₂CO₃ was required for the arylation of anisole with 2,6-dimethoxybenzoic acid (Scheme 28).⁸⁴ Limited by the severe reaction conditions (*ca.* 200 °C, microwave oven) and the poor regioselectivity related to the multiple active sites of anisole, Crabtree's method was subsequently improved by several groups using similar reaction conditions.



Scheme 28. Pd(II)/Ag(I) catalyzed decarboxylative C-H functionalization between anisole and 2,6-dimethoxybenzoic acid.

For instance, a wide range of benzoic acids involving electron-rich or electron-poor substituents can be used and coupled with various 5-membered heterocycles (indole,¹⁰² thiophenes,¹⁰³ furans, benzofurans, pyrroles,¹⁰⁴ thiazoles, benzoxazoles.¹⁰⁵ It is possible to direct the coupling position by tuning the nature of the benzoic acid: electron-rich benzoic acid favor C-2 arylated product (C-2: carbon atom adjacent to the nitrogen one) and electron-poor derivatives lead to arylation at C-3 position of the 5-membered heterocyclic species (Scheme 29).¹⁰²

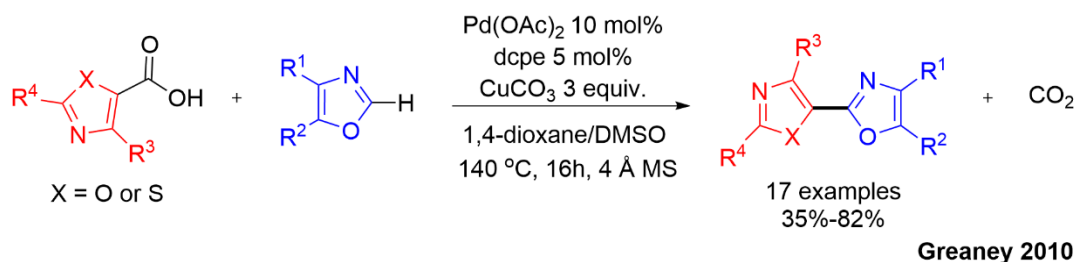


Scheme 29. Pd/Ag catalyzed regioselective arylation of electron-rich and -poor benzoic acids.

C–H arylation by decarboxylative coupling of acids with simple arenes such as benzene, toluene, xylene is also possible with polyfluorinated benzoic acids, but large amounts of arene partners are necessary and the yields are poor due to the low reactivity of these latter.¹⁰⁶ More reactive fluorobenzene could also be arylated with heteroaromatic carboxylic acid, provides a promising synthetic pathway to fluorobiaryl species.¹⁰⁷

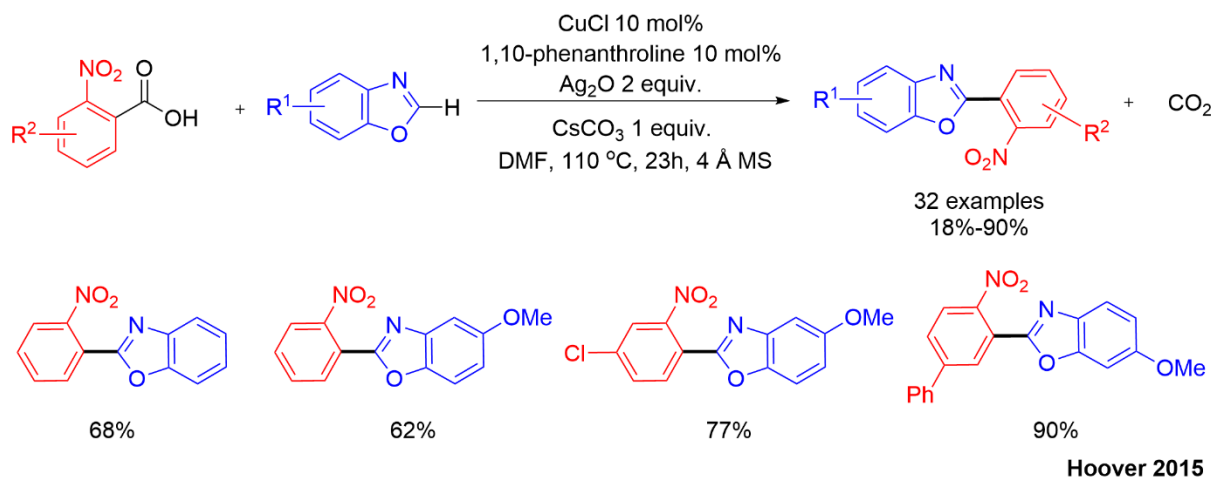
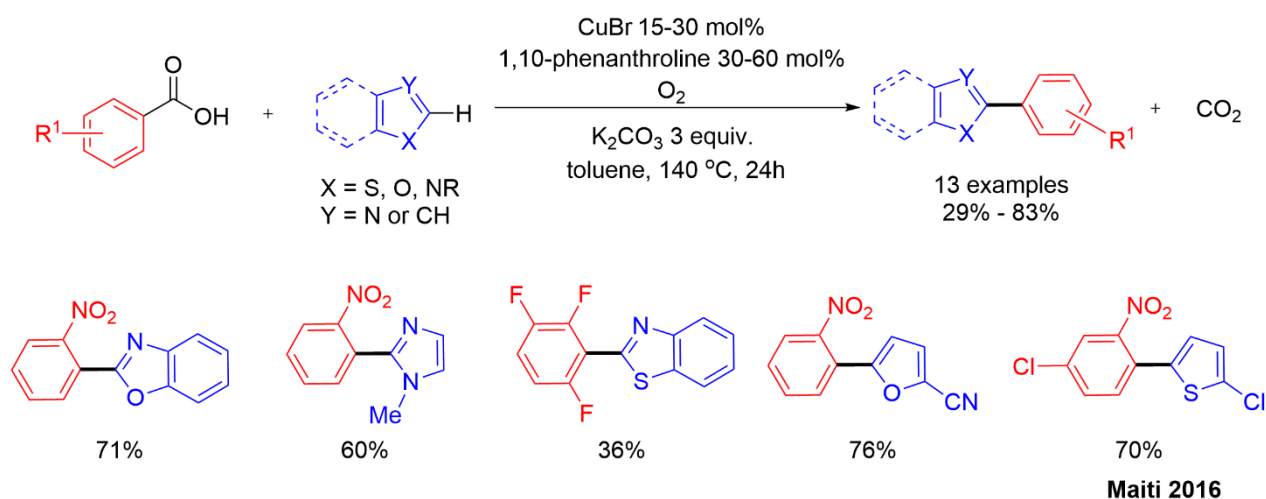
Inspired by the work of Greaney under radical conditions,¹⁰⁸ Su *et al.* developed another approach for the transformation of simple arenes to biaryl compounds by using silver catalyst and $K_2S_2O_8$ as one-electron oxidant.¹⁰⁹ With this work, Su had achieved something beautiful, which is the ability to decarboxylate non-ortho-substituted benzoic acids that tolerate various functional groups. Nonetheless, this *Minisci* type reaction afforded poor regioselectivity likely due to the radical nature of the reaction. Intramolecular decarboxylative arylation was also described for non-*ortho* substituted benzobenzonic acids using similar radical pathway mediated by Ag/ $K_2S_2O_8$ catalyst system¹⁰⁸ and for 2-phenoxybenzoic acid catalyzed by palladium complex and silver oxidant.¹¹⁰

There is one example of palladium catalyzed arylation of oxazoles with azole-5-carboxylic acids where $CuCO_3$ is employed as an oxidant and a base to mediate the decarboxylation process (*Scheme 30*).¹¹¹ Silver salts are also efficient for this reaction, however, they exhibit a lower reactivity compared to copper oxidizing agent.



Scheme 30. Pd/Cu catalyzed decarboxylative C–C bond formation of oxazole and azole-5-carboxylic acid.

On the basis of the known ability of copper to promote decarboxylation and its reactivity for C–H functionalization presented in several studies,^{112–116} Hoover *et al.* began study on the potential of the direct decarboxylative arylation of indoles catalyzed by copper species.¹¹⁷ Moderate to good yields of a variety of arylated benzoxazoles have been obtained by combining Cu (I and II) catalysts and Ag(I) oxidants in presence of bases (*Scheme 31*). Notwithstanding the availability of the copper catalyst, the reaction was limited to *ortho*-nitro benzoic acids and stoichiometric amounts of silver salts are required.¹¹⁷ Maiti *et al.* elegantly overcame this issue by the employment of oxygen as the oxidant while expanded the substrate scope to 5-membered heteroarenes with highly activated benzoic acid derivatives involving a number of electron-attracting substituents (*Scheme 32*).¹¹⁸

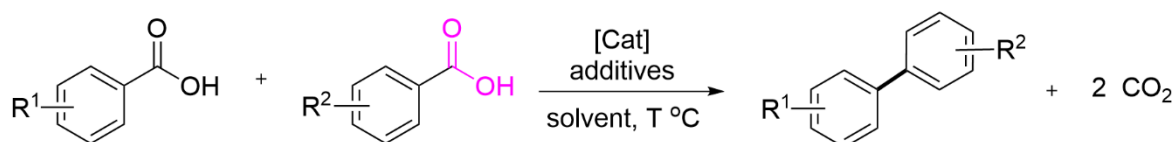
Scheme 31. Copper catalyzed decarboxylative arylation of 2- NO_2 -benzoic acid and indole.

Scheme 32. Copper-catalyzed C-C bond formation via decarboxylative C-H activation of heteroarene and benzoic acids.

Besides copper and palladium salts, Rh(III) ¹¹⁹ and Ni(II) ^{120,121} catalyzed arylation of thiophene or azole derivatives, respectively, with 2,4-(MeO)₂ $\text{C}_5\text{H}_3\text{CO}_2\text{H}$ or activated fluoro-benzoic acids, respectively, have also been reported. In the two cases, the utilization of Ag_2CO_3 is indispensable as oxidant but also as decarboxylating agent. With $[\text{Cp}^*\text{RhCl}_2]_2/\text{Ag}_2\text{CO}_3$, the reaction required 1 day at 100°C in DMF to give the products in a yield up to 82 % with K_2HPO_4 as a base in excess.¹¹⁹ The $\text{Ni(II)}/\text{Ag(I)}$ system also required additional bases; if the scope of azole derivatives is broad, the efficiency of the arylation with perfluorobenzoates is highly dependent on both the degree and position of fluorine atoms in the benzoate and high temperatures (120°C – 160°C) are needed.^{120,121}

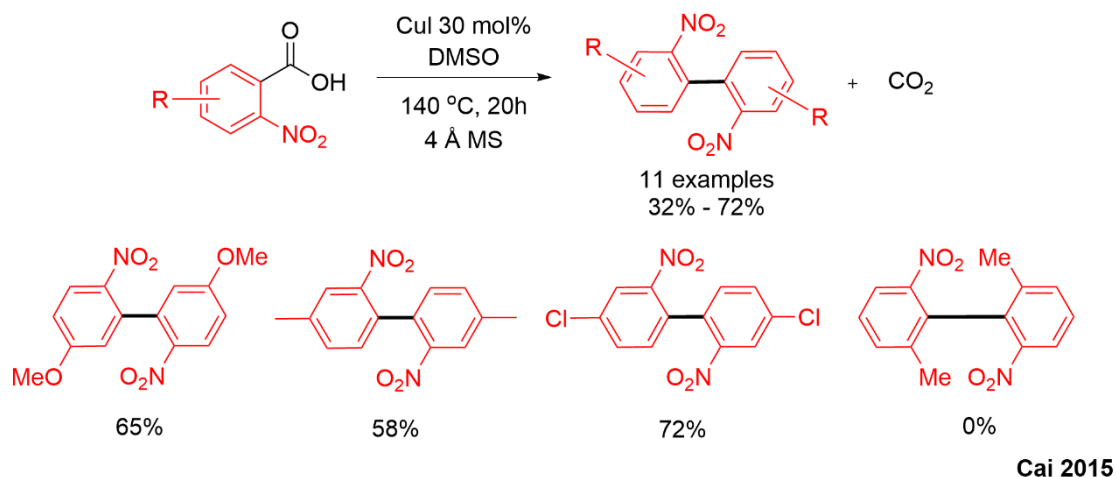
II. 4. 2. Decarboxylative C– CO_2H functionalization (homo-coupling and cross-coupling)

The decarboxylative C– CO_2H homo-coupling and cross-coupling involving two carboxylic acid substrates to undergo decarboxylation followed by a generation of a new C-C bond between them. In cross-coupling process, the chemoselectivity of the reaction is of importance since homocoupling is in competition (Scheme 33).



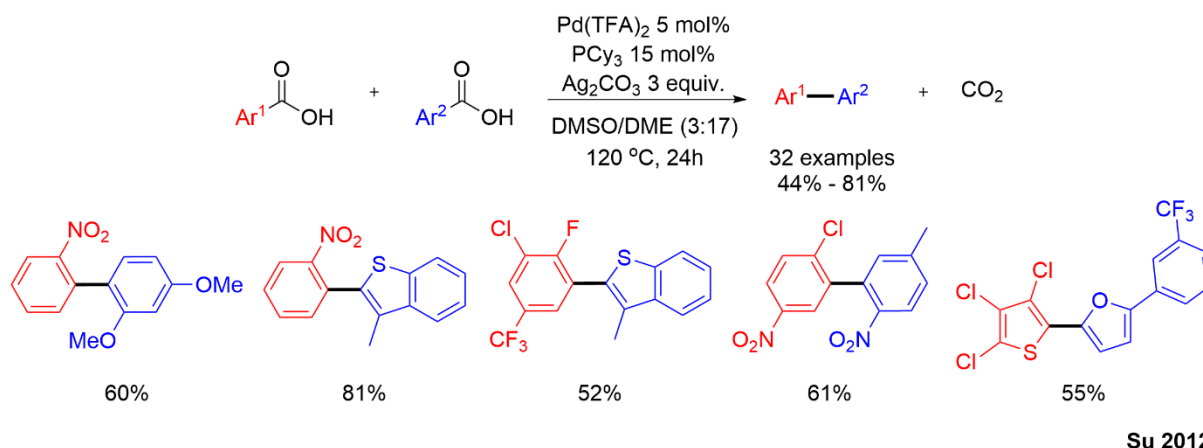
Scheme 33. A biaryl synthesis via a metal-catalyzed decarboxylative C-CO₂H coupling between carboxylic acids.

As for the C–C bond formation with arene compounds and under similar reaction conditions, the homo coupling of aryl fragments issued from decarboxylated benzoic acids has also been reported. In 2011, Larrosa *et al.* developed the first decarboxylative homocoupling of aromatic and heteroaromatic acids using Pd(II)/Ag(I) system.⁸⁵ This reaction required quantitative amount of Ag⁺ salt which acts as an oxidizing agent and promotes decarboxylation process. In view of the high loading of silver salts, Cai and co-workers explored another approach for the decarboxylative homocoupling of *ortho*-nitro benzoic acid derivatives with a copper catalyst (Scheme 34).¹²² This method is constrained by the need for a nitro group in *ortho*-position of the carboxylic moiety. Although there is a tolerance for both electron-donating and electron-withdrawing substituents on the aromatic ring, sterically congested benzoic acids were found unreactive.



Scheme 34. Copper-catalyzed decarboxylative homocoupling of 2-NO₂-benzoic acids.

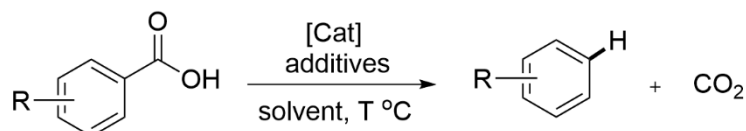
The strategy to obtain asymmetric biaryl compounds from the decarboxylative cross-coupling of aromatic acids was separately established by the groups of Tan¹²³ and Su.¹²⁴ In 2011, Tan *et al.* carried out the first cross-coupling between electron-rich or polyfluorinated benzoic acids with *ortho*-nitro benzoic acids in the presence of palladium catalyst and stoichiometric amount of silver base.¹²³ The chemoselectivity of this reaction remained however modest due to homocoupling reaction producing symmetrical biaryls. A year later, Su and co-workers reported the cross-coupling reaction between ArCO₂H species with substituents having similar and distinct electronic properties.¹²⁴ In their optimization study, the authors demonstrated that the combination of Pd(TFA)₂, PCy₃, and a mixture of solvents in a correct ratio afforded the unsymmetrical biaryl in the highest yield (Scheme 35). Although the yields are generally high, the author did not disclose the homocoupling levels in each case, hence, such conclusion regarding the chemoselectivity could not be unveiled.



Scheme 35. Unsymmetrical biaryl synthesis via Pd/Ag catalyzed decarboxylative cross-coupling of aromatic carboxylic acids.

Overall, decarboxylative oxidative coupling is a high atom-efficient transformation, in which the C–H functionalization of arenes is well developed with high regioselectivity. In particular, improvement of the chemoselectivity in the decarboxylative cross-coupling of two distinct benzoic acids is challenging. Even though the two C–H and C–CO₂H activation methodologies are straightforward and simple routes to biaryls or analogues, these processes suffer from the need for stoichiometric (or excess) amounts of oxidant and high temperatures.

II. 5. Protodecarboxylation

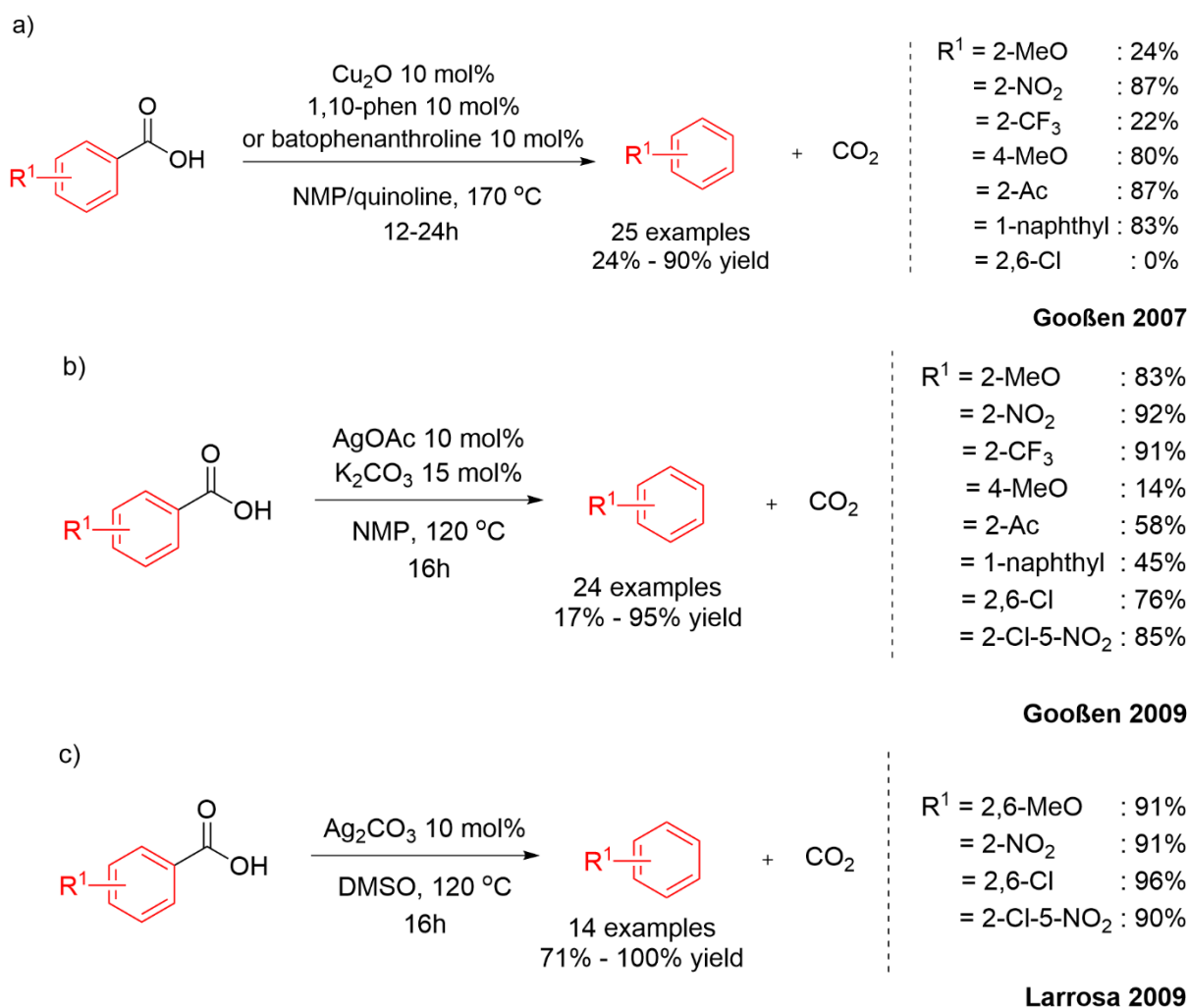


Scheme 36. General scheme of metal-catalyzed protodecarboxylation of carboxylic acid.

In the presence of proton sources, instead of the decarboxylative coupling process, a protodecarboxylation process, viewed as an unwanted pathway, can occur (Scheme 36). Nevertheless, when controlled, the protodecarboxylation reaction can be a convenient access to aromatics from benzoic acids. Therefore, this reaction attracted attention to gain deeper understanding and to use it as a means of detailing reactivity trends and limitations of transition metal-catalyzed decarboxylation.

A long time after Sheppard⁸⁰ pioneering contribution, Gooßen *et al.* evidenced that Cu₂O and bathophenanthroline ligand (4,7-diphenyl-1,10-phenanthroline) catalyzed protodecarboxylation of a range of substituted benzoic acids at elevated temperatures (*ca.* 170 °C) for around 12 to 24 h (Scheme 37a).⁵⁴ Microwave irradiation expedited the reaction, and with 5 mol% of an inexpensive Cu(I) catalyst, the smooth protodecarboxylation of diversely functionalized aromatic carboxylic acids occurred in a few minutes (5–15 min) instead of several hours. This efficient protocol can be suited in medicinal chemistry.¹²⁵ In 2009, Gooßen *et al.* disclosed the production of arenes from carboxylic acids via a decarboxylation step catalyzed by Ag(I) species in the presence of a base in NMP.⁵⁵ The Ag-system is much more effective than the Cu₂O/phen system since protodecarboxylation proceeded at lower temperatures (*ca.* 120 °C, 16 h), in high selectivity with at most, traces of side products arising from

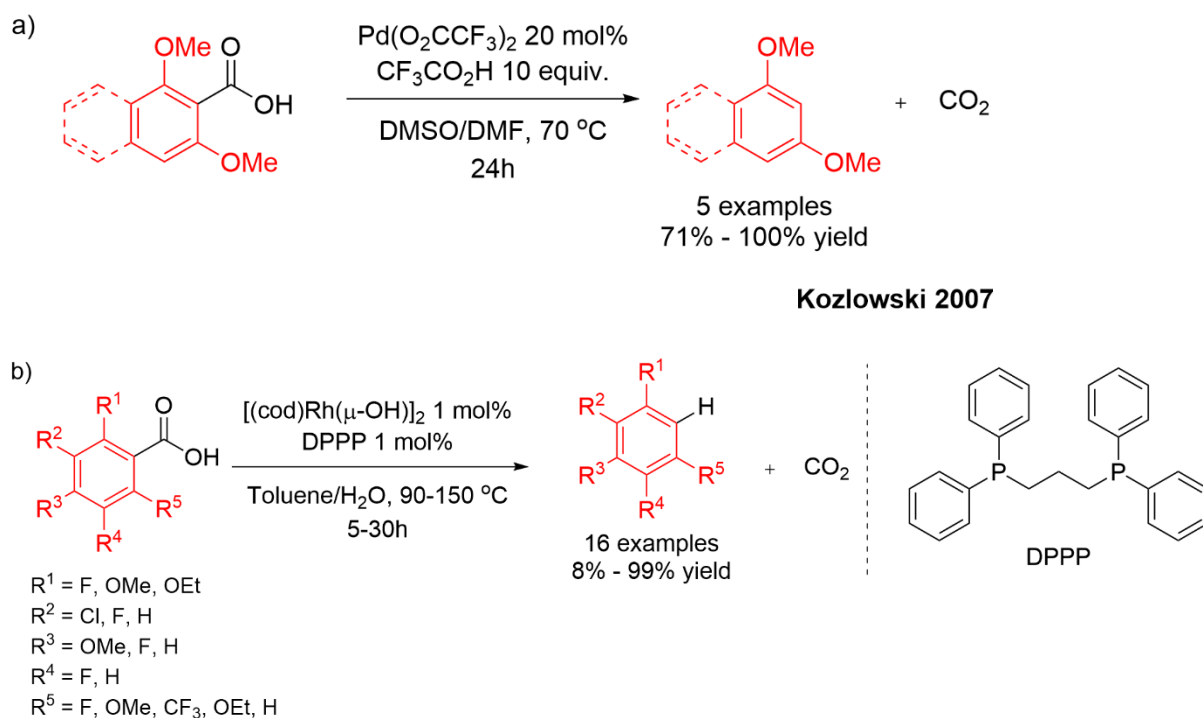
homocoupling and afforded better yields. However, it was only efficient with benzoic acids mainly substituted in ortho-positions by attracting groups (*Scheme 37b*). In the meantime, the copper catalyst system can be applied for a number of benzoic acid derivatives without the constraint of the functional group position (*Scheme 37a*). Similarly, Larrosa *et al.* developed a silver catalyst that works without additives. In DMSO at 120 °C, Ag₂O proved highly efficient for the protodecarboxylation of a variety of heteroaromatic carboxylic acids and the isolated yield of compounds are excellent; however, the number of benzoic acids reported is limited and most are *ortho*-substituted (*Scheme 37c*).⁵⁶ Interestingly, this reaction can also realized selective mono-protodecarboxylation of dicarboxylic acids.¹²⁶ Like copper and silver, gold salts in stoichiometric loading can also mediate the decarboxylation of aromatic and heteroaromatic carboxylic acids and at low temperatures (*ca.* 60 °C) much lower than those with Cu and Ag catalysts.^{127,128} However, the organometallic (Aryl)Au species thus obtained proved stable against protodemetalation.



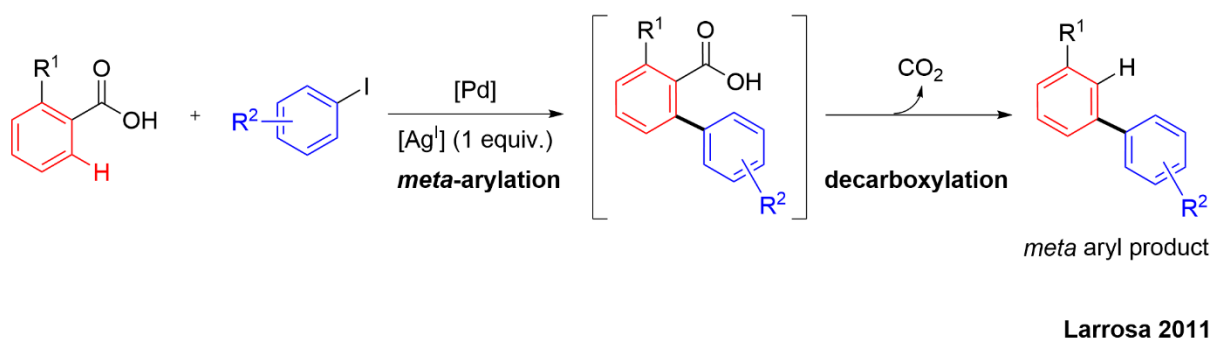
Scheme 37. Copper catalyzed protodecarboxylation of various aromatic carboxylic acid via a) copper catalyst system; b) silver catalyst with additives; and c) silver catalyst system without additives.

Besides group 11 transition metals, Pd(II) and Ru(II) catalysts operate at particularly mild conditions (*ca.* 70–110 °C), but are limited to a narrow scope of electron-rich 2,6-methoxy-disubstituted aromatic acids for the palladium system⁵⁷ as well as multi-substituted arene-carboxylic acids for the ruthenium

catalyst (Scheme 38).¹²⁹ This methodology has been applied in synthetic route for the *meta* functionalization of aryl scaffold in a tandem C-H activation and protodecarboxylation reactions (Scheme 39).^{130–133} The carboxylic acid group acts as a directing group in a first *ortho* C-H activation with haloarenes as coupling partner. It is followed by a protodecarboxylation reaction to remove the carboxylic group. Thus, challenging selectivity can be reached with a unique catalytic system and the support of the carboxylic function as traceless directing group. Regardless of its convenience as a one-pot strategy that provides a selective methodology for *meta*-functionalization, stoichiometric amount of oxidizing agent is required.



Scheme 38. a) Pd(II) catalyzed protodecarboxylation of 2,6-dimethoxy-aromatic carboxylic acids; b) Ru(II) catalyzed protodecarboxylation of multi-substituted arenecarboxylic acids.



Scheme 39. Tandem *ortho*-selective arylation/protodecarboxylation process leading to formal *meta*-selective C-H arylation.¹³⁰

In summary, general decarboxylative transformation for the synthesis of biaryl scaffolds has achieved remarkable results and versatility over the past decades. All studies are devoted to developing a large number of transformations that give access to a wide range of substrate classes starting from carboxylic acids. A number of challenges have been overcome, but the process still needs to be optimized to obtain more efficient and less costly catalytic systems. For instance, the elevated

temperatures for the reaction, functional group tolerance, and the availability of benzoic acid derivatives. Of all the transition metal catalysts, copper stands out as a promising catalyst for such a transformation under noble metal-free conditions, which is so far much more generally applicable. In recognition of copper's potential, much effort has gone into elucidating the mechanism of the copper-catalyzed decarboxylation step, in the hope of developing more practical generations of copper-based catalysts.

III. Mechanistic study of copper catalyzed decarboxylation step in catalysis

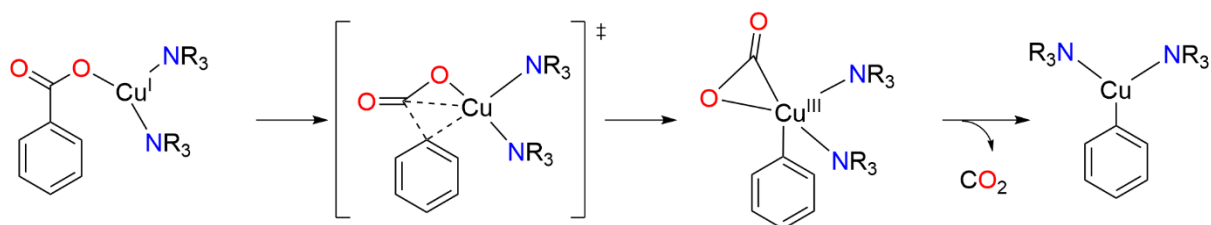
III. 1. Experimental study

The first mechanistic insight was reported by Nilsson *et al.* in 1966 when they discovered that 2-nitrobiphenyl can be formed by decarboxylation of *o*-nitrobenzoic acid in the presence of iodoarenes.⁷⁸ This combination of classic Ullmann reaction and copper-promoted decarboxylation of aromatic acids led to consider several points related to these two types of reaction. Firstly, the beneficial effect of *ortho*- group in the aromatic substrates, and secondly the nature of the intermediate, presumably a copper-aryl species, from the decarboxylation step. In 1970, Sheppard confirmed the hypothesis of an organocopper intermediate by isolating the [(quinoline)Cu-C₆F₅] complex (76%) resulting from the loss of CO₂ from the carboxylate [Cu(CO₂C₆F₅)] in the solvent quinoline at 60 °C.¹³⁴ This Cu-aryl complex was separately prepared by immersing (pentafluorophenyl)copper¹³⁵ in quinoline resulting a brown solid which has identical melting point with the decarboxylated product (mp 161–164 °C). It was the first evidence that the decarboxylation step took place via a copper-aryl intermediate. However, this [(quinoline)Cu-C₆F₅] is only characterized by melting point analysis.

Additionally, the important impact of the electronic properties of the aryl substituents on the stability of the copper-aryl species has been highlighted. Beside the tetramers [Cu(C₆F₅)₄] and the mesitylene analogue [Cu(Mes)₆] examples of well-defined and stable Aryl-Cu(I) copper species are very limited and generally involve additional ligands.^{136–140} In most of the case, the organocopper derivative degrades. The extrusion of CO₂ from copper carboxylate via homolytic C–C bond cleavage was initially ruled out to explain the distinct behavior of the aromatic and aliphatic carboxylic acid in the decarboxylative process. A similar observation was done by Cohen *et al.* through a kinetic study and stereochemical results that went against a radical process.^{81,82} Given that the reaction kinetic was measured to be first-order in cuprous benzoates, it was unlikely that radicals were involved. Moreover, the retention of configuration observed in the decarboxylation of pure isomeric diphenylpropenoic acids, that afforded separately the *cis*- or the *trans*- decarboxylated products in high yields, also supported a non-radical process.⁸¹ Recently, a work from Gooßen *et al.* involving the addition of the radical scavenger TEMPO showed no influence on the yield of the decarboxylation process.⁵⁴ Consequently, it is highly plausible that the cleavage of the C–C bond leading to the loss of CO₂ followed a heterolytic pathway via a copper-aryl intermediate.

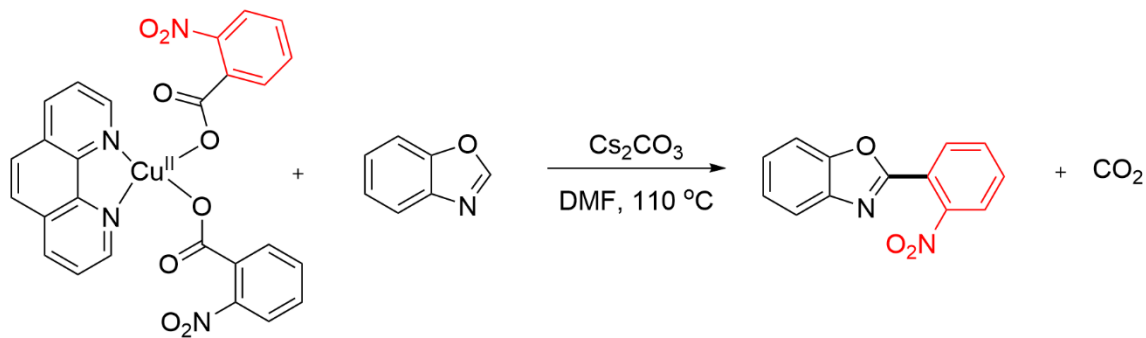
The oxidation state of the copper center of the active species is also somewhat controversial. Kinetic studies and ESR measurements by Cohen and co-workers suggested a copper (I) active species. This is evidenced first by a reduction of cupric carboxylates to copper(I) supposedly by quinoline solvent prior

to the decarboxylation step.⁸¹ Secondly, the kinetic is found to be first order in copper (I) carboxylate, whereas the decarboxylation proceeds 100 times slower when copper(II) is applied.⁸² Later, the same group proposed the passage to a transient copper(III) intermediate during the extrusion of CO₂ involving the oxidative addition of aryl carboxylate to copper(I) precursor.^{82,141} In fact, the shred of evidence to support this oxidative addition mechanism is mainly on the beneficial role of σ -donor ligand. Although the decarboxylative mechanism is not clear, Cahiez *et al.* considered as reasonable the proposal of Cohen⁸² concerning the oxidative addition of the copper atom to the C–COO bond of the carboxylate, via a π -complexation to the aromatic ring or not (Scheme 40).¹⁴² The instable copper (III) intermediate would indeed rapidly reductively eliminate carbon dioxide with formation of an aryl-copper(I) species. The loss of CO₂ would be induced by the π -back-donation of the metal center to the σ^* -orbitals of the C–C bond and this process favored by increasing the electronic density of the copper atom which is the role of strong σ -donor ligands such as the amines quinoline, bypyridine or 1,10-phenanthroline which gave the best results.



Scheme 40. Proposed mechanism for the copper-catalyzed decarboxylation via copper(III) intermediate.¹⁴²

Concerning the decarboxylation process involving the oxidant (*vide supra*, Chapter 1 – II. 4.), a recent investigation into the reactivity of copper(I) and copper(II) complexes by Hoover and co-workers gave more solid proofs for a pathway based on copper(II) reactive species.¹⁴³ In their study, they successfully isolated a series of 1,10-phenanthroline ligated copper(I) and copper(II) benzoates species [(phen)Cu(O₂CC₆H₄-*o*-NO₂)_x] (x = 1, 2) and the aryl derivative [(phen)Cu(C₆H₄-*o*-NO₂)]. They engaged the copper benzoate complexes in stoichiometric C–H functionalization reactions with benzoxazole in DMF in presence of Cs₂CO₃ at 110°C (Scheme 41). The higher yields observed while using Cu(II) species than Cu(I) suggests the cupric benzoate are important intermediates in reaction under oxidizing conditions. Nevertheless, the potential involvement of copper(III) benzoate generated via disproportionation¹⁴⁴ in the extrusion of CO₂ is not excluded.



Hoover 2017

Scheme 41. Stoichiometric reaction of copper(II) carboxylic acid and benzoxazole.¹⁴³

In short, experimental studies by Sheppard and Cohen in the 1970s have emphasized the intermediacy of copper(I) aryl species in the decarboxylation process by losing CO₂ of copper(I) carboxylate complex. So far only one example of copper(I) carboxylate undergoes CO₂ extrusion to produce a copper(I) aryl species was demonstrated, however without sufficient characterization analysis. Alternative, Cu(III) intermediate is proposed as well by Cohen and later agreed by Cahiez. This species is formed via the oxidative addition of carboxylate into a copper center to form a copper(III) aryl intermediate. However, due to the instability of copper(III) species, this complex is neither isolated nor observed. Regarding the oxidative decarboxylative process, copper(II) species is suggested to be the key intermediate as demonstrated by the group of Hoover. By observing a better reactivity of copper(II) benzoate in the C-H activation with benzoxazole substrate compared to copper(I) benzoate, they proposed that the loss of CO₂ is likely to occur at the copper (II) center. Nonetheless, the possible involvement of copper(III) intermediate is not excluded.

III. 2. DFT studies carried out for determining the mechanism of the copper catalyzed decarboxylation step in catalysis

Within the past decades, atomic- and molecular-level understanding of chemical processes by computational calculations led to meaningful predictions and calculations of chemical structures and were convenient for a clear understanding of the reactivity processes. Among the important types of modern calculations methods such as Hartree-Fock (HF), Moller-Plesset perturbation theory (MP), etc., density functional theory (DFT) calculations is considered to have sufficient accuracy and by far the most widely used method. DFT is a quantum-mechanical (QM) method used in chemistry and physics to compute some parts of the energy and the electron density of atoms and molecules. The huge impact of DFT in physics and chemistry had led to the Nobel Prize granted to Walter Kohn in 1998 for his development of the density-functional theory.

Understanding a chemical reaction mechanism has always been key to improve reaction conditions and to achieve a great scope in substrates. By employing the state-of-the-art computational tool, several studies dedicated to the redox-neutral decarboxylative process by looking at various energy profiles of different copper-catalyst systems were carried out. Consequently, the mystery behind the decarboxylation event and useful insight into experimental results are revealed.

In 2009, Liu *et al.* proposed a possible mechanism for the decarboxylative cross-coupling of potassium polyfluorobenzoates with haloarenes catalyzed by [(phen)Cu-I] (*Figure 15*).⁵⁸ The first step involves the salt exchange between potassium benzoate and the [(phen)Cu-X] (**I**) (X = Br, I) to form a copper benzoate [(phen)Cu-O₂C-Ar] (**II**) complex (Ar = polyfluoroarene) and KI salt. This copper benzoate species subsequently decarboxylates to release CO₂ and generating [(phen)Cu-Ar] (**III**) intermediate. The following oxidative addition of Ph-Br substrate into the copper aryl species leads to a pentacoordinated copper (III) intermediate (**IV**). Finally, reductive elimination of this copper species affords a coupling product and regenerate [(phen)Cu-X] (**I**) complex and closed the catalytic cycle.

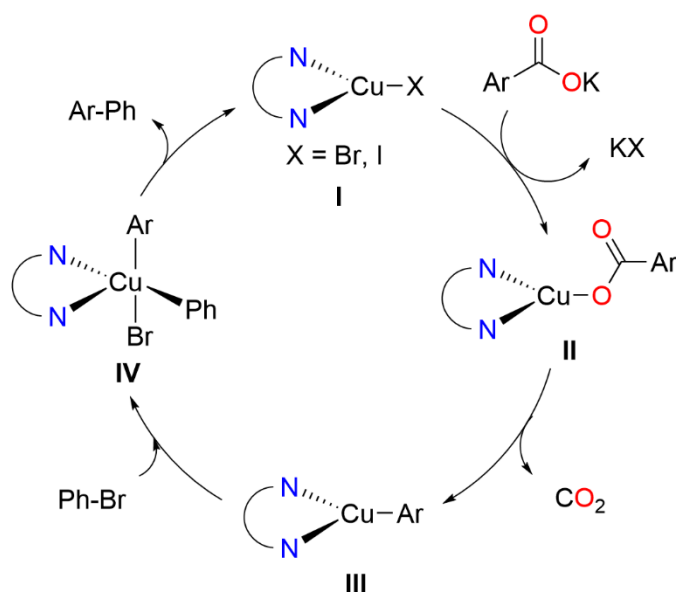


Figure 15. First proposed mechanisms for the copper-catalyzed decarboxylation of $C_6F_5CO_2K$ with haloarenes by $[(phen)Cu-I]$.⁵⁸

Alternatively, they considered a second pathway where oxidative addition of aryl halide compound occurs before the decarboxylation event (Figure 16). The catalytic cycle starts with the oxidative addition, resulting a pentacoordinated copper (III) complex **V**. Subsequently, the salt exchange takes place at the copper (III) center, forming a copper benzoate species (**VI**). The loss of CO_2 from this intermediate resulted complex **IV** as a pentacoordinated species. After the decarboxylation, intermediate **IV** undergoes reductive elimination to produce the final coupling compound and give back the copper(I) species.

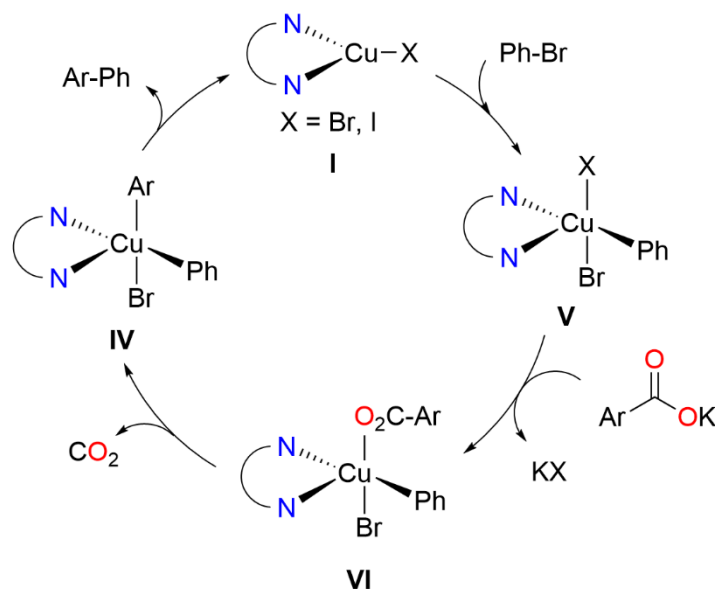


Figure 16. Second proposed mechanisms for the copper-catalyzed decarboxylation of $C_6F_5CO_2K$ with haloarenes by $[(phen)Cu-I]$.⁵⁸

DFT calculations were performed according on these pathways.⁵⁸ It was found that the first mechanism where decarboxylation occurs on copper(I) before oxidative addition of aryl halide compound is more

favorable with lower energy barriers for most of the steps, + 20.3 kcal.mol⁻¹ for decarboxylation and + 30.0 kcal.mol⁻¹ for oxidative addition, the latter being the limiting step. In the second pathway, where decarboxylation takes place after the oxidative addition via a copper(III) intermediate, the energy profile is much higher. The pentacoordinated copper(III) complex undergoes the extrusion of CO₂ via an extremely high activation barrier of + 51.1 kcal.mol⁻¹ and the energy gap of + 35.0 kcal.mol⁻¹ of this step is too high to be overcome. Therefore, in that case, decarboxylation at a copper(III) species is excluded.

In 2010, Gooßen and co-workers focused their attention on the decarboxylation event by computing the electronic structures and energy profiles of the starting materials, transition states and the products for the decarboxylation of the cuprous Cu(O₂CC₆H₄-o-F) complexes coordinated by 4,7-disubstituted 1,10-phenanthroline ligands (Figure 17).¹⁴⁵ A model system of these complexes with increasingly electron-donating substituents has been devised. The group focused on the computation of relevant parameters: the total energies of reaction (ΔE_{tot}^R) and activation (ΔE_{tot}^\ddagger), the free enthalpies of reaction (ΔG^R) and activation (ΔG^\ddagger), and the relative reaction rates (k) at room temperature (298 K) or higher temperature (443 K). These parameters were chosen in order to better understand the effect of ligand, particularly the electronic properties, on the thermodynamics and the kinetic of the decarboxylation event. The effect of ligand will be discussed later on. The analysis of these computed results also allowed rationalizing the reactivity pathway. Thus, an insightful conclusion was drawn and a general map of reactivity appeared.

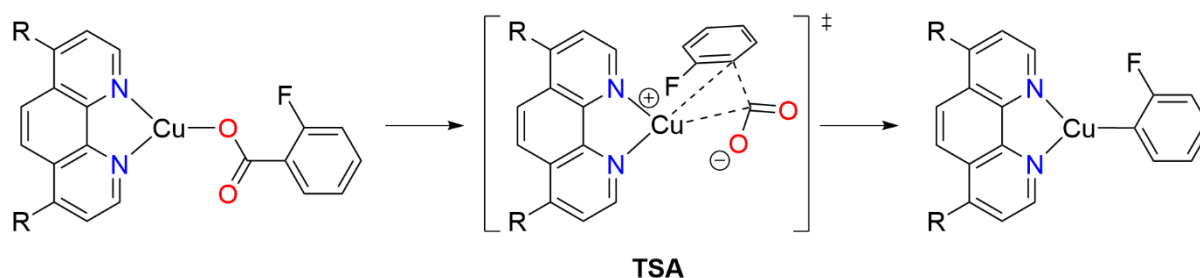


Figure 17. DFT calculations on the decarboxylation of 4,7-disubstituted-1,10-phenanthroline copper(I) 2-fluorobenzoats.¹⁴⁵

Generally, the loss of CO₂ is endergonic at room temperature and would proceed via a single transition state (TS). The structures of the TS are almost identical for all the substituted phenanthroline ligands. It is a distorted tetrahedral geometry where copper, coordinated by the two nitrogen atoms of the phenanthroline, the carbon atom of the CO₂ moiety and the C_{ipso} of the aryl group (Figure 18). It is noteworthy to mention that when they computed with unsubstituted phenanthroline, they obtained the same structure for TS and bond lengths. The C_{Ar}-C_{COO} bond lengths are around 1.90 Å and the Cu-C_{Ar} bond length is 2.03 Å for all cases. This, as indicated by the authors, are evidenced for an early transition state. Meanwhile, the Cu-C_{COO} and the Cu-O_{COO} distance are relatively long, which are 2.22 Å and 2.63 Å, respectively.

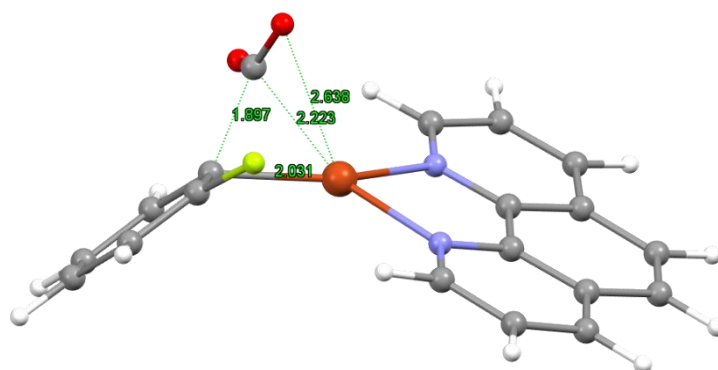


Figure 18. Calculated transition state structure of $\text{Cu}(\text{O}_2\text{C}_6\text{H}_4\text{-o-F})$ supported by phenanthroline in decarboxylation step calculated by Gooßen *et al.*¹⁴⁵

Orange sphere represent copper atom, red spheres: oxygen atoms, blue spheres: nitrogen atoms, grey spheres: carbon atoms, green sphere: fluorine atom, and white spheres: hydrogen atoms. Numbers in green are the distances between atoms in Å.

The optimized structure of the transition state (TS) proposed by Su *et al.* displays a similar coordination mode of the phenanthroline ligand, and the aryl carbon, however the carboxyl moiety is coordinated by the oxygen atom instead of the carbon atom.¹⁴⁶ All the computed TS for selected substituents at *ortho*, *para*, and *meta* position in the carboxylic acids have the similar structures. This TS adopts as well a distorted tetrahedron geometry, with $\text{C}_{\text{Ar}}\text{-C}_{\text{COO}}$ and Cu-C_{Ar} ($\text{Ar} = \text{C}_6\text{H}_5$) bond lengths are 2.06 Å and 1.96 Å, respectively, whereas the Cu-O_{COO} is relatively long with 2.66 Å (Figure 19). This transition state structure is in agreement with calculated model by Liu *et al.* with phenanthroline and $\text{C}_6\text{F}_5\text{COO}^-$ as ligands.⁵⁸ Despite having the same geometry and coordination sites, this TS has a shorter Cu-O_{COO} bond (2.09 Å) than that obtained by the Su group. The distances from C_{Ar} to the carboxyl moiety ($\text{C}_{\text{Ar}}\text{-C}_{\text{COO}}$) and to the copper center (Cu-C_{Ar}) have closed values of 2.01 Å and 2.00 Å respectively (Figure 19).

As seen above, two main transition states have been proposed, in which the key difference is the binding modes either via the oxygen atom or the carbon atom of the carboxyl group. Such different structures of between the two transition states can be due to different applied computational levels. So far, there is no definite conclusion on which TS could be considered.

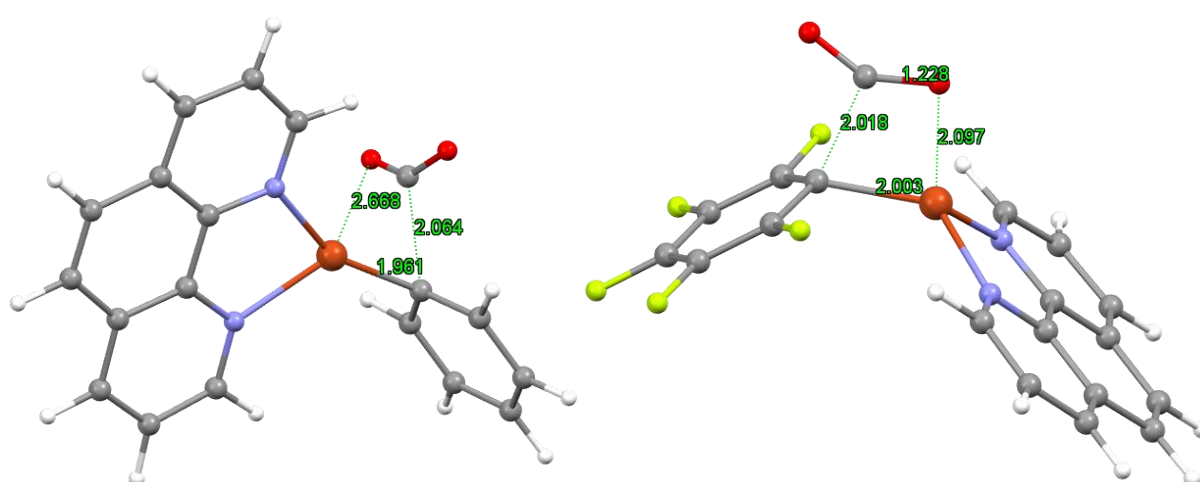


Figure 19. Calculated four-membered ring transition state structure of copper complex in decarboxylation step. Left: TS calculated by Su *et al.*¹⁴⁶ Right: TS calculated by Liu *et al.*⁵⁸

Orange sphere represent copper atom, red spheres: oxygen atoms, blue spheres: nitrogen atoms, grey spheres: carbon atoms, green spheres: fluorine atoms, and white spheres: hydrogen atoms. Numbers in green are the distances between atoms in Å.

The next question then turned to the electronic and steric effects of the substrates and the ligands, and more precisely to unveil the particular role of the substituents in *ortho*-position to the carboxylic fragment on the aromatic cycle, and the influence of the bidentate nitrogen ligands.

III. 2. 1. Ortho effect

During the early years in the development of copper-promoted decarboxylative reactions, *ortho*-substituted aromatic carboxylic acid was the best choice of substrate. As the improvements of reaction conditions and substrate scope progressed, the nature of the functional group and their position within the aromatic ring was recognized as one of the most significant point in the decarboxylation event. Computational studies have then been carried out by different research groups to gain insights on the influence of the *ortho*-substituents.

In 2010, Gooßen *et al.* calculated and compared by DFT the activation energies for the extrusion of CO₂ in Cu(O₂CC₆H₄-*o*-F) and Cu(O₂CC₆H₄-*m*-F) fluorobenzoate complexes coordinated with various 1,10-phenanthroline derivatives.¹⁴⁵ The choice of *meta*-substituted benzoate complex is to clarify the *ortho*-effect if it truly existed. Indeed, the activation energies for the (phen)Cu(O₂CC₆H₄-*m*-F) species were found higher than those calculated for the *ortho* derivatives, indicating of a decrease in the reaction rate.¹⁴⁵ These calculations matched their experimental results reported in 2007.⁵⁴ Shortly after this report, Su *et al.* took a giant step forward in exploring the electronic effects of a large range of substituents at different positions (*ortho*, *meta*, and *para*).¹⁴⁶ They first calculated the overall activation barriers for the transformation of the modeled copper-carboxylated complexes to the transition state of decarboxylation step. In general, copper-carboxylate complexes are calculated to adopt a T-shape structure with a 3-coordination mode by the bidentate phenanthroline ligand and the oxygen atom of a κ 1-carboxylate ligand (*Figure 20*, left). This copper carboxylate have relatively long Cu-O_{COO} bond of 1.88 Å and a short C_{Ar}-C_{COO} bond (1.50 Å). Similarly, when they calculated the structure of [(phen)Cu-C₆H₅] species, they obtained as well a 3-coordinated complex with a long Cu-C_{Ar} bond of 1.90 Å (*Figure 20*, right). For such a complex, the authors considered only a simple phenyl substrate, while other copper complexes with substituted aryls were not calculated. Meanwhile, as mentioned above, the calculated transition states (TS) feature a four-membered-ring structure (*Figure 19*, left).

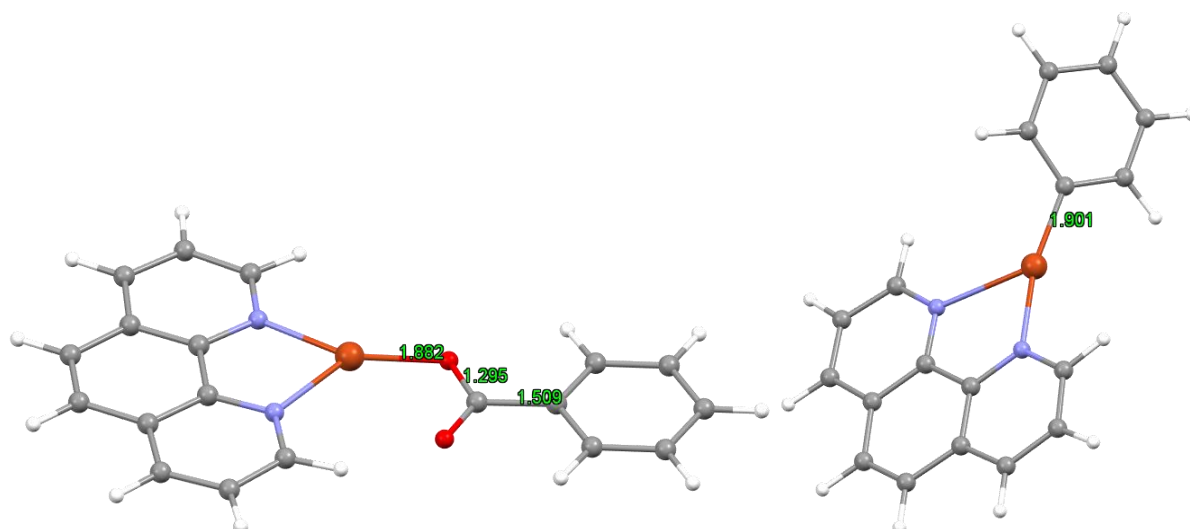


Figure 20. Left: Calculated T-shape structure of copper(I) benzoate complex; Right: Calculated structure of copper(I) phenyl complex.¹⁴⁶

Orange sphere represent copper atom, red sphere: oxygen atoms, blue spheres: nitrogen atoms, grey spheres: carbon atoms, and white spheres: hydrogen atoms. Numbers in green are the distances between atoms in Å.

To evaluate the substituent effect on the carboxylic acid, they considered various *ortho* substituents (e.g. NO₂, C(O)H, C(O)Me, C(O)NMe₂, OMe, Cl, Br, CN, Me, NH₂, and OH) on the aromatic ring of the aryl carboxylate and deduced their overall activation energies in the decarboxylation step by calculating their transition states. The calculated results showed that strongly electron donating groups, such as NH₂, and OH at have the highest activation energies (31.7 and 34.8 kcal.mol⁻¹, respectively), whereas OMe substituent gives similar barriers (25.7–26.9 kcal.mol⁻¹) with halogens. The C(O)R substituents (R = H, Me, NMe₂) have relatively low barriers (ca. 23.6 kcal.mol⁻¹) and the lowest among all the calculated substituents is NO₂, with the activation energy of 21.6 kcal.mol⁻¹. As result, there is no clear correlation between the electronic properties of the substituents and the calculated barriers to be detected. This observations are in agreement with the results published by the group of Gooßen.⁵⁴

Besides the substituent effect, the author also exploited the *ortho* effect by comparing the activation barriers from phenanthroline ligated copper carboxylate species [(phen)Cu-O₂CC₆H₄-R] to their decarboxylation transition states of a given substituents at *ortho*, *para*, and *meta* positions.¹⁴⁶ The calculations were performed for R = OMe, Me, NO₂, and CN substituents. The authors noticed that some substituents would help stabilize intermediates (or TS), namely stabilizing effect, while other would destabilize them, so-called destabilizing effect.

For instance, copper benzoate species with substituents at *para* and *meta* positions have similar free energy values (ca. 0.2 kcal.mol⁻¹) and activation barrier (ca. 31.4 kcal.mol⁻¹), regardless the electronic properties. Meanwhile, copper complex coordinated by *ortho*-substituted benzoates have higher free energies, about 2.2 to 5.9 kcal.mol⁻¹ depending on the substituents. The increment in energies of these complexes is caused by the steric hindrance imparted by an *ortho* substituent, which brings a primary destabilizing effect. A secondary stabilizing effect can take place for some substituents, by coordinating to the metal atom in the TS. Such destabilizing and stabilizing effects help lower the barrier of

decarboxylation by *ca.* 2.2 to 8.5 kcal.mol⁻¹, compared to the corresponding barriers for *para* and *meta* derivatives (*ca.* 33 kcal.mol⁻¹) (Figure 21).

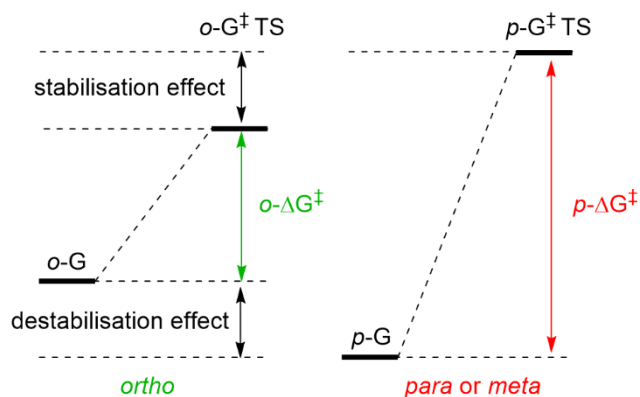


Figure 21. Destabilization effect by ortho substituent (1° effect) and stabilization effect by coordination of the ortho substituent to the copper center (2° effect).¹⁴⁷

Indeed, substituents such as –NO₂ and –C(O)R (R = H, Me, NMe₂) can provide an extra coordination site to the Cu metal center via the oxygen forming a stable five-membered-ring TS (Figure 22), hence decreasing its Gibbs free energy. One relevant example is NO₂ substituted benzoate copper complex. *Para* and *meta* isomers have similar level of energies, with respectively 0 and –0.3 kcal.mol⁻¹, and 30.1 and 30.5 kcal.mol⁻¹ for the corresponding TSs (Figure 23). Activation barriers of 30.1 and 30.8 kcal.mol⁻¹ are reported for them. In the case of *ortho* isomer, due to the additional coordination of the oxygen atom from the NO₂ group to the copper center, the transition state is stabilized and has a lower energy of 27.5 kcal.mol⁻¹. Furthermore, steric hindrance caused by the NO₂ moiety at the *ortho* position destabilized the copper benzoate derivatives, resulting in high energy level of 5.9 kcal.mol⁻¹ of this species. This overall brings a pronounced *ortho* effect, where the activation barrier is decreased to 21.6 kcal.mol⁻¹ (Figure 23).

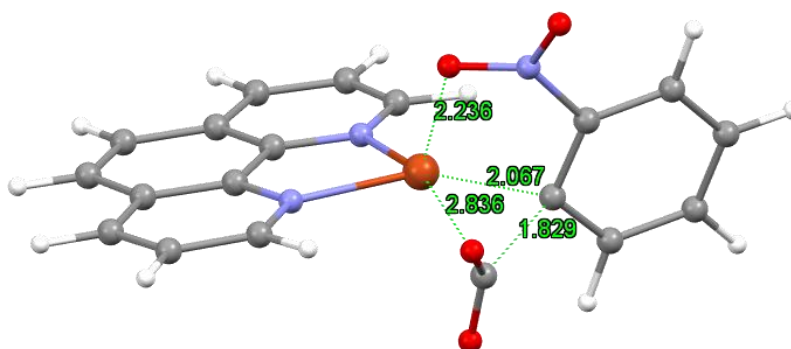


Figure 22. Calculated TS of copper complex with *o*-nitro-benzoate and phenanthroline as ligand.¹⁴⁶ Orange sphere represent copper atom, red spheres: oxygen atoms, blue spheres: nitrogen atoms, grey spheres: carbon atoms, and white spheres: hydrogen atoms. Numbers in green are the distances between atoms in Å.

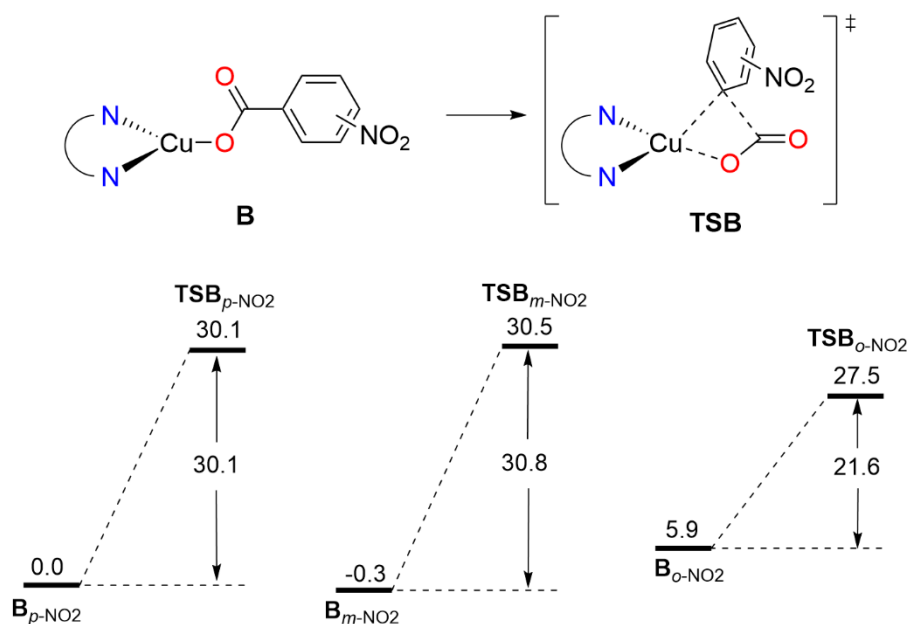


Figure 23. The relative energies (kcal.mol⁻¹) calculated for copper-catalyzed decarboxylation of some nitro-benzoic acids.¹⁴⁶

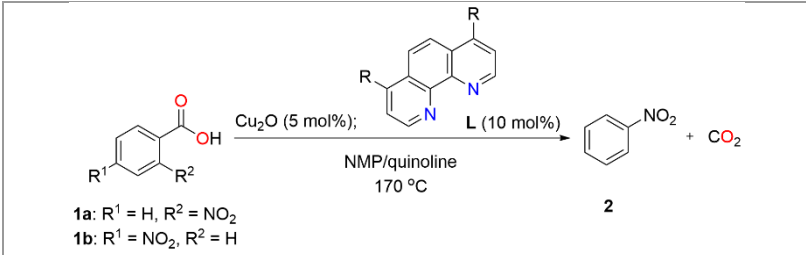
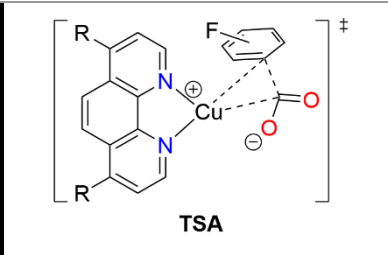
Overall, coordinating substituents in *ortho* position exert a primary destabilization effect of the carboxylate complex (favoring loss of CO₂) and a secondary stabilizing effect of the TS, thus, reducing the decarboxylation barriers. This emphasizes that the *ortho* effect exists and it is assumed to be an essential activating factor.

III. 2. 2. Effect of the nitrogen ligand:

All the works of the pioneering decarboxylation process had highlighted the key influence of the nitrogen ligand on the efficiency of the reaction. Gradually, with the help of innovating technologies, researchers started to investigate in more details the effects of the ligand upon the decarboxylation steps in the catalytic cycle.

Cohen noted, as early as 1978, the beneficial effect of chelating ligand such as 1,10-phenanthroline that enhanced the rate of decarboxylation.⁸² Since then, the employment of N-type bidentate ligand proved to be significant throughout years of developments of experimental catalysis. Taking the advantage of modern theoretical chemistry, Gooßen *et al.* carried out a computational investigations on the energy profile of the decarboxylation event to map the effect of the substituents on 4,7-positions of phenanthroline ligand.^{54,145} The calculated results showed in *Table 1* revealed no trend of electron-donating substituents on the aromatic rings of the ligand in the decarboxylation of copper(I) *o*- and *p*-fluorobenzoates.¹⁴⁵ The (ΔG[‡]) values calculated for the transition states of *ortho* and *para*-fluorobenzoates (TSA_{*o-p*} and TSA_{*p-F*} in *Table 1*) show only *ca.* 1 kcal.mol⁻¹ differences between substituents on the phenanthroline rings. On the other hand, the obtained experimental results showed little beneficial effect of electron-donating substituents (*Table 1*). For instance, in the copper catalyzed protodecarboxylation of *o*-nitrobenzoic acid, using 4,7-bis(dimethoxy)-phenanthroline as ligand gave 81 % yields and unsubstituted phenanthroline ligand afforded 65 % yield.¹⁴⁵

Table 1. Experimental results and DFT calculations of copper-catalyzed decarboxylation of carboxylic acids with 4,7-disubstituted 1,10-phenanthroline ligands.¹⁴⁵

				
R	Experimental results		DFT calculations results (ΔG^\ddagger) ^a	
	1a → 2 (%)	1b → 2 (%)	TSA _{o-F}	TSA _{p-F}
H	65	43	31.4	34.2
CN	64	10	32.0	35.1
Ph	55	57	31.1	34.3
Me	75	0	31.2	34.1
SPh	57	34	31.6	34.7
OPh	57	0	31.9	34.4
OMe	81	6	31.1	34.0
NMe ₂	--	--	30.6	33.7

^a ΔG^\ddagger are expressed in kcal.mol⁻¹ and calculated at reaction temperature of 443 K.

However, this trend is less evidence in the case of para-substituted benzoic acids as substrates, in which the use of electron-rich ligands gave very low conversions with 0 to 6 % yield compared to that obtained with phenanthroline ligand (43 %) (Table 1).¹⁴⁵ Such difference results can be explained by the *ortho*-effect which has been mentioned previously.

In contrast, the steric congestion afforded by substituents at 2,9-position on phenanthroline ring disabled the reactivity of copper complex due to the steric repulsion, whereas substituents on 4,7-positions proved generally beneficial.^{54,145} Only two reports by Cahiez¹⁴² and Cai¹⁴⁸, have described the advantages of non-aromatic and electronic rich nitrogen ligands such as TMEDA¹⁴² and NEt₃¹⁴⁸ in protodecarboxylation. These ligands, with stronger σ -donor characters, lower the reaction temperature however, with limited scope in benzoic substrates with NEt₃. So far, no computational study was carried out with these ligands.

Over decades, a consensus have been reached by the community on the general mechanisms for the copper-catalyzed decarboxylation reaction via one-step CO₂ extrusion, however through different possible transition states. Some main mechanistic key factors have been carefully considered and computed. For instance the involvement of copper(III) intermediates have been excluded due to the extremely high activation energy barrier via a hexacoordinated copper(III) transition state. The electronic properties of substituents on the benzoic acids rings proved to have little effect on the barrier energy levels, although *ortho* positions to the aromatic ring bring beneficial effects to the decarboxylation event. This was explained by the destabilizing effect and the stabilizing effect that lower the activation barrier in the decarboxylation process. Similarly, the choice of electron-rich ligand that favor the decarboxylative transformation is also exploited. However, the trend of electronic effect is less obvious and depends strongly on the carboxylic substrates. In term of substituted positions,

phenanthroline ligand with substituents at 2,9-position tends to hamper the copper reactivity by steric repulsion, which is not the case for 4,7-substituted isomers. Overall, these observations have brought insightful aspects to modulate the reactivity of the copper center, a result that would initiate a continuing and powerful trend in copper-promoted decarboxylation reaction.

Besides mononuclear copper(I) complexes, there are few research dedicated to the decarboxylation of dinuclear copper(I) carboxylates species. For instance, O'Hair *et al.* studied the decarboxylation in gas-phase of copper benzoate supported by 1,8-naphthyridine (napy) ligand $[(\text{napy})\text{Cu}_2(\text{O}_2\text{CC}_6\text{H}_4\text{X})]^+$ (X = H, F, Br, CN, NO₂, etc.) with X at *ortho*, *para*, or *meta* position combining mass spectrometry experiments and DFT calculations.¹⁴⁹ With mass spectrometry, the authors observed the corresponding $[(\text{napy})\text{Cu}_2(\text{C}_6\text{H}_4\text{X})]^+$ and CO₂ as main products from the decarboxylation of $[(\text{napy})\text{Cu}_2(\text{O}_2\text{CC}_6\text{H}_4\text{X})]^+$ at 250 °C. This is supported by DFT calculations where they found that the activation barriers for the decarboxylation step of $[(\text{napy})\text{Cu}_2(\text{O}_2\text{CC}_6\text{H}_4\text{X})]^+$ (**2oF**) to $[(\text{napy})\text{Cu}_2(\text{C}_6\text{H}_4\text{X})]^+$ (**3oF**) via transition state **TS_{2-3oF}** are relatively low (*ca.* 25 kcal.mol⁻¹) (Figure 24), compared to what have been reported by the groups of Gooßen, Su and Liu.^{58,145,146} However, the rate determining step is the breaking of one Cu-O bond of $[(\text{napy})\text{Cu}_2(\text{O}_2\text{CC}_6\text{H}_4\text{X})]^+$ **1oF**, in which the carboxylate ligands coordinate to two Cu centers via the two O atoms in a bridging mode, to generate the reactive conformer **2oF** via **TS_{1-2oF}** for the decarboxylation step (Figure 24).

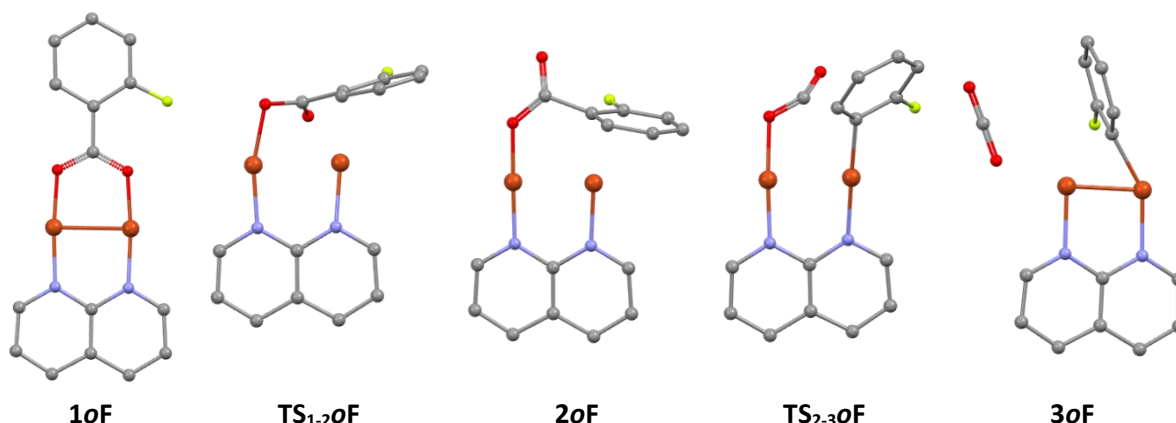


Figure 24. DFT calculated copper intermediates in the decarboxylation of $[(\text{napy})\text{Cu}_2(\text{O}_2\text{CC}_6\text{H}_4\text{X})]^+$.¹⁴⁹

Orange sphere represent copper atom, red sphere: oxygen atoms, blue spheres: nitrogen atoms, grey spheres: carbon atoms, and green spheres: fluorine atoms.

There is only one example where the dinuclear copper carboxylate complexes $[\text{Cu}(\mu\text{-O}_2\text{CC}_6\text{H}_4\text{X})(\text{quin})]_2$ (quin = quinoline, X = H, Me) were isolated and their structures were determined by X-ray diffractometer by van Koten in 1989.¹⁵⁰ In solid state, these binuclear complexes exist as dimers and bridged by two O-bonded carboxylate ligands. Each copper is coordinated by one quinoline compound, where the two N-coordinating ligand are almost parallel. In solution, these species are anticipated to be either in monomeric or dimeric structure. The reactivity of these complexes toward decarboxylation at elevated temperature has also been investigated in non-coordinating solvents, such as toluene, decalin or naphthalene. Although these copper carboxylate species did not decarboxylate in toluene and decalin, the authors observed successful extrusion of CO₂ (*ca.* 60 %) in naphthalene of these complexes in the presence of more than 1 equivalent of quinoline at 218 °C. Nevertheless, several quinoline containing products were obtained (*e.g.* biquinoline, 8-naphthylquinoline, 2-acylquinoline). A mechanism was proposed starting from the dimeric $[\text{Cu}(\mu\text{-O}_2\text{CC}_6\text{H}_4\text{X})(\text{quin})]_2$ species. Similar with

O'Hair proposal, the breaking of one Cu-O bond to afford an intermediate where two coppers are bridged by only one carboxylate ligand. The next steps are the rotation around the C-O and the C-Ar bonds of the non-bridging carboxylate group and its binding to the second copper center. This event brings the aromatic ring of the benzoate unit closer to the copper atom, thus enables the decarboxylation step. Nevertheless, there are several mechanistic pathways that can take place, neither via oxidative addition of the carboxylate group nor through single-electron transfer from the copper (I) ion to the π^* system.

Few studies have been published on the decarboxylation of dinuclear copper carboxylate complexes, and several plausible mechanisms have been proposed. Such mechanistic pathways have been reported for 1,8-naphthyridine and quinoline ligands, whereas more common copper-catalyzed decarboxylation process employs phenanthroline-based ligands. These ligands can bring distinct coordination modes to copper center, in which dimeric or monomeric copper species can be formed. This involvement of dinuclear copper species is outside the scope of our study, as our focus is on the generally accepted mechanism involving mononuclear copper species.

IV. Conclusion

Since the pioneering work of Shepard in 1930,⁷⁷ tremendous progress has been achieved within the decarboxylative copper-mediated C-C bond construction chemistry using carboxylic acids and aryl coupling partners. The interest of this decarboxylative transformation is originated from its benefit over traditional cross-coupling reactions as inexpensive, stable and easy to prepare benzoic acids in comparison to some pre-functionalized organometallic coupling partners. One main drawback of the decarboxylation process that has not been fixed are the elevated temperature required for the extrusion of CO₂, because such C-C bond cleavage needs high activation energy.

Many brilliant minds have put together important elements to create various pathways for the biaryl synthesis via decarboxylation of aromatic carboxylic acids, either via redox-neutral or oxidative process. Gooßen group has greatly contributed to achieve a direct cross-coupling between benzoic acids and aryl halides in particular under catalytic conditions. A common limitation observed is the need of coordinative substituents in *ortho* position of the carboxylic group. The transition state for the C_{Ar}-C_{COO} is usually high, however their presence decreases the energy required to reach the TS, and so supports the decarboxylative process. Dedicated studies enabled to design new catalytic conditions to broaden the substrate scope of aromatic carboxylic acids, including none *ortho*-substituted supporting groups

Within few years, their fruitful observation and studies eventually have finally made it possible to broaden the field of substrates to include para- and meta-substituted aromatic carboxylic acids.

In the field of decarboxylative oxidative coupling of a benzoic acid with an arene, it represents a more atom-economic approach than decarboxylative couplings with haloarenes, where no halide salts are produced as by-products. However, this field is still poor in efficient transformations, in which stoichiometric amount of transition metal are required, and lacks of mechanistic insights. To date, only two examples reported by the groups of Maiti and Su required catalytic amount of a transition metal, albeit with limitations in terms of substrate range or regioselectivity on the arene coupling partner.

Moreover, both fields of decarboxylative homocoupling and cross-coupling between aryl carboxylic acids are underdeveloped. The homocoupling of carboxylic acids via a double decarboxylation is possible with high copper catalyst loading, but it requires functional group in *ortho*-position on benzoic acids. While asymmetric biaryl molecules can be afforded from a wide range of (hetero)aromatic carboxylic acids, the reported protocol suffers from poor chemoselectivity and require stoichiometric amount of oxidant.

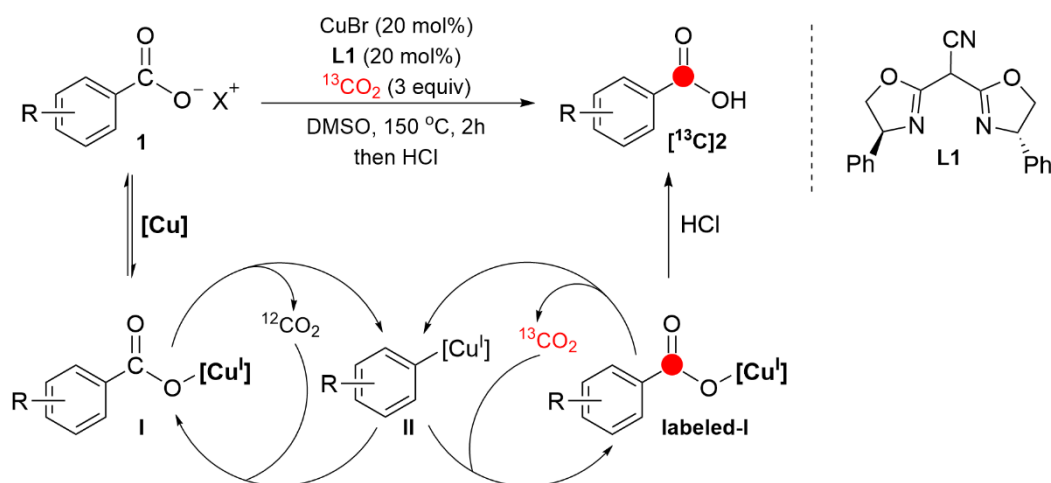
Initially seen as an undesired reaction during redox-neutral and oxidative decarboxylative coupling, the protodecarboxylation reaction has been include later in elegant synthetic strategy to remove carboxylic acid functions used as directing groups. Among the d-transition metals, copper and silver are the most efficient to promote this reaction. While copper-mediated protodecarboxylation is independent of *ortho*-substituted benzoic acid, silver-catalysed protodecarboxylation operates at lower temperatures but requires *ortho*-group.

Being essential in the decarboxylation process, copper metal species have received particular attention. Early mechanistic studies by Nilsson, Cohen and Sheppard focused mainly on the decarboxylation mechanism and the generation of organocopper intermediates. A few decades later, the observation of copper aryl species was confirmed by modern calculations carried out by the group of Gooßen and Su. They proposed a general mechanism in which decarboxylation occurs via the release of CO₂ from the copper (I) carboxylate complex and then generates a copper aryl species. In addition, the positive significance of *ortho* substituents in carboxylic acids has been explained by two different aspects and the influence of the ligand on copper activity was carefully calculated. The copper (II), crucial in some mediated decarboxylation, though is lacking of mechanistic study to decipher his role.

V. Objectives

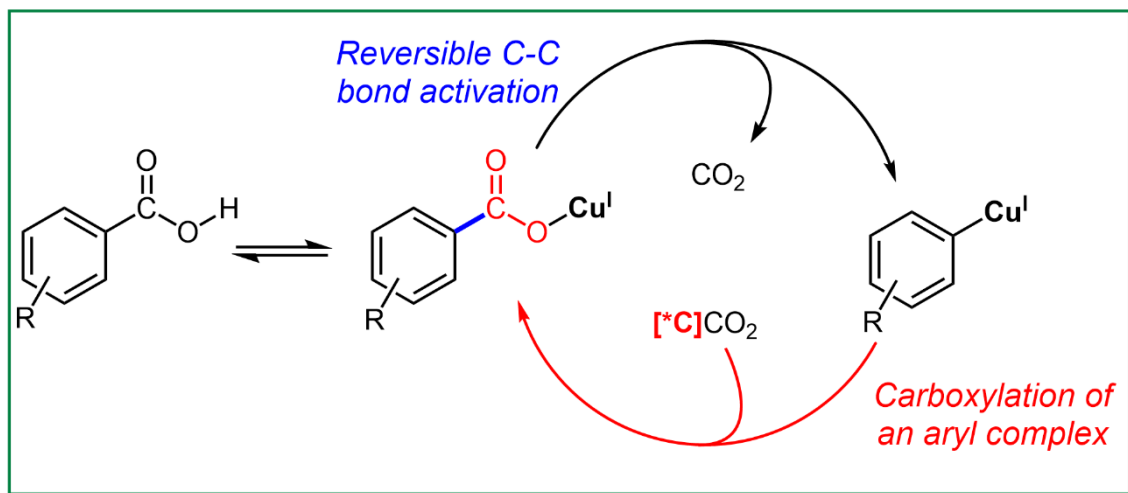
Experimental and theoretical studies brought to light the big picture of decarboxylation process, particularly centralized in copper-mediated system. Research has shown that not only copper metal can promote the breaking of strong C–C bond through decarboxylation but can also favor the making of C–C bonds by the insertion of CO₂ into a Cu–C bond. Since the first report by DePasquale *et al.* in the CO₂ insertion into [Cu–(C₆F₅)] in DMA at 70 °C,¹⁵¹ the fixation of CO₂ gas and its use as a C1 source in aromatic compound to generate transition metal-catalyzed benzoic acid derivatives, attracted considerable attention.^{152–155} The 2000's and 2010's have witnessed the evolution of synthetic methodologies towards carboxylation, thus adding new dimensions to copper-catalyzed addition reactions of carbon-nucleophiles to CO₂.^{156–158} Inspired by the work of Takaya *et al.*,¹⁵⁹ Hou and co-worker introduced a copper-catalyst system with N-heterocycle ligands (NHC) to prepare carboxylic acid compounds via CO₂ fixation into organoboron reagents.¹⁵⁶ Researchers proposed a catalytic cycle supported by stoichiometric control reactions. They displayed that both copper aryl and copper carboxylate are intermediates. Another strategy was developed by Daugulis *et al.* in 2013, where CuI/TMEDA catalyst system combined with Et₂Zn as reducing agent is employed for a reductive carboxylation of aryl iodides.¹⁵⁸ Without going further in the chemistry of CO₂ fixation, we will leave this topic here at the origins and developments, and refer the reader to Reviews in the evolving CO₂ insertion area.¹⁵⁷

As seen above, copper metal has been proved to be efficient for both decarboxylation and carboxylation reactions. The noteworthy similarities between the copper-catalyzed decarboxylation and carboxylation processes are nitrogen-containing ligands and copper intermediates. In this context, some groups have designed conditions allowing both decarboxylation and carboxylation do proceed simultaneously. Such conditions create a dynamic exchange favorable for the one-pot incorporation of labeled ¹¹C, ¹³C or ¹⁴C carbon dioxide into native ¹²C carboxylic acid molecules.¹⁶⁰ This carbon isotope exchange (CIE) was optimized to achieve carbon labeling of numerous arenes, heteroarenes with relatively high isotopic enrichment percentage. Such reactivity is strongly demanded for pharmaceutical application. Nevertheless, no mechanistic information is reported besides one general proposed catalytic cycle (*Scheme 42*).¹⁶⁰



Scheme 42. Copper-catalyzed ¹³CO₂ dynamic isotope exchange of benzoic acid.

We therefore set ourselves the goal of clarifying the mechanism and the species involved in the CIE process, starting by studying the behavior of copper(I) carboxylate and copper(I) aryl complexes in the reversible activation of the C–C bond. The current state of the art is based on an expensive and uncommon bisoxazoline ligand (**L1**). We therefore planned to isolate and characterize various copper(I) complexes using a more conventional nitrogen phenanthroline (phen) ligand that is well developed in copper chemistry. If successful, this will be the first direct insight into the reversible decarboxylation/carboxylation process via isolated copper(I) complexes.



VI. References

- (1) Bringmann, G.; Günther, C.; Ochse, M.; Schupp, O.; Tasler, S. Biaryls in Nature: A Multi-Faceted Class of Stereochemically, Biosynthetically, and Pharmacologically Intriguing Secondary Metabolites. In *Fortschritte der Chemie organischer Naturstoffe / Progress in the Chemistry of Organic Natural Products*; Herz, W., Falk, H., Kirby, G. W., Moore, R. E., Eds.; Fortschritte der Chemie organischer Naturstoffe / Progress in the Chemistry of Organic Natural Products; Springer Vienna: Vienna, 2001; Vol. 82, pp 1–249. https://doi.org/10.1007/978-3-7091-6227-9_1.
- (2) Brunel, J. M. BINOL: A Versatile Chiral Reagent. *Chem. Rev.* **2005**, *105* (3), 857–898. <https://doi.org/10.1021/cr040079g>.
- (3) Surry, D. S.; Buchwald, S. L. Dialkylbiaryl Phosphines in Pd-Catalyzed Amination: A User's Guide. *Chem. Sci.* **2011**, *2* (1), 27–50. <https://doi.org/10.1039/C0SC00331J>.
- (4) Hajduk, P. J.; Bures, M.; Praestgaard, J.; Fesik, S. W. Privileged Molecules for Protein Binding Identified from NMR-Based Screening. *J. Med. Chem.* **2000**, *43* (18), 3443–3447. <https://doi.org/10.1021/jm000164q>.
- (5) Grimsdale, A. C.; Leok Chan, K.; Martin, R. E.; Jokisz, P. G.; Holmes, A. B. Synthesis of Light-Emitting Conjugated Polymers for Applications in Electroluminescent Devices. *Chem. Rev.* **2009**, *109* (3), 897–1091. <https://doi.org/10.1021/cr000013v>.
- (6) Horton, D. A.; Bourne, G. T.; Smythe, M. L. The Combinatorial Synthesis of Bicyclic Privileged Structures or Privileged Substructures. *Chem. Rev.* **2003**, *103* (3), 893–930. <https://doi.org/10.1021/cr020033s>.
- (7) Kovacic, Peter.; Jones, M. B. Dehydro Coupling of Aromatic Nuclei by Catalyst-Oxidant Systems: Poly(p-Phenylene). *Chem. Rev.* **1987**, *87* (2), 357–379. <https://doi.org/10.1021/cr00078a005>.
- (8) Gomberg, M.; Bachmann, W. E. THE SYNTHESIS OF BIARYL COMPOUNDS BY MEANS OF THE DIAZO REACTION. *J. Am. Chem. Soc.* **1924**, *46* (10), 2339–2343. <https://doi.org/10.1021/ja01675a026>.
- (9) Ullmann, F.; Bielecki, J. Ueber Synthesen in der Biphenylreihe. *Ber. Dtsch. Chem. Ges.* **1901**, *34* (2), 2174–2185. <https://doi.org/10.1002/cber.190103402141>.
- (10) Hassan, J.; Sévignon, M.; Gozzi, C.; Schulz, E.; Lemaire, M. Aryl–Aryl Bond Formation One Century after the Discovery of the Ullmann Reaction. *Chem. Rev.* **2002**, *102* (5), 1359–1470. <https://doi.org/10.1021/cr000664r>.
- (11) McGlacken, G. P.; Bateman, L. M. Recent Advances in Aryl–Aryl Bond Formation by Direct Arylation. *Chem. Soc. Rev.* **2009**, *38* (8), 2447. <https://doi.org/10.1039/b805701j>.
- (12) García-López, J.-A.; Greaney, M. F. Synthesis of Biaryls Using Aryne Intermediates. *Chem. Soc. Rev.* **2016**, *45* (24), 6766–6798. <https://doi.org/10.1039/C6CS00220J>.
- (13) Yang, Y.; Lan, J.; You, J. Oxidative C–H/C–H Coupling Reactions between Two (Hetero)Arenes. *Chem. Rev.* **2017**, *117* (13), 8787–8863. <https://doi.org/10.1021/acs.chemrev.6b00567>.
- (14) Meerwein, H.; Büchner, E.; Van Emster, K. Über die Einwirkung aromatischer Diazoverbindungen auf α,β -ungesättigte Carbonylverbindungen. *J. Prakt. Chem.* **1939**, *152* (7–10), 237–266. <https://doi.org/10.1002/prac.19391520705>.
- (15) M. S., K.; E. K. J., F. *J. Am. Chem. Soc.* **63**, 2316–2320.
- (16) Corriu, R. J. P.; Masse, J. P. Activation of Grignard Reagents by Transition-Metal Complexes. A New and Simple Synthesis of Trans-Stilbenes and Polyphenyls. *J. Chem. Soc., Chem. Commun.* **1972**, No. 3, 144a. <https://doi.org/10.1039/c3972000144a>.

- (17) Tamao, K.; Sumitani, K.; Kumada, M. Selective Carbon-Carbon Bond Formation by Cross-Coupling of Grignard Reagents with Organic Halides. Catalysis by Nickel-Phosphine Complexes. *J. Am. Chem. Soc.* **1972**, *94* (12), 4374–4376. <https://doi.org/10.1021/ja00767a075>.
- (18) F., D.; P. J., S. *Metal-Catalyzed Cross-Coupling Reactions*; Wiley-VCH, New York, 1998.
- (19) Nicolaou, K. C.; Bulger, P. G.; Sarlah, D. Palladium-Catalyzed Cross-Coupling Reactions in Total Synthesis. *Angew. Chem. Int. Ed.* **2005**, *44* (29), 4442–4489. <https://doi.org/10.1002/anie.200500368>.
- (20) Hussain, N.; Hussain, A. Advances in Pd-Catalyzed C–C Bond Formation in Carbohydrates and Their Applications in the Synthesis of Natural Products and Medicinally Relevant Molecules. *RSC Adv.* **2021**, *11* (54), 34369–34391. <https://doi.org/10.1039/D1RA06351K>.
- (21) Cornella, J.; Zarate, C.; Martin, R. Metal-Catalyzed Activation of Ethers via C–O Bond Cleavage: A New Strategy for Molecular Diversity. *Chem. Soc. Rev.* **2014**, *43* (23), 8081–8097. <https://doi.org/10.1039/C4CS00206G>.
- (22) Fu, L.; Chen, Q.; Nishihara, Y. Recent Advances in Transition-metal-catalyzed C–C Bond Formation via C(sp^2)–F Bond Cleavage. *The Chemical Record* **2021**, *21* (12), 3394–3410. <https://doi.org/10.1002/tcr.202100053>.
- (23) Kambe, N.; Iwasaki, T.; Terao, J. Pd-Catalyzed Cross-Coupling Reactions of Alkyl Halides. *Chem. Soc. Rev.* **2011**, *40* (10), 4937. <https://doi.org/10.1039/c1cs15129k>.
- (24) Colacot, T. J. <|>The 2010 Nobel Prize in Chemistry: Palladium-Catalysed Cross-Coupling</|>. *platin met rev* **2011**, *55* (2), 84–90. <https://doi.org/10.1595/147106711X558301>.
- (25) Iglesias, J.; Martínez-Salazar, I.; Maireles-Torres, P.; Martín Alonso, D.; Mariscal, R.; López Granados, M. Advances in Catalytic Routes for the Production of Carboxylic Acids from Biomass: A Step Forward for Sustainable Polymers. *Chem. Soc. Rev.* **2020**, *49* (16), 5704–5771. <https://doi.org/10.1039/D0CS00177E>.
- (26) Kar, S.; Sanderson, H.; Roy, K.; Benfenati, E.; Leszczynski, J. Green Chemistry in the Synthesis of Pharmaceuticals. *Chem. Rev.* **2022**, *122* (3), 3637–3710. <https://doi.org/10.1021/acs.chemrev.1c00631>.
- (27) Petchey, M. R.; Grogan, G. Enzyme-Catalysed Synthesis of Secondary and Tertiary Amides. *Adv Synth Catal* **2019**, *361* (17), 3895–3914. <https://doi.org/10.1002/adsc.201900694>.
- (28) Zhang, M.; Xie, J.; Zhu, C. A General Deoxygenation Approach for Synthesis of Ketones from Aromatic Carboxylic Acids and Alkenes. *Nat Commun* **2018**, *9* (1), 3517. <https://doi.org/10.1038/s41467-018-06019-1>.
- (29) Qu, R.; Junge, K.; Beller, M. Hydrogenation of Carboxylic Acids, Esters, and Related Compounds over Heterogeneous Catalysts: A Step toward Sustainable and Carbon-Neutral Processes. *Chem. Rev.* **2023**, *123* (3), 1103–1165. <https://doi.org/10.1021/acs.chemrev.2c00550>.
- (30) Jerry, M. *Advanced Organic Chemistry*, third.; Wiley-VCH, New York, 1985.
- (31) Ni, W.; Zhu, G.; Liu, F.; Li, Z.; Xie, C.; Han, Y. Carboxylic Acids in Petroleum: Separation, Analysis, and Geochemical Significance. *Energy Fuels* **2021**, *35* (16), 12828–12844. <https://doi.org/10.1021/acs.energyfuels.1c01518>.
- (32) Lidén, G. Carboxylic Acid Production. *Fermentation* **2017**, *3* (3), 46. <https://doi.org/10.3390/fermentation3030046>.
- (33) Yang, S.-T.; Huang, H.; Tay, A.; Qin, W.; De Guzman, L.; Nicolas, E. C. S. Extractive Fermentation for the Production of Carboxylic Acids. In *Bioprocessing for Value-Added Products from Renewable Resources*; Elsevier, 2007; pp 421–446. <https://doi.org/10.1016/B978-044452114-9/50017-7>.

- (34) Kubitschke, J.; Lange, H.; Strutz, H. Carboxylic Acids, Aliphatic. In *Ullmann's Encyclopedia of Industrial Chemistry*; Wiley-VCH Verlag GmbH & Co. KGaA, Ed.; Wiley-VCH Verlag GmbH & Co. KGaA: Weinheim, Germany, 2014; pp 1–18. https://doi.org/10.1002/14356007.a05_235.pub2.
- (35) Keshav, A.; Norge, P.; Wasewar, K. L. Reactive Extraction of Citric Acid Using Tri-n-Octylamine in Nontoxic Natural Diluents: Part 1—Equilibrium Studies from Aqueous Solutions. *Appl Biochem Biotechnol* **2012**, *167* (2), 197–213. <https://doi.org/10.1007/s12010-012-9682-z>.
- (36) Khaw, K.-Y.; Parat, M.-O.; Shaw, P. N.; Falconer, J. R. Solvent Supercritical Fluid Technologies to Extract Bioactive Compounds from Natural Sources: A Review. *Molecules* **2017**, *22* (7), 1186. <https://doi.org/10.3390/molecules22071186>.
- (37) *Carboxylic acids*.
- (38) Gooßen, L. J.; Rodríguez, N.; Gooßen, K. Carboxylic Acids as Substrates in Homogeneous Catalysis. *Angew. Chem. Int. Ed.* **2008**, *47* (17), 3100–3120. <https://doi.org/10.1002/anie.200704782>.
- (39) 2017-Catalysts-Francos-Metalcatalyzed-Carboxylic Acid to Alkynes.Pdf.
- (40) Kennemur, J. L.; Maji, R.; Scharf, M. J.; List, B. Catalytic Asymmetric Hydroalkoxylation of C–C Multiple Bonds: Focus Review. *Chem. Rev.* **2021**, *121* (24), 14649–14681. <https://doi.org/10.1021/acs.chemrev.1c00620>.
- (41) Bruneau, C.; Dixneuf, P. H. Metal Vinylidenes and Allenylidenes in Catalysis: Applications in Anti-Markovnikov Additions to Terminal Alkynes and Alkene Metathesis. *Angew. Chem. Int. Ed.* **2006**, *45* (14), 2176–2203. <https://doi.org/10.1002/anie.200501391>.
- (42) Gooßen, L. J.; Gooßen, K.; Rodríguez, N.; Blanchot, M.; Linder, C.; Zimmermann, B. New Catalytic Transformations of Carboxylic Acids. *Pure and Applied Chemistry* **2008**, *80* (8), 1725–1733. <https://doi.org/10.1351/pac200880081725>.
- (43) Oe, Y.; Ohta, T.; Ito, Y. Ruthenium Catalyzed Addition Reaction of Carboxylic Acid across Olefins without β -Hydride Elimination. *Chem. Commun.* **2004**, No. 14, 1620–1621. <https://doi.org/10.1039/B404229H>.
- (44) Mitsudo, T.; Hori, Y.; Yamakawa, Y.; Watanabe, Y. Ruthenium-Catalyzed Selective Addition of Carboxylic Acids to Alkynes. A Novel Synthesis of Enol Esters. *J. Org. Chem.* **1987**, *52* (11), 2230–2239. <https://doi.org/10.1021/jo00387a024>.
- (45) Koschker, P.; Lumbroso, A.; Breit, B. Enantioselective Synthesis of Branched Allylic Esters via Rhodium-Catalyzed Coupling of Allenes with Carboxylic Acids. *J. Am. Chem. Soc.* **2011**, *133* (51), 20746–20749. <https://doi.org/10.1021/ja210149g>.
- (46) Cadierno, V. Gold-Catalyzed Addition of Carboxylic Acids to Alkynes and Allenes: Valuable Tools for Organic Synthesis. *Catalysts* **2020**, *10* (10), 1206. <https://doi.org/10.3390/catal10101206>.
- (47) Chary, B. C.; Kim, S. Gold(I)-Catalyzed Addition of Carboxylic Acids to Alkynes. *J. Org. Chem.* **2010**, *75* (22), 7928–7931. <https://doi.org/10.1021/jo101543q>.
- (48) Yang, C.-G.; He, C. Gold(I)-Catalyzed Intermolecular Addition of Phenols and Carboxylic Acids to Olefins. *J. Am. Chem. Soc.* **2005**, *127* (19), 6966–6967. <https://doi.org/10.1021/ja050392f>.
- (49) Smith, D. L.; Goundry, W. R. F.; Lam, H. W. Palladium-Catalyzed Hydroacyloxylation of Ynamides. *Chem. Commun.* **2012**, *48* (10), 1505–1507. <https://doi.org/10.1039/C1CC13595C>.
- (50) Lim, W.; Kim, J.; Rhee, Y. H. Pd-Catalyzed Asymmetric Intermolecular Hydroalkoxylation of Allene: An Entry to Cyclic Acetals with Activating Group-Free and Flexible Anomeric Control. *J. Am. Chem. Soc.* **2014**, *136* (39), 13618–13621. <https://doi.org/10.1021/ja508587f>.

- (51) Pradal, A.; Toullec, P. Y.; Michelet, V. Gold-Catalyzed Oxidative Acyloxylation of Arenes. *Org. Lett.* **2011**, *13* (22), 6086–6089. <https://doi.org/10.1021/ol202577c>.
- (52) Goossen, L. J.; Paetzold, J.; Koley, D. Regiocontrolled Ru-Catalyzed Addition of Carboxylic Acids to Alkynes: Practical Protocols for the Synthesis of Vinyl Esters We Thank Prof. Dr. M. T. Reetz for Generous Support and Constant Encouragement, and Gratefully Acknowledge the DFG, the FCI, and the BMBF for Financial Support. *Chem. Commun.* **2003**, No. 6, 706–707. <https://doi.org/10.1039/b211277a>.
- (53) Thiery, E.; Aouf, C.; Belloy, J.; Harakat, D.; Le Bras, J.; Muzart, J. Palladium-Catalyzed Allylic Acyloxylation of Terminal Alkenes in the Presence of a Base. *J. Org. Chem.* **2010**, *75* (5), 1771–1774. <https://doi.org/10.1021/jo902587u>.
- (54) Gooßen, L. J.; Thiel, W. R.; Rodríguez, N.; Linder, C.; Melzer, B. Copper-Catalyzed Protodecarboxylation of Aromatic Carboxylic Acids. *Adv. Synth. Catal.* **2007**, *349* (14–15), 2241–2246. <https://doi.org/10.1002/adsc.200700223>.
- (55) Gooßen, L. J.; Linder, C.; Rodríguez, N.; Lange, P. P.; Fromm, A. Silver-Catalysed Protodecarboxylation of Carboxylic Acids. *Chem. Commun.* **2009**, No. 46, 7173. <https://doi.org/10.1039/b912509d>.
- (56) Cornella, J.; Sanchez, C.; Banawa, D.; Larrosa, I. Silver-Catalysed Protodecarboxylation of Ortho-Substituted Benzoic Acids. *Chem. Commun.* **2009**, No. 46, 7176. <https://doi.org/10.1039/b916646g>.
- (57) Dickstein, J. S.; Mulrooney, C. A.; O'Brien, E. M.; Morgan, B. J.; Kozlowski, M. C. Development of a Catalytic Aromatic Decarboxylation Reaction. *Org. Lett.* **2007**, *9* (13), 2441–2444. <https://doi.org/10.1021/ol070749f>.
- (58) Shang, R.; Fu, Y.; Wang, Y.; Xu, Q.; Yu, H.-Z.; Liu, L. Copper-Catalyzed Decarboxylative Cross-Coupling of Potassium Polyfluorobenzoates with Aryl Iodides and Bromides. *Angew. Chem. Int. Ed.* **2009**, *48* (49), 9350–9354. <https://doi.org/10.1002/anie.200904916>.
- (59) Shang, R.; Xu, Q.; Jiang, Y.-Y.; Wang, Y.; Liu, L. Pd-Catalyzed Decarboxylative Cross Coupling of Potassium Polyfluorobenzoates with Aryl Bromides, Chlorides, and Triflates. *Org. Lett.* **2010**, *12* (5), 1000–1003. <https://doi.org/10.1021/ol100008q>.
- (60) Becht, J.-M.; Catala, C.; Le Drian, C.; Wagner, A. Synthesis of Biaryls via Decarboxylative Pd-Catalyzed Cross-Coupling Reaction. *Org. Lett.* **2007**, *9* (9), 1781–1783. <https://doi.org/10.1021/ol070495y>.
- (61) Gooßen, L. J.; Rudolphi, F.; Oppel, C.; Rodríguez, N. Synthesis of Ketones from α -Oxocarboxylates and Aryl Bromides by Cu/Pd-Catalyzed Decarboxylative Cross-Coupling. *Angew. Chem. Int. Ed.* **2008**, *47* (16), 3043–3045. <https://doi.org/10.1002/anie.200705127>.
- (62) Myers, A. G.; Tanaka, D.; Mannion, M. R. Development of a Decarboxylative Palladation Reaction and Its Use in a Heck-Type Olefination of Arene Carboxylates. *J. Am. Chem. Soc.* **2002**, *124* (38), 11250–11251. <https://doi.org/10.1021/ja027523m>.
- (63) Inoue, A.; Shinokubo, H.; Oshima, K. Oxidative Heck-Type Reaction Involving Cleavage of a Carbon–Phosphorus Bond of Arylphosphonic Acids. *J. Am. Chem. Soc.* **2003**, *125* (6), 1484–1485. <https://doi.org/10.1021/ja026758v>.
- (64) 1998-Nagayama-Direct Hydrogenation.Pdf.
- (65) Axelsson, L.; Veron, J.-B.; Sävmarker, J.; Lindh, J.; Odell, L. R.; Larhed, M. An Improved Palladium(II)-Catalyzed Method for the Synthesis of Aryl Ketones from Aryl Carboxylic Acids and

- Organonitriles. *Tetrahedron Letters* **2014**, *55* (15), 2376–2380. <https://doi.org/10.1016/j.tetlet.2014.02.109>.
- (66) Kakino, R.; Narahashi, H.; Shimizu, I.; Yamamoto, A. General and Greener Route to Ketones by Palladium-Catalyzed Direct Conversion of Carboxylic Acids with Organoboronic Acids. *Chem. Lett.* **2001**, *30* (12), 1242–1243. <https://doi.org/10.1246/cl.2001.1242>.
- (67) Gooßen, L. J.; Ghosh, K. Palladium-Catalyzed Synthesis of Aryl Ketones from Boronic Acids and Carboxylic Acids or Anhydrides. *Angewandte Chemie International Edition* **2001**, *40* (18), 3458–3460. [https://doi.org/10.1002/1521-3773\(20010917\)40:18<3458::AID-ANIE3458>3.0.CO;2-0](https://doi.org/10.1002/1521-3773(20010917)40:18<3458::AID-ANIE3458>3.0.CO;2-0).
- (68) Gooßen, L. J.; Winkel, L.; Döhning, A.; Ghosh, K.; Paetzold, J. Pd-Catalyzed Synthesis of Functionalized Arylketones from Boronic Acids and Carboxylic Acids Activated in Situ with Dimethyl Dicarboxylate. *Synlett* **2002**, No. 8, 1237–1240. <https://doi.org/10.1055/s-2002-32961>.
- (69) Miller, J. A.; Nelson, J. A.; Byrne, M. P. A Highly Catalytic and Selective Conversion of Carboxylic Acids to 1-Alkenes of One Less Carbon Atom. *J. Org. Chem.* **1993**, *58* (1), 18–20. <https://doi.org/10.1021/jo00053a008>.
- (70) Gooßen, L. J.; Rodríguez, N. A Mild and Efficient Protocol for the Conversion of Carboxylic Acids to Olefins by a Catalytic Decarbonylative Elimination Reaction. *Chem. Commun.* **2004**, No. 6, 724–725. <https://doi.org/10.1039/B316613A>.
- (71) 1982-J.Org. Chem-Blaser-The Palladium Catalyzed Arylation.Pdf.
- (72) Sugihara, T.; Satoh, T.; Miura, M. Mizoroki–Heck Type Arylation of Alkenes Using Aryl Chlorides under Base-Free Conditions. *Tetrahedron Letters* **2005**, *46* (48), 8269–8271. <https://doi.org/10.1016/j.tetlet.2005.09.179>.
- (73) Sugihara, T.; Satoh, T.; Miura, M.; Nomura, M. Rhodium-Catalyzed Coupling Reaction of Aryl Chlorides with Alkenes. *Adv Synth Catal* **2004**, *346* (13–15), 1765–1772. <https://doi.org/10.1002/adsc.200404145>.
- (74) Gooßen, L. J.; Paetzold, J. New Synthesis of Biaryls via Rh-Catalyzed Decarbonylative Suzuki-Coupling of Carboxylic Anhydrides with Arylboroxines. *Adv Synth Catal* **2004**, *346* (13–15), 1665–1668. <https://doi.org/10.1002/adsc.200404190>.
- (75) Cervantes-Reyes, A.; Smith, A. C.; Chinigo, G. M.; Blakemore, D. C.; Szostak, M. Decarbonylative Pd-Catalyzed Suzuki Cross-Coupling for the Synthesis of Structurally Diverse Heterobiaryls. *Org. Lett.* **2022**, *24* (8), 1678–1683. <https://doi.org/10.1021/acs.orglett.2c00267>.
- (76) Ruzi, R.; Liu, K.; Zhu, C.; Xie, J. Upgrading Ketone Synthesis Direct from Carboxylic Acids and Organohalides. *Nat Commun* **2020**, *11* (1), 3312. <https://doi.org/10.1038/s41467-020-17224-2>.
- (77) Shepard, A. F.; Winslow, N. R.; Johnson, J. R. THE SIMPLE HALOGEN DERIVATIVES OF FURAN. *J. Am. Chem. Soc.* **1930**, *52* (5), 2083–2090. <https://doi.org/10.1021/ja01368a057>.
- (78) 1966- ActaChem Scand, V20, 423-0426 NILSSON.Pdf.
- (79) 1968-Acta Chem Scand, V22, 2585 NILSSON.Pdf.
- (80) Sheppard, W. A. Pentafluorophenyl Group. Electronic Effect as a Substituent. *J. Am. Chem. Soc.* **1970**, *92* (18), 5419–5422. <https://doi.org/10.1021/ja00721a021>.
- (81) Cohen, T.; Schambach, R. A. Copper-Quinoline Decarboxylation. *J. Am. Chem. Soc.* **1970**, *92* (10), 3189–3190. <https://doi.org/10.1021/ja00713a047>.
- (82) Cohen, T.; Berninger, R. W.; Wood, J. T. Products and Kinetics of Decarboxylation of Activated and Unactivated Aromatic Cuprous Carboxylates in Pyridine and in Quinoline. *J. Org. Chem.* **1978**, *43* (5), 837–848. <https://doi.org/10.1021/jo00399a010>.

- (83) Gooßen, L. J.; Deng, G.; Levy, L. M. Synthesis of Biaryls via Catalytic Decarboxylative Coupling. *Science* **2006**, *313* (5787), 662–664. <https://doi.org/10.1126/science.1128684>.
- (84) Voutchkova, A.; Coplin, A.; Leadbeater, N. E.; Crabtree, R. H. Palladium-Catalyzed Decarboxylative Coupling of Aromatic Acids with Aryl Halides or Unactivated Arenes Using Microwave Heating. *Chem. Commun.* **2008**, No. 47, 6312. <https://doi.org/10.1039/b813998a>.
- (85) Cornella, J.; Lahlali, H.; Larrosa, I. Decarboxylative Homocoupling of (Hetero)Aromatic Carboxylic Acids. *Chem. Commun.* **2010**, *46* (43), 8276. <https://doi.org/10.1039/c0cc01943g>.
- (86) Goossen, L. J.; Rodríguez, N.; Melzer, B.; Linder, C.; Deng, G.; Levy, L. M. Biaryl Synthesis via Pd-Catalyzed Decarboxylative Coupling of Aromatic Carboxylates with Aryl Halides. *J. Am. Chem. Soc.* **2007**, *129* (15), 4824–4833. <https://doi.org/10.1021/ja068993+>.
- (87) Goossen, L. J.; Rodríguez, N.; Linder, C. Decarboxylative Biaryl Synthesis from Aromatic Carboxylates and Aryl Triflates. *J. Am. Chem. Soc.* **2008**, *130* (46), 15248–15249. <https://doi.org/10.1021/ja8050926>.
- (88) Gooßen, L. J.; Rodríguez, N.; Lange, P. P.; Linder, C. Decarboxylative Cross-Coupling of Aryl Tosylates with Aromatic Carboxylate Salts. *Angewandte Chemie* **2010**, *122* (6), 1129–1132. <https://doi.org/10.1002/ange.200905953>.
- (89) Gooßen, L. J.; Zimmermann, B.; Linder, C.; Rodríguez, N.; Lange, P. P.; Hartung, J. Synthesis of Biaryls and Aryl Ketones via Microwave-Assisted Decarboxylative Cross-Couplings. *Adv. Synth. Catal.* **2009**, *351* (16), 2667–2674. <https://doi.org/10.1002/adsc.200900337>.
- (90) Goossen, L.; Linder, C.; Rodríguez, N.; Lange, P. Biaryl and Aryl Ketone Synthesis via Pd-Catalyzed Decarboxylative Coupling of Carboxylate Salts with Aryl Triflates. *Chem. Eur. J.* **2009**, *15* (37), 9336–9349. <https://doi.org/10.1002/chem.200900892>.
- (91) Gooßen, L. J.; Zimmermann, B.; Knauber, T. Palladium/Copper-Catalyzed Decarboxylative Cross-Coupling of Aryl Chlorides with Potassium Carboxylates. *Angew. Chem. Int. Ed.* **2008**, *47* (37), 7103–7106. <https://doi.org/10.1002/anie.200800728>.
- (92) Becht, J.-M.; Drian, C. L. Biaryl Synthesis via Decarboxylative Pd-Catalyzed Reactions of Arenecarboxylic Acids and Diaryliodonium Triflates. *Org. Lett.* **2008**, *10* (14), 3161–3164. <https://doi.org/10.1021/ol8011293>.
- (93) Wang, Z.; Ding, Q.; He, X.; Wu, J. Pd-Catalyzed Decarboxylative Couplings of Arenecarboxylic Acids with Aryl Iodides. *Tetrahedron* **2009**, *65* (24), 4635–4638. <https://doi.org/10.1016/j.tet.2009.04.047>.
- (94) Zhang, F.; Greaney, M. F. Decarboxylative Cross-Coupling of Azoyl Carboxylic Acids with Aryl Halides. *Org. Lett.* **2010**, *12* (21), 4745–4747. <https://doi.org/10.1021/ol1019597>.
- (95) Gooßen, L. J.; Lange, P. P.; Rodríguez, N.; Linder, C. Low-Temperature Ag/Pd-Catalyzed Decarboxylative Cross-Coupling of Aryl Triflates with Aromatic Carboxylate Salts. *Chem. Eur. J.* **2010**, *16* (13), 3906–3909. <https://doi.org/10.1002/chem.200903319>.
- (96) Peschko, C.; Winkhofer, C.; Steglich, W. Biomimetic Total Synthesis of Lamellarin L by Coupling of Two Different Arylpyruvic Acid Units. *Chem. Eur. J.* **2000**, *6* (7), 1147–1152. [https://doi.org/10.1002/\(SICI\)1521-3765\(20000403\)6:7<1147::AID-CHEM1147>3.0.CO;2-1](https://doi.org/10.1002/(SICI)1521-3765(20000403)6:7<1147::AID-CHEM1147>3.0.CO;2-1).
- (97) Forgione, P.; Brochu, M.-C.; St-Onge, M.; Thesen, K. H.; Bailey, M. D.; Bilodeau, F. Unexpected Intermolecular Pd-Catalyzed Cross-Coupling Reaction Employing Heteroaromatic Carboxylic Acids as Coupling Partners. *J. Am. Chem. Soc.* **2006**, *128* (35), 11350–11351. <https://doi.org/10.1021/ja063511f>.

- (98) Bilodeau, F.; Brochu, M.-C.; Guimond, N.; Thesen, K. H.; Forgione, P. Palladium-Catalyzed Decarboxylative Cross-Coupling Reaction Between Heteroaromatic Carboxylic Acids and Aryl Halides. *J. Org. Chem.* **2010**, *75* (5), 1550–1560. <https://doi.org/10.1021/jo9022793>.
- (99) Miyasaka, M.; Fukushima, A.; Satoh, T.; Hirano, K.; Miura, M. Fluorescent Diarylindoles by Palladium-Catalyzed Direct and Decarboxylative Arylations of Carboxyindoles. *Chem. Eur. J.* **2009**, *15* (15), 3674–3677. <https://doi.org/10.1002/chem.200900098>.
- (100) Arroyave, F. A.; Reynolds, J. R. 3,4-Propylenedioxyppyrrrole-Based Conjugated Oligomers *via* Pd-Mediated Decarboxylative Cross Coupling. *Org. Lett.* **2010**, *12* (6), 1328–1331. <https://doi.org/10.1021/ol100231g>.
- (101) Miyasaka, M.; Hirano, K.; Satoh, T.; Miura, M. Synthesis of 2,3-Diarylbenzo[*b*]Thiophenes *via* Nickel-Catalyzed Suzuki-Miyaura Cross-Coupling and Palladium-Catalyzed Decarboxylative Arylation. *Adv. Synth. Catal.* **2009**, *351* (16), 2683–2688. <https://doi.org/10.1002/adsc.200900480>.
- (102) Zhou, J.; Hu, P.; Zhang, M.; Huang, S.; Wang, M.; Su, W. A Versatile Catalyst for Intermolecular Direct Arylation of Indoles with Benzoic Acids as Arylating Reagents. *Chemistry - A European Journal* **2010**, *16* (20), 5876–5881. <https://doi.org/10.1002/chem.201000529>.
- (103) Hu, P.; Zhang, M.; Jie, X.; Su, W. Palladium-Catalyzed Decarboxylative C–H Bond Arylation of Thiophenes. *Angew. Chem. Int. Ed.* **2012**, *51* (1), 227–231. <https://doi.org/10.1002/anie.201106451>.
- (104) Pei, K.; Jie, X.; Zhao, H.; Su, W. Palladium-Catalyzed Decarboxylative C–H Bond Arylation of Furans: Pd-Catalyzed Decarboxylative C–H Bond Arylation of Furans. *Eur. J. Org. Chem.* **2014**, *2014* (20), 4230–4233. <https://doi.org/10.1002/ejoc.201402278>.
- (105) Xie, K.; Yang, Z.; Zhou, X.; Li, X.; Wang, S.; Tan, Z.; An, X.; Guo, C.-C. Pd-Catalyzed Decarboxylative Arylation of Thiazole, Benzoxazole, and Polyfluorobenzene with Substituted Benzoic Acids. *Org. Lett.* **2010**, *12* (7), 1564–1567. <https://doi.org/10.1021/ol100296b>.
- (106) Luo, H.-Q.; Dong, W.; Loh, T.-P. Pd-Catalyzed Decarboxylative Cross-Coupling of Perfluorobenzoic Acids with Simple Arenes. *Tetrahedron Letters* **2013**, *54* (22), 2833–2836. <https://doi.org/10.1016/j.tetlet.2013.03.086>.
- (107) Zhao, H.; Wei, Y.; Xu, J.; Kan, J.; Su, W.; Hong, M. Pd/PR₃-Catalyzed Cross-Coupling of Aromatic Carboxylic Acids with Electron-Deficient Polyfluoroarenes *via* Combination of Decarboxylation with Sp² C–H Cleavage. *J. Org. Chem.* **2011**, *76* (3), 882–893. <https://doi.org/10.1021/jo102175f>.
- (108) Seo, S.; Slater, M.; Greaney, M. F. Decarboxylative C–H Arylation of Benzoic Acids under Radical Conditions. *Org. Lett.* **2012**, *14* (10), 2650–2653. <https://doi.org/10.1021/ol3010694>.
- (109) Kan, J.; Huang, S.; Lin, J.; Zhang, M.; Su, W. Silver-Catalyzed Arylation of (Hetero)Arenes by Oxidative Decarboxylation of Aromatic Carboxylic Acids. *Angew. Chem. Int. Ed.* **2015**, *54* (7), 2199–2203. <https://doi.org/10.1002/anie.201408630>.
- (110) Wang, C.; Piel, I.; Glorius, F. Palladium-Catalyzed Intramolecular Direct Arylation of Benzoic Acids by Tandem Decarboxylation/C–H Activation. *J. Am. Chem. Soc.* **2009**, *131* (12), 4194–4195. <https://doi.org/10.1021/ja8100598>.
- (111) Zhang, F.; Greaney, M. F. Decarboxylative C–H Cross-Coupling of Azoles. *Angewandte Chemie International Edition* **2010**, *49* (15), 2768–2771. <https://doi.org/10.1002/anie.200906921>.
- (112) Daugulis, O.; Do, H.-Q.; Shabashov, D. Palladium- and Copper-Catalyzed Arylation of Carbon–Hydrogen Bonds. *Acc. Chem. Res.* **2009**, *42* (8), 1074–1086. <https://doi.org/10.1021/ar9000058>.

- (113) Do, H.-Q.; Daugulis, O. Copper-Catalyzed Cyanation of Heterocycle Carbon–Hydrogen Bonds. *Org. Lett.* **2010**, *12* (11), 2517–2519. <https://doi.org/10.1021/ol100772u>.
- (114) Do, H.-Q.; Daugulis, O. A General Method for Copper-Catalyzed Arene Cross-Dimerization. *J. Am. Chem. Soc.* **2011**, *133* (34), 13577–13586. <https://doi.org/10.1021/ja2047717>.
- (115) Wendlandt, A. E.; Suess, A. M.; Stahl, S. S. Copper-Catalyzed Aerobic Oxidative C–H Functionalizations: Trends and Mechanistic Insights. *Angew. Chem. Int. Ed.* **2011**, *50* (47), 11062–11087. <https://doi.org/10.1002/anie.201103945>.
- (116) Daugulis, O.; Roane, J.; Tran, L. D. Bidentate, Monoanionic Auxiliary-Directed Functionalization of Carbon–Hydrogen Bonds. *Acc. Chem. Res.* **2015**, *48* (4), 1053–1064. <https://doi.org/10.1021/ar5004626>.
- (117) Chen, L.; Ju, L.; Bustin, K. A.; Hoover, J. M. Copper-Catalyzed Oxidative Decarboxylative C–H Arylation of Benzoxazoles with 2-Nitrobenzoic Acids. *Chem. Commun.* **2015**, *51* (81), 15059–15062. <https://doi.org/10.1039/C5CC06645J>.
- (118) Patra, T.; Nandi, S.; Sahoo, S. K.; Maiti, D. Copper Mediated Decarboxylative Direct C–H Arylation of Heteroarenes with Benzoic Acids. *Chem. Commun.* **2016**, *52* (7), 1432–1435. <https://doi.org/10.1039/C5CC08367B>.
- (119) Zhang, Y.; Zhao, H.; Zhang, M.; Su, W. Carboxylic Acids as Traceless Directing Groups for the Rhodium(III)-Catalyzed Decarboxylative C–H Arylation of Thiophenes. *Angew. Chem.* **2015**, *127* (12), 3888–3892. <https://doi.org/10.1002/ange.201411701>.
- (120) Crawford, J. M.; Shelton, K. E.; Reeves, E. K.; Sadarananda, B. K.; Kalyani, D. Nickel-Catalyzed Decarboxylative Arylation of Azoles with Perfluoro- and Nitrobenzoates. *Org. Chem. Front.* **2015**, *2* (6), 726–729. <https://doi.org/10.1039/C5QO00040H>.
- (121) Yang, K.; Wang, P.; Zhang, C.; Kadi, A. A.; Fun, H.-K.; Zhang, Y.; Lu, H. Nickel-Catalyzed Decarboxylative Arylation of Heteroarenes through Sp² C–H Functionalization: Nickel-Catalyzed Decarboxylative Arylation of Heteroarenes. *Eur. J. Org. Chem.* **2014**, *2014* (34), 7586–7589. <https://doi.org/10.1002/ejoc.201403234>.
- (122) Fu, Z.; Li, Z.; Xiong, Q.; Cai, H. Facile Synthesis of 2,2'-Dinitrosubstituted Biaryls through Cu-Catalyzed Ligand-Free Decarboxylative Homocoupling of Ortho-Nitrobenzoic Acids. *RSC Adv.* **2015**, *5* (64), 52101–52104. <https://doi.org/10.1039/C5RA07771K>.
- (123) Xie, K.; Wang, S.; Yang, Z.; Liu, J.; Wang, A.; Li, X.; Tan, Z.; Guo, C.-C.; Deng, W. Synthesis of Biaryls by Pd-Catalyzed Decarboxylative Homo- and Heterocoupling of Substituted Benzoic Acids. *Eur. J. Org. Chem.* **2011**, *2011* (29), 5787–5790. <https://doi.org/10.1002/ejoc.201100913>.
- (124) Hu, P.; Shang, Y.; Su, W. A General Pd-Catalyzed Decarboxylative Cross-Coupling Reaction between Aryl Carboxylic Acids: Synthesis of Biaryl Compounds. *Angew. Chem. Int. Ed.* **2012**, *51* (24), 5945–5949. <https://doi.org/10.1002/anie.201200153>.
- (125) Goossen, L. J.; Manjolinho, F.; Khan, B. A.; Rodríguez, N. Microwave-Assisted Cu-Catalyzed Protodecarboxylation of Aromatic Carboxylic Acids. *J. Org. Chem.* **2009**, *74* (6), 2620–2623. <https://doi.org/10.1021/jo802628z>.
- (126) Lu, P.; Sanchez, C.; Cornella, J.; Larrosa, I. Silver-Catalyzed Protodecarboxylation of Heteroaromatic Carboxylic Acids. *Org. Lett.* **2009**, *11* (24), 5710–5713. <https://doi.org/10.1021/ol902482p>.

- (127) Dupuy, S.; Lazreg, F.; Slawin, A. M. Z.; Cazin, C. S. J.; Nolan, S. P. Decarboxylation of Aromatic Carboxylic Acids by Gold(I)-*N*-Heterocyclic Carbene (NHC) Complexes. *Chem. Commun.* **2011**, 47 (19), 5455–5457. <https://doi.org/10.1039/C1CC10917K>.
- (128) Cornella, J.; Rosillo-Lopez, M.; Larrosa, I. A Novel Mode of Reactivity for Gold(I): The Decarboxylative Activation of (Hetero)Aromatic Carboxylic Acids. *Adv. Synth. Catal.* **2011**, 353 (8), 1359–1366. <https://doi.org/10.1002/adsc.201100109>.
- (129) Sun, Z.-M.; Zhang, J.; Zhao, P. Rh(I)-Catalyzed Decarboxylative Transformations of Arenecarboxylic Acids: Ligand- and Reagent-Controlled Selectivity toward Hydrodecarboxylation or Heck–Mizoroki Products. *Org. Lett.* **2010**, 12 (5), 992–995. <https://doi.org/10.1021/ol100001b>.
- (130) Cornella, J.; Righi, M.; Larrosa, I. Carboxylic Acids as Traceless Directing Groups for Formal Meta-Selective Direct Arylation. *Angew. Chem. Int. Ed.* **2011**, 50 (40), 9429–9432. <https://doi.org/10.1002/anie.201103720>.
- (131) Luo, J.; Preciado, S.; Larrosa, I. Overriding Ortho–Para Selectivity via a Traceless Directing Group Relay Strategy: The Meta-Selective Arylation of Phenols. *J. Am. Chem. Soc.* **2014**, 136 (11), 4109–4112. <https://doi.org/10.1021/ja500457s>.
- (132) Luo, J.; Preciado, S.; Larrosa, I. Salicylic Acids as Readily Available Starting Materials for the Synthesis of Meta-Substituted Biaryls. *Chem. Commun.* **2015**, 51 (15), 3127–3130. <https://doi.org/10.1039/C4CC09674F>.
- (133) Luo, J.; Preciado, S.; Araromi, S. O.; Larrosa, I. A Domino Oxidation/Arylation/Protodecarboxylation Reaction of Salicylaldehydes: Expanded Access to *Meta*-Arylphenols. *Chem. Asian J.* **2016**, 11 (3), 347–350. <https://doi.org/10.1002/asia.201500506>.
- (134) Cairncross, A.; Roland, J. R.; Henderson, R. M.; Sheppard, W. A. Organocopper Intermediates via Decarboxylation of Cuprous Carboxylates. *J. Am. Chem. Soc.* **1970**, 92 (10), 3187–3189. <https://doi.org/10.1021/ja00713a046>.
- (135) Cairncross, A.; Sheppard, W. A. Fluorinated Organocopper Compounds. *J. Am. Chem. Soc.* **1968**, 90 (8), 2186–2187. <https://doi.org/10.1021/ja01010a050>.
- (136) Tsuda, T.; Yazawa, T.; Watanabe, K.; Fujii, T.; Saegusa, T. Preparation of Thermally Stable and Soluble Mesitylcopper(I) and Its Application in Organic Synthesis. *J. Org. Chem.* **1981**, 46 (1), 192–194. <https://doi.org/10.1021/jo00314a048>.
- (137) Stollenz, M.; Gehring, H.; Konstanzer, V.; Fischer, S.; Dechert, S.; Grosse, C.; Meyer, F. From Pyrazolate-Based Binuclear Copper(I) Complexes to Octanuclear σ -Mesityl-Bridged μ_4 -Oxo-Cuprocuprates: Controlled Dioxygen Splitting by Organocopper Scaffolds. *Organometallics* **2011**, 30 (14), 3708–3725. <https://doi.org/10.1021/om100836j>.
- (138) Plotzitzka, J.; Kleeberg, C. [(NHC)Cu^I–ER₃] Complexes (ER₃ = SiMe₂Ph, SiPh₃, SnMe₃): From Linear, Mononuclear Complexes to Polynuclear Complexes with Ultrashort Cu^I...Cu^I Distances. *Inorg. Chem.* **2016**, 55 (10), 4813–4823. <https://doi.org/10.1021/acs.inorgchem.6b00210>.
- (139) Leoni, P.; Pesquali, M.; Ghilardi, C. A. Isolation and Crystal and Molecular Structure of a Rare Example of a Mononuclear Organo-Cuprate. *J. Chem. Soc., Chem. Commun.* **1983**, No. 5, 240. <https://doi.org/10.1039/c39830000240>.
- (140) Niemeyer, M. Ein ungewöhnlicher ambivalenter Zinn(II)-oxo-Cluster. *Z. anorg. allg. Chem.* **2004**, 630 (2), 252–256. <https://doi.org/10.1002/zaac.200300230>.
- (141) Casitas, A.; Ribas, X. The Role of Organometallic Copper(III) Complexes in Homogeneous Catalysis. *Chem. Sci.* **2013**, 4 (6), 2301. <https://doi.org/10.1039/c3sc21818j>.

- (142) Cahiez, G.; Moyeux, A.; Gager, O.; Poizat, M. Copper-Catalyzed Decarboxylation of Aromatic Carboxylic Acids: En Route to Milder Reaction Conditions. *Adv. Synth. Catal.* **2013**, *355* (4), 790–796. <https://doi.org/10.1002/adsc.201201018>.
- (143) Baur, A.; Bustin, K. A.; Aguilera, E.; Petersen, J. L.; Hoover, J. M. Copper and Silver Benzoate and Aryl Complexes and Their Implications for Oxidative Decarboxylative Coupling Reactions. *Org. Chem. Front.* **2017**, *4* (4), 519–524. <https://doi.org/10.1039/C6QO00678G>.
- (144) Ribas, X.; Jackson, D. A.; Donnadieu, B.; MahÑ-a, J.; Parella, T.; Xifra, R.; Hedman, B.; Hodgson, K. O.; Llobet, A.; Stack, T. D. P. Aryl CbH Activation by CuI To Form an Organometallic Aryl–CuIII Species: A Novel Twist on Copper Disproportionation. *Angew. Chem. Int. Ed.* **2002**, *41* (16), 2991. [https://doi.org/10.1002/1521-3773\(20020816\)41:16<2991::AID-ANIE2991>3.0.CO;2-6](https://doi.org/10.1002/1521-3773(20020816)41:16<2991::AID-ANIE2991>3.0.CO;2-6).
- (145) Gooßen, L. J.; Rodríguez, N.; Linder, C.; Lange, P. P.; Fromm, A. Comparative Study of Copper- and Silver-Catalyzed Protodecarboxylations of Carboxylic Acids. *ChemCatChem* **2010**, *2* (4), 430–442. <https://doi.org/10.1002/cctc.200900277>.
- (146) Xue, L.; Su, W.; Lin, Z. Mechanism of Silver- and Copper-Catalyzed Decarboxylation Reactions of Aryl Carboxylic Acids. *Dalton Trans.* **2011**, *40* (44), 11926. <https://doi.org/10.1039/c1dt10771b>.
- (147) Perry, G. J. P.; Larrosa, I. Recent Progress in Decarboxylative Oxidative Cross-Coupling for Biaryl Synthesis: Recent Progress in Decarboxylative Oxidative Cross-Coupling for Biaryl Synthesis. *Eur. J. Org. Chem.* **2017**, *2017* (25), 3517–3527. <https://doi.org/10.1002/ejoc.201700121>.
- (148) Li, Z.; Fu, Z.; Zhang, H.; Long, J.; Song, Y.; Cai, H. A Simple Protocol for Cu-Catalyzed Protodecarboxylation of (Hetero)Aromatic Carboxylic Acids. *New J. Chem.* **2016**, *40* (4), 3014–3018. <https://doi.org/10.1039/C5NJ02792F>.
- (149) Jin, Q.; Li, J.; Ariaferd, A.; Canty, A. J.; O’Hair, R. A. J. Substituent Effects in the Decarboxylation Reactions of Coordinated Arylcarboxylates in Dinuclear Copper Complexes, [(Napy)Cu₂(O₂CC₆H₄X)]. **2017**, *23* (6), 351–358.
- (150) Aalten, H. L.; Van Koten, G.; Tromp, J.; Stam, C. H.; Goubitz, K.; Mak, A. N. S.; Van Der Kerk-van Hoof, A. Dinuclear Copper(I) Benzoate Quinoline Complexes as Intermediates in the Copper-Quinoline Decarboxylation Reaction. *Recl. Trav. Chim. Pays-Bas* **1989**, *108* (9), 295–303. <https://doi.org/10.1002/recl.19891080903>.
- (151) DePasquale, R. J.; Tamborski, C. Reactions of Pentafluorophenylcopper Reagent. *J. Org. Chem.* **1969**, *34* (6), 1736–1740. <https://doi.org/10.1021/jo01258a046>.
- (152) Tsuji, Y.; Fujihara, T. Carbon Dioxide as a Carbon Source in Organic Transformation: Carbon–Carbon Bond Forming Reactions by Transition-Metal Catalysts. *Chem. Commun.* **2012**, *48* (80), 9956. <https://doi.org/10.1039/c2cc33848c>.
- (153) Börjesson, M.; Moragas, T.; Gallego, D.; Martin, R. Metal-Catalyzed Carboxylation of Organic (Pseudo)Halides with CO₂. *ACS Catal.* **2016**, *6* (10), 6739–6749. <https://doi.org/10.1021/acscatal.6b02124>.
- (154) Zhang, L.; Hou, Z. N-Heterocyclic Carbene (NHC)–Copper-Catalysed Transformations of Carbon Dioxide. *Chem. Sci.* **2013**, *4* (9), 3395. <https://doi.org/10.1039/c3sc51070k>.
- (155) Cokoja, M.; Bruckmeier, C.; Rieger, B.; Herrmann, W. A.; Kühn, F. E. Transformation of Carbon Dioxide with Homogeneous Transition-Metal Catalysts: A Molecular Solution to a Global Challenge? *Angew. Chem. Int. Ed.* **2011**, *50* (37), 8510–8537. <https://doi.org/10.1002/anie.201102010>.

- (156) Ohishi, T.; Nishiura, M.; Hou, Z. Carboxylation of Organoboronic Esters Catalyzed by N-Heterocyclic Carbene Copper(I) Complexes. *Angew. Chem. Int. Ed.* **2008**, *47* (31), 5792–5795. <https://doi.org/10.1002/anie.200801857>.
- (157) Zhang, L.; Li, Z.; Takimoto, M.; Hou, Z. Carboxylation Reactions with Carbon Dioxide Using N-Heterocyclic Carbene-Copper Catalysts. *Chem. Rec.* **2020**, *20* (6), 494–512. <https://doi.org/10.1002/tcr.201900060>.
- (158) Tran-Vu, H.; Daugulis, O. Copper-Catalyzed Carboxylation of Aryl Iodides with Carbon Dioxide. *ACS Catal.* **2013**, *3* (10), 2417–2420. <https://doi.org/10.1021/cs400443p>.
- (159) Takaya, J.; Tadami, S.; Ukai, K.; Iwasawa, N. Copper(I)-Catalyzed Carboxylation of Aryl- and Alkenylboronic Esters. *Org. Lett.* **2008**, *10* (13), 2697–2700. <https://doi.org/10.1021/ol800829q>.
- (160) Destro, G.; Loreau, O.; Marcon, E.; Taran, F.; Cantat, T.; Audisio, D. Dynamic Carbon Isotope Exchange of Pharmaceuticals with Labeled CO₂. *J. Am. Chem. Soc.* **2019**, *141* (2), 780–784. <https://doi.org/10.1021/jacs.8b12140>.

Chapter 2 – Syntheses, structures and reactivity of complexes [(2,9-(^tBu)₂-phen)Cu(O₂CAryl)] and [(2,9-(^tBu)₂-phen)Cu(Aryl)]: Experimental and theoretical investigation of the CO₂ extrusion or insertion

Abstract:

The development of copper-catalyzed decarboxylative coupling has been fully described, in which the mechanism for the loss of CO₂ is proposed to proceed via copper(I) carboxylate species and copper(I) aryl intermediates. Meanwhile, few examples of these copper(I) complexes have been described, with a limited numbers of carboxylic acids.

In 2019, Destro *et al.* demonstrated a dynamic carbon isotopic exchange (CIE) reaction catalyzed by a copper-bisoxazoline system, where a variety of carboxylic acids were successfully enriched in ¹³CO₂ or ¹⁴CO₂ fragment.¹ This reaction is suggested to proceed via an initial decarboxylation event of the copper(I) carboxylates species transformed into copper(I) aryl intermediates, that further react with labelled CO₂ to give the ¹³C or ¹⁴C enriched copper(I) carboxylate complexes. Nevertheless, the mechanism is not clearly established and efforts to isolate a bisoxazoline copper(I) species were proven to be fruitless.

This challenge led us to try to clarify the CIE reaction mechanism, with the isolation of copper(I) carboxylate and their copper(I) aryl derivatives. To avoid the use of bisoxazoline ligands that are costly and difficult to prepare, we turned our attention on more accessible copper(I) phenanthrolines species, that are much more common and well-described in copper chemistry.

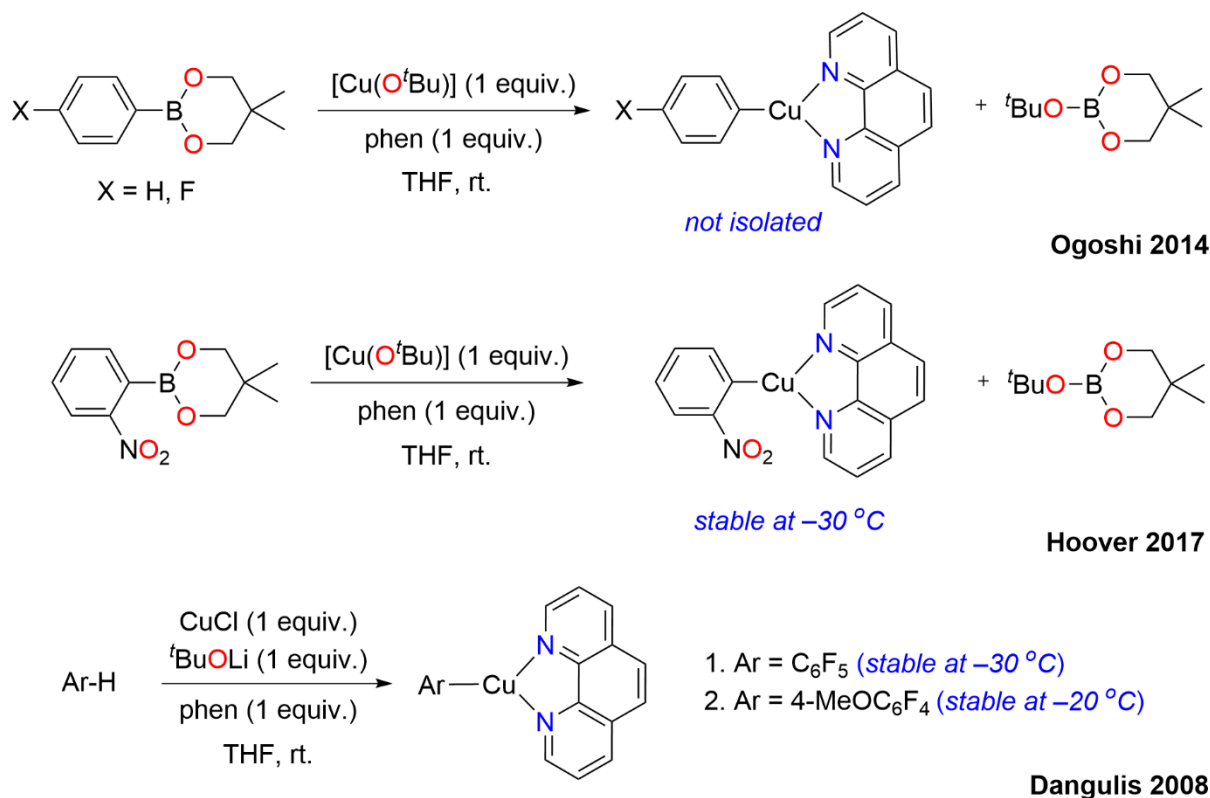
Table of Contents

Abstract:	86
I. State-of-the-art of the synthesis of copper(I) complexes supported by phenanthroline ligand.	88
II. Choice for the nitrogened ligand	90
III. Results and discussion	93
III. 1. Syntheses and crystal structures of the phen* (1) ligand	93
III. 2. Synthesis of the carboxylic complexes [(phen*)Cu(O ₂ CR)] (R = <i>o</i> -F-C ₆ H ₄ (2), <i>p</i> -F-C ₆ H ₄ (3), C ₆ F ₅ (4), <i>o</i> -NO ₂ -C ₆ H ₄ (5), <i>p</i> -NO ₂ -C ₆ H ₄ (6), CF ₃ (7)) and characterization.....	94
III. 3. Synthesis and structure of the aryl and alkyl [(phen*)Cu-R] complexes, R = C ₆ F ₅ (8), <i>o</i> -NO ₂ -C ₆ H ₄ (9), CF ₃ (11) & structure of the fluoride solvate [(phen*)CuF(HF)]·C ₆ H ₆ (10).....	100
III. 4. Study of the decarboxylation of the [(phen*)Cu(O ₂ CR)] complexes (R = C ₆ H ₄ - <i>o</i> -F (2), C ₆ H ₄ - <i>o</i> -NO ₂ (5), C ₆ F ₅ (4), CF ₃ (7)).....	107
III. 4. 1. Decarboxylation in THF.....	107
III. 4. 2. Decarboxylation in other solvents.....	109
III. 5. Study of the carboxylation of the [(phen*)Cu-R] complexes 8 , 9 , and 11	115
III. 6. DFT calculation	118
III. 7. Proposed mechanism	121
IV. Conclusion	124
V. References	126

I. State-of-the-art of the synthesis of copper(I) complexes supported by phenanthroline ligand.

Copper(I) carboxylates can be synthesized by many different routes.² One way is the halide substitution of Cu–X species with carboxylate (generated *in situ* or not),^{3,4} another way is the treatment of Cu₂O with the carboxylic acid. A more facile and general synthesis of copper carboxylates, has also been described via the reaction of RCO₂H with the extremely oxygen- and water-sensitive Cu(I)(aryl) (aryl = C₆F₅, Mesityl), which prevents formation of water or salts that can make the purification step difficult).⁵ Indeed, this procedure only generates Cu(I) carboxylates and volatiles that can be easily removed by evaporation. However, this method requires the formation of starting Cu(I)(aryl), which can be delicate and time consuming, releases toxic aromatics and shows a low atom economy. Since its first report in 1972, the copper(I) *tert*-butoxide aggregate [Cu(O^tBu)]₄, inexpensive and readily synthesized, has proven a useful synthon in synthetic chemistry.⁶ Indeed, the alkoxide group, as a strong base, can react readily with carboxylic acids with release of a volatile alcohol. Although [Cu(O^tBu)]₄ is not very stable and must be stored at low temperature (*ca.* –30 °C) under inert gas, it proved to be a convenient precursor towards copper complexes.^{7–9}

The preparation of (phen)Cu–aryl (phen = 1,10-phenanthroline) complexes is well known and may employ [Cu(O^tBu)] as precursor. In 2014, Ogoshi and co-workers observed the generation of [(phen)Cu(C₆H₄-*p*-X)] (X = H, F) by ¹H, ¹¹B, and ¹⁹F NMR analyses when mixing [Cu(O^tBu)], phen and arylboronates as aryl transfer reagents in THF (*Scheme 43*).¹⁰ However, these species were not isolated since their objective was to form fluoroalkyl copper(I) complexes by subsequently exposure of [(phen)Cu(C₆H₄-*p*-X)] to a tetrafluoroethylene (TFE) atmosphere. Nonetheless, Hoover *et al.* succeeded to synthesize [(phen)Cu(C₆H₄-*o*-NO₂)] in a good yield (73 %) using a protocol similar to that reported by Ogoshi (*Scheme 43*).¹¹ Notwithstanding the efficiency of the procedure, this thermally unstable complex must be stored at –30 °C, and no crystal structure has been described. Daugulis *et al.* developed another approach for the formation of phen-ligated copper aryl complexes bearing highly fluorinated aryl ligands (*Scheme 43*).¹² By adding [Cu(O^tBu)], generated *in situ* from the reaction of CuCl and ^tBuOLi in a THF solution of ArH and phenanthroline, they obtained [(phen)Cu(C₆F₅)] and [(phen)Cu(C₆F₄-*p*-OMe)] in moderate yields of 52% and 38%, respectively. Similar to what has been observed by Hoover *et al.*, these complexes exist as moisture- and temperature-sensitive solids with very poor solubility in common organic solvents (*i.e.* THF, CH₂Cl₂). Interestingly, the crystal structure of [(phen)Cu(C₆F₄-*p*-OMe)] has been shown to be dimeric (*Figure 25*). However, the structure of the [(phen)Cu(C₆F₅)] derivative has not been elucidated due to twinning of the crystals.¹²



Scheme 43. Synthesis of different phenanthroline ligated copper complexes.

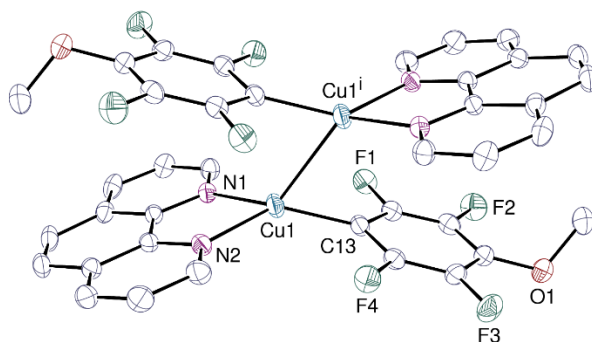
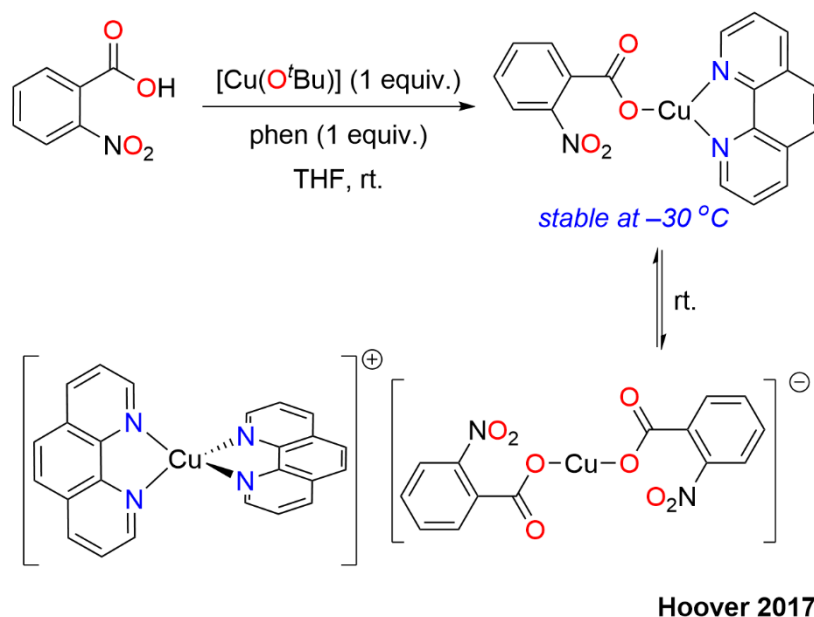


Figure 25. ORTEP view of $[(\text{phen})\text{Cu}(\text{C}_6\text{F}_4\text{-}p\text{-OMe})]$. Selected interatomic distances (\AA) and angles (deg): $\text{Cu1-C}(13) = 1.932(2)$, $\text{Cu1-N}(2) = 2.0720(18)$, $\text{Cu1-N}(1) = 2.0949(19)$, $\text{Cu1-Cu1}^i = 2.5770(6)$, $\text{C}(13)\text{-Cu-N}(2) = 135.68(9)$, $\text{C}(13)\text{-Cu-N}(1) = 132.69(8)$.¹²

In 2017, Hoover *et al.* reported the high yield (93%) synthesis of $[(\text{phen})\text{Cu}(\text{O}_2\text{CC}_6\text{H}_4\text{-}o\text{-NO}_2)]$, isolated as a dark purple solid, starting from $[\text{Cu}(\text{O}^t\text{Bu})]$, phen, and 2-nitrobenzoic acid in THF at room temperature (Scheme 44).¹¹ However, in solution, an equilibrium between $[(\text{phen})\text{Cu}(\text{O}_2\text{CC}_6\text{H}_4\text{-}o\text{-NO}_2)]$ and its isomer $[(\text{phen})_2\text{Cu}]^+[\text{Cu}(\text{O}_2\text{CC}_6\text{H}_4\text{-}o\text{-NO}_2)_2]^-$ is observed at room temperature, as evidenced by the broadened ^1H NMR signals (Scheme 44). Only at $-30\text{ }^\circ\text{C}$, the sharp ^1H NMR signals of the ligand and the benzoate moiety are recorded, which corresponds to a neutral form of the copper(I)-benzoate complex.

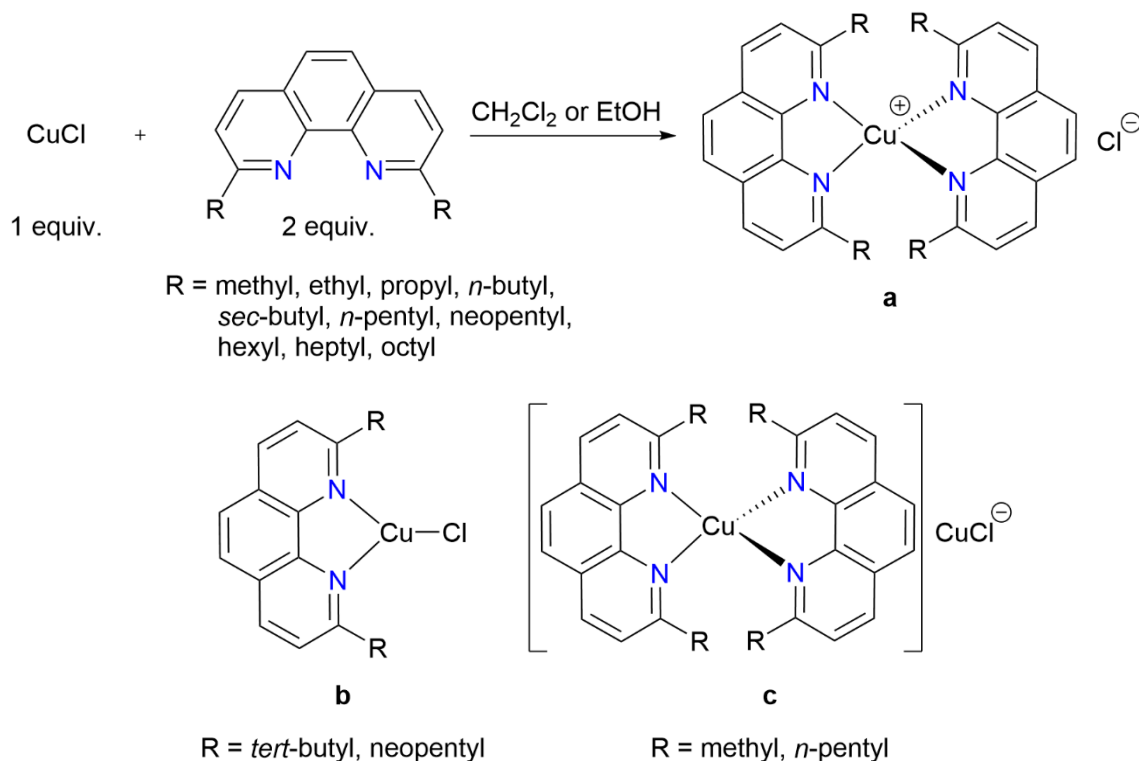


Scheme 44. Synthesis of $[(phen)Cu(O_2CC_6H_4-o-NO_2)]$ and the equilibrium between the neutral and the ion pair species in solution.¹¹

In conclusion, all these results showed that $[Cu(O^tBu)]$ is a convenient precursor to obtain carboxylate or aryl-copper species, without the formation of toxic by-products. As seen above, $[Cu(O^tBu)]$ can react rapidly with aryl boronic esters or benzoic acids at room temperature in the presence of phenanthroline ligand to form phenanthroline copper(I) complexes. Nevertheless, in most cases, these complexes are difficult to isolate due to low thermal stability and air-sensitivity. Whereas copper(I) benzoate complexes can be isolated in the solid state, they tend to exist in an anionic form in solution at 25 °C, as observed with $[(phen)_2Cu]^+[Cu(O_2CC_6H_4-o-NO_2)_2]^-$. Furthermore, only the crystal structure of the phenanthroline copper(I) polyfluorinated phenyl complex has been described so far. Therefore, it can be surmised that phenanthroline is not a suitable ligand to support a tri-coordinated copper(I) center. In addition, another cited drawback is the low solubility of the phenanthroline copper(I) complexes. A strategy to overcome those limitations consists in using substituted phenanthroline ligands.

II. Choice for the nitrogened ligand

Early in 1995, Pallenberd *et al.* reported the synthesis and characterization of some copper(I) phenanthroline complexes.¹³ In their study, they revealed that different copper complexes can be formed depending on the amount of ligand and the size of its alkyl-substituent groups at the 2,9-positions. In most cases, in the presence of two phenanthrolines per copper atom, in chloroform or ethanol solvent, the formation of complex $[(2,9-dialkyl-1,10-phenanthroline)_2Cu]^+Cl^-$ is favorable (with $CuCl$ as precursor) (Scheme 45, **a**).¹³ With the 1:1 ligand:copper stoichiometry, two possible structures of copper complexes can be observed, in which the isomer **b** is favored by bulky phenanthroline systems (Scheme 45, **b** and **c**).



Pallenberg 1995

Scheme 45. Copper(I) phenanthroline complexes formed by reaction of phenanthroline with CuCl. The 2:1 ligand:copper stoichiometry gives **a** and the 1:1 stoichiometry gives **b** or **c**.

Among the tested substituents, they observed the formation of mono-ligated [(2,9-dialkyl-1,10-phenanthroline)CuCl] complex analogue to structure of **b** only with *tert*-butyl and *neopentyl* groups. Interestingly, the use of *tert*-butyl groups led to complete transformation to [(phen*)CuCl] (phen* = 2,9-di-*tert*butyl-1,10-phenanthroline), notwithstanding the 2:1 (ligand:copper) ratio. Meanwhile, the di-*neopentyl*-substituted phenanthroline ligand afforded a mixture of structures of type **a** and **b** depending on the stoichiometry of the reaction (2:1 and 1:1, respectively). The bulkier *tert*-butyl groups thus led only to the formation of the isomer **b** as a pseudotrigonal complex, even with a ratio ligand/copper superior to 1.

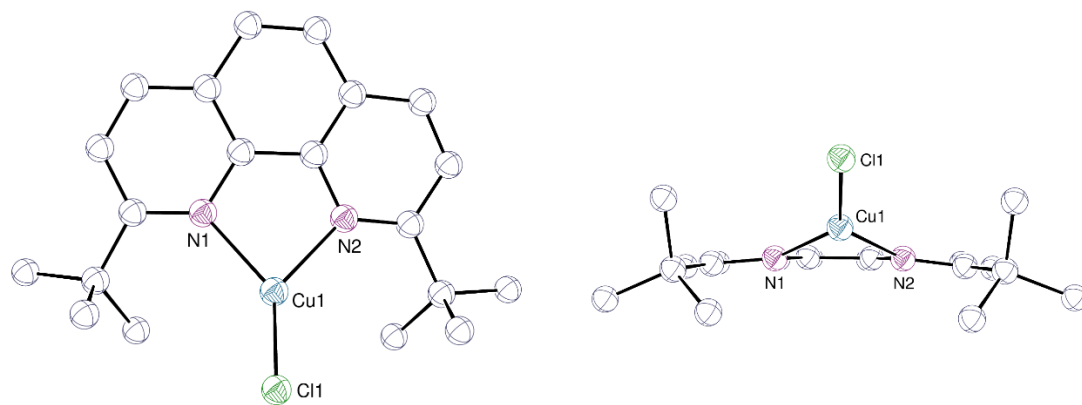
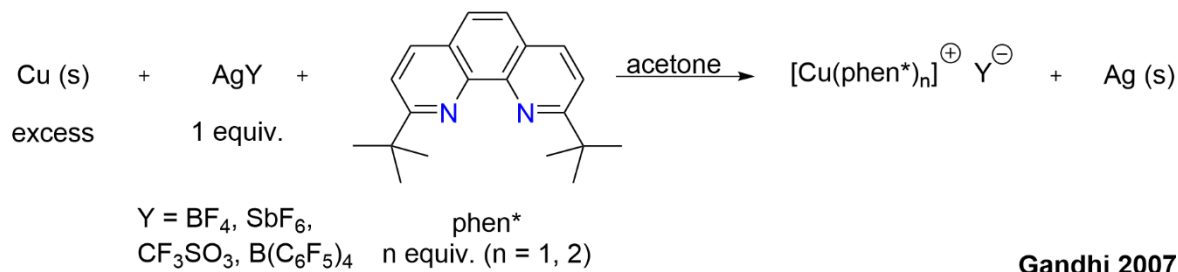


Figure 26. ORTEP view of [(2,9-di-tert-butyl-1,10-phenanthroline)CuCl]. Selected interatomic distances (Å) and angles (deg): Cu1–Cl1 = 2.147(4), Cu1–N(1) = 2.077(10), Cu1–N(2) = 2.093(10), N(1)–Cu–N(2) = 82.2(4).¹³

Later in 2007, Gandhi *et al.* proved that [(phen*)CuCl] complex was unable to give [(phen*)CuY] by treatment with a silver salt AgY (Y = BF₄, SbF₆, CF₃SO₃) and their explanation relied on the strong affinity of Cu⁺ for the chloride anion.¹⁴ They developed a new method for the preparation of [(phen*)CuY] (Y = BF₄, SbF₆, CF₃SO₃, B(C₆F₅)₄) by a controlled oxidation of metallic copper powder using a stoichiometric amount of silver(I) salt in the presence of different equivalents of phen* ligand (Scheme 46). Interestingly, this protocol also offered access to the extremely bulky cation [(phen*)₂Cu]⁺ species, which was previously considered unattainable by the method of Pallenberg.¹³ However, the reaction proceeded smoothly within 30 min to give [(phen*)₂Cu][B(C₆F₅)₄]·CH₂Cl₂ in 81% yield (crystal structure shown in Figure 25).



Scheme 46. Synthesis of [(phen*)CuY] (Y = BF₄, SbF₆, CF₃SO₃, B(C₆F₅)₄).

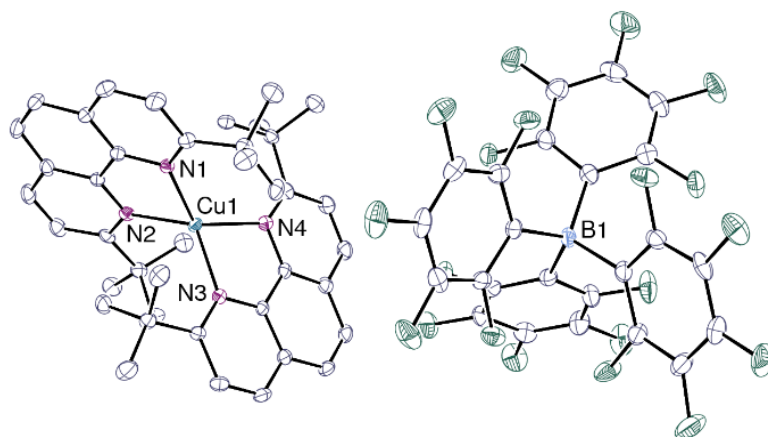


Figure 27. View of the complex $[\text{Cu}(\text{phen}^*)_2][\text{B}(\text{C}_6\text{F}_5)_4]$ in the crystal $[\text{Cu}(\text{phen}^*)_2][\text{B}(\text{C}_6\text{F}_5)_4]\cdot\text{CH}_2\text{Cl}_2(4\cdot\text{CH}_2\text{Cl}_2)$ with 50% probability thermal ellipsoids. The two phen* ligands are arranged in a pseudotetrahedral fashion. H atoms have been omitted for clarity. Selected interatomic distances (Å) and angles (deg): $\text{Cu1-N}(1) = 2.096(3)$, $\text{Cu1-N}(2) = 2.115(3)$, $\text{Cu1-N}(3) = 2.076(3)$, $\text{Cu1-N}(4) = 2.139(3)$, $\text{N}(1)\text{-Cu-N}(2) = 82.2(4)$.¹⁴

Overall, these results have shown that the structures of phenanthroline-based copper(I) complexes can be controlled through the amount of added ligand. Generally, with two equivalents of ligand, the formation of the bis-phenanthroline $[(2,9\text{-dialkyl-1,10-phenanthroline})_2\text{Cu}]^+$ is favorable, whereas the neutral tri-coordinated copper(I) or its isomer are generated when one equivalent of ligand is employed. Importantly, the formation of tri-coordinated copper(I) complex is more favored when the bulky *tert*-butyl groups are introduced, regardless of the amount of added ligand. Alternatively, Gandhi *et al.* proposed a new pathway where it is possible to obtain $[(\text{phen}^*)_2\text{Cu}]^+$ via an oxidation-based synthetic route. In conclusion, among the tested alkyls, *tert*-butyl groups exhibit the steric characteristics best suited to promote a pseudotrigonal geometry (similar to **b**, Scheme 43) in which only one ligand is coordinated to the copper(I) center.

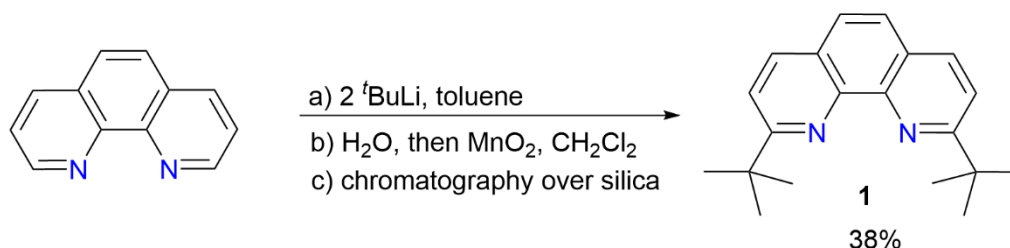
Finally, all the gathered evidence incited us to choose the 2,9-di-*tert*butyl-1,10-phenanthroline ligand which also bring increased solubility for our study. Moreover, due to the great stability of $[(\text{phen}^*)\text{CuCl}]$ against substitution reaction, we decided to use $[\text{Cu}(\text{O}^t\text{Bu})]$ as a precursor to synthesize both copper(I) carboxylate and aryl species.

III. Results and discussion

III. 1. Syntheses and crystal structures of the phen* (**1**) ligand

The 2,9-di-*tert*butyl-1,10-phenanthroline (phen*) ligand was prepared by a modified method from the literature (Scheme 47).^{13,15,16} Instead of an excess of $^t\text{BuLi}$, we used only 2 equivalents to substitute phen and thus produce phen* as a pale-yellow solid with an improved yield (38%, compared to the 28% reported in the literature).^{13,15,16} It is important to highlight that its ^1H NMR spectrum in $\text{THF-}d_8$ evidences two signals for the aromatic hydrogen, a doublet at 8.23 ppm and a singlet that overlaps with a doublet at 7.76 ppm and which account for 2H and 4H, respectively, while the ^tBu group is a singlet at δ 1.60 ppm. Because the signal of the ligand will be shifted downfield upon coordination to copper(I), this will be one proof for the coordination of phen* (*vide infra*, Chapter 2 – III. 2.). Compound **1** is soluble in a number of organic solvents such as pentane, diethylether, THF, toluene or

dichloromethane. It crystallized readily as thin pale yellow needles by slow evaporation of an isopropanol, ethanol or CH_2Cl_2 solution. Single crystals suitable for X-ray diffraction were obtained by slow evaporation of a dichloromethane solution of **1**.



Scheme 47. Synthesis of 2,9-di-tertbutyl-1,10-phenanthroline (phen*) (**1**) ligand.

The structure of **1** is shown in Figure 28, and selected bond lengths and angles are listed in Table 2. The phenanthroline fragment is quasi-planar (rms deviation, 0.022 Å). The molecules are arranged in layers parallel to (001) and no π -stacking interaction is present, as can be seen in Figure 28 (right), all centroid...centroid distances being larger than 4.8 Å, in contrast to the presence of π -stacking interactions with 2,9-bis(hydroxymethyl)-1,10-phenanthroline (2,9-(CH_2OH)₂phen).¹⁷ The C–N distances, which average 1.34(2) Å, are quite classical and the C–C bond lengths inside the aromatic cycles are also similar to those found in other free phenanthroline molecules.¹⁷

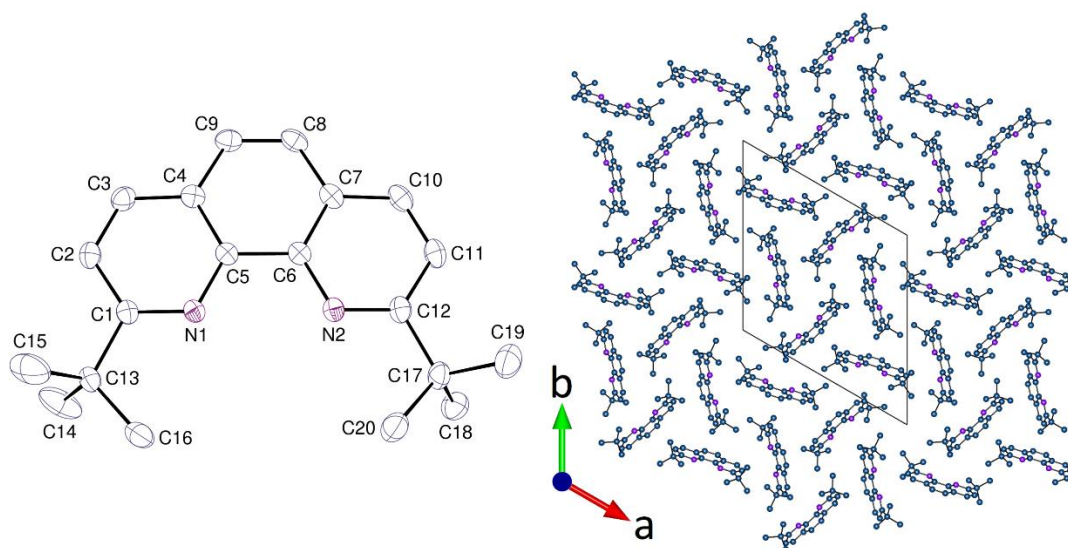
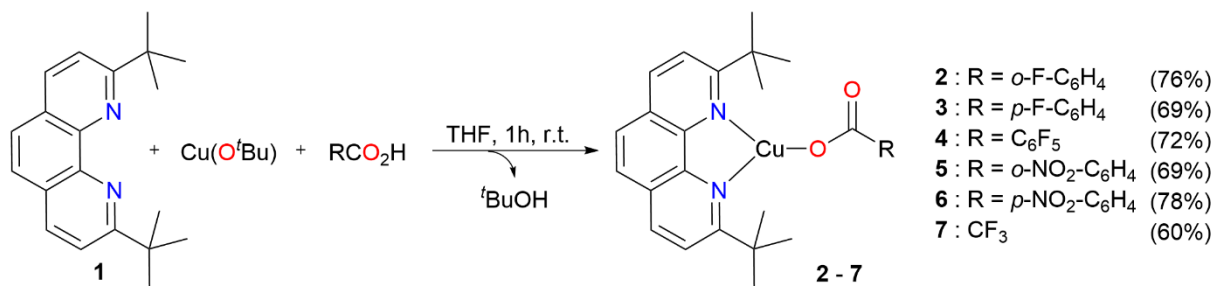


Figure 28. (Left) Crystal structure of **1** with hydrogen atoms omitted. Displacement ellipsoids are drawn at the 50% probability level. (Right) View of one layer in the crystal packing (N, purple; C, blue).

III. 2. Synthesis of the carboxylic complexes [(phen*)Cu(O₂CR)] (R = *o*-F-C₆H₄ (**2**), *p*-F-C₆H₄ (**3**), C₆F₅ (**4**), *o*-NO₂-C₆H₄ (**5**), *p*-NO₂-C₆H₄ (**6**), CF₃ (**7**)) and characterization.

The preparation of [(phen*)Cu(O₂CR)] (**2–7**) complexes was performed by reaction of [Cu(O^{*t*}Bu)], and phen* with the corresponding acids. The complexes [(phen*)Cu(O₂CR)] (R = *o*-F-C₆H₄ (**2**), *p*-F-C₆H₄ (**3**), C₆F₅ (**4**), *o*-NO₂-C₆H₄ (**5**), *p*-NO₂-C₆H₄ (**6**), CF₃ (**7**)) have been obtained readily by treating a pale yellow THF solution of [Cu(O^{*t*}Bu)] with 1 equiv. of 2,9-di-tertbutyl-1,10-phenanthroline (phen*) and then 1 equiv. of the corresponding acid (Scheme 48). The resulting light brown solution obtained by addition

of phen* to $[\text{Cu}(\text{O}^t\text{Bu})]$ is not the stable coordination compound $[(\text{phen}^*)\text{Cu}(\text{O}^t\text{Bu})]$, as indicated by the ^1H NMR, which actually suggests an equilibrium between free and coordinated ligand to the Cu(I) alkoxide (see SI). In addition, all attempts at crystallization of the complex in THF or benzene were unsuccessful, affording only crystals of free phen*. Stoichiometric addition of the corresponding benzoic acid derivative to the previous mixture resulted in an immediate change of color which varied from orange to red. After 1 h stirring at room temperature and evaporation of the solvent, the residual colored solid was washed with pentane and dried under vacuum overnight to afford the desired pure product $[(\text{phen}^*)\text{Cu}(\text{O}_2\text{CR})]$ ($\text{R} = o\text{-F-C}_6\text{H}_4$ (**2**), $p\text{-F-C}_6\text{H}_4$ (**3**), C_6F_5 (**4**), $o\text{-NO}_2\text{-C}_6\text{H}_4$ (**5**), $p\text{-NO}_2\text{-C}_6\text{H}_4$ (**6**), CF_3 (**7**)).



Scheme 48. Synthesis of the $[(\text{phen}^*)\text{Cu}(\text{O}_2\text{CR})]$ complexes **2-7**

All the carboxylate complexes **2-7** have been characterized by ^1H , $^{13}\text{C}\{^1\text{H}\}$ and $^{19}\text{F}\{^1\text{H}\}$ NMR, by infrared spectroscopy, and by elemental analysis as well as by their crystal structure. The ^1H NMR spectra of the complexes show that all the phen* signals are shifted downfield relatively to those of the free ligand, as evidenced by a clear separation of the doublet and singlet that overlap in **1** (Figure 29).

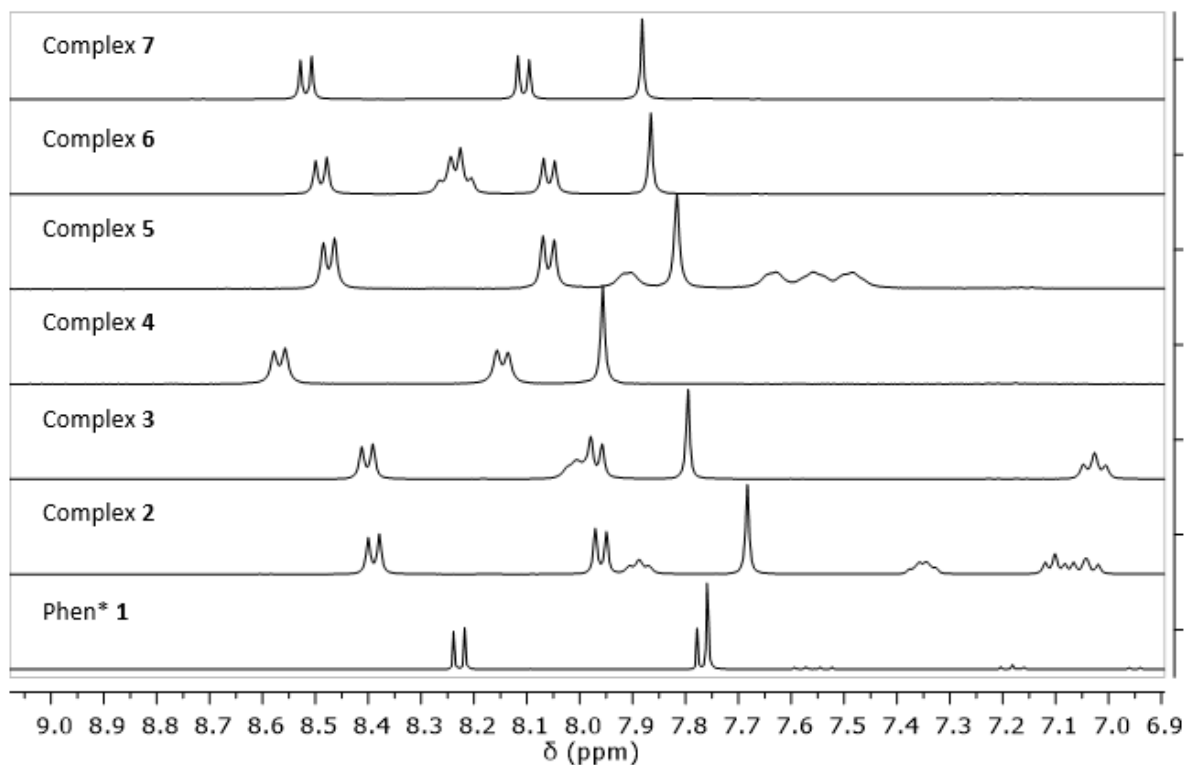


Figure 29. ^1H NMR stacked spectra of compound **1** to **7** in THF-d_8 which show the aromatic regions of the free ligand and the coordinated ligands within the copper complexes.

Dark orange crystals of compounds **3**, **4**, **5**·THF and **6**·THF were grown by slowly cooling a heated THF solution of the corresponding complex or by slow diffusion of pentane into a toluene solution for **2**·0.5(toluene) and **7**. The structures of **2–7** are shown in *Figure 30* to *Figure 35*.

All the complexes **2–7** are mononuclear and tri-coordinated with the Cu(I) ion bound to the N1, N2 and O1 atoms in a distorted trigonal geometry. All structures display π -stacking interactions between phen* molecules or between phen* and C₆F₅ cycles (as in **4**) and even with the co-crystallized toluene molecule (in **2**·0.5(toluene)) that lead to distinct packings. In **2**, **5**, **6** and **7**, pairs of molecules related by inversion are held by π -interactions between the phenanthroline ligands, with intermolecular distances between phenanthroline mean planes of 3.48 Å in **2**, 3.36 Å in **5**, 3.59 Å in **6** and 3.46 Å in **7**, comparable to the range of values found in other [(phen*)CuX] (X = Cl, Br, I) complexes [3.42–3.63 Å].¹⁸ The distance between the centroid of the C₆F₅ ring and the phenanthroline mean plane of a close neighboring molecule in **4** is 3.40 Å. The packing in **7**, which displays columns of molecules related by inversion parallel to [100], is shown as an example in *Figure 35*.

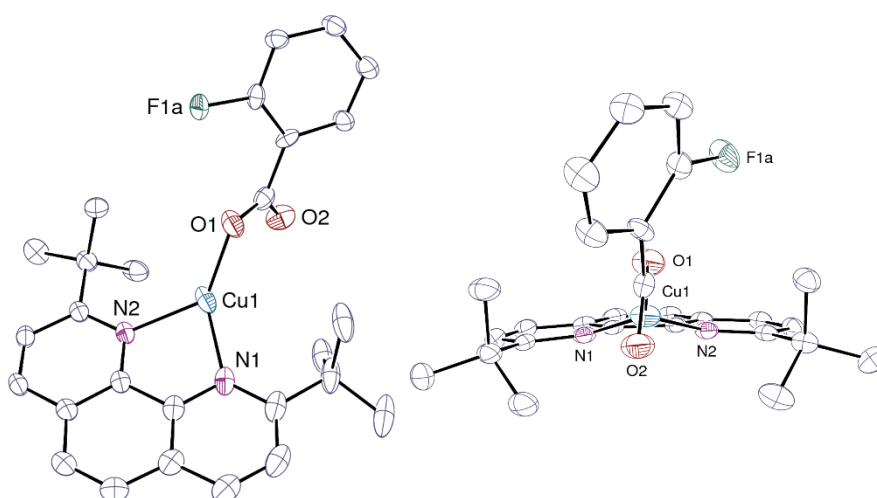


Figure 30. Two views of complex **2** with solvent molecule and hydrogen atoms omitted. Only one position of the disordered group is represented. Displacement ellipsoids are drawn at the 50% probability level.

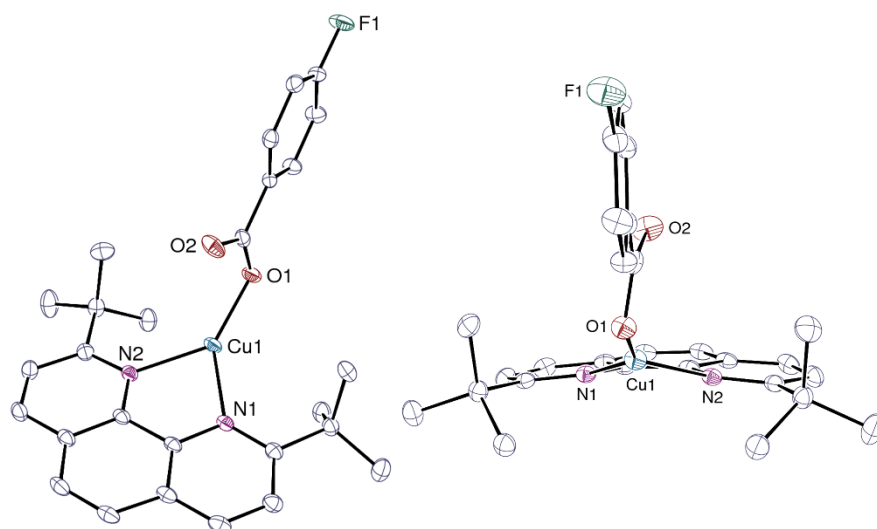


Figure 31. Two views of complex **3** with hydrogen atoms omitted. Displacement ellipsoids are drawn at the 50% probability level.

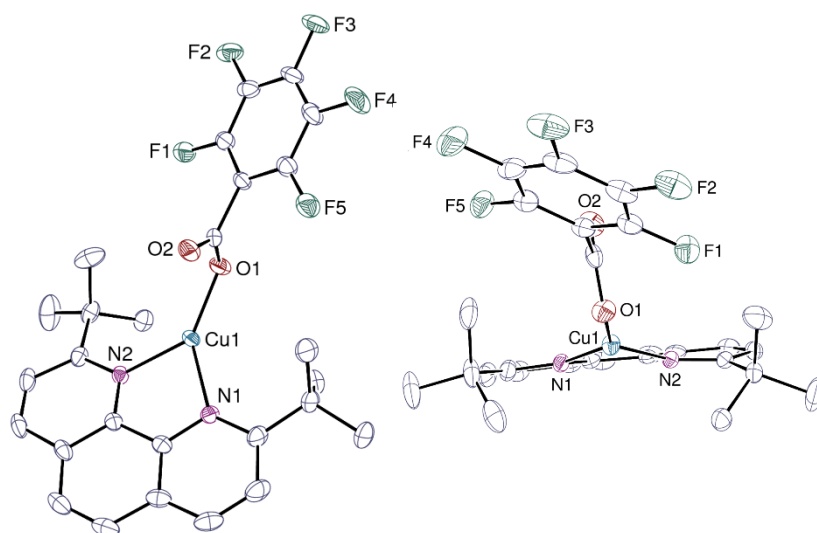


Figure 32. Two views of complex **4** with hydrogen atoms omitted. Displacement ellipsoids are drawn at the 50% probability level.

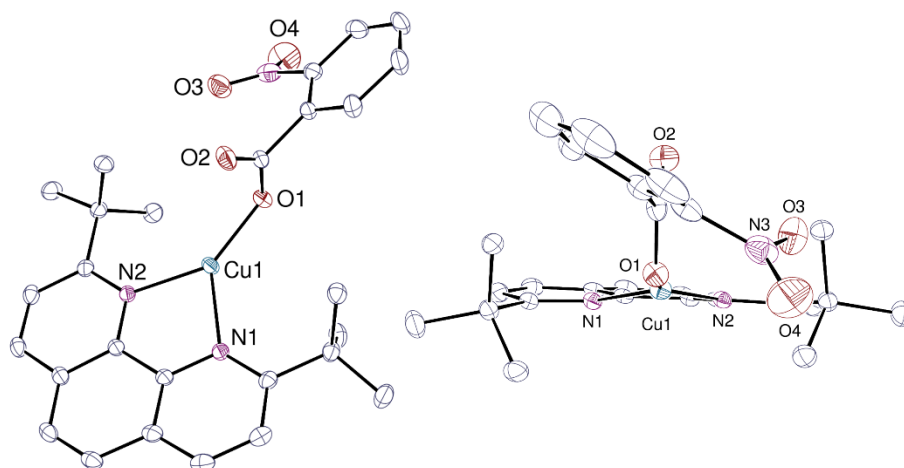


Figure 33. Two views of complex 5 with solvent molecule and hydrogen atoms omitted. Displacement ellipsoids are drawn at the 50% probability level.

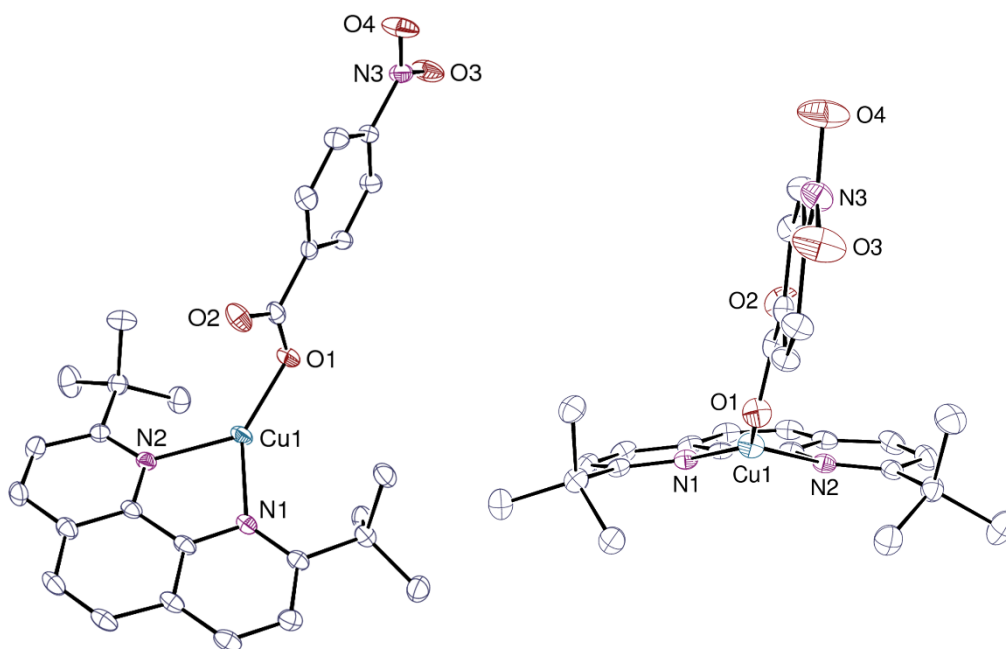


Figure 34. Two views of complex 6 with solvent molecule and hydrogen atoms omitted. Displacement ellipsoids are drawn at the 50% probability level.

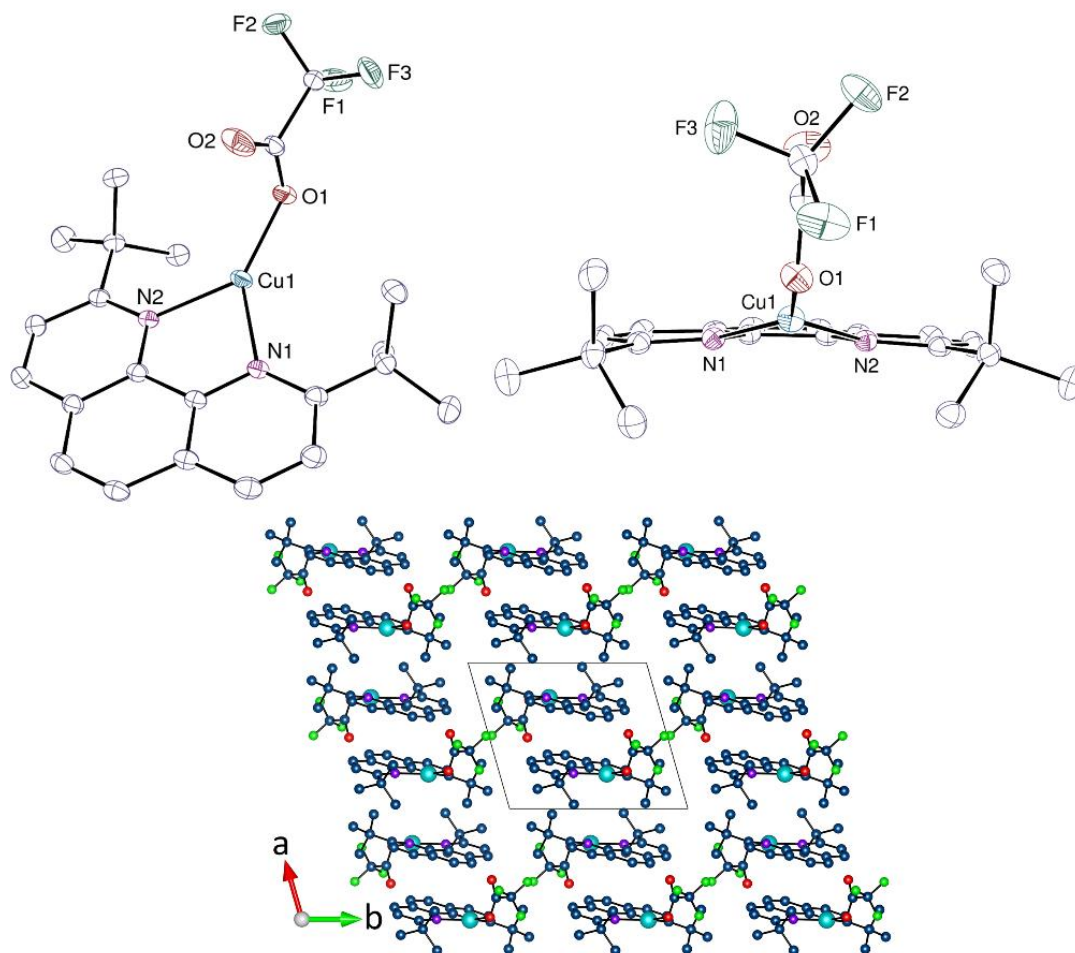


Figure 35. (Top) Two views of complex **7** with hydrogen atoms omitted. Displacement ellipsoids are drawn at the 50% probability level. (Bottom) View of the packing (Cu, light blue; F, green; O, red; N, purple; C, blue).

It was previously assessed that the steric congestion of the $t\text{Bu}$ groups in the 2,9-position of the phenanthroline ligand was responsible for the displacement of the halide anion (Cl, Br, I) out of the ligand plane. Here again, the κ^1 -carboxylate ligand stands outside the plane of the aromatic ligand. While in the tricoordinate $\{[(\text{Medpq})\text{Cu}]_2\{1,3(\text{O}_2\text{C})_2\text{C}_6\text{H}_4\}\}$ (Medpq= 2-methyldipyrido[3,2-f:2'3'-h]quinoxaline), where the Medpq ligand (derivative of phenanthroline) is less congested than phen*, the Cu center is displaced out of the phenanthroline plane by 0.079 Å only,¹⁹ in the bulky derivatives **2–7**, this displacement is much more pronounced and reaches values in the range of 0.3462(7) Å (for **5**) to 0.6769(11) Å (for **6**), the extreme values being found for the two NO_2 -substituted complexes **5** and **6**. In **5**, the aromatic fragment of the carboxylate ligand makes a dihedral angle of 62.44(10)° with respect to the COO plane, while this ligand is nearly planar in **6** (Figure 33 and Figure 34).

The Cu–N distances are asymmetric in complexes **2–7** and vary in the range 2.0164(15)–2.0958(14) Å. The distances from the Cu(I) center to the O1-coordinating atom of the carboxylate are quite similar in these κ^1 -tricoordinate complexes with values in the range of 1.9031(15)–1.9417(11) Å. Meanwhile, the Cu \cdots O2 distances are larger than 2.77 Å, *i.e.* larger than the sum of the ionic radii of copper and oxygen (1.95 Å), indicating at best a weak interaction. These values can be compared to the longer Cu–O bond lengths (1.967 Å and 2.686 Å) in the bidentate carboxylate ligand of the dimeric complex $\{[(\text{phen})\text{Cu}(\kappa^2\text{-O}_2\text{CC}_6\text{HF}_4)(\kappa^1\text{-O}_2\text{CC}_6\text{HF}_4)]\{\mu\text{-MeOH}\}\}$.²⁰ As expected, the copper atom and the

carboxylate ligand in **2–7** are located on the same side of the phenanthroline moiety. The N1 and N2 atoms as well as the C13 and C17 atoms of the ^tBu groups are also more or less displaced from this mean plane. While the N1 and N2 atoms are found in or above the phen mean plane, the ^tBu groups are above or below this plane (Table 2). Of interest, to minimize steric interaction with the carboxylate ligand, the ^tBu groups are oriented in such a way that two methyl groups point away from the carboxylate ligand. This remark will be valid for all the phen* complexes in this study. Distortion in the coordinating environment of the metal center can be characterized by the sum of the angles formed with O1, N1 and N2, which indicates near-planarity in all cases, the lowest value of 352° being found in the *ortho*-fluoro derivative **2**.

Table 2. Selected distances (Å) and angles (°) in the carboxylate complexes **2**-0.5(toluene), **3**, **4**, **5**-THF, **6**-THF, **7** and in the fluoride complex **10**-C₆H₆.

Complex	2 -0.5(toluene)	3	4	5 -THF	6 -THF	7	10 -C ₆ H ₆
Cu–O1/F1	1.9031(15)	1.9417(11)	1.9128(14)	1.9403(8)	1.9265(12)	1.9297(10)	1.8970(16)
Cu–N1	2.0395(18)	2.0356(13)	2.0530(16)	2.0863(9)	2.0164(15)	2.0432(11)	2.040(2)
Cu–N2	2.0622(15)	2.0823(13)	2.0300(16)	2.0409(9)	2.0958(14)	2.0560(11)	2.0613(19)
<Cu–N>	2.053(8)	2.06(2)	2.042(11)	2.06(2)	2.06(4)	2.050(6)	2.051(11)
<i>d</i> (Cu) ^a	+0.6146(12)	+0.6593(10)	+0.4958(13)	+0.3462(7)	+0.6769(11)	+0.5148(8)	+0.1466(16)
<i>d</i> (N1) ^a	+0.0667(13)	+0.1228(11)	+0.1154(15)	–0.0459(8)	+0.1508(13)	+0.0483(10)	+0.0317(18)
<i>d</i> (N2) ^a	+0.0681(13)	+0.0620(11)	–0.0286(15)	+0.1022(8)	+0.0320(13)	+0.0558(10)	+0.0149(18)
<i>d</i> (C13) ^a	–0.068(3)	+0.074(19)	+0.110(3)	–0.2324(14)	+0.062(2)	–0.1475(17)	+0.089(3)
<i>d</i> (C17) ^a	–0.083(2)	–0.125(2)	–0.454(3)	+0.2464(14)	–0.225(2)	–0.0370(16)	+0.001(3)
O1/F1–Cu–N1	136.63(7)	141.02(5)	137.38(6)	133.79(4)	142.96(6)	139.19(5)	139.13(7)
O1/F1–Cu–N2	132.25(6)	135.63(5)	137.72(6)	142.88(4)	133.45(6)	136.46(4)	136.39(7)
N1–Cu–N2	83.38(6)	82.68(5)	83.70(6)	83.33(4)	82.87(6)	83.65(4)	84.38(8)
Σ ^b	352.26	359.33	358.80	360.00	359.28	359.30	359.90

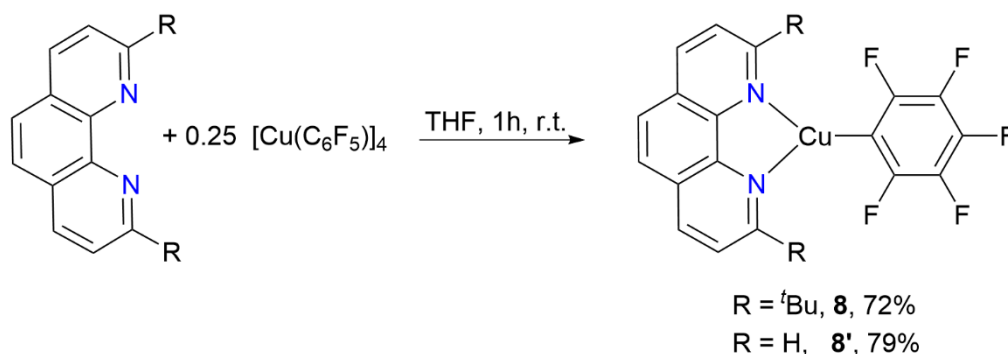
^a *d* is the displacement from the phen mean plane. ^b Sum of the three angles around the Cu centre.

We can note that, if hundreds of structurally characterized copper(II) carboxylate complexes involving bidentate nitrogen aromatic cycles (bipy, phen...) can be found in the Cambridge Structural Database,²¹ carboxylate complexes of copper(I) are very rare. To our knowledge, only the above mentioned bimetallic compound $\{[(\text{Medpq})\text{Cu}]_2\{1,3(\text{O}_2\text{C})_2\text{C}_6\text{H}_4\}\}$ and the monomeric complex $[(\text{bipy})\text{Cu}(\kappa^1\text{-O}_2\text{C-C}_6\text{H}_4\text{-2,5}(\text{CO}_2\text{H})_2)]$ have been crystallographically characterized.^{19,22} In the latter compound, the geometrical parameters are quite different from those in **2–7** and the carboxylate ligand tends to lie in the plane of the bipy ligand. Moreover, the Cu–N distances (2.274 Å and 2.348 Å) as well as Cu–O1 (2.20 Å) and Cu...O2 (2.782 Å) are much larger than expected while the sum of the angles around the metal center reaches 357.7°.²² In the Cu(II) complexes $[(2,9\text{-Me}_2\text{-phen})\text{Cu}(\kappa^1\text{-O}_2\text{CC}_6\text{H}_4\text{-}o\text{-OH})_2]$ and $[(2,9\text{-Me}_2\text{-phen})\text{Cu}(\kappa^1\text{-O}_2\text{CC}_6\text{H}_4\text{-}m\text{-OH})_2]$, the Cu²⁺ ion is in a tetragonal coordination environment.^{23,24} Their Cu–O distances of 1.931(2)–1.9509(18) Å are slightly larger than those found in the Cu(I) complexes **2–7**, despite distinct ionic radii and coordination number of the metal ions.²⁵

III. 3. Synthesis and structure of the aryl and alkyl [(phen*)Cu-R] complexes, R = C₆F₅ (**8**), *o*-NO₂-C₆H₄ (**9**), CF₃ (**11**) & structure of the fluoride solvate [(phen*)CuF(HF)]·C₆H₆ (**10**).

The complex $[(\text{phen}^*)\text{Cu-C}_6\text{F}_5]$ (**8**) was synthesized starting from $[\text{Cu}(\text{C}_6\text{F}_5)_4]$ precursor, which was prepared following a literature procedure by the metathetical reaction of Grignard C₆F₅MgBr with CuCl halide in ether (Scheme 49).^{26,27} Indeed, coordination of the neutral nitrogen ligand L (L = substituted pyridines or 2,2'-bipy) to $[\text{Cu}(\text{C}_6\text{F}_5)_4]$ was previously reported to proceed readily and to form the corresponding $[\text{pyridine}]_2[\text{Cu}(\text{C}_6\text{F}_5)_4]$ and $[(2,2'\text{-bipy})\text{Cu}(\text{C}_6\text{F}_5)]$ complexes which have been isolated in good yields and structurally characterized.²⁸ By following this procedure, addition of 1 equivalent of

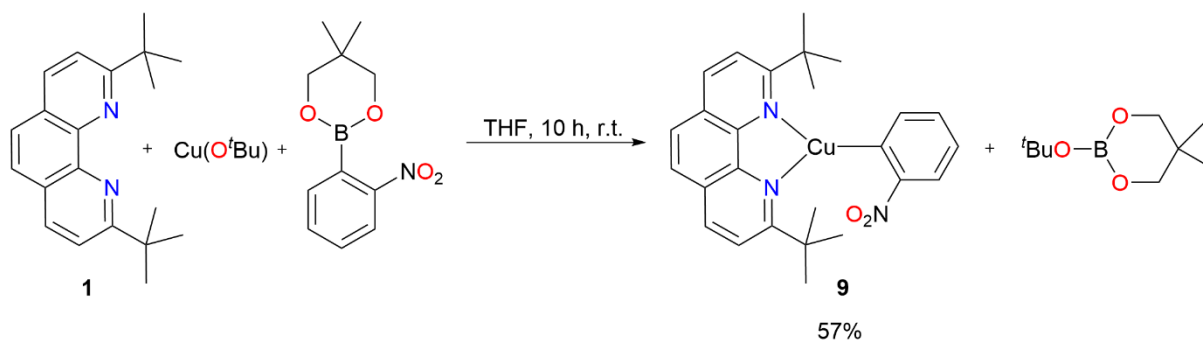
phen* to 0.25 equivalent of $[\text{Cu}(\text{C}_6\text{F}_5)]_4$ led to an immediate orange suspension. Simple filtration of the solid afforded pure **8** in a non-optimized yield of 75% and large orange crystals of **8** could be obtained by slow cooling down a hot toluene solution.



Scheme 49. Synthesis of complex $[(\text{phen}^*)\text{Cu}-\text{C}_6\text{F}_5]$ (**8**) and $[(\text{phen})\text{Cu}-\text{C}_6\text{F}_5]$ (**8'**).

Following a similar protocol with 1,10-phenanthroline, the poorly soluble analogue $[(\text{phen})\text{Cu}(\text{C}_6\text{F}_5)]$ (**8'**) could be obtained almost quantitatively and crystallized as red crystalline needles (Scheme 49). This species was previously synthesized by treatment of CuI with a mixture of K_3PO_4 , $\text{C}_6\text{F}_5\text{H}$ and phen in refluxing DMF.¹²

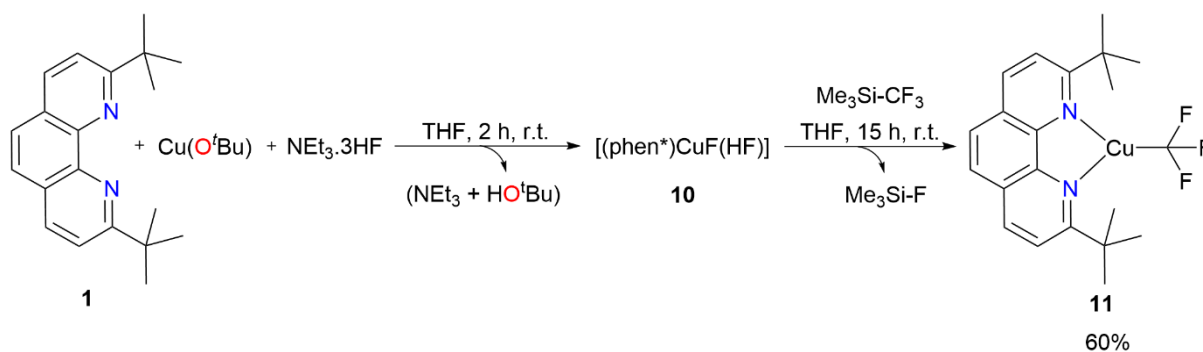
The copper(I) species $[(\text{phen}^*)\text{Cu}(\text{C}_6\text{H}_4\text{-}o\text{-NO}_2)]$ (**9**) was synthesized in a different way because the aryl precursor $[\text{Cu}(\text{C}_6\text{H}_4\text{-}o\text{-NO}_2)]_n$ is not reported. We used the method published by the group of Hoover for the preparation of the copper(I) species $[(\text{phen})\text{Cu}(\text{C}_6\text{H}_4\text{-}o\text{-NO}_2)]$.¹¹ After usual purification, compound **9** was obtained pure in 57% yield from the addition of 5,5-dimethyl-2-(2-nitrophenyl)-[1,3,2]-dioxaborinane to a mixture of phen* and of the freshly sublimed $[\text{Cu}(\text{O}^t\text{Bu})]$ in THF (Scheme 50). It crystallized as orange blocks by cooling down a refluxed THF solution of the complex.



Scheme 50. Synthesis of complex $[(\text{phen}^*)\text{Cu}(\text{C}_6\text{H}_4\text{-}o\text{-NO}_2)]$ (**9**).

Complex $[(\text{phen}^*)\text{Cu}(\text{CF}_3)]$ (**11**) was synthesized in a slightly distinct manner from the procedure reported by the group of Hartwig in 2011.²⁹ If $[(\text{phen})\text{Cu}(\text{CF}_3)]$ is obtained almost quantitatively by treatment of the *in situ* generated $[(\text{phen})\text{Cu}(\text{O}^t\text{Bu})]$ with 1 equiv. of Me_3SiCF_3 in benzene, this protocol proved unsuccessful for giving the analogous phen* derivative **11**. As we saw above, the non-coordination of phen* to $[\text{Cu}(\text{O}^t\text{Bu})]$ is likely the key for this difference. To drive the reaction toward **11**, we thus substituted the congested O^tBu group with the smaller fluorine anion whose affinity for silicon ion is well known. Copper(I) fluoride complexes ligated by substituted phenanthrolines have been synthesized and structurally characterized previously.³⁰ In particular, the orange compound

[(phen*)Cu–F] has been isolated in 38% yield from the reaction of [Cu(O^tBu)] with the phen* ligand in THF, followed by the addition of 1 equiv. NEt₃·3HF.^{30,31} This air- and moisture-sensitive complex crystallized with one molecule of NEt₃·3HF in the cell. During one synthesis in benzene, we also crystallized the fluorine solvate complex with the formula [(phen*)CuF](HF)·C₆H₆ (**10**·C₆H₆). Treatment of the in-situ generated complex **10** at room temperature for 1 h with excess TMSCF₃ (3 equiv.) afforded the pure compound **11** as a yellow solid (60.3 mg, 60 %) after usual work up. Yellow crystals of **11** were obtained by cooling down a hot THF solution of the complex.



Scheme 51. Synthesis of complex [(phen)Cu(CF₃)] (**11**) from the “in situ” preparation of [(phen*)CuF](HF) (**10**).

All the copper(I) complexes **8–11** are sensitive to air and moisture and degrade after prolonged heating, as evidenced by a rapid color change of the solutions with formation of a black deposit. They are soluble in THF and in less polar solvents, such as benzene and Et₂O. They were fully characterized by ¹H, ¹³C, and ¹⁹F NMR spectroscopies and/or elemental analysis, and X-ray diffraction. Views of the structures of the alkyl/aryl complexes **8**, **8'**, **9**, **10** and **11** are shown in Figure 36–Figure 40 and distances and angles are reported in Table 3 (Table 2 for **10**). All the alkyl/aryl complexes **8**, **8'**, **9** and **11** are mononuclear and tricoordinated.

The structures of the two analogous complexes [(L)Cu(κ¹-C₆F₅)] (L = phen* (**8**), phen (**8'**)) are different, the Cu(I) ion being found in an environment either perfectly trigonal in **8'** or slightly distorted in **8**. In **8'**, columns parallel to [100] are formed by molecules stacked in top to tail fashion (Figure 37 right), with π-interactions between the facing phen* and C₆F₅ ligands. A nearly linear chain of Cu atoms is thus formed, with alternating Cu⋯Cu distances of 3.2886(4) and 3.3431(4) Å.

In contrast, in complex **8**, the two aromatic ligands are not coplanar (Figure 36). Their mean planes form a dihedral angle of 71.36(4)°. The Cu atom and the C₆F₅ ligand are located on the same side of the mean plane of the phen fragment, with a displacement of 0.8033(12) Å for Cu(I). The N1 and N2 atoms are displaced on the same side by 0.1497(14) and 0.0170(14) Å while the two ^tBu groups are on either side of the plane (Table 3). The π-stacking interactions in **8** are different from those in **8'**, with formation of columns, directed along [100], of inversion-related molecules with only partial overlap of phen* moieties involved in π-stacking (Figure 36).

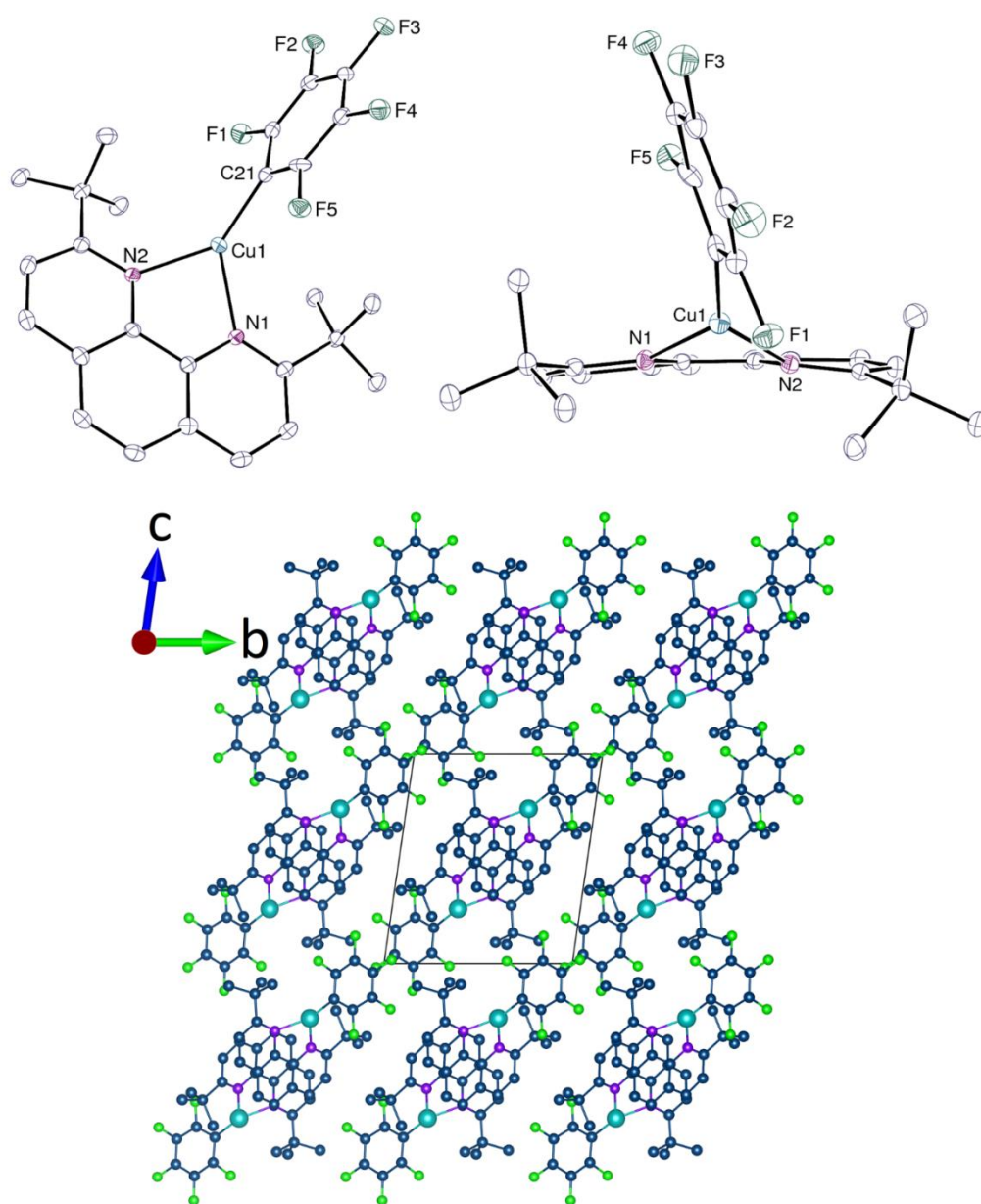


Figure 36. (Top) Two views of complex **8** with hydrogen atoms omitted. Displacement ellipsoids are drawn at the 50% probability level. (Bottom) View of the packing (Cu, light blue; F, green; N, purple; C, blue).

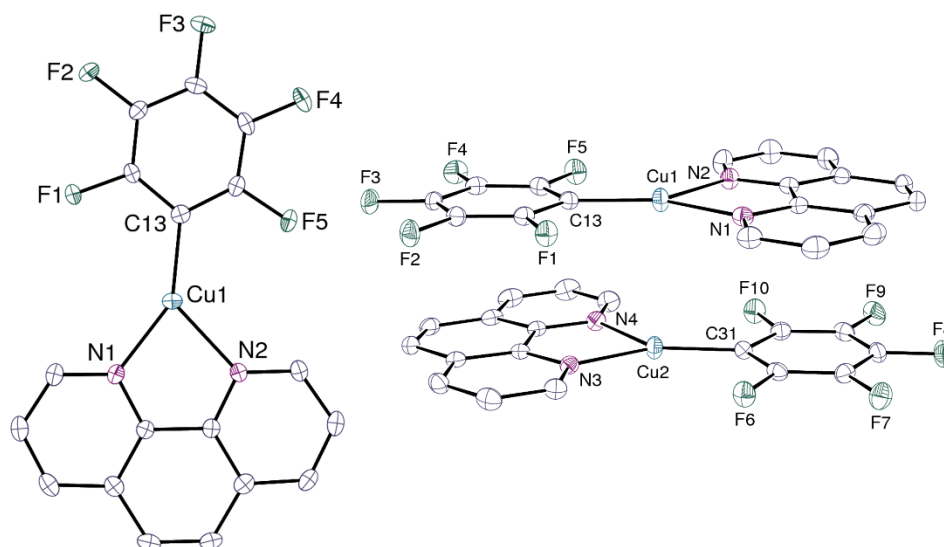


Figure 37. Views of one of the two independent molecules (left) and of the arrangement of the two molecules (right) in complex **8'**, with hydrogen atoms omitted. Displacement ellipsoids are drawn at the 50% probability level.

Here also, there is an asymmetry in the Cu–N bond lengths, with differences of 0.097 Å (mean value) in **8'** and 0.063 Å in **8**. They are however in the range of values reported in phen and bipy derivatives (see Table 3). As expected, the Cu–C distance is slightly longer in the more congested complex **8**, by ~ 0.015 Å, the value for both compounds being similar to those found in the complexes [(bipy)Cu(C₆F₅)] (1.907(2) Å) and [(phen)Cu(C₆F₄-*p*-OMe)] (1.932(2) Å).^{12,28} The sum of the angles around the tri-coordinate metal ion are 360 and 356° for **8'** and **8**, respectively.

Table 3. Selected distances (Å) and angles (°) in the aryl and alkyl complexes **8**, **8'**, **9**, **11** and in [(bipy)Cu(C₆F₅)] and [(phen)Cu(C₆F₄-*p*-OMe)].^{12,28}

Complex	[(bipy)Cu(C ₆ F ₅)]	[(phen)Cu(C ₆ F ₄ - <i>p</i> -OMe)]	8'	8	9	11
Cu–C(C ₆ F ₅)	1.907(2)	1.932(2)	1.9076(19)/1.9092(19)	1.9230(19)	1.9080(17)	1.9296(13)
Cu–N1/N3	2.017(2)	2.072(2)	2.0118(17)/2.0258(15)	2.1105(15)	2.0131(14)	2.0503(11)
Cu–N2/N4	2.082(2)	2.094(2)	2.1262(16)/2.1056(17)	2.0473(15)	2.1633(14)	2.1106(11)
<Cu–N>	2.05(3)	2.08(1)	2.07(5)	2.08(3)	2.09(8)	2.08(3)
<i>d</i> (Cu) ^a			–0.0016(14)/+0.0401(13)	+0.8033(12)	+1.0031(10)	+0.8368(8)
<i>d</i> (N1/N3) ^a			+0.0127(15)/+0.0259(14)	+0.1497(14)	+0.1470(12)	+0.1157(9)
<i>d</i> (N2/N4) ^a			–0.0079(15)/–0.0148(15)	+0.0170(14)	–0.0634(12)	+0.0229(10)
<i>d</i> (C13) ^a				+0.143(2)	+0.177(2)	+0.0164(16)
<i>d</i> (C17) ^a				–0.450(2)	–0.283(2)	–0.3552(17)
C–Cu–N1/N3	131.35(7)	135.68(9)	147.95(7)/144.84(7)	134.32(7)	149.51(6)	143.02(5)
C–Cu–N2/N4	148.30(7)	132.69(8)	131.49(7)/134.54(7)	140.12(7)	123.95(6)	132.52(5)
N1/N3–Cu–N2/N4	79.69(6)	80.02	80.55(6)/80.61(6)	81.60(6)	80.87(5)	81.25(4)
Σ ^b	359.34	348.39	360.00	356.04	354.33	356.79

^a *d* is the displacement from the phen mean plane. ^b Sum of the angles around the Cu centre. For complex **8'**, values are given for the two independent molecules.

The important role of the bidentate nitrogen ligand as well as that of the fluorinated-aryl in the geometry of the complexes must be emphasized. Indeed, the geometry of the non-planar [(κ²-bipy)Cu(C₆F₅)] is notably different to that of **8'**.²⁸ Likewise, replacing C₆F₅ with C₆F₄-*p*-OMe in the [(κ²-phen)Cu(Aryl)] species also considerably modifies the geometry of the complex, [(phen)Cu(C₆F₄-*p*-OMe)] being a dimer with a Cu–Cu bond length of 1.932(2) Å.¹²

The Cu(I) coordination mode in [(phen*)Cu(κ¹-C₆H₄-*o*-NO₂)] (**9**) (Figure 38) is similar to that in **8** (Figure 37). The molecules are loosely held by π-stacking interactions between the phen moieties, so as to form centrosymmetric dimers. These dimers are further stacked into columns parallel to [010]. The

Cu–N1 and Cu–N2 distances are strongly asymmetric and differ by 0.15 Å which is, by far, the largest gap found in all the phen* complexes reported here. The Cu–C distance of 1.9080(17) Å is close to that in **8'** and shorter than in **8** and even **11**, while the large Cu⋯O1(NO₂) distance of 2.6593(13) Å suggests the absence of any interaction. Indeed, this distance is extremely long when compared to the Cu–O distances of 1.927(2) Å or 1.929(3) Å found respectively in the triflate complex [(phen*)Cu(κ¹-O₃SCF₃)] or in the acetone adduct [(phen*)Cu(O=CMe₂)] [SbF₆].¹⁴ As in all the above mentioned complexes (except **8'**), both the metal ion and the aryl ligand are located on the same side of the phen* ligand, with an out-of-plane displacement of 1.0031(10) Å for Cu(I), the largest found in the present series. The displacements are 0.1470(12), –0.0634(12), 0.177(2) and –0.283(2) Å for N1, N2, C13 and C17 (the *tert*-butyl attachments), respectively, and two pairs of methyl groups point away from the anionic ligand. The NO₂ substituent is twisted from the aryl plane while the mean planes of phen* and the aryl ligand form a dihedral angle of 62.38(4)°. The N–Cu–N angle of 80.87(5)° is in the range of those found in **8'**, **8**, and **11**. Strong distortion in this complex can be visualized by the sum of the angles around the Cu atom of 354°, one of the lowest values with that measured in the carboxylate complex **2**.

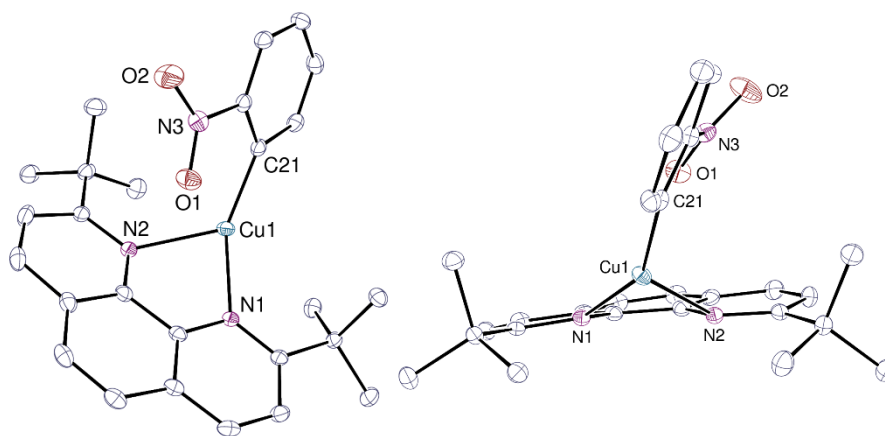


Figure 38. Two views of complex **9** with hydrogen atoms omitted. Displacement ellipsoids are drawn at the 50% probability level.

The mononuclear complex [(phen*)Cu(CF₃)] (**11**) is shown in Figure 39. Here again, π -stacking leads to formation of centrosymmetric dimers, with a distance of 3.56 Å between the mean planes of the phen* ligands. The Cu atom and the CF₃ ligand are on the same side of the mean plane of phen*, with a displacement of 0.8368(8) Å for Cu(I), a value similar to that found in **8**, these two complexes showing close structural analogies. The displacements for N1, N2, C13 and C17 (the *tert*-butyl attachments) are 0.1157(9), 0.0229(10), 0.0164(16) and –0.3552(17) Å, respectively. The Cu–N1 and Cu–N2 distances in **11** and **8** are very close, as well as the Cu–C distances which differ by 0.007 Å. They also have similar N–Cu–N angles and sum of the angles around the Cu atom (357° in **11**).

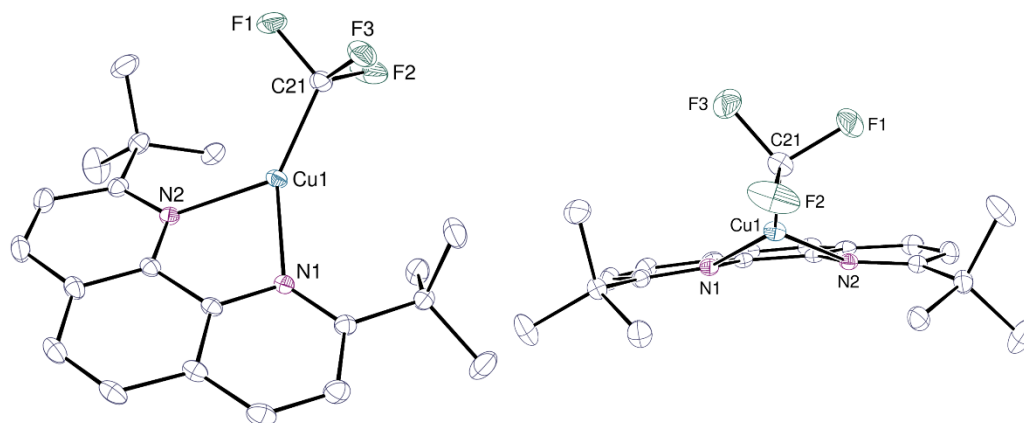


Figure 39. Two views of complex **11** with hydrogen atoms omitted. Displacement ellipsoids are drawn at the 50% probability level.

The structure of the Cu–F(HF) complex **10** in the solvate $[(\text{phen}^*)\text{CuF}](\text{HF})\cdot\text{C}_6\text{H}_6$ (Figure 40) is quite similar to that of $[(\text{phen}^*)\text{CuF}]$ which co-crystallizes with one molecule of $(\text{HF})_3\cdot\text{NEt}_3$.³⁰ Complex **10** is a very rare example of a phenanthroline copper fluoride compound with a true Cu–F bond.³² The solid-state structure reveals a neutral species where the Cu(I) ion, coordinated to a bidentate phen* and a fluoride ion, is found in an almost planar trigonal geometry (sum of the three angles, 360°). A hydrogen atom is located between the two fluorine atoms, with F1–H1 and F2–H1 bond lengths of 1.21(4) and 1.14(4) Å, respectively. Here again, the Cu and N atoms are displaced on the same side of the mean plane of the phen moiety, by 0.1466(16), 0.0317(18) and 0.0149(18) Å, respectively, while the anionic fluoride ligand is at 0.376(3) Å on the same side and the C13 and C17 atoms of the *t*Bu groups are almost in the plane. The Cu–F bond length of 1.8970(16) Å is quite similar to the distance of 1.891 Å reported in the Cu(II) species $(\text{phen})\text{CuF}_2(\text{H}_2\text{O})$ ³² or in the analogous $[(\text{phen}^*)\text{CuF}]$ complex (1.870(8) Å).³⁰ The difference is more pronounced when compared to other Cu–F bonds of complexes involving different ligands such as in the biscoordinate carbene (NHC)CuF complexes (1.7865(10)–1.872 Å)^{31,33,34} or $(\text{PPh}_3)_3\text{CuF}$ (2.062(6) Å).³⁵ The two Cu–N bonds are not symmetrical, differing by 0.02 Å. The N–Cu–N angle of $84.38(8)^\circ$ is similar to the angle reported in $[(\text{phen}^*)\text{CuF}]$ (84.1°) and slightly larger than the angles found in the carboxylate complexes **2–7** (Table 2).

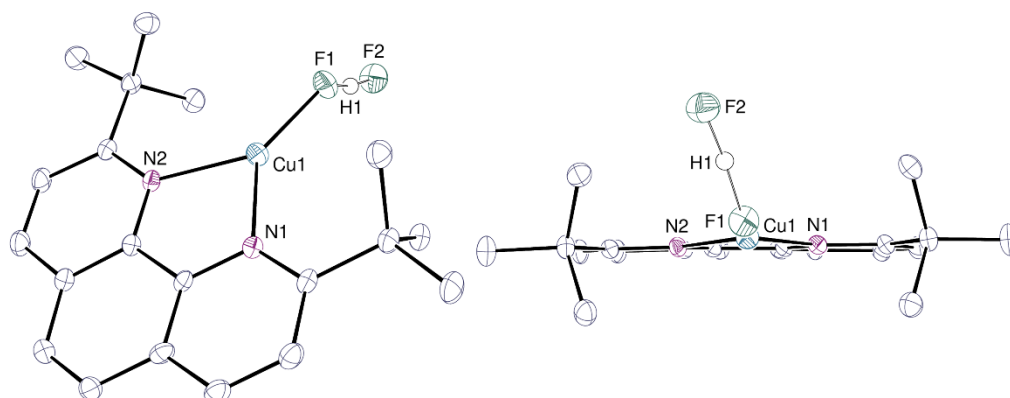


Figure 40. Two views of complex **10** with solvent molecule and carbon-bound hydrogen atoms omitted. Displacement ellipsoids are drawn at the 50% probability level.

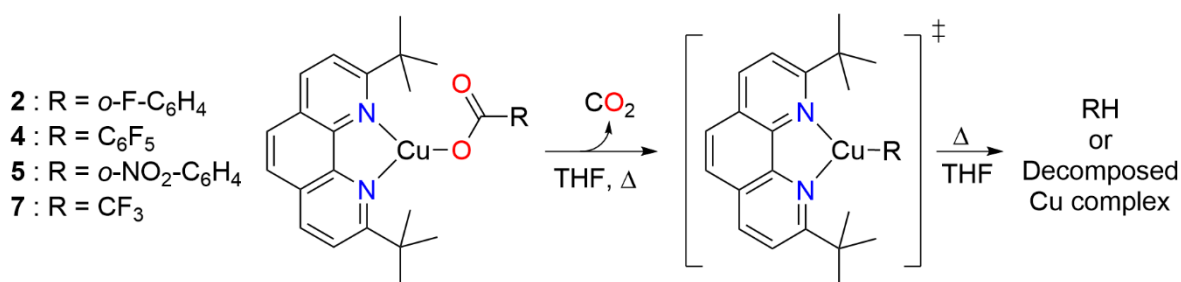
Overall, a simple and general method for the preparation of several copper(I) carboxylate species has been described, leading to good or even excellent yields. Thanks to the steric demand of *tert*-butyl

groups at 2,9-positions of phen, the copper(I) center is stabilized with an appropriate hindrance inhibiting coordination of a second phen* ligand. However, the synthetic routes for the generation of complexes involving copper-carbon bonds are not straightforward. Although being isolated in moderate yields, these [(phen*)CuR] (R = C₆F₅, *o*-NO₂-C₆H₄, CF₃) are representative examples of potential key intermediates for our mechanistic study of decarboxylation in the next step.

III. 4. Study of the decarboxylation of the [(phen*)Cu(O₂CR)] complexes (R = C₆H₄-*o*-F (2), C₆H₄-*o*-NO₂ (5), C₆F₅ (4), CF₃ (7)).

III. 4. 1. Decarboxylation in THF

Since carboxylate ligands with *ortho*-substituents are favorable to the loss of CO₂ (*vide supra*, Chapter 1 – III. 2. 1.),³⁶ the decarboxylation behavior of complexes 2, 4, 5 and 7 were first tested in the range of temperatures 25 °C to 175 °C in THF-*d*₈ in order to track their evolution by ¹⁹F NMR analysis (Table 4). However, as mentioned by Petrukhina *et al.*,² we must be aware that copper(I) carboxylates may readily disproportionate to produce copper(II) salts and metallic copper, as the process is facilitated by high temperatures and long reaction times in coordinating solvents.



Entry	Complex	T (°C)	Time (h)	Results and Observations
1	2	75	2	Free ligand, disproportionation
2	4	50	5	Free ligand and complex 4 in the ratio ~ 1/1
3		100	3	Presence of C ₆ F ₅ H and free phen* with Cu ⁰
4	5	50	2	Stable complex
5		100	72	Free ligand, disproportionation
6	7	50	2	Slight degradation
7		175	2	Partial degradation

Table 4. Decarboxylation tests in THF-*d*₈ for the complexes 2, 4, 5 and 7.

Due to the distinct ¹⁹F NMR signals in THF-*d*₈ of the carboxylate complexes 4 (–143.49 ppm, –161.20 ppm, –165.37 ppm) and 7 (–75.14) in comparison with those of the organometallic derivatives [(phen*)Cu(C₆F₅)] (–111.59, –164.70, –168.83), [(phen*)Cu(CF₃)] (–26.79) and of pentafluorobenzene (C₆F₅H) (–140.61, –156.70, –164.65), the thermal behavior of the carboxylate complexes was monitored by ¹⁹F NMR and ¹H NMR spectroscopy.

Complexes 2, 4, 5 and 7 have distinct thermal stabilities (see Table 4) and did not afford, by heating, the corresponding [(phen*)CuR] (R = Aryl, CF₃) derivatives since they could not be detected in THF-*d*₈ or in other deuterated organic solvents. These latter having poor thermal stability, they rapidly

degraded upon warming, affording a black copper(0) deposit, and in some cases, forming green solutions of Cu(II) and free ligands (phen* and aryl compounds).

Complexes **2** and **4** are less stable than **5** and **7** and are rapidly decomposed upon low heating ($T = 50$ – 75°C), affording a black deposit and free phen* (Figure 41c–f for **4**) and with the clear release of $\text{C}_6\text{F}_5\text{H}$ (for **4**) as observed by $^{19}\text{F}\{^1\text{H}\}$ NMR (Table 4, entries 1–3, and Figure 42e–d for **4**) (See SI for **2**). Because free phen* is readily formed in mild conditions (5 h at 50°C) prior to the generation of pentafluorobenzene (3 h at 100°C), it might suggest possible loss of CO_2 from the uncoordinated and possibly less stable species $[\text{Cu}(\text{O}_2\text{CC}_6\text{F}_5)]$ (Figure 41 and Figure 42). The green solution obtained from **2** likely suggests formation of copper(II) carboxylate species via disproportionation, which could not be characterized and crystallized. Formation of $\text{C}_6\text{F}_5\text{H}$ genuinely indicated initial extrusion of CO_2 from **4** with a subsequent hydrolytic cleavage of the Cu–C bond. On the other hand, after 2 h at 50°C , decomposition of **7** in $\text{THF-}d_8$ can be detected with formation of free phen* but was not completely transformed even after further 2 h at 175°C (57 % of **7** vs 43 % free phen*) (Table 4, entry 6) (See SI). In contrast, the *o*-nitro complex **5**, appeared much more stable and was fully destroyed after 3 days at 100°C to form copper(0) and copper(II) carboxylate via disproportionation (Table 4, entries 4 and 5) (See SI).

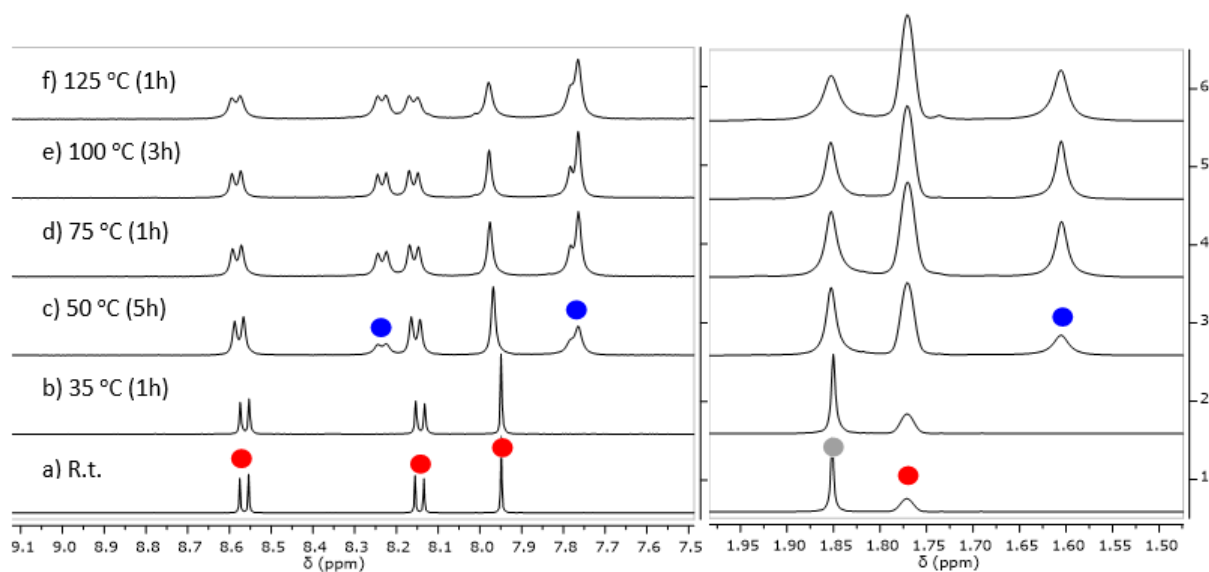


Figure 41. Zoom on ^1H NMR stacked spectra of the thermal evolution of complex $[(\text{phen}^*)\text{Cu}(\text{O}_2\text{CC}_6\text{F}_5)]$ **4** in $\text{THF-}d_8$ and the release of free phen*.

Orange circle: $[(\text{phen}^*)\text{Cu}(\text{C}_6\text{F}_5)]$, blue circle: free phen*, gray circle: $\text{THF-}d_8$.

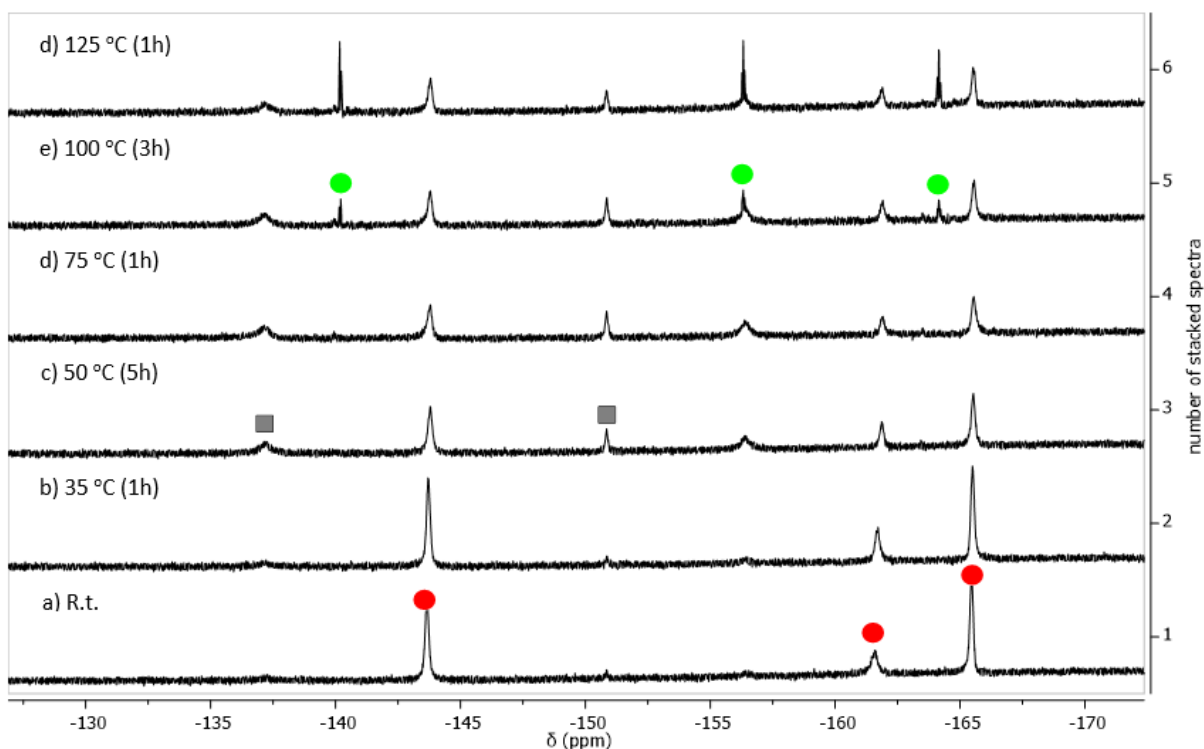
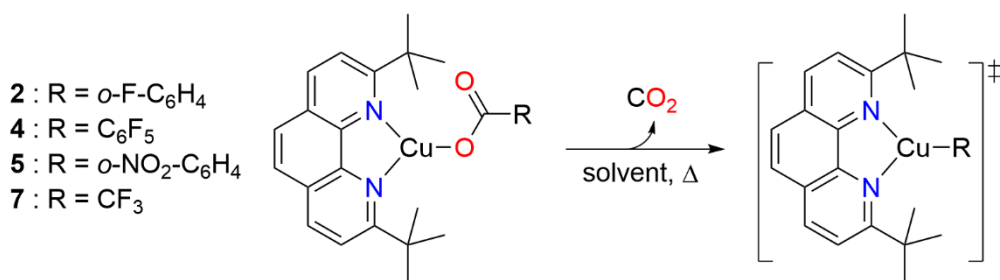


Figure 42. $^{19}\text{F}\{^1\text{H}\}$ NMR stacked spectra of the thermal evolution of complex $[(\text{phen}^*)\text{Cu}(\text{O}_2\text{CC}_6\text{F}_5)]$ (**4**) in quinoline and evidence for the generation of $\text{C}_6\text{F}_5\text{H}$.

Red circle: $[(\text{phen}^*)\text{Cu}(\text{O}_2\text{CC}_6\text{F}_5)]$, green circle: $\text{C}_6\text{F}_5\text{H}$, gray square: unidentified byproducts.

III. 4. 2. Decarboxylation in other solvents

Strongly coordinating solvents with higher boiling point than THF, such as $\text{DMF-}d_7$, quinoline and NMP (*N*-methyl-2-pyrrolidone) were reported to be more favorable for the decarboxylation process³⁷ and have thus been considered (Table 5). Here again, complex **7** showed the greatest stability and stayed remarkably robust in NMP or quinoline even after ~ 6 h at temperatures exceeding 150 °C (Table 5, entries 8 and 9).



Entry	Compound	Solvent	T (°C)	Time (h)	Result
1	2	quinoline	120	72	Protodecarboxylation
2		quinoline		1	Protodecarboxylation
3	4	NMP	35	4	and formation of [(phen*)Cu(C ₆ F ₅)]
4		DMF- <i>d</i> ₇		1	
5	5	quinoline	120	10	No reaction
6				150	
7		DMF- <i>d</i> ₇	50	2	Stable complex
8	7	NMP	150	6	Stable complex
9		quinoline		170	

Table 5. Decarboxylation tests in quinoline, NMP or DMF for the complexes **2**, **4**, **5** and **7**.

In these solvents, complex **4** proved to be the least stable (Table 5, entries 2–4). To understand its stability, we particularly focused on studying its thermal behavior in quinoline by ¹⁹F NMR spectroscopy (Figure 43a). In quinoline, complex **4** began to decarboxylate at the low temperature of 35 °C and after hardly ~ 1 h, the presence of C₆F₅H species was clearly evidenced (Figure 43b). The solution was then kept at 50 °C for another hour and then 2 h at 75 °C, respectively (Figure 43c and d). These spectra show the disappearance of **4** into a new species and C₆F₅H. This new species has ¹⁹F signals seemingly identical to those of [(phen*)Cu(C₆F₅)] (**8**) in quinoline.

To verify if this new species is actually the desired decarboxylated product **8**, a ¹⁹F NMR study of [Cu(C₆F₅)₄] in quinoline with subsequent addition of phen* was monitored. When [Cu(C₆F₅)] was solubilized in quinoline, the [Cu(C₆F₅)(quinoline)_n] species was expected to form (¹⁹F NMR signals in Figure 43e). By addition of 1 equivalent phen*, resonances of the three distinct fluorine atoms were slightly shifted low-field, indicating the coordination of phen* to [Cu(C₆F₅)(quinoline)_n] (Figure 43f). As expected, these signals are identical to those of [(phen*)Cu(C₆F₅)] (**8**) (Figure 44), indicating successful decarboxylation of [(phen*)Cu(O₂CC₆F₅)] (**4**) to **8**. It is noted that the ¹⁹F signals of **8** are slightly deshielded by *ca.* 0.3 ppm compared to the [(phen*)Cu(C₆F₅)] samples obtained by thermal decarboxylation of **4** or by coordination of phen* to [Cu(C₆F₅)(quinoline)_n]. These results suggest that the CO₂ extrusion reaction proceeds preferably in quinoline compared to THF, and phen* is not fully displaced by quinoline solvent. Moreover, a possible coordination of quinoline to [(phen*)Cu(O₂CC₆F₅)] (**4**) and [(phen*)Cu(C₆F₅)] (**8**) is not completely excluded. Interestingly, C₆F₅H is formed spontaneously already at room temperature when phen* is added into the quinoline solution of [Cu(C₆F₅)(quinoline)_n] (Figure 43f). This evidences a facile protodecarboxylation process which is concomitant with the decarboxylation of **4**.

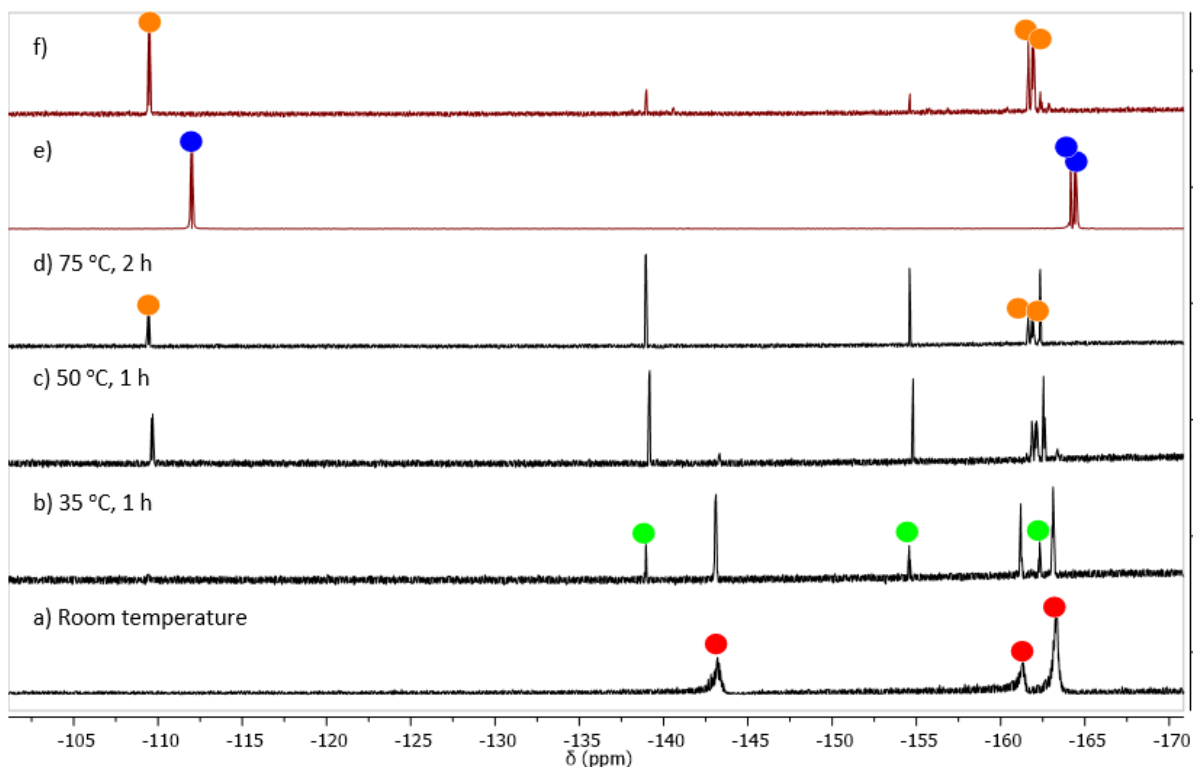


Figure 43. In black (a to d spectra): $^{19}\text{F}\{^1\text{H}\}$ NMR stacked spectra of the thermal evolution of complex $[(\text{phen}^*)\text{Cu}(\text{O}_2\text{CC}_6\text{F}_5)]$ (**4**) in quinoline and evidence for the generation of $[(\text{phen}^*)\text{Cu}(\text{C}_6\text{F}_5)]$.

In red: spectrum of $[\text{Cu}(\text{C}_6\text{F}_5)(\text{quinoline})_n]$ (e) and of the 1:1 mixture $[\text{Cu}(\text{C}_6\text{F}_5)(\text{quinoline})_n] + \text{phen}^*$ (f).

Red circle: $[(\text{phen}^*)\text{Cu}(\text{O}_2\text{CC}_6\text{F}_5)]$, green circle: $\text{C}_6\text{F}_5\text{H}$, orange circle: $[(\text{phen}^*)\text{Cu}(\text{C}_6\text{F}_5)]$, blue circle: $[\text{Cu}(\text{C}_6\text{F}_5)(\text{quinoline})_n]$.

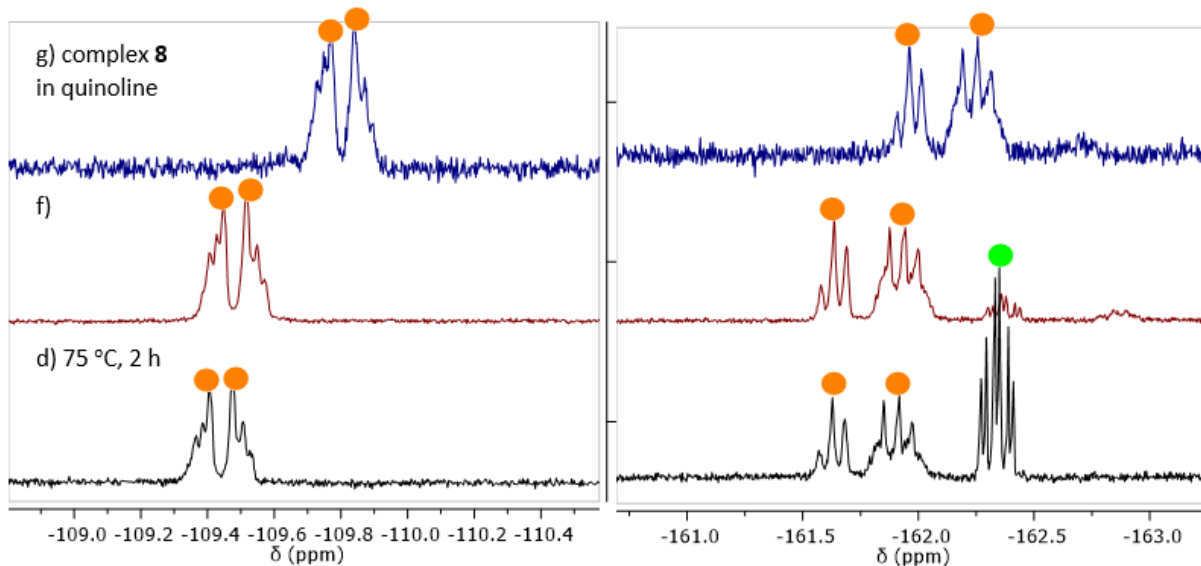


Figure 44. Zoom on $^{19}\text{F}\{^1\text{H}\}$ NMR stacked spectra of Figure 31 (d) and (f) and complex **8** in quinoline (g) evidence for the generation of $[(\text{phen}^*)\text{Cu}(\text{C}_6\text{F}_5)]$. Orange circle: $[(\text{phen}^*)\text{Cu}(\text{C}_6\text{F}_5)]$, green circle: 1 signal of $\text{C}_6\text{F}_5\text{H}$.

It is important to mention that, continuous heating of a quinoline solution of complex **4** to $150\text{ }^\circ\text{C}$ led to the complete consumption of the generated species $[(\text{phen}^*)\text{Cu}(\text{C}_6\text{F}_5)]$, while the resonances of the $\text{C}_6\text{F}_5\text{H}$ compound remained after 9 h (Figure 45). This observation suggests that $[(\text{phen}^*)\text{Cu}(\text{C}_6\text{F}_5)]$ may decompose upon heating with release of $\text{C}_6\text{F}_5\text{H}$. This point further emphasizes the role of

$[(\text{phen}^*)\text{Cu}(\text{C}_6\text{F}_5)]$ as a key intermediate in both decarboxylation and protodecarboxylation processes. The slightly shifted signals in these spectra can again be explained by the evolution of the mixture, as underlined by the change in color of the solution from orange (after 2 h at 75 °C) to brown (after 9 h at 150 °C).

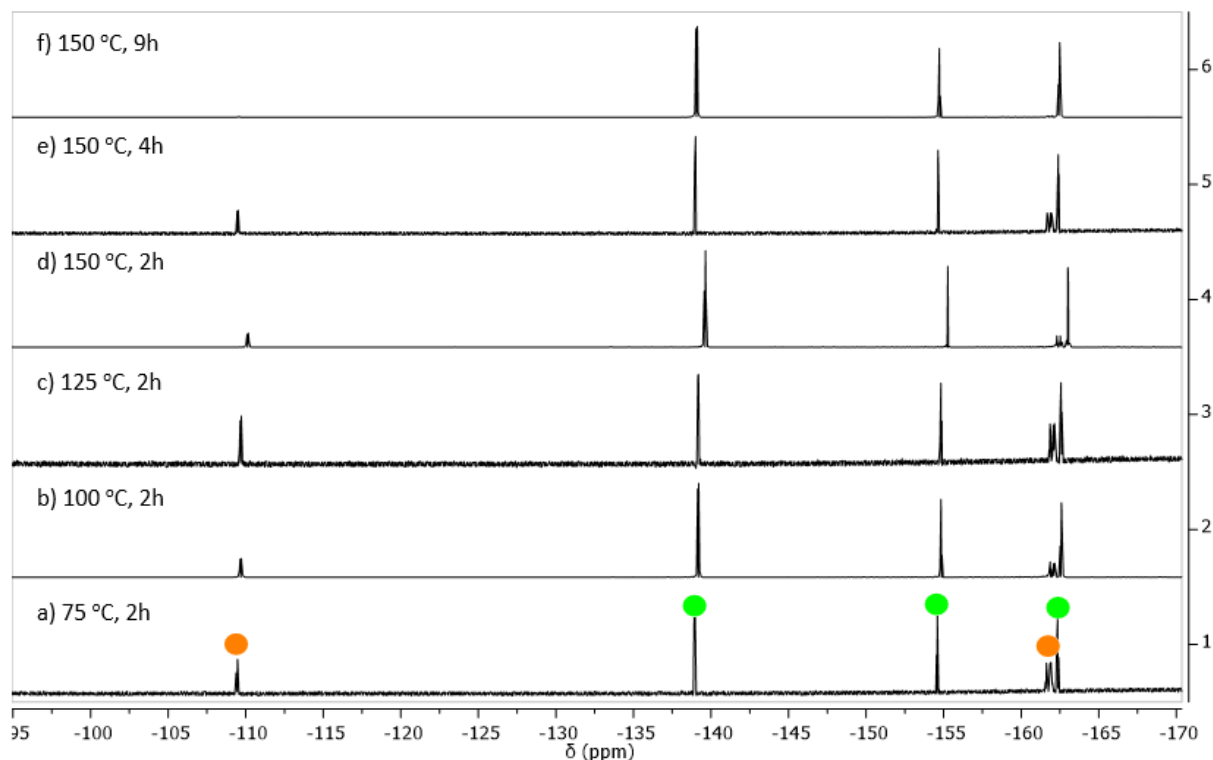


Figure 45. $^{19}\text{F}\{^1\text{H}\}$ NMR stacked spectra of the thermal evolution of complex **4** in quinoline: after 2 h at 75 °C **4** has been totally transformed into $[(\text{phen}^*)\text{Cu}(\text{C}_6\text{F}_5)]$ (**8**) and $\text{C}_6\text{F}_5\text{H}$. Spectra b to f evidence complete degradation of **8** with release of $\text{C}_6\text{F}_5\text{H}$.

Similar formation of $[(\text{phen}^*)\text{Cu}(\text{C}_6\text{F}_5)]$ (**8**) and $\text{C}_6\text{F}_5\text{H}$ from thermal degradation of $[(\text{phen}^*)\text{Cu}(\text{O}_2\text{CC}_6\text{F}_5)]$ (**4**) in NMP (4 h at 35 °C) or in $\text{DMF-}d_7$ (1 h at 35 °C) were also observed (Table 5, entries 3 and 4). Interestingly, $\text{DMF-}d_7$ favored over quinoline and NMP, the rapid and simultaneously formation of a $[\text{Cu}(\text{C}_6\text{F}_5)]$ species and $\text{C}_6\text{F}_5\text{H}$ (Figure 46b) while the precursor **4** was almost completely consumed after 1 h at 35 °C (Figure 46b compared to Figure 43b). With new set of ^{19}F signals at -110.95 , and two signals at around -164 ppm that superimposed with that of $\text{C}_6\text{F}_5\text{H}$ resonances, $[(\text{phen}^*)\text{Cu}(\text{C}_6\text{F}_5)(\text{DMF})_n]$ species is supposed to form (Figure 47). Because its ^{19}F signals are closed to that of $[(\text{phen}^*)\text{Cu}(\text{C}_6\text{F}_5)]$ (**8**) in quinoline (-109.84 , -161.96 , -162.26). Additionally, ^1H NMR analysis in $\text{DMF-}d_7$ showed shifted signals of the phen^* ligand in **4** during the reaction which are different from the resonances of free phen^* , suggesting formation of a new phen^* ligated copper species (See SI). This led us to believe that the $[(\text{phen}^*)\text{Cu}(\text{C}_6\text{F}_5)(\text{DMF})_n]$ may exist as seen in quinoline. One important drawback of DMF solvent is that more unidentified byproducts are formed than in quinoline (Figure 46c).

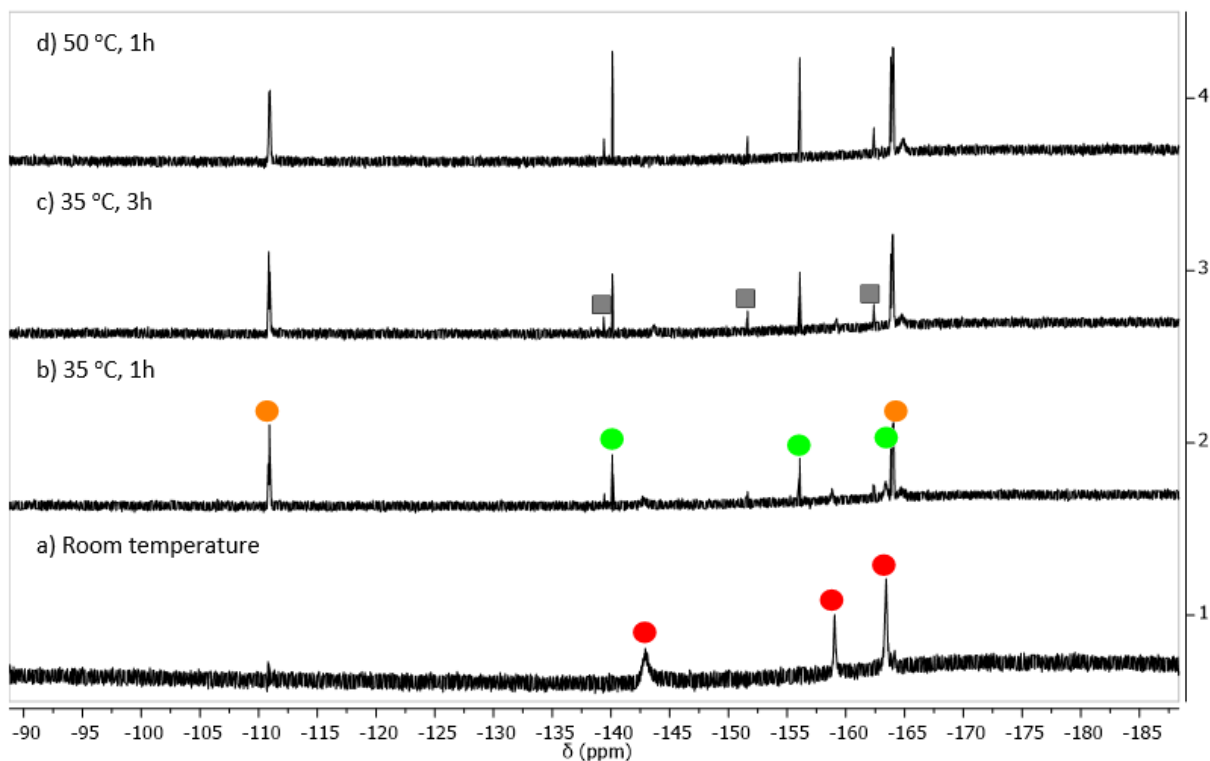


Figure 46. $^{19}\text{F}\{^1\text{H}\}$ NMR stacked spectra of the thermal evolution of **4** in DMF-d_7 and evidence for the generation of $[(\text{phen}^*)\text{Cu}(\text{C}_6\text{F}_5)]$ and $\text{C}_6\text{F}_5\text{H}$. Red circle: $[(\text{phen}^*)\text{Cu}(\text{O}_2\text{CC}_6\text{F}_5)]$ (**4**), green circle: $\text{C}_6\text{F}_5\text{H}$, orange circle: $[(\text{phen}^*)\text{Cu}(\text{C}_6\text{F}_5)(\text{DMF})_n]$, gray square: unidentified byproducts.

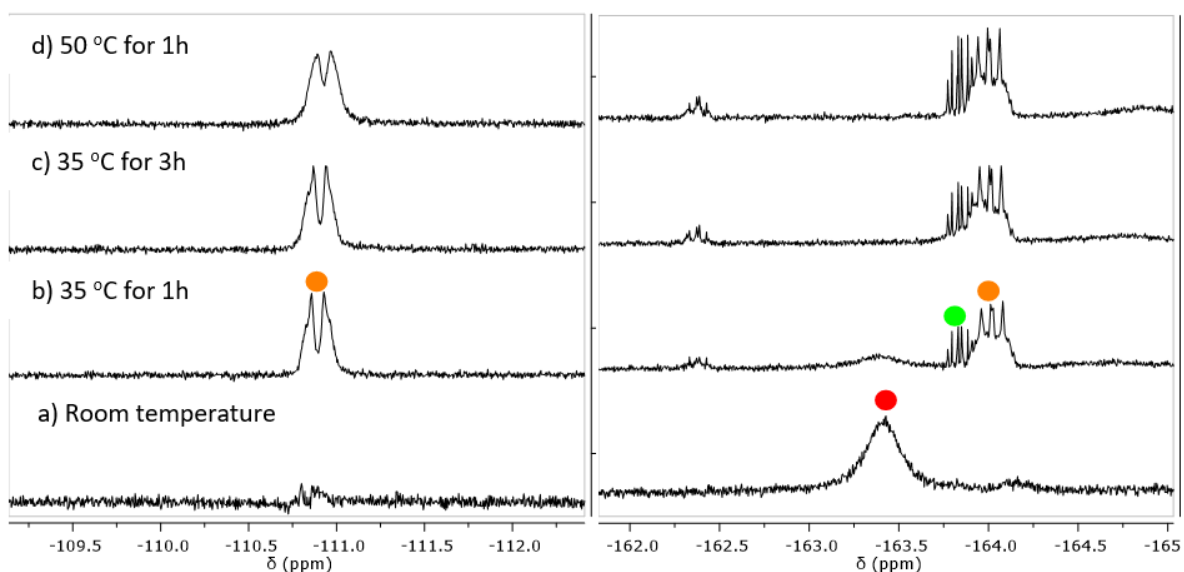


Figure 47. Zoom on Figure 34.

In the case of the solvent NMP, the decarboxylation process is less efficient, as evidenced by the longer reaction time (10 h at 35 °C) required to reach full conversion (Figure 48b–c).

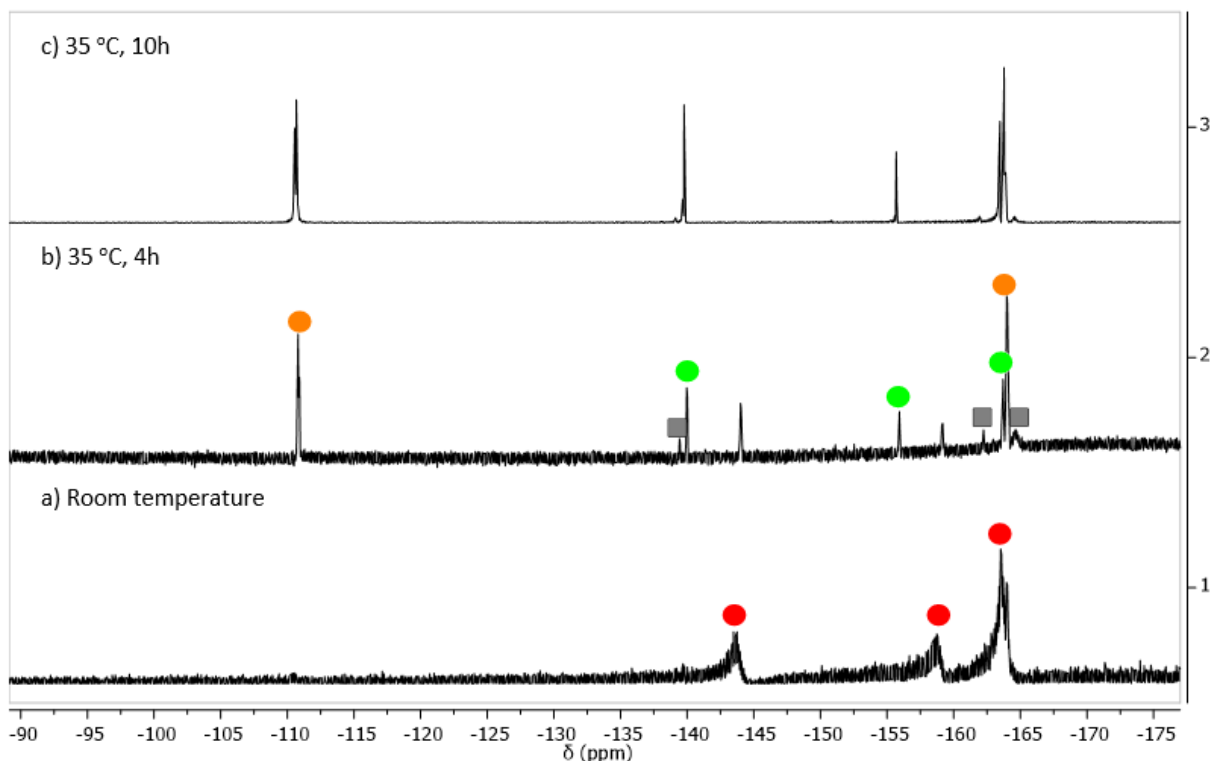


Figure 48. $^{19}\text{F}\{^1\text{H}\}$ NMR stacked spectra of the thermal evolution of complex **4** in NMP and evidence for the generation of $[(\text{phen}^*)\text{Cu}(\text{C}_6\text{F}_5)]$. Red circle: $[(\text{phen}^*)\text{Cu}(\text{O}_2\text{CC}_6\text{F}_5)]$, green circle: $\text{C}_6\text{F}_5\text{H}$, orange circle: $[(\text{phen}^*)\text{Cu}(\text{C}_6\text{F}_5)]$, gray square: unidentified byproducts.

In order to highlight the beneficial effect of copper on the decarboxylation process of carboxylic acids, a control experiment was performed. The pentafluorobenzoic acid $\text{C}_6\text{F}_5\text{CO}_2\text{H}$ was added in quinoline in the absence of copper source. The substrate evolution was followed by ^{19}F NMR and recorded at specific time points. Interestingly, after 1 h at 35 °C, pentafluorobenzene could be detected thus indicating a strong influence of copper on the process. However, formation of the protodecarboxylation product $\text{C}_6\text{F}_5\text{H}$ was observed after 2 h at 80 °C and fully consumed after 3,5 h at 100 °C (see SI).

For the first time, we bring in this work an NMR proof for the decarboxylation event. Sheppard reported in 1969 the decarboxylation of $[\text{Cu}(\text{CO}_2\text{C}_6\text{F}_5)]$ in quinoline at 60 °C and he isolated the $[\text{Cu}(\text{C}_6\text{F}_5)]$ product (72% yield) which was characterized by a melting point analysis.³⁷ Moreover, the use of phen* is of significance for the stabilization of the copper(I) species, that coordinates to copper(I) center without being displaced by quinoline solvent.

The source of proton for the generation of $\text{C}_6\text{F}_5\text{H}$ has been already discussed in the literature. It was first pointed out by Cohen and Wood *et al.*³⁸ that basic solvents (quinoline, pyridine, etc.) could act as protons reservoir for the hydrolytic cleavage step, and that they promoted the reaction with their coordinating ability. Meanwhile, study on the decarboxylation of $\text{C}_6\text{F}_5\text{CO}_2\text{X}$ salts ($\text{X} = \text{NHET}_3, \text{Na}$) in DMF by Bower *et al.* showed the significant role of proton sources for the protodecarboxylation process.³⁹ They found that only 25 % of $\text{C}_6\text{F}_5\text{CO}_2\text{Na}$ converted into $\text{C}_6\text{F}_5\text{H}$ after 1 h at 80 °C, whereas protodecarboxylation of $\text{C}_6\text{F}_5\text{CO}_2(\text{NHET}_3)$ was over than 95 % complete after 100 s in the same conditions. Moreover, addition of water (1 equiv.) into the former case enhanced the reaction rate and led to full conversion after *ca.* 200 s, suggesting a protodecarboxylation promoted by water.³⁹ At

last, the source of protons may originate from adventitious traces of water in the reagents or solvents.³⁸ In this study, the solvents have been thoroughly dried.

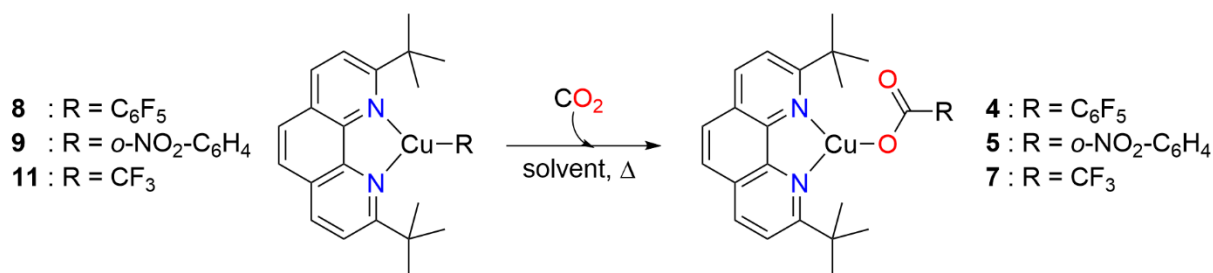
In quinoline, the *o*-fluoro (**2**) and *o*-nitro (**5**) derivatives were also protodecarboxylated affording the corresponding C₆H₅X (X = F, NO₂) arene (*Table 5*, entries 1, 5–6). The formation of fluorobenzene in quinoline was confirmed by ¹⁹F NMR spectroscopy and the presence of a signal ($\delta_F = -112.73$) identical to that of a commercial sample. In addition, CO₂ gas was also detected by gas chromatography analysis at the end of the reaction. The thermal behavior of the *o*-NO₂ derivative **5** was difficult to follow by ¹H NMR since its signals were weak compared to those of the solvent quinoline. The CO₂ gas was not detected neither by ¹³C NMR nor by gas chromatography (GC) upon heating a solution of **5** in quinoline for several hours at 120 °C (*Table 5*, entry 5) but was found by GC after 17 h at 150 °C (*Table 5*, entry 6). Nitrobenzene was also detected in the GC-MS spectra (gas chromatography-mass spectrometry) after hydrolysis of the reaction mixture.

In summary, the use of quinoline as solvent facilitated the loss of CO₂ in complexes **2**, **4** and **5**. While complex **2** and **5** only underwent protodecarboxylation under harsh conditions, complex **4** decarboxylated at remarkably low temperature to form [(phen*)Cu(C₆F₅)] (**8**) together with C₆F₅H. It is clear that the essential role of quinoline is undeniable in these reactions in which several copper-catalysed homogeneous decarboxylative cross-coupling reactions have been widely used.^{36,40–44}

III. 5. Study of the carboxylation of the [(phen*)Cu-R] complexes **8**, **9**, and **11**

Reverse to the decarboxylation process, the carboxylation of copper(I) aryl complexes **8**, **9** and **11** was considered and the possible insertion of CO₂ into the Cu–C bond was monitored by NMR.

A few reports^{45,46} have highlighted the beneficial effect of the solvent DMA (Dimethylamide = HCONMe₂) versus common solvents such as THF for the insertion of CO₂ (1 atm) into the copper-carbon bond at room temperature. In our study, all attempts to insert CO₂ in the Cu–C bond of the organometallic species **8**, **9** and **11** to afford the corresponding carboxylate derivatives **4**, **5** or **7** were unsuccessful regardless of the solvent (THF, quinoline, DMA or toluene), the pressure of CO₂, and the reaction temperature (*Table 6*). In most cases, decomposition of the complexes was detected, as indicated by the generation of black copper deposits and/or the change in color of the solution to green or brown. The thermal sensitivity of the organometallic complexes led to their decomposition when heated and prior to CO₂ insertion if this latter reaction is thermodynamically favored.



Entry	Compound	CO ₂ (bar)	Solvent	T (°C)	t(h)	Result
1	8	10	THF- <i>d</i> ₈	rt. - 50 °C 100 °C	2 2	Formation of C ₆ F ₅ H (50 °C) Partial decomposition to Cu ⁰
2		10	Quinoline	rt.	1	Formation of C ₆ F ₅ H No insertion
3		10	DMA	rt.	8 9 days	Formation of C ₆ F ₅ H No insertion
4	9	10	Benzene- <i>d</i> ₆	rt.	8	Decomposition to Cu ⁰
5		4*	Tol- <i>d</i> ₈	rt. - 75 °C	10	Partial decomposition to Cu ⁰
6		4*	DMA	rt. - 75 °C	10	Decomposition to Cu ⁰
7	11	1.5	Benzene- <i>d</i> ₆	rt. - 75 °C	7	Decomposition to Cu ⁰
8		10	THF- <i>d</i> ₈	rt. - 150 °C	2	Decomposition to Cu ⁰ (75 °C)
9		10	DMA	rt.	6 days	No insertion

* ¹³CO₂: apply to better track the insertion in the Cu-C bond by ¹³C NMR

Table 6. Attempts at carboxylation of copper(I) aryl/alkyl complexes **8**, **9** and **11** with ¹²CO₂ and ¹³CO₂.

For instance, complex **9** decomposed readily at 25 °C in benzene and at 75 °C in DMA to form copper(0) (Table 6, entries 4 and 6). However, this complex displays higher stability in toluene, as evidenced by its robust signals in ¹H NMR that are seen even after 10 h of heating at 75 °C (Table 6, entry 5 and see SI). Despite small formation of black solid (copper(0)), no signal for the free ligand was detected by ¹H NMR (see SI). Unlike **9**, complex **11** species exhibited a higher robustness toward thermal degradation. It showed however a weak stability when heated up to 75 °C in benzene and THF, evidenced by its degradation into Cu(0) and the release of free phen* (Table 6, entries 7 and 8, see SI). To avoid decomposition of **11**, the carboxylation of [(phen*)Cu(CF₃)] (**11**) was then attempted in DMA at room temperature for several days. Under 10 bar of CO₂, it was found inert and CO₂ insertion was not observed after 10 days of reaction in DMA (Table 6, entry 9).

Complex [(phen*)Cu(C₆F₅)] (**8**) showed the lowest stability among all. This can be observed by the generation of pentafluorobenzene at room temperature from a quinoline or DMA solution of **8** (Table 6, entry 2 and 3). For instance, when diluted in quinoline, complex **8** spontaneously released C₆F₅H (Figure 49a) but these two compounds remained visible by ¹H NMR after three days with continuous mixing at 25 °C (Figure 49b). Disappointingly, when CO₂ (10 bar) was added to the solution, no reaction was observed except the formation of C₆F₅H (Figure 49c).

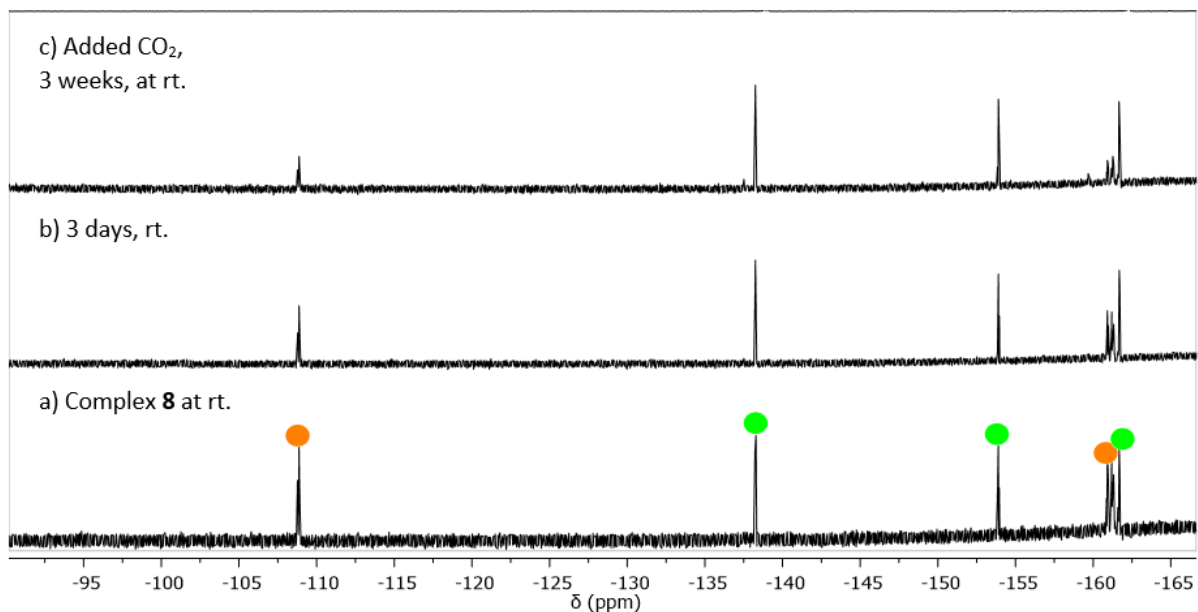


Figure 49. $^{19}\text{F}\{^1\text{H}\}$ NMR stacked spectra of the thermal evolution of complex **8** in quinoline and evidence for the generation of $\text{C}_6\text{F}_5\text{H}$. Green circle: $\text{C}_6\text{F}_5\text{H}$, orange circle: $[(\text{phen}^*)\text{Cu}(\text{C}_6\text{F}_5)]$.

In contrast, **8** seems to be more stable in THF (Figure 50), proved by the fact that it is smoothly converted into $\text{C}_6\text{F}_5\text{H}$ at $50\text{ }^\circ\text{C}$ (Figure 50b) and partially decomposed when heated up to $100\text{ }^\circ\text{C}$ for 2 h (Table 6, entry 1 and Figure 50d). Degradation evidenced the release of free phen*, indicated by ^1H NMR, and formation of a black solid deposit (Figure 51d).

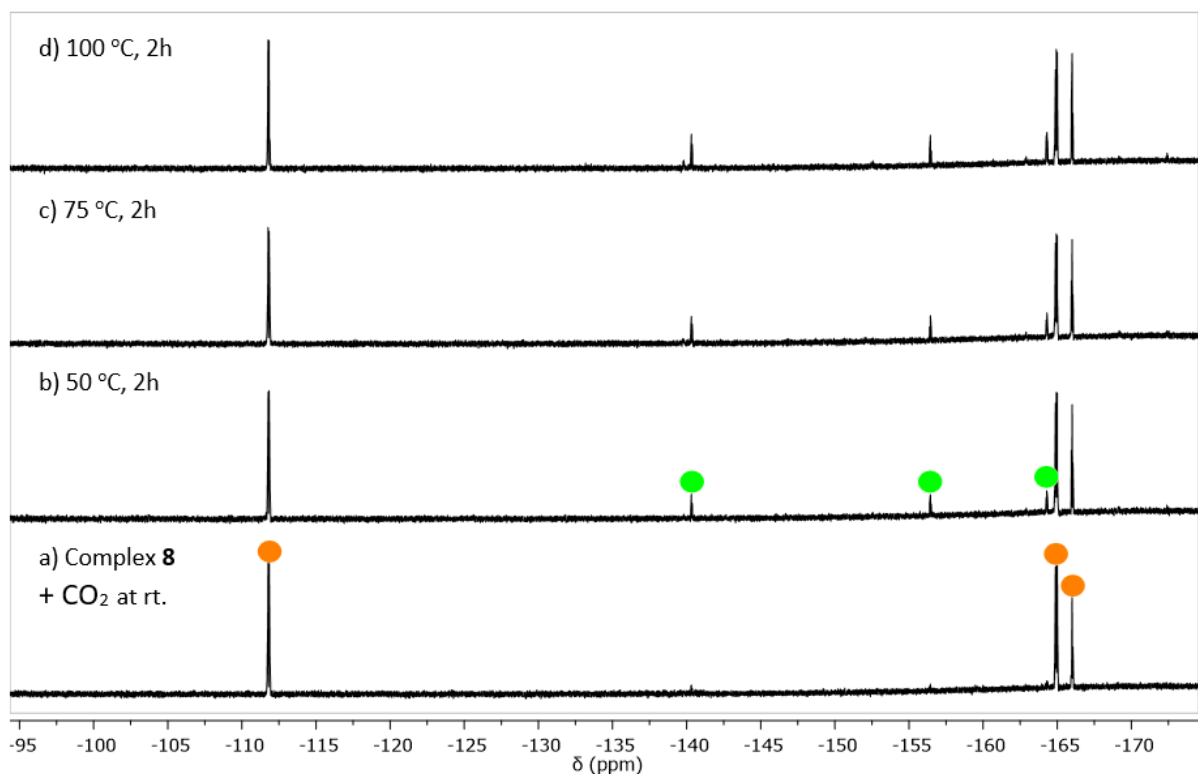


Figure 50. $^{19}\text{F}\{^1\text{H}\}$ NMR stacked spectra of the thermal evolution of complex **8** in THF-d_8 and the release of $\text{C}_6\text{F}_5\text{H}$. Green circle: $\text{C}_6\text{F}_5\text{H}$, orange circle: $[(\text{phen}^*)\text{Cu}(\text{C}_6\text{F}_5)]$.

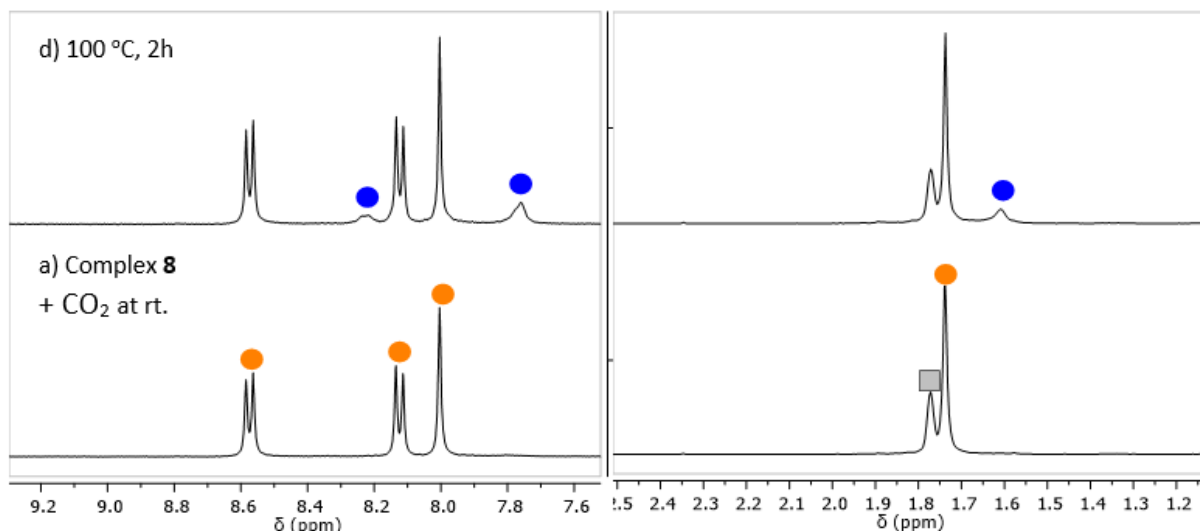


Figure 51. Zoom on ^1H NMR stacked spectra of the thermal evolution of complex **8** in THF-d_8 and the release of free phen*. Orange circle: $[(\text{phen}^*)\text{Cu}(\text{C}_6\text{F}_5)]$, blue circle: free phen*, gray square: THF-d_8 .

The carboxylation of copper(I) aryl complexes **8**, **9** and **11** proved unsuccessful regardless the applied pressure of CO_2 gas (1 to 10 bar). These complexes degraded with or without heating and their thermal sensitivity is related to the nature of the aryl group and the coordinating solvent. Next, we turned to computational studies of the decarboxylation and carboxylation processes to rationalize and further understand the reactivity of these copper complexes.

III. 6. DFT calculation

Generally, the calculated energy activation barriers for the decarboxylation of aromatic acids are high (ca. + 30 kcal.mol^{-1}),⁴⁷ which explained the need for high temperatures in copper catalyzed processes^{36,42,47} or non-catalyzed reactions.^{48,49} Numerous computational investigations have been made to uncover the transitions states structures of the decarboxylation event.^{36,42} We therefore turned our attention to the thermodynamics of the reaction in order to rationalize our experimental results.

In order to obtain thermodynamic information on the CO_2 extrusion/insertion process in the above $(\text{phen}^*)\text{Cu}(\text{I})$ compounds, we therefore investigated, by density functional theory (DFT) calculations, the decarboxylation step in complexes $[(\text{phen}^*)\text{Cu}(\text{O}_2\text{CR})]$ ($\text{R} = \text{C}_6\text{H}_5$, C_6F_5 , $o/p\text{-F-C}_6\text{H}_4$, CF_3 , $o/p\text{-NO}_2\text{-C}_6\text{H}_4$). Our first step was to optimize and obtain the Gibbs free energies of all copper complexes and of $[(\text{phen}^*)\text{Cu}(\text{O}_2\text{CC}_6\text{H}_5)]$ for comparison as a non-substituted benzoate substrate at the DFT M06L/Def2TZVP/W06⁵⁰⁻⁵² level. To understand the electronic influences of the *ortho* and *para*-substituents R on the phenyl ring, we next calculated the enthalpy and Gibbs free energy of the reaction, e.g. ΔH_r and ΔG_r .

In the case of $[(\text{phen}^*)\text{Cu}(\text{C}_6\text{F}_5)]$ (**8**), $[(\text{phen}^*)\text{Cu}(\text{C}_6\text{H}_4\text{-}o\text{-NO}_2)]$ (**9**), and $[(\text{phen}^*)\text{Cu}(\text{CF}_3)]$ (**11**), the DFT optimized geometries are in good agreement with the X-ray structures (Figure 52). The structures of these complexes have copper centers out of the phenanthroline ligand plane. In addition, the calculated phenanthroline moieties of **8** and **9** show a slight deviation of planarity, which is effectively observed in the corresponding crystal structures. The differences in distances from copper atom to the phen mean plane between the calculated structures and the crystal structures are likely due to crystal

packing effects in the solid state, which is not accounted in our level of calculations. In fact, all the calculated geometries of $[(\text{phen}^*)\text{Cu}(\text{R})]$ complexes show the copper ion out of the phen mean plane and a longer Cu1–C21 bond (Table 7, see more details in SI). This suggests an important role of steric factors in the interactions of the copper ion with the R ligand caused by the *tert*-butyl groups rather than electronic effects of substituents. For the carboxylate complexes (**0–7**), the optimized geometries showed a completely planar phenanthroline moiety and very small ($\text{R} = \text{C}_6\text{H}_5$, C_6F_5 , *o*- $\text{F-C}_6\text{H}_4$, *o*- $\text{NO}_2\text{-C}_6\text{H}_4$, CF_3) or no copper displacement ($\text{R} = p\text{-F-C}_6\text{H}_4$, *p*- $\text{NO}_2\text{-C}_6\text{H}_4$). It is noteworthy that the *p*- NO_2 and *p*- F substituents gave the optimized structures with the aromatic rings of benzoic acid in the same plane with the phen moiety. Again, these results can be attributed to the steric bulk around the copper ion, which is minimized with *p*- NO_2 and *p*- F substituents. Nonetheless, additional insights into the impact of electronic properties of the substituents on the R group by DFT calculations are required to support our hypothesis.

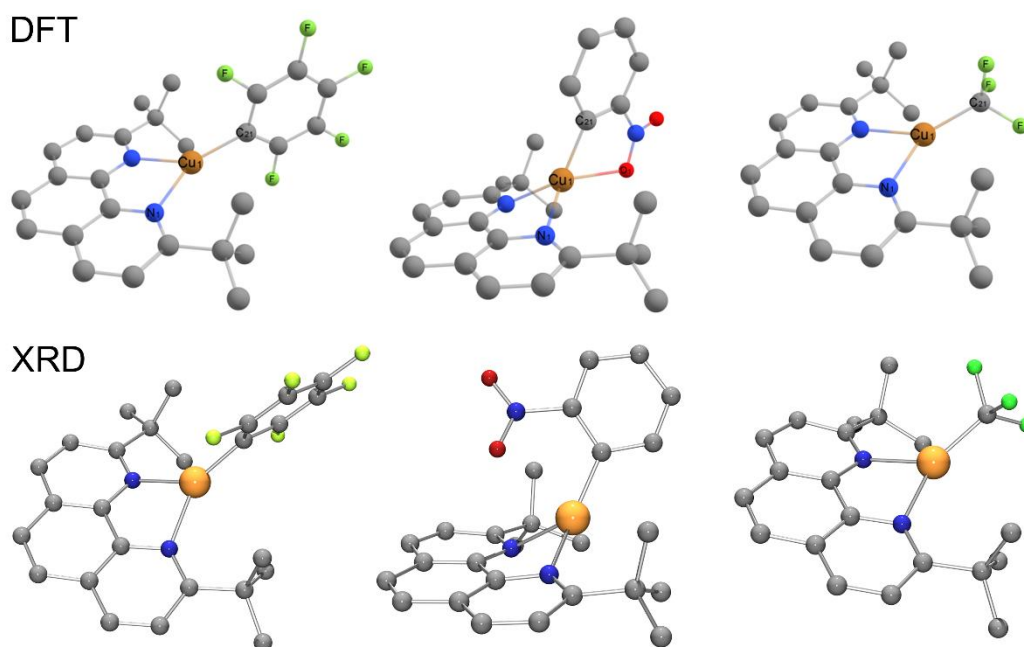


Figure 52. Top: Calculated structures of complexes (from left to right) $[(\text{phen}^*)\text{Cu}(\text{C}_6\text{F}_5)]$ (**8**), $[(\text{phen}^*)\text{Cu}(\text{C}_6\text{H}_4\text{-}o\text{-NO}_2)]$ (**9**), and $[(\text{phen}^*)\text{Cu}(\text{CF}_3)]$ (**11**) by DFT calculations. Bottom: Single crystal structures by XRD of (from left to right) $[(\text{phen}^*)\text{Cu}(\text{C}_6\text{F}_5)]$ (**8**), $[(\text{phen}^*)\text{Cu}(\text{C}_6\text{H}_4\text{-}o\text{-NO}_2)]$ (**9**), and $[(\text{phen}^*)\text{Cu}(\text{CF}_3)]$ (**11**).

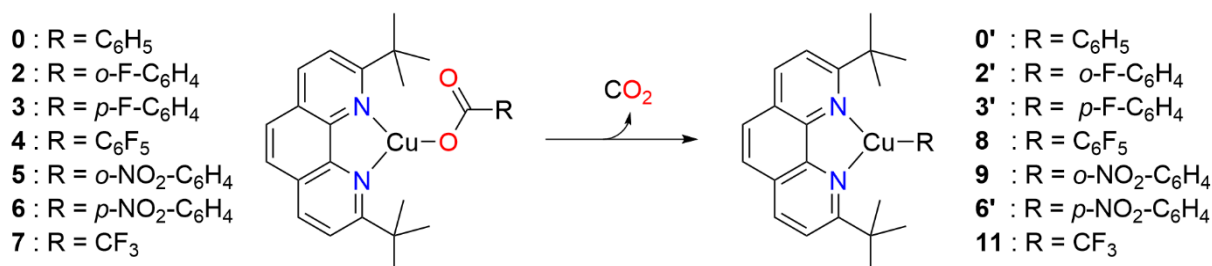
^a Numbers in blue color were computed at the M06L/Def2TZVP/W06 level of theory

Complex	Cu1–C (Å)	Cu1–N1(Å)	Cu1⋯O1(Å)	Cu1–phen*(plane) (Å)
$[(\text{phen}^*)\text{Cu}(\text{C}_6\text{F}_5)]$ (8)	1.9230(19) 1.956	2.1105(15) 2.146	-- --	0.8033(12) 0.314
$[(\text{phen}^*)\text{Cu}(\text{C}_6\text{H}_4\text{-}o\text{-NO}_2)]$ (9)	1.9080(17) 1.982	2.0131(14) 2.060	2.6593(13) 2.677	1.0031(10) 0.578
$[(\text{phen}^*)\text{Cu}(\text{CF}_3)]$ (11)	1.9296(13) 1.986	2.0503(11) 2.167	-- --	0.8368(8) 0.291

Table 7. Selected bond lengths and copper displacement from the phen mean plane for $[(\text{phen}^*)\text{Cu}(\text{C}_6\text{F}_5)]$ (**8**) and $[(\text{phen}^*)\text{Cu}(\text{C}_6\text{H}_4\text{-}o\text{-NO}_2)]$ (**9**) from single crystal X-ray diffraction experiments and DFT calculation.^a

In term of reactivity, the Gibbs free energy (ΔG) and free enthalpies (ΔH) of the reaction in the two solvents quinoline and THF, at room temperature ($T = 298$ K) are computed and the results are displayed in Table 8.

A view from Table 8 shows that the decarboxylation reaction is thermodynamically favored only with the polyfluoro-complexes **4** and **7** and the *ortho*- and *para*-nitro benzoate species **5** and **6** while for the other compounds the thermodynamics is not favorable. The overall reaction of complex **4** is an exergonic process with the reaction free energy of -11.62 kcal.mol⁻¹, whereas the well-known *o*-NO₂ substituent is second to favor the decarboxylation process ($\Delta G_r = -1.72$ kcal.mol⁻¹). The *ortho* effect was detected, where *o*-NO₂ ($\Delta G_r = -1.72$ kcal.mol⁻¹) and *o*-F ($\Delta G_r = 0.52$ kcal.mol⁻¹) give lower reaction free energy than the *para*-substituents (*p*-NO₂ and *p*-F, $\Delta G_r = -0.49$ and 6.58 kcal.mol⁻¹, respectively). Interestingly, electronic effects seem to dominate over *ortho* effects since the *p*-NO₂ of complex **6** gives a lower ΔG_r (-0.49 kcal.mol⁻¹) than *o*-F, which is an endergonic process of $\Delta G_r = 0.52$ kcal.mol⁻¹. In fact, a clear correlation between the thermodynamics of the reaction and the electronic properties of the substituent is observed, that follows the trend: H < F < NO₂ < F₅, where withdrawing substituents significantly reduce ΔG_r . The alkyl carboxylate complex **7** (CF₃) lies between the aryl derivatives with F₅ and *o*-NO₂ substituents with $\Delta G_r = -3.44$ kcal.mol⁻¹. It is noteworthy that studies by the groups of Gooßen and Xue on the *ortho* effect of substituents on the decarboxylation reactions gave similar results.^{36,53} Moreover, these values of ΔG_r (-11.62 , -3.44 , -1.72 , and -0.49 kcal.mol⁻¹) underline that decarboxylation would be more favorable for the [(phen*)Cu(O₂CR)] complexes than for their [(phen)Cu(O₂CR)] counterparts. For instance, the decarboxylation step of [(phen)Cu(O₂CR)] when R = C₆H₅, C₆H₄-*o*/*p*-NO₂, C₆H₄-*o*/*p*-F, C₆H₄-*o*/*p*-OMe, or C₆H₄-*p*-Me is endergonic at room temperature.³⁶



Complex	R	ΔH_r	ΔG_r	ΔH_r	ΔG_r
		in quinoline	in quinoline	in THF	in THF
0	R = C ₆ H ₅	21.45	8.80	21.02	10.41
2	R = <i>o</i> -F-C ₆ H ₄	11.52	0.52	11.04	1.75
3	R = <i>p</i> -F-C ₆ H ₄	16.86	6.58	17.09	6.89
4	R = C ₆ F ₅	0.48	-11.62	0.73	-11.39
5	R = <i>o</i> -NO ₂ -C ₆ H ₄	8.92	-1.72	9.21	-1.37
6	R = <i>p</i> -NO ₂ -C ₆ H ₄	12.16	-0.49	--	--
7	R = CF ₃	7.77	-3.44	7.98	-3.37

Computational parameters: Gaussian 16 suite of software, Rev. C01;⁵⁴ M06L-D3,⁵⁵ Def2TZVP/W06,⁵⁰⁻⁵² Solvation effects were accounted for with the SMD model;⁵⁶ ΔH_r and ΔG_r are expressed in kcal.mol⁻¹

Table 8. Selected results from the DFT calculations on the decarboxylation of [(phen*)Cu(O₂CC₆H₄R)].

The ΔG_r values in THF are close to those found in quinoline and follow the same pattern. However, as observed experimentally, the solvent is crucial: none of the isolated copper carboxylate underwent CO₂ extrusion in THF while the complexes [(phen*)Cu(O₂CC₆F₅)] (**4**), [(phen*)Cu(O₂CC₆H₄-*o*-NO₂)] (**5**) and [(phen*)Cu(O₂CC₆H₄-*o*-F)] (**2**) decarboxylated readily in quinoline at different applied temperatures.

In agreement with our experimental results, we found that the decarboxylation of [(phen*)Cu(O₂CC₆F₅)] is exergonic ($\Delta G_r = -11.62 \text{ kcal.mol}^{-1}$), and complex **4** is the most prone to CO₂ loss in the series we studied. This is in agreement with the previous reports by Liu who demonstrated experimentally and theoretically that copper-mediated decarboxylation process is energetically favored with the electron deficient C₆F₅ fragment.⁴² The energy barrier for the decarboxylation of [(phen)Cu(O₂CC₆F₅)] was +20.3 kcal.mol⁻¹,⁴² which is a gap easily overcome by heating. In addition, the strongly favorable thermodynamics for the formation of [(phen*)Cu(C₆F₅)] (**8**) from its carboxylate ($\Delta G_r = -11.39 \text{ kcal.mol}^{-1}$) explained why this complex could not give back **4** under CO₂ (*vide supra*, III. 5. – Table 6, entries 1–3).

Decarboxylation of **5** bearing an *ortho* nitro group is only slightly exergonic ($\Delta G_r = -1.72 \text{ kcal.mol}^{-1}$), which is matched with our experimental observation where [(phen*)Cu(O₂CC₆H₄-*o*-NO₂)] decarboxylate in quinoline at higher temperature (170 °C) (*vide supra*, III. 4. 2. – Table 5, entries 5 and 6). Calculated ΔG_r for the decarboxylation of compound **2** suggests a slightly endothermic process of $\Delta G = 0.52 \text{ kcal.mol}^{-1}$ at 298 K in quinoline. This is plausible as decarboxylated product from **2** is accessible energetically and can react further experimentally (*vide supra*, III. 4. 2. – Table 5, entry 1). Moreover, it has been reported that the decarboxylation process using copper-phenanthroline catalyst, while endergonic at room temperature, became exergonic at high temperature (170 °C, 443 K), as calculated on 2-fluoro-substituted benzoic acid.⁴⁷ Additionally, the same report also gave some insight into the ligand effect: electron-rich substituents on the 4,7-positions of phenanthroline favor decarboxylation, while neocuproine can decrease the reactivity due to its steric hindrance.³⁶

Overall, DFT calculations for a general thermodynamic overview of the stoichiometric decarboxylation of [(phen*)Cu(O₂CR)] to [(phen*)Cu(R)], with R = H, *o/p*-NO₂, *o/p*-F, C₆F₅ and CF₃ has been computed. The reaction is exergonic for complexes bearing electron-withdrawing substituents in the benzoic rings with ΔG_r is in a range of -11.62 to $-0.49 \text{ kcal.mol}^{-1}$ (complex **4–7**). Meanwhile, decarboxylation of non-substituted and *ortho*- and *para*-fluoro benzoate species **0**, **2** and **3** is thermodynamically unfavorable. It is evident that the reactivity of these complexes have a strong correlation with electronic properties of the substituents on the aromatic rings. The famous *ortho* effect is evidenced, but is less important than the electronic effect. Importantly, the calculated reaction energies are in agreement with our experimental results, supporting a plausible decarboxylation event occur via [(phen*)Cu(O₂CR)] (R = C₆F₅, *o*-NO₂, *o*-F).

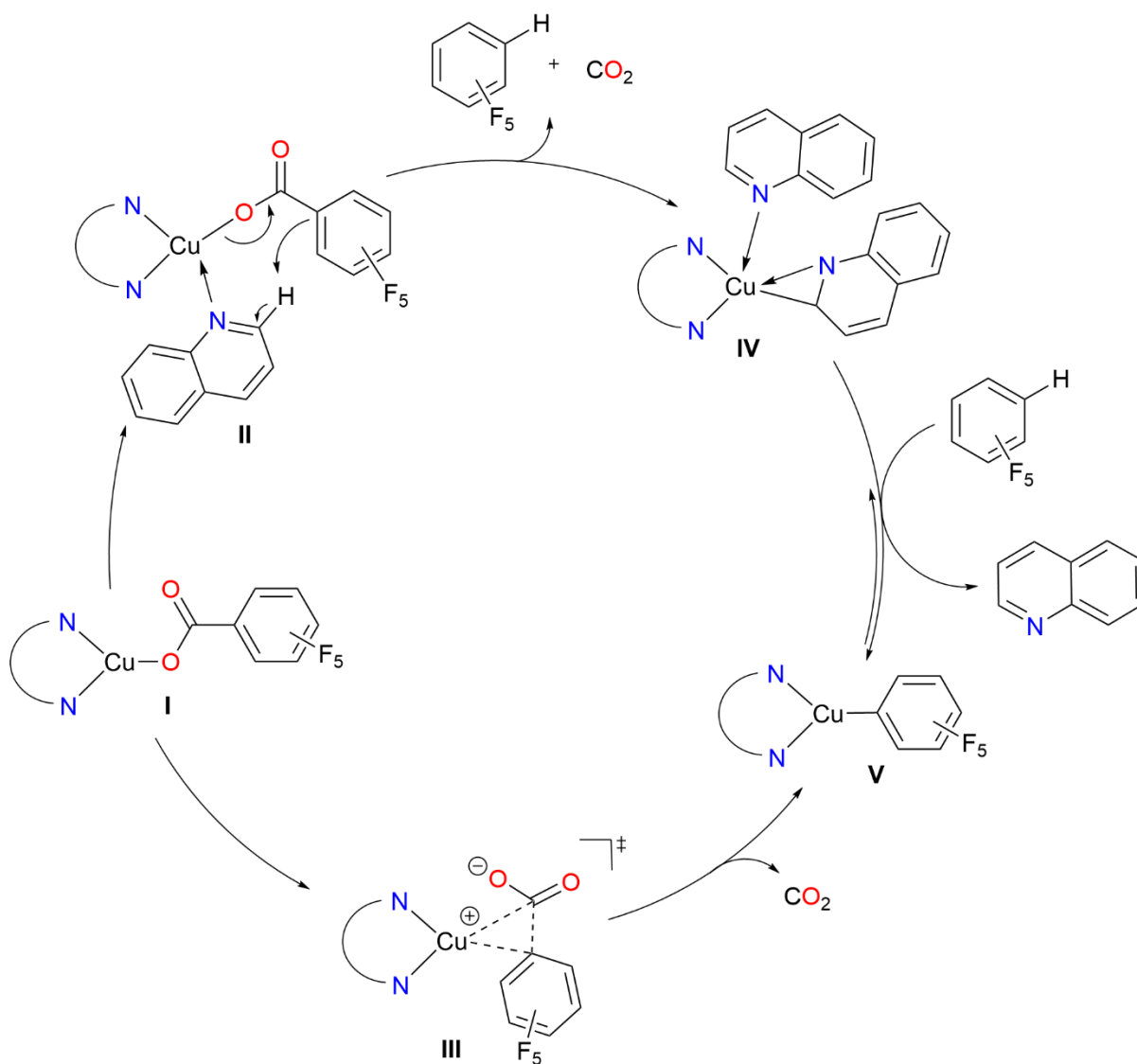
III. 7. Proposed mechanism

Here, based on the results obtained from the two complexes **4** and **5**, we focus on rationalizing the decarboxylation and protodecarboxylation processes. It is important to reiterate that there are differences in term of reactivity related to the choice of solvent, namely THF and quinoline. Furthermore, it is evident that the protodecarboxylation process preceds the formation of the copper-

aryl complex (Table 5, entries 2–4), we thus assumed there are several possible mechanisms via different potential intermediates.

On the basis of our observations, and the conclusion of previous studies,^{38,47,53} the mechanism could be described as follows (Scheme 52).

Based on the reactivity of complex **4** [(phen*)Cu(O₂CC₆F₅)] in quinoline, we proposed a general decarboxylation and protodecarboxylation mechanism with two pathways connected by a copper(I) aryl intermediate (*Scheme 52*). We first considered that CO₂ extrusion of copper carboxylate complex **I** occurs via a concerted mechanism, as proposed by Gooßen and Lin,^{47,53} to form an organocopper species (**V**) via a transition state **III**. This TS is drawn closely based on the computed structure done by Gooßen.⁴⁷ However, this mechanistic approach cannot explain why the formation of C₆F₅H is observed before the formation of the complex [(phen*)Cu(C₆F₅)] (**8**) if traces of water present in the reaction medium are excluded (*vide supra*, III. 4. 2.).

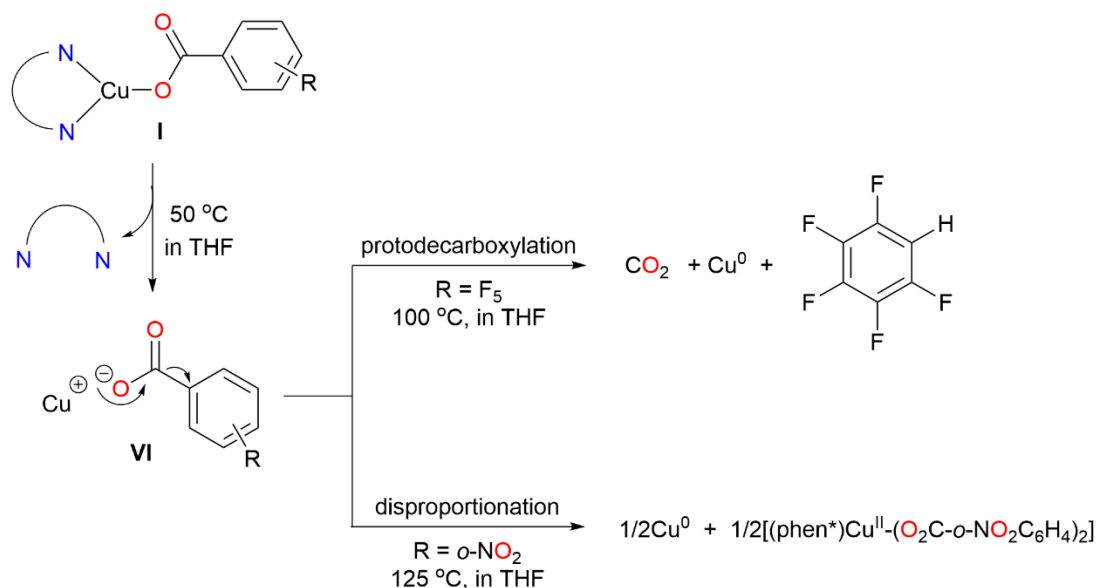


Scheme 52. Proposed mechanism for the decarboxylation of [(phen*)Cu(O₂CC₆F₅)] (**4**) in quinoline.

Alternatively, a second path emerged (*Scheme 52*). It started with the coordination of quinoline (Q) into copper carboxylate **I** to generate intermediate **II** [(phen*)Cu(O₂CC₆F₅)(Q)]. The coordination of quinoline, would completely displace the phen* ligand, as evidenced by the broadened fluorine signals C₆F₅⁻ moiety (*Figure 43a*). We assumed that a fourth coordination into the copper (I) center is possible, although there is no solid evidence for this species. This is because the tetracoordinated copper complexes are well described in the literature, where numerous structures of copper at oxidation state +2 have been published.^{57–60} The next step in the second pathway is the protodecarboxylation of species **II** to give CO₂ and arene in a single step. The abstracted hydrogen of quinoline can be at the 2-position (*ortho* to the pyridine ring) or in the 8-position, since these are acidic protons. This hypothesis is supported by Cohen's investigation of the proton source, in which they obtained a monodeuterated product using 2-deuterioquinoline as a solvent.³⁸ After the deprotonation, anionic quinoline (Q⁻) binded to copper and made an ionic complex **IV** [(phen*)Cu]⁺[Q]⁻. This complex would be stabilized as [(phen*)Cu(Q)_n]⁺[Q]⁻ by additional coordination of quinoline. A proton abstraction by anionic quinoline (Q⁻) from the generated arene finally yields the copper(I) aryl species (**V**). Experimental evidence has shown that the copper aryl complex **8** can indeed be easily converted into C₆F₅H in quinoline at room temperature (*vide supra*, *III. 4. 2.*), suggesting that the reverse transformation of intermediate **V** into **IV** is possible. In this pathway, the order of formation of the protodecarboxylation product and the copper aryl species would be in accordance with the experimental results.

Nonetheless, the concerted pathway is not excluded since the calculated mechanisms involved various benzoic acid derivatives^{47,53} rather than pentafluoro-substituted carboxylate. In the meantime, the results obtained from the complex [(phen*)Cu(O₂CC₆F₅)] (**4**) are the sole basis of our hypothesis. In addition, CO₂ extrusion of other copper carboxylate complexes [(phen*)Cu(O₂CC₆H₄-*o*-F)] (**2**) and [(phen*)Cu(O₂CC₆H₄-*o*-NO₂)] (**5**) only afforded arene compounds without the formation of corresponding decarboxylated copper aryl species [(phen*)Cu(C₆H₄-*o*-F)], and [(phen*)Cu(C₆H₄-*o*-NO₂)] (**9**), respectively.

Experimental results showed that the decoordination of the phen* ligand precedes the protodecarboxylation event in particular in THF (*vide supra*, *III. 4. 1.*, *Figure 41* and *Figure 42*). We therefore hypothesized that in THF, the CO₂ extrusion might occurs via intermediate [Cu(O₂C-Ar)], followed by degradation of the copper complex at higher temperatures (*ca.* 100 °C). This may be due to the poor stability of the copper intermediate provided by the THF ligand. The proposed mechanism starts with the displacement of phen* from the copper species (**I**) to form the ionic species **VI** (*Scheme 53*). At elevated temperatures, this species either goes through protodecarboxylation and degradation (in the case of complex **4**) or disproportionation (in the case of complex **5**) to ultimately produced Cu⁰.



Scheme 53. Proposal for the decarboxylation of $[(\text{phen}^*)\text{Cu}(\text{O}_2\text{CC}_6\text{F}_5)]$ (**4**) and $[(\text{phen}^*)\text{Cu}(\text{O}_2\text{CC}_6\text{H}_4\text{-}o\text{-NO}_2)]$ (**5**) in THF.

IV. Conclusion

In summary, the crystal structure of the bulky phenanthroline 2,9-*t*Bu₂phen (phen*) has been determined and a series of copper(I) complexes involving this ligand have been synthesized, isolated and structurally characterized. The species $[(\text{phen}^*)\text{Cu}(\text{O}_2\text{CR})]$ (R = *o*-F-C₆H₄ (**2**), *p*-F-C₆H₄ (**3**), C₆F₅ (**4**), *o*-NO₂-C₆H₄ (**5**), *p*-NO₂-C₆H₄ (**6**), CF₃ (**7**)) and aryl/alkyl counterparts $[(\text{phen}^*)\text{CuR}]$ (R = C₆F₅ (**8**), *o*-NO₂-C₆H₄ (**9**), CF₃ (**11**)) are among the rare isolated copper(I) complexes with higher thermal stability and solubility than existing copper complexes. These improvements allow us to carry out mechanistic studies in common solvents such as THF or in thermal condition.

Using these compounds, we studied decarboxylation reaction of $[(\text{phen}^*)\text{Cu}(\text{O}_2\text{CR})]$ complexes and the reverse carboxylation process with the organometallic derivatives. The loss of CO₂ in the $[(\text{phen}^*)\text{Cu}(\text{O}_2\text{CR})]$ complexes (R = *o*-F-C₆H₄ (**2**), C₆F₅ (**4**), *o*-NO₂-C₆H₄ (**5**), CF₃ (**7**)) was successful, except for complex **7**, especially in quinoline. However, the carboxylation of the alkyl and aryl $[(\text{phen}^*)\text{CuR}]$ complexes did not take place as expected. This can be explained by different factors, such as the stability of the complexes and the competitive protodecarboxylation reaction. Rationalization of these data using DFT corroborates the experimental results.

We can propose for $[(\text{phen}^*)\text{Cu}(\text{O}_2\text{CC}_6\text{F}_5)]$ (**4**) a decarboxylation process via the intermediate $[(\text{phen}^*)\text{Cu}(\text{C}_6\text{F}_5)]$ (**8**) when using quinoline as solvent. However, the loss of CO₂ from the complexes $[(\text{phen}^*)\text{Cu}(\text{O}_2\text{CC}_6\text{H}_4\text{-}o\text{-F})]$ (**2**) and $[(\text{phen}^*)\text{Cu}(\text{O}_2\text{CC}_6\text{H}_4\text{-}o\text{-NO}_2)]$ (**5**) in quinoline did not afford the desired decarboxylated species $[(\text{phen}^*)\text{Cu}(\text{C}_6\text{H}_4\text{-}o\text{-F})]$ and $[(\text{phen}^*)\text{Cu}(\text{C}_6\text{H}_4\text{-}o\text{-NO}_2)]$ (**9**) but only the protodecarboxylation products fluorobenzene and nitrobenzene, respectively. Nonetheless, in THF, only $[(\text{phen}^*)\text{Cu}(\text{O}_2\text{CC}_6\text{F}_5)]$ (**4**) underwent protodecarboxylation.

DFT calculations with including solvent effects gave similar results regarding the thermodynamic of the reactions with both quinoline and THF. On the other hand, experimental results showed that copper carboxylate complexes decarboxylate more readily in quinoline than in THF. For example,

protodecarboxylation was observed only for complex **4** at 100 °C (1 h) in THF, whereas the process occurred at 35 °C (1 h) in quinoline. In addition, complexes **2** and **5** underwent protodecarboxylation in quinoline (120 °C after 72 h, and 150 °C after 17 h, respectively), while the reactions were not observed in THF. Quinoline did not displace phen* but proved a better solvent than THF for the decarboxylation of the carboxylic complexes [(phen*)Cu(O₂CAr)]. This might support, through additional coordination at the metal center, the formation of intermediate more stabilized against degradation and which are thus more prone to decarboxylation. It is also thought that protodecarboxylation predominates over decarboxylation because quinoline acts as a proton source. Thus, quinoline solvent is critical for CO₂ extrusion, while phen* ligand has the ability to stabilize intermediates that capture aryl moiety. Both elements are critical to decarboxylation.

Regarding the mechanism, three different pathways have been proposed, devoted to the decarboxylation and protodecarboxylation process of complexes **4** and **5**, particularly in quinoline and THF solvents. We considered the concerted decarboxylation mechanism proposed by the Gooßen and Lin groups,^{47,53} where CO₂ is extruded from the copper carboxylate complex to the copper aryls in one single step. However, this mechanism does not explain the formation of the protodecarboxylate C₆F₅ before the generation of the copper aryl species. Therefore, we proposed a second pathway, in which the role of quinoline is highlighted: quinoline first coordinates to the copper carboxylate complex, followed by concerted CO₂ extrusion and proton abstraction to produce C₆F₅H and an ionic [(phen*)Cu]⁺[Q]⁻ species (Q = quinoline). Alternatively, in THF, a distinct mechanism has emerged in which phen* is first displaced by the solvent to form [Cu(O₂CR)(THF)_n] (R = C₆F₅ (**4**), *o*-NO₂-C₆H₄ (**5**)). This latter species, not stabilized by the phen* ligand, rapidly disproportionates to form copper(0) and the copper(II) carboxylate [Cu(O₂CR)₂(THF)_n] (in the case of complex **5**). In contrast, protodecarboxylation is mainly observed for complex **4**.

V. References

- (1) Destro, G.; Loreau, O.; Marcon, E.; Taran, F.; Cantat, T.; Audisio, D. Dynamic Carbon Isotope Exchange of Pharmaceuticals with Labeled CO₂. *J. Am. Chem. Soc.* **2019**, *141* (2), 780–784. <https://doi.org/10.1021/jacs.8b12140>.
- (2) Hietsoi, O.; Filatov, A. S.; Dubceac, C.; Petrukhina, M. A. Structural Diversity and Photoluminescence of Copper(I) Carboxylates: From Discrete Complexes to Infinite Metal-Based Wires and Helices. *Coordination Chemistry Reviews* **2015**, *295*, 125–138. <https://doi.org/10.1016/j.ccr.2015.03.009>.
- (3) Edwards, D., A.; Richards, R. Copper(I) Carboxylates: Preparations and Infrared and Mass Spectral Features. *J. Chem. Soc., Dalton Trans* **1973**, 2463–2468.
- (4) Louka, F. R.; Haq, S. J.; Guidry, H. R.; Williams, B. R.; Henary, M. M.; Fischer, R. C.; Torvisco, A.; Massoud, S. S.; Mautner, F. A. Polynuclear and Coordination Polymers of Copper(II) Complexes Assembled by Flexible Polyamines and Bridging Rigid N-Heterocyclic Multicarboxylates. *Inorganica Chimica Acta* **2020**, *500*, 119240. <https://doi.org/10.1016/j.ica.2019.119240>.
- (5) Aalten, H. L.; Van Koten, G.; Goubitz, K.; Stam, C. H. The Hurtley Reaction. 1. Synthesis and Characterization of Copper(I) Benzoates Containing Reactive Ortho C-X (X = Cl, Br) Bonds and Their Reactivity toward Organocopper(I) Compounds: Crystal Structure of a Thermally Stable Trinuclear Hetero Copper(I) Cluster, Bis(Benzoato)Mesityltricopper(I). *Organometallics* **1989**, *8* (10), 2293–2299. <https://doi.org/10.1021/om00112a001>.
- (6) Tsuda, T.; Hashimoto, T.; Saegusa, T. Cuprous Tert-Butoxide. New and Useful Metalation Reagent. *J. Am. Chem. Soc.* **1972**, *94* (2), 658–659. <https://doi.org/10.1021/ja00757a069>.
- (7) Whitesides, G. M.; Sadowski, J. S.; Lilburn, J. Copper(I) Alkoxides. Synthesis, Reactions, and Thermal Decompositions. *J. Am. Chem. Soc.* **1974**, *96* (9), 2829–2835. <https://doi.org/10.1021/ja00816a027>.
- (8) Greiser, T.; Weiss, E. Kristallstruktur des Kupfer(I) -tert -butoxids, [CH₃]₃COCu]₄. *Chem. Ber.* **1976**, *109* (9), 3142–3146. <https://doi.org/10.1002/cber.19761090920>.
- (9) Jeffries, P. M.; Dubois, L. H.; Girolami, G. S. Metal-Organic Chemical Vapor Deposition of Copper and Copper(I) Oxide from Copper(I)Tert-Butoxide. *Chem. Mater.* **1992**, *4* (6), 1169–1175. <https://doi.org/10.1021/cm00024a013>.
- (10) Saijo, H.; Ohashi, M.; Ogoshi, S. Fluoroalkylcopper(I) Complexes Generated by the Carbocupration of Tetrafluoroethylene: Construction of a Tetrafluoroethylene-Bridging Structure. *J. Am. Chem. Soc.* **2014**, *136* (43), 15158–15161. <https://doi.org/10.1021/ja5093776>.
- (11) Baur, A.; Bustin, K. A.; Aguilera, E.; Petersen, J. L.; Hoover, J. M. Copper and Silver Benzoate and Aryl Complexes and Their Implications for Oxidative Decarboxylative Coupling Reactions. *Org. Chem. Front.* **2017**, *4* (4), 519–524. <https://doi.org/10.1039/C6QO00678G>.
- (12) Do, H.-Q.; Khan, R. M. K.; Daugulis, O. A General Method for Copper-Catalyzed Arylation of Arene C–H Bonds. *J. Am. Chem. Soc.* **2008**, *130* (45), 15185–15192. <https://doi.org/10.1021/ja805688p>.
- (13) Pallenberg, A. J.; Koenig, K. S.; Barnhart, D. M. Synthesis and Characterization of Some Copper(I) Phenanthroline Complexes. *Inorg. Chem.* **1995**, *34* (11), 2833–2840. <https://doi.org/10.1021/ic00115a009>.

- (14) Gandhi, B. A.; Green, O.; Burstyn, J. N. Facile Oxidation-Based Synthesis of Sterically Encumbered Four-Coordinate Bis(2,9-Di-*Tert*-Butyl-1,10-Phenanthroline)Copper(I) and Related Three-Coordinate Copper(I) Complexes. *Inorg. Chem.* **2007**, *46* (10), 3816–3825. <https://doi.org/10.1021/ic0615224>.
- (15) Wang, T.; Chen, F.; Qin, J.; He, Y.-M.; Fan, Q.-H. Asymmetric Ruthenium-Catalyzed Hydrogenation of 2- and 2,9-Substituted 1,10-Phenanthrolines. *Angew. Chem. Int. Ed.* **2013**, *52*, 7172–7176.
- (16) Dietrick-Buchecker, C. O.; Marnot, P. A.; Sauvage, J. P. Direct Synthesis of Disubstituted Aromatic Polyimine Chelates. *Tetrahedron Letters* **1982**, *23* (50), 5291–5294. [https://doi.org/10.1016/S0040-4039\(00\)85821-9](https://doi.org/10.1016/S0040-4039(00)85821-9).
- (17) Williams, N. J.; Gephart Iii, R. T.; Hames, A. E.; Reibenspies, J. H.; Luckay, R. C.; De Sousa, A. S.; Hancock, R. D. Affinity of Two Highly Preorganized Ligands for the Base Metal Ions Co(II), Ni(II) and Cu(II): A Thermodynamic, Crystallographic and Fluorometric Study. *Polyhedron* **2012**, *46* (1), 139–148. <https://doi.org/10.1016/j.poly.2012.08.013>.
- (18) Nitsch, J.; Kleeberg, C.; Fröhlich, R.; Steffen, A. Luminescent Copper(I) Halide and Pseudohalide Phenanthroline Complexes Revisited: Simple Structures, Complicated Excited State Behavior. *Dalton Trans.* **2015**, *44* (15), 6944–6960. <https://doi.org/10.1039/C4DT03706E>.
- (19) Huang, Y.-J.; Gui, Y.-C.; Du, G. Hydrothermal Synthesis and Crystal Structure of a Zero-Dimensional Copper(I) Complex with Isophthalic Acid and Medpq Ligands. *Chinese J. Inorg. Chem.* **2009**, *25* (10), 1882–1884.
- (20) Sun, J. μ_2 -Methanol- $\kappa^2 O$:*O*-Bis[(1,10-Phenanthroline- $\kappa^2 N, N'$)Bis(2,3,4,5-Tetrafluorobenzoato)- κO ; $\kappa^2 O, O'$]-Copper(II)]. *IUCrData* **2019**, *4* (11), x191583. <https://doi.org/10.1107/S2414314619015839>.
- (21) Groom, C. R.; Bruno, I. J.; Lightfoot, M. P.; Ward, S. C. The Cambridge Structural Database. *Acta Crystallogr B Struct Sci Cryst Eng Mater* **2016**, *72* (2), 171–179. <https://doi.org/10.1107/S2052520616003954>.
- (22) Zhang, S.; Wang, Z.; Zhang, H.; Cao, Y.; Sun, Y.; Chen, Y.; Huang, C.; Yu, X. Self-Assembly of Two Fluorescent Supramolecular Frameworks Constructed from Unsymmetrical Benzene Tricarboxylate and Bipyridine. *Inorganica Chimica Acta* **2007**, *360* (8), 2704–2710. <https://doi.org/10.1016/j.ica.2007.01.023>.
- (23) Zhai, C.; Yan, F.; Zhao, P. (2,9-Dimethyl-1,10-Phenanthroline- $\kappa^2 N, N'$)Bis(2-Hydroxybenzoato- κO)Copper(II). *Acta Crystallogr E Struct Rep Online* **2008**, *64* (12), m1526–m1527. <https://doi.org/10.1107/S1600536808036283>.
- (24) Zhao, P.; Yan, F.; Xuan, X.-P.; Tang, Q.-H. (2,9-Dimethyl-1,10-Phenanthroline) $\kappa^2 N, N'$)Bis(3-Hydroxybenzoato- κO) Copper(II). *Acta Crystallographica Section E Structure Reports Online* **2007**, *E63*, m2523.
- (25) Shannon, R. D. Revised Effective Ionic Radii and Systematic Studies of Interatomic Distances in Halides and Chalcogenides. *Acta crystallographica* **1976**, *A32*, 751–767.
- (26) Cairncross, A.; Sheppard, W. A. Fluorinated Organocopper Compounds. *J. Am. Chem. Soc.* **1968**, *90* (8), 2186–2187. <https://doi.org/10.1021/ja01010a050>.
- (27) Jäkle, F. Pentafluorophenyl Copper: Aggregation and Complexation Phenomena, Photoluminescence Properties, and Applications as Reagent in Organometallic Synthesis. *Dalton Trans.* **2007**, No. 27, 2851–2858. <https://doi.org/10.1039/B704372D>.

- (28) Doshi, A.; Sundararaman, A.; Venkatasubbaiah, K.; Zakharov, L. N.; Rheingold, A. L.; Myahkostupov, M.; Piotrowiak, P.; Jäkle, F. Pentafluorophenyl Copper–Pyridine Complexes: Synthesis, Supramolecular Structures via Cuprophilic and π -Stacking Interactions, and Solid-State Luminescence. *Organometallics* **2012**, *31* (4), 1546–1558. <https://doi.org/10.1021/om200989b>.
- (29) Morimoto, H.; Tsubogo, T.; Litvinas, N. D.; Hartwig, J. F. A Broadly Applicable Copper Reagent for Trifluoromethylations and Perfluoroalkylations of Aryl Iodides and Bromides. *Angew. Chem. Int. Ed.* **2011**, *50* (16), 3793–3798. <https://doi.org/10.1002/anie.201100633>.
- (30) Liu, Y.; Chen, C.; Li, H.; Huang, K.-W.; Tan, J.; Weng, Z. Efficient S_N2 Fluorination of Primary and Secondary Alkyl Bromides by Copper(I) Fluoride Complexes. *Organometallics* **2013**, *32* (21), 6587–6592. <https://doi.org/10.1021/om4008967>.
- (31) Fujihara, T.; Xu, T.; Semba, K.; Terao, J.; Tsuji, Y. Copper-Catalyzed Hydrocarboxylation of Alkynes Using Carbon Dioxide and Hydrosilanes. *Angew. Chem. Int. Ed.* **2011**, *50* (2), 523–527. <https://doi.org/10.1002/anie.201006292>.
- (32) Emsley, J.; Arif, M.; Bates, P. A.; Hursthouse, M. B. Aquadifluoro(1,10-Phenanthroline)Copper(II) Dihydrate: X-Ray Crystal Structure Reveals Strong Hydrogen Bonds between Ligand Fluoride and Lattice Water Molecules. *Journal of Crystallographic and Spectroscopic Research* **1987**, *17* (5), 605–613. <https://doi.org/10.1007/BF01167118>.
- (33) Vergote, T.; Nahra, F.; Welle, A.; Luhmer, M.; Wouters, J.; Mager, N.; Riant, O.; Leysens, T. Unprecedented Copper(I) Bifluoride Complexes: Synthesis, Characterization and Reactivity. *Chem. Eur. J.* **2012**, *18* (3), 793–798. <https://doi.org/10.1002/chem.201102655>.
- (34) Hall, J. W.; Seeberger, F.; Mahon, M. F.; Whittlesey, M. K. (Carbene)CuF Complexes Featuring Bulky Arduengo-Type, Ring-Expanded, and Cyclic (Alkyl)(Amino)Carbenes: Applications in Catalytic Aldehyde Allylation. *Organometallics* **2020**, *39* (1), 227–233. <https://doi.org/10.1021/acs.organomet.9b00772>.
- (35) Gulliver, D. J.; Levason, W.; Webster, M. Coordination Stabilised Copper(I) Fluoride. Crystal and Molecular Structure of Fluorotris(Triphenylphosphine)Copper(I)*Ethanol (I/2), Cu(PPh₃)₃F·2EtOH. **1981**, *52*, 153–159.
- (36) Gooßen, L. J.; Thiel, W. R.; Rodríguez, N.; Linder, C.; Melzer, B. Copper-Catalyzed Protodecarboxylation of Aromatic Carboxylic Acids. *Adv. Synth. Catal.* **2007**, *349* (14–15), 2241–2246. <https://doi.org/10.1002/adsc.200700223>.
- (37) Cairncross, A.; Roland, J. R.; Henderson, R. M.; Sheppard, W. A. Organocopper Intermediates via Decarboxylation of Cuprous Carboxylates. *J. Am. Chem. Soc.* **1970**, *92* (10), 3187–3189. <https://doi.org/10.1021/ja00713a046>.
- (38) Cohen, T.; Berninger, R. W.; Wood, J. T. Products and Kinetics of Decarboxylation of Activated and Unactivated Aromatic Cuprous Carboxylates in Pyridine and in Quinoline. *J. Org. Chem.* **1978**, *43* (5), 837–848. <https://doi.org/10.1021/jo00399a010>.
- (39) Faulkner, A.; Scott, J. S.; Bower, J. F. An Umpolung Approach to Alkene Carboamination: Palladium Catalyzed 1,2-Amino-Acylation, -Carboxylation, -Arylation, -Vinylolation, and -Alkynylation. *J. Am. Chem. Soc.* **2015**, *137* (22), 7224–7230. <https://doi.org/10.1021/jacs.5b03732>.
- (40) Gooßen, L. J.; Deng, G.; Levy, L. M. Synthesis of Biaryls via Catalytic Decarboxylative Coupling. *Science* **2006**, *313* (5787), 662–664. <https://doi.org/10.1126/science.1128684>.

- (41) Goossen, L. J.; Rodríguez, N.; Linder, C. Decarboxylative Biaryl Synthesis from Aromatic Carboxylates and Aryl Triflates. *J. Am. Chem. Soc.* **2008**, *130* (46), 15248–15249. <https://doi.org/10.1021/ja8050926>.
- (42) Shang, R.; Fu, Y.; Wang, Y.; Xu, Q.; Yu, H.-Z.; Liu, L. Copper-Catalyzed Decarboxylative Cross-Coupling of Potassium Polyfluorobenzoates with Aryl Iodides and Bromides. *Angew. Chem. Int. Ed.* **2009**, *48* (49), 9350–9354. <https://doi.org/10.1002/anie.200904916>.
- (43) Fu, Z.; Li, Z.; Xiong, Q.; Cai, H. Facile Synthesis of 2,2'-Dinitrosubstituted Biaryls through Cu-Catalyzed Ligand-Free Decarboxylative Homocoupling of Ortho-Nitrobenzoic Acids. *RSC Adv.* **2015**, *5* (64), 52101–52104. <https://doi.org/10.1039/C5RA07771K>.
- (44) Gooßen, L. J.; Zimmermann, B.; Knauber, T. Pd-Catalyzed Decarboxylative Heck Vinylation of 2-Nitrobenzoates in the Presence of CuF₂. *Beilstein J. Org. Chem.* **2010**, *6*. <https://doi.org/10.3762/bjoc.6.43>.
- (45) DePasquale, R. J.; Tamborski, C. Reactions of Pentafluorophenylcopper Reagent. *J. Org. Chem.* **1969**, *34* (6), 1736–1740. <https://doi.org/10.1021/jo01258a046>.
- (46) Tran-Vu, H.; Daugulis, O. Copper-Catalyzed Carboxylation of Aryl Iodides with Carbon Dioxide. *ACS Catal.* **2013**, *3* (10), 2417–2420. <https://doi.org/10.1021/cs400443p>.
- (47) Gooßen, L. J.; Rodríguez, N.; Linder, C.; Lange, P. P.; Fromm, A. Comparative Study of Copper- and Silver-Catalyzed Protodecarboxylations of Carboxylic Acids. *ChemCatChem* **2010**, *2* (4), 430–442. <https://doi.org/10.1002/cctc.200900277>.
- (48) Li, J.; Brill, T. B. Spectroscopy of Hydrothermal Reactions 23: The Effect of OH Substitution on the Rates and Mechanisms of Decarboxylation of Benzoic Acid. *J. Phys. Chem. A* **2003**, *107* (15), 2667–2673. <https://doi.org/10.1021/jp0220231>.
- (49) Chuchev, K.; BelBruno, J. J. Mechanisms of Decarboxylation of Ortho-Substituted Benzoic Acids. *Journal of Molecular Structure: THEOCHEM* **2007**, *807* (1–3), 1–9. <https://doi.org/10.1016/j.theochem.2006.12.004>.
- (50) Weigend, F.; Ahlrichs, R. Balanced Basis Sets of Split Valence, Triple Zeta Valence and Quadruple Zeta Valence Quality for H to Rn: Design and Assessment of Accuracy. *Phys. Chem. Chem. Phys.* **2005**, *7* (18), 3297. <https://doi.org/10.1039/b508541a>.
- (51) Weigend, F. Accurate Coulomb-Fitting Basis Sets for H to Rn. *Phys. Chem. Chem. Phys.* **2006**, *8* (9), 1057. <https://doi.org/10.1039/b515623h>.
- (52) Rappoport, D.; Furche, F. Property-Optimized Gaussian Basis Sets for Molecular Response Calculations. *The Journal of Chemical Physics* **2010**, *133* (13), 134105. <https://doi.org/10.1063/1.3484283>.
- (53) Xue, L.; Su, W.; Lin, Z. Mechanism of Silver- and Copper-Catalyzed Decarboxylation Reactions of Aryl Carboxylic Acids. *Dalton Trans.* **2011**, *40* (44), 11926. <https://doi.org/10.1039/c1dt10771b>.
- (54) Gaussian 16 Rev C.01, M. J. Frisch, G. W. Trucks, H. B. Schlegel, G. E. Scuseria, M. A. Robb, J. R. Cheeseman, G. Scalmani, V. Barone, G. A. Petersson, H. Nakatsuji, X. Li, M. Caricato, A. V. Marenich, J. Bloino, B. G. Janesko, R. Gomperts, B. Mennucci, H. P. Hratchian, J. V. Ortiz, A. F. Izmaylov, J. L. Sonnenberg, D. Williams-Young, F. Ding, F. Lipparini, F. Egidi, J. Goings, B. Peng, A. Petrone, T. Henderson, D. Ranasinghe, V. G. Zakrzewski, J. Gao, N. Rega, G. Zheng, W. Liang, M. Hada, M. Ehara, K. Toyota, R. Fukuda, J. Hasegawa, M. Ishida, T. Nakajima, Y. Honda, O. Kitao, H. Nakai, T. Vreven, K. Throssell, J. A. Montgomery, Jr., J. E. Peralta, F. Ogliaro, M. J. Bearpark, J. J. Heyd, E. N. Brothers, K. N. Kudin, V. N. Staroverov, T. A. Keith, R. Kobayashi, J. Normand, K. Raghavachari, A. P. Rendell, J. C.

- Burant, S. S. Iyengar, J. Tomasi, M. Cossi, J. M. Millam, M. Klene, C. Adamo, R. Cammi, J. W. Ochterski, R. L. Martin, K. Morokuma, O. Farkas, J. B. Foresman, and D. J. Fox, Gaussian, Inc., Wallingford CT, 2016.
- (55) Zhao, Y.; Truhlar, D. G. A New Local Density Functional for Main-Group Thermochemistry, Transition Metal Bonding, Thermochemical Kinetics, and Noncovalent Interactions. *The Journal of Chemical Physics* **2006**, *125* (19), 194101. <https://doi.org/10.1063/1.2370993>.
- (56) Marenich, A. V.; Cramer, C. J.; Truhlar, D. G. Universal Solvation Model Based on Solute Electron Density and on a Continuum Model of the Solvent Defined by the Bulk Dielectric Constant and Atomic Surface Tensions. *J. Phys. Chem. B* **2009**, *113* (18), 6378–6396. <https://doi.org/10.1021/jp810292n>.
- (57) Giordana, A.; Priola, E.; Bonometti, E.; Benzi, P.; Operti, L.; Diana, E. Structural and Spectroscopic Study of the Asymmetric 2-(2'-Pyridyl)-1,8-Naphthyridine Ligand with Closed-Shell Metals. *Polyhedron* **2017**, *138*, 239–248. <https://doi.org/10.1016/j.poly.2017.09.032>.
- (58) Salinas-Uber, J.; Barrios, L. A.; Estrader, M.; Roubeau, O.; Aromí, G. Dinuclear Cu(II) Molecules Exhibiting Reversible Photochromism.
- (59) Murphy, B.; Roberts, G.; Tyagi, S.; Hathaway, B. J. The Crystal Structures and Electronic Properties of Three New [Cu(Bipy)2(ONO)][Y] Complexes. The Structural Pathway of the [Cu(Bipy)2(ONO)][Y] Series of Complexes. Further Insights into the Pseudo Jahn–Teller Model. *Journal of Molecular Structure* **2004**, *698* (1–3), 25–36. <https://doi.org/10.1016/j.molstruc.2004.02.025>.
- (60) Hathaway, B. J.; Ray, N.; Kennedy, D.; O'Brien, N.; Murphy, B. The Structures of Acetatobis(2,2'-Bipyridyl)Eopper(II) Perchlorate Monohydrate and Tetrafluoroborate - Cation Distortion Isomers.

Chapter 3 – The isolation of a copper (I) formate complex and its reactivity in dynamic isotopic exchange and formic acid dehydrogenation

Abstract:

Formic acid (FA) is considered as a promising candidate for liquid hydrogen storage, which has a great potential in hydrogen fuel applications. Many researches have been devoted to the development of efficient catalytic systems for the selective conversion of FA to H₂ and CO₂, with precious metal catalysts, such as Ir, Ru, being the most successful. Unlike other metal-based catalysts, copper complexes have received little attention and only three examples are known that exhibit low catalytic activity. Mechanistic studies on copper species for the catalytic hydrogenation of FA have suggested the formation of transient copper hydride and copper formate species. Nonetheless, only a handful of copper-formate complexes have been successfully isolated. While the insertion of CO₂ into copper hydride is well documented, the reverse decarboxylation reaction of copper formate is uncommon.¹

Since we have successfully isolated mono-ligated copper(I) carboxylate complexes using the bulky 2,9-di-*tert*butyl-1,10-phenanthroline (phen*) ligand, we targeted the phen* ligated copper(I) formate, *e.g.* [(phen*)Cu^I(O₂CH)], to see its potential activity in the dehydrogenation of formic acid. Being a catalyst, formation of the transient copper-hydride species [(phen*)Cu–H] issued from the decarboxylation of [(phen*)Cu^I(O₂CH)], has been tracked by different methods including dynamic isotopic exchange with ¹³CO₂.

Table of Contents

Abstract:	131
I. Introduction	133
I. 1. Physical and chemical methods to store dihydrogen.....	133
I. 2. State-of-the-art on the dehydrogenation of formic acid (FA).....	135
I. 2. 1. Formic acid as liquid hydrogen carrier	135
I. 2. 2. Transition metal-catalyzed dehydrogenation of formic acid	137
I. 2. 3. Copper-catalyzed dehydrogenation of formic acid and hydrogenation of CO ₂	140
I. 2. 4. Synthesis of monomeric copper(I) formate complexes	142
II. Results and discussions	147
II. 1. Synthesis and characterization of [(phen*)Cu(κ^1 -O ₂ CH)] (12)	147
II. 2. Attempts to the copper monohydride [(phen*)Cu-H].....	149
II. 3. Stoichiometric reaction with ¹³ CO ₂	150
II. 4. Catalytic dehydrogenation of formic acid (FA).....	158
III. Conclusion and perspectives	164
III. 1. Conclusion	164
III. 2. Perspectives.....	164
IV. References	165

I. Introduction

I. 1. Physical and chemical methods to store dihydrogen

In the urge to develop a sustainable energy system to replace fossil resources (coal, oil, gas, etc.) that directly contribute to increasing global warming, hydrogen (H_2) stood out as a suitable and renewable carbon-free energy vector. Since Jones published the first report on using hydrogen as an energy carrier in 1976,² several studies have been released looking at different aspects of using hydrogen as an energy carrier. A review carried out by Bockris in 2013 has summarized the developments in the direction of a future hydrogen economy.³ The efficient conversion of H_2 to electricity, with only water as a by-product, makes it an attractive fuel candidate as an energy vector for mobile and power generation applications.⁴ Indeed, H_2 is a fuel of choice since its combustion in air is capable of generating $120\text{--}142 \text{ MJ.kg}^{-1}$ (i.e. 33.33 kWh.m^{-3}) against $42\text{--}47 \text{ MJ.kg}^{-1}$ for standard gasoline (Figure 53). It can also be a source of electricity through direct use in fuel cells for power, mobility, and home applications.

However, H_2 is the lightest gas in the universe, which has an extremely low energy density by volume around $0.011\text{--}0.013 \text{ MJ.L}^{-1}$ (i.e. 3.05 kWh.m^{-3}) compare to standard gasoline (ca. 34.2 MJ.L^{-1}). This low volumetric density has been measured to be 0.0898 g.L^{-1} (at $25 \text{ }^\circ\text{C}$, 1 bar) under atmospheric pressure. In other words, hydrogen requires about 3,000 times more space than petrol for the same amount of energy and a concentrated volumetric density of H_2 is required to exploit its fuel potential efficiently. Large-scale hydrogen transportation and storage are technically challenging processes and energy consuming.⁵

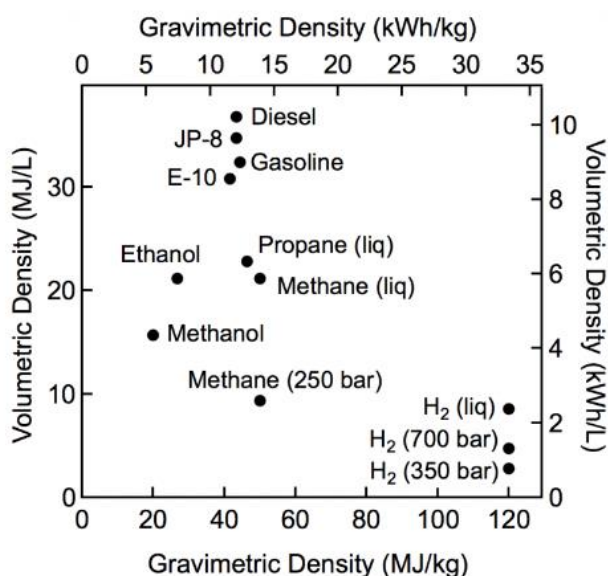


Figure 53. Comparison of specific energy (per mass or per gravimetric density) and energy density (energy per volume or volumetric density) for several fuels based on lower heating values. (original image taken from energy.gov)⁶

For this reason, hydrogen energy storage should not only increase the volumetric energy content while maintaining the same gravimetric energy density, but it should also be safe and secure for transport

and handling. Numerous hydrogen storage technologies have been developed, including compressed gas, cryogenic hydrogen, solid-state storage or liquid hydrogen method.^{7,8}

Although compressed gas is a well-established technology for storing hydrogen in its natural form (200 to 700 bar), there are still a few unresolved problems. For instance, it has a volumetric energy density of 5.6 MJ.L^{-1} ($\rho_V(\text{H}_2) = 40 \text{ g H}_2.\text{L}^{-1}$), which is far less than 32.0 MJ.L^{-1} for gasoline.⁹ Furthermore, high-pressure delivery with potential leakage, and required low temperature or high pressure to store have to be complied.⁸ On the other hand, hydrogen can be stored as a liquid at $-253 \text{ }^\circ\text{C}$ (20 K), which has an energy density by volume (9 MJ.L^{-1}) 4 times smaller than hydrocarbon fuels such as gasoline (*ca.* 34.2 MJ.L^{-1}). Nevertheless, the liquefaction process costs about 30-40 % of the energy content of the hydrogen.¹⁰ Alternatively, the solid-state method offers storage with a hydrogen density greater than that of cryogenic hydrogen at moderate temperature and pressure. This allows a large amount of hydrogen to be stored in a small volume. The solid-state storage method consist in trapping the hydrogen atoms into chemical compounds (metal hydrides, hydride complexes) or by adsorption in the cavity of porous materials (MOFs, zeolites, etc.).¹¹ In the latter case, the H_2 adsorption capacity is strongly affected by ligand functionalization, catenation, open metal sites, and pore size of the material, and generally requires low temperatures and high pressures to work.¹² Hydrogen can also be stored in inorganic hydrides (*e.g.* MgH_2 , LiAlH_4 , NaBH_4) or chemical hydrides (*e.g.* $\text{NH}_3\bullet\text{BH}_3$), which have relatively high energy volume density. They are also relatively safer and more easily handled than compressed gas or liquid hydrogen. For example, $\text{NH}_3\bullet\text{BH}_3$ has a H_2 storage capacity of 19.6 wt% (100 $^\circ\text{C}$), which translates into a volumetric energy density of about 35.6 MJ.L^{-1} , a value close to that of gasoline.¹³ The most significant shortcoming of these systems is the irreversible nature of the storage, which makes it difficult to regenerate the hydride carriers once they have released their hydrogen content.^{14,15} Consequently, off-board regeneration of the H_2 carrier is required.

Among the H_2 chemical traps, liquid organic hydrogen carriers (LOHC) are promising storage sources that are predicted to be more efficient than gaseous compressed hydrogen.^{8,16} For instance, the advantages of LOHC systems are long storage time and no hydrogen loss in long-distance transportation.¹⁷ This method is based on a two-step cycle involving the hydrogenation, in which hydrogen is covalently bound to the liquid carrier (typically C-H), and dehydrogenation. The use of catalysts is essential to facilitate these reactions that are generally performed at elevated temperatures (*ca.* 200 $^\circ\text{C}$). Several examples of LOHC compounds have been developed,¹⁷ such as methylcyclohexane-toluene, cycloalkanes, *N*-ethylcarbazole (NEC), dibenzyltoluene (DBT), methanol etc., in which methanol has more hydrogen storage capacity than others (*i.e.* 10 wt%). *N*-ethylcarbazole which has a hydrogen storage capacity of 5.8 wt% corresponding to a low 2.5 kWh.L^{-1} energy density is however the best understood LOHC and can be stored, transported and handled as a liquid diesel-like substance.¹⁷ Numerous catalytic systems have been developed where the reversible hydrogenation and dehydrogenation of *N*-ethylcarbazole and its dehydrogenated pair (perhydro-*N*-ethylcarbazole, H_{12} -NEC) can be achieved with full conversion using $\text{Ru/Al}_2\text{O}_3$ and $\text{Pd/Al}_2\text{O}_3$ respectively, but with degradation after 10 cycles (*Figure 54*).¹⁸ In comparison with other LOHC systems, DBT has a superior hydrogen storage capacity (6.2 wt%), an energy density of 1.9 kWh.L^{-1} with excellent thermal stability, high boiling point (390 $^\circ\text{C}$) and low toxicity.¹⁹ Due to the elevated temperature in the reactor of the LOHC dehydrogenation process (*ca.* 200 $^\circ\text{C}$), the hydrogenation and dehydrogenation of DBT can proceed in its liquid form without undergoing the vaporization such as in

the case of toluene as LOHC.¹⁷ For the hydrogenation of DBT, precious metals based heterogeneous catalysts such as Pt or Ru supported by Al₂O₃ are employed. For instance, Brückner *et al.* reported a hydrogenation of DBT to afford perhydro-dibenzyltoluene (H₁₈-DBT) with full conversion at 150 °C for 4 h (Ru/Al₂O₃ catalyst).²⁰ Dehydrogenation of H₁₈-DBT can be done by Ru or Pd catalysts supported by carbon.²⁰ A catalyst system was developed by the group of Brückner using Pd/C, where the dehydrogenation process can be achieved with excellent yield of 97% after 2 h at 310 °C.²⁰ Alternatively, Milstein *et al.* proposed an interesting approach where 2-aminoethanol is used as a hydrogen carrier with hydrogen capacity of 6.6 wt%.²¹ Under mild reaction conditions (*ca.* 135 °C, 10-70 bar H₂), this LOHC system is catalytically converted to the cyclic peptide glycine anhydride and release H₂ gas by a single Ru-based complex. Using the same catalyst, the peptide hydrogenation regenerates 2-aminoethanol as hydrogen carrier.²¹⁻²³ Nevertheless, the system cannot reach high selectivity and conversion rates.

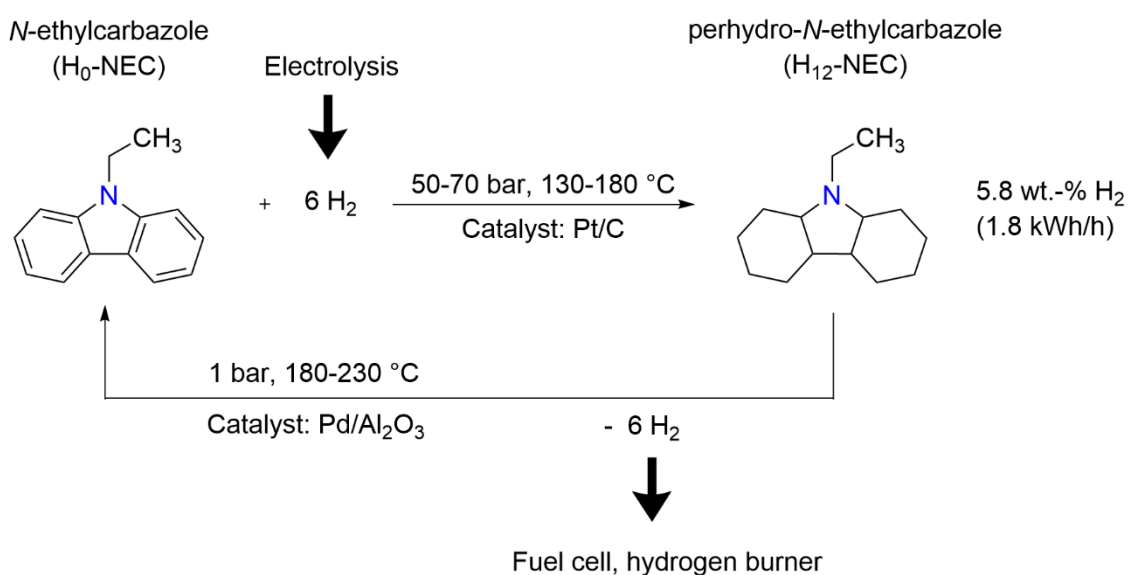


Figure 54. Storage process of the N-ethylcarbazole: perhydro-N-ethylcarbazole system.¹⁷

Formic acid (FA) is considered as a promising liquid organic hydrogen carrier. Its notable volumetric hydrogen content (4.4 wt%) is in line with the targets set for 2020 by the US Department of Energy (4.5% hydrogen by weight). Moreover, since FA is relatively dense ($\rho = 1.22 \text{ g.cm}^{-3}$) and has an usable/net capacity of 53 g hydrogen *per* liter, it surpasses most standard storage materials.²⁴ If fully converted, FA can potentially generate 6.48 MJ.L^{-1} of energy, which exceeds that of a compressed cylinder (5.6 MJ.L^{-1}).¹⁷ Its stability, its low toxicity and the ease to store it under ambient conditions offer also interest. Moreover, this liquid, which is chemically similar to vinegar (acetic acid), has a flash point of +69 °C. This characteristic of formic acid evidences the gain in terms of safety compared with other fuels, since the flash points are much lower: +12 °C for methanol and -40 °C for gasoline.²⁵

I. 2. State-of-the-art on the dehydrogenation of formic acid (FA)

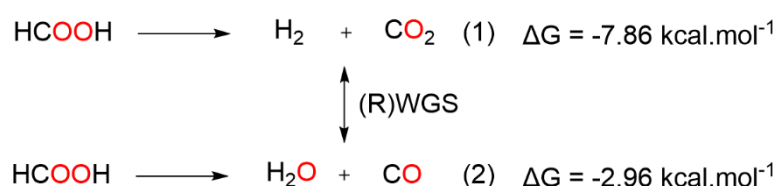
I. 2. 1. Formic acid as liquid hydrogen carrier

Formic acid HCOOH, is a colorless liquid completely miscible with water and many polar solvents but partially miscible with hydrocarbons. Formic acid derived its name from the ant in which it was

discovered in the XVIIth century and has further been detected in the poison or defense systems of bees and insects. Formic acid was first synthesized from hydrocyanic acid by Gay Lussac and at the end of the XIXth century by Marcellin Berthelot who developed a synthesis from carbon dioxide similar to the process used today. Formic acid is produced by hydrolysis of methyl formate (BASF, Kemira – Leonard Process) or formamide (BASF) or from its salts.²⁶ It is also a byproduct of acetic acid production by liquid-phase oxidation of hydrocarbons.²⁶ HCO₂H is used as intermediate in the chemical and pharmaceutical industries, as dyeing in the textile and leather industries, in agriculture etc. The worldwide production of formic acid was about 621,000 t/a in 2012.²⁶

FA can also be produced by the hydrogenation of CO₂,²⁶ an abundant and inexpensive gas massively released by some industries and human activities. The use of CO₂ as a C₁ building block however offers huge potential for reducing the carbon footprint of chemical industry in the biosphere. CO₂ being strongly oxidized and chemically poorly reactive, its hydrogenation into formic acid is strongly endergonic in the gas phase ($\Delta G_{298}^0 = +32.8 \text{ kJ}\cdot\text{mol}^{-1}$) but the reaction becomes thermodynamically favorable in basic solution ($\Delta G_{298}^0 = -35.4 \text{ kJ}\cdot\text{mol}^{-1}$).^{24,27} As hydrogenation is efficiency limited by the solubility of the gas H₂ and CO₂, homogeneous catalysts have been introduced to improve FA production. Generally, most of these catalysts are based on noble metals (Rh, Ru, and Ir) under a pressure range from 1 to 100 bar and operate at temperatures from 50 to 100 °C.^{28,29} Besides homogenous catalysts, heterogeneous catalysts have been well investigated.^{30–32}

The decomposition of FA can take place through two distinct pathways, producing H₂ and CO₂ (dehydrogenation) or dehydration to release water and carbon monoxide (*Scheme 54*).^{33,34} For an efficient hydrogen storage system, the second route must be avoided because the CO byproduct is harmful to fuel cells. A fuel cell is a clean and efficient device, which uses the chemical energy of hydrogen to generate electricity by electrochemical conversion. Both dehydrogenation and dehydration processes are thermodynamically favorable ($\Delta G_{298}^0 = -7.86 \text{ kcal}\cdot\text{mol}^{-1}$ for dehydrogenation and $\Delta G_{298}^0 = -2.96 \text{ kcal}\cdot\text{mol}^{-1}$ for dehydration) and interchangeable at high temperatures *via* water-gas shift reaction (WGS) (*Scheme 54*).



Scheme 54. Two pathways for the decomposition of formic acid: (1) dehydrogenation and (2) dehydration.

The selective decomposition of FA into H₂ and CO₂ is an essential part of a LOHC system. Beller and co-workers³⁵ as well as Laurency and co-workers³⁶ independently proposed a catalytic system that can selectively catalyze the dehydrogenation of FA and the re-generation of formic acid from carbon dioxide. This opens up a new concept for hydrogen storage system: FA/CO₂ (*Figure 55*).

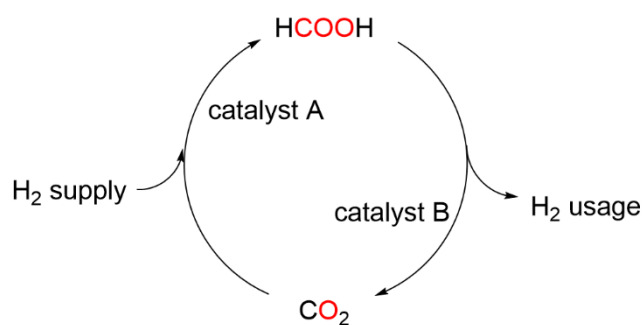


Figure 55. Hydrogen storage based on carbon dioxide/formic acid.

I. 2. 2. Transition metal-catalyzed dehydrogenation of formic acid

It was in 1967 when Coffey reported the pioneering work on the homogeneous catalysis of the dehydrogenation of FA by iridium-phosphine complex with the TOF of 1187 h^{-1} .³⁷ Since then, the development of noble metal complexes catalyzing the selective decomposition of FA has been successful. They exhibited excellent activity with impressive TON and TOF.³⁸ For instance, Huang and Zheng *et al.* developed a Ru complex with PNP-pincer ligand (**Ru-1**) that catalyzed FA dehydrogenation in the presence of NEt_3 as a base, for a production of H_2 with a TOF of 7333 h^{-1} and TON of 1,100,000 in 150 h at 90°C (Figure 56).³⁹ Alternatively, Huang *et al.* demonstrated that a Ru(II) species bearing a bisimidazole ligand (**Ru-2**) was effective for FA dehydrogenation with a TOF of $12,000 \text{ h}^{-1}$ and TON of 350,000 (35 h) at 90°C in H_2O .⁴⁰ Recently, another example was reported by Milstein *et al.* with a Ru-ligated 9H-acridine pincer ligand (**Ru-3**).⁴¹ This catalytic system achieved the selective dehydrogenation of FA with a high TON > 1.7 million and TOF of 3067 h^{-1} at 95°C .⁴¹

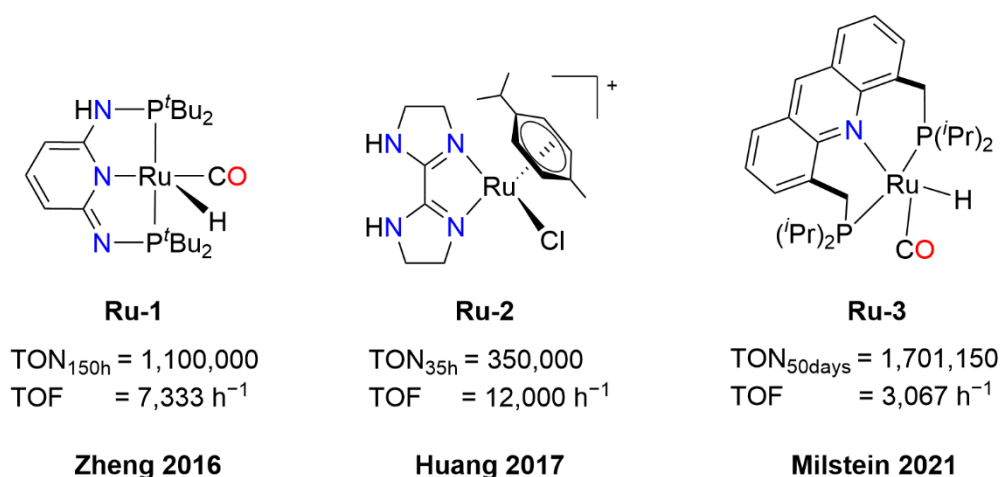


Figure 56. Examples of Ru complexes catalyzing dehydrogenation of formic acid

In parallel, several generations of iridium catalyst systems have been investigated (Figure 57). Fujita *et al.* developed an Ir complex bearing a bipyrimidine ligand (**Ir-1**) that catalytically decomposes FA with a TOF of $158,000 \text{ h}^{-1}$ and TON of 308,000 at 80°C in acidic conditions after 12 h.⁴² Interestingly, by increasing the pH of the reaction to basic conditions, the same catalyst system promotes the reverse reaction, *e.g.* the hydrogenation of CO_2 to formate.⁴² It was previously shown that the introduction of an electron-donating substituent on 2,2'-bipyridine is an effective method to improve the catalytic activity favoring the dehydrogenation of FA. The highly electron-donating hydroxyl (OH) substituent

favors much better the FA decomposition than other substituents such as methyl or methoxy under basic conditions. Thus, in a buffered basic medium (above pH 5), the hydroxyl cation substituents of complex in *Figure 58* (left) evolves towards its neutral form by deprotonation of the OH (*Figure 58*, right). This latter mediates the hydrogenation of CO₂ with a TOF of 53,800 h⁻¹ and TON of 153,000 at 80 °C and 5 MPa pressure of CO₂.⁴² In 2019, Himeda *et al.* demonstrated that the hydroxyl-pyridyl complex **Ir-2** could serve as catalyst for both carbon dioxide hydrogenation to formate and formic acid dehydrogenation in water (*Figure 57*, center).⁴³ In a basic medium, the hydrogenation of CO₂ can be achieved with a low final concentration of FA (*ca.* 0.037 M) after 1 h at 80 °C (TON of 1350). Meanwhile, this catalyst showed a high catalytic activity in FA dehydrogenation that is maintained during a long period (*i.e.* 35 days) at pH 3.5. In fact, after 35 days of continuous FA addition, the Ir catalyst was capable of producing 2.5 m³ of gas with a total TON of 10 millions, the highest values ever reported.⁴³

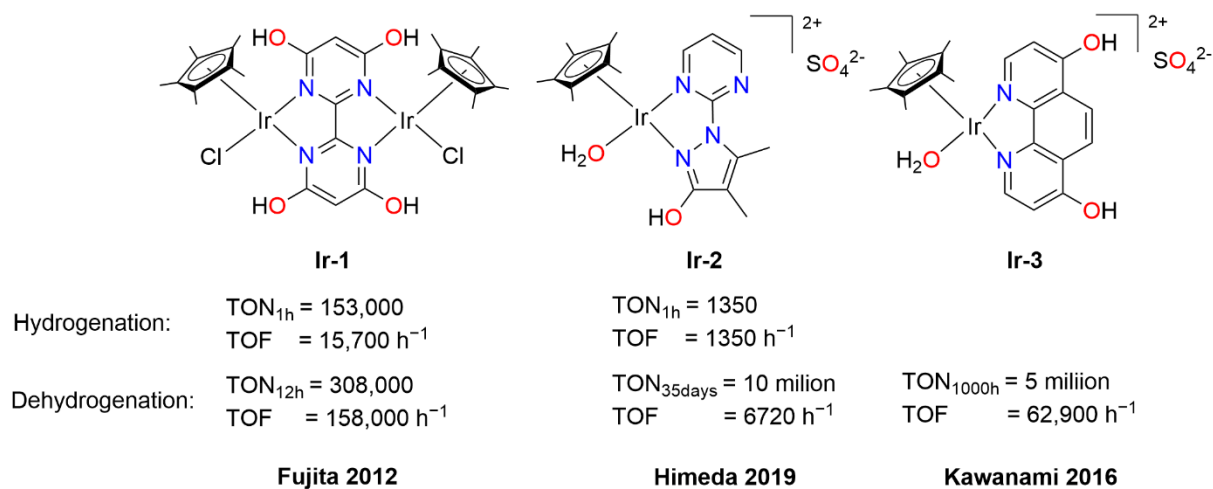


Figure 57. Examples of Ir catalysts for formic acid dehydrogenation.

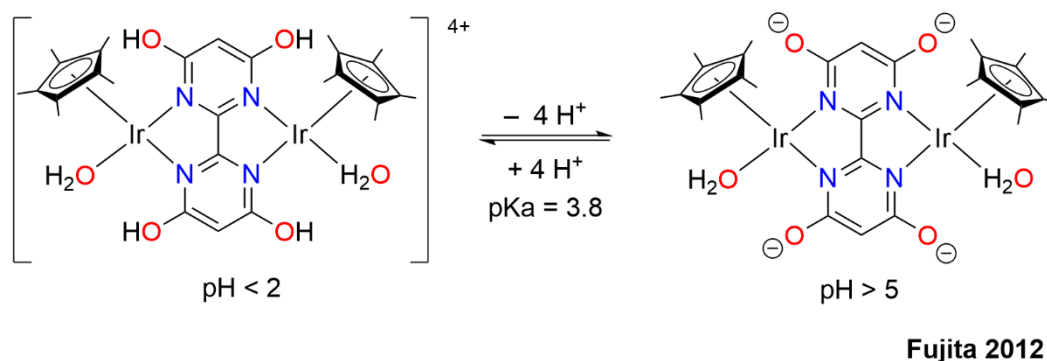


Figure 58. Reversible formation of protonated and deprotonated bimetallic Ir catalysts under acidic and basic conditions.

Another Ir complex involving the 4,7-(HO)₂-1,10-phenanthroline ligand (**Ir-3**), described by Kawanami *et al.*, can be used for the generation of high-pressure H₂ from FA.⁴⁴ The complex is active in water for 2600 h (*≈* 3.5 months) and gives the highest TON value of 5,000,000 (*Figure 57*) and a high TOF of 62,900 h⁻¹ at 80 °C. Interestingly, the catalytic activity was maintained under high pressure (*i.e.* 22 MPa), over a reaction time of 200 h. The iridium complex precipitated due to the change in pH at the

end of the reaction when all the formic acid was consumed. The precipitated complex can be easily separated and the catalyst regenerated and recycled more than 10 times without losing any activity.⁴⁴

While precious metal catalysts have been widely reported with excellent TON and TOF, the choice of non-precious metals attract interest in terms of resource depletion. The 2010's have seen a great development of a variety of non-noble transition metal catalysts of iron, nickel, cobalt, aluminum, and copper.⁴⁵

In 2011, Beller *et al.* demonstrated that $\text{Fe}(\text{BF}_4)_2 \cdot 6\text{H}_2\text{O}$ with a tetradentate phosphine (**Fe-1**) catalyzed the dehydrogenation of FA (80 °C, 16 h) in propylene carbonate as solvent with a TOF of 5390 h^{-1} and a total TON of 92,000 (Figure 59).⁴⁶ Similarly, Laurenczy *et al.* reported a water soluble iron catalyst bearing a tetradentate phosphine derivatives (**Fe-2**), in which the total TONs of 13,000 is reached after 8 weeks (30 dehydrogenation cycles at 80 °C) (Figure 59).⁴⁷ When the ligand : metal ratio was increased from 1:1 to 2:1, the TOF increased from 66 h^{-1} to 240 h^{-1} , a values lower than the one obtained by Beller and coworkers with their iron species.⁴⁶ In 2013, Milstein *et al.* introduced a new iron catalyst with a pincer ligand (**Fe-3**) for the dehydrogenation of FA.⁴⁸ They obtained a TOF of 653 h^{-1} and a TON of 100,000 after 10 days of reaction at 40°C in 1,4-dioxane in presence of the base NEt_3 for deprotonating the FA. A slight decrease in TOF (*ca.* 500 h^{-1}) is observed when tested in a closed system with pressure build-up (range 0 to 10 bar) compared to the open system (Figure 59). Later in 2014, Hazari *et al.* developed another PNP-pincer ligated Fe catalyst (**Fe-4**) efficient in dioxane in presence of the Lewis acid LiBF_4 (10 mol%) as a co-catalyst for FA decomposition. They achieved an impressive TOF and TON of $196,700 \text{ h}^{-1}$ and 1 million respectively within 9.5 h at 80 °C (Figure 59).^{49,50}

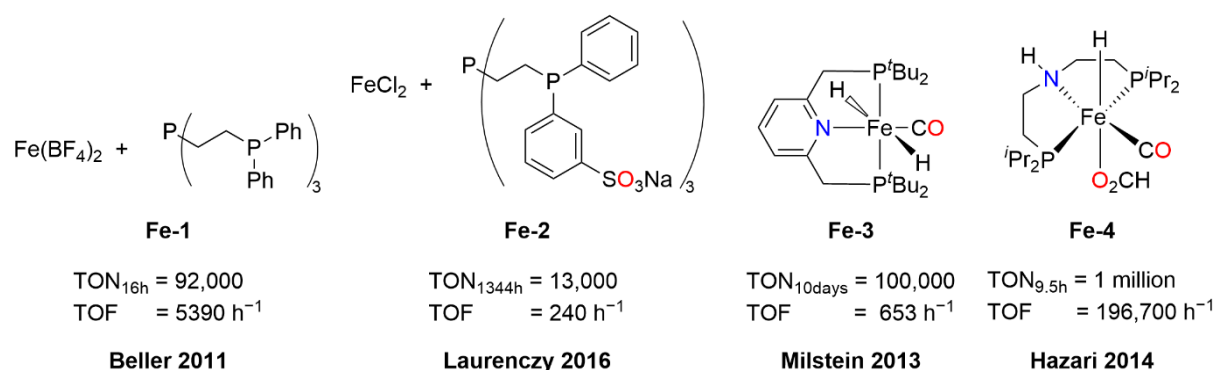


Figure 59. Examples of Fe catalysts for formic acid dehydrogenation.

Enthaler and co-workers developed a Ni(II) complex coordinated with a pincer-type ligand (**Ni-1**) that promotes the production of H_2 from FA with a TON of 626 and TOF of 209 h^{-1} after 3 h in propylene carbonate in the presence of NEt_3 as a base (Figure 60).⁵¹ In addition, they proposed nickel-hydride and nickel-formate species as active intermediates of the catalytic cycle. Furthermore, this nickel-hydride is capable of hydrogenating sodium bicarbonate with a TON of 3,000 after 20 h under high pressure of H_2 (55 bar) at 150 °C. Parkin and co-workers reported a simple zerovalent $\text{Ni}(\text{PMe}_3)_4$ catalyst system that can facilitate the decomposition of FA selectively in the absence of a base.⁵² However, the catalytic activity of this nickel complex is much less than that reported by Enthaler.⁵¹

In addition to iron and nickel, the catalytic activity of manganese(II) in the dehydrogenation of FA has also been studied. (Figure 60). For instance, in 2019, Tondreau *et al.* described a Mn bearing a pincer-

type ligand (**Mn-1**) that can efficiently convert FA into H₂ and CO₂ with a high TOF of 8,500 h⁻¹ and TON of 20,000, in the presence of a base (NEt₃) in chlorobenzene as solvent at 80 °C for 24 h.⁵³ Alternatively, Beller *et al.* proposed another approach with the Mn(II) imidazoline species **Mn-2** which dehydrogenates FA with a TON of 5,736 and TOF of 188 h⁻¹.⁵⁴

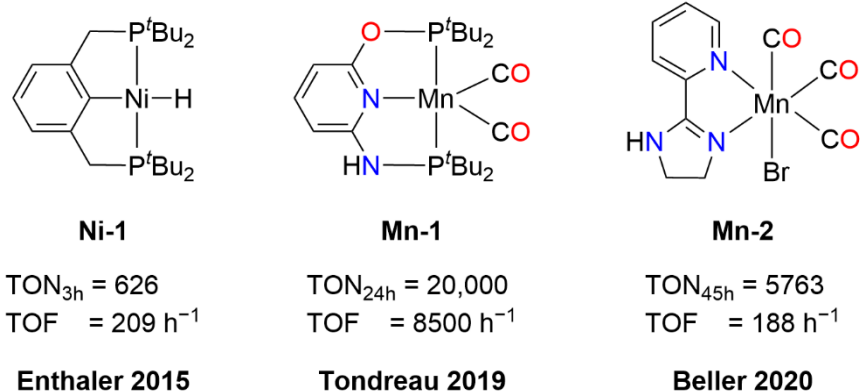


Figure 60. Examples of Ni and Mn catalysts for formic acid dehydrogenation.

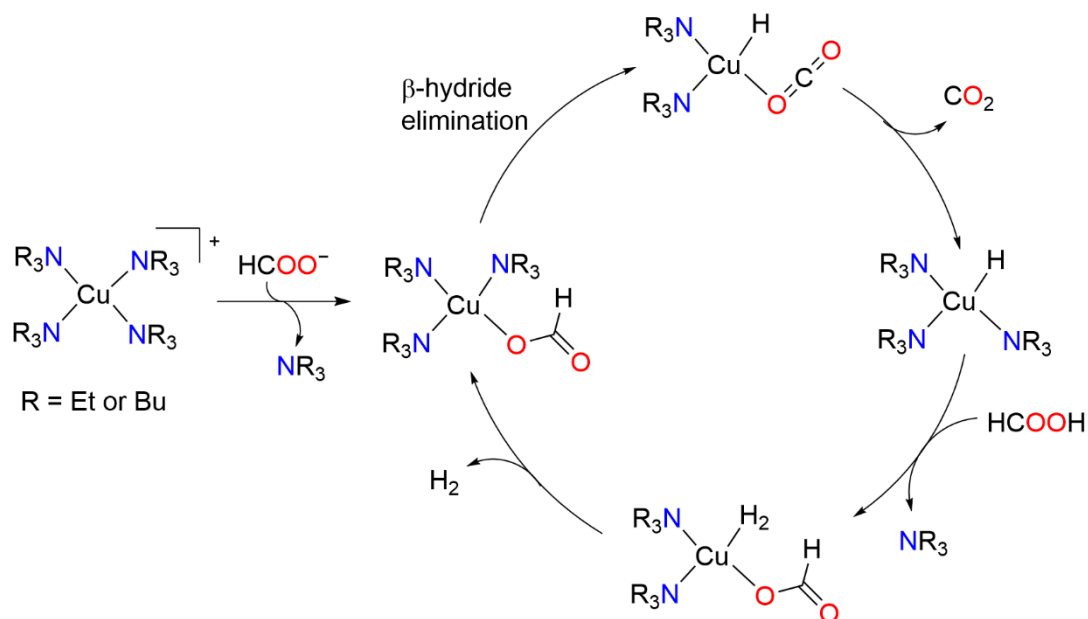
Of all the reported transition metals with high reactivity for FA dehydrogenation, only a few examples focused on mononuclear copper species,⁵⁵ while copper aggregates catalysts are more exploited.^{56,57}

1. 2. 3. Copper-catalyzed dehydrogenation of formic acid and hydrogenation of CO₂

Examples of catalytic dehydrogenation of FA by copper complexes are unusual. In 2014, Scotti *et al.* reported a copper-based catalyzed (**Cu-1**) hydrogen production from FA/amine adducts (Figure 61).⁵⁵ In their study, they investigated the different effects of the amines on the catalytic performances. Interestingly, reactivity did not depend on the sole basicity of the amine as the activity was enhanced with a decreasing nucleophilicity and increasing steric hindrance (cone angle) of the NR₃. For example, NEt₃ has a nucleophilic constant⁵⁸ of 4.09 and a cone angle⁵⁹ of 150° affording a 17.2 % conversion of FA after 22 h.⁵⁵ Meanwhile, piperidine (greater basicity than NEt₃) possesses a higher nucleophilic constant and a smaller cone angle (5.59, and 121°, respectively) giving a lower conversion of 12 % under the same reaction conditions. This result therefore indicates that the role of the amine can be only related to the deprotonation of FA. Even though **Cu-1** is selective for hydrogen production, with their best example of CuI as catalyst (1 mol%) and the 1/1 ratio in HCOOH/NEt₃, only 36.2 % conversion was obtained after 22 h, corresponding to a TON value of 72. Furthermore, the calculated TOFs for all examples are considerably low and smaller than 1 h⁻¹.⁵⁵

The same group proposed later a mechanistic study by DFT calculations for the FA dehydrogenation induced by a copper-amino based system.⁶⁰ In their study, they calculated the thermodynamic of all the steps in the proposed catalytic cycle for three different amino compounds, namely NEt₃, NBU₃, and NHPH₂ (Scheme 55). They showed that the FA conversion is multistep and generally exergonic, the rate-determining step being the formation of the key intermediate [(NR₃)₂Cu(H)(CO₂)] (with R = NEt₃, NBU₃, NHPH₂, and ΔE = +8.3, +6.1, +14.1, respectively) *via* β-hydride elimination of copper formate [(NR₃)₃Cu(O₂CH)]. Interestingly, they also evaluated the oxidation state of the copper ion. The

calculated energies suggested a decrease in stability of the key intermediate $[(\text{NR}_3)_2\text{Cu}(\text{H})(\text{CO}_2)]$ as the oxidation state of copper decreased from +2 to +1.⁶⁰



Scheme 55. Proposed catalytic cycle for Cu/NR₃ catalyst system of FA dehydrogenation.⁶⁰

This result also emphasized and confirmed their experimental results where the amine not only was useful to deprotonate FA, but acted a stabilizing ligand for the transient copper hydride intermediate $[\text{L}_2\text{Cu}(\text{H})(\text{CO}_2)]$ (L = NBu₃, NEt₃, and diphenylamine).⁶⁰ However, neither the copper-formate nor the copper-hydride have been isolated.

Tilley *et al.* successfully isolated a pentanuclear copper hydride supported by a bulky hexadentate naphthyridine-based ligand (**Cu-2**) (Figure 61) which proved efficient to catalytically dehydrogenate FA under mild conditions without the need for additives.⁵⁶ However, no TON and TOF values were reported and this copper hydride species was unreactive with CO₂. Tanase and colleagues reported another synthetic method starting from CuCl and RCN (R = ^tBu, Cy) for the isolation of a hexanuclear copper hydride (**Cu-3**) supported by a linear tetradentate phosphine ligand dpmpbb in the presence of NaBH₄ and NH₄PF₆ (Figure 61).⁵⁷ By testing a variety of phosphine (dpmpbm, dpmppe, dpmpbb), they evidence that the copper-hydride **Cu-3** displayed the highest catalytic activity in the dehydrogenation of FA (TON of 720 and a TOF of 240 h⁻¹ after 3 h at 70 °C) (Figure 61). The stoichiometric reaction of **Cu-3** and CO₂ (1 bar, rt.) in MeCN generated the discrete copper formate species $[\text{Cu}_2(\text{O}_2\text{CH})(\text{dpmpbb})\text{L}_2]^+[(\text{PF}_6)_4]^-$ (L = ^tBuNC, MeCN) after 30 h. Interestingly, exposure of the latter species to N₂ (30 h, 1 bar, rt.) in the same solvent regenerated the copper hydride **Cu-3**, indicating facile decarboxylation into the hexacopper-dihydride. Nevertheless, this copper formate cation $[\text{Cu}_2(\text{O}_2\text{CH})(\text{dpmpbb})\text{L}_2]^+$ was only identified using ESI-MS and NMR analysis without crystal structure determination.⁵⁷

These rare examples show the interconversion between copper hydride and copper formate, which are likely key intermediates in the catalytic dehydrogenation of FA. The choice of ancillary ligands to further stabilize or increase the reactivity of the reactive copper intermediates in this catalysis is of importance. Mechanistic insights to deeply apprehend and clarified the nature of the true active

species and eventual (un)suspected redox intermediates required further developments and in particular of well-defined, stable and soluble monomolecular species.

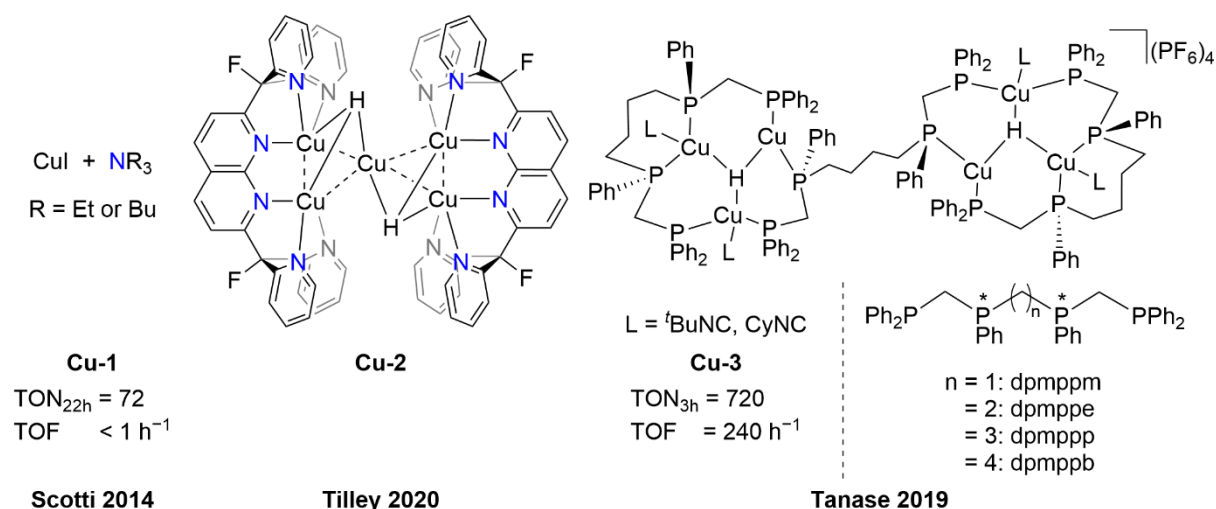
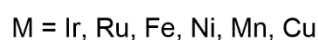
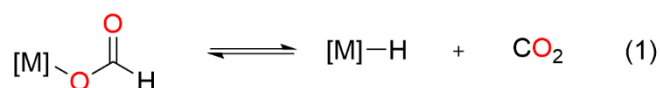


Figure 61. Examples of Cu catalysts for formic acid dehydrogenation.

I. 2. 4. Synthesis of monomeric copper(I) formate complexes

In recent years, formate complexes have aroused considerable interest and several molecular species have been synthesized and isolated in the d- and f-transition metal as well as in non-metal series (B, Si,...).^{61–69} Their particular chemical behavior and reactivity make them attractive for applications in coordination chemistry, catalysis, and in various fields ranging from energy storage^{25,28,33,38,45,70} to reduction chemistry.^{71–74}

For example, in stark contrast to the stable carboxylate complexes $[\text{M}](\text{O}_2\text{CR})$ ($\text{R} = \text{alkyl}$), decarboxylation of the $[\text{M}](\text{O}_2\text{CH})$ species (Eq.1 below) is much easier and is a classical reaction in the catalytic decomposition of formic acid (HCO_2H) into H_2 and CO_2 .^{45,70,75}



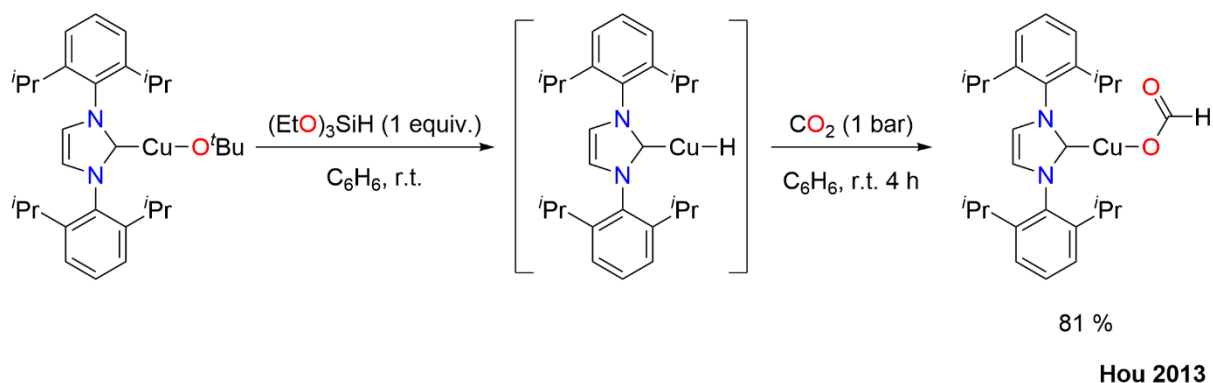
These complexes also proved crucial intermediates in reductive chemistry by promoting hydrogen transfer reactions with CO_2 release particularly when using liquid hydrogen surrogates such as HCO_2H , $\text{HCO}_2\text{H}-\text{NEt}_3$, or solid sources containing the formate ion HCO_2^- .^{76–82} Redox transformations of CO_2 and carbonyl molecules into methanol were thus performed but also the isomerization of methyl formate (HCO_2Me) into acetic acid^{83–85} and recently recyclable silylformates (SiO_2CH) were shown to favor disproportionation of acid formic into methanol derivatives in presence of a Ru(II) catalyst.⁶⁹ Some metal formates have also gained interest as new synthons in the deposition of thin metal films by chemical vapor deposition (CVD), spin-coating processes,...as those of Cu(I) and Cu(II), Ag(I) and Au(I).^{86–88}

Easily obtained from different routes, mainly substitution reaction from halide derivatives with formate ion, reaction of HCO_2H with compounds involving hydrogen-sensitive $[\text{M}]-\text{R}$ bonds ($\text{R} = \text{H, NR}_2$,

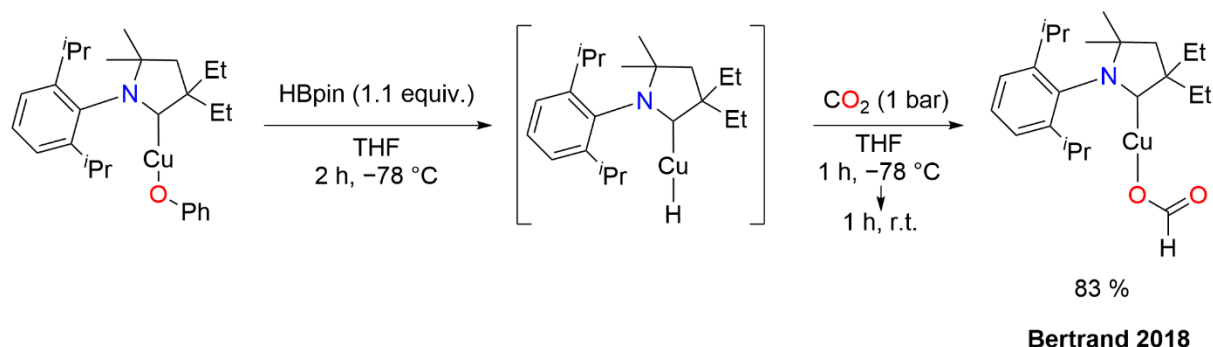
R) species, or insertion of CO₂ into the [M]–H bond, formate complexes can be viewed as convenient synthons to generate transient or stable hydride complexes by decarboxylation, provided that the release of CO₂ is thermodynamically favorable.^{1,85,89}

Although well documented for copper(II),^{90–94} only a fistful of copper(I) formate complexes have been reported. These latter Cu(I) complexes are coordinated with phosphine,^{95–98} carbene (NHC type),^{99–104} [(η⁵-C₅H₄SiMe₃)₂Ti](C≡CSiMe₃)₂,^{105,106} or nitrogenated molecules as ancillary ligands.^{1,89} In the latter case, only the mixed-N,P-phosphane complex [(P(C₆H₂CH₂NMe₂-2)₃)Cu(O₂CH)]⁸⁹ and the dimer (BBN^TTACN^{tBu})Cu(μ-O₂CH)₂ (BBN^TTACN^{tBu} = substituted triazacyclononane)¹⁰⁶ which has been structurally characterized.

A few monometallic formate species of Cu(I) are known with phosphines,^{107–109} phosphanes⁸⁹ and above all NHC ligands.^{99,101,102} For instance, the groups of Hou *et al.*¹⁰² and Bertrand *et al.*¹⁰⁴ by using NHC carbene as ancillary ligands have isolated [(IPr)Cu(κ¹-O₂CH)] (IPr = 1,3-bis(2,6-diisopropylphenyl)imidazol-2-ylidene)¹⁰² and [(CAAC₁)Cu(κ¹-O₂CH)] (CAAC₁ = cyclic(alkyl)(amino)carbene)¹⁰⁴ as described in Scheme 56 and Scheme 57, respectively.



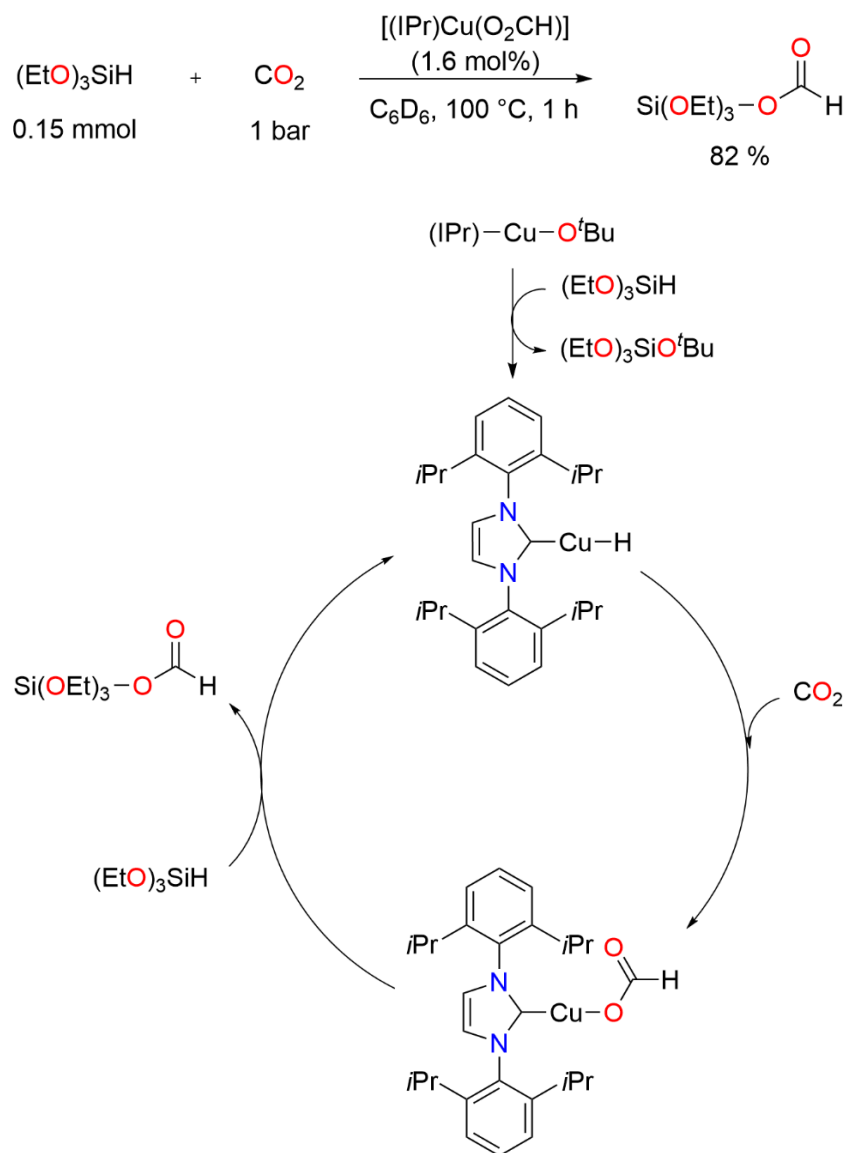
Scheme 56. Formation of [(IPr)Cu(κ¹-O₂CH)] from [(IPr)Cu(O^tBu)] and triethoxysilane under CO₂.



Scheme 57. Formation of [(CAAC₁)Cu(κ¹-O₂CH)] from [(CAAC₁)Cu(OPh)] and pinacolborane under CO₂.

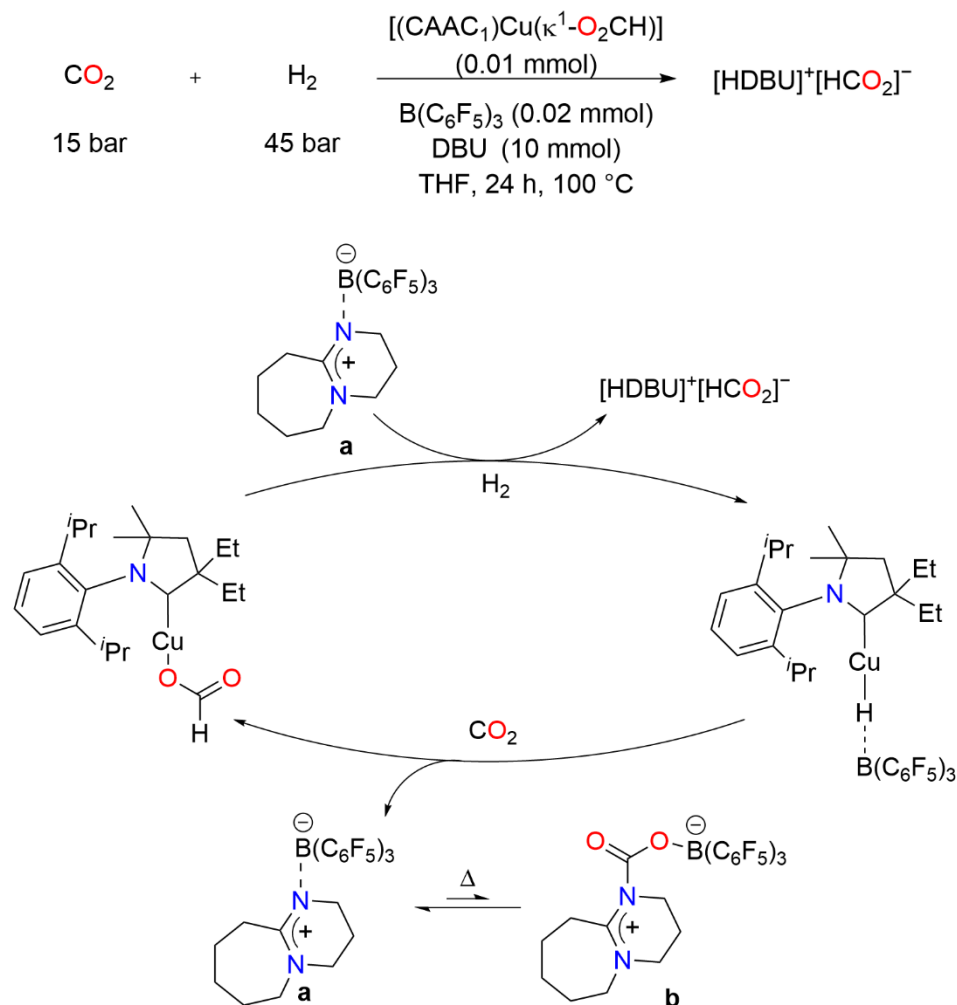
The isolated species [(IPr)Cu(κ¹-O₂CH)] showed high catalytic activity toward the hydrosilylation of CO₂ to afford the silyl formate (EtO)₃SiO₂CH in a yield of 82 % (Scheme 58).¹⁰² However, the yield can be increased to 94 % with [(IPr)Cu(O^tBu)], under the same conditions. In their mechanistic study, the authors proposed that [(IPr)Cu(O^tBu)] is a pre-catalyst affording the hydride [(IPr)Cu(H)] (Scheme 58) by reaction with the hydrosilane. Formation of this hydride was confirmed by NMR observation. The

latter species inserts readily CO_2 to yield the formate derivative $[(\text{IPr})\text{Cu}(\kappa^1\text{-O}_2\text{CH})]$ transformed back into the hydride with release of the SiO_2CH species by reaction with the hydrosilane.



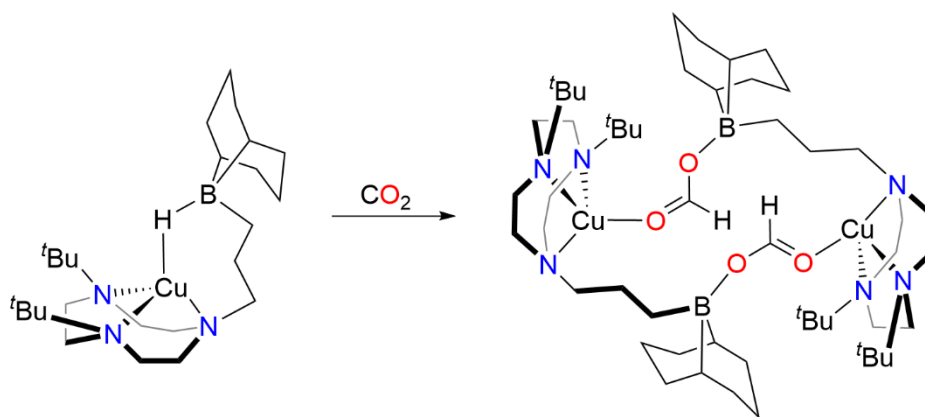
Scheme 58. Reaction conditions and proposed mechanism for the hydrosilylation of CO_2 catalyzed by $[(\text{IPr})\text{Cu}(\text{O}^t\text{Bu})]$ as pre-catalyst.¹⁰²

The complex $[(\text{CAAC}_1)\text{Cu}(\kappa^1\text{-O}_2\text{CH})]$ isolated by Bertrand *et al.* also showed excellent catalytic activity in the hydrogenation of CO_2 to the formate (TON of 387 after 24 h at 100°C) in the presence of a Frustrated Lewis Pair (FLP) composed of $\text{B}(\text{C}_6\text{F}_5)_3$ (strong Lewis acid) and the base DBU (1,8-diazabicyclo[5.4.0]undec-7-ene) (Scheme 59).¹⁰⁴ In this reaction, hydrogen and carbon dioxide are activated by the FLP. The proposed mechanism involves conversion of copper formate to copper hydride by reaction with H_2 , which is activated by the Lewis adduct **a** (Scheme 59). A following reaction of copper hydride with activated CO_2 -Lewis adduct **b** by Lewis adduct **a** regenerated the copper formate.

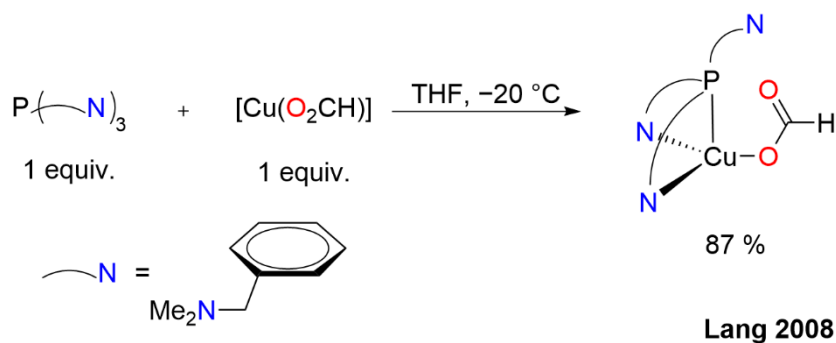


Scheme 59. Reaction conditions and proposed mechanism for the hydrogenation of CO_2 catalyzed by $[(\text{IPr})\text{Cu}(\text{O}^t\text{Bu})]$ as pre-catalyst.¹⁰⁴

There are two copper formate complexes of Cu(I) involving ancillary ligand with N-coordinating atoms, e.g. $[(^t\text{Bu}_2\text{C}_6\text{N}_3\text{-CH}_2\text{CH}_2\text{CH}_2\text{BC}_8\text{H}_{14})\text{Cu}(\mu\text{-O}_2\text{CH})]_2$ ¹⁰⁶ and $[(\text{P}(\text{C}_6\text{H}_2\text{CH}_2\text{NMe}_2\text{-2})_3)\text{Cu}(\text{O}_2\text{CH})]$ ⁸⁹. In the former case, the triazacyclononane has a pending boron Lewis acid fragment and the formate ligand is bridging between the Cu and B centers (Scheme 60).¹⁰⁶ The second complex with a mixed-N,P-phosphane ligand, is the unique monometallic formate species that has been reported and crystallographically characterized. It has been obtained, by Lang *et al.*, in good yield by reacting $[\text{Cu}(\text{O}_2\text{CH})]$ ¹¹⁰ and the phosphane at a low temperature in THF (Scheme 61).⁸⁹ It is fairly stable and tends to react further with FA (in excess) to form the adduct $[(\text{P}(\text{C}_6\text{H}_2\text{CH}_2\text{NMe}_2\text{-2})_3)\text{-CuOC}(\text{O})\text{H}\cdot 2\text{HOC}(\text{O})\text{H}]$, characterized by X-ray diffraction on single crystal. It decomposes at 200 °C to release CO_2 and H_2 and elemental copper via two possible pathways, a) by loss of the ligand and the regenerated starting $[\text{Cu}(\text{O}_2\text{CH})]$ degrades with release of hydrogen and carbon dioxide gases, b) or through the decarboxylation of $[(\text{P}(\text{C}_6\text{H}_2\text{CH}_2\text{NMe}_2\text{-2})_3)\text{Cu}(\text{O}_2\text{CH})]$ to form an unstable the copper-hydride species $[(\text{P}(\text{C}_6\text{H}_2\text{CH}_2\text{NMe}_2\text{-2})_3)\text{Cu}(\text{H})]$. However, there is no proof to support these hypotheses.



Scheme 60. Formation of the triazacyclononane $[(^t\text{Bu}_2\text{C}_6\text{N}_3\text{-CH}_2\text{CH}_2\text{CH}_2\text{BC}_8\text{H}_{14})\text{Cu}(\mu\text{-O}_2\text{CH})]$ by insertion of CO_2 .



Scheme 61. Formation of the phosphane complex $[\text{P}(\text{C}_6\text{H}_2\text{CH}_2\text{NMe}_2\text{-}2)_3\text{Cu}(\text{O}_2\text{CH})]$ from the $[\text{Cu}(\text{O}_2\text{CH})]$ precursor.

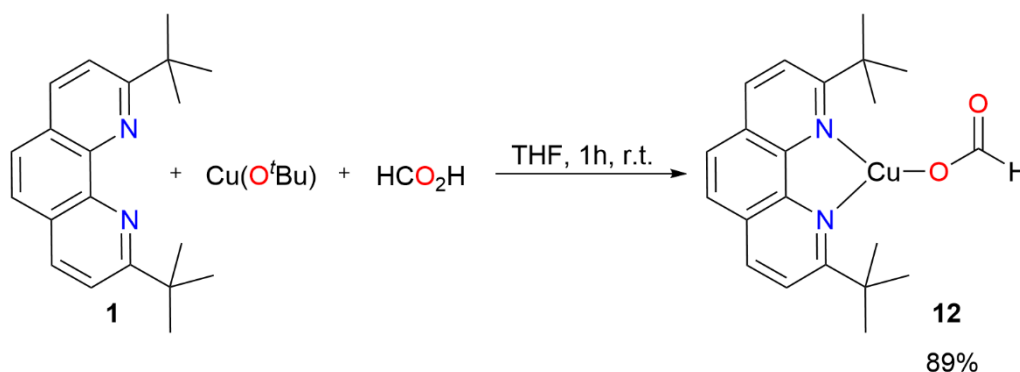
The use of copper catalysts in the field of hydrogen storage has been investigated. The ability of multinuclear copper hydride complexes to promote FA dehydrogenation, albeit with modest TONs and TOFs, have been presented in two examples by the groups of Tanase and Tilley.^{56,57} The formation of copper formates as key intermediates was suggested by their insightful observations. Only a few examples of copper formate active in hydrogenation and hydrosilylation of CO_2 into the corresponding formate and silylformate have been reported.^{102,104} Here, the loss of CO_2 from the copper formate species leads to the formation of a transient copper hydride, isolated by addition of the strong Lewis acid $\text{B}(\text{C}_6\text{F}_5)_3$ that stabilize the hydroborane copper species.¹⁰⁴ These results suggest that copper-catalytic dehydrogenation of FA and the CO_2 hydrogenation likely proceed *via* the copper formate and copper hydride intermediates which are chemically related. Depending on the nature of the ligand, these complexes can be more or less stable. Transient copper hydrides are generally more stable in polynuclear entities, whereas monometallic or polymetallic copper formate complexes can be stabilized by a variety of ligands (carbene, phosphine...). To date, the reversible passage from a copper formate and its hydride counterpart has not been directly observed. Furthermore, there are no report on copper formate catalyzing the dehydrogenation of FA into CO_2 and H_2 .

Our present study focuses on the synthesis and full characterization of the complex $[(\text{phen}^*)\text{Cu}(\kappa^1\text{-O}_2\text{CH})]$ (**12**), with the ligand $\text{phen}^* = 2,9\text{-di-}t\text{-tertbutyl-}1,10\text{-phenanthroline}$. Attempts to synthesize or trap the bulky monomeric hydride $[(\text{phen}^*)\text{CuH}]$, in particular through the reversible incorporation of labeled $^{13}\text{CO}_2$, are also presented. Furthermore, the reactivity of this copper formate to selectively dehydrogenate FA without the need for additives is discussed.

II. Results and discussions

II. 1. Synthesis and characterization of $[(\text{phen}^*)\text{Cu}^{\text{I}}(\text{O}_2\text{CH})]$ (**12**)

We previously observed that the bulky phenanthroline ligand 2,9-di-*tert*butyl-1,10-phenanthroline (phen^*) could form highly soluble $(\text{phen}^*)\text{CuX}$ monomeric complexes that are stable toward ligand redistribution (*vide supra*, Chapter 2 – III. 2. and III. 3.). We thus aimed at the isolation of the copper formate $[(\text{phen}^*)\text{Cu}^{\text{I}}(\text{O}_2\text{CH})]$ (**12**) species, and study its thermal decarboxylation to determine if it would yield a stable or detectable copper monohydride derivative. Indeed, Meyer *et al.* recently reported a synthesis of a $\mu_{1,3}$ -formate-bridged dicopper(II) complex $[\text{LCu}^{\text{II}}_2(\mu\text{-O}_2\text{CH})](\text{ClO}_4)_2$, with ligand (L) is a tetradentate N-donor with a central pyrazolate bridge and two appended 1,4,7-triazacyclonone (tacn) chelate arms.¹ A reduction of this species by Cp_2Co or Cp^*Co (Cp^* = pentamethylcyclopentadienide) spontaneously form a stable hexanuclear hydride copper(I) derivative $[\text{L}_2\text{Cu}^{\text{I}}_6(\text{H})_2](\text{ClO}_4)_2$ and releasing CO_2 .¹ Such decarboxylation process could be a promising approach to unusual monocopper(I) hydride complexes. We hypothesized this latter could be monomeric due to the congestion of the *t*Bu groups and because all the $[(\text{phen}^*)\text{CuX}]$ ($X = \text{Cl}, \text{F}, \text{OTf}$) or $[(\text{phen}^*)\text{Cu}(\text{L})]^+$ ($\text{L} = \text{CO}, \text{Me}_2\text{CO}$) derivatives reported so far are monomeric in the solid state.^{111–113}



Scheme 62. Synthesis of $[(\text{phen}^*)\text{Cu}^{\text{I}}(\text{O}_2\text{CH})]$ (**12**).

Complex $[(\text{phen}^*)\text{Cu}^{\text{I}}(\text{O}_2\text{CH})]$ (**12**) was readily obtained by the addition of 1 equiv. of phen^* to a THF solution of the yellow tetramer $[\text{Cu}(\text{O}^t\text{Bu})_4]$ (1 equiv.) and then by treatment with formic acid (1 equiv.) at room temperature (Scheme 62). The change of color (yellow to orange) was immediate. After stirring 1 h at room temperature and then evaporation of the volatiles and washing of the residue with pentane, complex **12** was readily isolated in good yield (89 %) as a dark-orange solid which still retained traces of FA despite prolonged drying. It has been characterized in solution by ^1H NMR and $^{13}\text{C}\{^1\text{H}\}$ NMR spectra and in the solid state by its infra-red spectrum and by elemental analysis. The ^1H NMR signal of the formate anion appears as a broad singlet at $\delta = 8.17$, a value displaced upfield compared to those of other $[\text{Cu}^{\text{I}}(\text{O}_2\text{CH})]$ species (range 9.01–8.40 ppm)^{89,102,104,108} and the signals of phen^* are shifted downfield in comparison with those of the free ligand. The $^{13}\text{C}\{^1\text{H}\}$ NMR spectrum only evidences signals of phen^* and the carbon atom of the formate is undetectable. The strong band at 1620 cm^{-1} in the infra-red spectrum is assigned to the $\nu_{\text{asym}}(\text{CO}_2)$ stretching mode of the coordinated formate (see SI). This value is close to those reported for example in the complexes $[(\text{triphos})\text{Cu}_2\text{O}_2\text{CH}]$ (1620 cm^{-1}),¹⁰⁸ $[\text{Cu}(\text{PPh}_3)_2\text{O}_2\text{CH}]\cdot\text{EtOH}$ (1607 cm^{-1}),⁹⁶ the phosphane $[(\text{P}(\text{C}_6\text{H}_2\text{CH}_2\text{NMe}_2)_3)\text{CuO}_2\text{CH}]$

(1607 cm^{-1}),⁸⁹ and $[\text{LCu}_2(\mu\text{-HCO}_2)](\text{ClO}_4)_2$ ($\text{L} = (\text{N},\text{N}'\text{-Me}_2\text{-C}_6\text{H}_{12}\text{N}_3)\text{CH}_2(\text{C}_3\text{HN}_2)(\text{N},\text{N}'\text{-Me}_2\text{-C}_6\text{H}_{12}\text{N}_3)$) (1570 cm^{-1}).¹

Single crystals of $[(\text{phen}^*)\text{Cu}(\kappa^1\text{-O}_2\text{CH})_{0.8}\text{I}_{0.2}]\cdot(\text{THF})_{0.5}$ (**12'**) could be grown in an NMR tube by slow diffusion of pentane into a crude THF mixture of **12** prepared in situ. The iodine atom presence in the crystal likely results from residual KI impurity contained in $[\text{Cu}(\text{O}^t\text{Bu})]$, the latter being synthesized from treatment of CuI with KO^tBu . Views of the structure of **12'** determined by X-ray diffraction are in Figure 62 with selected bond lengths and angles.

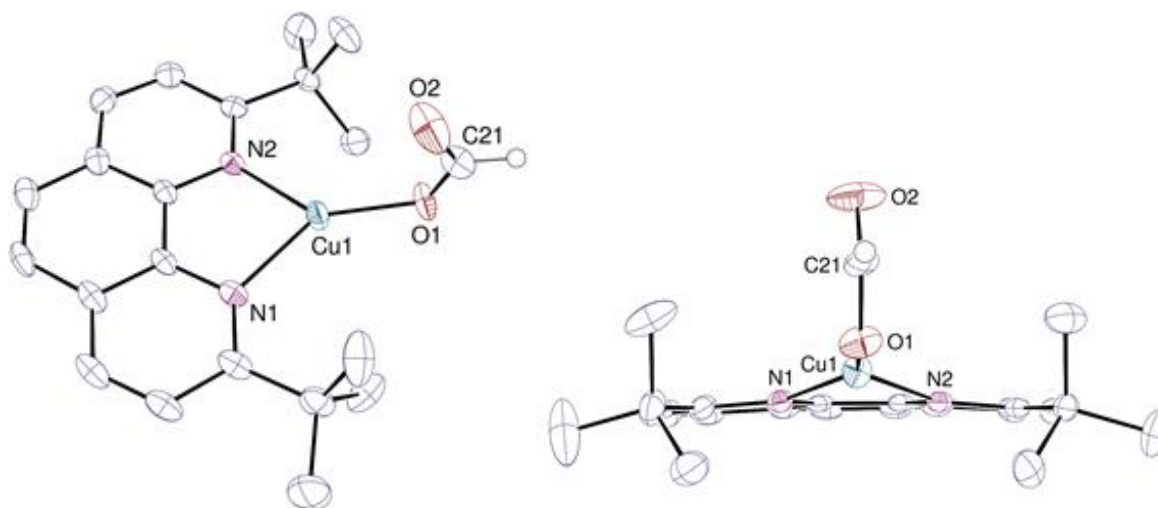


Figure 62. Two views of the crystal structure of complex **12'**. Displacement ellipsoids are drawn at the 50% probability level and hydrogen atoms are omitted except for that of formate. The minor iodide component is not shown. Selected bond distances (\AA) and angles (deg): Cu1–O1 1.883(3), Cu1–N1 2.029(3), Cu1–N2 2.080(3), O1–C21 1.248(5), O2–C21 1.242(4); N1–Cu1–N2 83.44(10), N1–Cu1–O1 140.69(13); N2–Cu1–O1 135.23(12).

12' is a monomeric, three-coordinate complex with the Cu^+ ion ligated to the N1, N2 and O1 atoms in a distorted trigonal geometry, with the minor iodide component being close to the formate carbon atom. As in other reported carbene-copper complexes^{102,104} the formate unit bonds to the copper center in an κ^1 -coordination mode through one of the oxygen atoms, with a Cu1–O1 bond length of 1.883(3) \AA , which is longer than in the 2-coordinate carbene species $[(\text{IPr})\text{Cu}(\kappa^1\text{-O}_2\text{CH})]$ (IPr = 1,3-bis(2,6-diisopropylphenyl)imidazol-2-ylidene) (**a**) (1.848(2) \AA)¹⁰² and $[(\text{CAAC}_1)\text{Cu}(\kappa^1\text{-O}_2\text{CH})]$ ($\text{CAAC}_1 = \text{cyclic(alkyl)(amino)carbene}$) (**b**) (1.863 \AA),¹⁰⁴ but smaller than that found in the tetracoordinate phosphane compound $[(\text{P}(\text{C}_6\text{H}_2\text{CH}_2\text{NMe}_2)_2)_3\text{Cu}(\kappa^1\text{-O}_2\text{CH})]$ (**c**) (2.041(2) \AA).⁸⁹ Unlike in the IPr-ligated copper formate¹⁰² where the two C–O distances are distinct by 0.085 \AA , there is no significant difference between the C21–O1 and C21–O2 distances (1.248(5) \AA , 1.242(4) \AA , respectively), indicating charge delocalization over the carboxylic moiety. However, the formate ligand is not coordinated in chelating κ^2 -fashion as shown by the long Cu1...O2 distance of 3.112(4) \AA . The Cu–N distances are in the range of values found in $[(\text{phen}^*)\text{CuX}]$ complexes. In addition, steric hindrance due to the bulky *tert*-butyl substituents caused the copper center to deviate from the mean plane of the phen* by 0.520(2) \AA . This typical coordination mode can also be observed in other $[(\text{phen}^*)\text{CuX}]$ ($\text{X} = \text{halide}$) copper complexes.^{106,112,114} In the packing, centrosymmetric dimers are formed through π -stacking interactions [centroid...centroid distances, 3.5660(19)–4.1058(19) \AA ; dihedral angles, 0–7.40(15) $^\circ$] and the distance between the phenanthroline mean planes reaches 3.412 \AA .

II. 2. Attempts to the copper monohydride [(phen*)Cu–H]

The use of bulky ancillary ligands or encapsulating ligands is a helpful strategy to stabilize very reactive species. It has been considered in copper chemistry by the groups of Bertrand¹¹⁵ and Sollogoub¹¹⁶ to generate or isolate mono copper hydride species in organic solution. We thus expected that the steric bulk of the phen* ligand could be promising to afford such hydride species.

All attempts to generate [(phen*)Cu–H] by reacting [(phen*)Cu–I] with the super hydride KBHET₃ or KH (with or without the 18-crown-6 ether), proved unsuccessful in THF, leading to rapid degradation and formation of a Cu(0) black deposit. Addition of 1 equiv. phen* (per Cu⁺) to the Stryker's reagent [(C₆H₅)₃P]CuH₆ in benzene also led to decomposition while hydrogenation (1 bar) of a 1:1 mixture of [Cu(O^tBu)] and phen* under H₂ (in THF) or its treatment with 1 equiv. pinBH (in benzene) led rapidly to black precipitates.

We thus tried to detect the [(phen*)Cu–H] complex by heating a solution of **12** in THF at 50 °C for hours. Complex **12** decomposed slowly by releasing CO₂ and H₂. No other species could be detected by ¹H NMR and after further 7 h at 60 °C, only free phen* was present in solution with a dark deposit (see SI). The CO₂ release suggested formation of a transient Cu–H species. We tried to capture it using reactive groups like the Lewis acids BEt₃, B(C₆F₅)₃ or the unsaturated molecules Et–NCO or phenylacetylene.¹¹⁷ Indeed, the transient [(P₃N)CuH] hydride was trapped with B(C₆F₅)₃ as the unusual but stable triethylborohydride copper complex [(P₃N)Cu(μ–H–BEt₃)] (P₃N = N,N'-(2,4,6-C₆H₂Me₃)₂C₃H₆N₂C).¹¹⁷ In contrast, in the carbene series, [(IPr)Cu(O^tBu)] underwent hydrosilylation to give the stable dimer [(IPr)CuH]₂, which easily converts to the monoformate derivative under 1 atm CO₂.¹⁰² Unfortunately, the expected hydride reaction products were not obtained in this case, but rather undetermined and intractable mixtures. For example, with EtNCO (4 h at 50 °C), no formation of the expected [Cu]–NEtCHO complex could be identified.¹¹⁸ In the presence of phenylacetylene, the immediate formation of greenish solution and phen* decoordination are observed. With BEt₃, **12** degraded instead of forming a copper borohydride product.

It is only with B(C₆F₅)₃ that a complex could be characterized: [(phen*)Cu]₂(μ–O₂CH)[(HCO₂–κ¹)B(C₆F₅)₃] (**13**) was isolated as light orange crystals, indicating initial formate abstraction by the Lewis acidic boron center. A view of the structure of **13** determined by X-ray diffraction is represented in *Figure 63* with selected bond lengths and angles. The Cu–N distances are classical and similar to those found in **12'**. The mean distance of 1.918 (7) Å for the Cu–O bond lengths is notably longer than the corresponding average values of 1.859 (2) Å measured in the bridged NHC dimer [(IDipp)Cu]₂(μ–O₂CH)[BF₄] (IDipp = {2,6-ⁱPr₂C₆H₃}₂(C₃N₂H₂)).¹¹⁹ Of interest are the C–O bond lengths in the bridging and monodentate formate ligands of **13**. In the former entity, the two C–O distances are quite identical and similar to those found in the monodentate complex **12'** and suggest charge delocalization. In contrast, in the anionic moiety [(HCO₂)B(C₆F₅)₃][–] the difference of 0.1 Å between the two C–O bonds likely reflects single and double bond character as in the species [(IPr)Cu(κ¹–O₂CH)].¹¹⁴ The ¹H NMR spectrum of **13** in THF-*d*₈ revealed two broad ¹H NMR signals at 8.19 ppm and 8.43 ppm^{120–122} for the boron and copper formate, respectively, and the attribution was made possible with the synthesis of the ammonium salt [HNEt₃][(HCO₂)B(C₆F₅)₃]. We also observed for **13** upfield shifted signals for the C₆F₅ moiety and B center in ¹⁹F NMR and ¹¹B NMR (see SI).^{121–123}

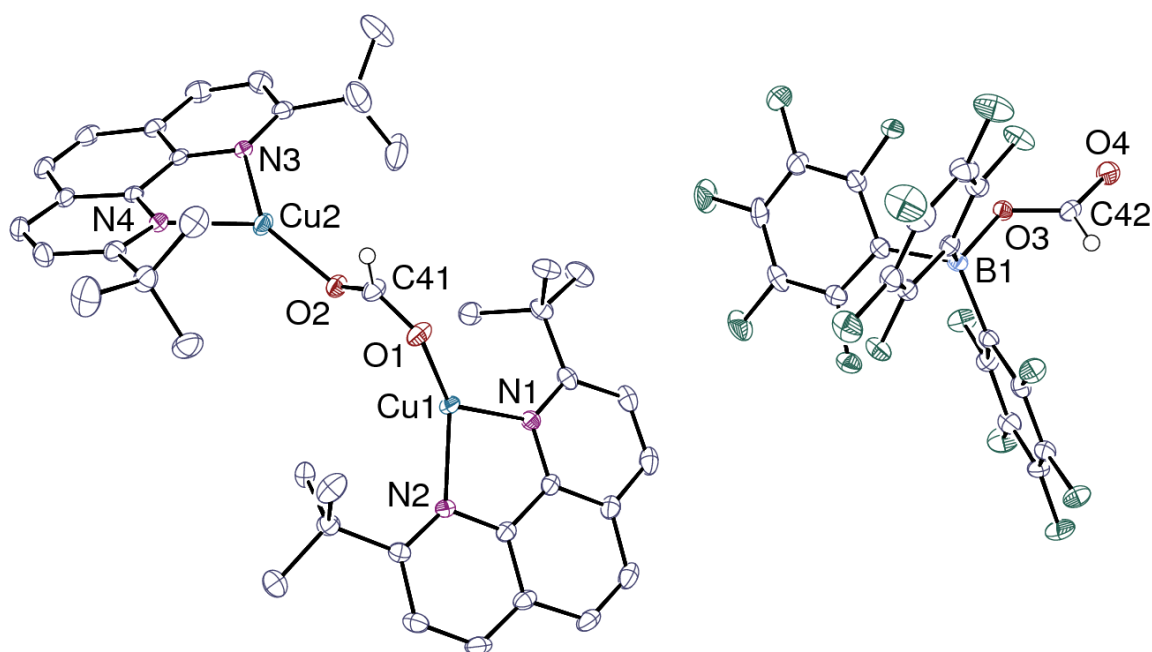
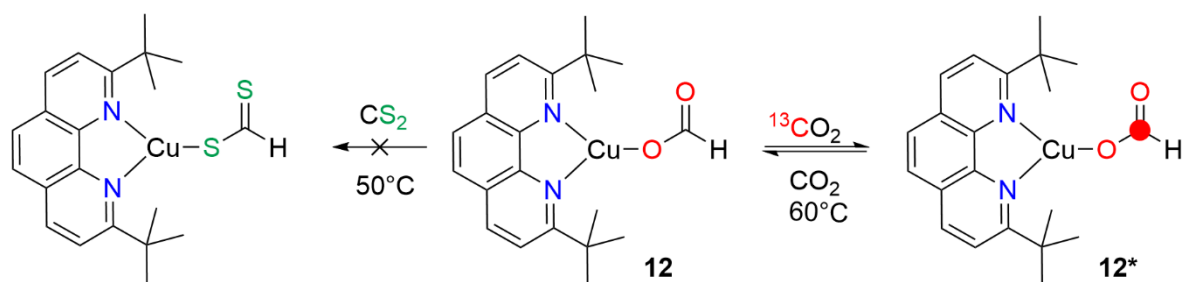


Figure 63. View of the crystal structure of complex **13**. Displacement ellipsoids are drawn at the 50% probability level and hydrogen atoms are omitted except for that of formate. Selected bond distances (Å) and angles (deg): Cu1–O1 1.9116(13), Cu1–N1 2.0508(15), Cu1–N2 2.0458(15), Cu2–O2 1.9260(13), Cu2–N3 2.0584(15), Cu2–N4 2.0585(15), \langle Cu–N \rangle 2.053(5), O1–C41 1.245(2), O2–C41 1.251(2), B1–O3 1.513(2), O3–C42 1.301(2), O4–C42 1.207(2); N1–Cu1–N2 83.20(6), O1–Cu1–N1 135.82(6), O1–Cu1–N2 135.17(6), N3–Cu2–N4 82.85(6), O2–Cu2–N3 136.43(6); O2–Cu2–N4 137.44(6).

II. 3. Stoichiometric reaction with $^{13}\text{CO}_2$

As our attempts to chemically trap a hydride were not successful, we thus considered the dynamic isotope exchange method¹²⁴ with $^{13}\text{CO}_2$ and its related CS_2 as a means of revealing this transient species.

In 2016, Guan *et al.* tracked the decarboxylation of the nickel formate $[(\text{POCOP})\text{Ni}(\kappa^1\text{-O}_2\text{CH})]$ ($\text{POCOP} = \{2,6\text{-}(\text{R}_2\text{PO})_2\text{C}_6\text{H}_3\}$; $\text{R} = \text{}^t\text{Bu}, \text{}^i\text{Pr}$) by using CS_2 instead of the expensive labeled $^{13}\text{CO}_2$.⁷³ They observed the formation of the stable dithioformate $[(\text{POCOP})\text{Ni}(\text{S}_2\text{CH})]$ derivative, plausibly *via* the transient formation of a nickel hydride.⁷³ Because of the higher reactivity of liquid CS_2 versus CO_2 gas for the insertion reaction,^{125,126} and because these authors claimed that the method is applicable to many d-trans complexes, we performed similar reaction. Disappointingly, **12** proved inert to an excess of CS_2 in THF at room temperature (Scheme 63). The NMR spectra effectively showed no evolution, and further warming at 50 °C for 3 h only evidenced the slow decomposition into free ligand and black elemental copper.



Scheme 63. Insertion reactions of **12** with CS_2 and $^{13}\text{CO}_2$ at 50 and 60 °C, respectively.

We thus changed our strategy to detect a potentially active copper hydride intermediate by considering a dynamic isotopic exchange procedure with labeled $^{13}\text{CO}_2$ (Scheme 63). This method, recently developed with copper(I) catalysts, is based on the reversible carboxylation and decarboxylation processes for efficient one-step insertion of a carbon tag into carboxylate substrates without structural modification.¹²⁴ If working, such a method would be useful to access the marked formate anion from the corresponding labeled CO_2 .

A J-Young NMR tube containing a $\text{THF-}d_8$ solution of **12** was pressurized with 1 atm $^{13}\text{CO}_2$ and heated at 60 °C for *ca* 4 h. ^1H and ^{13}C NMR monitoring did not show degradation of the starting complex, but evidenced slow replacement of the unlabeled HCO_2^- with $\text{H}^{13}\text{CO}_2^-$. Enrichment of the formate ligand in ^{13}C supports the initial decarboxylation of **12** into the putative hydride $[(\text{phen}^*)\text{Cu}-\text{H}]$ that would immediately trap $^{13}\text{CO}_2$ to give the ^{13}C -labeled formate derivative **12***. The evolution of **12** into **12*** is confirmed by ^{13}C NMR. Indeed, while the formate carbon atom of **12** is not detected, the $^{13}\text{C}\{^1\text{H}\}$ NMR spectra showed a singlet at $\delta = 164.65$ (in the expected range for a formate anion) that grew up continuously with time (Figure 64a). The signal appeared as a doublet with a coupling constant $J = 198$ Hz in the non-decoupled ^{13}C NMR spectrum (20 % isotopic enrichment, IE, by ^1H NMR integration after 4h30) (Figure 64c). The ^1H NMR signal for the formate unit of **12** appears as a broad singlet at 8.27 ppm (Figure 64b) that splits by coupling with the ^{13}C atom during the exchange process, and with a constant $J = 198$ Hz identical to that measured for the C atom of the coordinated $\text{H}^{13}\text{CO}_2^-$ ligand in the ^{13}C spectrum (Figure 64c, top). Continuous heating of the reaction for 3 more hours enhanced the ^{13}C enrichment (30 % IE) along with the degradation of **12** observed by the formation of free phen^* .

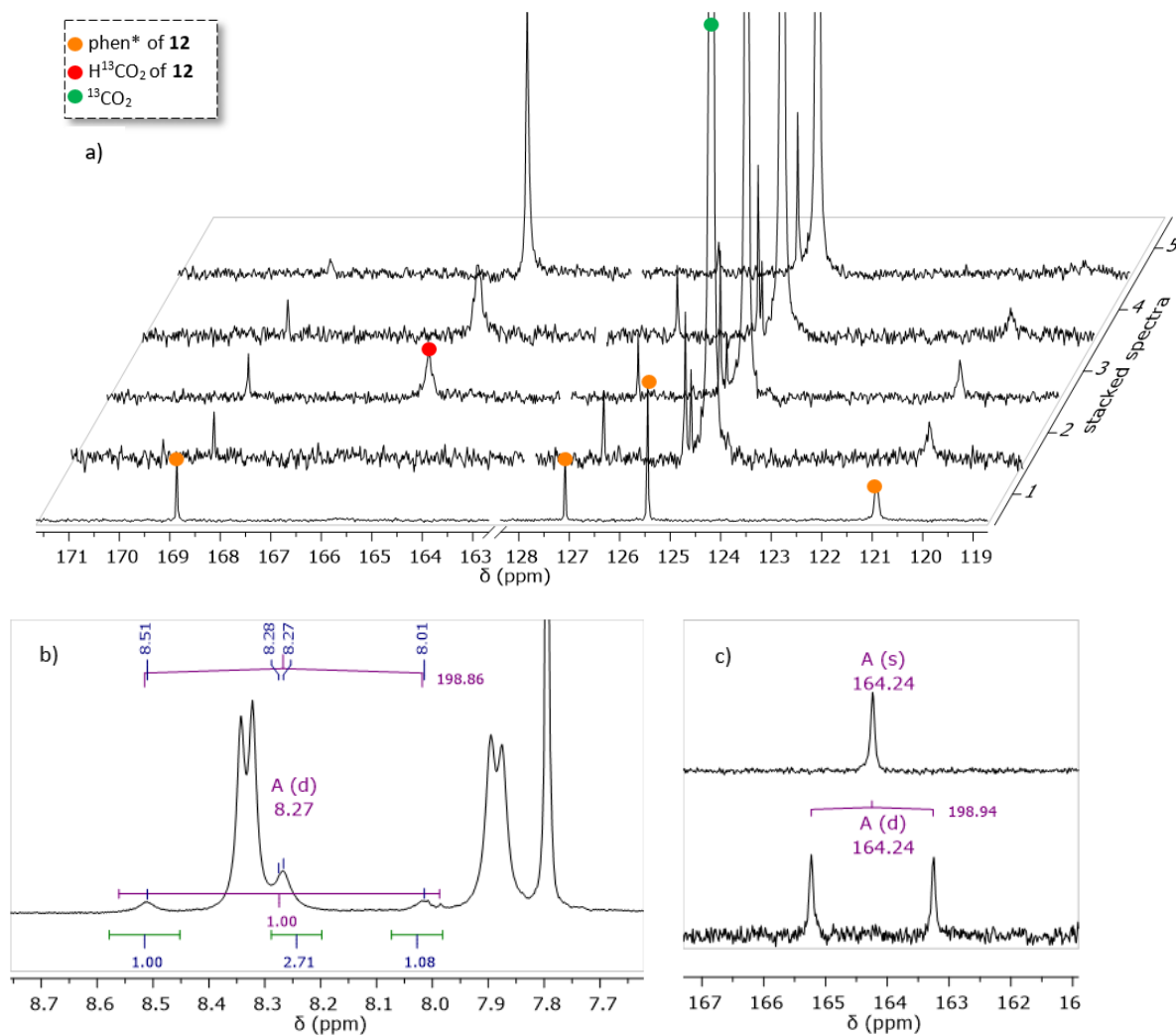


Figure 64. a- $^{13}\text{C}\{^1\text{H}\}$ NMR spectrum showing the increase with time of the H^{13}CO_2 signal at 164 ppm (the signal increases from top to down). b- ^1H NMR signal of the H^{12}CO_2 ligand of **12** which is split in the labelled analogue **12***. c- Singlet signal (bottom) in ^{13}C NMR spectrum and doublet signal (top) in $^{13}\text{C}\{^1\text{H}\}$ NMR of H^{13}CO_2 in **12***.

The ^1H - ^{13}C HSQC (heteronuclear single quantum coherence) analysis evidenced the correlation between the labeled carbon atom of the formate ion ($\delta = 164.72$) and its neighboring proton ($\delta = 8.28$) (Figure 65). These observations provide solid proof for a successful $^{12}\text{CO}_2/^{13}\text{CO}_2$ exchange in $[(\text{phen}^*)\text{Cu}(\text{O}_2\text{CH})]$, and clearly suggest the involvement of a copper hydride as transient intermediate. In their investigations into the copper-catalyzed hydrosilylation of CO_2 to silyl formate,¹²⁷ Motokura *et al.* also reported the capture of CO_2 by a tricoordinated copper diphosphine hydride to give the corresponding formate. This hydride was regenerated from the formate by treatment with a polymethylhydrosiloxane (PMHS).¹²⁷

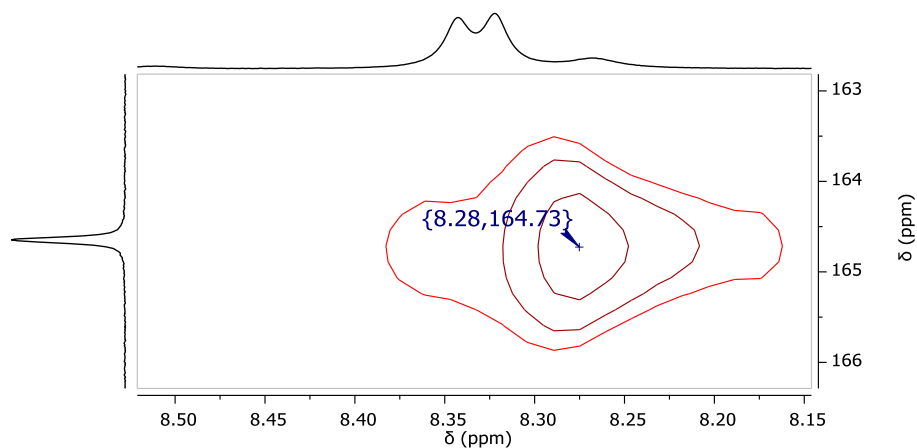
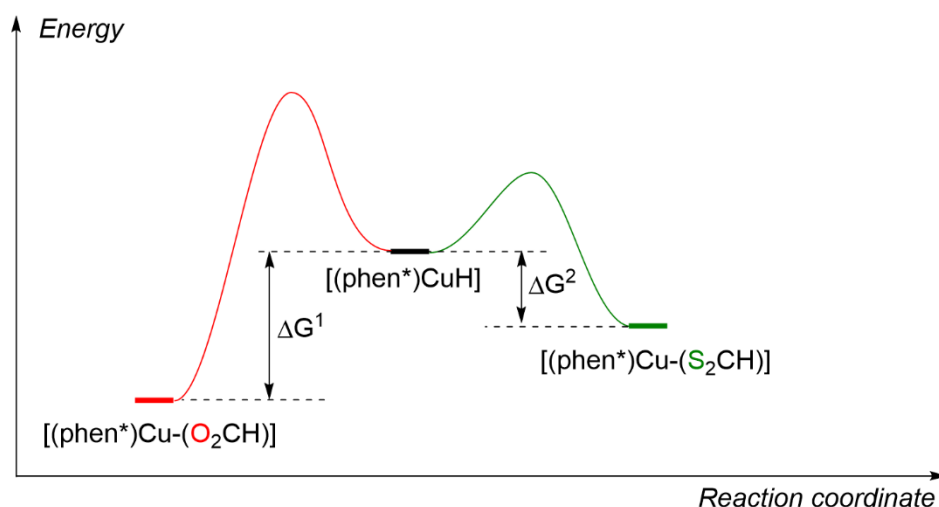
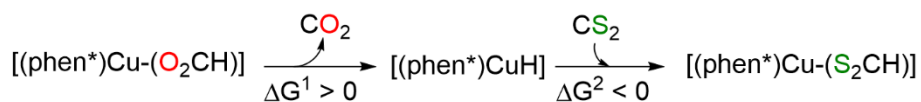


Figure 65. Zoom of the ^1H - ^{13}C HSQC spectrum of the crude mixture of **12** under $^{13}\text{CO}_2$ (after 60 °C at 4.5 h) in THF- d_8 evidences a correlation between the $\{^1\text{H}\}^{13}\text{C}$ NMR signal of the formate (at $\delta = 164$) and its H signal in the ^1H NMR spectrum (centered at $\delta = 8.2$).

The above results show that the copper formate easily undergo $\text{CO}_2/^{13}\text{CO}_2$ exchange producing 30 % of the labeled copper formate **12***, but does not react with CS_2 in THF and even degrades at 50 °C. These distinct reactivities of **12** toward CO_2 and CS_2 in the same solvent (THF) may be first surprising as CS_2 is reported to be more reactive than CO_2 toward nucleophilic attack. We can tentatively bring some hypotheses to explain this.

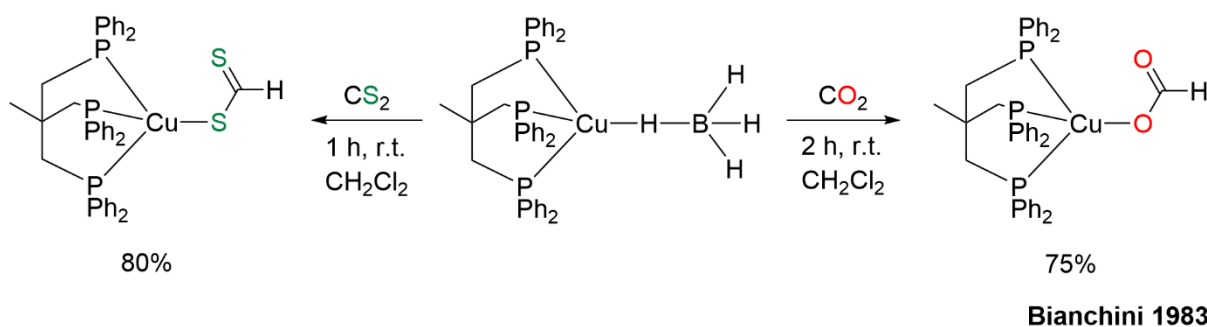
CS_2 is more electrophilic than CO_2 and thus more favorable to hydride attack. The possibility that CS_2 insertion proceeds *via* a higher activation energy pathway than CO_2 is unlikely. The CS_2 insertion is therefore believed to be under thermodynamic control and to have an energy profile such as that proposed in *Scheme 64*. The reaction would start with the decarboxylation of **12** to generate the copper hydride. This reaction is known to be endergonic ($\Delta G^1 > 0$)¹²⁸ and requires a relatively high activation energy barrier (*vide supra*, Chapter 1 – III. 2. and Chapter 2 – III. 6.).

The insertion of CS_2 into the $[\text{Cu}]\text{--H}$ should be a favor exergonic process ($\Delta G^2 < 0$) because the H ligand has a strong hydride character and the instable copper hydride is certainly at a higher energy level than $[(\text{phen}^*)\text{Cu}(\text{S}_2\text{CH})]$. The latter species would be on the energy profile at the level: $\Delta G = \Delta G^1 + \Delta G^2$. In the thermal reaction of **12** and CS_2 , the transient hydride can add CS_2 reversibly, but the thermodynamic is pushed to the left, towards the regeneration of formate **12**. Due to the release of CO_2 into the gas when **12** is heated (the solubility of CO_2 decreases with increasing temperature), regeneration of the latter is impossible and, ultimately, the hydride and dithioformate complexes are the only ones in solution that can interconvert each other rapidly. Under heating (50 °C), the unstable hydride and the likely thermally sensitive dithioformate progressively degrade, with release of H_2 , as observed experimentally.



Scheme 64. Schematic energy profile for the reaction of $[(\text{phen}^*)\text{Cu}(\text{O}_2\text{CH})]$ (**12**) with CS_2 .

The lower stability of copper dithioformate vs **12** could also be explained by the weak Cu–S bond (285 kcal.mol⁻¹) in comparison to the Cu–O bond (343 kcal.mol⁻¹).¹²⁹ However, a few dithioformate complexes of Cu(I) are existing.^{108,130–132} All of them involve bulky phosphine ligands and have been synthesized by metathesis of the precursor $[\text{Cu}]\text{X}$ and dithiocarbamate salts or by insertion of CS_2 in copper(I) borohydride species.^{108,132} The latter case adds fuel to our fire concerning the formation of $[(\text{phen}^*)\text{Cu}(\text{S}_2\text{CH})]$. Bianchini *et al.* reported the formation of $[(\text{triphos})\text{Cu}(\kappa^1\text{-S}_2\text{CH})]$ by treating $[(\text{triphos})\text{Cu}(\text{BH}_4)]$ with CS_2 (Scheme 65).¹⁰⁸ Its molecular structure has not been elucidated but, from NMR and IR data, it is thought to be similar to that of the formate derivative $[(\text{triphos})\text{Cu}(\kappa^1\text{-O}_2\text{CH})]$ (Scheme 65).¹⁰⁸ A research in the Cambridge Data Base revealed a unique structure for a $[\text{Cu}](\text{S}_2\text{CH})$ complex that is the trimetallic $[(\text{R}_2\text{PNHPR}_2)_3\text{Cu}_3(\mu^3\text{-H})(\mu\text{-}\kappa^2\text{-S}_2\text{CH})]$, where the HCS_2^- ligand is bridging.¹³²



Scheme 65. The insertion of CO_2 and CS_2 into a $[(\text{triphos})\text{Cu}(\text{BH}_4)]$ complex.

We carried out reaction in THF. We might hypothesized that coordination of CS_2 vs CO_2 onto the Cu^+ center could be more hindered by the coordinating solvent and also because the sulfur atom has a larger size than the oxygen atom. But the hydride opens up space in the coordination sphere, and the values of ionization potential and electron affinity show that CS_2 is a relatively better σ -donor and a better π -acceptor than CO_2 .¹²⁶

With regard to the mechanism of the CX_2 ($X = O, S$) insertion in Cu–H bond, there are numerous reports dealing with the insertion of CO_2 into copper hydrides. Most are dimeric copper hydride bearing carbene-NHC ligand (i.e. IPr, 6Dipp, 7Dipp)^{102,104,133} or copper hydride cluster supported by phenanthroline⁹⁷ or tetrakisphosphine ligand.⁹⁸ Monomeric copper hydride species has never been isolated except one trapped in the cavity of a NHC-capped cyclodextrin.¹¹⁶

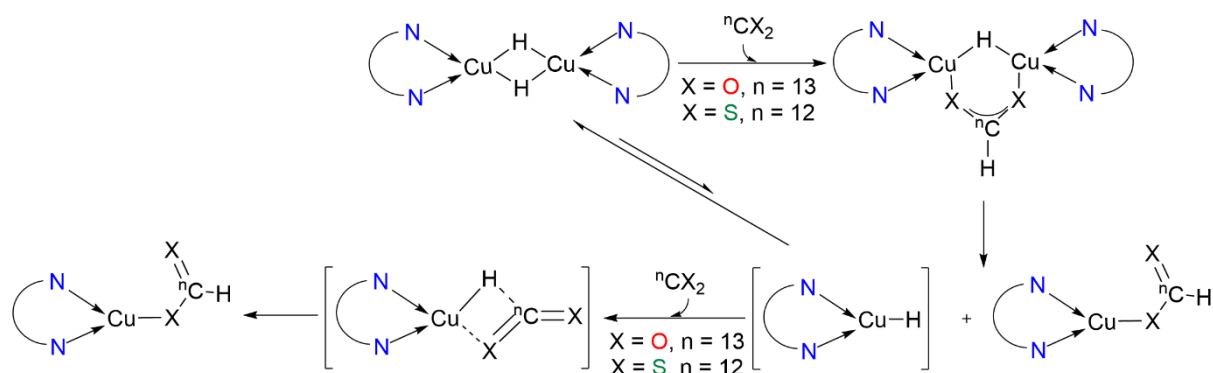
Based on the literature, we can propose two possible routes (*Scheme 66*) for the decarboxylation of the formate **12** and further insertion of CO_2/CS_2 molecules into the putative hydride $[(phen^*)CuH]$. The two pathways rely on a first step where the formate ligand of **12** would undergo a classical β -H elimination (*Scheme 66, 1*) or would proceed via intramolecular rearrangement and displacement of the H-bound formate (*Scheme 66, 2*), as proposed by Milstein and Schneider groups with iron complexes, to generate the copper hydride.^{48,49}

The CO_2 and CS_2 molecules can coordinate in a “end on” or “side on” fashion to the copper ion and transfer of the hydride leads to the corresponding complexes $[(phen^*)Cu(O_2CH)]$ or $[(phen^*)Cu(S_2CH)]$, respectively. Their formation is reversible as discussed above.

This pathway can support formation of the adducts $[(phen^*)Cu(H)(X_2C)]$ ($X = O, S$). The insertion of CO_2 is rapid so that under thermal condition and under $^{13}CO_2$, we did not observed degradation but instead $^{13}C/^{12}C$ exchange on the formate. In presence of CS_2 , yet expected to be more reactive than CO_2 , the rapid interconversion between $[(phen^*)Cu(S_2C)]$ and $[(phen^*)CuH]$ which are less stable than the formate precursor, would bring decomposition into elemental copper, free ligand and H_2 as observed experimentally. If the hydride proves inert toward CS_2 , then decomposition is self-evident.

monomer would either dimerize again into the dimer, repeating the process, or would insert directly $^{13}\text{CO}_2$ or CS_2 to form the related products.

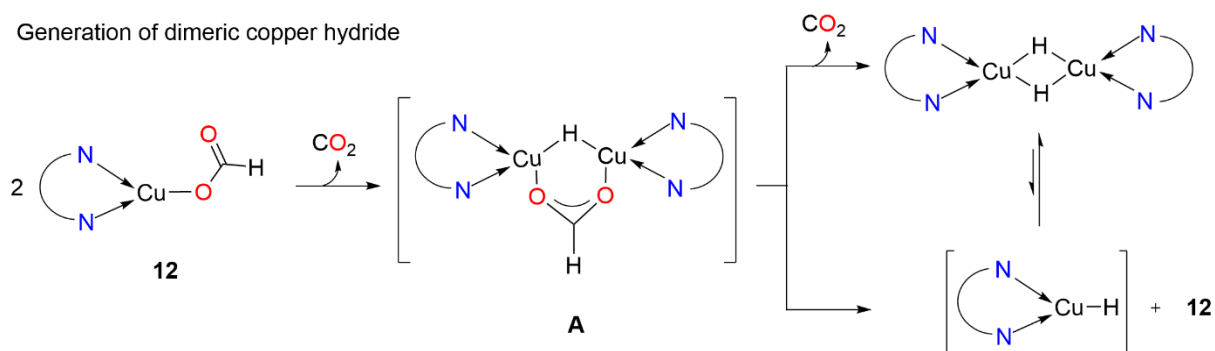
Insertion via dimeric copper hydride



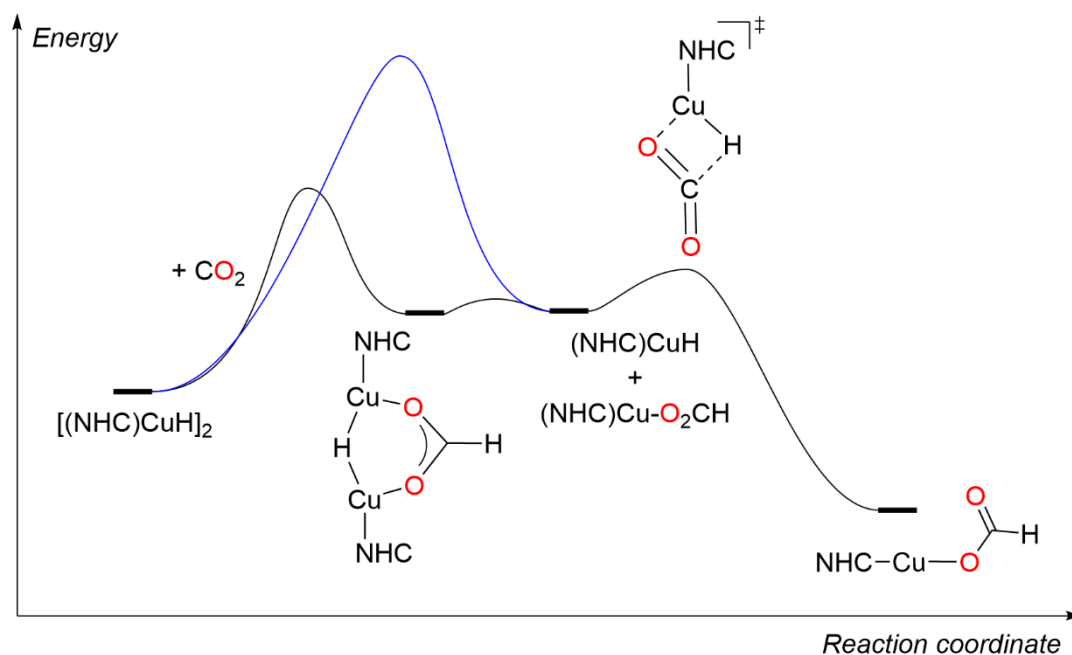
Scheme 67. Proposed insertion mechanism of $^{13}\text{CO}_2/\text{CS}_2$ from $[(\text{phen}^*)\text{Cu}(\kappa^1\text{-O}_2\text{CH})]$ (**12**) via dimeric copper hydride species.

Formation of $[(\text{phen}^*)\text{CuH}]_2$ from the formate complex **12**, may proceed by decarboxylation of **12** into $[(\text{phen}^*)\text{Cu}(\text{H})]$ which might be trapped, reversibly, with 1 equivalent of **12** to form the intermediate $[(\text{phen}^*)\text{Cu}]_2(1,3\text{-}\mu\text{-O}_2\text{CH})(\mu\text{-H})$ (**A**) (Scheme 68). Decarboxylation of the latter would afford $[(\text{phen}^*)\text{CuH}]_2$. Considering the energy profile proposed by Bullock's group (Scheme 69, in black),¹⁰¹ since the decarboxylation of **A** would require a higher activation pathway, formation of $[(\text{phen}^*)\text{CuH}]_2$ by this way is unlikely. Conversely, decomposition of **A** into monomeric copper hydride and copper formate requires less energy. Although the copper hydride may tend to dimerize rapidly to gain kinetic stability, the high energy barrier to overcome is an impediment (Scheme 69, in blue). In contrast, insertion of CX_2 ($\text{X} = \text{O}, \text{S}$) into the Cu-H bond of the monomer is energetically favorable and would bring the copper formate (or dithioformate) product. Consequently, the insertion of CX_2 into the Cu-H bond probably takes place from the monomeric species $[(\text{phen}^*)\text{Cu}(\text{H})]$ and dimerisation of the latter must be disregarded.

Generation of dimeric copper hydride



Scheme 68. Proposed mechanism for the formation of dimeric copper hydride $[(\text{phen}^*)\text{Cu}(\text{H})]_2$ via $[(\text{phen}^*)\text{Cu}(\text{O}_2\text{CH})]$ **12**.



Scheme 69. Energy profile implication of CO_2 insertion into $[(\text{NHC})\text{CuH}]_2$ (in black) and the dissociation of $[(\text{NHC})\text{CuH}]_2$ into monomer $[(\text{NHC})\text{CuH}]$ (in blue). (modified scheme from the original image taken from Bullock et al.¹⁰¹)

One way to clarify this hypothesis would be to prepare $[(\text{phen}^*)\text{CuH}]_2$ and test its reactivity towards CO_2 insertion. However, all our attempts to generate $[(\text{phen}^*)\text{Cu-H}]$ were unsuccessful, as mentioned above (*vide supra*, Chapter 3 – II. 2.)

In summary, formation of the intermediate $[(\text{phen}^*)\text{CuH}]$ from the decarboxylation of $[(\text{phen}^*)\text{Cu}(\kappa^1\text{-O}_2\text{CH})]$ (**12**) was not detected directly but indirectly by the ^{13}C enrichment of the formate ligand in **12** when placed under $^{13}\text{CO}_2$. The labelled copper formate $[(\text{phen}^*)\text{Cu}(\text{O}_2^{13}\text{CH})]$ was identified by NMR analysis and the equilibrium between the two complexes **12** and **12*** was indicated by an isotopic enrichment of 30%. In contrast, complex **12** was not reactive with CS_2 and the reaction did not deliver the insertion product $[(\text{phen}^*)\text{Cu}(\text{S}_2\text{CH})]$. The lower stability of $[(\text{phen}^*)\text{Cu}(\text{S}_2\text{CH})]$ compared to that of the starting material **12** may be the key factor. Different mechanisms have been proposed for the behavior of **12** and $^{13}\text{CO}_2$ and involve a transient hydride $[(\text{phen}^*)\text{CuH}]$. The pathway considering dimerization of the copper hydride monomer to $[(\text{phen}^*)\text{Cu}(\text{H})]_2$ would be unlikely, as energy profile proposed by Bullock proved a decarboxylation via a dimeric $[\{(\text{NHC})\text{Cu}\}_2(1,3\text{-}\mu\text{-O}_2\text{CH})(\mu\text{-H})]$ species is less favorable. The other mechanistic views are plausible but remain inconclusive.

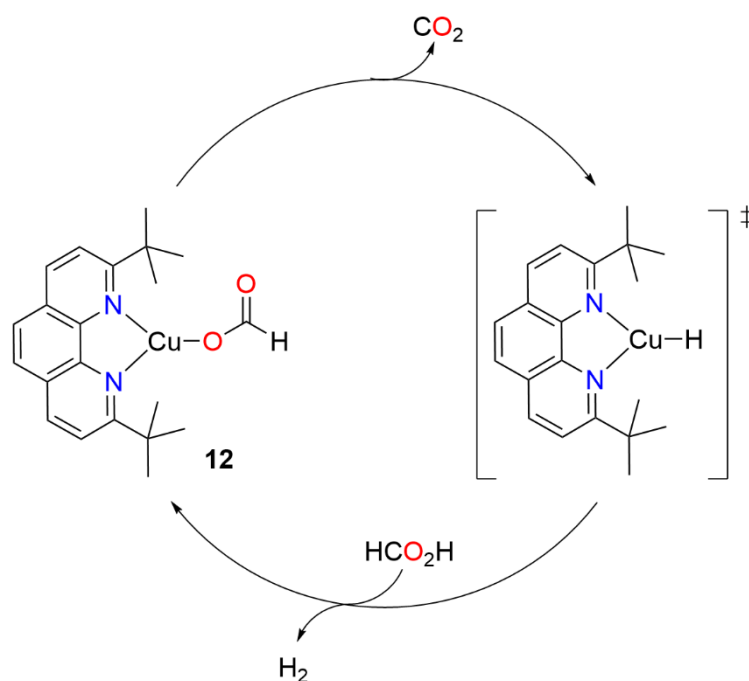
The dynamic exchange process of **12** under CO_2 suggested that it could be a rare copper catalyst for the dehydrogenation of formic acid. We reasoned that if the hydride intermediate could trap gaseous CO_2 , it should also react quickly with the liquid acid HCO_2H , which was more abundant in the reaction medium.

II. 4. Catalytic dehydrogenation of formic acid (FA)

Most homogeneous catalysts for FA dehydrogenation are based on noble metals such as Ru, Rh and Ir. However, less expensive and more abundant metals have been less explored, especially copper. The first Cu-catalyzed homogeneous systems for HCO_2H decomposition were reported only in 2014.⁵⁵ The

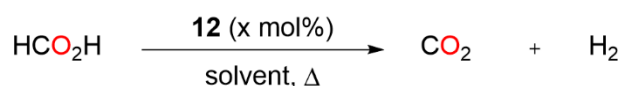
Cu(I) and Cu(II) precursors ($\text{Cu}(\text{OAc})_2$, $\text{Cu}(\text{acac})_2$, $\text{Cu}(\text{O}_2\text{CH})_2$, $\text{Cu}(\text{NO}_3)_2$, CuCl_2 , CuO , CuCl , CuI , $\{\text{CuH}(\text{PPh}_3)\}_6$) in solution in $\text{HCO}_2\text{H}/\text{Et}_3\text{N}$ displayed a low catalytic activity⁵⁵ which was found dependent on the nature of the amine as confirmed later by a DFT study (*vide supra*, Chapter 3 – I. 2. 3.).⁶⁰ In 2019, the hexanuclear cationic copper hydride $[\text{Cu}_6(\mu^3\text{-H})_2(\text{L})_3(\text{tBNC})_4][\text{PF}_6]_4$, involving a linear tetradentate phosphine ($\text{L} = \text{meso-Ph}_2\text{PCH}_2\text{P}(\text{Ph})(\text{CH}_2)_4\text{P}(\text{Ph})\text{-CH}_2\text{PPh}_2$), showed low catalytic activity for H_2 release from HCO_2H at 70°C in acetonitrile solution with tBuNC and NEt_3 additives.⁵⁷ At last, in 2023, O'Hair *et al.* revealed that the mononuclear cuprate hydride anions $[(\text{X})\text{CuH}]^-$ ($\text{X} = \text{H}^-, \text{O}_2\text{CH}^-, \text{BH}_4^-$ and CN^-) reacted in the gas-phase with formic acid to release H_2 with formation of the formate $[(\text{X})\text{Cu}(\text{O}_2\text{CH})]^-$ compound.¹³⁴ The latter decarboxylates readily *via* collision-induced dissociation to regenerate the initial copper hydride.

Our approach to selective composition of FA into CO_2 and H_2 promoted by copper formates complex (**12**) without the need of additives is shown in Scheme 70.



Scheme 70. Proposed catalytic cycles for the dehydrogenation of formic acid catalyzed by **12**.

Table 1 summarizes the catalytic activity of **12** under different reaction conditions. Gas evolution was measured by ^1H NMR spectra and GC analysis (gas chromatography analysis) and the consumption of HCO_2H (FA) was followed by ^1H NMR with mesitylene as internal standard. The appearance and evolution of H_2 was detected at $\delta = 4.59$ ppm in ^1H NMR, along with the diminution of the signals of HCO_2H (Figure 66 and Figure 67).



Entry	x (mol%)	Solvent	T (°C)	Time (h)	Conversion ^a (%)
1	0	THF- <i>d</i> ₈	100	16	0
2	10	THF- <i>d</i> ₈	100	2,5	100 ^{b,c}
3	5	THF- <i>d</i> ₈	100	3	27
				8	90 ^c
4	1	THF- <i>d</i> ₈	100	15	40 ^c
5	5	THF- <i>d</i> ₈	80	4	4
6	5	THF- <i>d</i> ₈	60	15	0
7	14	MeCN- <i>d</i> ₃	60	15	0
8	5	MeCN- <i>d</i> ₃	100	8	0

^a Conversions measured by ¹H NMR against mesitylene (10 mol%) as internal standard. ^b TOF = 4 h⁻¹; ^c **12** is degraded

Table 1. Optimization of the reaction conditions for the dehydrogenation of formic acid with complex **12**.

When heated to 100 °C, which is a temperature favoring decarboxylation of **12** (see above), the ¹H NMR spectra of a THF-*d*₈ solution of **12** (10 mol%) containing 18 μL of HCO₂H evidenced the selective release of H₂ and no trace of CO was detected by GC analysis. In the absence of **12**, HCO₂H was not degraded (Table 1, entries 1–2). NMR monitoring of the dehydrogenation of formic acid and of the behavior of the catalyst **12** was recorded by following the aromatic signals of the phen* ligand concomitantly with the degradation of FA (Figure 66). At first (t = 0), the phen* signals of **12** in the HCO₂H-THF-*d*₈ solution are shifted downfield (by 0.08–0.1 ppm) by comparison to those of isolated **12** in THF-*d*₈, suggesting a possible interaction between **12** and the acid *via* the formate ligand (Figure 66). Such interaction would explain why **12** is always contaminated with formic acid. In fact, [Cu](O₂CH)⋯HO₂CH interactions have been clearly established in some structurally characterized copper(I) formate, such as [Cu(PPh₃)₃O₂CH]•HCO₂H and the phosphane [(P(C₆H₂CH₂NMe₂-2)₃)CuO₂CH]•2HO₂CH,^{89,96} or recently in a Pd(II) complex.¹³⁵ It can also be observed in the crystal structure of [(phen*)Cu–F⋯HF] (**10**) (*vide supra*, Chapter 2 – III. 3.).¹³⁶ During the course of the reaction, these signals slowly moved to lower frequencies (upfield shifted) and broadened. By the end of the reaction when almost all of the formic acid has been consumed, the signal of free phen* emerged, reflecting decomposition of the catalyst **12**. Catalyst degradation was confirmed by further addition of FA, which was not dehydrogenated (see SI).

Decomposition of HCO₂H with a 10 mol% charge in **12** was complete after 2.5 h at 100 °C (Figure 67). Decreasing the catalyst loading to 5 mol% increased the reaction time (total conversion after 8 h). In contrast, for a charge of 1 mol%, the catalyst is totally degraded after 15 h while only 40 % of the acid was dehydrogenated (Table 1, Entries 3–4).

The thermal input is of importance (Table 1, Entries 3, 5–6). By reducing the temperature to 80 °C, a low conversion of FA (4 %) can be measured after 4 h, and no reaction occurred below the boiling point of THF (66 °C). The influence of the solvent is also important as highlighted by the distinct reactivity in THF and acetonitrile. The latter seems to completely prevent the dehydrogenation process at 60 °C or 100 °C (Table 1, Entries 7–8).

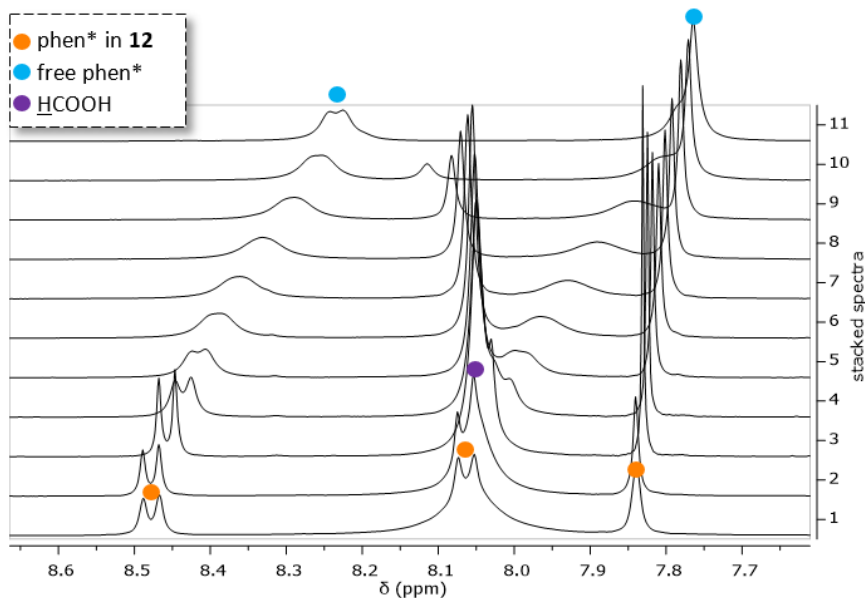


Figure 66. ^1H NMR spectrum showing the aromatic signals of the phen* moiety of **12** (10 mol%) in the formic acid dehydrogenation catalysis. Spectra were recorded every 15 min (total reaction time, 2h30).

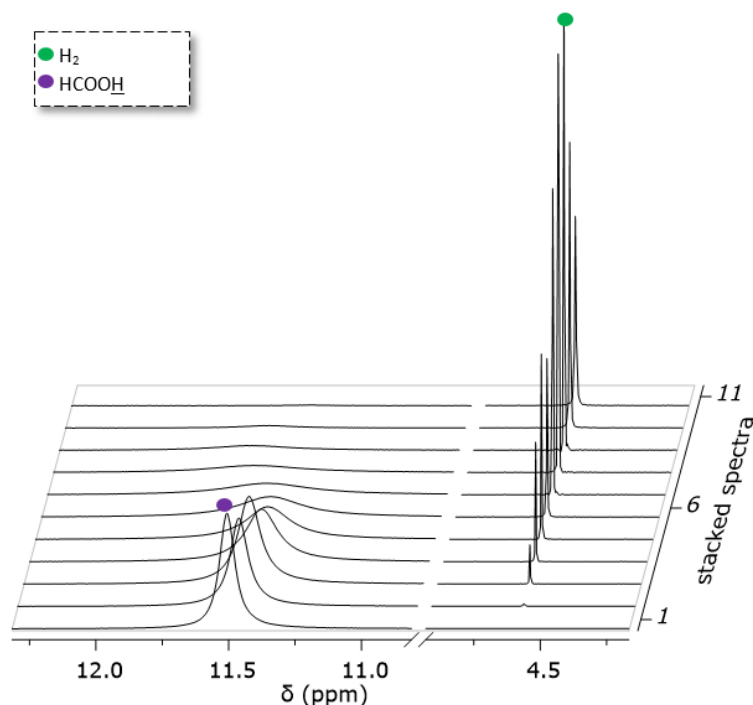


Figure 67. ^1H NMR spectrum showing disappearance of the acidic signal of formic acid and concomitant release of H_2 . Spectra were recorded every 15 min (total reaction time, 2h30).

These results underlined that complex **12** is reactive in the catalytic decomposition of HCO_2H into CO_2 and H_2 . The catalysis does not require any additive or base to proceed, because **12** spontaneously

releases CO₂ under heating with formation of a transient hydride [Cu]–H that has sufficient hydride character to deprotonate formic acid and regenerate **12** with evolution of H₂.

The downfield shifted signals of the phen* ligand of **12** in the presence of excess of FA in comparison with complex **12** alone in THF-*d*₈ (Figure 68) can suggest formation of a FA adduct [(phen*)Cu-(κ¹-O₂CH)(HO₂CH)] (**I**).

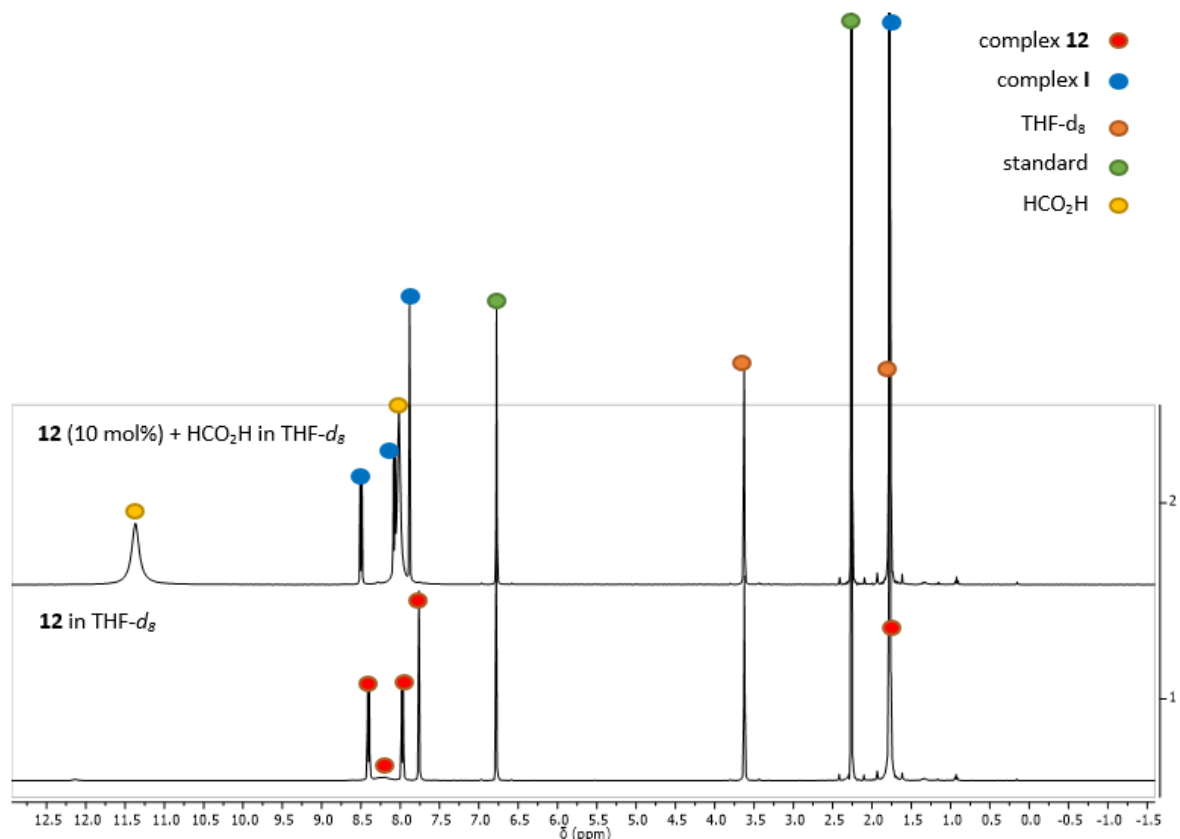
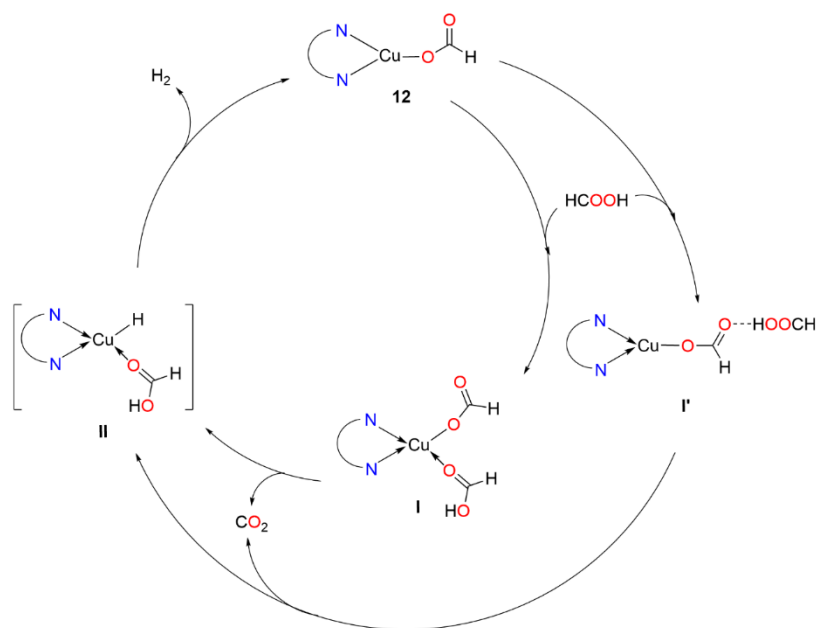


Figure 68. ¹H NMR stacked spectra of **12** (10 mol%) in THF-*d*₈ (bottom) and the following addition of FA (18 μL) (top) in the presence of mesitylene as internal standard.

A catalytic cycle can then be proposed (Scheme 71): At first, a molecule of FA coordinates or interacts with complex **12** to give either the adduct **I** or the species **I'**. These two compounds decarboxylate under heating to form the copper hydride (**II**) which immediately reacts with the neighboring acid to release dihydrogen with regeneration of **12**.

The interaction of copper complex with an acid, as schematized in **I'**, has already been observed in copper(I) formate complexes and some of them have been structurally characterized such as [Cu(PPh₃)₃O₂CH]•HCO₂H⁸⁹ and the phosphane [(P(C₆H₂CH₂NMe₂-2)₃CuO₂CH]•2HO₂CH.⁹⁶ Such interaction was also noticed in the fluoride species [(phen*)Cu-F(HF)] (**10**) (*vide supra*, Chapter 2 – III. 3.) which is also reported in the literature.¹³⁶ The crystal structure of this adduct shows that the molecule of HF is not coordinated to the copper center but interacts with the fluorine ligand through its proton. Similar interaction was also reported in 2023 by Belkova *et al.* between formic acid and the formate ligand in the pincer complex Pd [(^tBuPXCYP)-Pd(OCHO)] (X and Y = CH₂, O) which is a catalyst for the dehydrogenation of FA.¹³⁵ Based on NMR and IR analyses, they proposed a mechanistic pathway where the species [Pd]–OCH=O···HOCH is formed and assists the hydride abstraction and

CO₂ release. The hydrogen bonding of this intermediate was evidenced by ³¹P{¹H} NMR analysis : the phosphorus resonance in [Pd]–OCH=O…HOOCH is shifted downfield (higher values) compared to that of [Pd]–OCH=O.



Scheme 71. Proposed catalytic cycle for the dehydrogenation of formic acid by [(phen*)Cu(κ1-O₂CH)] **12** as pre-catalyst.

Degradation of the catalyst can occur by different pathways, the dihydride **II** can be in equilibrium with the adduct [(phen*)Cu-(κ¹-O₂CH)(S)] (S = solvent) or [(phen*)Cu-H] which decomposes under the conditions of the catalysis into Cu(0) and free phen*. We can also hypothesize that displacement of phen* may occur in THF and its decoordination from **I** would give [Cu(O₂CH)(HO₂CH)] species that would oxidize into Cu(II) derivatives under heating. We have indeed observed that treatment of a mixture of phen* and Cu(O^tBu) with FA in toluene led to **12** containing green Cu(II) species. Moreover, these copper formate species are not thermally stable. Previous investigations on the solid state behavior of Cu(O₂CH)₂(H₂O)_n species under thermal treatment (445 K) have shown their decomposition into Cu(0) and the gas H₂ and CO₂.^{137,138}

Complex **12** is not very active in FA decomposition to H₂ since it shows a TOF of 4 h⁻¹ at 100 °C for a catalyst loading of 10 mol%. This activity is however superior to that reported for some simple Cu(0), Cu(I) and Cu(II) precursors in presence of NEt₃ and which displayed TOFs lower than 1 h⁻¹ at 95 °C.^{45,55,60} The species [Cu(NCMe)₄][PF₆] with the presence of various phosphine ligands and additives (^tBuNC-NEt₃) at 70 °C in acetonitrile, showed greater activities in the decomposition of HCO₂H with reported TOFs in the range 10–240 h⁻¹.⁵⁷ However, all these copper catalysts exhibit activities significantly lower than the TOF values of 5,000 – 10,000 h⁻¹ required for an economically viable process.⁷⁰ Iron catalytic systems have TOFs of ca 10,000 h⁻¹ and TONs of 10⁵,⁴⁶ and the most efficient complexes are currently based on noble metals (Ru and Ir), with TON values exceeding 10⁶.^{70,139} For example, Williams and coworkers in 2016 and Li *et al.* in 2015, reported a binuclear iridium(III) and two organometallic mononuclear (C₅Me₅)Ir(III) catalysts exhibiting, at 90 °C, TOF of 2.28 × 10⁵ h⁻¹ (TON = 2.16 × 10⁶) and 4.88 × 10⁵ h⁻¹ (TON = 2.4 × 10⁶ at 80 °C), respectively.^{140,141}

III. Conclusion and perspectives

III. 1. Conclusion

In conclusion, we synthesized a monomeric copper(I) formate complex involving a bulky substituted phenanthroline as ancillary ligand (phen*) that provides solubility and stability. Such Cu^I(O₂CH) species with simple nitrogen ligands are uncommon. Complex [(phen*)Cu(O₂CH)] (**12**) displayed catalytic activity in the decomposition of formic acid into H₂ and CO₂ without the need for additional agents. Expected to be generated in the decarboxylation of **12**, the hydride intermediate [(phen*)Cu–H] could not be detected or trapped with organic scavengers. However, the steady increase of the ¹³C{H} NMR signal of the formate anion when **12** is placed under 1 atm. Carbon isotopic exchange reaction with ¹³CO₂ brings strong evidence for the decarboxylation of **12** into the putative copper(I) hydride. In contrast, the carbon dioxide analog CS₂ did not insert into the [Cu–H] to produce the expected copper dithioformate [(phen*)Cu(S₂CH)]. The CS₂ reaction with the hydride is presumably inhibited for thermodynamic considerations or possibly because of its lower thermal stability versus that of **12**.

III. 2. Perspectives

As previously mentioned, copper was found to be less reactive than other metal catalysts in dehydrogenating FA to produce H₂/CO₂. However, being cheap and abundant, the development of copper chemistry, with applications in catalysis will continue and expand strongly.

As far as our current system is concerned, the role of the phen* ligand is undeniably important in maintaining the copper center during the transformation process. However, there have been indications that the bulkiness and lability of phen* may not be efficient in providing adequate stability to the copper center without compromising its reactivity.^{142,143} Therefore, another generation of phen derivatives can be considered, such as neocuproine or a 2,9-di-*neopentyl*-1,10-phenanthroline ligand. With similar rigidity but less steric hindrance provided in the coordination sphere, these phen-based ligands might enhance the catalytic activity of copper metal while avoiding decoordination from the copper center that leads to complex degradation. Alternatively, NNO, NNN pincer ligands is also an option, such as (E)-N'-(phenyl(pyridin-2-yl)methylene)isonicotinohydrazide (Figure 69, a) (NNO type),¹⁴⁴ pyridine bridged bis(imidazolin-2-imine) (NNN type) (Figure 69, b),¹⁴⁵ and (2,6-bis(diisopropylaminomethyl)-pyridine) (NNN type) (Figure 69, c).¹⁴⁶ This type of ligand has three coordination sites *via* N and/or O atoms that are hemilabile. These ligands offer more flexibility in the coordination sphere, allowing additional bonds to be added or removed depending on the copper center's requirements. Therefore, a new generation of copper catalysts can be developed based on the nitrogen-type pincer ligands.

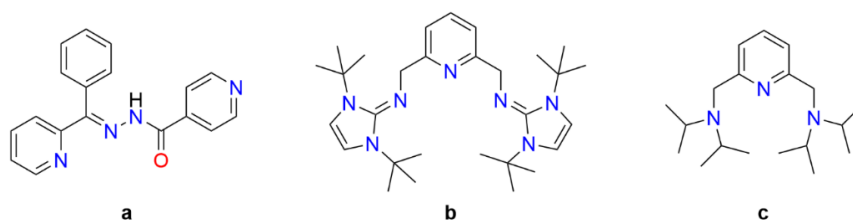


Figure 69. Examples of proposed pincer type ligands.

IV. References

- (1) Lücken, J.; Auth, T.; Mozzi, S. I.; Meyer, F. Hexanuclear Copper(I) Hydride from the Reduction-Induced Decarboxylation of a Dicopper(II) Formate. *Inorg. Chem.* **2020**, *59* (19), 14347–14354. <https://doi.org/10.1021/acs.inorgchem.0c02126>.
- (2) Jones, L. W. Perspectives on the Evolution into a Hydrogen Economy. *Energy Commun* **1976**, *2* (6), 573–584.
- (3) Bockris, J. O. M. The Hydrogen Economy: Its History. *International Journal of Hydrogen Energy* **2013**, *38* (6), 2579–2588. <https://doi.org/10.1016/j.ijhydene.2012.12.026>.
- (4) Singh, S.; Jain, S.; Ps, V.; Tiwari, A. K.; Nouni, M. R.; Pandey, J. K.; Goel, S. Hydrogen: A Sustainable Fuel for Future of the Transport Sector. *Renewable and Sustainable Energy Reviews* **2015**, *51*, 623–633. <https://doi.org/10.1016/j.rser.2015.06.040>.
- (5) Armaroli, N.; Balzani, V. The Hydrogen Issue. *ChemSusChem* **2011**, *4* (1), 21–36. <https://doi.org/10.1002/cssc.201000182>.
- (6) <https://www.nobelprize.org/prizes/chemistry/1998/kohn/facts/>.
- (7) Usman, M. R. Hydrogen Storage Methods: Review and Current Status. *Renewable and Sustainable Energy Reviews* **2022**, *167*, 112743. <https://doi.org/10.1016/j.rser.2022.112743>.
- (8) Tarhan, C.; Çil, M. A. A Study on Hydrogen, the Clean Energy of the Future: Hydrogen Storage Methods. *Journal of Energy Storage* **2021**, *40*, 102676. <https://doi.org/10.1016/j.est.2021.102676>.
- (9) Mazloomi, K.; Gomes, C. Hydrogen as an Energy Carrier: Prospects and Challenges. *Renewable and Sustainable Energy Reviews* **2012**, *16* (5), 3024–3033. <https://doi.org/10.1016/j.rser.2012.02.028>.
- (10) Midilli, A.; Ay, M.; Dincer, I.; Rosen, M. A. On Hydrogen and Hydrogen Energy Strategies I: Current Status and Needs. *Fuel and Energy Abstracts* **2005**, *46* (4), 255–271. [https://doi.org/10.1016/S0140-6701\(05\)81477-8](https://doi.org/10.1016/S0140-6701(05)81477-8).
- (11) He, T.; Pachfule, P.; Wu, H.; Xu, Q.; Chen, P. Hydrogen Carriers. *Nature Reviews Materials* **2016**, *1* (16059), 1–17.
- (12) Shet, S. P.; Shanmuga Priya, S.; Sudhakar, K.; Tahir, M. A Review on Current Trends in Potential Use of Metal-Organic Framework for Hydrogen Storage. *International Journal of Hydrogen Energy* **2021**, *46* (21), 11782–11803. <https://doi.org/10.1016/j.ijhydene.2021.01.020>.
- (13) Sanyal, U.; Demirci, U. B.; Jagirdar, B. R.; Miele, P. Hydrolysis of Ammonia Borane as a Hydrogen Source: Fundamental Issues and Potential Solutions Towards Implementation. *ChemSusChem* **2011**, *4* (12), 1731–1739. <https://doi.org/10.1002/cssc.201100318>.
- (14) Jena, P. Materials for Hydrogen Storage: Past, Present, and Future. *J. Phys. Chem. Lett.* **2011**, *2* (3), 206–211. <https://doi.org/10.1021/jz1015372>.
- (15) Singh, R. Reversible Chemical Hydrogen Storage in Borohydrides via Thermolysis and Hydrolysis: Recent Advances, Challenges, and Perspectives. *International Journal of Hydrogen Energy* **2022**, *47* (62), 26549–26573. <https://doi.org/10.1016/j.ijhydene.2021.10.022>.
- (16) Bano, S.; Siluvai Antony, P.; Jangde, V.; Biniwale, R. B. Hydrogen Transportation Using Liquid Organic Hydrides: A Comprehensive Life Cycle Assessment. *Journal of Cleaner Production* **2018**, *183*, 988–997. <https://doi.org/10.1016/j.jclepro.2018.02.213>.
- (17) Niermann, M.; Beckendorff, A.; Kaltschmitt, M.; Bonhoff, K. Liquid Organic Hydrogen Carrier (LOHC) – Assessment Based on Chemical and Economic Properties. *International Journal of Hydrogen Energy* **2019**, *44* (13), 6631–6654. <https://doi.org/10.1016/j.ijhydene.2019.01.199>.

- (18) Yang, M.; Han, C.; Ni, G.; Wu, J.; Cheng, H. Temperature Controlled Three-Stage Catalytic Dehydrogenation and Cycle Performance of Perhydro-9-Ethylcarbazole. *International Journal of Hydrogen Energy* **2012**, *37* (17), 12839–12845. <https://doi.org/10.1016/j.ijhydene.2012.05.092>.
- (19) Shi, L.; Qi, S.; Qu, J.; Che, T.; Yi, C.; Yang, B. Integration of Hydrogenation and Dehydrogenation Based on Dibenzyltoluene as Liquid Organic Hydrogen Energy Carrier. *International Journal of Hydrogen Energy* **2019**, *44* (11), 5345–5354. <https://doi.org/10.1016/j.ijhydene.2018.09.083>.
- (20) Brückner, N.; Obesser, K.; Bösmann, A.; Teichmann, D.; Arlt, W.; Dungs, J.; Wasserscheid, P. Evaluation of Industrially Applied Heat-Transfer Fluids as Liquid Organic Hydrogen Carrier Systems. *ChemSusChem* **2014**, *7* (1), 229–235. <https://doi.org/10.1002/cssc.201300426>.
- (21) Hu, P.; Fogler, E.; Diskin-Posner, Y.; Iron, M. A.; Milstein, D. A Novel Liquid Organic Hydrogen Carrier System Based on Catalytic Peptide Formation and Hydrogenation. *Nat Commun* **2015**, *6* (1), 6859. <https://doi.org/10.1038/ncomms7859>.
- (22) Gunanathan, C.; Milstein, D. Applications of Acceptorless Dehydrogenation and Related Transformations in Chemical Synthesis. *Science* **2013**, *341* (6143), 1229712. <https://doi.org/10.1126/science.1229712>.
- (23) Hu, P.; Ben-David, Y.; Milstein, D. Rechargeable Hydrogen Storage System Based on the Dehydrogenative Coupling of Ethylenediamine with Ethanol. *Angew. Chem. Int. Ed.* **2016**, *55* (3), 1061–1064. <https://doi.org/10.1002/anie.201505704>.
- (24) Laurency, G.; Dyson, P. J. Homogeneous Catalytic Dehydrogenation of Formic Acid: Progress Towards a Hydrogen-Based Economy. *Journal of the Brazilian Chemical Society* **2014**. <https://doi.org/10.5935/0103-5053.20140235>.
- (25) Grasemann, M.; Laurency, G. Formic Acid as a Hydrogen Source – Recent Developments and Future Trends. *Energy Environ. Sci.* **2012**, *5* (8), 8171. <https://doi.org/10.1039/c2ee21928j>.
- (26) Hietala, J.; Vuori, A.; Johnsson, P.; Pollari, I.; Reutemann, W.; Kieczka, H. Formic Acid. In *Ullmann's Encyclopedia of Industrial Chemistry*; Wiley-VCH, Ed.; Wiley, 2016; pp 1–22. https://doi.org/10.1002/14356007.a12_013.pub3.
- (27) Jessop, P. G.; Joó, F.; Tai, C.-C. Recent Advances in the Homogeneous Hydrogenation of Carbon Dioxide. *Coordination Chemistry Reviews* **2004**, *248* (21–24), 2425–2442. <https://doi.org/10.1016/j.ccr.2004.05.019>.
- (28) Singh, T.; Jalwal, S.; Chakraborty, S. Homogeneous First-row Transition-metal-catalyzed Carbon Dioxide Hydrogenation to Formic Acid/Formate, and Methanol. *Asian J Org Chem* **2022**, *11* (9). <https://doi.org/10.1002/ajoc.202200330>.
- (29) Enthaler, S. Carbon Dioxide-The Hydrogen-Storage Material of the Future? *ChemSusChem* **2008**, *1* (10), 801–804. <https://doi.org/10.1002/cssc.200800101>.
- (30) Verma, P.; Zhang, S.; Song, S.; Mori, K.; Kuwahara, Y.; Wen, M.; Yamashita, H.; An, T. Recent Strategies for Enhancing the Catalytic Activity of CO₂ Hydrogenation to Formate/Formic Acid over Pd-Based Catalyst. *Journal of CO₂ Utilization* **2021**, *54*, 101765. <https://doi.org/10.1016/j.jcou.2021.101765>.
- (31) Chatterjee, S.; Dutta, I.; Lum, Y.; Lai, Z.; Huang, K.-W. Enabling Storage and Utilization of Low-Carbon Electricity: Power to Formic Acid. *Energy Environ. Sci.* **2021**, *14* (3), 1194–1246. <https://doi.org/10.1039/D0EE03011B>.

- (32) Bulushev, D. A.; Ross, J. R. H. Heterogeneous Catalysts for Hydrogenation of CO₂ and Bicarbonates to Formic Acid and Formates. *Catalysis Reviews* **2018**, *60* (4), 566–593. <https://doi.org/10.1080/01614940.2018.1476806>.
- (33) Mellmann, D.; Sponholz, P.; Junge, H.; Beller, M. Formic Acid as a Hydrogen Storage Material – Development of Homogeneous Catalysts for Selective Hydrogen Release. *Chem. Soc. Rev.* **2016**, *45* (14), 3954–3988. <https://doi.org/10.1039/C5CS00618J>.
- (34) Jessop, P. G. *Homogeneous Hydrogenation of Carbon Dioxide*. In *The Handbook of Homogeneous Hydrogenation*; de Vries, J. G., Elsevier, C. J., Eds.; Wiley: Weinheim, 2007.
- (35) Loges, B.; Boddien, A.; Junge, H.; Beller, M. Controlled Generation of Hydrogen from Formic Acid Amine Adducts at Room Temperature and Application in H₂/O₂ Fuel Cells. *Angew. Chem. Int. Ed.* **2008**, *47* (21), 3962–3965. <https://doi.org/10.1002/anie.200705972>.
- (36) Fellay, C.; Dyson, P.; Laurency, G. A Viable Hydrogen-Storage System Based On Selective Formic Acid Decomposition with a Ruthenium Catalyst. *Angew. Chem. Int. Ed.* **2008**, *47* (21), 3966–3968. <https://doi.org/10.1002/anie.200800320>.
- (37) Coffey, R. S. The Decomposition of Formic Acid Catalysed by Soluble Metal Complexes. *Chem. Commun. (London)* **1967**, No. 18, 923b. <https://doi.org/10.1039/c1967000923b>.
- (38) Onishi, N.; Kanega, R.; Kawanami, H.; Himeda, Y. Recent Progress in Homogeneous Catalytic Dehydrogenation of Formic Acid. *Molecules* **2022**, *27* (2), 455. <https://doi.org/10.3390/molecules27020455>.
- (39) Pan, Y.; Pan, C.; Zhang, Y.; Li, H.; Min, S.; Guo, X.; Zheng, B.; Chen, H.; Anders, A.; Lai, Z.; Zheng, J.; Huang, K. Selective Hydrogen Generation from Formic Acid with Well-Defined Complexes of Ruthenium and Phosphorus–Nitrogen PN³-Pincer Ligand. *Chemistry An Asian Journal* **2016**, *11* (9), 1357–1360. <https://doi.org/10.1002/asia.201600169>.
- (40) Guan, C.; Zhang, D.-D.; Pan, Y.; Iguchi, M.; Ajitha, M. J.; Hu, J.; Li, H.; Yao, C.; Huang, M.-H.; Min, S.; Zheng, J.; Himeda, Y.; Kawanami, H.; Huang, K.-W. Dehydrogenation of Formic Acid Catalyzed by a Ruthenium Complex with an *N,N'*-Diimine Ligand. *Inorg. Chem.* **2017**, *56* (1), 438–445. <https://doi.org/10.1021/acs.inorgchem.6b02334>.
- (41) Kar, S.; Rauch, M.; Leitus, G.; Ben-David, Y.; Milstein, D. Highly Efficient Additive-Free Dehydrogenation of Neat Formic Acid. *Nat Catal* **2021**, *4* (3), 193–201. <https://doi.org/10.1038/s41929-021-00575-4>.
- (42) Hull, J. F.; Himeda, Y.; Wang, W.-H.; Hashiguchi, B.; Periana, R.; Szalda, D. J.; Muckerman, J. T.; Fujita, E. Reversible Hydrogen Storage Using CO₂ and a Proton-Switchable Iridium Catalyst in Aqueous Media under Mild Temperatures and Pressures. *Nature Chem* **2012**, *4* (5), 383–388. <https://doi.org/10.1038/nchem.1295>.
- (43) Onishi, N.; Kanega, R.; Fujita, E.; Himeda, Y. Carbon Dioxide Hydrogenation and Formic Acid Dehydrogenation Catalyzed by Iridium Complexes Bearing Pyridyl-pyrazole Ligands: Effect of an Electron-donating Substituent on the Pyrazole Ring on the Catalytic Activity and Durability. *Adv Synth Catal* **2019**, *361* (2), 289–296. <https://doi.org/10.1002/adsc.201801323>.
- (44) Iguchi, M.; Himeda, Y.; Manaka, Y.; Kawanami, H. Development of an Iridium-Based Catalyst for High-Pressure Evolution of Hydrogen from Formic Acid. *ChemSusChem* **2016**, *9* (19), 2749–2753. <https://doi.org/10.1002/cssc.201600697>.
- (45) Iglesias, M.; Fernández-Alvarez, F. J. Advances in Nonprecious Metal Homogeneously Catalyzed Formic Acid Dehydrogenation. *Catalysts* **2021**, *11*, 1288.

- (46) Boddien, A.; Mellmann, D.; Gärtner, F.; Jackstell, R.; Junge, H.; Dyson, P. J.; Laurency, G.; Ludwig, R.; Beller, M. Efficient Dehydrogenation of Formic Acid Using an Iron Catalyst. *Science* **2011**, 333 (6050), 1733–1736. <https://doi.org/10.1126/science.1206613>.
- (47) Montandon-Clerc, M.; Dalebrook, A. F.; Laurency, G. Quantitative Aqueous Phase Formic Acid Dehydrogenation Using Iron(II) Based Catalysts. *Journal of Catalysis* **2016**, 343, 62–67. <https://doi.org/10.1016/j.jcat.2015.11.012>.
- (48) Zell, T.; Butschke, B.; Ben-David, Y.; Milstein, D. Efficient Hydrogen Liberation from Formic Acid Catalyzed by a Well-Defined Iron Pincer Complex under Mild Conditions. *Chem. Eur. J.* **2013**, 19 (25), 8068–8072. <https://doi.org/10.1002/chem.201301383>.
- (49) Bielinski, E. A.; Lagaditis, P. O.; Zhang, Y.; Mercado, B. Q.; Würtele, C.; Bernskoetter, W. H.; Hazari, N.; Schneider, S. Lewis Acid-Assisted Formic Acid Dehydrogenation Using a Pincer-Supported Iron Catalyst. *J. Am. Chem. Soc.* **2014**, 136 (29), 10234–10237. <https://doi.org/10.1021/ja505241x>.
- (50) Curley, J. B.; Smith, N. E.; Bernskoetter, W. H.; Hazari, N.; Mercado, B. Q. Catalytic Formic Acid Dehydrogenation and CO₂ Hydrogenation Using Iron PN^RP Pincer Complexes with Isonitrile Ligands. *Organometallics* **2018**, 37 (21), 3846–3853. <https://doi.org/10.1021/acs.organomet.8b00534>.
- (51) Enthaler, S.; Brück, A.; Kammer, A.; Junge, H.; Irran, E.; Gülak, S. Exploring the Reactivity of Nickel Pincer Complexes in the Decomposition of Formic Acid to CO₂/H₂ and the Hydrogenation of NaHCO₃ to HCOONa. *ChemCatChem* **2015**, 7 (1), 65–69. <https://doi.org/10.1002/cctc.201402716>.
- (52) Neary, M. C.; Parkin, G. Nickel-Catalyzed Release of H₂ from Formic Acid and a New Method for the Synthesis of Zerovalent Ni(PMe₃)₄. *Dalton Trans.* **2016**, 45 (37), 14645–14650. <https://doi.org/10.1039/C6DT01499B>.
- (53) Anderson, N. H.; Boncella, J.; Tondreau, A. M. Manganese-Mediated Formic Acid Dehydrogenation. *Chemistry A European J* **2019**, 25 (45), 10557–10560. <https://doi.org/10.1002/chem.201901177>.
- (54) Léval, A.; Agapova, A.; Steinlechner, C.; Alberico, E.; Junge, H.; Beller, M. Hydrogen Production from Formic Acid Catalyzed by a Phosphine Free Manganese Complex: Investigation and Mechanistic Insights. *Green Chem.* **2020**, 22 (3), 913–920. <https://doi.org/10.1039/C9GC02453K>.
- (55) Scotti, N.; Psaro, R.; Ravasio, N.; Zaccheria, F. A New Cu-Based System for Formic Acid Dehydrogenation. *RSC Adv.* **2014**, 4 (106), 61514–61517. <https://doi.org/10.1039/C4RA11031E>.
- (56) Desnoyer, A. N.; Nicolay, A.; Ziegler, M. S.; Torquato, N. A.; Tilley, T. D. A Dicopper Platform That Stabilizes the Formation of Pentanuclear Coinage Metal Hydride Complexes. *Angew Chem Int Ed* **2020**, 59 (31), 12769–12773. <https://doi.org/10.1002/anie.202004346>.
- (57) Nakajima, T.; Kamiryo, Y.; Kishimoto, M.; Imai, K.; Nakamae, K.; Ura, Y.; Tanase, T. Synergistic Cu₂ Catalysts for Formic Acid Dehydrogenation. *J. Am. Chem. Soc.* **2019**, 141 (22), 8732–8736. <https://doi.org/10.1021/jacs.9b03532>.
- (58) Hall, H. K.; Bates, R. B. Correlation of Alkylamine Nucleophilicities with Their Basicities. *Tetrahedron Letters* **2012**, 53 (14), 1830–1832. <https://doi.org/10.1016/j.tetlet.2012.01.128>.
- (59) Seligson, A. L.; Trogler, W. C. Cone Angles for Amine Ligands. X-Ray Crystal Structures and Equilibrium Measurements for Ammonia, Ethylamine, Diethylamine, and Triethylamine Complexes with the [Bis(Dimethylphosphino)Ethane]Methylpalladium(II) Cation. *J. Am. Chem. Soc.* **1991**, 113 (7), 2520–2527. <https://doi.org/10.1021/ja00007a028>.

- (60) Correa, A.; Cascella, M.; Scotti, N.; Zaccheria, F.; Ravasio, N.; Psaro, R. Mechanistic Insights into Formic Acid Dehydrogenation Promoted by Cu-Amino Based Systems. *Inorganica Chimica Acta* **2018**, *470*, 290–294. <https://doi.org/10.1016/j.ica.2017.06.043>.
- (61) Kinzel, N. W.; Werlé, C.; Leitner, W. Transition Metal Complexes as Catalysts for the Electroconversion of CO₂: An Organometallic Perspective. *Angew. Chem. Int. Ed.* **2021**, *60* (21), 11628–11686. <https://doi.org/10.1002/anie.202006988>.
- (62) Creutz, C.; Chou, M. H. Hydricities of d⁶ Metal Hydride Complexes in Water. *J. Am. Chem. Soc.* **2009**, *131* (8), 2794–2795. <https://doi.org/10.1021/ja809724s>.
- (63) Godou, T.; Chauvier, C.; Thuéry, P.; Cantat, T. Iron-Catalyzed Silylation of Alcohols by Transfer Hydrosilylation with Silyl Formates. *Synlett* **2017**, *28* (18), 2473–2477. <https://doi.org/10.1055/s-0036-1591508>.
- (64) Darensbourg, D. J.; Wiegrefe, P.; Riordan, C. G. Mechanistic Aspects of Decarboxylation Reactions of Group 10 Metal Formate Hydrido Tricyclohexylphosphine [(PCy₃)₂M(H)O₂CH] Derivatives. *J. Am. Chem. Soc.* **1990**, *112* (15), 5759–5762. <https://doi.org/10.1021/ja00171a014>.
- (65) Merrifield, J. H.; Gladysz, J. A. Synthesis and Decarboxylation Mechanism of the Chiral Rhenium Formate (.Eta.-C₅H₅)Re(NO)(PPh₃)(OCHO). *Organometallics* **1983**, *2* (6), 782–784. <https://doi.org/10.1021/om00078a022>.
- (66) Takao, S.; Takao, K.; Kraus, W.; Emmerling, F.; Scheinost, A. C.; Bernhard, G.; Hennig, C. First Hexanuclear U^{IV} and Th^{IV} Formate Complexes – Structure and Stability Range in Aqueous Solution. *Eur. J. Inorg. Chem.* **2009**, *2009* (32), 4771–4775. <https://doi.org/10.1002/ejic.200900899>.
- (67) Chauvier, C.; Tlili, A.; Das Neves Gomes, C.; Thuéry, P.; Cantat, T. Metal-Free Dehydrogenation of Formic Acid to H₂ and CO₂ Using Boron-Based Catalysts. *Chem. Sci.* **2015**, *6* (5), 2938–2942. <https://doi.org/10.1039/C5SC00394F>.
- (68) Chauvier, C.; Thuéry, P.; Cantat, T. Silyl Formates as Surrogates of Hydrosilanes and Their Application in the Transfer Hydrosilylation of Aldehydes. *Angew. Chem. Int. Ed.* **2016**, *55* (45), 14096–14100. <https://doi.org/10.1002/anie.201607201>.
- (69) Chauvier, C.; Imberdis, A.; Thuéry, P.; Cantat, T. Catalytic Disproportionation of Formic Acid to Methanol by Using Recyclable Silylformates. *Angew. Chem. Int. Ed.* **2020**, *59* (33), 14019–14023. <https://doi.org/10.1002/anie.202002062>.
- (70) Guan, C.; Pan, Y.; Zhang, T.; Ajitha, M. J.; Huang, K. An Update on Formic Acid Dehydrogenation by Homogeneous Catalysis. *Chem. Asian J.* **2020**, *15* (7), 937–946. <https://doi.org/10.1002/asia.201901676>.
- (71) Savourey, S.; Lefèvre, G.; Berthet, J.-C.; Thuéry, P.; Genre, C.; Cantat, T. Efficient Disproportionation of Formic Acid to Methanol Using Molecular Ruthenium Catalysts. *Angew. Chem. Int. Ed.* **2014**, *53* (39), 10466–10470. <https://doi.org/10.1002/anie.201405457>.
- (72) Wang, L.; Sun, H.; Zuo, Z.; Li, X.; Xu, W.; Langer, R.; Fuhr, O.; Fenske, D. Activation of CO₂, CS₂, and Dehydrogenation of Formic Acid Catalyzed by Iron(II) Hydride Complexes. *Eur. J. Inorg. Chem.* **2016**, *2016* (33), 5205–5214. <https://doi.org/10.1002/ejic.201600642>.
- (73) Ma, Q.-Q.; Liu, T.; Adhikary, A.; Zhang, J.; Krause, J. A.; Guan, H. Using CS₂ to Probe the Mechanistic Details of Decarboxylation of Bis(Phosphinite)-Ligated Nickel Pincer Formate Complexes. *Organometallics* **2016**, *35* (24), 4077–4082. <https://doi.org/10.1021/acs.organomet.6b00759>.

- (74) Liu, W.; Huang, H.; Ouyang, T.; Jiang, L.; Zhong, D.; Zhang, W.; Lu, T. A Copper(II) Molecular Catalyst for Efficient and Selective Photochemical Reduction of CO₂ to CO in a Water-Containing System. *Chem. Eur. J.* **2018**, *24* (18), 4503–4508. <https://doi.org/10.1002/chem.201705566>.
- (75) Al-Nayili, A.; Majdi, H. Sh.; Albayati, T. M.; Saady, N. M. C. Formic Acid Dehydrogenation Using Noble-Metal Nanoheterogeneous Catalysts: Towards Sustainable Hydrogen-Based Energy. *Catalysts* **2022**, *12* (3), 324. <https://doi.org/10.3390/catal12030324>.
- (76) Wienhöfer, G.; Sorribes, I.; Boddien, A.; Westerhaus, F.; Junge, K.; Junge, H.; Llusar, R.; Beller, M. General and Selective Iron-Catalyzed Transfer Hydrogenation of Nitroarenes without Base. *J. Am. Chem. Soc.* **2011**, *133* (32), 12875–12879. <https://doi.org/10.1021/ja2061038>.
- (77) Shen, R.; Chen, T.; Zhao, Y.; Qiu, R.; Zhou, Y.; Yin, S.; Wang, X.; Goto, M.; Han, L.-B. Facile Regio- and Stereoselective Hydrometalation of Alkynes with a Combination of Carboxylic Acids and Group 10 Transition Metal Complexes: Selective Hydrogenation of Alkynes with Formic Acid. *J. Am. Chem. Soc.* **2011**, *133* (42), 17037–17044. <https://doi.org/10.1021/ja2069246>.
- (78) Broggi, J.; Jurčik, V.; Songis, O.; Poater, A.; Cavallo, L.; Slawin, A. M. Z.; Cazin, C. S. J. The Isolation of [Pd{OC(O)H}(H)(NHC)(PR₃)₃] (NHC = N-Heterocyclic Carbene) and Its Role in Alkene and Alkyne Reductions Using Formic Acid. *J. Am. Chem. Soc.* **2013**, *135* (12), 4588–4591. <https://doi.org/10.1021/ja311087c>.
- (79) Zeng, M.; Li, L.; Herzon, S. B. A Highly Active and Air-Stable Ruthenium Complex for the Ambient Temperature Anti-Markovnikov Reductive Hydration of Terminal Alkynes. *J. Am. Chem. Soc.* **2014**, *136* (19), 7058–7067. <https://doi.org/10.1021/ja501738a>.
- (80) Guo, S.; Yang, P.; Zhou, J. (Steve). Nickel-Catalyzed Asymmetric Transfer Hydrogenation of Conjugated Olefins. *Chem. Commun.* **2015**, *51* (60), 12115–12117. <https://doi.org/10.1039/C5CC01632K>.
- (81) Wang, D.; Astruc, D. The Golden Age of Transfer Hydrogenation. *Chem. Rev.* **2015**, *115* (13), 6621–6686. <https://doi.org/10.1021/acs.chemrev.5b00203>.
- (82) Touge, T.; Nara, H.; Fujiwhara, M.; Kayaki, Y.; Ikariya, T. Efficient Access to Chiral Benzhydrols via Asymmetric Transfer Hydrogenation of Unsymmetrical Benzophenones with Bifunctional Oxo-Tethered Ruthenium Catalysts. *J. Am. Chem. Soc.* **2016**, *138* (32), 10084–10087. <https://doi.org/10.1021/jacs.6b05738>.
- (83) Li, Y.-N.; Ma, R.; He, L.-N.; Diao, Z.-F. Homogeneous Hydrogenation of Carbon Dioxide to Methanol. *Catal. Sci. Technol.* **2014**, *4* (6), 1498–1512. <https://doi.org/10.1039/C3CY00564J>.
- (84) Kar, S.; Goepfert, A.; Prakash, G. K. S. Integrated CO₂ Capture and Conversion to Formate and Methanol: Connecting Two Threads. *Acc. Chem. Res.* **2019**, *52* (10), 2892–2903. <https://doi.org/10.1021/acs.accounts.9b00324>.
- (85) Eberhardt, N. A.; Guan, H. Nickel Hydride Complexes. *Chem. Rev.* **2016**, *116* (15), 8373–8426. <https://doi.org/10.1021/acs.chemrev.6b00259>.
- (86) Mouche, M.-J.; Mermet, J.-L.; Romand, M.; Charbonnier, M. Metal–Organic Chemical Vapor Deposition of Copper Using Hydrated Copper Formate as a New Precursor. *Thin Solid Films* **1995**, *262* (1–2), 1–6. [https://doi.org/10.1016/0040-6090\(95\)05813-3](https://doi.org/10.1016/0040-6090(95)05813-3).
- (87) Grodzicki, A.; Łakomska, I.; Piszczek, P.; Szymańska, I.; Szłyk, E. Copper(I), Silver(I) and Gold(I) Carboxylate Complexes as Precursors in Chemical Vapour Deposition of Thin Metallic Films. *Coordination Chemistry Reviews* **2005**, *249* (21–22), 2232–2258. <https://doi.org/10.1016/j.ccr.2005.05.026>.

- (88) Mokhtari, O.; Conti, F.; Saccon, R.; Bhogaraju, S. K.; Elger, G. Formic Acid and Formate Salts for Chemical Vapor Deposition of Copper on Glass Substrates at Atmospheric Pressure. *New J. Chem.* **2021**, *45* (43), 20133–20139. <https://doi.org/10.1039/D1NJ02476K>.
- (89) Lang, H.; Shen, Y.; Ruffer, T.; Walfort, B. Phosphane Copper(I) Formate Complexes Stabilized by Formic Acid and Acetic Acid through H···O···H Bridges. *Inorganica Chimica Acta* **2008**, *361* (1), 95–102. <https://doi.org/10.1016/j.ica.2007.06.028>.
- (90) Casarin, M.; Corvaja, C.; Di Nicola, C.; Falcomer, D.; Franco, L.; Monari, M.; Pandolfo, L.; Pettinari, C.; Piccinelli, F. One-Dimensional and Two-Dimensional Coordination Polymers from Self-Assembling of Trinuclear Triangular Cu(II) Secondary Building Units. *Inorg. Chem.* **2005**, *44* (18), 6265–6276. <https://doi.org/10.1021/ic050678l>.
- (91) Barquín, M.; Cocera, N.; González Garmendia, M. J.; Larrínaga, L.; Pinilla, E.; Seco, J. M.; Torres, M. R. Acetato and Formato Copper(II) Complexes with 4,4'-Dimethyl-2,2'-Bipyridine and 5,5'-Dimethyl-2,2'-Bipyridine: Synthesis, Crystal Structure, Magnetic Properties and EPR Results. A New 1D Polymeric Water Chain. *Inorganica Chimica Acta* **2010**, *363* (1), 127–133. <https://doi.org/10.1016/j.ica.2009.09.034>.
- (92) Di Nicola, C.; Garau, F.; Gazzano, M.; Guedes da Silva, M. F. C.; Lanza, A.; Monari, M.; Nestola, F.; Pandolfo, L.; Pettinari, C.; Pombeiro, A. J. L. New Coordination Polymers and Porous Supramolecular Metal Organic Network Based on the Trinuclear Triangular Secondary Building Unit $[\text{Cu}_3(\mu_3\text{-OH})(\mu\text{-Pz})_3]^{2+}$ and 4,4'-Bypiridine. 1°. *Crystal Growth & Design* **2012**, *12* (6), 2890–2901. <https://doi.org/10.1021/cg300080a>.
- (93) Marchal, W.; Longo, A.; Briois, V.; Van Hecke, K.; Elen, K.; Van Bael, M. K.; Hardy, A. Understanding the Importance of Cu(I) Intermediates in Self-Reducing Molecular Inks for Flexible Electronics. *Inorg. Chem.* **2018**, *57* (24), 15205–15215. <https://doi.org/10.1021/acs.inorgchem.8b02493>.
- (94) Fujita, W. Crystal Structures, and Magnetic and Thermal Properties of Basic Copper Formates with Two-Dimensional Triangular-Lattice Magnetic Networks. *RSC Adv.* **2018**, *8* (57), 32490–32496. <https://doi.org/10.1039/C8RA07134A>.
- (95) Ghilardi, C. A. Unprecedented Intramolecular Attack by a Phosphine on a N2-Dithiomethyl Ester Group. X-Ray Crystal Structure of the Complex $[\text{Ph}_2\text{PCH}_2\text{CH}_2\text{N}(\text{CH}_2\text{CH}_2\text{PPh}_2)_2\text{Ni}(\text{CS}_2\text{Me})]\text{BPh}_4$. *Journal of Organometallic Chemistry* **1983**, *246*, C13–C15.
- (96) Bowmaker, G. A.; Hanna, J. V.; Healy, P. C.; Reid, J. C.; Rickard, C. E. F.; White, A. H. Crystal Structures and Vibrational and Solid-State (CPMAS) NMR Spectroscopic Studies in the Tris(Triphenylphosphine)-Copper(I) and -Silver(I) Formate Systems. *J. Chem. Soc., Dalton Trans.* **2000**, No. 5, 753–762. <https://doi.org/10.1039/a908427d>.
- (97) Nguyen, T.-A. D.; Goldsmith, B. R.; Zaman, H. T.; Wu, G.; Peters, B.; Hayton, T. W. Synthesis and Characterization of a Cu_{14} Hydride Cluster Supported by Neutral Donor Ligands. *Chem. Eur. J.* **2015**, *21* (14), 5341–5344. <https://doi.org/10.1002/chem.201500422>.
- (98) Nakamae, K.; Kure, B.; Nakajima, T.; Ura, Y.; Tanase, T. Facile Insertion of Carbon Dioxide into $\text{Cu}_2(\mu\text{-H})$ Dinuclear Units Supported by Tetrphosphine Ligands. *Chem. Asian J.* **2014**, *9* (11), 3106–3110. <https://doi.org/10.1002/asia.201402900>.
- (99) Beamer, A. W.; Buss, J. A. Synthesis, Structural Characterization, and CO_2 Reactivity of a Constitutionally Analogous Series of Tricopper Mono-, Di-, and Trihydrides. *J. Am. Chem. Soc.* **2023**, *145* (23), 12911–12919. <https://doi.org/10.1021/jacs.3c04170>.

- (100) Tran, B. L.; Neisen, B. D.; Speelman, A. L.; Gunasekara, T.; Wiedner, E. S.; Bullock, R. M. Mechanistic Studies on the Insertion of Carbonyl Substrates into Cu-H: Different Rate-Limiting Steps as a Function of Electrophilicity. *Angew Chem Int Ed* **2020**, *59* (22), 8645–8653. <https://doi.org/10.1002/anie.201916406>.
- (101) Patrick, E. A.; Bowden, M. E.; Erickson, J. D.; Bullock, R. M.; Tran, B. L. Single-Crystal to Single-Crystal Transformations: Stepwise CO₂ Insertions into Bridging Hydrides of [(NHC)CuH]₂ Complexes. *Angew Chem Int Ed* **2023**, *62* (30), e202304648. <https://doi.org/10.1002/anie.202304648>.
- (102) Zhang, L.; Cheng, J.; Hou, Z. Highly Efficient Catalytic Hydrosilylation of Carbon Dioxide by an N-Heterocyclic Carbene Copper Catalyst. *Chem. Commun.* **2013**, *49* (42), 4782–4784. <https://doi.org/10.1039/c3cc41838c>.
- (103) Jordan, A. J.; Wyss, C. M.; Bacsa, J.; Sadighi, J. P. Synthesis and Reactivity of New Copper(I) Hydride Dimers. *Organometallics* **2016**, *35* (5), 613–616. <https://doi.org/10.1021/acs.organomet.6b00025>.
- (104) Romero, E. A.; Zhao, T.; Nakano, R.; Hu, X.; Wu, Y.; Jazzar, R.; Bertrand, G. Tandem Copper Hydride–Lewis Pair Catalysed Reduction of Carbon Dioxide into Formate with Dihydrogen. *Nat Catal* **2018**, *1* (10), 743–747. <https://doi.org/10.1038/s41929-018-0140-3>.
- (105) Tuchscherer, A.; Shen, Y.; Jakob, A.; Mothes, R.; Al-Anber, M.; Walfort, B.; Rüffer, T.; Frühauf, S.; Ecke, R.; Schulz, S. E.; Gessner, T.; Lang, H. Lewis-Base Copper(I) Formates: Synthesis, Reaction Chemistry, Structural Characterization and Their Use as Spin-Coating Precursors for Copper Deposition. *Inorganica Chimica Acta* **2011**, *365* (1), 10–19. <https://doi.org/10.1016/j.ica.2010.05.048>.
- (106) Norwine, E. E.; Kiernicki, J. J.; Zeller, M.; Szymczak, N. K. Distinct Reactivity Modes of a Copper Hydride Enabled by an Intramolecular Lewis Acid. *J. Am. Chem. Soc.* **2022**, *144* (33), 15038–15046. <https://doi.org/10.1021/jacs.2c02937>.
- (107) Marsich, N.; Camus, A.; Nardin, G. REACTION OF CARBON DIOXIDE WITH ARYL COPPER(I) COMPLEXES CONTAINING TERTIARY PHOSPHINES.
- (108) Ghilardi, A. FACILE REDUCTION OF CARBON DIOXIDE, CARBONYL SULFIDE, AND CARBON DISULFIDE BY COPPER(I) BOROHYDRIDE. X-RAY CRYSTAL STRUCTURE OF THE COMPLEX [(Triphos)Cu(O₂CH)]. *Journal of Organometallic Chemistry* **1983**, No. 248, C13–C16.
- (109) Bianchini, C.; Ghilardi, C. A.; Meli, A.; Midollini, S.; Orlandini, A. Reactivity of Copper(I) Tetrahydroborates toward Carbon Dioxide and Carbonyl Sulfide. Structure of (Triphos)Cu(η¹-O₂CH). *Inorg. Chem.* **1985**, *24* (6), 924–931. <https://doi.org/10.1021/ic00200a025>.
- (110) Edwards, D., A.; Richards, R. Copper(I) Carboxylates: Preparations and Infrared and Mass Spectral Features. *J. Chem. Soc., Dalton Trans* **1973**, 2463–2468.
- (111) Pallenberg, A. J.; Koenig, K. S.; Barnhart, D. M. Synthesis and Characterization of Some Copper(I) Phenanthroline Complexes. *Inorg. Chem.* **1995**, *34* (11), 2833–2840. <https://doi.org/10.1021/ic00115a009>.
- (112) Gandhi, B. A.; Green, O.; Burstyn, J. N. Facile Oxidation-Based Synthesis of Sterically Encumbered Four-Coordinate Bis(2,9-Di-*Tert*-Butyl-1,10-Phenanthroline)Copper(I) and Related Three-Coordinate Copper(I) Complexes. *Inorg. Chem.* **2007**, *46* (10), 3816–3825. <https://doi.org/10.1021/ic0615224>.
- (113) Green, O.; Gandhi, B. A.; Burstyn, J. N. Photophysical Characteristics and Reactivity of Bis(2,9-Di-*Tert*-Butyl-1,10-Phenanthroline)Copper(I). *Inorg. Chem.* **2009**, *48* (13), 5704–5714. <https://doi.org/10.1021/ic802361q>.

- (114) Nitsch, J.; Kleeberg, C.; Fröhlich, R.; Steffen, A. Luminescent Copper(I) Halide and Pseudohalide Phenanthroline Complexes Revisited: Simple Structures, Complicated Excited State Behavior. *Dalton Trans.* **2015**, *44* (15), 6944–6960. <https://doi.org/10.1039/C4DT03706E>.
- (115) Romero, E. A.; Olsen, P. M.; Jazzar, R.; Soleilhavoup, M.; Gembicky, M.; Bertrand, G. Spectroscopic Evidence for a Monomeric Copper(I) Hydride and Crystallographic Characterization of a Monomeric Silver(I) Hydride. *Angew. Chem. Int. Ed.* **2017**, *56* (14), 4024–4027. <https://doi.org/10.1002/anie.201700858>.
- (116) Xu, G.; Leloux, S.; Zhang, P.; Meijide Suárez, J.; Zhang, Y.; Derat, E.; Ménand, M.; Bistri-Aslanoff, O.; Roland, S.; Leysens, T.; Riant, O.; Sollogoub, M. Capturing the Monomeric (L)CuH in NHC-Capped Cyclodextrin: Cavity-Controlled Chemoselective Hydrosilylation of α,β -Unsaturated Ketones. *Angew Chem Int Ed* **2020**, *59* (19), 7591–7597. <https://doi.org/10.1002/anie.202001733>.
- (117) Aloisi, A.; Crochet, É.; Nicolas, E.; Berthet, J.-C.; Lescot, C.; Thuéry, P.; Cantat, T. Copper–Ligand Cooperativity in H₂ Activation Enables the Synthesis of Copper Hydride Complexes. *Organometallics* **2021**, *40* (13), 2064–2069. <https://doi.org/10.1021/acs.organomet.1c00212>.
- (118) English, L. E.; Horsley Downie, T. M.; Lyall, C. L.; Mahon, M. F.; McMullin, C. L.; Neale, S. E.; Saunders, C. M.; Liptrot, D. J. Selective Hydroboration of Electron-Rich Isocyanates by an NHC-Copper(I) Alkoxide. *Chem. Commun.* **2023**, *59* (8), 1074–1077. <https://doi.org/10.1039/D2CC04742J>.
- (119) Wyss, C. M.; Tate, B. K.; Bacsa, J.; Gray, T. G.; Sadighi, J. P. Bonding and Reactivity of a μ -Hydrido Dicopper Cation. *Angew. Chem. Int. Ed.* **2013**, *52* (49), 12920–12923. <https://doi.org/10.1002/anie.201306736>.
- (120) Voss, T.; Mahdi, T.; Otten, E.; Fröhlich, R.; Kehr, G.; Stephan, D. W.; Erker, G. Frustrated Lewis Pair Behavior of Intermolecular Amine/B(C₆F₅)₃ Pairs. *Organometallics* **2012**, *31* (6), 2367–2378. <https://doi.org/10.1021/om300017u>.
- (121) Zhao, T.; Hu, X.; Wu, Y.; Zhang, Z. Hydrogenation of CO₂ to Formate with H₂: Transition Metal Free Catalyst Based on a Lewis Pair. *Angew. Chem. Int. Ed.* **2019**, *58* (3), 722–726. <https://doi.org/10.1002/anie.201809634>.
- (122) Dermot, O. Non-Metal-Mediated Homogeneous Hydrogenation of CO₂ to CH₃OH. *Angew. Chem. Int. Ed.* 2009, pp 9839–9843.
- (123) Lorber, C.; Choukroun, R.; Vendier, L. Reactivity of B(C₆F₅)₃ with Simple Early Transition Metal Alkoxides: Alkoxide-Aryl Exchange, THF Ring-Opening, or Acetonitrile CC Coupling. *Organometallics* **2008**, *27* (19), 5017–5024. <https://doi.org/10.1021/om800234z>.
- (124) Destro, G.; Loreau, O.; Marcon, E.; Taran, F.; Cantat, T.; Audisio, D. Dynamic Carbon Isotope Exchange of Pharmaceuticals with Labeled CO₂. *J. Am. Chem. Soc.* **2019**, *141* (2), 780–784. <https://doi.org/10.1021/jacs.8b12140>.
- (125) Butler, I. S.; Fenster, A. E. Activation of Carbon Disulphide by Transition Metal Complexes. *Journal of Organometallic Chemistry* **1974**, *66* (2), 161–194. [https://doi.org/10.1016/S0022-328X\(00\)91482-7](https://doi.org/10.1016/S0022-328X(00)91482-7).
- (126) Pandey, K. K. Reactivities of Carbonyl Sulfide (COS), Carbon Disulfide (CS₂) and Carbon Dioxide(CO₂)with Transition Metal Complexes. *Coordination Chemistry Reviews* **1995**, *140*, 37–114. [https://doi.org/10.1016/0010-8545\(94\)01120-Z](https://doi.org/10.1016/0010-8545(94)01120-Z).
- (127) Motokura, K.; Kashiwame, D.; Takahashi, N.; Miyaji, A.; Baba, T. Highly Active and Selective Catalysis of Copper Diphosphine Complexes for the Transformation of Carbon Dioxide into Silyl Formate. *Chem. Eur. J.* **2013**, *19* (30), 10030–10037. <https://doi.org/10.1002/chem.201300935>.

- (128) Gooßen, L. J.; Thiel, W. R.; Rodríguez, N.; Linder, C.; Melzer, B. Copper-Catalyzed Protodecarboxylation of Aromatic Carboxylic Acids. *Adv. Synth. Catal.* **2007**, *349* (14–15), 2241–2246. <https://doi.org/10.1002/adsc.200700223>.
- (129) <https://Labs.Chem.Ucsb.Edu/Zakarian/Armen/11---BondDissociationEnergy.Pdf>.
- (130) Rajput, G.; Singh, V.; Singh, S. K.; Prasad, L. B.; Drew, M. G. B.; Singh, N. Cooperative Metal–Ligand-Induced Properties of Heteroleptic Copper(I) Xanthate/Dithiocarbamate PPh₃ Complexes. *Eur. J. Inorg. Chem.* **2012**, *2012* (24), 3885–3891. <https://doi.org/10.1002/ejic.201200307>.
- (131) Gupta, A. N.; Singh, V.; Kumar, V.; Prasad, L. B.; Drew, M. G. B.; Singh, N. Syntheses, Crystal Structures and Optical Properties of Heteroleptic Copper(I) Dithio/PPh₃ Complexes. *Polyhedron* **2014**, *79*, 324–329. <https://doi.org/10.1016/j.poly.2014.04.068>.
- (132) Ma, H. Z.; Li, J.; Canty, A. J.; O’Hair, R. A. J. Cluster Transformation of [Cu₃(μ₃-H)(μ₃-BH₄)(PPh₂)₂NH₃](BF₄) to [Cu₃(μ₃-H)(μ₂,μ₁-S₂CH)(PPh₂)₂NH₃](BF₄) via Reaction with CS₂. X-Ray Structural Characterisation and Reactivity of Cationic Clusters Explored by Multistage Mass Spectrometry and Computational Studies. *Dalton Trans.* **2017**, *46* (43), 14995–15003. <https://doi.org/10.1039/C7DT03510A>.
- (133) Shintani, R.; Nozaki, K. Copper-Catalyzed Hydroboration of Carbon Dioxide. *Organometallics* **2013**, *32* (8), 2459–2462. <https://doi.org/10.1021/om400175h>.
- (134) Ma, H. Z.; Canty, A. J.; O’Hair, R. A. J. Near Thermal, Selective Liberation of Hydrogen from Formic Acid Catalysed by Copper Hydride Ate Complexes. *Dalton Trans.* **2023**, *52* (6), 1574–1581. <https://doi.org/10.1039/D2DT03764E>.
- (135) Osipova, E. S.; Sedlova, D. V.; Gutsul, E. I.; Nelyubina, Y. V.; Dorovatovskii, P. V.; Epstein, L. M.; Filippov, O. A.; Shubina, E. S.; Belkova, N. V. Reactivity of Heterobimetallic Ion Pairs in Formic Acid Dehydrogenation. *Organometallics* **2023**, *42* (18), 2651–2660. <https://doi.org/10.1021/acs.organomet.3c00125>.
- (136) Liu, Y.; Chen, C.; Li, H.; Huang, K.-W.; Tan, J.; Weng, Z. Efficient S_N2 Fluorination of Primary and Secondary Alkyl Bromides by Copper(I) Fluoride Complexes. *Organometallics* **2013**, *32* (21), 6587–6592. <https://doi.org/10.1021/om4008967>.
- (137) Pascher, T. F.; Ončák, M.; Van Der Linde, C.; Beyer, M. K. Decomposition of Copper Formate Clusters: Insight into Elementary Steps of Calcination and Carbon Dioxide Activation. *ChemistryOpen* **2019**, *8* (12), 1453–1459. <https://doi.org/10.1002/open.201900282>.
- (138) Galwey, A. K.; Jamieson, D.; Brown, M. E. Thermal Decomposition of Three Crystalline Modifications of Anhydrous Copper(II) Formate. *J. Phys. Chem.* **1974**, *78* (26), 2664–2670. <https://doi.org/10.1021/j100619a006>.
- (139) Sponholz, P.; Mellmann, D.; Junge, H.; Beller, M. Towards a Practical Setup for Hydrogen Production from Formic Acid. *ChemSusChem* **2013**, *6* (7), 1172–1176. <https://doi.org/10.1002/cssc.201300186>.
- (140) J., C.; Z., L.; E., K. A Prolific Catalyst for Dehydrogenation of Neat Formic Acid. *Nature Communication* **2016**, No. 7, 11308–11314. <https://doi.org/doi/10.1038/ncomms11308>.
- (141) Wang, Z.; Lu, S.-M.; Li, J.; Wang, J.; Li, C. Unprecedentedly High Formic Acid Dehydrogenation Activity on an Iridium Complex with an N, N’-Diimine Ligand in Water. *Chem. Eur. J.* **2015**, *21* (36), 12592–12595. <https://doi.org/10.1002/chem.201502086>.

- (142) Colton, R.; James, B. D.; Potter, I. D.; Traeger, J. C. Copper(I) Tetrahydroborate Derivatives Containing Phosphine and Phenanthroline Ligands: An Electrospray Mass Spectrometric Study of Species in Solution. *Inorg. Chem.* **1993**, *32* (12), 2626–2629. <https://doi.org/10.1021/ic00064a009>.
- (143) Scaltrito, D. V.; Thompson, D. W.; O’Callaghan, J. A.; Meyer, G. J. MLCT Excited States of Cuprous Bis-Phenanthroline Coordination Compounds. *Coordination Chemistry Reviews* **2000**, *208* (1), 243–266. [https://doi.org/10.1016/S0010-8545\(00\)00309-X](https://doi.org/10.1016/S0010-8545(00)00309-X).
- (144) Shukla, S. N.; Gaur, P.; Raidas, M. L.; Chaurasia, B.; Bagri, S. S. Novel NNO Pincer Type Schiff Base Ligand and Its Complexes of Fe(III), Co(II) and Ni(II): Synthesis, Spectroscopic Characterization, DFT, Antibacterial and Anticorrosion Study. *Journal of Molecular Structure* **2021**, *1240*, 130582. <https://doi.org/10.1016/j.molstruc.2021.130582>.
- (145) Petrovic, D.; Bannenberg, T.; Randoll, S.; Jones, P. G.; Tamm, M. Synthesis and Reactivity of Copper(I) Complexes Containing a Bis(Imidazolin-2-Imine) Pincer Ligand. *Dalton Trans.* **2007**, No. 26, 2812–2822. <https://doi.org/10.1039/b703183a>.
- (146) Vedernikov, A. N.; Wu, P.; Huffman, J. C.; Caulton, K. G. Cu(I) and Cu(II) Complexes of a Pyridine-Based Pincer Ligand. *Inorganica Chimica Acta* **2002**, *330* (1), 103–110. [https://doi.org/10.1016/S0020-1693\(01\)00825-8](https://doi.org/10.1016/S0020-1693(01)00825-8).

Conclusion and Perspectives

Table of Contents

I. Conclusion	177
I. 1. The synthesis of copper(I) carboxylate and copper(I) aryl complex supported by 2,9- ^t Bu ₂ phen (phen*) ligand and their reactivity toward decarboxylation and CO ₂ insertion (Chapter 2)	177
I. 2. The synthesis of phen* ligated copper formate complex (12) and its reactivity in dynamic isotopic exchange and formic acid dehydrogenation (Chapter 3)	178
II. Perspectives.....	179
II. 1. Decarboxylation of copper carboxylate complexes supported by quinoline ligand.	179
II. 2. Insertion SO ₂ into copper complexes	180
III. References.....	182

I. Conclusion

Since the first report by Shepard in 1930,¹ significant progresses have been achieved in the 21st century on the development of transition metals catalyzed decarboxylative cross-coupling and related protodecarboxylation reactions.²⁻⁴ Though they have provided efficient synthetic methods for the transformation of carboxylic acids into valuable biaryl compounds, some challenges remain related to the high reaction temperatures and substrates scope that requires *ortho* substituents on the aromatic ring. There have been efforts over the years to optimize the reaction conditions and widen the range of functionalized carboxylic acids to *para*- and *meta*-derivatives. Copper-based catalysts supported by nitrogenated ancillary ligands have been particularly successful and have offered new catalytic systems enabling the coupling reaction with non *ortho*-substituted carboxylic acids, however at elevated temperatures.

Investigations on the mechanism of the decarboxylation process when a copper catalyst is employed were also pursued. All mechanistic studies have been carried out with phenanthroline-based ligand and activated benzoic acids, such as pentafluorobenzoic acid, *o*-nitro benzoic acid, *etc.* Such studies have allowed for the identification of potentially active copper intermediates, namely copper(I) carboxylate and copper(I) aryl species, and the beneficial influence of *ortho*-substituted benzoic acids. However, these studies did not bring conclusive proofs due to the instability of copper(I) complexes but a general consensus mechanism relying on a one-step CO₂ extrusion via these copper intermediates.

The development of copper-catalyzed dynamic carbon isotopic exchange by Destro *et al.*, where the gas ¹⁴CO₂ exchanges with the ¹²CO₂ fragment in carboxylic acids in a single step, has brought insightful observation in the decarboxylation process since the two steps proceed simultaneously.⁵ It suggested that the loss of ¹²CO₂ in copper carboxylate complexes, and its further reinsertion as ¹⁴CO₂, proceeded via copper carboxylate and copper aryl intermediates, respectively. Since the detection or identification of the reaction intermediates using their bioxazoline-based ligand were not attempted or were unsuccessful, the view on the mechanism remained incomplete.

With the goal to clearly identify the active species (their nature and oxidation state of the copper ions), we envisioned the synthesis of the carboxylate and aryl copper(I) pairs involving a bulky phenanthroline ligand, *e.g.* 2,9-^tBu₂phen (phen*), which would bring greater stability of the complexes and be useful for NMR investigations.

I. 1. The synthesis of copper(I) carboxylate and copper(I) aryl complex supported by 2,9-^tBu₂phen (phen*) ligand and their reactivity toward decarboxylation and CO₂ insertion (Chapter 2)

In chapter 2, I reported the synthesis of a variety of (phen*)copper(I) carboxylate and copper(I) aryl complexes, in particular pairs of compounds with the same aryl fragment. Most of them have been characterized by their crystal structures.

With this series of complexes, studies on the decarboxylation process from copper carboxylates [(phen*)Cu(O₂CAr)] complexes as well as the insertion of CO₂ in copper aryl [(phen*)Cu-Ar] derivatives

was possible. I demonstrated that some copper carboxylate species $[(\text{phen}^*)\text{Cu}(\text{O}_2\text{C}\text{Ar})]$ ($\text{Ar} = o\text{-F-C}_5\text{H}_4$ (**2**), C_6F_5 (**4**), $o\text{-NO}_2\text{-C}_5\text{H}_4$ (**5**)) could decarboxylate in quinoline solvent at different temperatures, and that the protodecarboxylation side reaction (formation of Ar-H) inevitably occur. The decarboxylation of the *ortho*-substituted complexes **2** and **5** was evidenced by the release of CO_2 gas by GC analysis and the formation of corresponding arene compounds, fluorobenzene and nitrobenzene, respectively. Through the CO_2 extrusion in complex **4**, the corresponding copper aryl complex (**8**) has been detected, along with the protodecarboxylation side product $\text{C}_6\text{F}_5\text{H}$. Influence of the solvent is crucial and compared to THF, quinoline considerably promotes both decarboxylation and protodecarboxylation processes. However, I have never observed the insertion of CO_2 in the other copper(I) aryl, a point that likely reflect the lower stability of these aryl compounds which are rapidly degraded under heating and/or because of a unfavorable thermodynamic.

Based on the experiments, two plausible pathways are proposed for the decarboxylation of **4**. The first is in agreement with the literature and would proceed via a concerted CO_2 extrusion where the copper center interacts both with the ipso carbon of the aryl and the CO_2 fragment. The second possibility involves coordination of quinoline to the copper center that favor first protodecarboxylation side reaction. The quinoline anion in $[(\text{phen}^*)\text{Cu}(\text{quin})]$ then reacts with $\text{C}_6\text{F}_5\text{-H}$ to generate $[(\text{phen}^*)\text{Cu}(\text{C}_6\text{F}_5)]$ and quinoline.

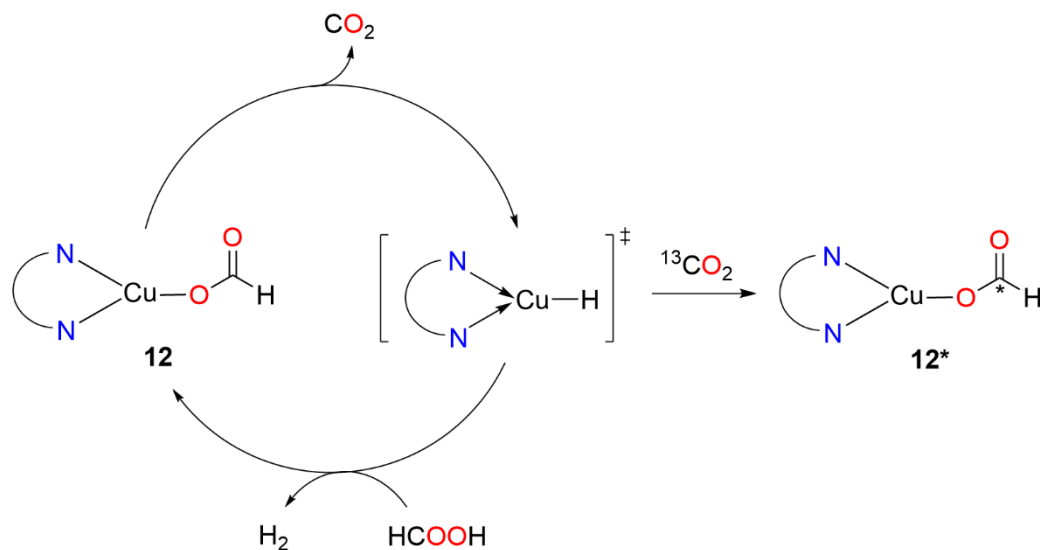
There are therefore still unresolved questions about the reversibility of the reaction and whether the concerted decarboxylation pathway is through a copper (III) intermediate.

1. 2. The synthesis of phen* ligated copper formate complex (**12**) and its reactivity in dynamic isotopic exchange and formic acid dehydrogenation (Chapter 3)

I report the synthesis of the copper formate complex $[(\text{phen}^*)\text{Cu}(\text{O}_2\text{CH})]$ (**12**) and its solid state structure obtained by X-ray diffraction one single crystal. It is a very rare monometallic formate complex supported by a nitrogen ligand. We hypothesize that a formate species, compared with a true carboxylate derivative, would be more sensitive and reactive toward decarboxylation. Dynamic isotopic exchange of **12** with $^{13}\text{CO}_2$ resulted in a mixture of **12** and its labeled derivative $[(\text{phen}^*)\text{Cu}(\text{O}_2^{13}\text{CH})]$ (**12***). This result clearly evidenced decarboxylation of **12** and, because of the reversibility of the process under CO_2 , the transient formation of the copper hydride intermediate $[(\text{phen}^*)\text{Cu-H}]$ (*Scheme CP1*). This latter reactive hydride would immediately insert $^{13}\text{CO}_2$ to afford $[(\text{phen}^*)\text{Cu}(\text{O}_2^{13}\text{CH})]$ (**12***). Suspected to be monomeric, I tried to isolate or detect the hydride $[(\text{phen}^*)\text{Cu-H}]$ because reactive monometallic $[\text{Cu}]\text{-H}$ species are actively sought after for years. However, this instable species remained inaccessible and could not be obtained even by other synthetic pathways which all gave elemental copper.

I have also shown that complex **12** is an active catalyst in the dehydrogenation of formic acid. Of interest, the reaction did not require any additives to proceed. However, this catalyst degrades at the end of the reaction with the liberation of phen* ligand. From the reports in the literature and our results, we have proposed a catalytic cycle for the FA dehydrogenation catalyzed by **12**. It involves either the coordination of FA to the copper ion or the solvate species $[(\text{phen}^*)\text{Cu}(\text{O}_2\text{CH})]\cdot n(\text{HCO}_2\text{H})$ where the formate ligand interacts with the proton of the acid through hydrogen bonding. Such

interaction of copper and d-transition metal species with FA is well documented. After the CO₂ extrusion, the generated copper hydride is immediately trapped by the acid to produce H₂ with regeneration of **12**.



Scheme CP1. Combination of proposed mechanism for the dehydrogenation of FA by $[(phen^*)Cu(\kappa^1-O_2CH)]$ **12** and dynamic isotopic exchange of **12** with $^{13}CO_2$ via copper hydride intermediate.

II. Perspectives

II. 1. Decarboxylation of copper carboxylate complexes supported by quinoline ligand.

In 1989, van Koten *et al.* isolated the dinuclear copper carboxylate complexes $[Cu(\mu-O_2CC_6H_4X)(quin)]_2$ (quin = quinoline; X = H, Me) and study their reactivity in decarboxylation process.⁶ As mentioned in Chapter 1, they observed the decarboxylation only in naphthalene solvent with the addition of 1.1 extra equivalent of quinoline at 218 °C. They obtained a mixture of quinoline and quinoline containing products (2-acylquinolines, 2,2'-diquinolyl ether and three different coupling products between naphthalene and quinoline, naphthylquinoline being the major coupling product) along with CO₂ gas and no arene or biaryl compound was detected. They proposed three plausible pathways from the dinuclear copper(I) species, that would lead to Cu(II)/Cu(II), Cu(I)/Cu(III) or Cu(II)/Cu(I) intermediates by oxidative addition event or single-electron transfer step. Nevertheless, their study lacks detailed NMR observations and although highly interesting, these works should be continued to access to a conclusive mechanism.

In this study, I have shown that ortho-substituted complexes with electron-attracting groups such as $[(phen^*)Cu(O_2C-C_6H_4\{o-F\})]$ (**2**), $[(phen^*)Cu(O_2CC_6F_5)]$ (**4**), and $[(phen^*)Cu(O_2C-C_6H_4\{o-NO_2\})]$ (**5**) can readily decarboxylate into the corresponding arene (with release of CO₂) in particular in quinoline solvent. With regard to the results of van Koten *et al.*, we recognized that the mechanism of decarboxylation by copper species may be highly subject to the nature of solvent, and quinoline is particularly fitted. We thus envisioned that such copper carboxylates $[Cu(O_2CR)]$ species, supported by quinoline ligands instead of phen*, might be more convenient precursors for studying the decarboxylation process and afford detailed examination on the mechanism. At the end of my PhD, I

have thus isolated the quinoline copper(I) carboxylates complexes $[\text{Cu}(\mu\text{-O}_2\text{C-C}_6\text{H}_4\{\text{o-NO}_2\})\{\text{quin}\}]_2$ (**14**) and $[\text{Cu}(\mu\text{-O}_2\text{C-C}_6\text{H}_4\{\text{o-F}\})\{\text{quin}\}]_2$ (**15**) and obtained their crystal structures (see *Figure CP1*). The decarboxylation behaviour of these complexes should be studied in non-coordinating solvents such as toluene or in quinoline and followed by NMR analysis. Additional mechanistic probes such as $^{13}\text{CO}_2$ could be introduced to track the CO_2 extrusion along with computational studies to address the putative intermediates.

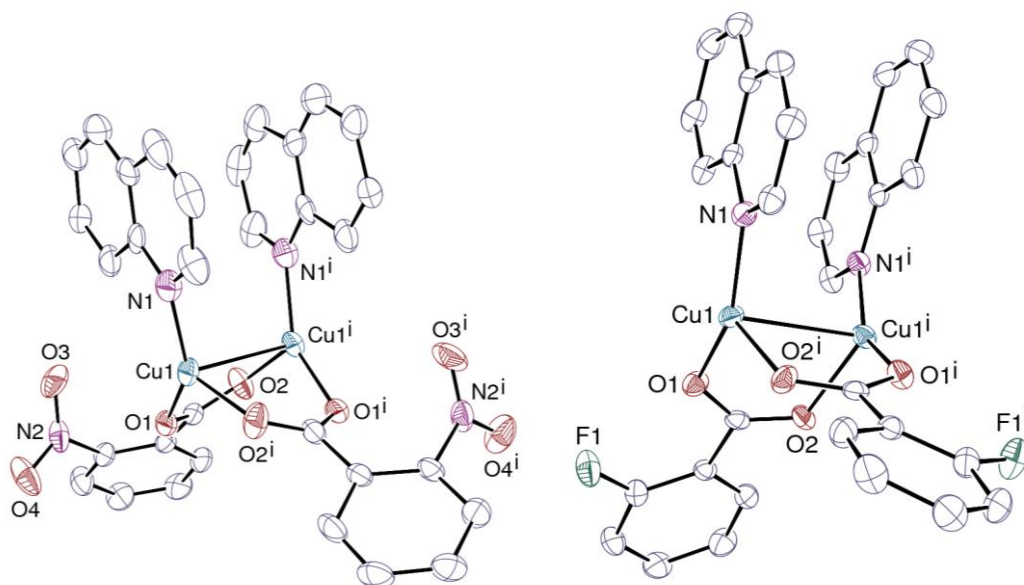
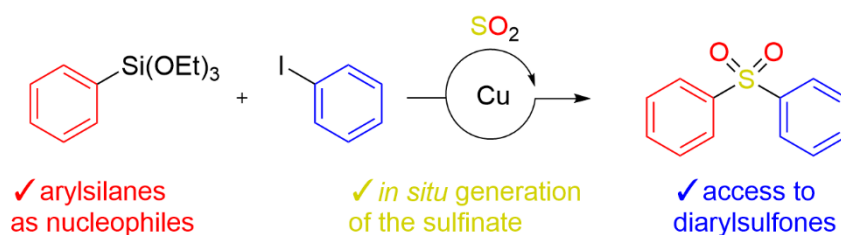


Figure CP1. Views of $[(\text{quin})\text{Cu}(\text{O}_2\text{C-o-NO}_2\text{-C}_6\text{H}_4)]_2$ (**14**) (left) and of $[(\text{quin})\text{Cu}(\text{O}_2\text{C-o-F-C}_6\text{H}_4)]_2$ (**15**) (right). Displacement ellipsoids are drawn at the 50% probability level. (Cu, light blue; F, green; O, red; N, purple; C, blue).

II. 2. Insertion SO_2 into copper complexes

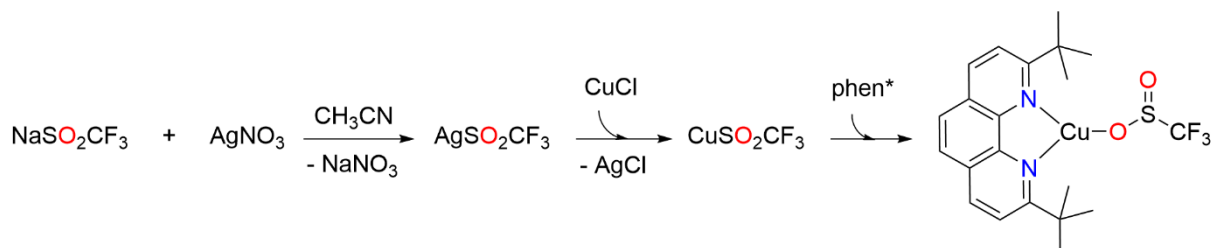
Our group has recently reported the copper(I)-catalyzed sulfonylative Hiyama cross-coupling for the production of sulfones by reacting organosilanes, sulfur dioxide (SO_2) and iodoarenes (Scheme CP2).⁷



Scheme CP2. A $\text{Cu}(\text{I})$ -catalyzed sulfonylative Hiyama cross-coupling for the direct synthesis of diaryl sulfones from aryl silanes, SO_2 surrogate, and aryl iodides.

This methodology was efficient to form a variety of diaryl sulfones, using an inexpensive catalytic system involving $[\text{Cu}(\text{MeCN})_4]\text{BF}_4$ and dmeda (1,2-dimethyl ethylenediamine). Based on experimental and computational mechanistic studies, they proposed a mechanism involving the insertion of SO_2 into an aryl copper(I) species to generate a copper(I) sulfinate intermediate. Their effort to isolate a copper(I) sulfinate complex was successful with the use of 1,10-phenanthroline as ligand and 4-toluenesulfonic acid. They isolated the dimeric species $[(\text{phen})\text{Cu}(\text{SO}_2\text{Tol})]_2$.

In this context, another perspective can be opened from my PhD study. It is the mechanistic investigation on the sulfonylation of copper(I) aryl and copper(I) alkyl species. My first attempts with the copper aryl and alkyl species $[(\text{phen}^*)\text{Cu}(\text{C}_6\text{F}_5)]$ (**8**) and $[(\text{phen}^*)\text{Cu}(\text{CF}_3)]$ (**11**), respectively, have shown the insertion of SO_2 into complex **11**, in THF at 70°C . I generated a new species $[(\text{phen}^*)\text{Cu}]_2[(\mu\text{-O}_2\text{S-CF}_3)]^+[\text{HSO}_4]^-$ (**17**) that I have structurally characterized by X-ray diffraction study (Figure CP2, right and SI). I also prepared the monomeric $[(\text{phen}^*)\text{Cu}(\kappa^1\text{-O}_2\text{SCF}_3)]$ complex (**16**) (Scheme CP3) and is presented in Figure CP2 (left) (see SI). These results may offer a starting basis for the mechanistic investigation of the desulfonylation/sulfonylation process by copper that could be complementary to the decarboxylation/carboxylation process.



Scheme CP3. Synthesis of $[(\text{phen}^*)\text{Cu}(\kappa^1\text{-O}_2\text{S-CF}_3)]$.

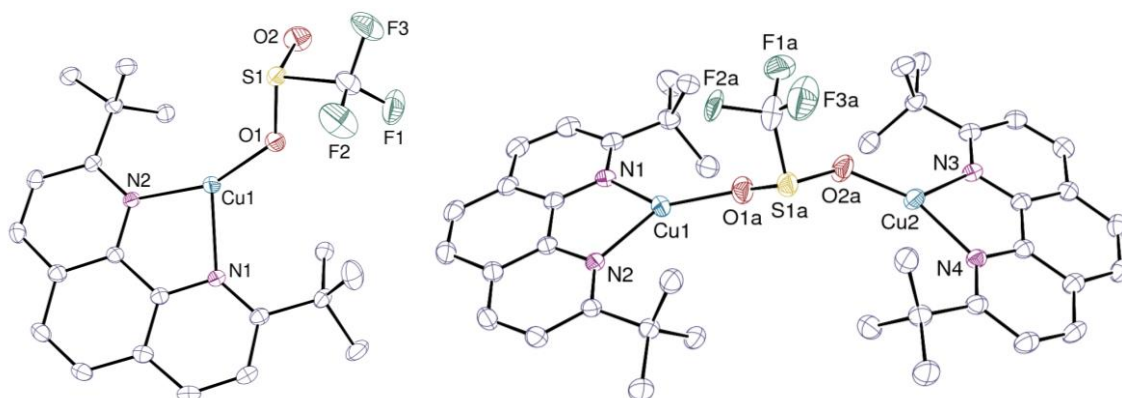


Figure CP2. Views of $[(\text{phen}^*)\text{Cu}(\text{O}_2\text{S-CF}_3)]$ (**16**) (left) and of $[(\text{phen}^*)\text{Cu}]_2[(\mu\text{-O}_2\text{SCF}_3)]^+$ (**17**) (right), with anion HSO_4^- and hydrogen atoms are omitted. Displacement ellipsoids are drawn at the 50% probability level. (Cu, light blue; F, green; O, red; N, purple; C, blue).

III. References

- (1) Shepard, A. F.; Winslow, N. R.; Johnson, J. R. THE SIMPLE HALOGEN DERIVATIVES OF FURAN. *J. Am. Chem. Soc.* **1930**, *52* (5), 2083–2090.
- (2) Zhang, T.; Wang, N.-X.; Xing, Y. Advances in Decarboxylative Oxidative Coupling Reaction. *J. Org. Chem.* **2018**, *83* (15), 7559–7565.
- (3) Wei, Y.; Hu, P.; Zhang, M.; Su, W. Metal-Catalyzed Decarboxylative C–H Functionalization. *Chem. Rev.* **2017**, *117* (13), 8864–8907..
- (4) Rodríguez, N.; Goossen, L. J. Decarboxylative Coupling Reactions: A Modern Strategy for C–C Bond Formation. *Chem. Soc. Rev.* **2011**, *40* (10), 5030.
- (5) Destro, G.; Loreau, O.; Marcon, E.; Taran, F.; Cantat, T.; Audisio, D. Dynamic Carbon Isotope Exchange of Pharmaceuticals with Labeled CO₂. *J. Am. Chem. Soc.* **2019**, *141* (2), 780–784.
- (6) Aalten, H. L.; Van Koten, G.; Tromp, J.; Stam, C. H.; Goubitz, K.; Mak, A. N. S.; Van Der Kerk-van Hoof, A. Dinuclear Copper(I) Benzoato Quinoline Complexes as Intermediates in the Copper-Quinoline Decarboxylation Reaction. *Recl. Trav. Chim. Pays-Bas* **2010**, *108* (9), 295–303.
- (7) Adenot, A.; Anthore-Dalion, L.; Nicolas, E.; Berthet, J.; Thuéry, P.; Cantat, T. A Copper(I)-Catalyzed Sulfonylative Hiyama Cross-Coupling. *Chemistry A European J* **2021**, *27* (72), 18047–18053.

Experimental Part

Table of Contents

I. General information	186
II. Experimental part of chapter 2.....	186
II. 1. Synthese of phen* (1) ligand and [Cu(O ^t Bu)]	186
II. 1. 1. Spectra of 2,9-di- <i>tert</i> butyl-1,10-phenanthroline (1), (Formula: C ₂₀ H ₂₄ N ₂ , M= 292.19 g/mol)	186
II. 1. 2. Synthesis of [Cu(O ^t Bu)] ₄	188
II. 1. 3. Data of complex [(phen*)Cu-O ^t Bu]:	189
II. 2. General synthesis procedure for the formation of carboxylate complexes (phen*)Cu ^I (O ₂ CR) (R = C ₆ H ₄ - <i>o</i> -F (2), C ₆ H ₄ - <i>p</i> -F (3), C ₆ F ₅ (4), C ₆ H ₄ - <i>o</i> -NO ₂ (5), C ₆ H ₄ - <i>p</i> -NO ₂ (6), CF ₃ (7)).	190
II. 2. 1. Data for complex [(phen*)Cu-(O ₂ CC ₆ H ₄ - <i>o</i> -F)] (2):.....	190
II. 2. 2. Data for complex [(phen*)Cu-(O ₂ CC ₆ H ₄ - <i>p</i> -F)] (3):.....	193
II. 2. 3. Data for complex [(phen*)Cu(O ₂ CC ₆ F ₅)] (4):.....	195
II. 2. 4. Data for complex [(phen*)Cu(O ₂ CC ₆ H ₄ - <i>o</i> -NO ₂)] (5):	198
II. 2. 5 Data for complex [(phen*)Cu(O ₂ CC ₆ H ₄ - <i>p</i> -NO ₂)] (6):	200
II. 2. 6. Data for complex [(phen*)Cu(O ₂ CCF ₃)] (7):	202
II. 3. Synthesis of the [(phen*)Cu-R] complexes.....	205
II. 3. 1. Data for complex [(phen*)Cu-C ₆ F ₅] (8):	205
II. 3. 2. Data for complex [(phen)Cu-C ₆ F ₅] (8'):	208
II. 3. 3. Data for complex [(phen*)Cu(C ₆ H ₄ - <i>o</i> -NO ₂)] (9):	209
II. 3. 4. Data for complex [(phen*)Cu-CF ₃] (11):	213
II. 3. 5. Crystal structure of [(phen*)Cu-F(HF)]•C ₆ H ₆ and NMR of [(phen*)Cu-F(HF)] (10).....	216
II. 4. Decarboxylation of the [(phen*)Cu(O ₂ CR)] complexes (R = C ₆ H ₄ - <i>o</i> -F, C ₆ F ₅ , C ₆ H ₄ - <i>o</i> -NO ₂ , CF ₃) .	218
II. 4. 1. Decarboxylation in THF:.....	218
<i>a. Thermal decarboxylation of [(phen*)Cu(O₂CC₆H₄-<i>o</i>-F)] (2)</i>	<i>218</i>
<i>b. Thermal decarboxylation of [(phen*)Cu(O₂CC₆F₅)] (4):</i>	<i>220</i>
<i>c. Thermal decarboxylation of [(phen*)Cu(O₂CC₆H₄-<i>o</i>-NO₂)] (5)</i>	<i>222</i>
<i>d. Thermal decarboxylation of [(phen*)Cu(O₂CCF₃)] (7).....</i>	<i>223</i>
II. 4. 2. Decarboxylation in quinoline:.....	225
<i>a. Control experiment</i>	<i>225</i>
<i>b. [Cu(C₆F₅)(quinoline)_n]</i>	<i>226</i>

c. Reaction of $[Cu(C_6F_5)(quinoline)_n]$ and 1 equiv. phen*	227
d. Thermal decarboxylation of $[(phen^*)Cu(O_2CC_6H_4-o-F)]$ (2) in quinoline	230
e. Thermal decarboxylation of $[(phen^*)Cu(O_2CC_6F_5)]$ (4) in quinoline	230
g. Thermal decarboxylation of $[(phen^*)Cu(O_2CCF_3)]$ (11) in quinoline	233
h. Thermal decarboxylation of $[(phen^*)Cu(O_2CCF_3)]$ (11) in DMF- d_7	234
II. 5. Carboxylation of the $[(phen^*)Cu-R]$ complexes 8 , 9 , and 11	234
II. 5. 1. Carboxylation of $[(phen^*)Cu(C_6F_5)]$ (8)	234
a. Carboxylation of $[(phen^*)Cu(C_6F_5)]$ (8) in DMA	235
b. Carboxylation of $[(phen^*)Cu(C_6F_5)]$ (8) in quinoline	235
c. Carboxylation of $[(phen^*)Cu(C_6F_5)]$ (8) in THF- d_8	236
II. 5. 2. Carboxylation of $[(phen^*)Cu(C_6H_4-o-NO_2)]$ (9)	237
a. Carboxylation of $[(phen^*)Cu(C_6H_4-o-NO_2)]$ (9) in C_6D_6	238
b. Carboxylation of $[(phen^*)Cu(o-NO_2-C_6H_4)]$ (9) in Tol- d_8	239
II. 5. 3. Carboxylation of $[(phen^*)Cu(CF_3)]$ (11) in DMA	240
III. Experimental part of Chapter 3	243
III. 1. Synthesis of $[(phen^*)Cu(\kappa^1-O_2CH)]$ (12) (Formula : $C_{21}H_{25}CuN_2O_2$, M= 400.99 g/mol)	243
III. 2. $[(phen^*)Cu-(O_2CH)]$ in THF- d_8 at low temperatures	245
III. 2. 1. Solution of $[(phen^*)Cu(O_2CH)]$ in THF- d_8 at 210 K (-63 °C)	247
III. 3. Thermal decomposition of $[(phen^*)Cu(O_2CH)]$ (12)	248
III. 4. Attempts to isolate/detect copper hydride	249
III. 4. 1. Reaction of $Cu(O^tBu) + Phen^*$ with dihydrogen:	249
III. 4. 2. Reaction of $Cu(O^tBu) + Phen^*$ with HBpin:	249
III. 4. 3. Reaction of $Phen^*$ with Stryker reagent $[Cu(PPh_3)H]_6$:	250
III. 4. 4. Reaction of $[(phen^*)CuI]$ with hydride reagents:	251
III. 4. 5. Thermal behavior of 12 in presence of BEt_3 :	252
III. 4. 6. Synthesis of $\{[(phen^*)Cu]_2(\mu-O_2CH)\}[(HCO_2-\kappa^1)B(C_6F_5)_3]$ (13) by reaction of 12 with $B(C_6F_5)_3$:	252
III. 4. 7. Synthesis of $[HNEt_3][(HCO_2-\kappa^1)B(C_6F_5)_3]$:	255
III. 4. 8. Thermal behavior of 12 in presence of with phenylacetylene:	257
III. 4. 9. Stoichiometric reaction of 12 with $^{13}CO_2$:	257
III. 4. 10. Stoichiometric reaction with CS_2	262
III. 5. Procedure for the catalytic dehydrogenation of formic acid	262
III. 5. 1. General catalysis experiment	262
III. 5. 2. Representative procedure for the catalytic dehydrogenation	262
III. 5. 3. GC analysis for catalytic dehydrogenation of formic acid	266
III. 5. 4. Proof for the decomposition of complex 12 after catalysis	267

VI. Experimental part of Perspectives	269
VI. 1. Formation of $[\text{Cu}(\mu\text{-O}_2\text{C-C}_6\text{H}_4\{\text{o-NO}_2\})_2(\text{quin})]_2$ (14) and $[\text{Cu}(\mu\text{-O}_2\text{C-C}_6\text{H}_4\{\text{o-F}\})_2(\text{quin})]_2$ (15) ...	269
IV. 1. 1. Data for $[\text{Cu}(\mu\text{-O}_2\text{C-C}_6\text{H}_4\{\text{o-NO}_2\})_2(\text{quin})]_2$ (14):	269
IV. 1. 2. Data for $[\text{Cu}(\mu\text{-O}_2\text{C-C}_6\text{H}_4\{\text{o-F}\})_2(\text{quin})]_2$ (15):.....	270
IV. 2. SO_2 insertion into $[(\text{phen}^*)\text{Cu-CF}_3]$ (11) for the formation of $[(\text{phen}^*\text{-Cu})_2\text{-O}_2\text{S-CF}_3]$ (17). ...	271
IV. 3. Synthesis of $[(\text{phen}^*)\text{Cu}(\kappa^1\text{-O}_2\text{SCF}_3)]$ complex (16)	273
V. Computational details	275
VI. Crystallography	275

I. General information

The solvents (toluene, pentane, diethyl ether and tetrahydrofuran) were carefully dried over a mixture of sodium-benzophenone, and over KH for acetonitrile, and were distilled prior to use. Deuterated toluene, benzene and tetrahydrofuran (Eurisotop) were distilled over potassium. Deuterated acetonitrile was distilled over KH and then stored over 3 Å molecular sieves in a glove box. The 4 Å molecular sieve (Aldrich) was activated by drying under dynamic vacuum at 250 °C for 48 h prior to use.

Mesitylene (Aldrich) was stored over activated 4 Å molecular sieves and used directly without further purification. All other reagents were purchased from commercial suppliers (Sigma Aldrich, Carlo Erba, Thermo Fischer Scientific, and Alfa Aesar), and used as received.

$[\text{Cu}(\text{C}_6\text{F}_5)]_4$, were prepared from literature methods.^{1–3} The organic acids RCO_2H ($\text{R} = o/p\text{-F-phenyl}$, $o/p\text{-NO}_2\text{-phenyl}$, C_6F_5 , CF_3), and CF_3SiMe_3 , $\text{NEt}_3 \cdot \text{HF}$, 1,10-phenanthroline, $^t\text{Bu-Li}$ (1.7 M solution in pentane), CuCl , CuI , $\text{C}_6\text{F}_5\text{MgBr}$ (0.5 M in Et_2O) were purchased from Sigma-Aldrich and generally used as received. Compound 5,5-dimethyl-2-(2-nitrophenyl)-1,3,2-dioxaborinane was synthesis according to the literature.⁴

CO_2 and $^{13}\text{CO}_2$ gas were purchased from Messer and Eurisotop.

The ^1H , ^{31}P and $^{13}\text{C}\{^1\text{H}\}$ NMR spectra were recorded on a *Bruker AVANCE Neo 400 MHz* spectrometer and referenced internally using the residual protio solvent resonances relative to tetramethylsilane (δ 0). The spectra were recorded at 25 °C when not otherwise specified. The ^1H NMR signals of THF- d_6 are referenced at values given in the literature. The ^{19}F NMR signals were referenced from CCl_3F ($\delta = 0$). All the δ values are in ppm. Elemental analyses were performed by Medac Ltd at Chobham (Surrey, UK). IR spectra were recorded on a Nicolet 6700 FT-IR with ATR diamond accessory.

II. Experimental part of chapter 2

II. 1. Synthese of phen* (1) ligand and $[\text{Cu}(\text{O}^t\text{Bu})]$

II. 1. 1. Spectra of 2,9-di-*tert*butyl-1,10-phenanthroline (1), (Formula: $\text{C}_{20}\text{H}_{24}\text{N}_2$, $M = 292.19$ g/mol)

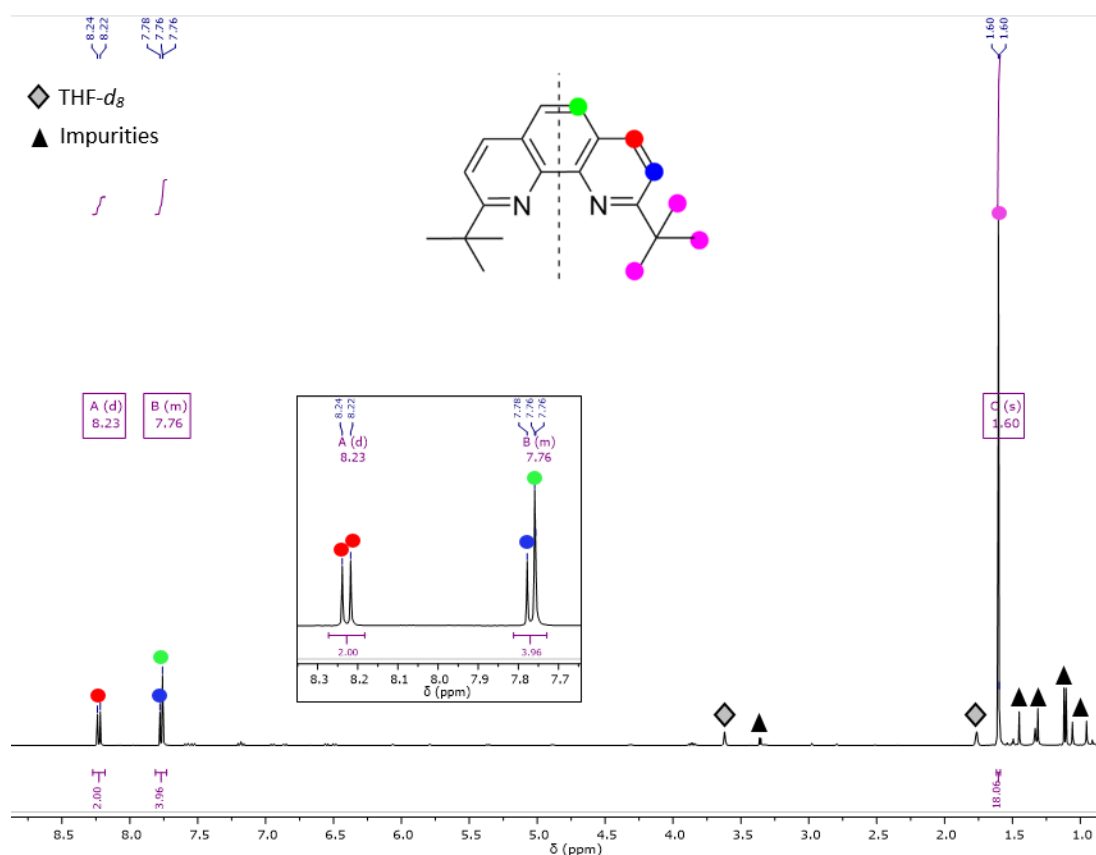
The following synthesis was inspired by Barnhart et al.,⁵ Quing-Hua Fan et al.,⁶ and Sauvage et al.⁷ with modification.

To a clear colorless solution of 1,10-phenanthroline (5g, 27.75 mmol, 1 equiv.) in toluene (200 mL) cooled down at -40 °C for 2 h, 2 equiv. of $^t\text{Bu-Li}$ in pentane (35.3 mL, 1.7 M solution in pentane, 55.5 mmol, 2 equiv.) were added dropwise. The solution rapidly turned to a red suspension (2 min during the addition) which was stirred continuously at room temperature overnight (8 h). Distilled H_2O (50 mL) was then added, in a single addition, to the red suspension. The red solution turned yellow within

5 min and was further stirred for 10 min to obtain two separate layers of yellow organic phase (above) and clear colorless aqueous phase (below) which were separated. The aqueous phase was extracted with dichloromethane (10 mL x 3) and all the organic fractions (toluene and CH₂Cl₂ fractions) were combined together. Black powder of MnO₂ (57.89 g, 0.66 mol, 24 equiv.) was then added to the yellow organic phase and the suspension stirred at room temperature for 7 h before MnO₂ was filtrated off on a glass filter frit with a layer of Celite. The resulting yellow solution was then dried over MgSO₄ (4.3 g, 35.7 mmol, 1.3 equiv.) for 1 h. The solution was finally filtrated to remove MgSO₄ and the solvent evaporated off. The yellow residue was mixed with silica gel and poured out on the top of the silica gel column. Chromatography purification was perform with the mixture of solvents (petroleum ether/ethyl acetate : 30/1 in volume) as eluent. Presence of the product was checked by chromatography by TLC (thin layer chromatography, petroleum ether/ethyl acetate : 30/1 in volume). All the fractions containing the pure product were combined. After evaporation of the solvent, a solid orange residue is obtained which was recrystallized in isopropanol and washed by cold pentane (−4 °C) to afford 2,9-di-tertbutyl-1,10-phenanthroline as a pale yellow fluffy powder (2.7 g , 38 %). Colorless parallelepiped crystals suitable for an X-ray diffraction study were grown by slow evaporation of a dichloromethane solution of phen*.

¹H NMR (400 MHz, THF-*d*₈, δ/ppm) 8.23 (d, *J* = 8.4 Hz, 2H), 7.82 – 7.72 (m, 4H), 1.60 (s, ^tBu, 18H).

¹³C{¹H} NMR (101 MHz, THF-*d*₈, δ/ppm) 168.18, 145.31, 135.51, 126.57, 125.09, 118.51, 62.62, 38.29, 29.76.



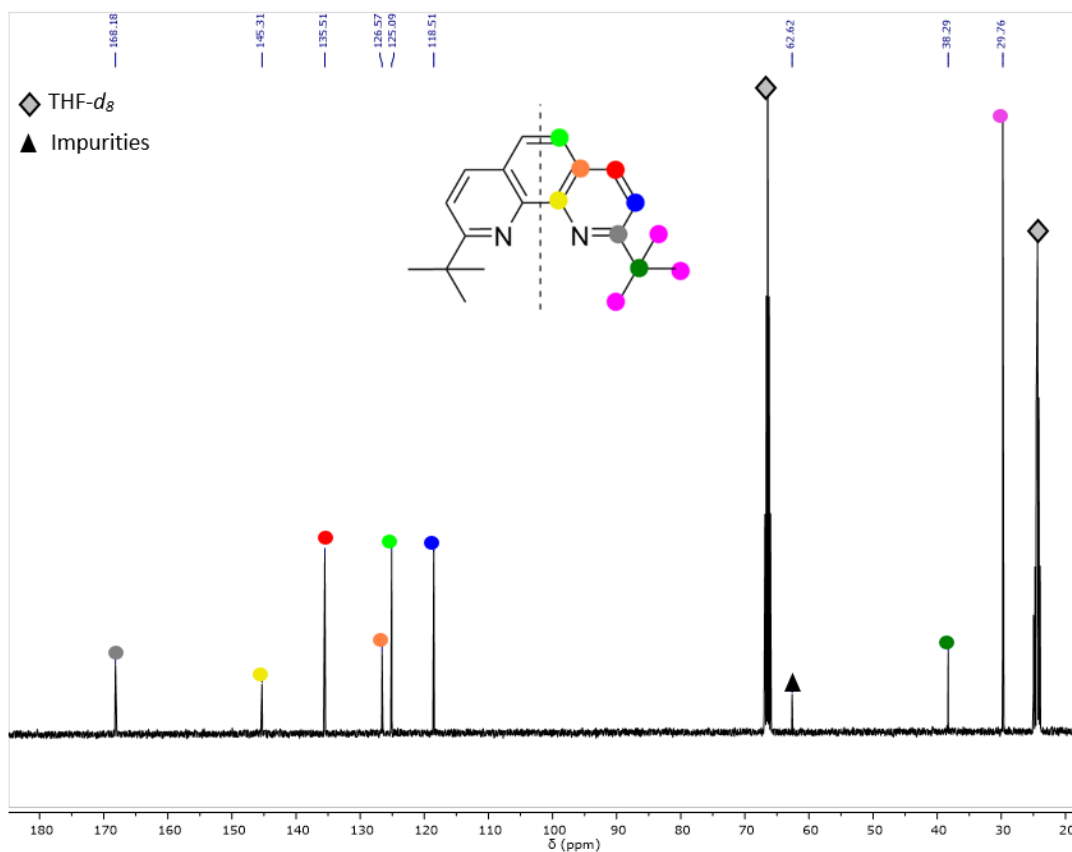


Figure S2. $^{13}\text{C}\{^1\text{H}\}$ NMR spectra of 2,9-di-tert-butyl-1,10-phenanthroline (**1**) in $\text{THF-}d_8$.

II. 1. 2. Synthesis of $[\text{Cu}(\text{O}^t\text{Bu})]_4$

The following synthesis was inspired by literature.⁸

To a suspension of CuI (1.0 g, 5.2 mmol) in THF (around 30 mL) was added $^t\text{BuOK}$ (0.6 g, 5.2 mmol) to obtain a pale brown solution. The mixture was then kept stirring at room temperature overnight. The resulting brown suspension was evaporated to remove all the solvent and obtain a mixture of solid CuO^tBu and KI . The desired product was purified by sublimation under static vacuum at 170 °C for 8 hours to yield the product as a pale white powder (0.56 g, 78 %).

^1H NMR (400 MHz, $\text{THF-}d_8$, δ /ppm): δ 1.31 (s, 9H).

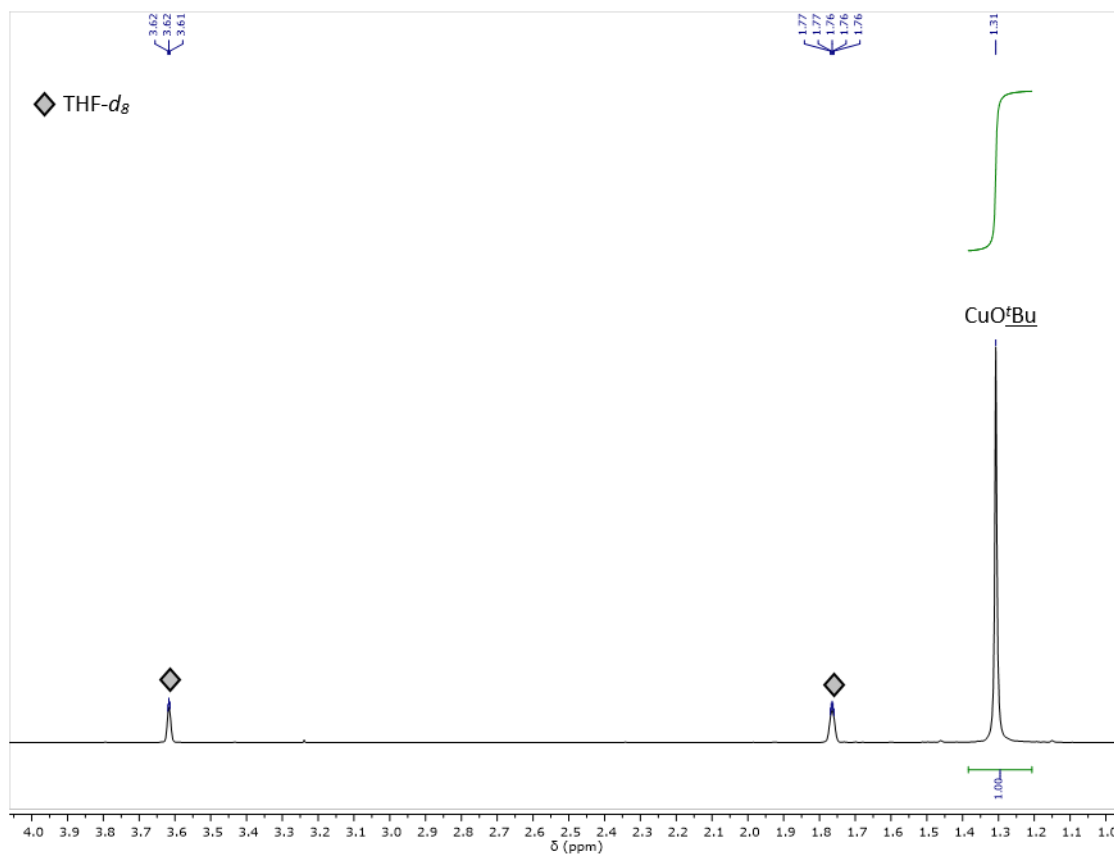


Figure S3. ^1H NMR spectra of $[\text{Cu}(\text{O}^t\text{Bu})_4]$ in $\text{THF-}d_8$.

II. 1. 3. Data of complex $[(\text{phen}^*)\text{Cu-O}^t\text{Bu}]$:

The addition of phen^* (10.7 mg, 1 equiv.) to $\text{Cu}(\text{O}^t\text{Bu})$ (5 mg, 1 equiv.) resulted a light brown solution which showed a weakly coordinated phen^* ligand to $\text{Cu}(\text{O}^t\text{Bu})$ by ^1H NMR.

^1H NMR (400 MHz, $\text{THF-}d_8$, δ/ppm) 8.23 (d, $J = 8.4$ Hz, 2H), 7.81 – 7.73 (m, 4H), 1.61 (s, 18H), 1.32 (s, 9H).

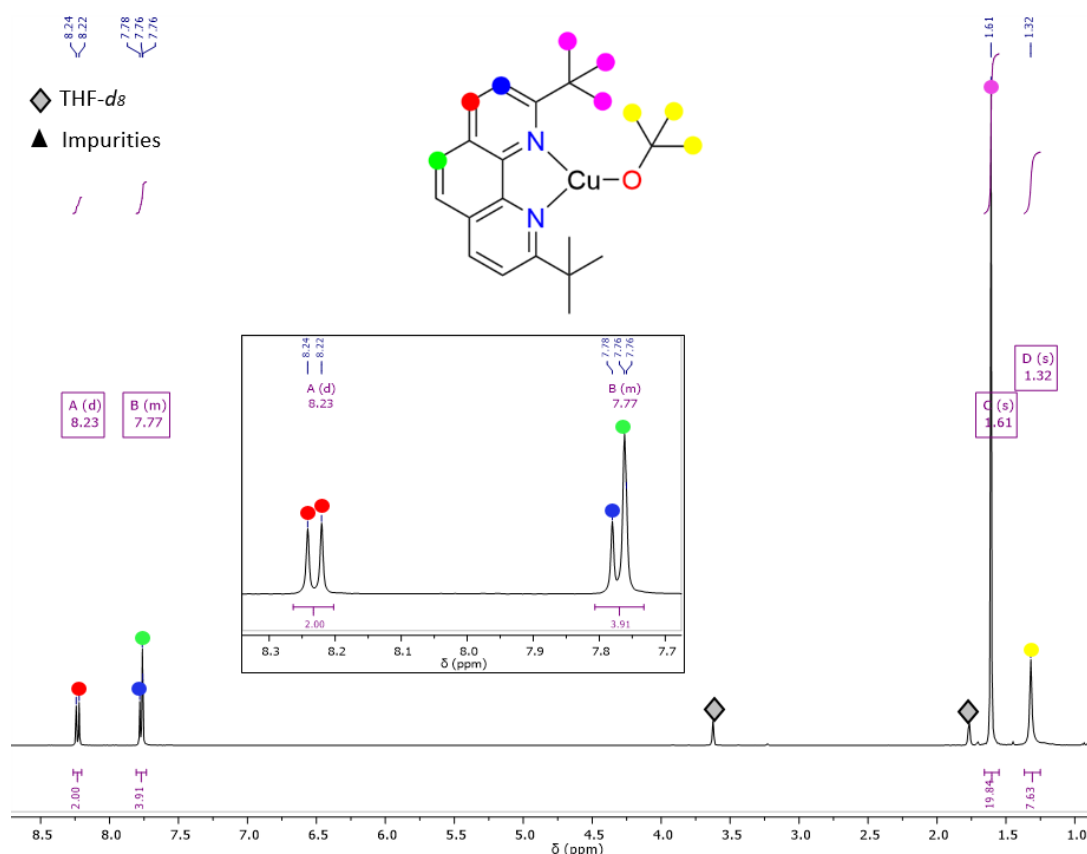


Figure S4. ^1H NMR spectra of $[(\text{phen}^*)\text{Cu}-\text{O}^t\text{Bu}]$ in $\text{THF}-d_8$.

II. 2. General synthesis procedure for the formation of carboxylate complexes $(\text{phen}^*)\text{Cu}^{\text{I}}(\text{O}_2\text{CR})$ ($\text{R} = \text{C}_6\text{H}_4\text{-}o\text{-F}$ (**2**), $\text{C}_6\text{H}_4\text{-}p\text{-F}$ (**3**), C_6F_5 (**4**), $\text{C}_6\text{H}_4\text{-}o\text{-NO}_2$ (**5**), $\text{C}_6\text{H}_4\text{-}p\text{-NO}_2$ (**6**), CF_3 (**7**)).

To a light yellow solution of **1** (106.9 mg, 0.36 mmol) in THF (10 mL), 1 equiv. $\text{Cu}(\text{O}^t\text{Bu})$ (50 mg, 0.36 mmol) was added. The resulted light brown solution was stirred at room temperature for 2 h. Addition of the substituted benzoic acid (0.36 mmol, 1 equiv.) resulted in an immediately change of color (color change from orange to red depending on the substituted benzoic acid) and the mixture was stirred at room temperature for another hour. The solvent was evaporated off under vacuum to give an orange-red solid which was washed with pentane (10 mL x 2) and dried under vacuum overnight (*ca.* 15 h) to afford the desired pure product as an orange-red solid.

II. 2. 1. Data for complex $[(\text{phen}^*)\text{Cu}(\text{O}_2\text{CC}_6\text{H}_4\text{-}o\text{-F})]$ (**2**):

Quantity of $(o\text{-F-Ph})\text{CO}_2\text{H}$ added for the reaction (0.30 mmol, 42.5 mg, 1 equiv.) Complex **2** isolated as an orange solid (115 mg, 76 %). Orange crystals of $\mathbf{2}\cdot\mathbf{0.5}(\text{toluene})$ were obtained by slowly cooling down a hot THF solution of the complex.

^1H NMR (400 MHz, $\text{THF}-d_8$, rt, δ/ppm) 8.39 (d, $J = 8.5$ Hz, 2H), 7.96 (d, $J = 8.5$ Hz, 2H), 7.89 (t, $J = 7.5$ Hz, 1H), 7.68 (s, 2H), 7.35 (ddd, $J = 8.1, 4.6, 2.2$ Hz, 1H), 7.17 – 6.98 (m, 2H), 1.81 (s, 18H).

$^{13}\text{C}\{^1\text{H}\}$ NMR (101 MHz, THF- d_8 , rt, δ /ppm): 168.79, 162.89, 160.36, 144.01, 134.72, 132.36, 130.42, 130.34, 126.99, 125.35, 122.65, 115.82, 115.60, 38.30, 30.04.

$^{19}\text{F}\{^1\text{H}\}$ NMR (377 MHz, THF- d_8 , rt, δ /ppm): -111.80

IR data (ν cm^{-1}): 2945 (vs), 1604 (s, CO_2), 1463 (vs, C-F), 1367 (s), 1136 (w), 858 (w), 771 (w), 615 (w).

Elemental analysis for $\text{C}_{27}\text{H}_{28}\text{CuFN}_2\text{O}_2$, (M= 495.08 g/mol), found (theoretical) %: C, 61.72 (65.50); H, 5.49 (5.70); N, 5.43 (5.66).

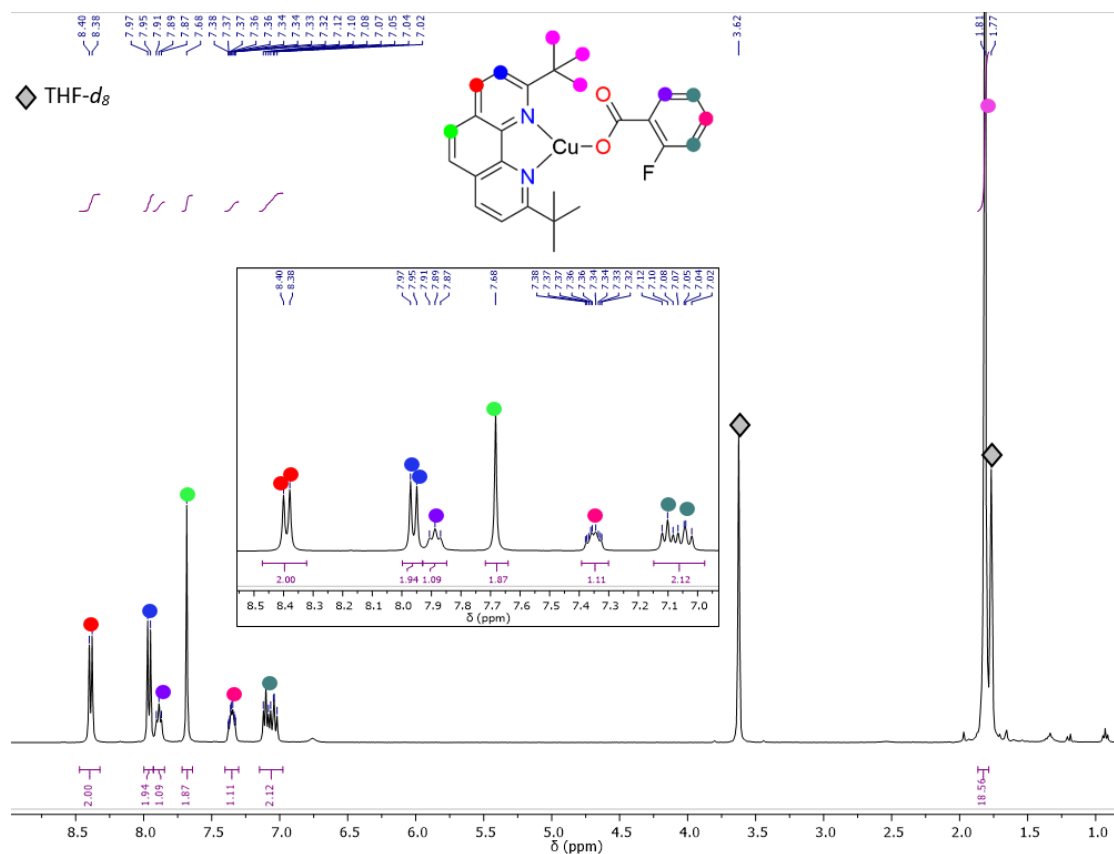


Figure S5. ^1H NMR spectra of $[(\text{phen}^*)\text{Cu}-(\text{O}_2\text{C}_6\text{H}_4\text{-O-F})]$ (2) in THF- d_8 .

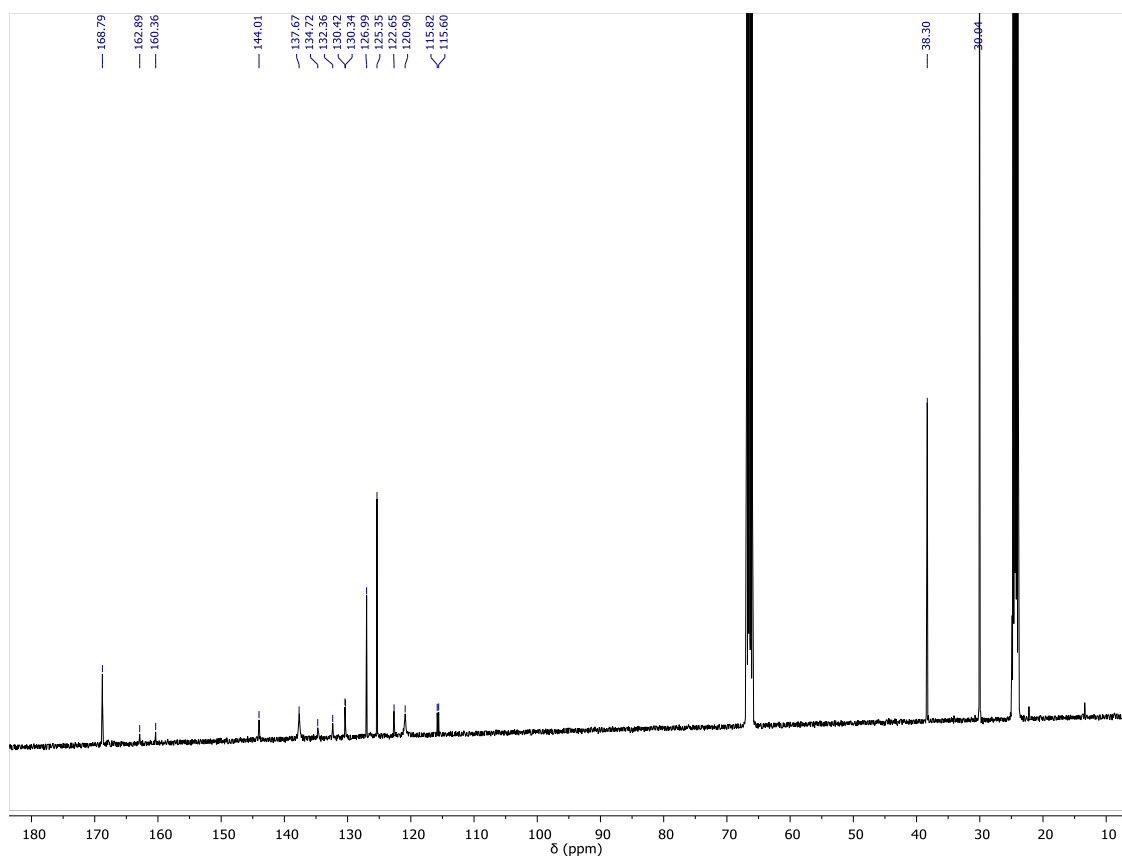


Figure S6. $^{13}\text{C}\{^1\text{H}\}$ NMR spectra of $[(\text{phen}^*)\text{Cu}-(\text{O}_2\text{C}\text{C}_6\text{H}_4\text{-o-F})]$ (**2**) in THF-d_8 .

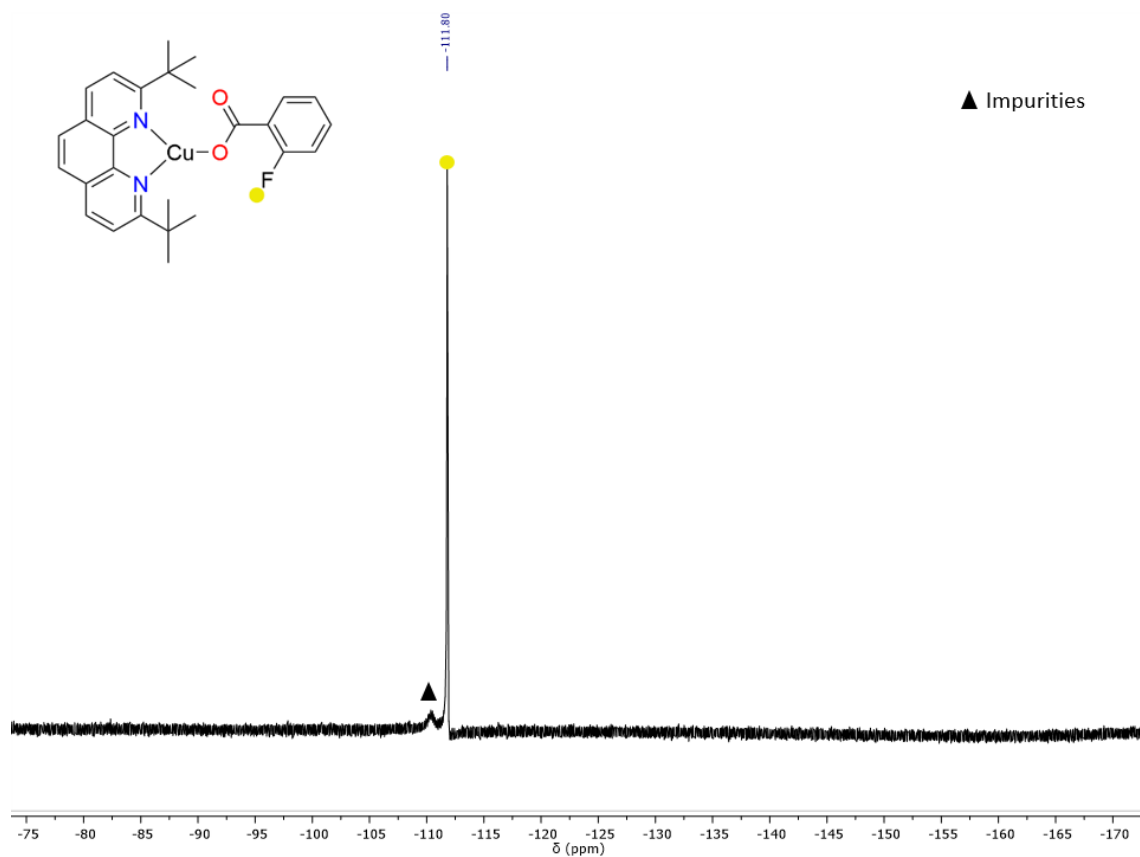


Figure S7. $^{19}\text{F}\{^1\text{H}\}$ NMR spectra of $[(\text{phen}^*)\text{Cu}-(\text{O}_2\text{C}\text{C}_6\text{H}_4\text{-o-F})]$ (**2**) in THF-d_8 .

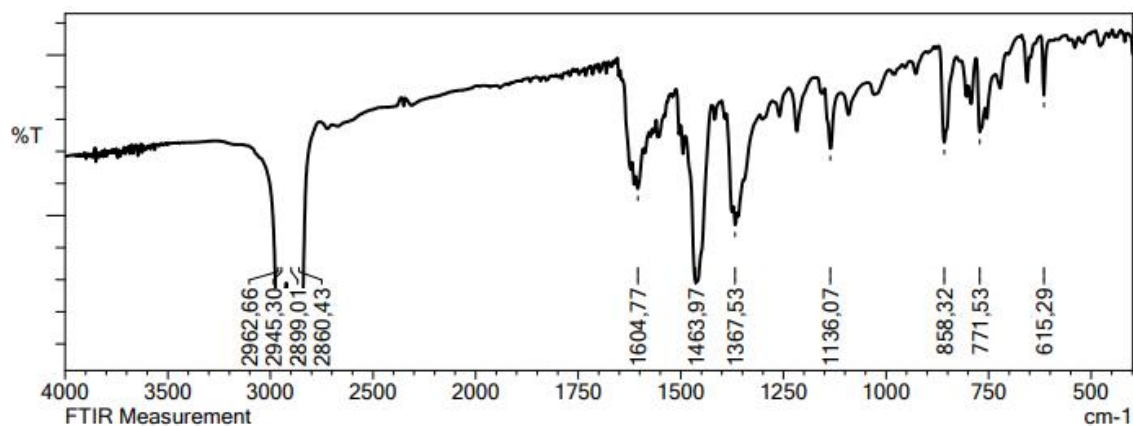


Figure S8. IR data of $[(\text{phen}^*)\text{Cu}-(\text{O}_2\text{CC}_6\text{H}_4\text{-o-F})]$ (**2**) in heavy paraffin oil (nujol).

II. 2. 2. Data for complex $[(\text{phen}^*)\text{Cu}-(\text{O}_2\text{CC}_6\text{H}_4\text{-p-F})]$ (**3**):

Quantity of the acid (*p*-F-Ph) CO_2H added for the reaction (0.36 mmol, 48.8 mg, 1 equiv.) Complex **3** isolated as an orange solid (122 mg, 69 %). Orange parallelepiped crystals of **3** were obtained by slowly cooling down a hot THF solution of the complex.

^1H NMR (400 MHz, THF- d_8 , rt, δ /ppm): 8.39 (d, $J = 8.5$ Hz, 2H), 8.03 (t, $J = 7.1$ Hz, 2H), 7.96 (d, $J = 8.5$ Hz, 2H), 7.76 (s, 2H), 7.03 (t, $J = 8.5$ Hz, 2H), 1.77 (s, ^tBu , 18H).

$^{13}\text{C}\{^1\text{H}\}$ NMR (101 MHz, THF- d_8 , rt, δ /ppm): 168.95, 165.37, 162.92, 144.30, 137.42, 132.01, 127.04, 125.41, 120.69, 113.72, 113.51, 38.29, 29.97.

$^{19}\text{F}\{^1\text{H}\}$ NMR (377 MHz, THF- d_8 , rt, δ /ppm): -113.7

IR data (ν cm^{-1}): 2970 (w), 1614 (s, CO_2), 1583 (m), 1558 (w), 1496 (m), 1365 (s), 1217 (m), 1151 (w), 1138 (m), 1083 (w), 858 (s), 840 (m), 777 (s), 623 (m).

Elemental analysis for $\text{C}_{27}\text{H}_{28}\text{CuFN}_2\text{O}_2$, ($M = 495.08$ g/mol) found (theoretical) %: C, 62.70 (65.50); H, 5.87 (5.70); N, 5.54 (5.66).

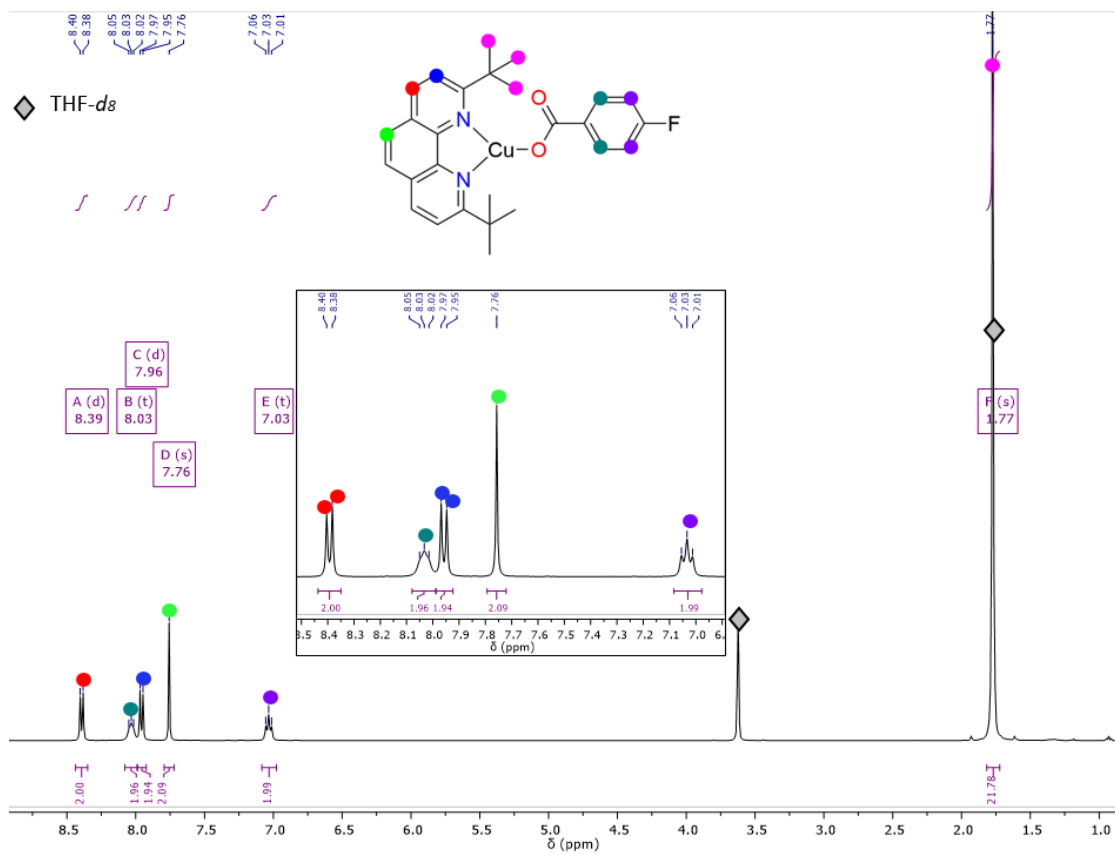


Figure S9. 1H NMR spectra of $[(phen^*)Cu-(O_2CC_6H_4-p-F)]$ (3) in $THF-d_8$.

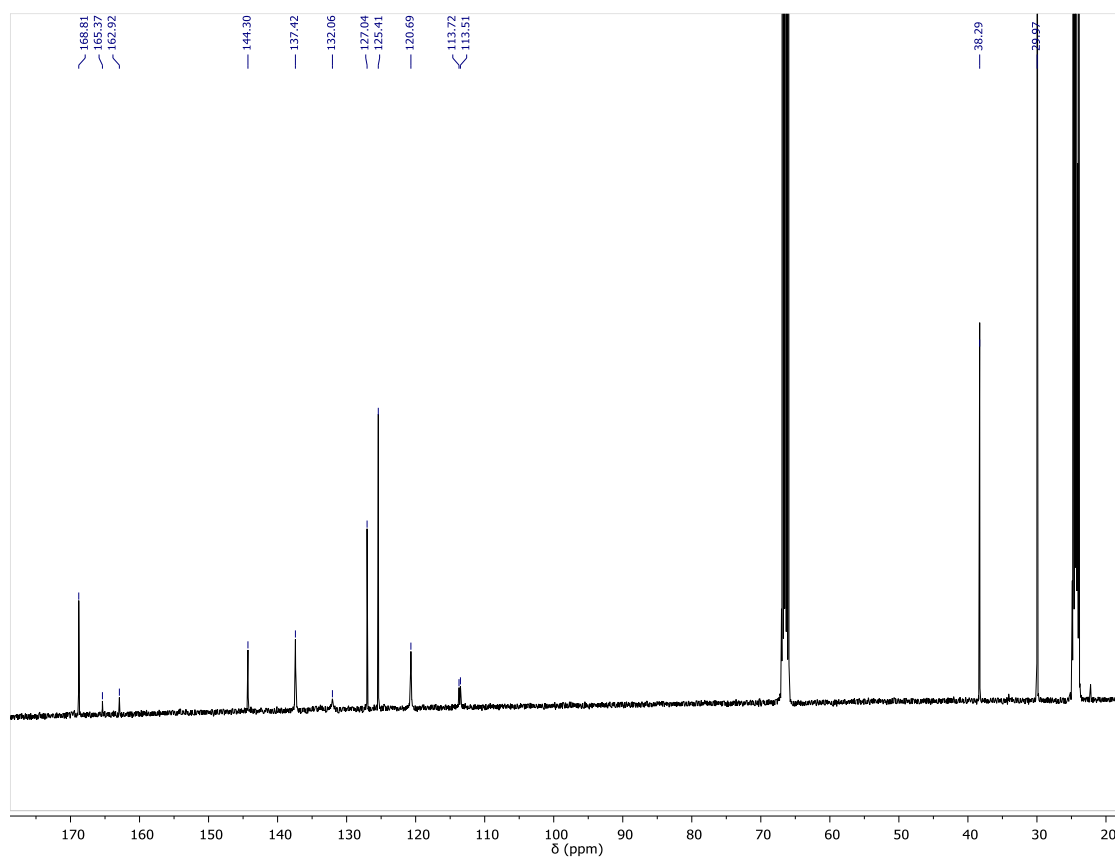


Figure S10. ^{13}C NMR spectra of $[(phen^*)Cu-(O_2CC_6H_4-p-F)]$ (3) in $THF-d_8$.

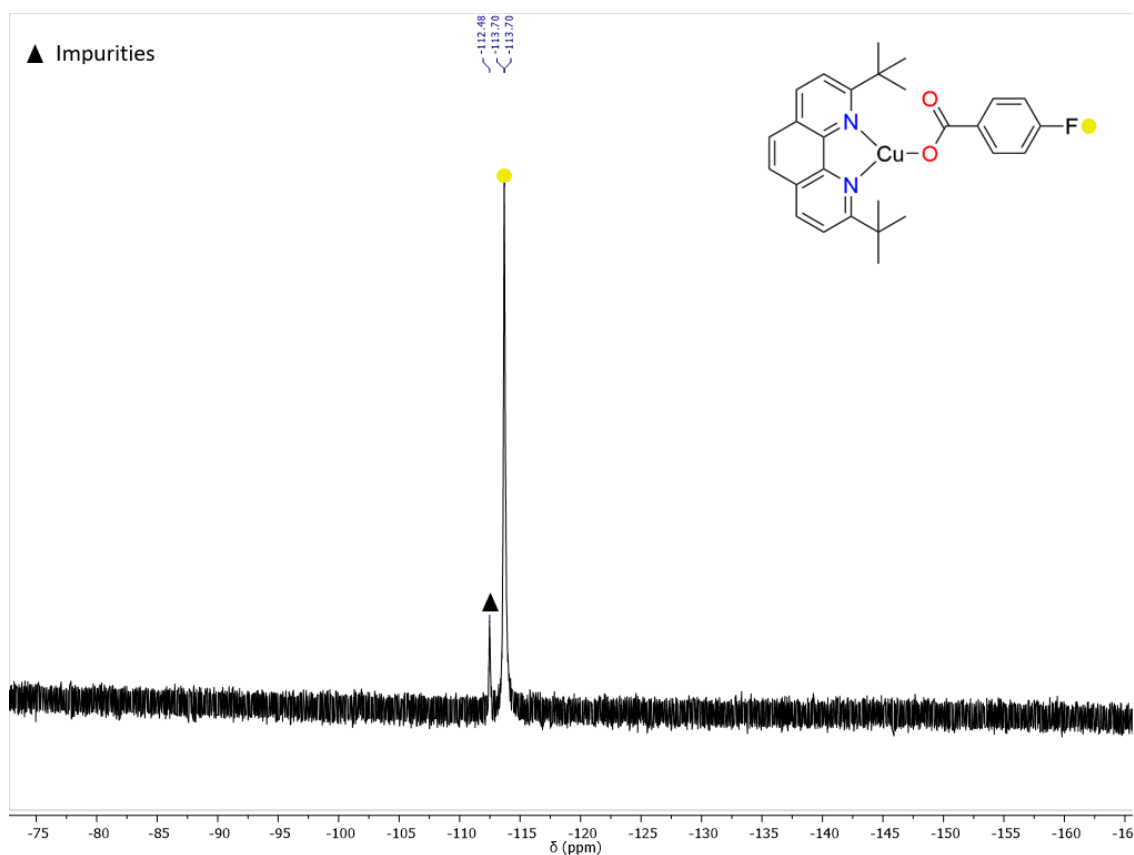


Figure S11. $^{19}\text{F}\{^1\text{H}\}$ NMR spectra of $[(\text{phen}^*)\text{Cu}(\text{O}_2\text{CC}_6\text{H}_4\text{-p-F})]$ (**3**) in THF-d_8 .

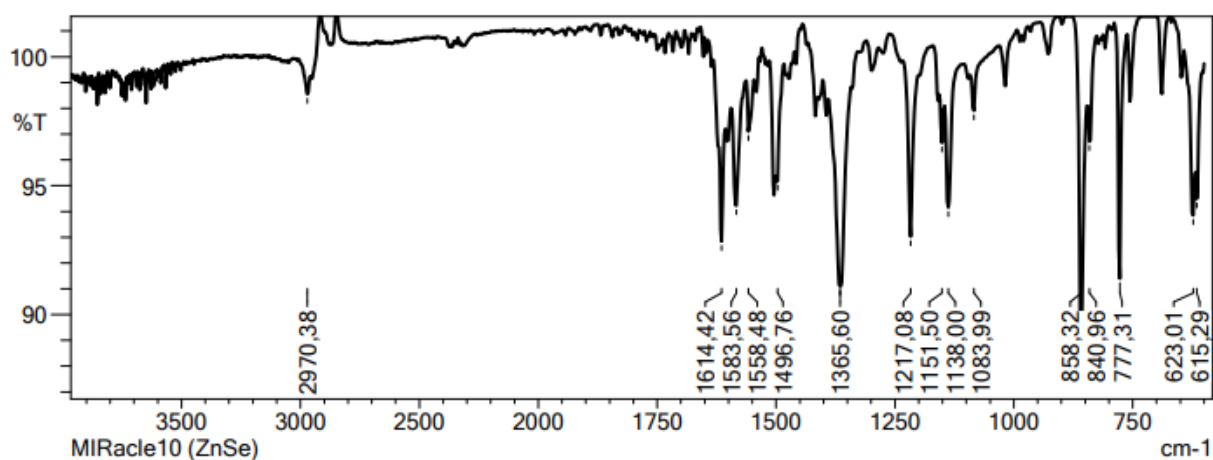


Figure S12. IR spectra of $[(\text{phen}^*)\text{Cu}(\text{O}_2\text{CC}_6\text{H}_4\text{-p-F})]$ (**3**).

II. 2. 3. Data for complex $[(\text{phen}^*)\text{Cu}(\text{O}_2\text{CC}_6\text{F}_5)]$ (**4**):

Quantity of the acid $(\text{C}_6\text{F}_5)\text{CO}_2\text{H}$ added for the reaction (0.36 mmol, 76.3 mg, 1 equiv.) Complex **4** isolated as a light orange powder (150 mg, 72 %). Orange crystalline platelets of **4** were obtained by heating at $100\text{ }^\circ\text{C}$ (*ca* 5 min) a THF solution of **4** and slowly cooling down in a hot water bath overnight.

^1H NMR (400 MHz, THF-d_8 , rt, δ/ppm): 8.56 (d, $J = 8.6$ Hz, 2H), 8.15 (d, $J = 8.6$ Hz, 2H), 7.96 (s, 2H), 1.85 (s, ^tBu , 18H).

$^{13}\text{C}\{^1\text{H}\}$ NMR (101 MHz, THF- d_8 , rt, δ /ppm): 169.57, 143.98, 138.46, 127.45, 125.78, 121.87, 38.36, 30.20. (only see signal of phen* ligand)

$^{19}\text{F}\{^1\text{H}\}$ NMR (377 MHz, THF- d_8 , rt, δ /ppm): -143.79, -161.84, -165.54.

IR data (ν cm^{-1}): 2956 (m), 2927 (m), 1631 (s, CO_2), 1490 (s, CF), 1361 (s), 1141 (w), 1099 (w), 985 (s), 921 (w), 860 (s), 748 (s), 613 (s).

Elemental analysis for $\text{C}_{27}\text{H}_{24}\text{CuF}_5\text{N}_2\text{O}_2$, M= 567.04 g/mol, found (theoretical) %: C, 57.65 (57.19); H, 4.33 (4.27); N, 4.97 (4.94).

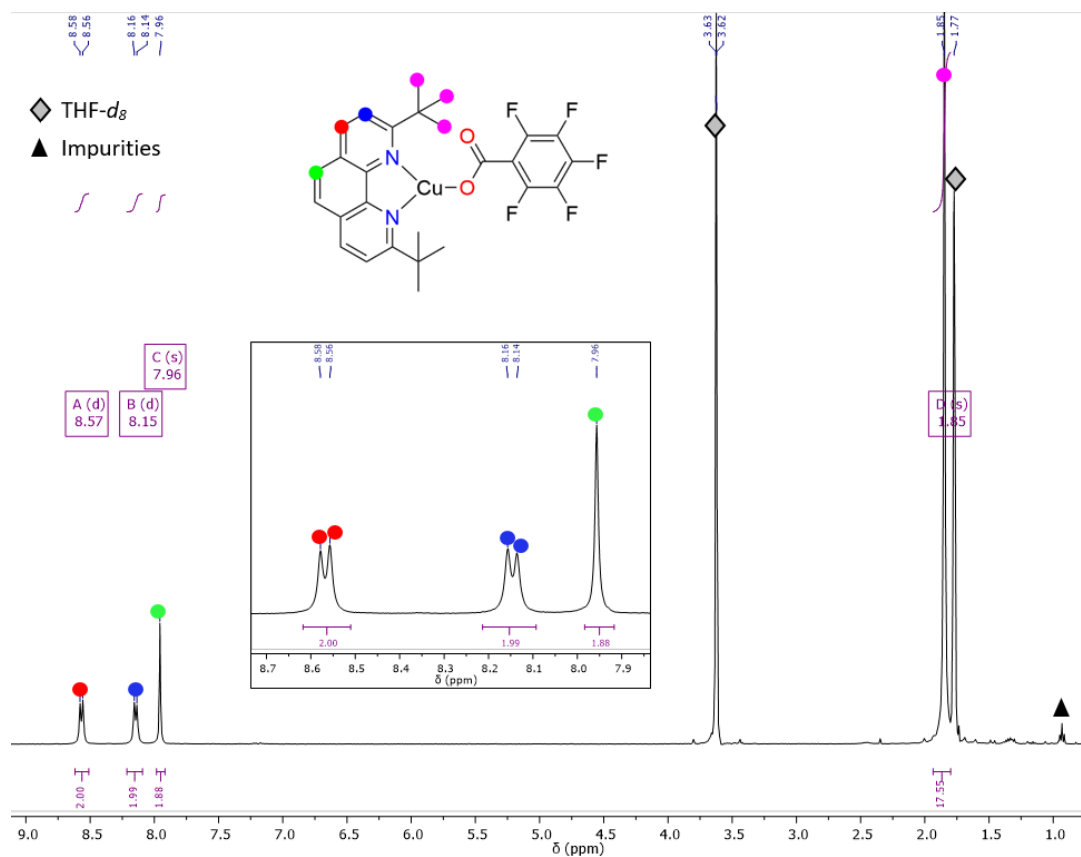


Figure S13. ^1H NMR spectra of $[(\text{phen}^*)\text{Cu}-\text{O}_2\text{C}-\text{C}_6\text{F}_5]$ (**4**) in THF- d_8 .

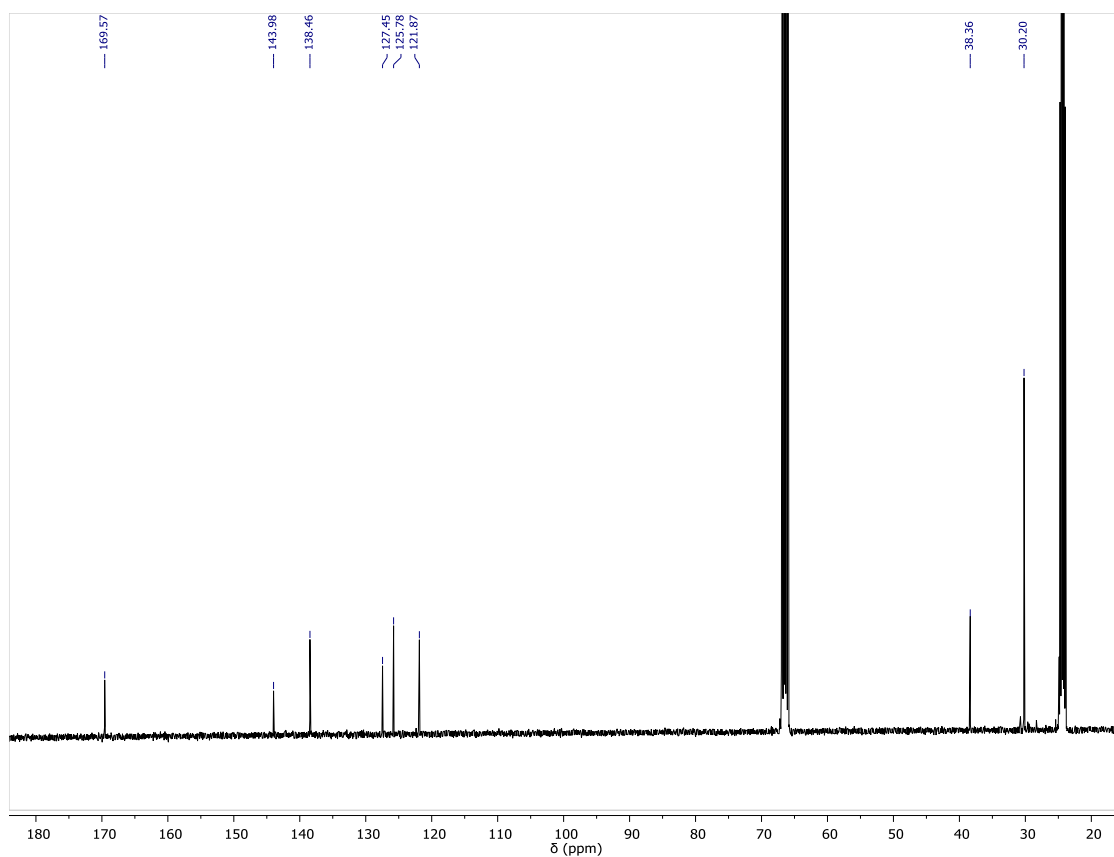


Figure S14. $^{13}\text{C}\{^1\text{H}\}$ NMR spectra of $[(\text{phen}^*)\text{Cu}-\text{O}_2\text{C}-\text{C}_6\text{F}_5]$ (**4**) in $\text{THF}-d_8$.

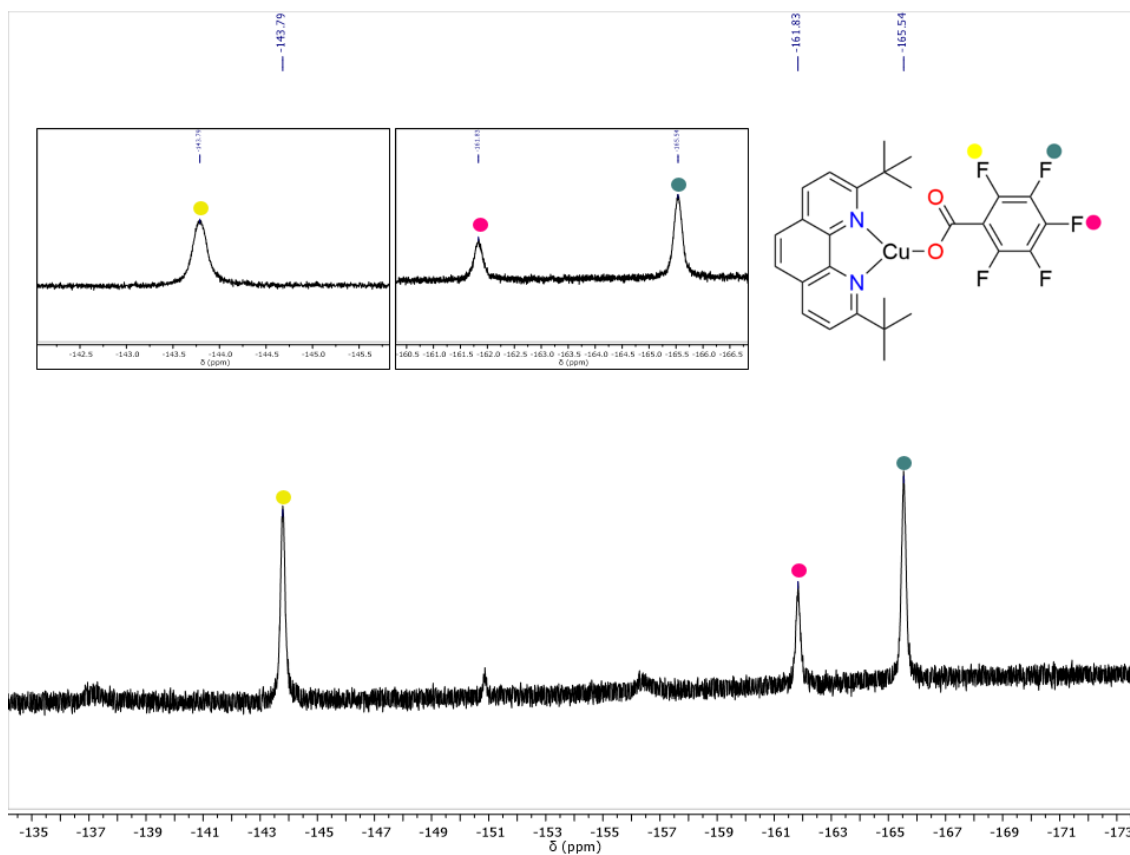


Figure S15. $^{19}\text{F}\{^1\text{H}\}$ NMR spectra of $[(\text{phen}^*)\text{Cu}-\text{O}_2\text{C}-\text{C}_6\text{F}_5]$ (**4**) in $\text{THF}-d_8$.

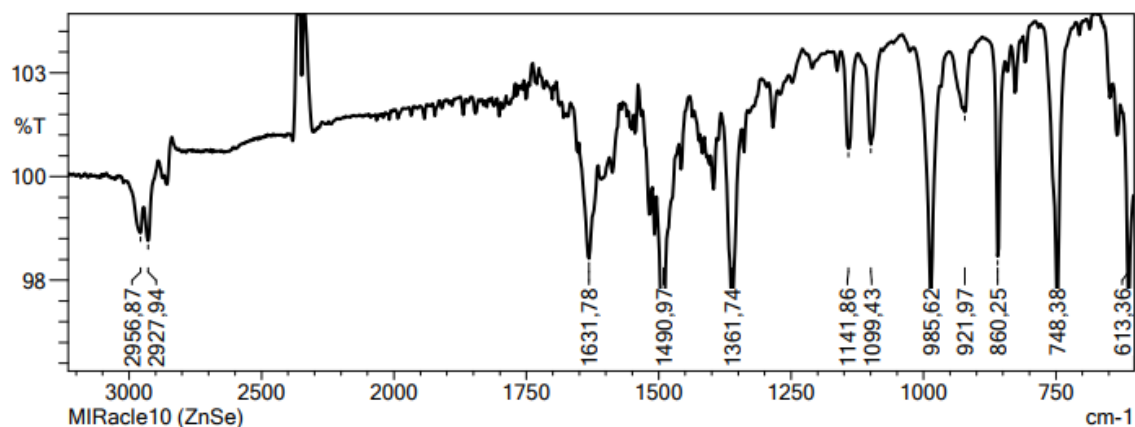


Figure S16. IR spectra of [(phen*)Cu-O₂C-C₆F₅] (4) in THF-*d*₈.

II. 2. 4. Data for complex [(phen*)Cu(O₂CC₆H₄-*o*-NO₂)] (5):

¹H NMR (400 MHz, THF-*d*₈, rt, δ/ppm): 8.47 (d, *J* = 8.5 Hz, 2H), 8.06 (d, *J* = 8.5 Hz, 2H), 7.91 (s, 1H), 7.82 (s, 2H), 7.74 – 7.37 (m, 3H), 1.83 (s, 18H).

¹³C{¹H} NMR (101 MHz, THF-*d*₈, rt, δ/ppm): 169.25, 128.44, 127.15, 125.52, 122.23, 38.32, 34.08, 30.02, 22.22, 13.38. (some carbon signals of phen* ligand and the aromatic of benzoic acid cannot be observed)

IR data (ν cm⁻¹): 2927 (m), 1627 (s, CO₂), 1521 (s, NO₂), 1361 (s, NO₂), 1143 (m), 862 (s), 827 (m), 786 (m), 744 (m), 698 (m), 615 (s).

Elemental analysis for C₂₇H₂₈CuN₃O₂, (M= 522.08 g/mol) found (theoretical) %: C, 61.57 (62.12); H, 5.42 (5.41); N, 8.05 (8.05).

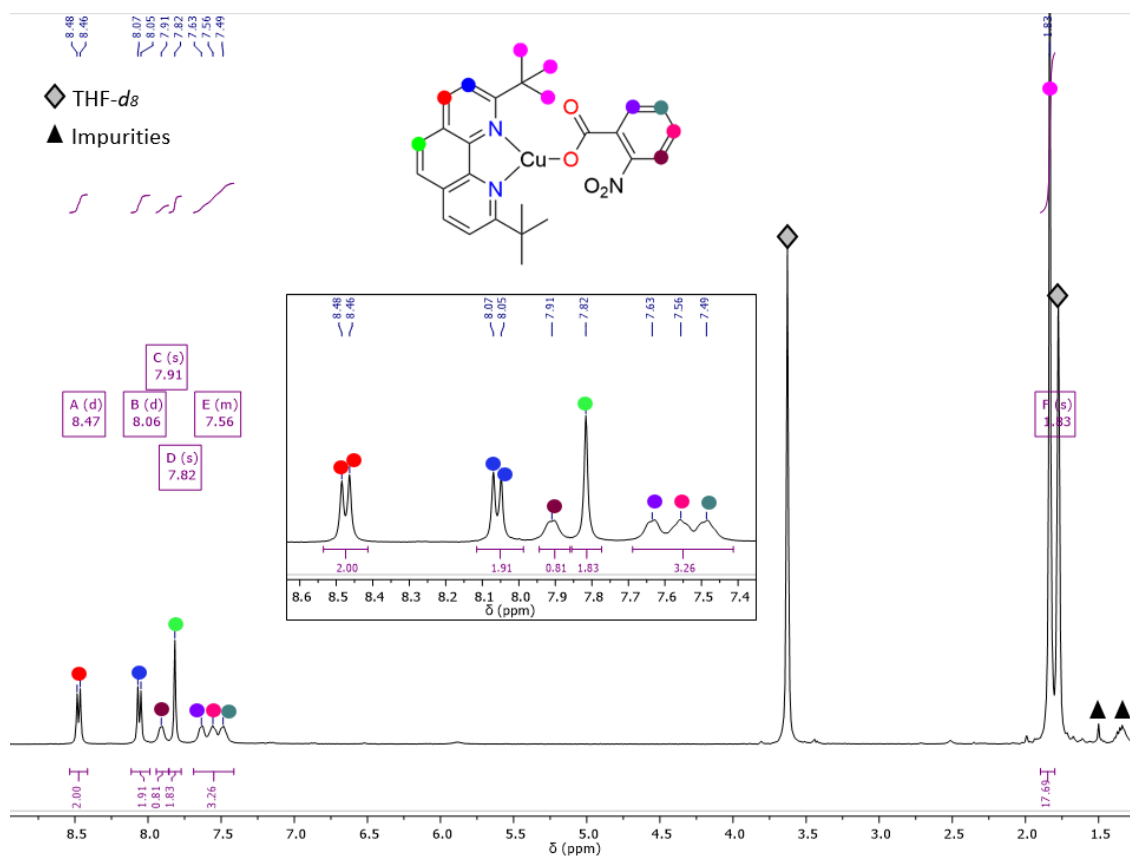


Figure S17. ^1H NMR spectra of $[(\text{phen}^*)\text{Cu}-(\text{O}_2\text{CC}_6\text{H}_4\text{-o-NO}_2\text{-Ph})]$ (**5**) in THF- d_8 .

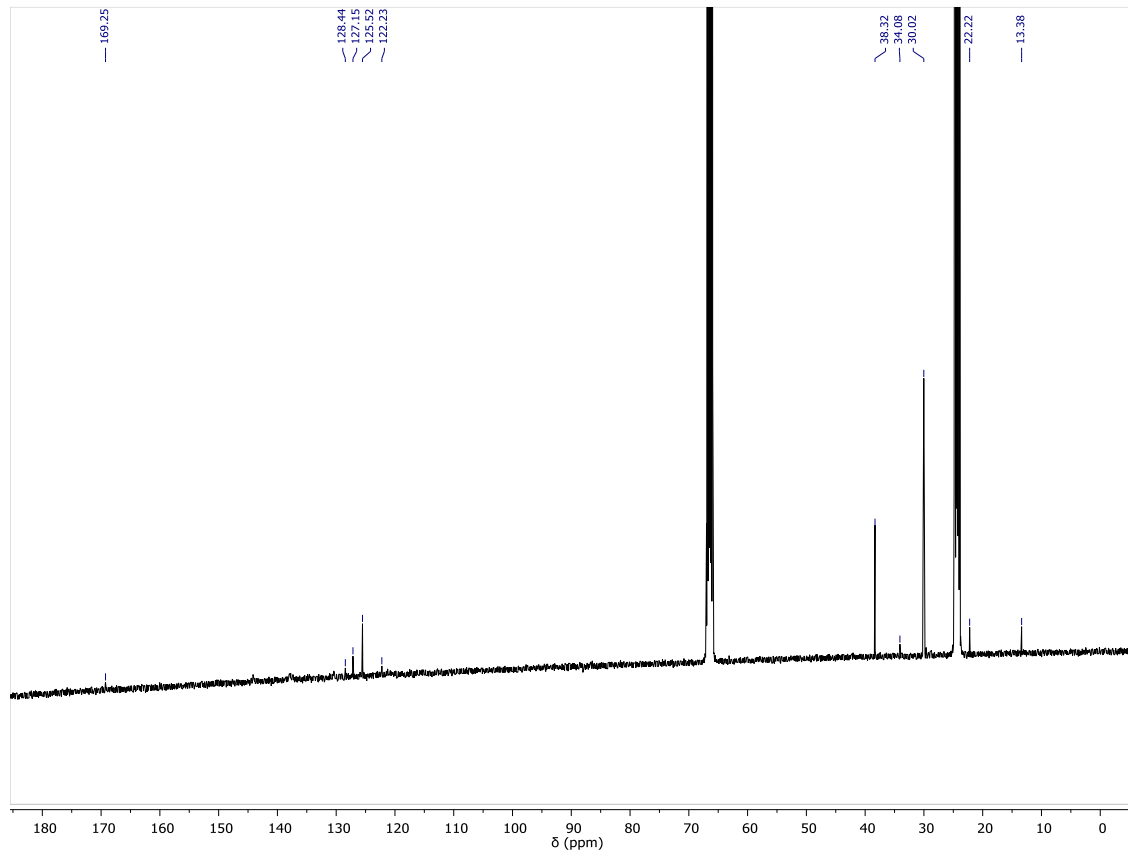


Figure S18. $^{13}\text{C}\{^1\text{H}\}$ NMR spectra of $[(\text{phen}^*)\text{Cu}-(\text{O}_2\text{CC}_6\text{H}_4\text{-o-NO}_2\text{-Ph})]$ (**5**) in THF- d_8 .

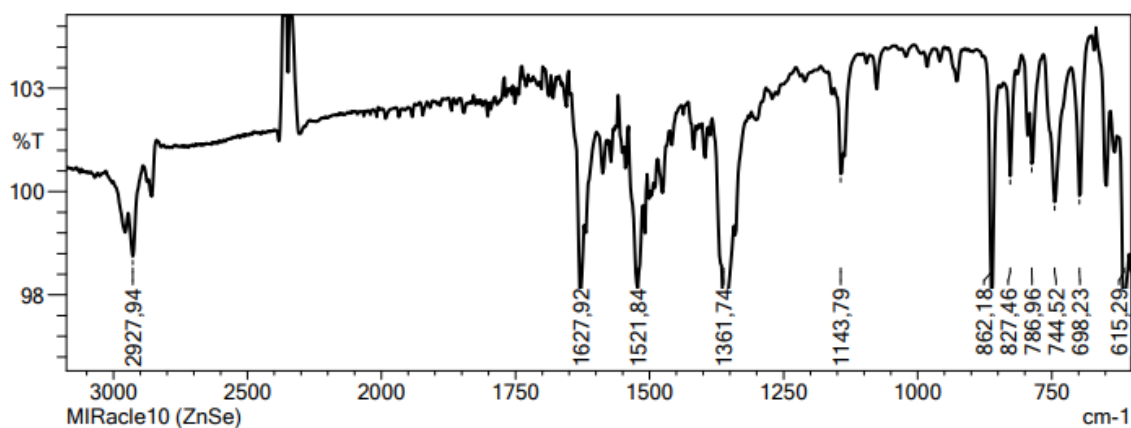


Figure S19. IR spectra of $[(phen^*)Cu-(O_2CC_6H_4-o-NO_2-Ph)]$ (**5**) in $THF-d_8$.

II. 2. 5 Data for complex $[(phen^*)Cu(O_2CC_6H_4-p-NO_2)]$ (**6**):

Quantity of the acid $(Ph-p-NO_2)CO_2H$ added for the reaction (0.39 mmol, 59.7 mg, 1 equiv.) Complex **6** isolated as a light orange powder (160 mg, 78 %). Orange parallelepiped crystals of **6**•THF were obtained by slowly cooling down a hot THF solution (60 °C) of the complex.

1H NMR (400 MHz, $THF-d_8$, rt, δ/ppm): 8.49 (d, $J = 8.5$ Hz, 2H), 8.24 (t, $J = 7.9$ Hz, 4H), 8.06 (d, $J = 8.5$ Hz, 2H), 7.87 (s, 2H), 1.80 (s, tBu , 18H).

$^{13}C\{^1H\}$ NMR (101 MHz, $THF-d_8$, rt, δ/ppm): 169.21, 149.00, 143.99, 138.23, 130.55, 127.32, 125.65, 122.34, 121.61, 38.29, 30.03.

IR data ($\nu\ cm^{-1}$): 2966 (m), 1627 (m, CO_2), 1591 (m), 1517 (s), 1498 (m), 1363 (m), 1340 (s), 1138 (s), 873 (m), 856 (s), 821 (m), 790 (m), 729 (s).

Elemental analysis for $C_{27}H_{28}CuN_3O_2$, (M= 522.08 g/mol), found (theoretical) %: C, 60.42 (62.12); H, 5.59 (5.41); N, 8.24 (8.05).

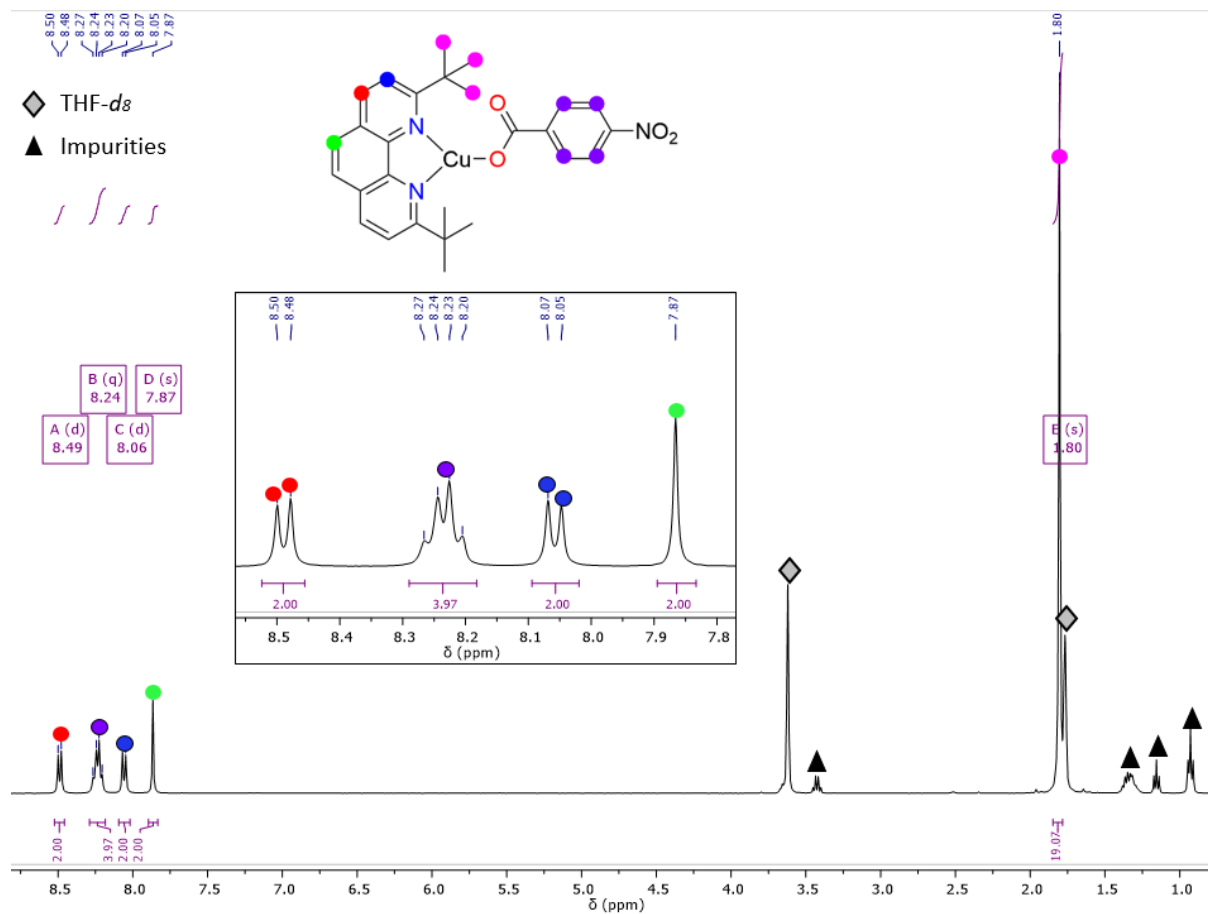


Figure S20. 1H NMR spectra of $[(phen^*)Cu-O_2C(p-NO_2-Ph)]$ (6) in THF-*d*₈.

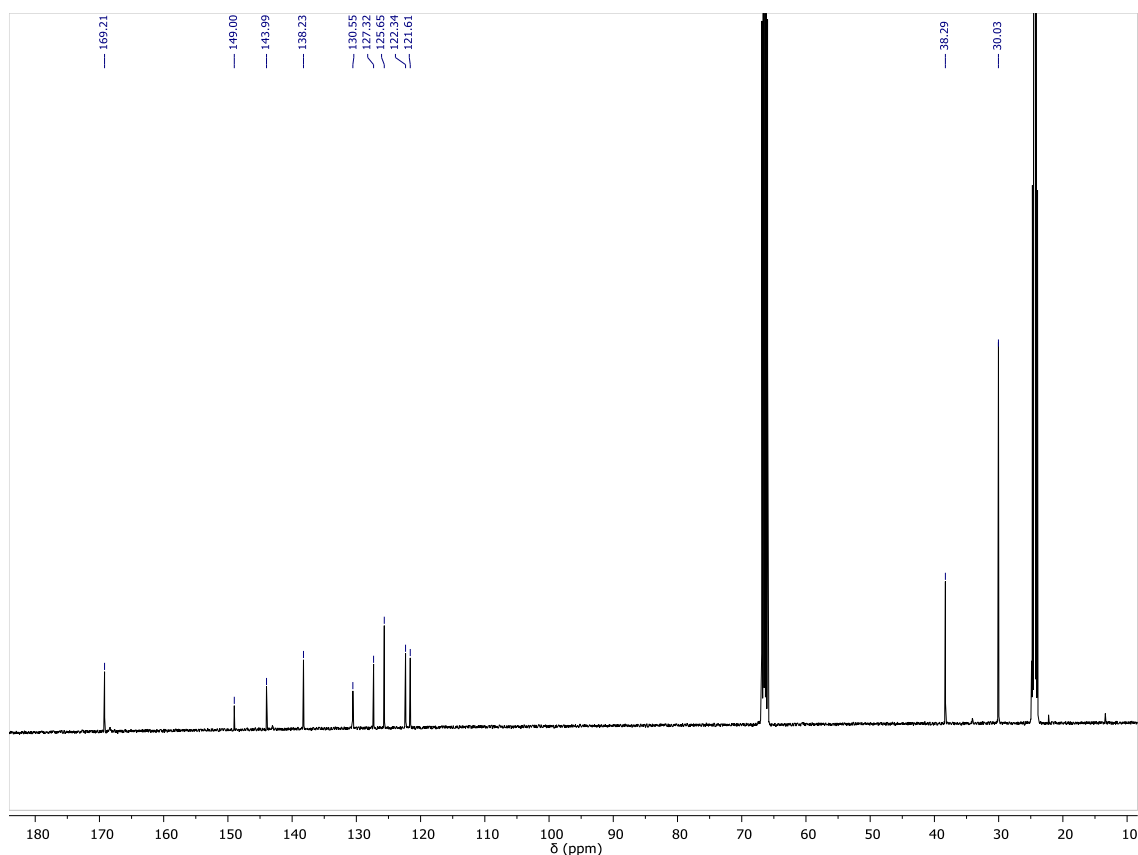


Figure S21. $^{13}\text{C}\{^1\text{H}\}$ NMR spectra of $[(\text{phen}^*)\text{Cu}-\text{O}_2\text{C}(p\text{-NO}_2\text{-Ph})]$ (**6**) in THF-d_8 .

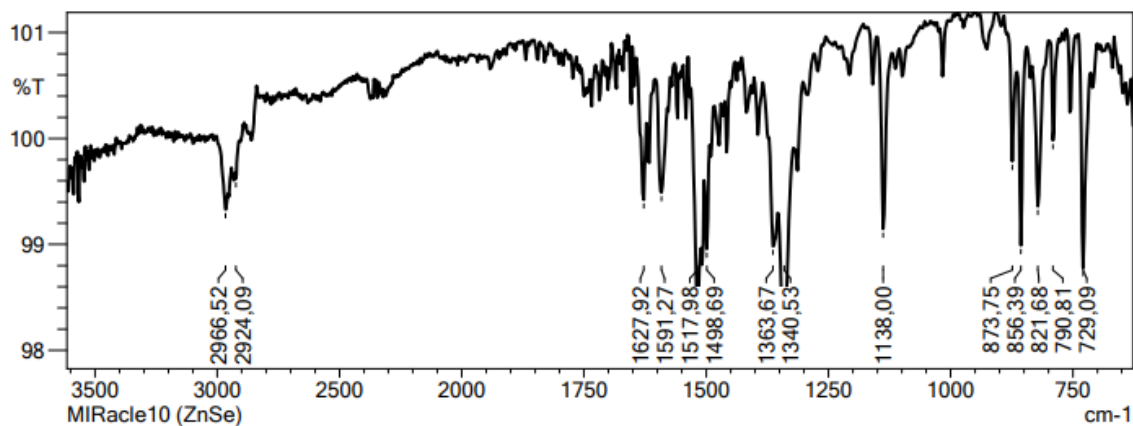


Figure S22. IR spectra of $[(\text{phen}^*)\text{Cu}-\text{O}_2\text{C}(p\text{-NO}_2\text{-Ph})]$ (**6**) in THF-d_8 .

II. 2. 6. Data for complex $[(\text{phen}^*)\text{Cu}(\text{O}_2\text{CCF}_3)]$ (**7**):

Complex **7** is prepared by following the general procedure, and trifluoroacetic acid (28.0 μL , 0.36 mmol, 1 equiv.) diluted in toluene (10 mL) was added to the THF solution of phen* and Cu(O^tBu). After evaporation of the solvent and washing of the residue with Et₂O (10 mL x 3) instead of pentane, pure **7** was isolated as an orange powder (100.2 mg, 60 %). Orange crystalline platelets were obtained after a few days by slow diffusion of pentane to a toluene solution of the complex.

^1H NMR (400 MHz, THF-d_8 , rt, δ /ppm): 8.52 (d, $J = 8.6$ Hz, 2H), 8.11 (d, $J = 8.5$ Hz, 2H), 7.88 (s, 2H), 1.79 (s, ^tBu, 18H).

$^{13}\text{C}\{^1\text{H}\}$ NMR (101 MHz, THF- d_8 , rt, δ /ppm): 169.64, 143.90, 138.55, 127.48, 125.83, 121.92, 38.27, 30.01. (carbon signals of CF_3 and CO_2 cannot be observed, only see the signals of phen* ligand).

$^{19}\text{F}\{^1\text{H}\}$ NMR (377 MHz, THF- d_8 , rt, δ /ppm): -75.33.

IR data ($\nu \text{ cm}^{-1}$): 2926 (m), 2856 (m), 1689 (s, CO_2), 1587 (w), 1508 (w), 1498 (w), 1417 (w), 1193 (s), 1138 (s), 860 (s), 721 (m), 613 (s).

Elemental analysis for $\text{C}_{22}\text{H}_{24}\text{CuF}_3\text{N}_2\text{O}_2$, (M= 468.99 g/mol), found (theoretical) %: C, 56.44 (56.34); H, 5.52 (5.70); N, 5.98 (5.97).

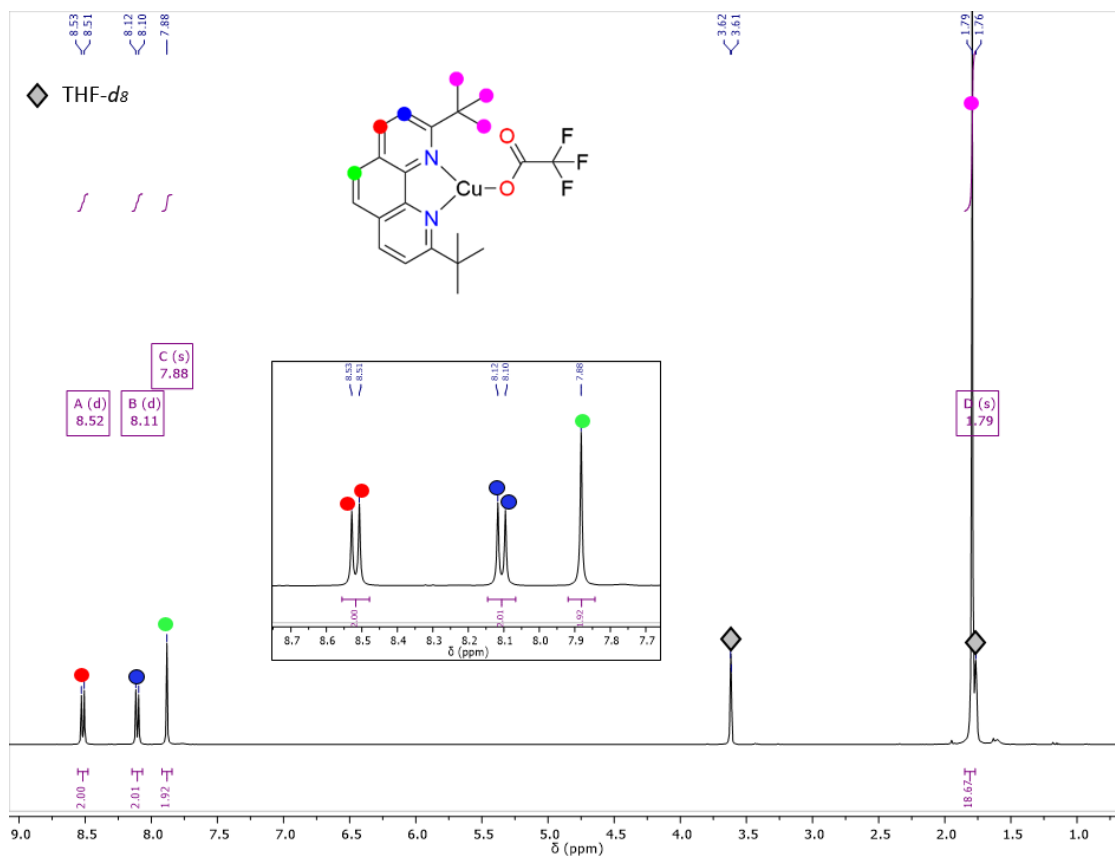


Figure S23. ^1H NMR spectra of $[(\text{phen}^*)\text{Cu}-\text{O}_2\text{CCF}_3]$ (7) in THF- d_8 .

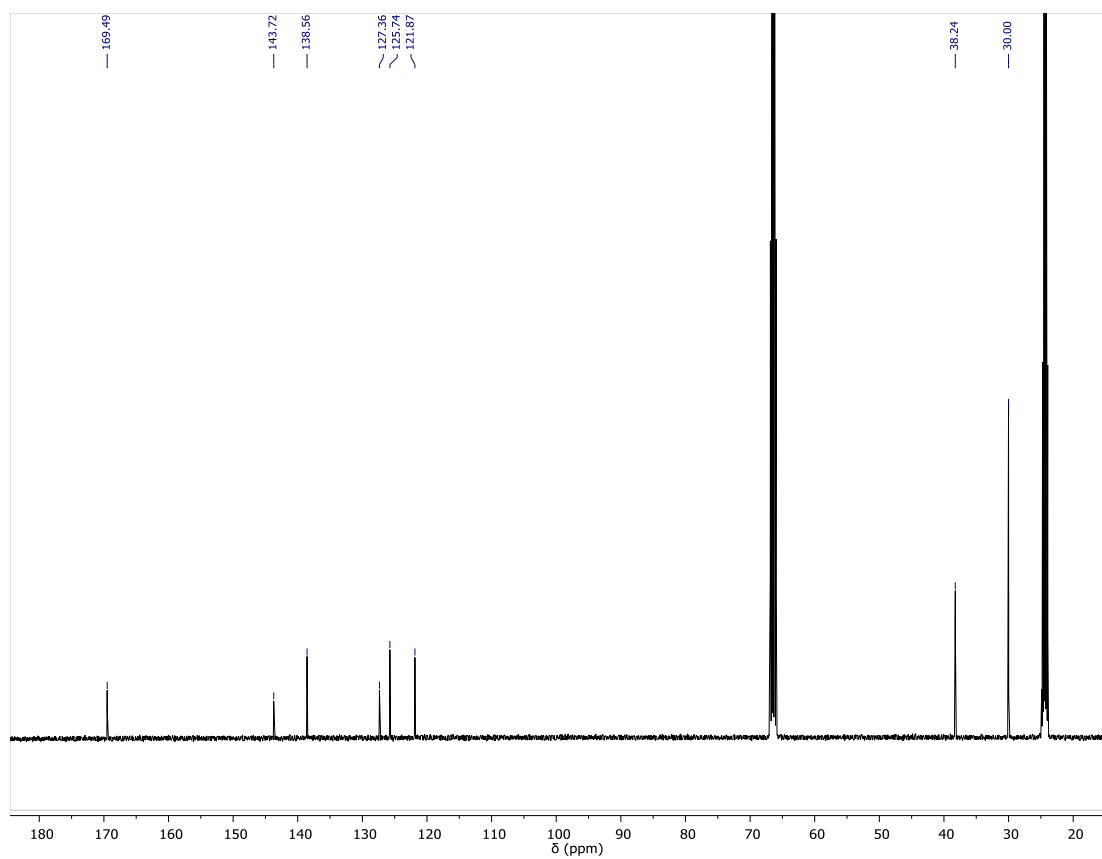


Figure S24. $^{13}\text{C}\{^1\text{H}\}$ NMR spectra of $[(\text{phen}^*)\text{Cu}-\text{O}_2\text{CCF}_3]$ (**7**) in $\text{THF}-d_8$.

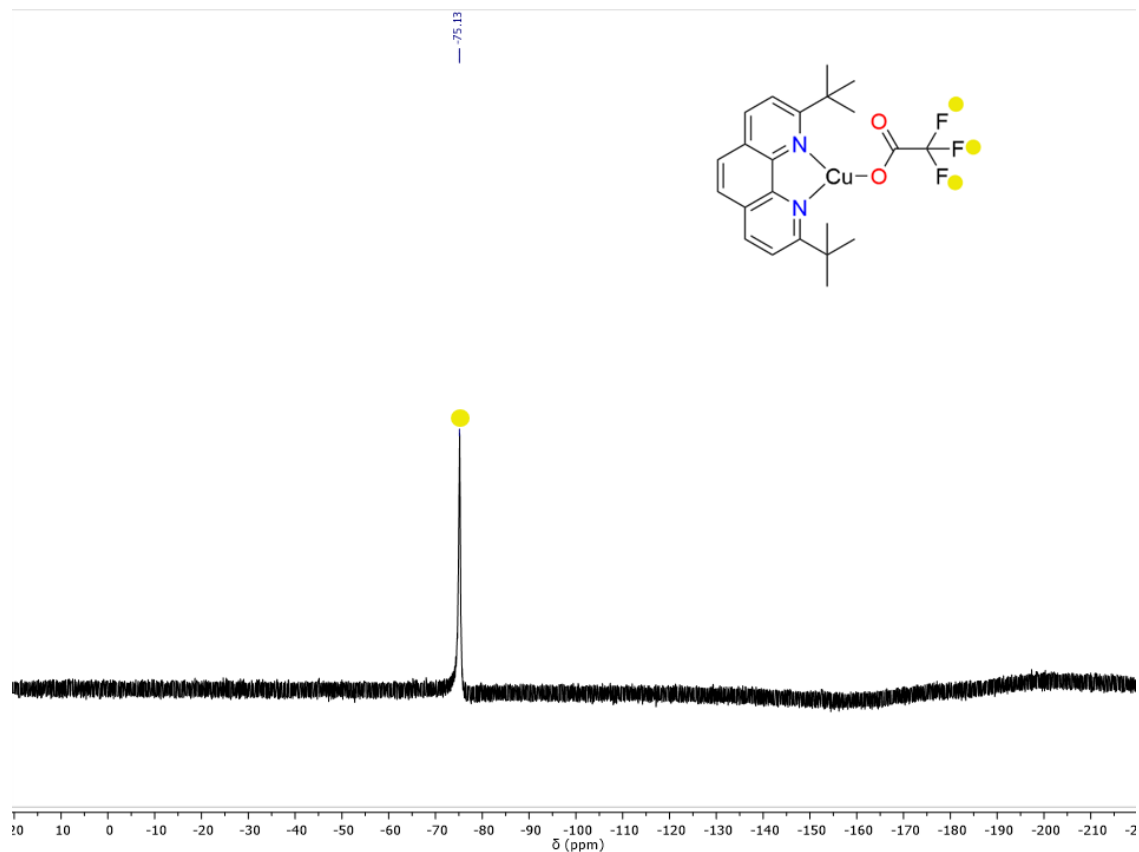


Figure S25. $^{19}\text{F}\{^1\text{H}\}$ NMR spectra of $[(\text{phen}^*)\text{Cu}-\text{O}_2\text{CCF}_3]$ (7) in $\text{THF}-d_8$.

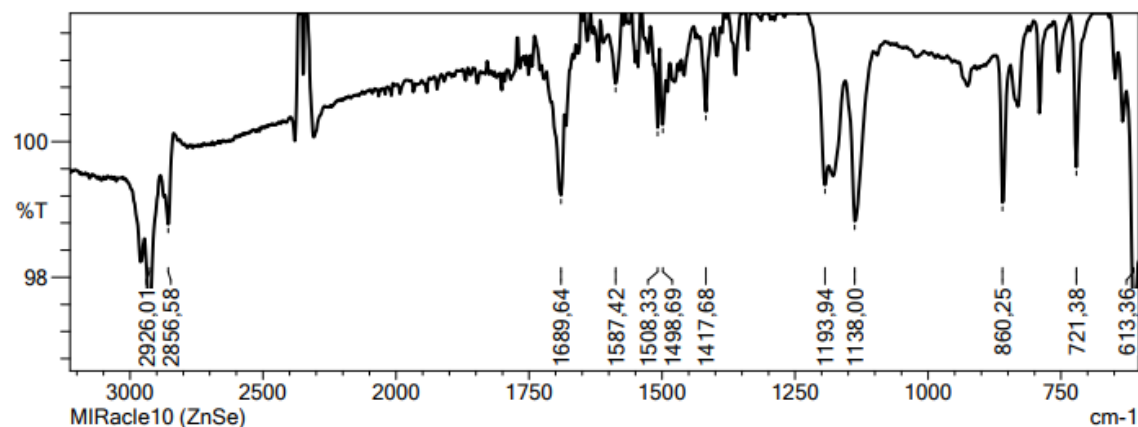


Figure S26. IR spectra of $[(\text{phen}^*)\text{Cu}-\text{O}_2\text{CCF}_3]$ (7) in $\text{THF}-d_8$.

II. 3. Synthesis of the $[(\text{phen}^*)\text{Cu}-\text{R}]$ complexes

II. 3. 1. Data for complex $[(\text{phen}^*)\text{Cu}-\text{C}_6\text{F}_5]$ (8):

In a round balloon flask was charged with $[\text{Cu}(\text{C}_6\text{F}_5)_4]$ (66 mg, 0.29 mmol) and **1** (85.2 mg, 0.29 mmol, 1 equiv.) and benzene (2 mL) was condensed in it. The orange suspension was stirred for 1h at room temperature. Pentane (5 mL) was then condensed in it, and the suspension stirred overnight at room temperature. The powder was then filtrated off, washed with pentane (3 mL) and dried for 1h under vacuum at room temperature. Complex **8** was isolated as an orange powder (110 mg, 72%).

^1H NMR (400 MHz, $\text{THF-}d_8$, rt, δ/ppm): 8.54 (d, $J = 8.6$ Hz, 2H), 8.09 (d, $J = 8.6$ Hz, 2H), 7.97 (s, 2H), 7.30 (trace of benzene), 1.70 (s, ^tBu , 18H).

$^{13}\text{C}\{^1\text{H}\}$ NMR (101 MHz, $\text{THF-}d_8$, rt, δ/ppm): 169.68, 143.95, 138.23, 128.05, 127.44, 125.79, 121.98, 38.49, 29.93.

$^{19}\text{F}\{^1\text{H}\}$ NMR (377 MHz, $\text{THF-}d_8$, rt, δ/ppm): -111.59 , -164.70 , -168.83 .

Elemental analysis for $\text{C}_{26}\text{H}_{24}\text{CuF}_5\text{N}_2$ ($M = 523.03$), found (theoretical) %: C, 57.28 (59.71); H, 4.92 (4.63); N, 5.55 (5.36).

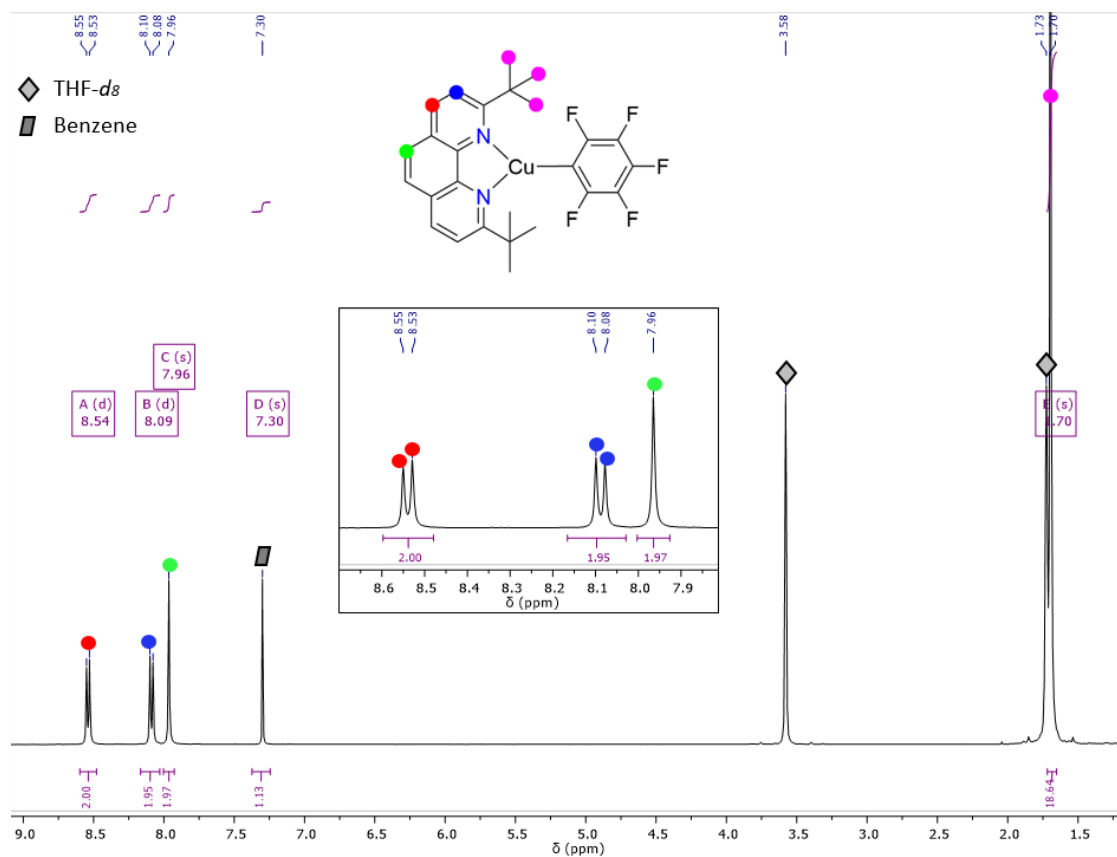


Figure S27. ^1H NMR spectra of $[(\text{phen}^*)\text{Cu-C}_6\text{F}_5]$ (**8**) in $\text{THF-}d_8$.

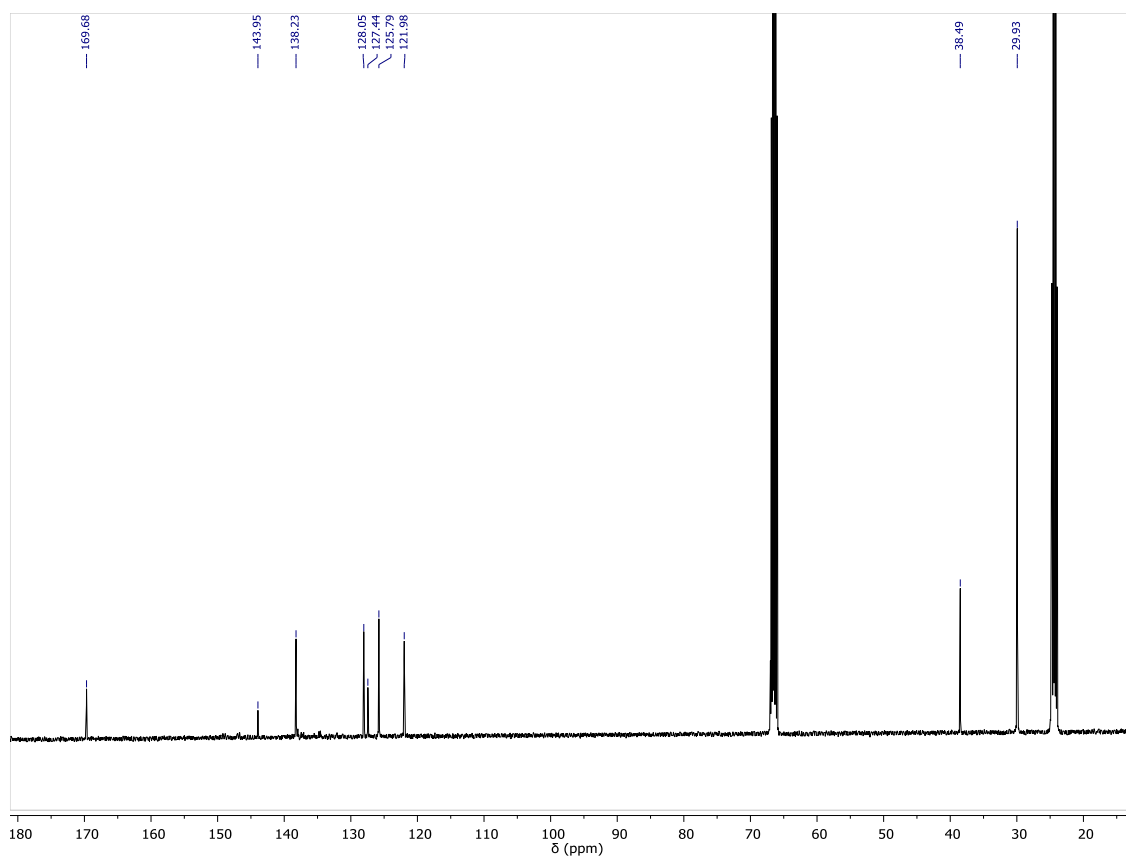


Figure S28. $^{13}\text{C}\{^1\text{H}\}$ NMR spectra of $[(\text{phen}^*)\text{Cu}-\text{C}_6\text{F}_5]$ (**8**) in $\text{THF}-d_8$.

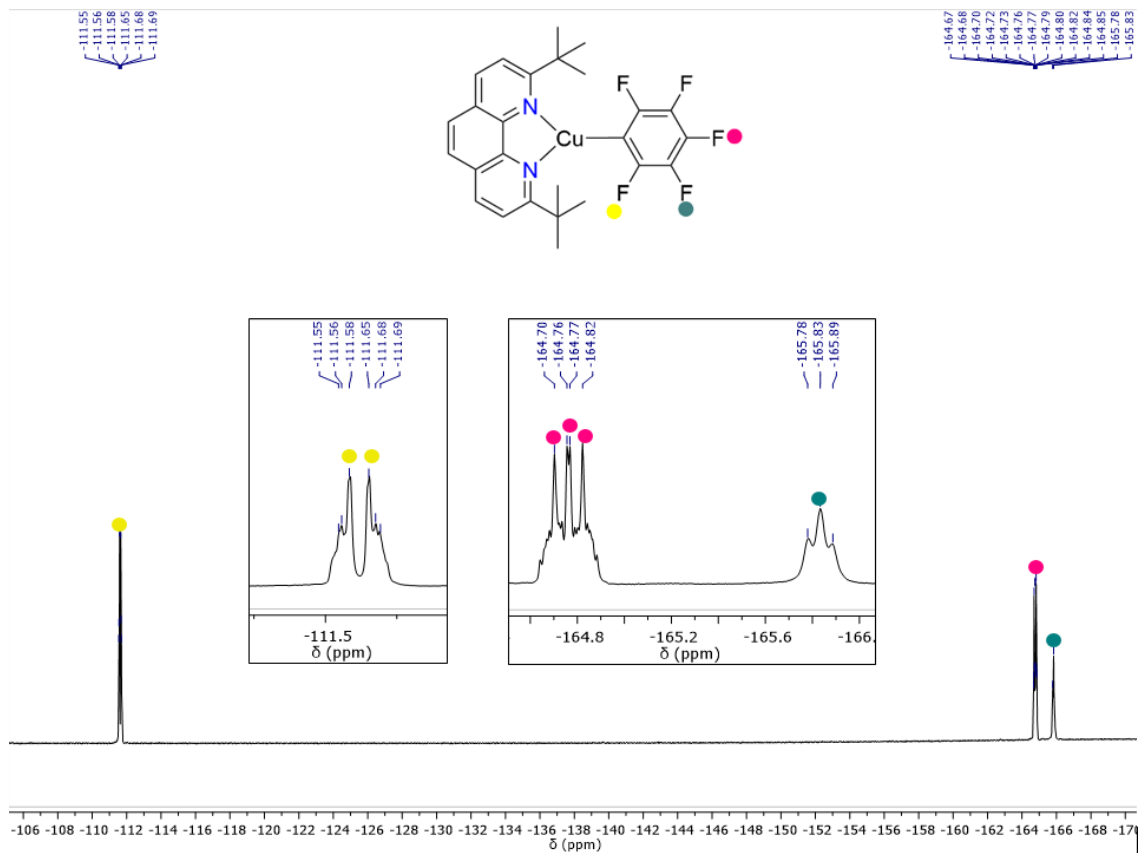


Figure S29. $^{19}\text{F}\{^1\text{H}\}$ NMR spectra of $[(\text{phen}^*)\text{Cu}-\text{C}_6\text{F}_5]$ (**8**) in $\text{THF}-d_8$.

II. 3. 2. Data for complex $[(\text{phen})\text{Cu}-\text{C}_6\text{F}_5]$ (**8'**):

This complex was previously synthesized by another protocol.⁹

In a round balloon flask was charged with $[\text{Cu}(\text{C}_6\text{F}_5)]_4$ (100 mg, 0.14 mmol) and 1,10-phenanthroline (24 mg, 0.13 mmol, <1 eq) and toluene (5 mL) was condensed in it. A red-orange suspension formed immediately and was stirred for 90 min at room temperature. Et_2O (5 mL) was then condensed in it to induce increased precipitation of the product. The powder was then filtrated off, washed by Soxhlet with the toluene-ether mixture followed by Et_2O (3 mL) and then dried overnight (*ca* 10h) under vacuum at room temperature. Complex **8'** was isolated as an orange powder (120 mg, 79%).

^1H NMR (400 MHz, $\text{THF}-d_8$, rt, δ/ppm): 9.29 (d, $J = 4.6$ Hz, 2H), 8.71 (dd, $J = 8.1, 1.6$ Hz, 2H), 8.14 (s, 2H), 8.04 (dd, $J = 8.2, 4.6$ Hz, 2H).

$^{19}\text{F}\{^1\text{H}\}$ NMR (377 MHz, $\text{THF}-d_8$, rt, δ/ppm): $-109.5, -164.8$.

These NMR are in agreement with those previously published. Elemental analysis for $\text{C}_{18}\text{H}_8\text{CuF}_5\text{N}_2$ ($M = 410.81$): The complex was previously said to be sensitive to temperature and atmospheric moisture and satisfactory elemental analyses could not be obtained.⁹

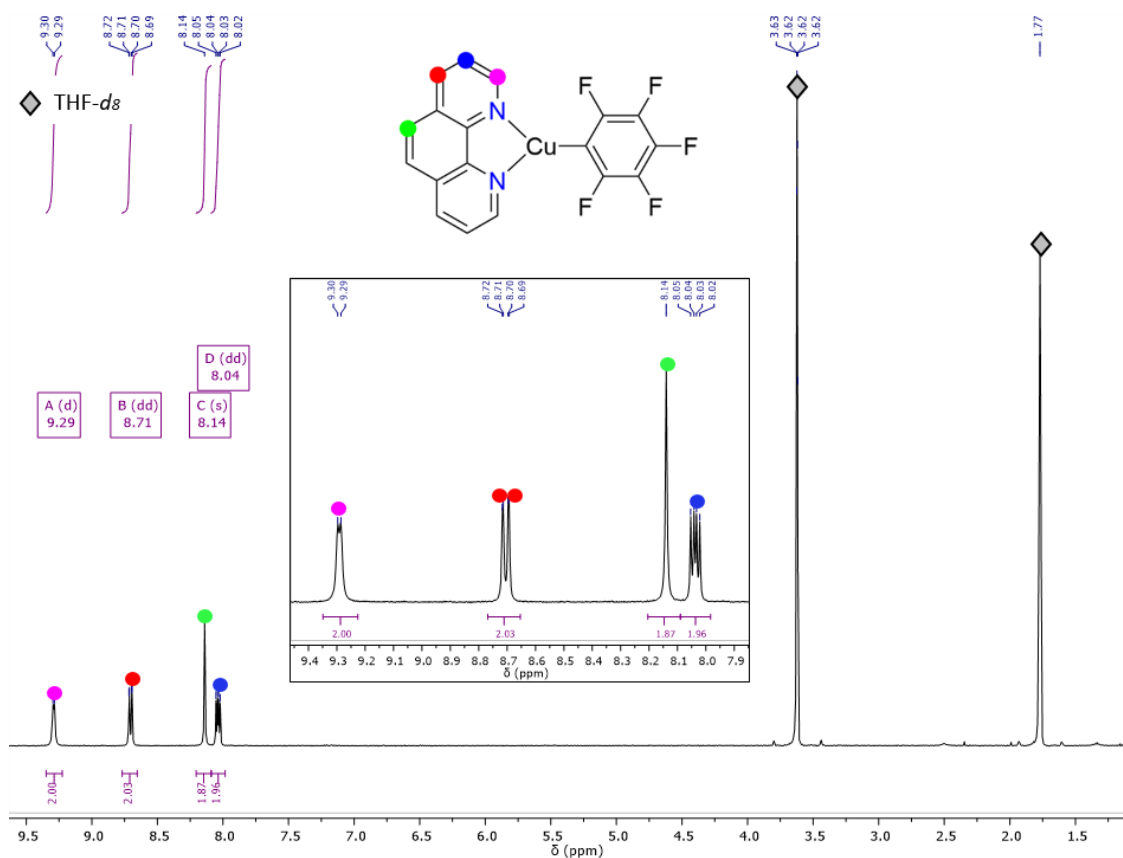


Figure S30. ^1H NMR spectra of $[(\text{phen})\text{Cu}-\text{C}_6\text{F}_5]$ (**8'**) in $\text{THF}-d_8$.

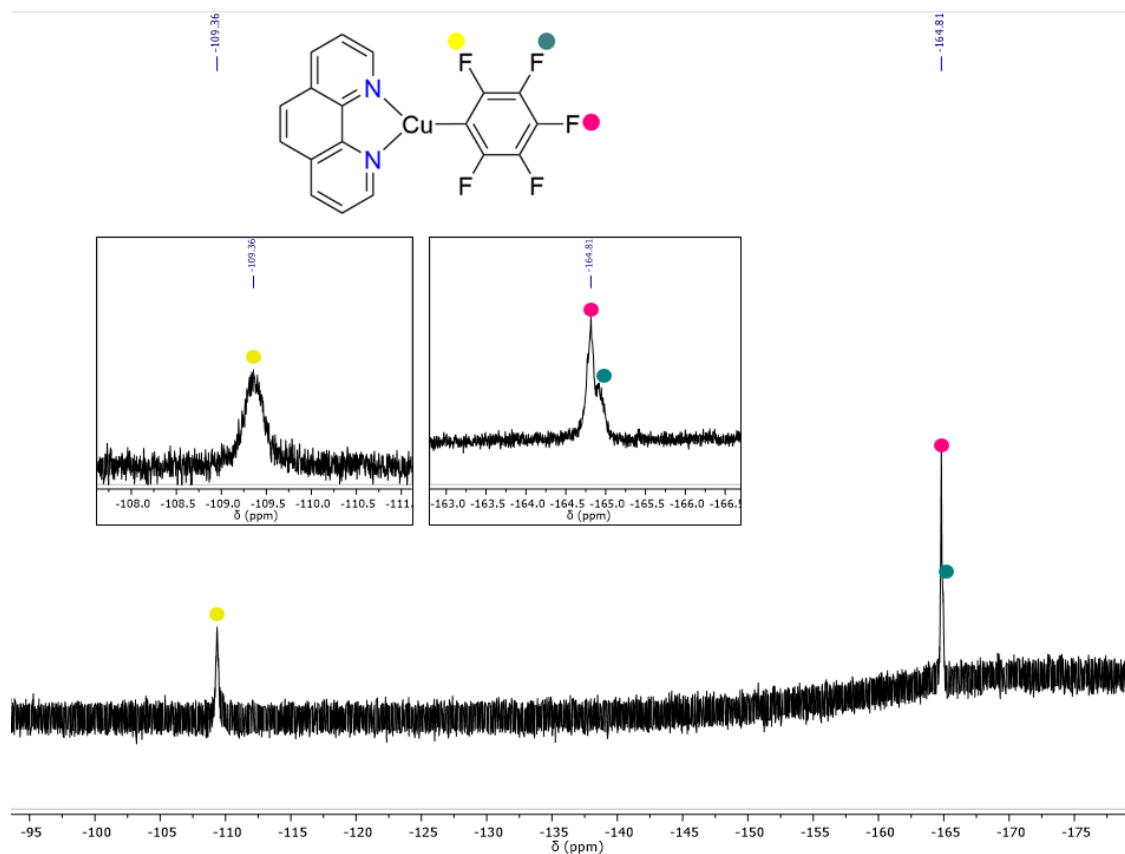
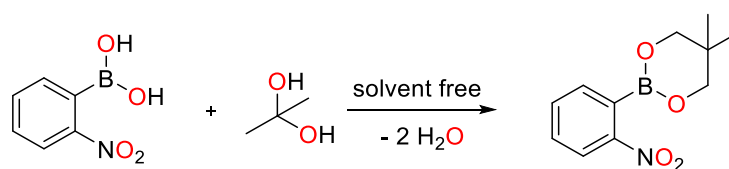


Figure S31. $^{19}\text{F}\{^1\text{H}\}$ NMR spectra of $[(\text{phen})\text{Cu}-\text{C}_6\text{F}_5]$ (**8'**) in $\text{THF}-d_8$.

II. 3. 3. Data for complex $[(\text{phen}^*)\text{Cu}(\text{C}_6\text{H}_4-o\text{-NO}_2)]$ (**9**):

a. Data for 5,5-dimethyl-2-(2-nitrophenyl)-1,3,2-dioxaborinane⁴



^1H NMR (400 MHz, chloroform- d_3 , rt, δ/ppm): 8.13 (dd, $J = 8.3, 1.0$ Hz, 1H), 7.66 (td, $J = 7.3, 1.1$ Hz, 1H), 7.59 (dd, $J = 7.4, 1.6$ Hz, 1H), 7.52 (ddd, $J = 8.3, 7.2, 1.6$ Hz, 1H), 3.83 (s, 4H), 1.15 (s, 6H).

$^{13}\text{C}\{^1\text{H}\}$ NMR (101 MHz, chloroform- d_3 , rt, δ/ppm): 151.06, 133.69, 132.36, 129.51, 122.92, 72.76, 31.97, 22.12. (missing one C in aromatic ring)

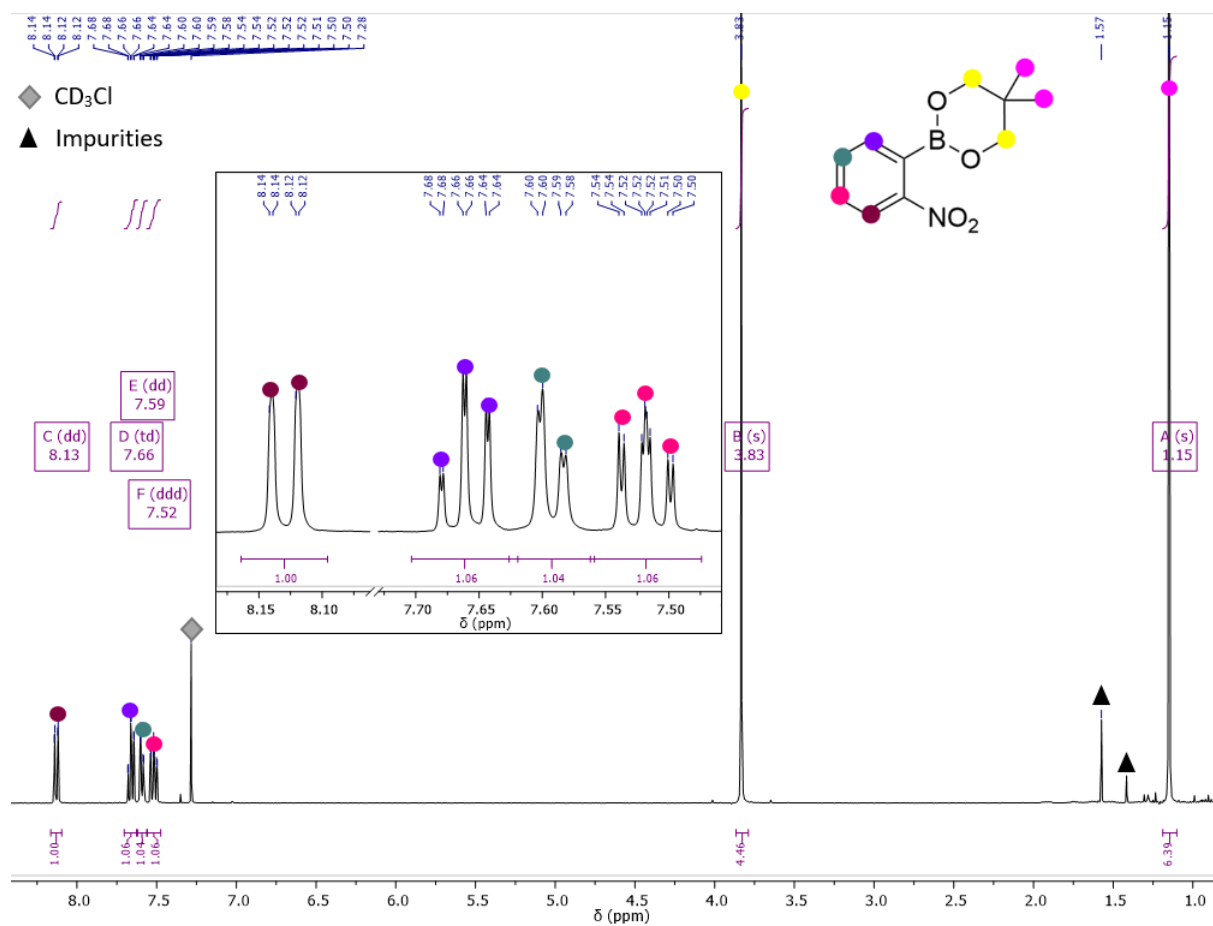


Figure S32. ¹H NMR spectra of 5,5-dimethyl-2-(2-nitrophenyl)-1,3,2-dioxaborinane in chloroform-d₃.

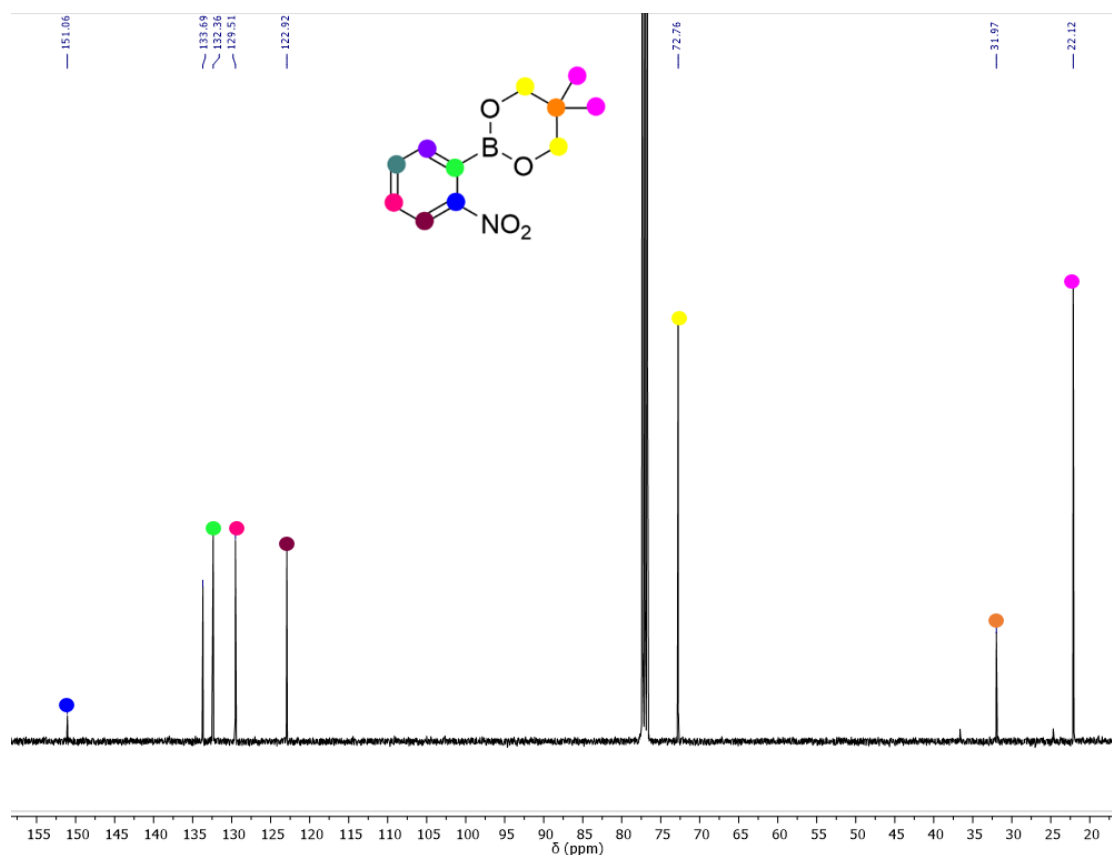


Figure S33. $^{13}\text{C}\{^1\text{H}\}$ NMR spectra of 5,5-dimethyl-2-(2-nitrophenyl)-1,3,2-dioxaborinane in chloroform- d_3 .³

b. Synthesis of [(phen)Cu(C₆H₄-o-NO₂)] (9):*

^1H NMR (400 MHz, THF- d_8 , rt, δ /ppm): 8.52 (d, J = 8.6 Hz, 2H), 8.23 (t, J = 7.1 Hz, 1H), 8.08 – 7.95 (m, 4H), 7.92 (d, J = 8.3 Hz, 1H), 7.81 – 7.71 (m, 1H), 7.31 (t, J = 7.2 Hz, 1H), 6.93 (t, J = 7.8 Hz, 1H), 1.67 (s, 18H), 1.60 (s, 8H, impurity, free phen* and remained of boronic substrate).

$^{13}\text{C}\{^1\text{H}\}$ NMR (101 MHz, THF- d_8 , rt, δ /ppm): 169.01, 156.71, 141.39, 137.56, 135.50, 134.39, 129.30, 125.59, 123.11, 121.62, 121.50, 121.44, 118.51, 38.42, 34.08, 29.57, 22.22, 14.69, 13.37. (impurity included free phen* and boronic substrate signals are underlines).

IR data (ν cm^{-1}): 3018 (m), 2796 (m), 1506 (w), 1467 (w), 1446 (w), 1363 (w), 1182 (w), 1024 (m), 877 (w), 871 (w).

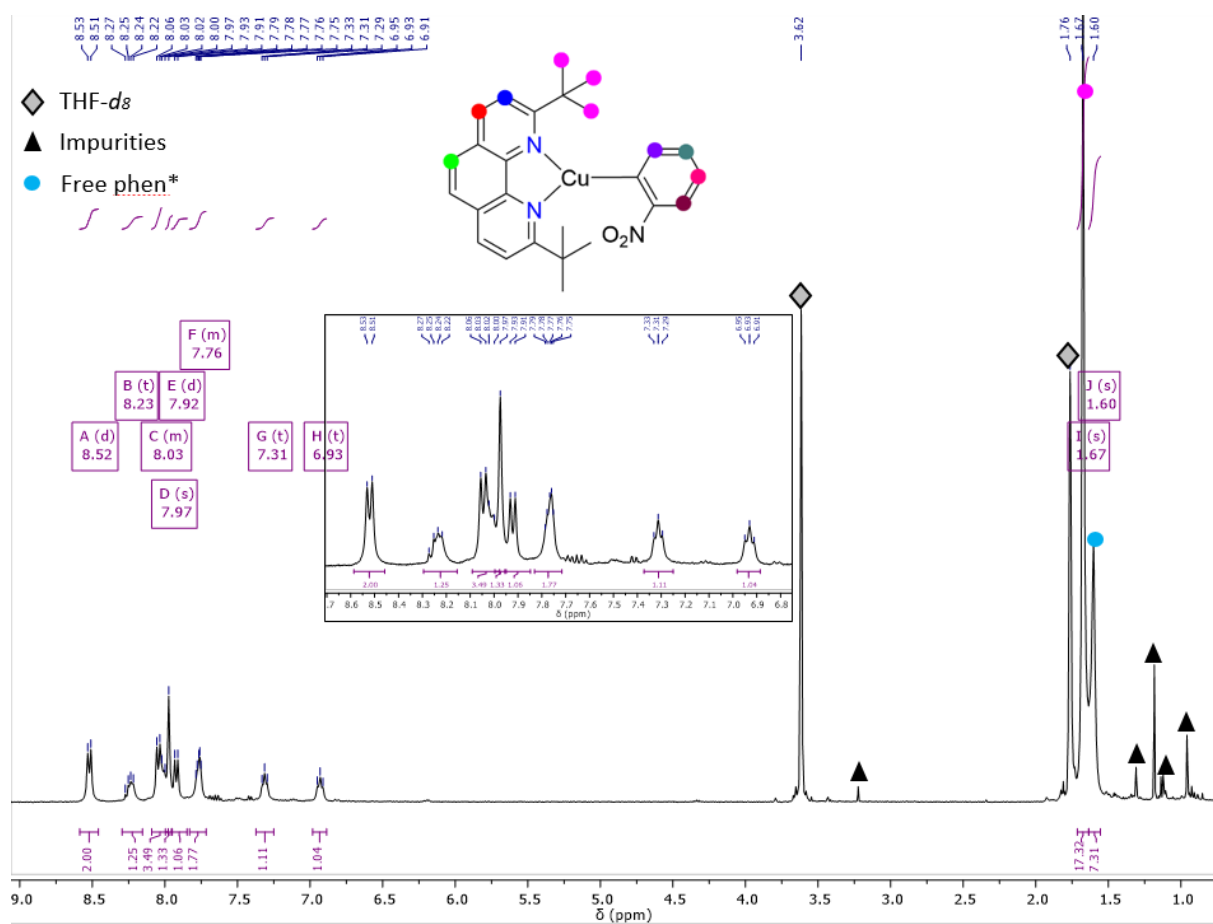


Figure S34. ¹H NMR spectra of [(phen*)Cu(C₆H₄-o-NO₂)] (9) in THF-*d*₈.

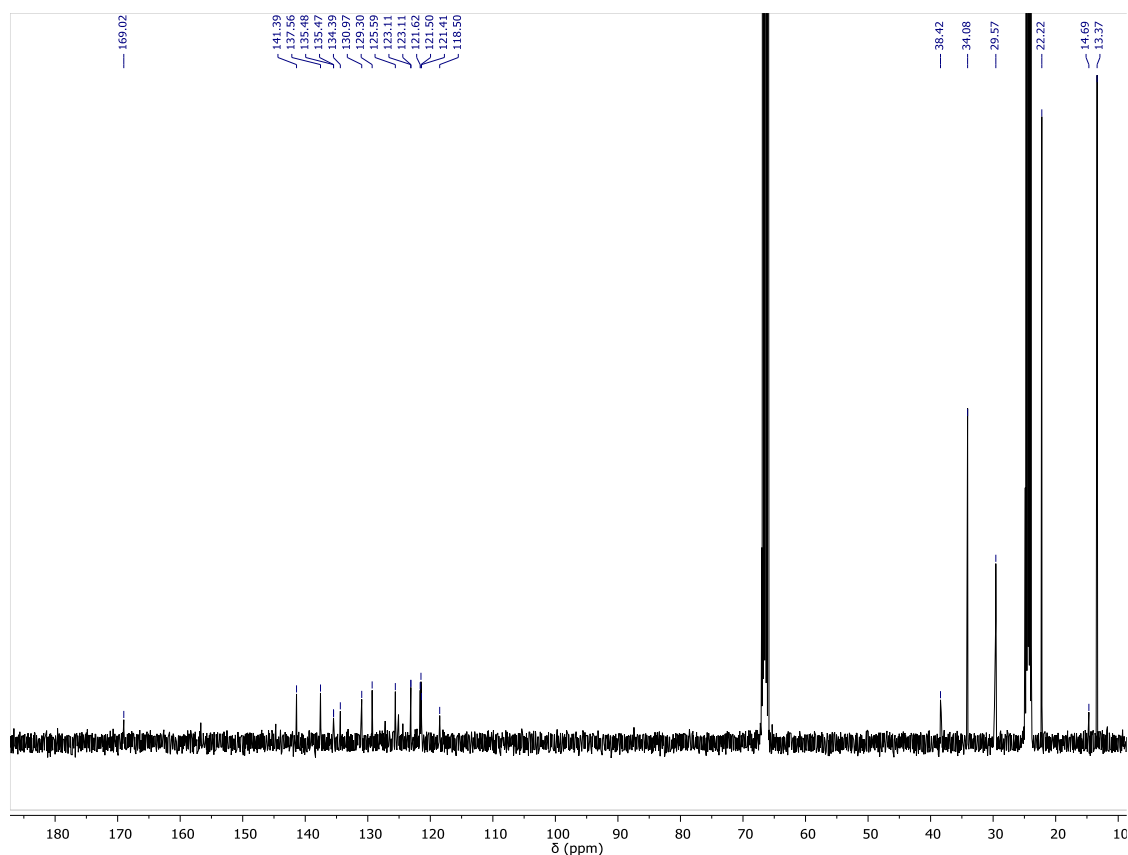


Figure S35. $^{13}\text{C}\{^1\text{H}\}$ NMR spectra of $[(\text{phen}^*)\text{Cu}(\text{C}_6\text{H}_4\text{-o-NO}_2)]$ (9) in THF-d_8 .

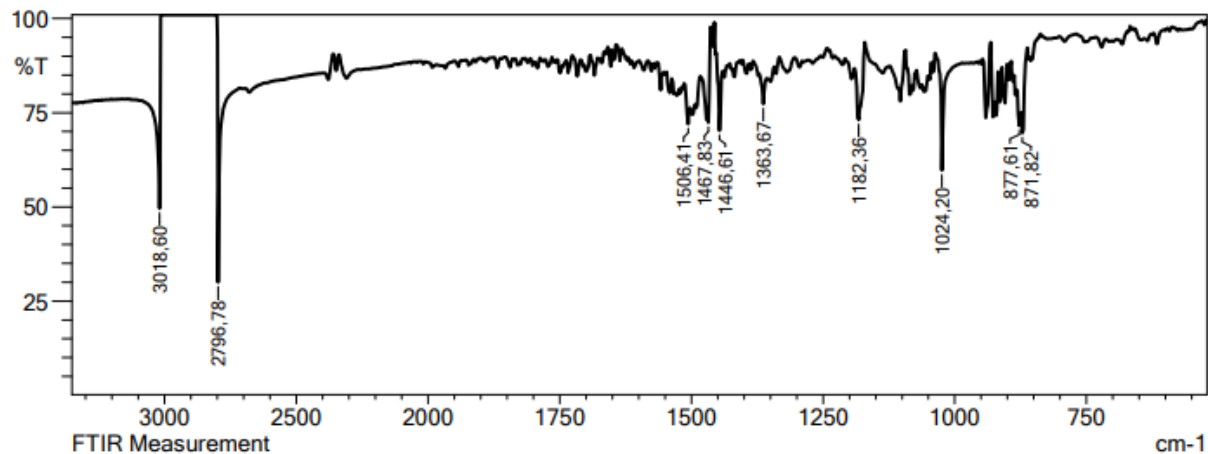


Figure S36. IR spectra of $[(\text{phen}^*)\text{Cu}(\text{C}_6\text{H}_4\text{-o-NO}_2)]$ (9).

II. 3. 4. Data for complex $[(\text{phen}^*)\text{Cu-CF}_3]$ (11):

To a solution of 2,9-di-*tert*butyl-1,10-phenanthroline (68.8 mg, 0.23 mmol, 1 equiv.) in THF (10 mL) was added $[\text{Cu}(\text{O}^t\text{Bu})]$ (pale yellow sublimed solid, 32.2 mg, 0.23 mmol, 1 eq.). The resulted light brown solution mixture was stirred at room temperature for 2 h. To the mixture, a solution of $\text{NEt}_3 \cdot 3\text{HF}$ (25.5 μL , 0.16 mmol, 2/3 equiv.) was added and the solution turned immediately red-orange. This treatment generated the complex $[(\text{phen}^*)\text{Cu-FHF}]$ which has been previously reported and crystallographically characterized.¹⁰ We prepared it in-situ and used it immediately to form $[(\text{phen}^*)\text{Cu-CF}_3]$. Thus, the red-orange solution of $[(\text{phen}^*)\text{Cu-FHF}]$ was stirred at room temperature for 1 h and TMSCF_3 (104.3 μL ,

0.69 mmol, 3 equiv.) was then syringed into it. The resulted red-orange mixture was kept stirring at room temperature for another hour to obtained a red-orange suspension. The solvent was then evaporated off and the solid residue dried under vacuum for 30 minute to give a crude yellow solid. This later was washed with pentane (10 mL x 3) and dried under primary vacuum for 2 h to afford pure complex **11** as a yellow solid (60.3 mg, 60 %). Yellow crystalline platelets of **11** were obtained by heating at 100 °C (less than 5 min) a THF solution of **11** and slowly cooling down in a hot water bath overnight.

^1H NMR (400 MHz, THF- d_8 , rt, δ /ppm): 8.52 (d, $J = 8.6$ Hz, 2H), 8.13 (d, $J = 8.8$ Hz, 2H), 7.94 (s, 2H), 1.83 (s, ^tBu , 18H).

$^{13}\text{C}\{^1\text{H}\}$ NMR (101 MHz, THF- d_8 , rt, δ /ppm): 169.94, 143.69, 137.92, 127.13, 125.58, 122.15, 38.44, 29.90.

$^{19}\text{F}\{^1\text{H}\}$ NMR (377 MHz, THF- d_8 , rt, δ /ppm): -26.79.

IR data (ν cm^{-1}): 3022 (m), 2792 (m), 1595 (s), 1562 (m), 1467 (w), 1444 (w), 1107 (m), 947 (m), 860 (m).

Elemental analysis for $\text{C}_{21}\text{H}_{24}\text{CuF}_3\text{N}_2$, ($M = 424.98$ g/mol), found (theoretical) %: C, 59.79 (59.35); H, 6.80 (5.69); N, 7.50 (6.59).

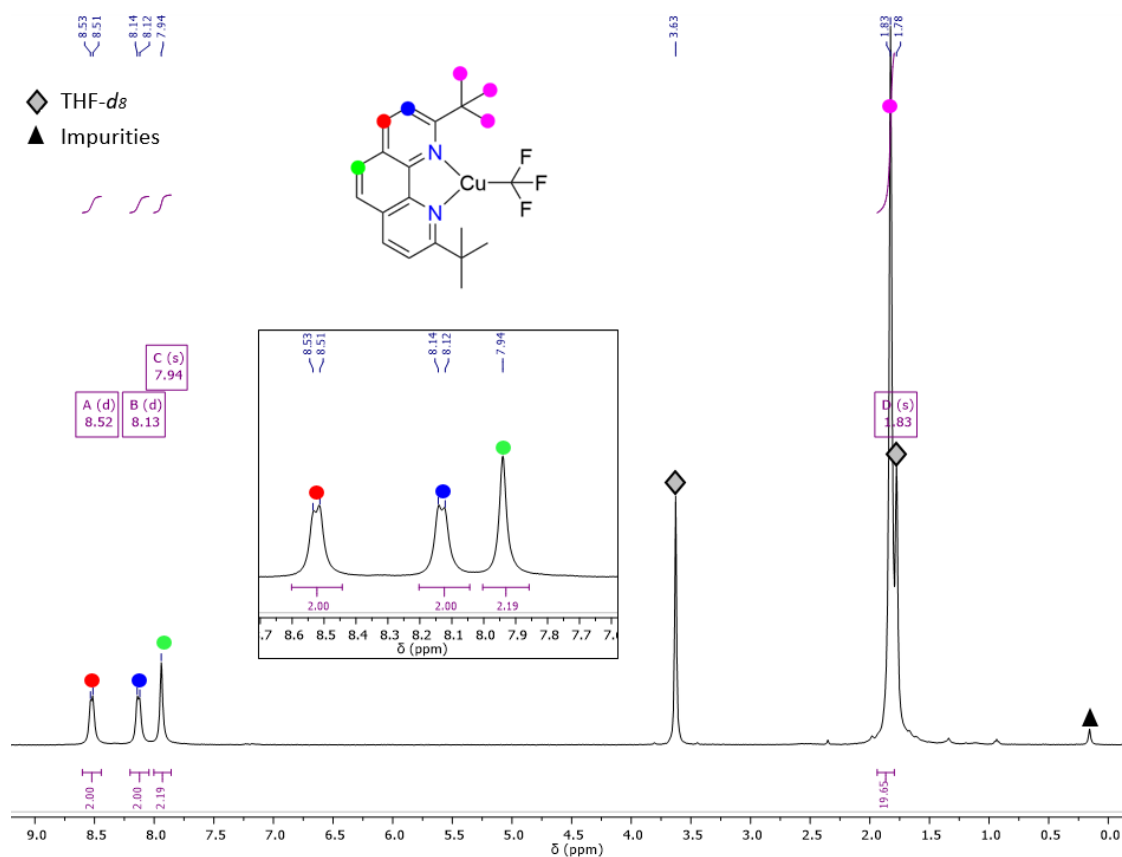


Figure S37. ^1H NMR spectra of $[(\text{phen}^*)\text{CuCF}_3]$ (**11**) in THF- d_8 .

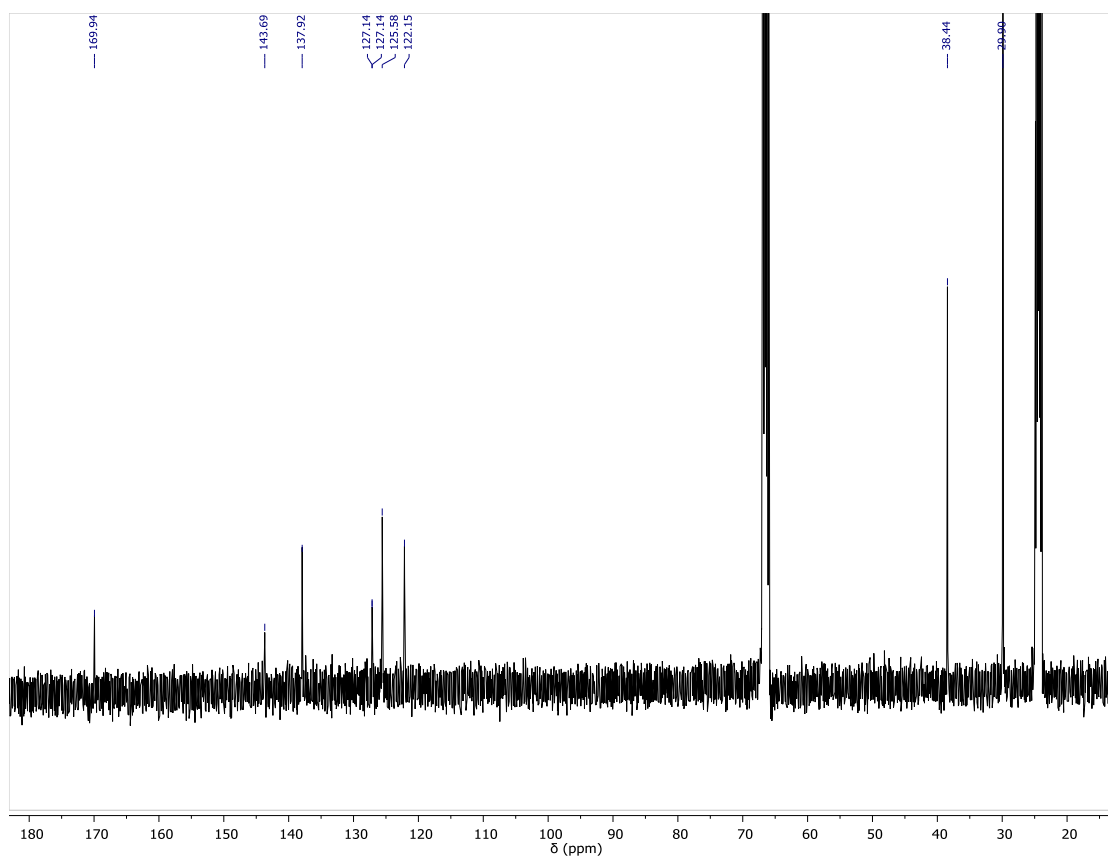


Figure S38. $^{13}\text{C}\{^1\text{H}\}$ NMR spectra of $[(\text{phen}^*)\text{CuCF}_3]$ (**11**) in THF-d_8 .

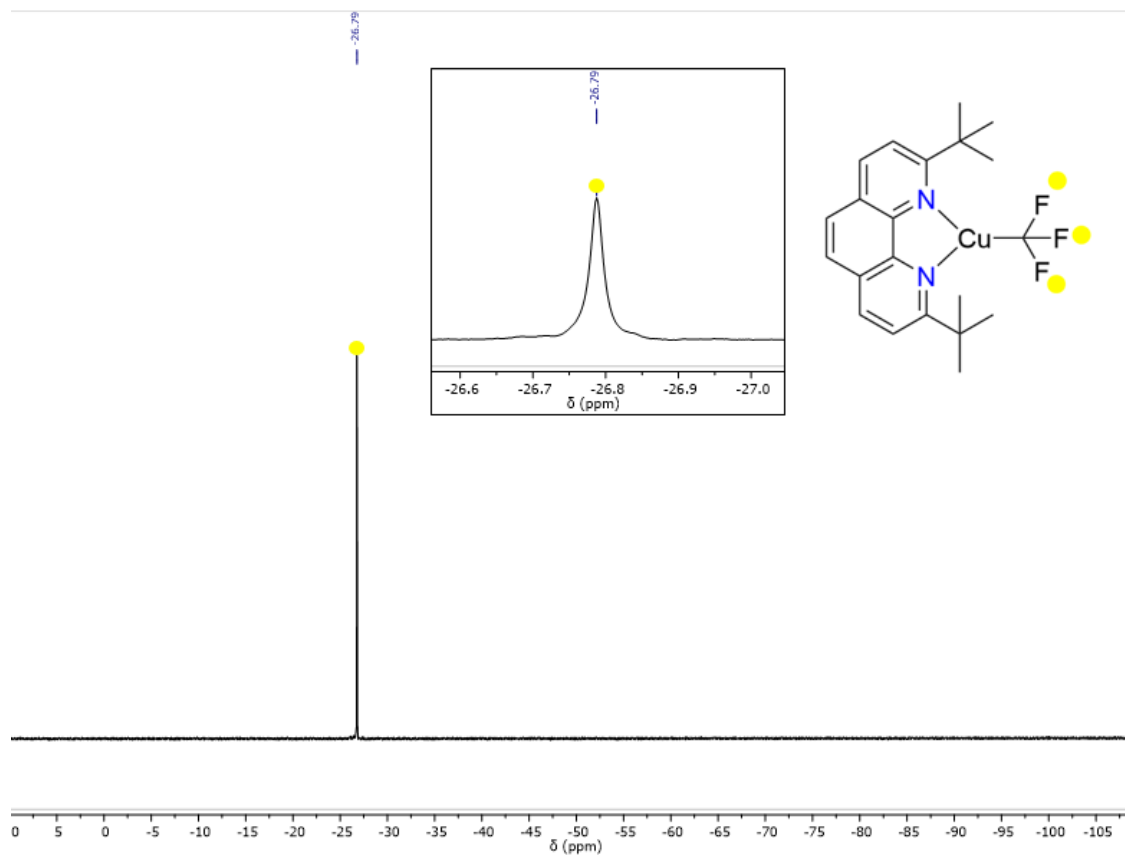


Figure S39. $^{19}\text{F}\{^1\text{H}\}$ NMR spectra of $[(\text{phen}^*)\text{CuCF}_3]$ (**11**) in THF-d_8 .

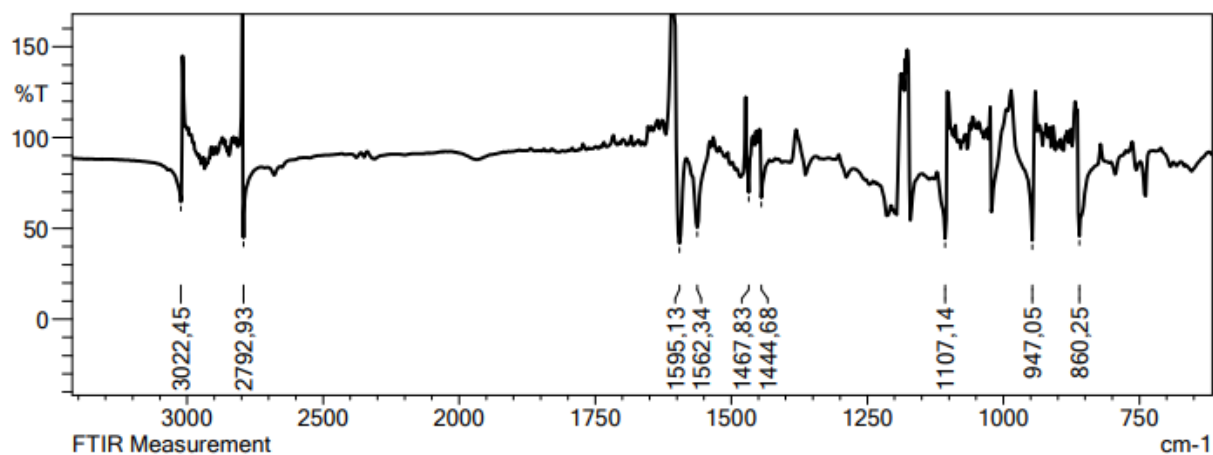


Figure S40. IR spectra of $[(phen^*)CuCF_3]$ (**11**).

II. 3. 5. Crystal structure of $[(phen^*)Cu-F(HF)] \cdot C_6H_6$ and NMR of $[(phen^*)Cu-F(HF)]$ (**10**)

The formation of $[(phen^*)Cu-F(HF)]$ as described above. Crystal structure of $[(phen^*)Cu-F(HF)] \cdot C_6H_6$ was crystallized by heating at 80 °C (less than 5 min) a solution of $[(phen^*)Cu-F(HF)]$ in benzene and cooling down slowly in hot water bath overnight.

1H NMR (400 MHz, THF- d_8 , rt, δ /ppm): 11.87 (s, 1H, HF), 8.59 (d, $J = 8.6$ Hz, 2H), 8.24 (d, $J = 8.4$ Hz, 1H), 8.15 (d, $J = 8.6$ Hz, 2H), 7.98 (s, 2H), 7.78 (d, $J = 7.9$ Hz, 2H), 1.86 (s, t Bu, 18H), 1.61 (s, 9H). (the underlined signals are belongs to free phen* that cannot be eliminated definitively by washing with pentane)

$^{19}F\{^1H\}$ NMR (377 MHz, THF- d_8 , rt, δ /ppm): -208.70

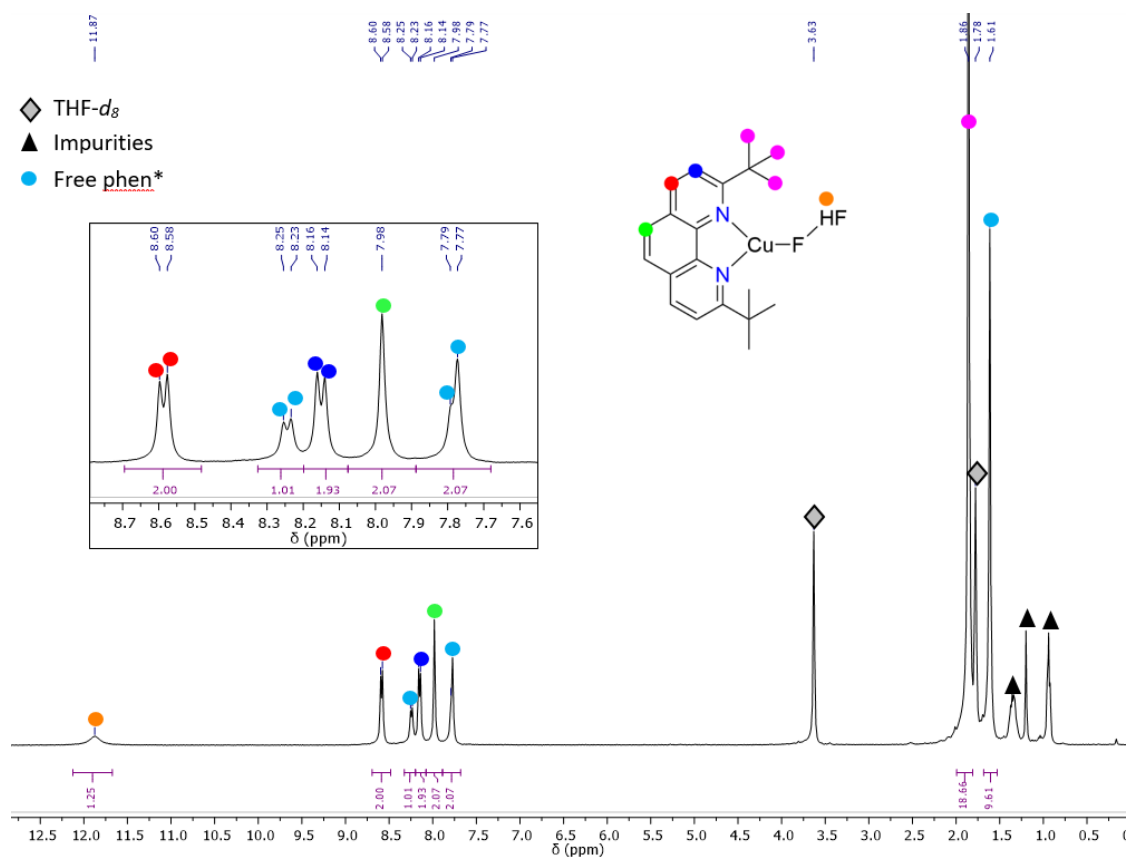


Figure S41. 1H NMR spectra of $[(phen^*)CuF(HF)]$ (10) in THF- d_8 .

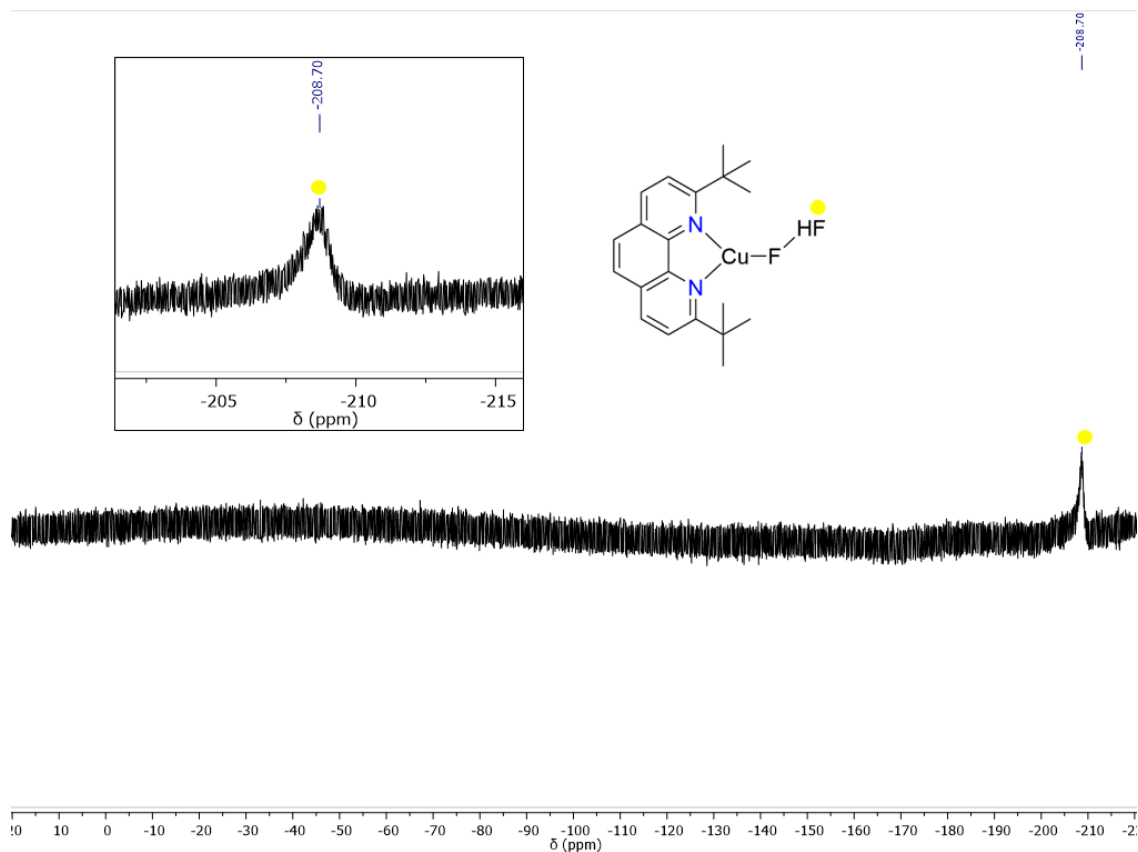


Figure S42. $^{19}\text{F}\{^1\text{H}\}$ NMR spectra of $[(\text{phen}^*)\text{CuF}(\text{HF})]$ (**10**) in $\text{THF-}d_8$.

II. 4. Decarboxylation of the $[(\text{phen}^*)\text{Cu}(\text{O}_2\text{CR})]$ complexes ($\text{R} = \text{C}_6\text{H}_4\text{-}o\text{-F}$, C_6F_5 , $\text{C}_6\text{H}_4\text{-}o\text{-NO}_2$, CF_3)

II. 4. 1. Decarboxylation in THF:

In different NMR Young tubes, all tested complexes (**2**, **4**, **5**, and **7**) (~ 5 mg) were solubilized in $\text{THF-}d_8$ (~ 5 mL) and heated from 35 °C to 175 °C depending on the complex. The evolution of each complex was monitored by ^1H NMR and $^{19}\text{F}\{^1\text{H}\}$ NMR at indicated time.

a. Thermal decarboxylation of $[(\text{phen}^*)\text{Cu}(\text{O}_2\text{CC}_6\text{H}_4\text{-}o\text{-F})]$ (**2**)

Thermal decarboxylation of **2** is recorded every 2.5h at different temperatures. After 2.5 h at 75 °C, started to observe the change of solution color from clear yellow to green and the formation of small amount of black solid. At the end of the reaction (2.5 h at 175 °C), solution turned to clear green and the larger amount of black solid with the formation of free phen^* .

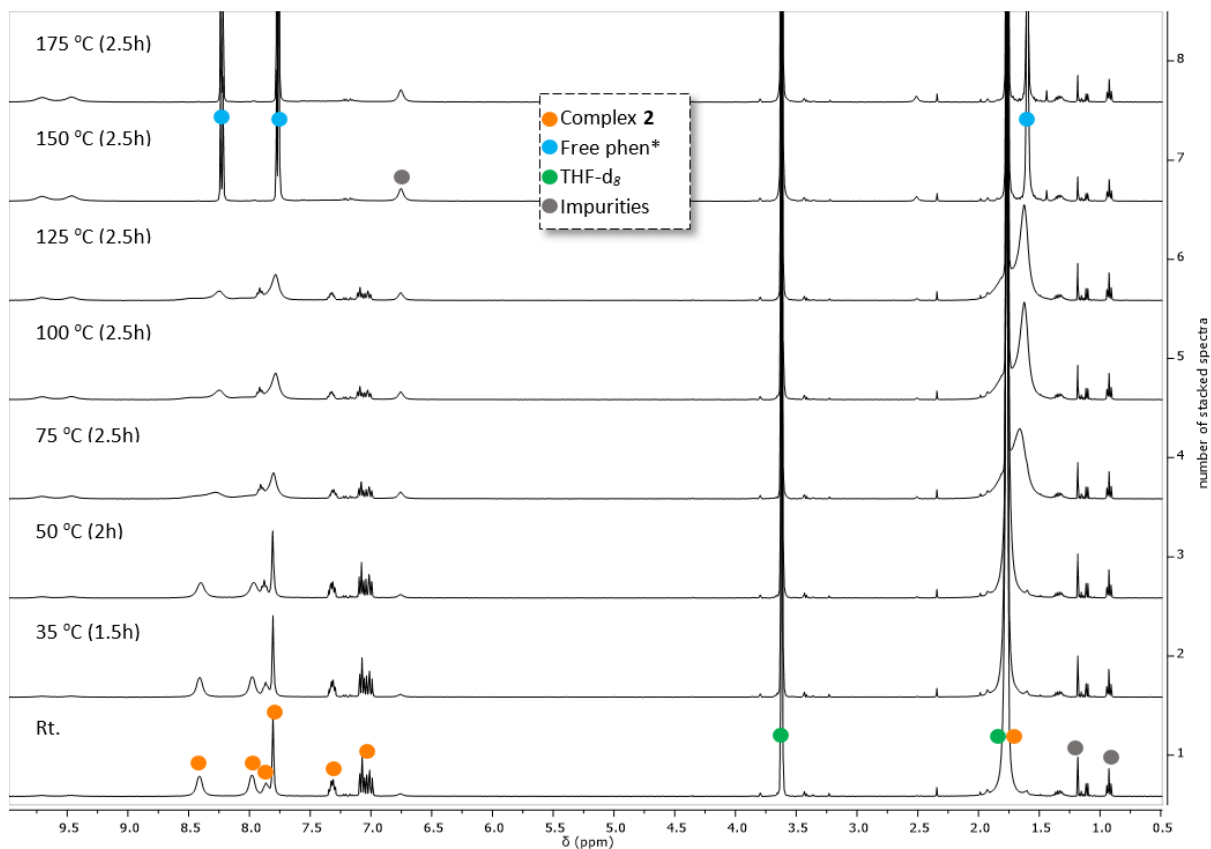


Figure S43. ^1H NMR stacked spectrum of the thermal evolution of **2** in THF-d_8 .

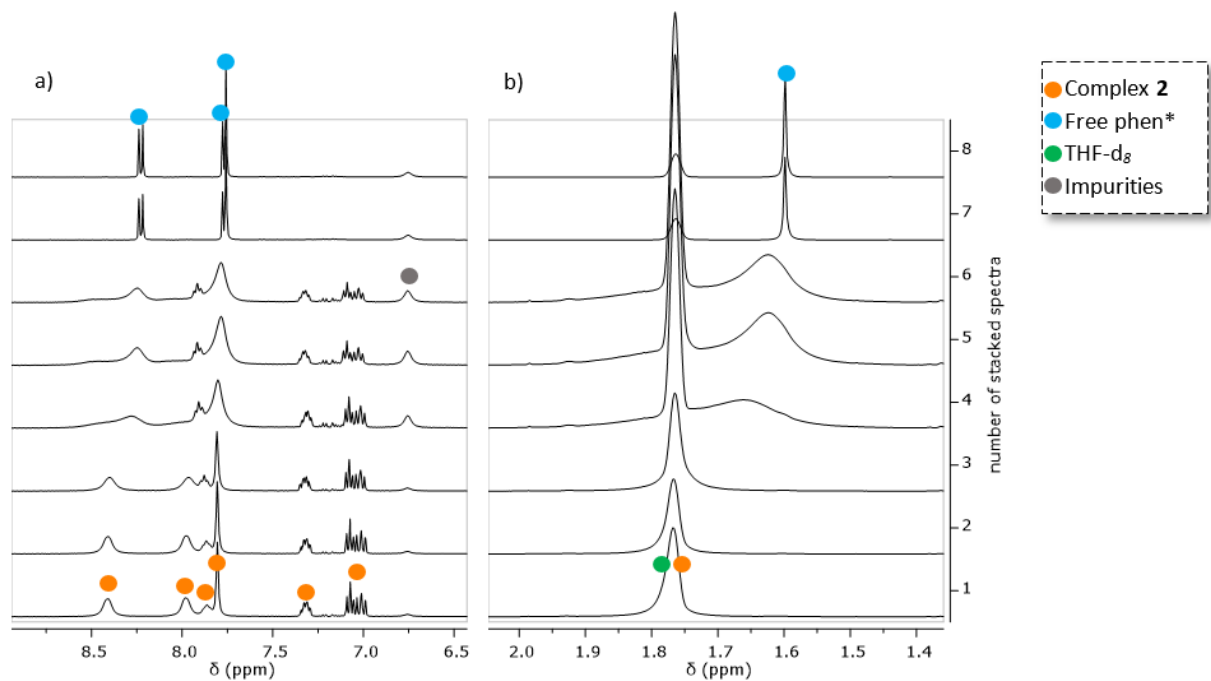


Figure S44. Zoom on Figure S43: a) aromatic region; b) aliphatic regions.

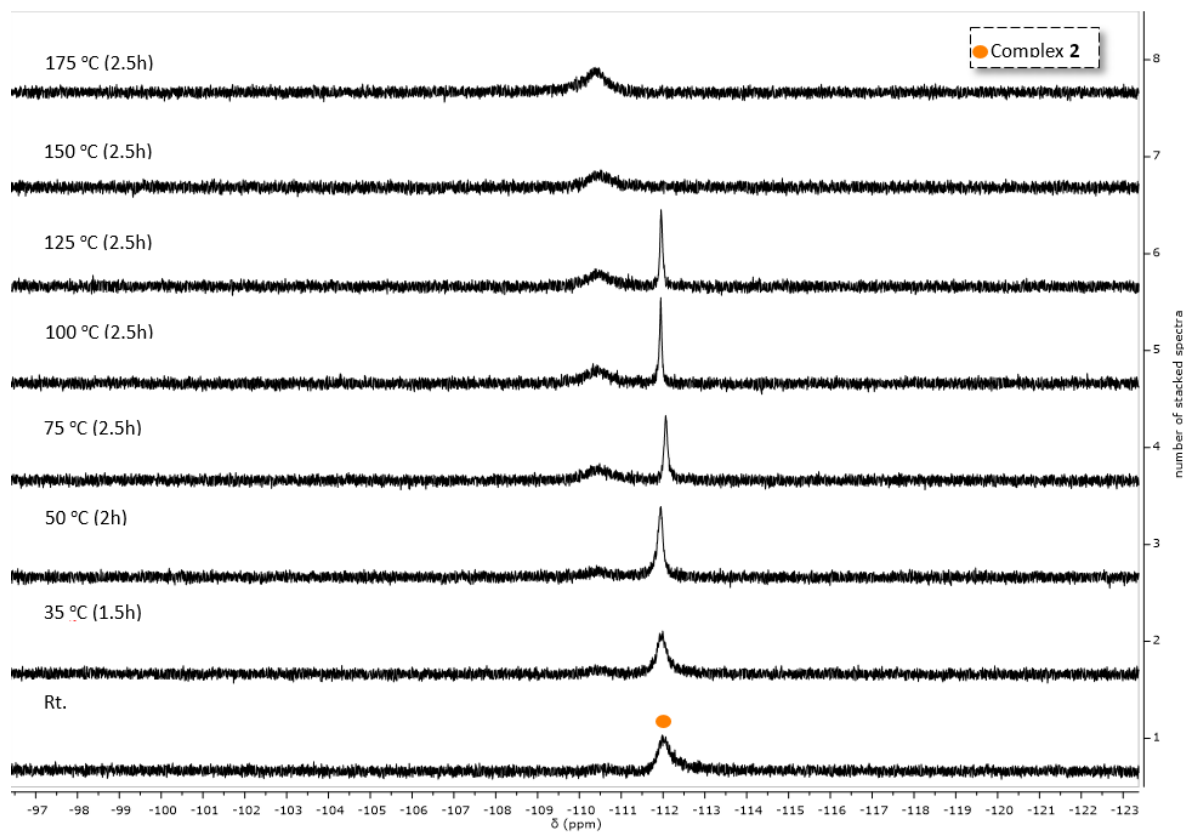


Figure S45. $^{19}\text{F}\{^1\text{H}\}$ NMR spectra of the thermal evolution of **2** in $\text{THF-}d_8$.

b. Thermal decarboxylation of $[(\text{phen}^)\text{Cu}(\text{O}_2\text{CC}_6\text{F}_5)]$ (**4**):*

A clear orange solution of **4** (5 mg, 8.8 μmol) in $\text{THF-}d_8$ was heated at 35 °C for 1h and then continued at 50 to 125 °C at different times. There was no change of solution color upon heating and the resulted solution at the end of the reaction remained. The formation of free ligand is observed after heating at 35 °C (1h) and then at 50 °C (5h). At the end of the reaction, the ratio between complex **4** and ligand is 1:1, respectively. The formation of $\text{C}_6\text{F}_5\text{H}$ is detected by ^{19}F NMR after 3h at 100 °C along with an unidentified fluorinated species.

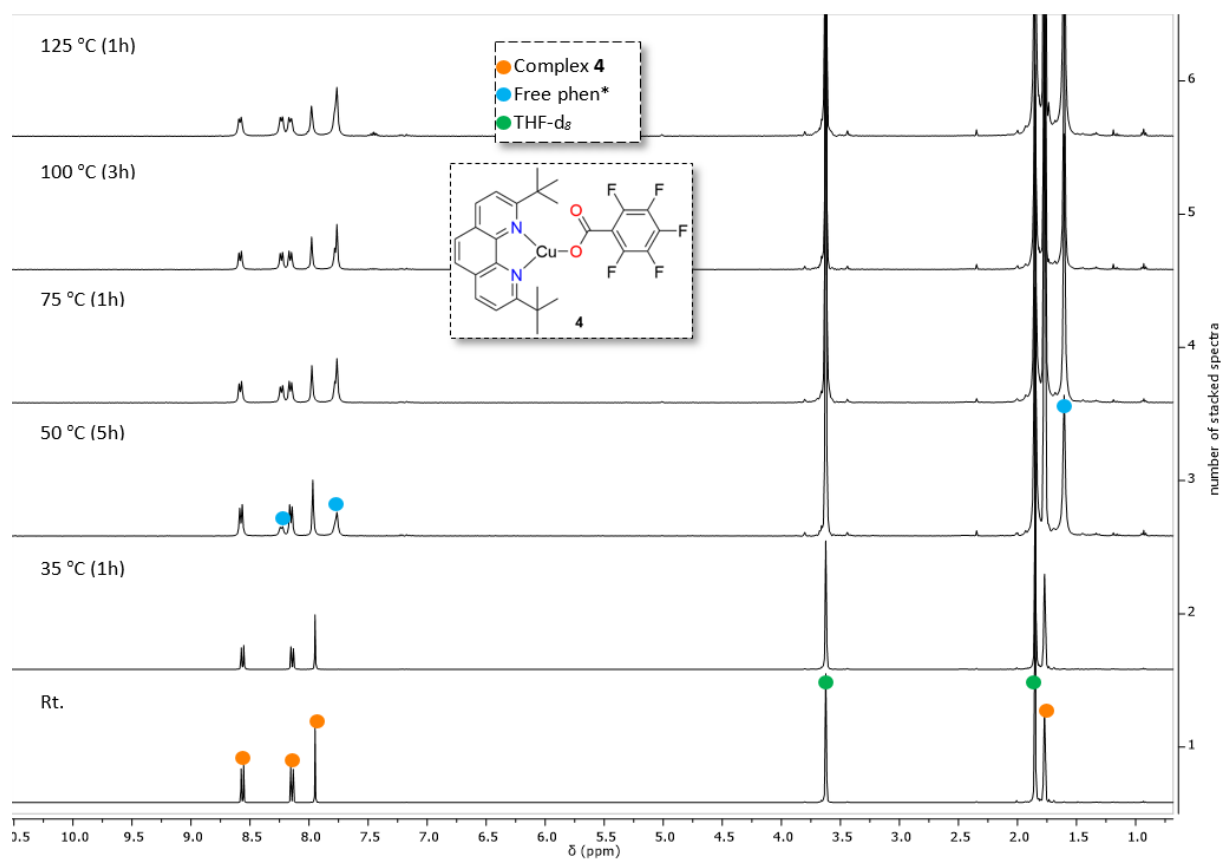


Figure S46. ^1H NMR spectra of the thermal evolution of **4** in THF-d_8 .

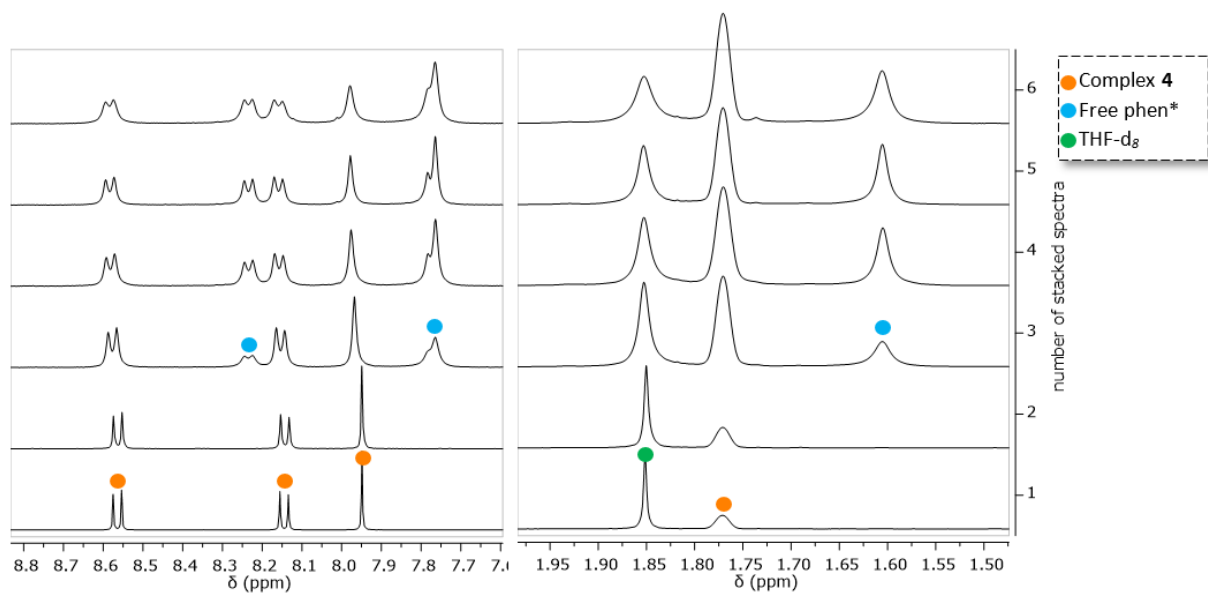


Figure S47. Zoom on Figure S46 (the intensity of some spectrum have been modified for clarification).

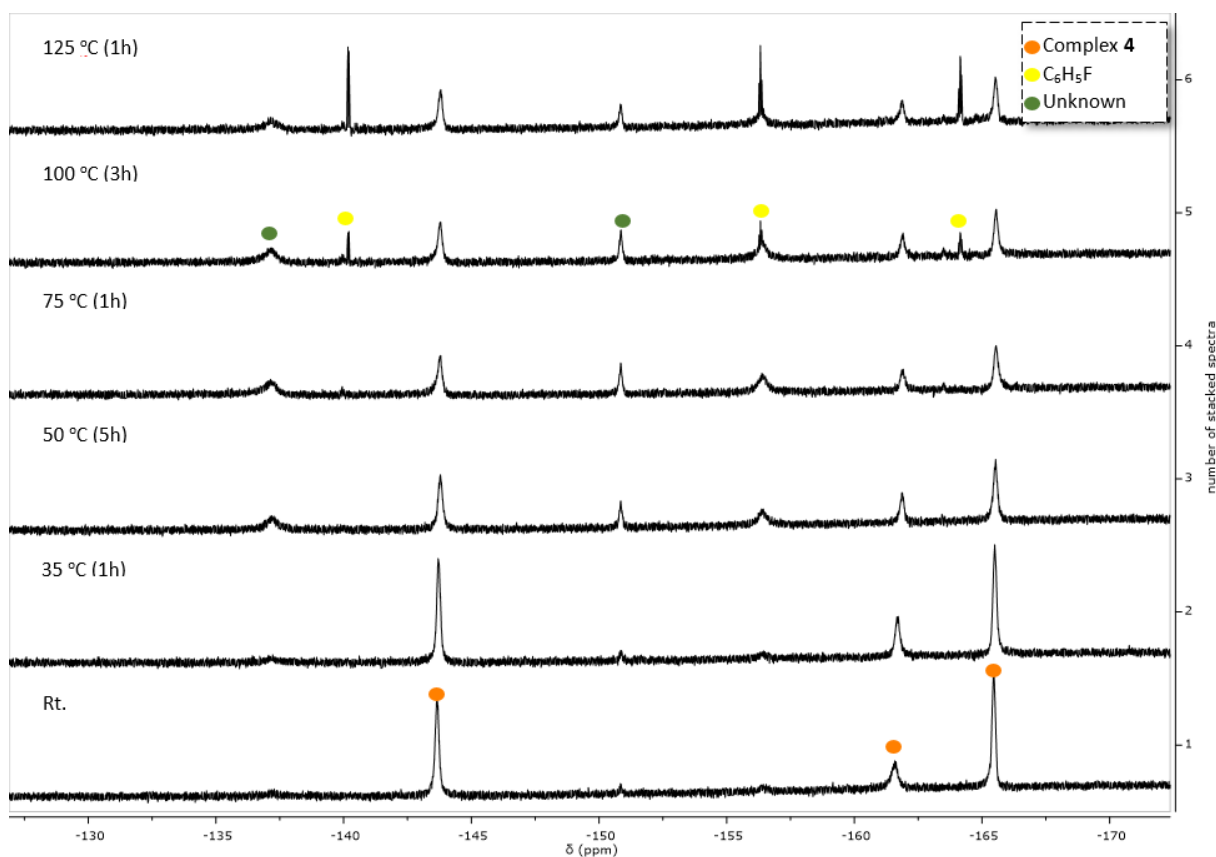


Figure S48. $^{19}\text{F}\{^1\text{H}\}$ NMR spectra of the thermal evolution of **4** in $\text{THF-}d_8$.

c. Thermal decarboxylation of $[(\text{phen}^)\text{Cu}(\text{O}_2\text{CC}_6\text{H}_4\text{-o-NO}_2)]$ (**5**)*

A clear light yellow solution of **5** (5 mg, 9.6 μmol) was heated from 35 – 100 °C for different amount of time. No change of solution color was observed upon heating up to 50 °C for 2 h and the degradation of the complex only observed starting at 80 °C for (10 h). At the end of the reaction (100 °C for 72 h), the solution turned to clear green indicated the dead of complex **5**.

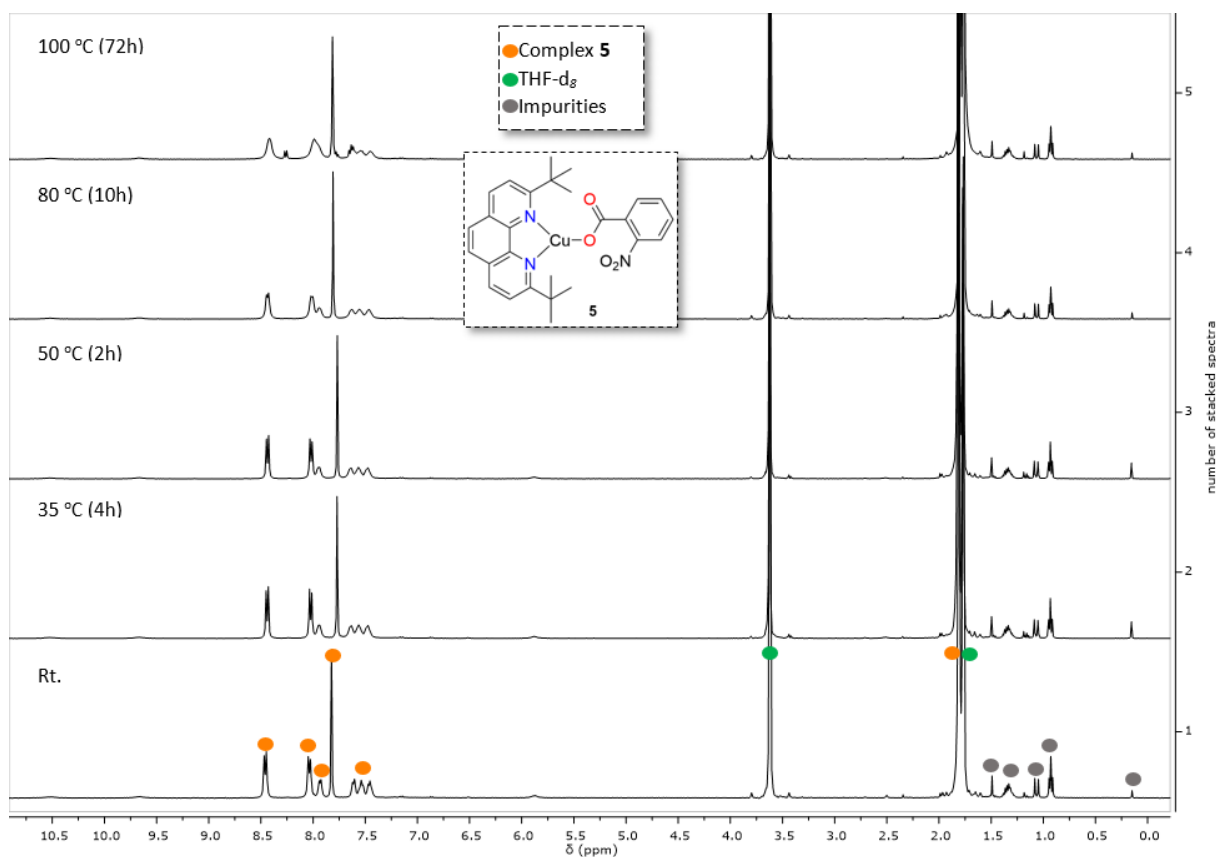


Figure S49. ^1H NMR spectra of the thermal evolution of **5** in THF-d_8 .

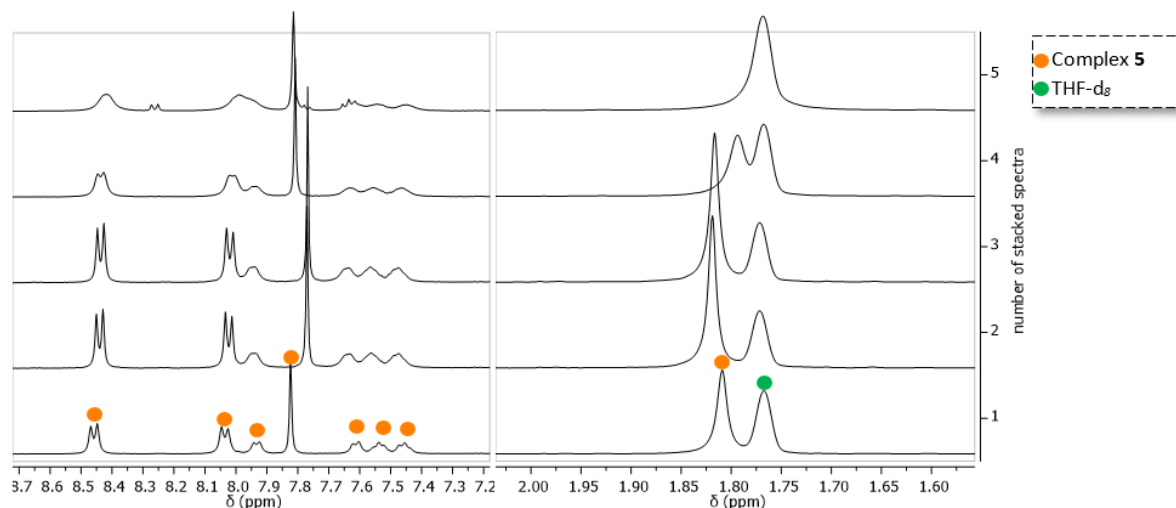


Figure S50. Zoom on Figure S49.

d. Thermal decarboxylation of $[(\text{phen}^*)\text{Cu}(\text{O}_2\text{CCF}_3)]$ (**7**)

Thermal decarboxylation of **7** is recorded every 2.5 h at different temperatures. The orange solution of **7** was heated at 50 °C for 2 h where free ligand started to form. Upon heating the reaction solution at higher temperature (75–175 °C), the liberation of free ligand continued however, up to 175 °C after 2 h, complex **7** remained the majority in clear yellow solution and only a small amount of black solid is generated. Nevertheless, the ^{19}F NMR signal of **7** became undetectable after heating for 2 h at 50 °C.

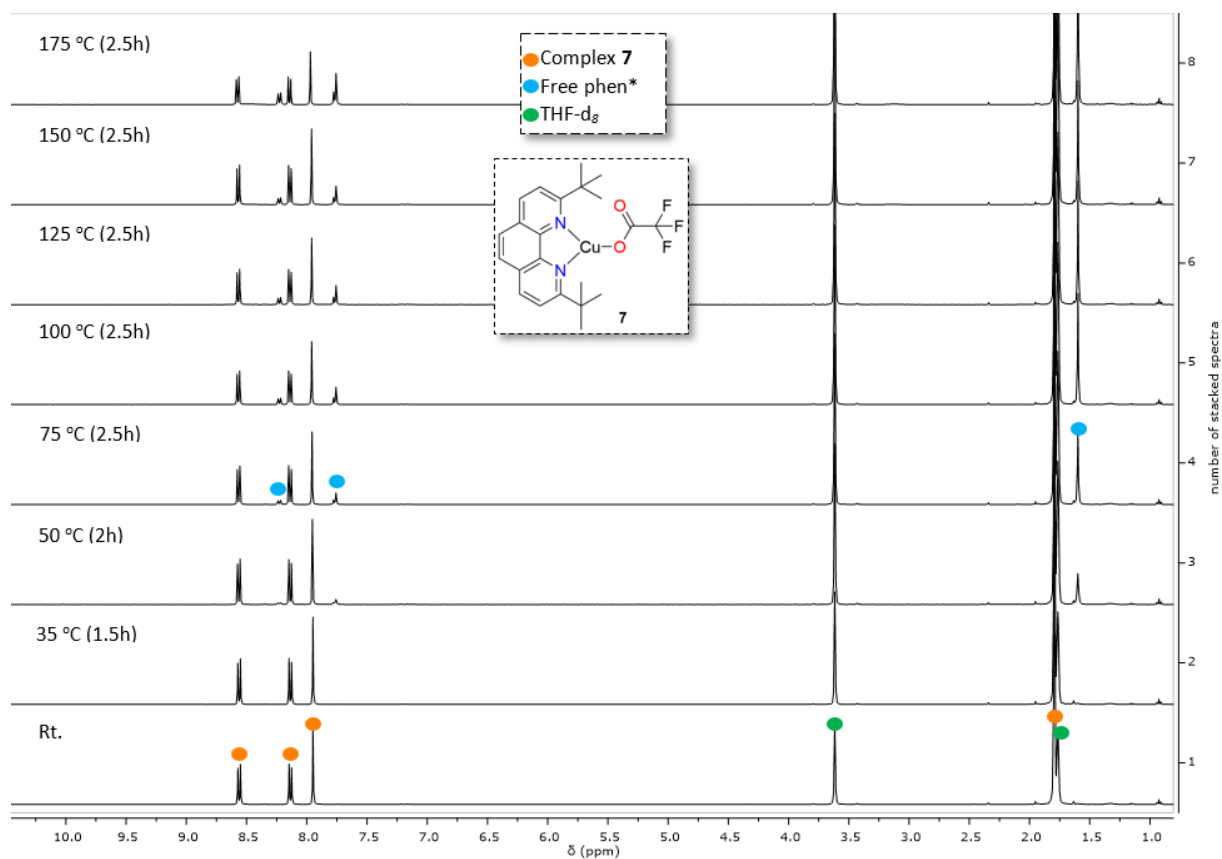


Figure S51. ^1H NMR spectra of the thermal evolution of **7** in THF-d_8 .

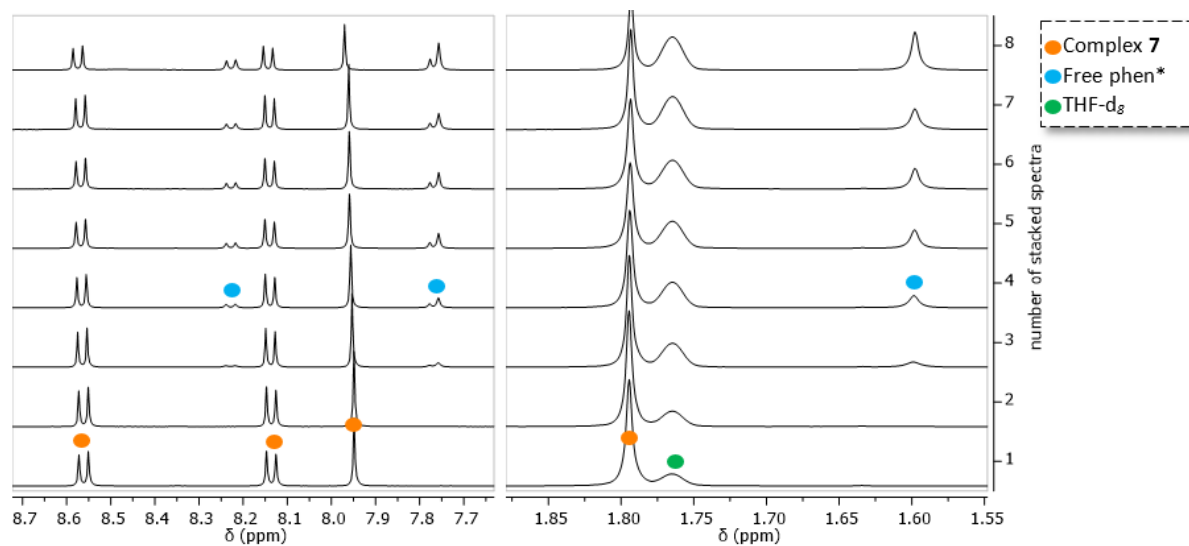


Figure S52. Zoom on Figure S51.

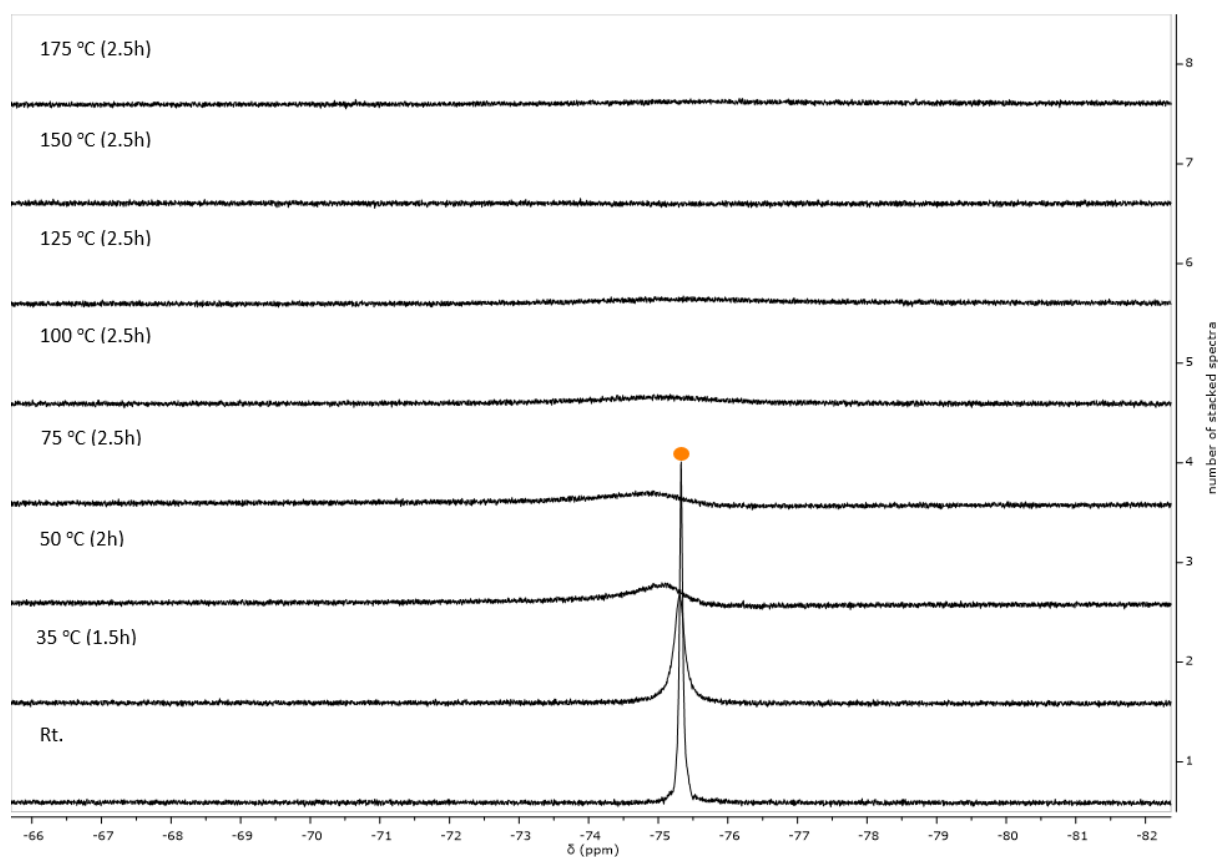


Figure S53. $^{19}\text{F}\{^1\text{H}\}$ NMR spectra of the thermal evolution of **7** in THF-d_8 .

II. 4. 2. Decarboxylation in quinoline:

a. Control experiment:

A clear colorless solution of $\text{C}_6\text{F}_5\text{CO}_2\text{H}$ (13 mg, 0.06 mol) in quinoline (5 mL) was heated from 35 °C to 100 °C for several hours. The reaction was monitored by ^{19}F NMR spectroscopy at certain time. At the end of the reaction (100 °C for 3.5 h), ^{19}F NMR spectra indicated full conversion of carboxylic acids to form pentafluorobenzene.

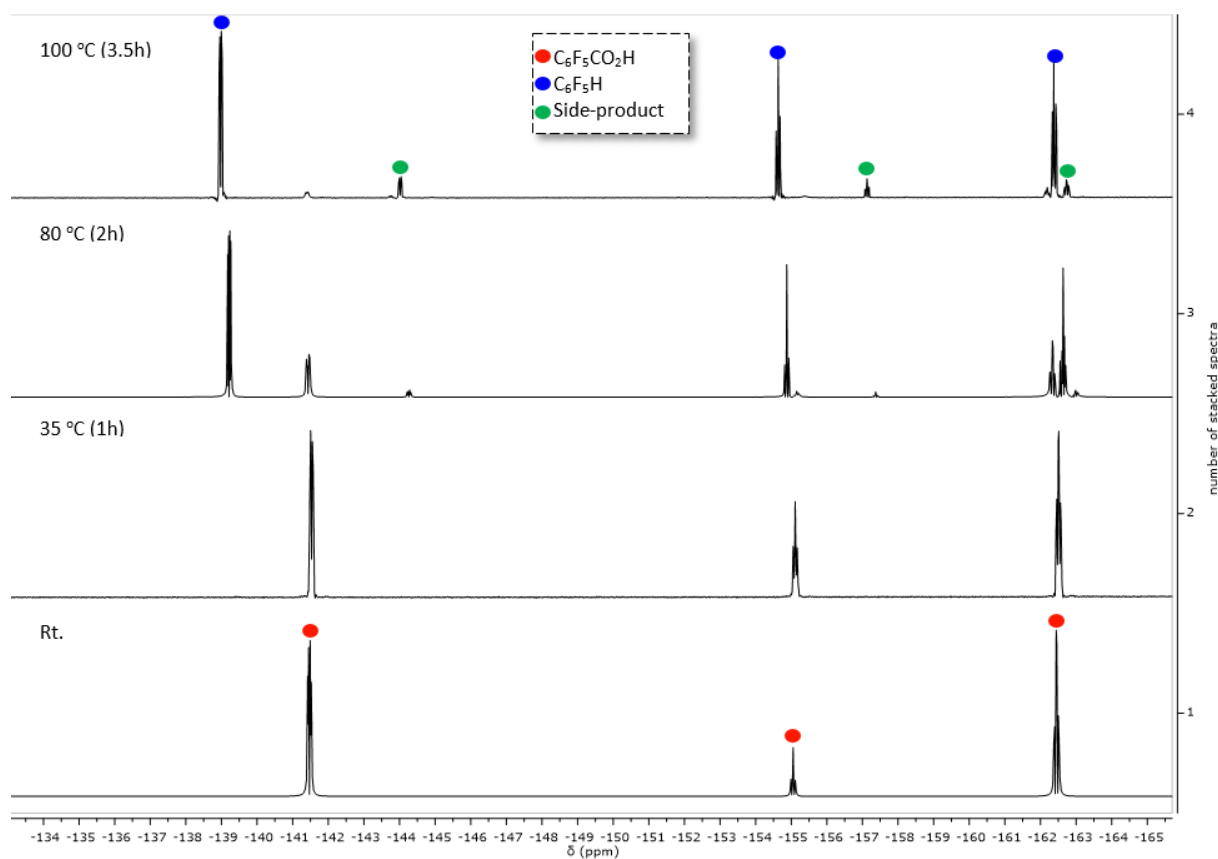


Figure S54. $^{19}\text{F}\{^1\text{H}\}$ NMR spectra of the thermal evolution of $\text{C}_6\text{F}_5\text{CO}_2\text{H}$ in quinoline.

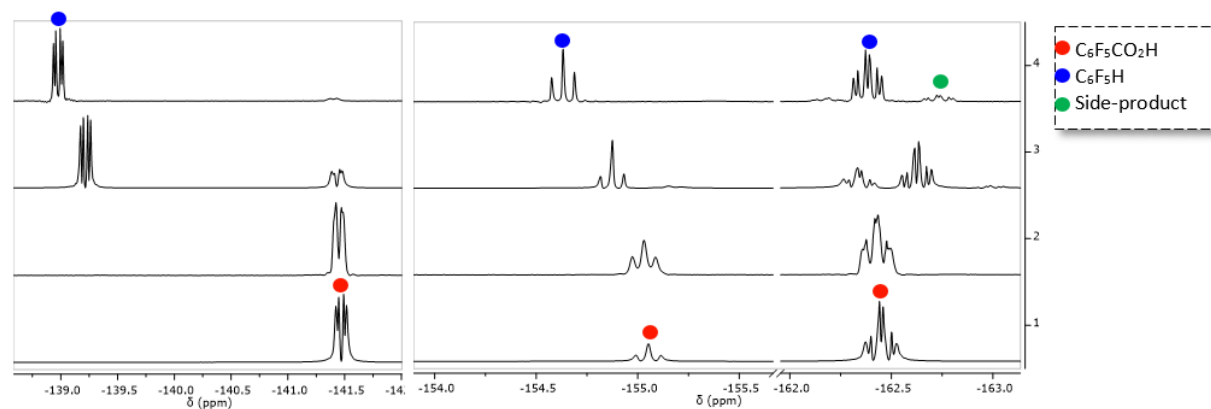


Figure S55. Zoom on Figure S54.

b. $[\text{Cu}(\text{C}_6\text{F}_5)(\text{quinoline})_n]$

In an NMR tube, $[\text{Cu}(\text{C}_6\text{F}_5)]_4$ (5 mg, 0.02 mmol) was solubilized in quinoline (5 mL, in excess) to obtain a clear yellow solution.

$^{19}\text{F}\{^1\text{H}\}$ NMR (377 MHz, $\text{THF}-d_8$, rt, δ/ppm): -112.03 , -164.15 , -164.46 .

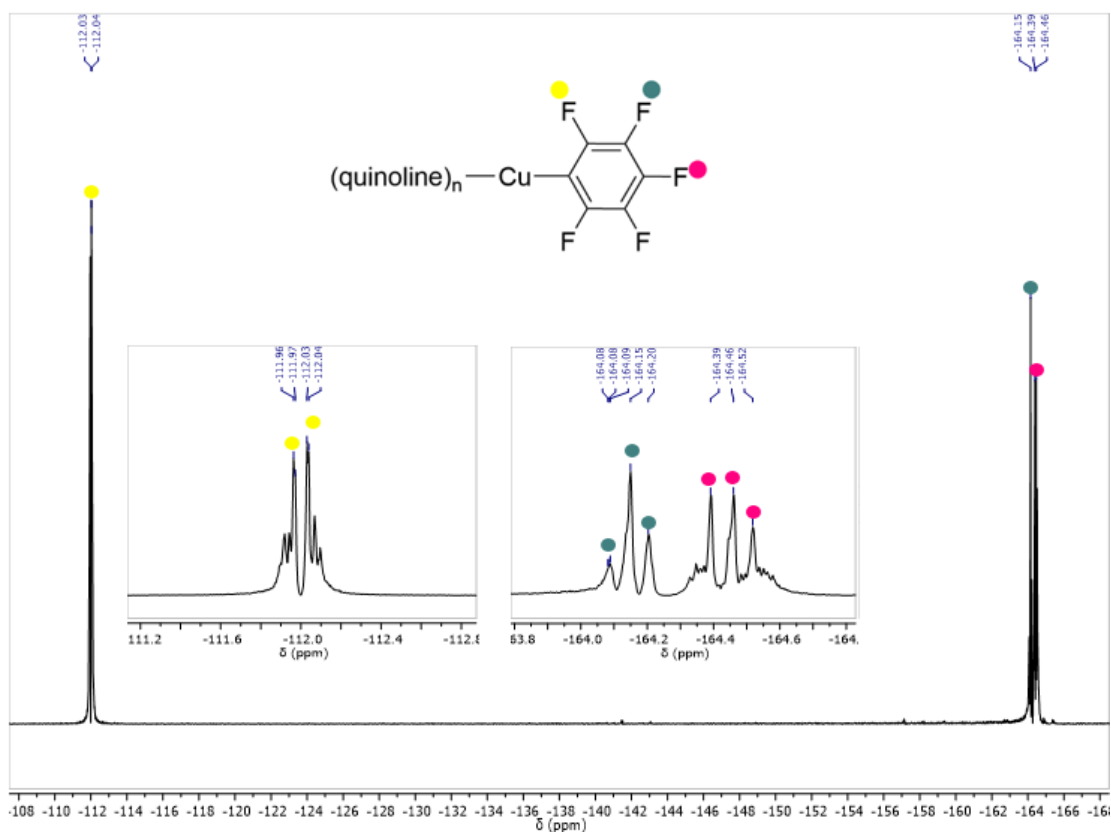


Figure S56. $^{19}\text{F}\{^1\text{H}\}$ NMR spectra of $[\text{Cu}(\text{C}_6\text{F}_5)]$ in quinoline.

c. Reaction of $[\text{Cu}(\text{C}_6\text{F}_5)(\text{quinoline})_n]$ and 1 equiv. phen:*

In an NMR tube, $[\text{Cu}(\text{C}_6\text{F}_5)]_4$ ($M = 731.387$ g/M for the tetramer, 5 mg, 5.7 μmol) was solubilized in quinoline (4 mL) to obtain a clear yellow solution. To this mixture was added phen* (1.7 mg, 5.7 μmol , 1 equiv *per* $\text{Cu}(\text{C}_6\text{F}_5)$ fragment) to result a clear yellow solution. Immediately after the addition, the solution mixture was analyzed by ^{19}F NMR. Two set of ^{19}F signals of $[(\text{phen}^*)\text{Cu}(\text{C}_6\text{F}_5)]$ and $\text{C}_6\text{F}_5\text{H}$ is detected.

$^{19}\text{F}\{^1\text{H}\}$ NMR (377 MHz, $\text{THF-}d_8$, rt, δ/ppm): $-109.45, -138.95, -154.62, -161.63, -161.94, -162.38$.

Note: The addition of phen* is not fully replace quinoline to form $[(\text{phen}^*)\text{Cu}(\text{C}_6\text{F}_5)]$ as the set of signals ($-109.45, -161.63, -161.94$) is different from what have been observed of complex **8** in $\text{THF-}d_8$ ($-111.59, -164.70, -168.83$).

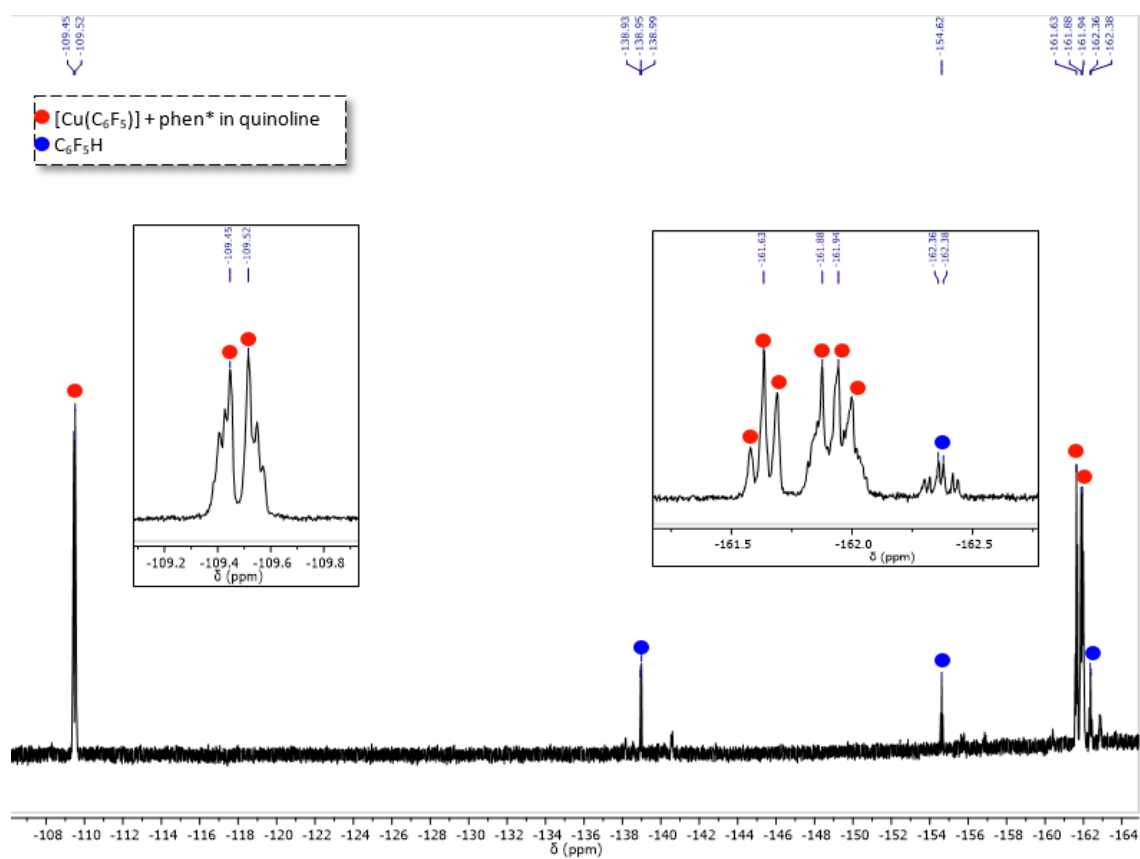


Figure S57. $^{19}\text{F}\{^1\text{H}\}$ NMR spectra of [Cu(C₆F₅)] and 1 equiv. phen* in quinoline.

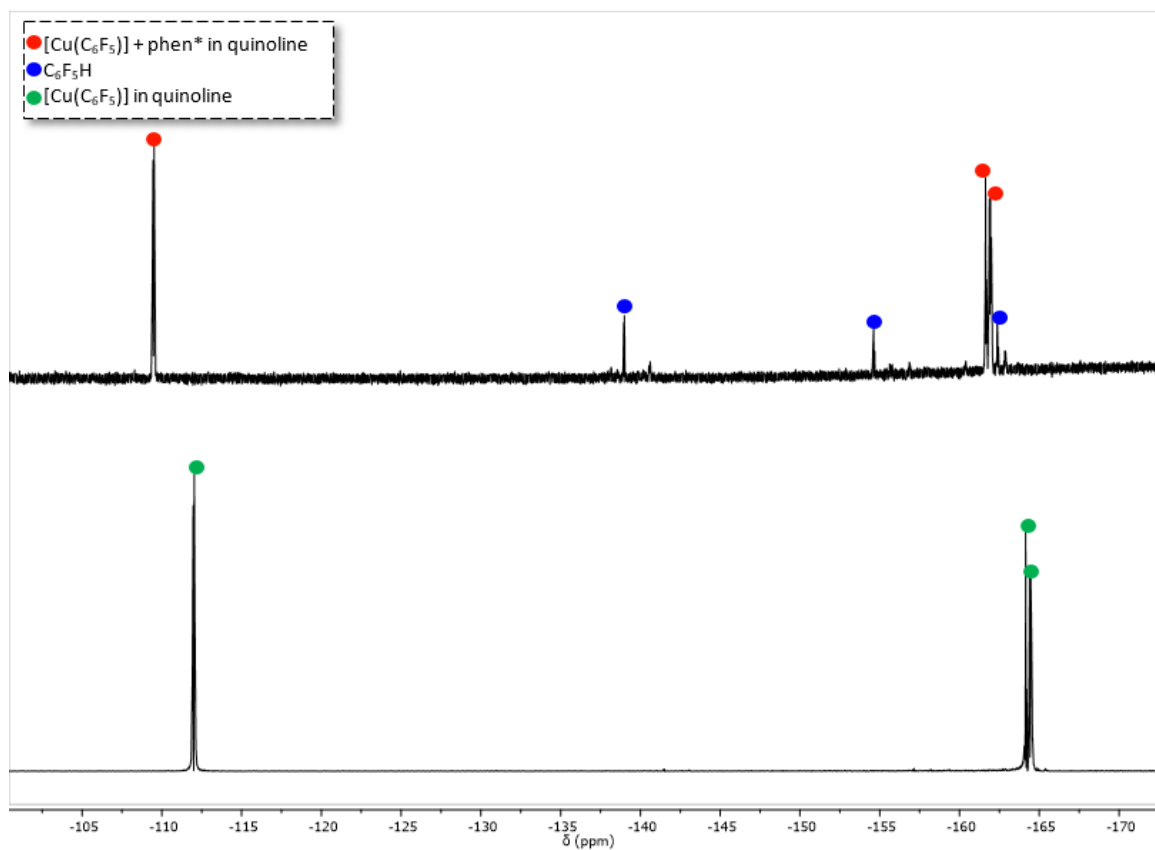


Figure S58. $^{19}\text{F}\{^1\text{H}\}$ NMR stacked spectra of: top: $[\text{Cu}(\text{C}_6\text{F}_5)]$ and 1 equiv. phen^* in quinoline; bottom: $[\text{Cu}(\text{C}_6\text{F}_5)]$ in quinoline.

d. Thermal decarboxylation of $[(\text{phen}^*)\text{Cu}(\text{O}_2\text{CC}_6\text{H}_4\text{-o-F})]$ (**2**) in quinoline

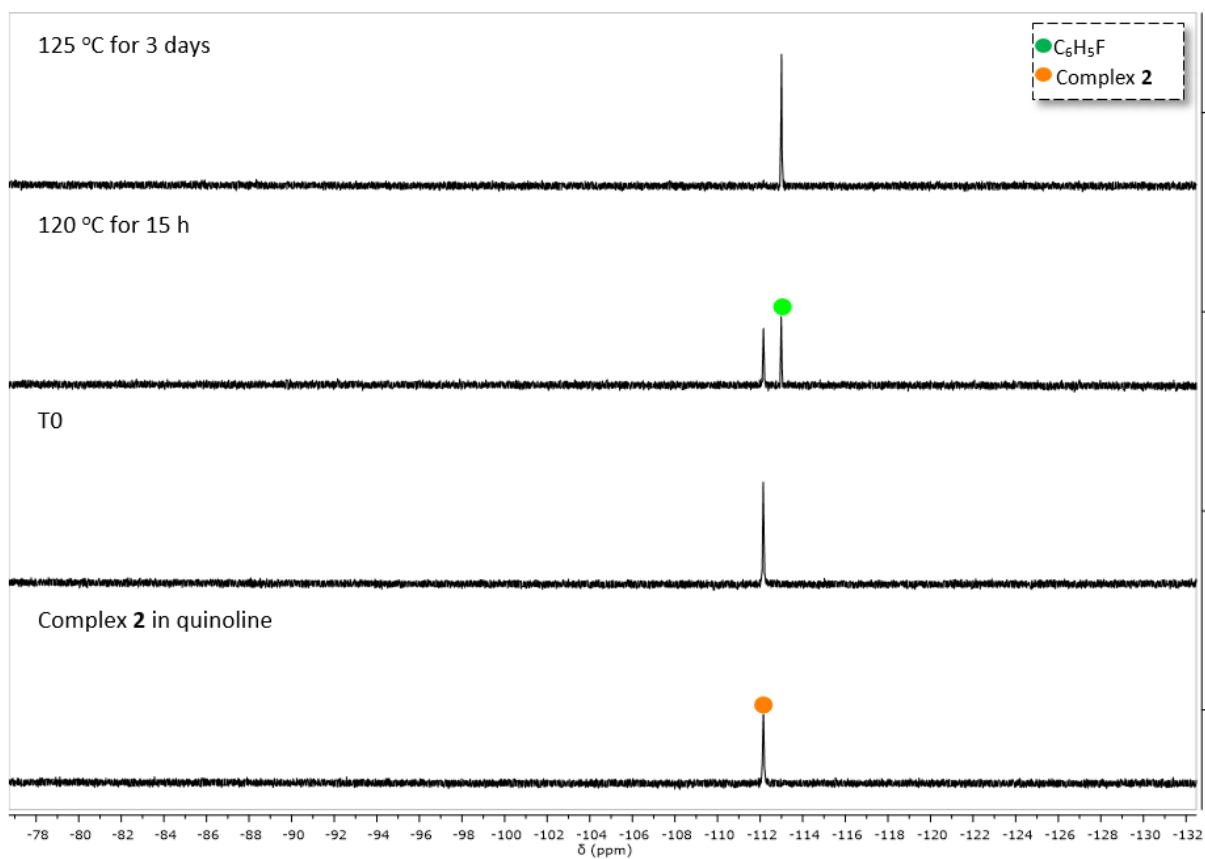


Figure S59. $^{19}\text{F}\{^1\text{H}\}$ NMR stacked spectra of the thermal evolution of complex **2** in quinoline.

e. Thermal decarboxylation of $[(\text{phen}^*)\text{Cu}(\text{O}_2\text{CC}_6\text{F}_5)]$ (**4**) in quinoline

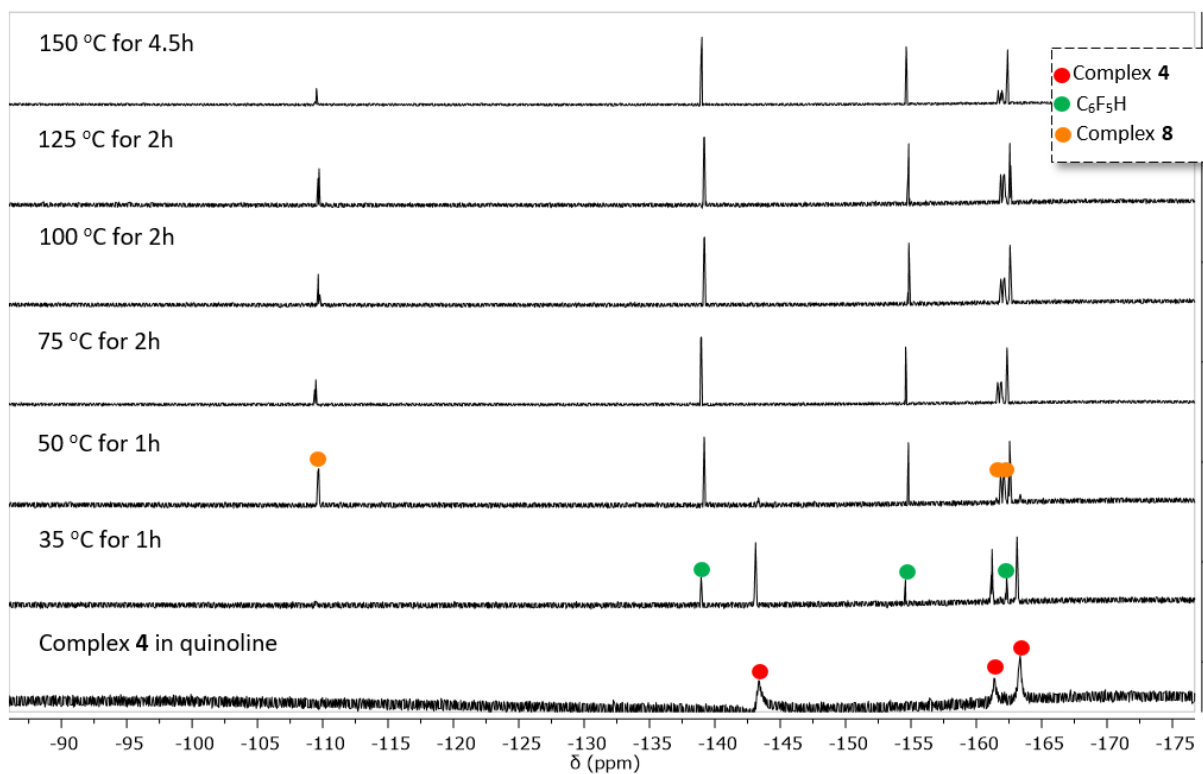


Figure S60. $^{19}\text{F}\{^1\text{H}\}$ NMR stacked spectra of the thermal evolution of complex **4** in quinoline.

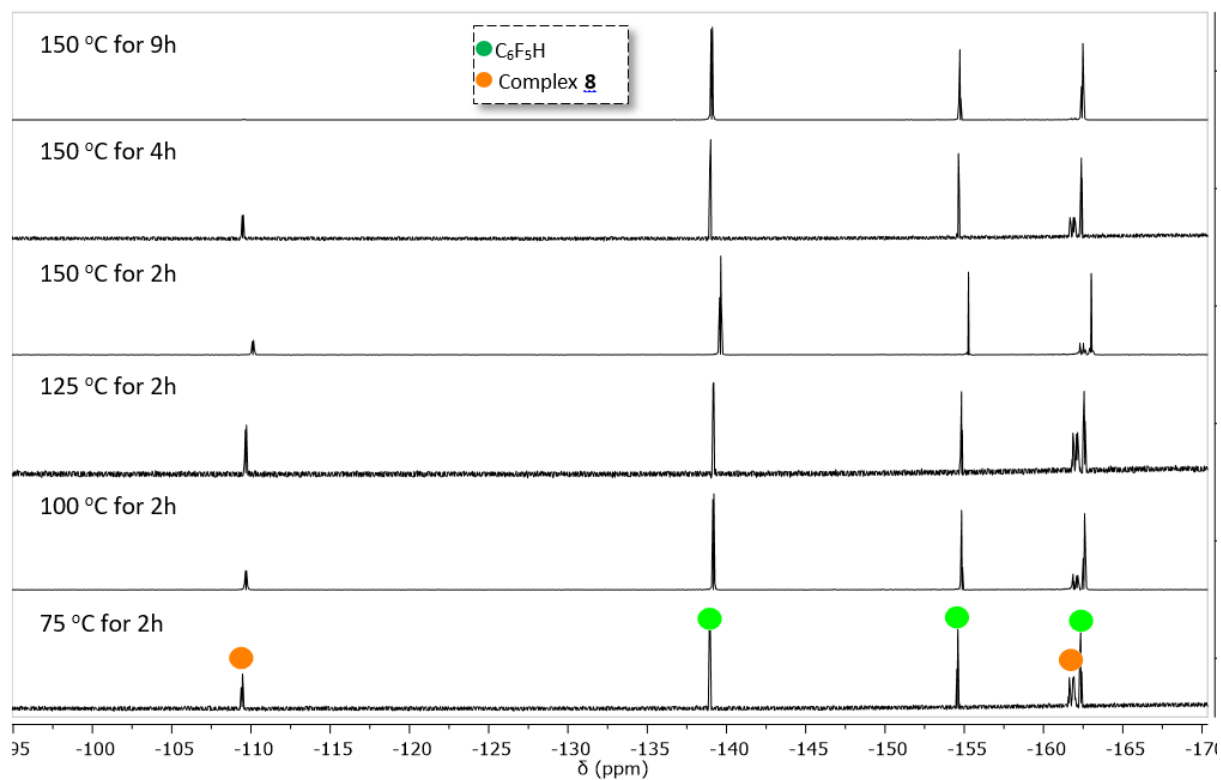


Figure S61. Continue of Figure S60: $^{19}\text{F}\{^1\text{H}\}$ NMR stacked spectra of the thermal evolution of complex **4** in quinoline: after 2 h at 75 °C **4** has been totally transformed into $[(\text{phen}^*)\text{Cu}(\text{C}_6\text{F}_5)]$ (**8**) and $\text{C}_6\text{F}_5\text{H}$.

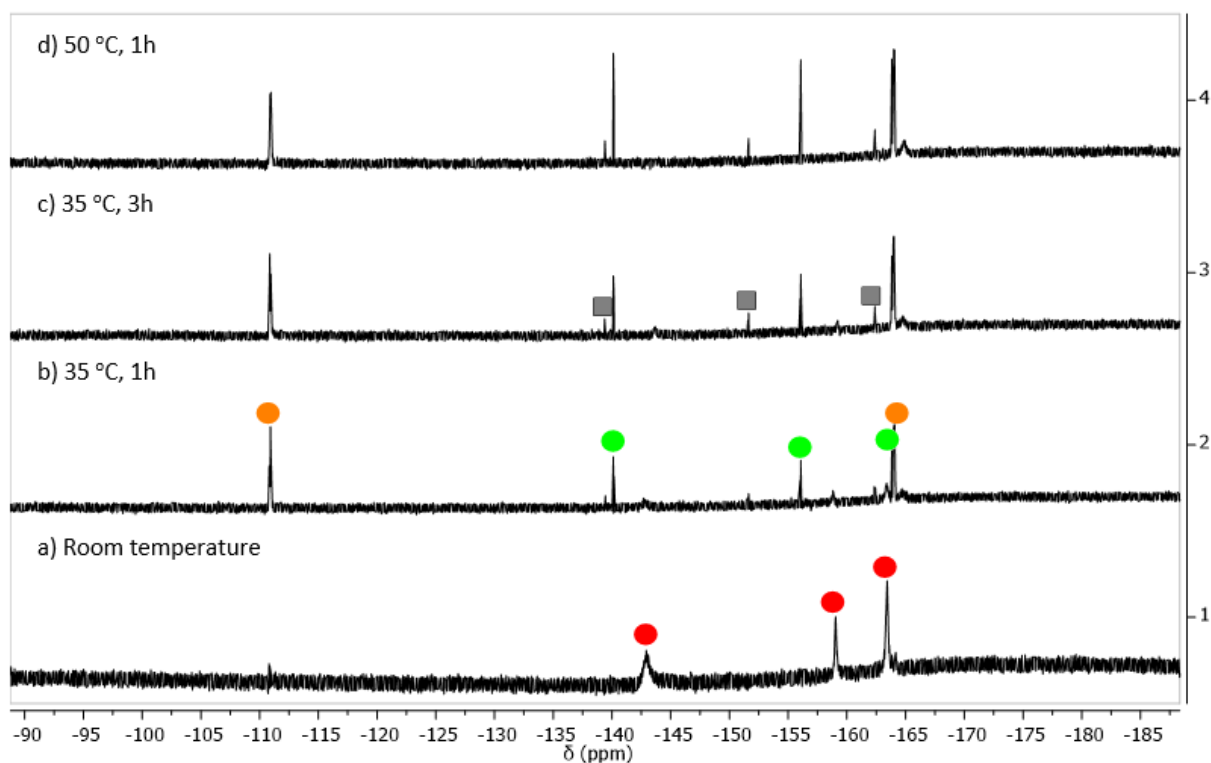


Figure S62. $^{19}\text{F}\{^1\text{H}\}$ NMR stacked spectra of the thermal evolution of **4** in DMF-d_7 and evidence for the generation of $[(\text{phen}^*)\text{Cu}(\text{C}_6\text{F}_5)(\text{DMF})_n]$ and $\text{C}_6\text{F}_5\text{H}$. Red circle: $[(\text{phen}^*)\text{Cu}(\text{O}_2\text{CC}_6\text{F}_5)]$ (**4**), green circle: $\text{C}_6\text{F}_5\text{H}$, orange circle: $[(\text{phen}^*)\text{Cu}(\text{C}_6\text{F}_5)]$, gray square: unidentified byproducts.

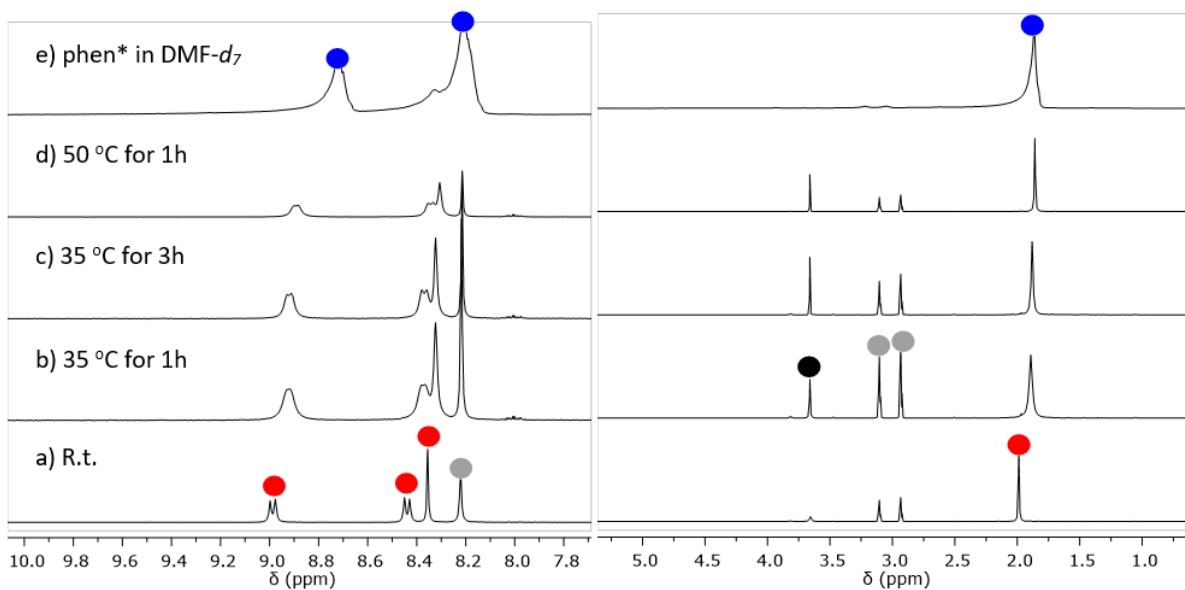


Figure S63. Zoom on ^1H NMR stacked spectra of the thermal evolution of **4** in DMF-d_7 and evidence for the generation of $[(\text{phen}^*)\text{Cu}(\text{C}_6\text{F}_5)(\text{DMF})_n]$ and $\text{C}_6\text{F}_5\text{H}$. Red circle: $[(\text{phen}^*)\text{Cu}(\text{O}_2\text{CC}_6\text{F}_5)]$ (**4**), orange circle: $[(\text{phen}^*)\text{Cu}(\text{C}_6\text{F}_5)(\text{DMF})_n]$, gray circle: DMF-d_7 , black circle: unidentified species.

g. Thermal decarboxylation of $[(\text{phen}^*)\text{Cu}(\text{O}_2\text{CCF}_3)]$ (**11**) in quinoline

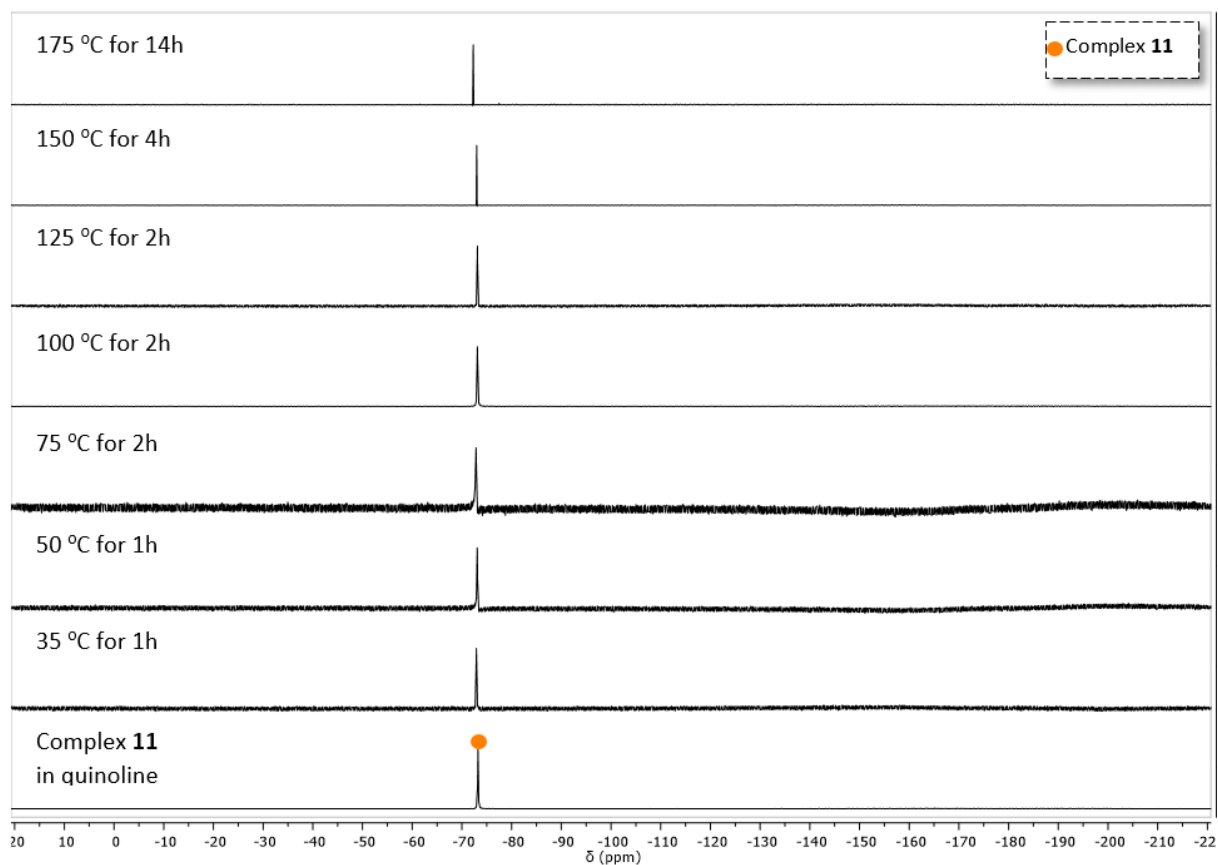
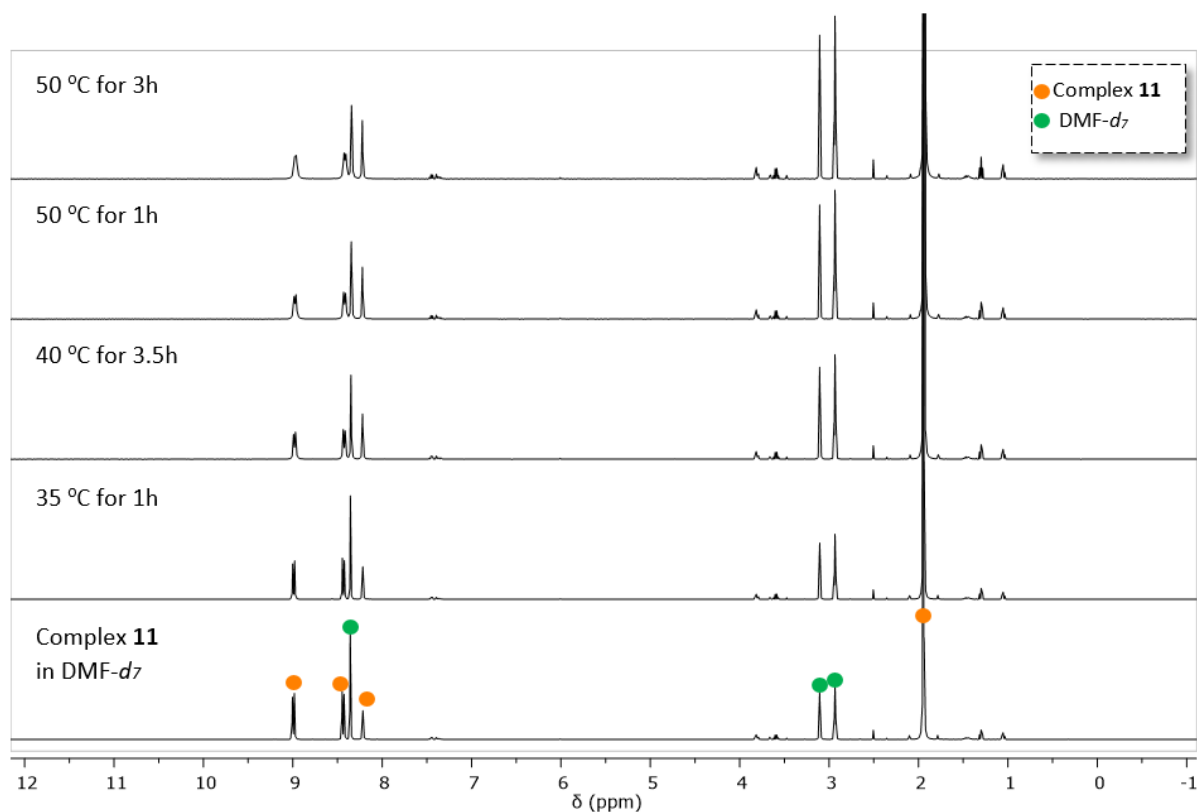


Figure S64. $^{19}\text{F}\{^1\text{H}\}$ NMR stacked spectra of the thermal evolution of complex **11** in quinoline.

h. Thermal decarboxylation of $[(\text{phen}^*)\text{Cu}(\text{O}_2\text{CCF}_3)]$ (**11**) in DMF-d_7 Figure S65. ^1H NMR stacked spectra of the thermal evolution of complex **11** in DMF-d_7

Note: Complex **11** remained stable in NMP solvent as observed in quinoline.

II. 5. Carboxylation of the $[(\text{phen}^*)\text{Cu-R}]$ complexes **8**, **9**, and **11**II. 5. 1. Carboxylation of $[(\text{phen}^*)\text{Cu}(\text{C}_6\text{F}_5)]$ (**8**)

In a NMR tube (Young or New Era depending on the pressure of CO_2), complex **8** was dissolved in the tested solvent (quinoline or THF-d_8 , or DMA) to result a clear yellow solution. The mixture then was added CO_2 (10 bar). For all the experiment, no immediate change of solution color is noted after the addition of CO_2 gas. The resulted mixture was then followed at certain reaction times by ^1H NMR and/or $^{19}\text{F}\{^1\text{H}\}$ NMR.

a. Carboxylation of $[(phen^*)Cu(C_6F_5)]$ (**8**) in DMA

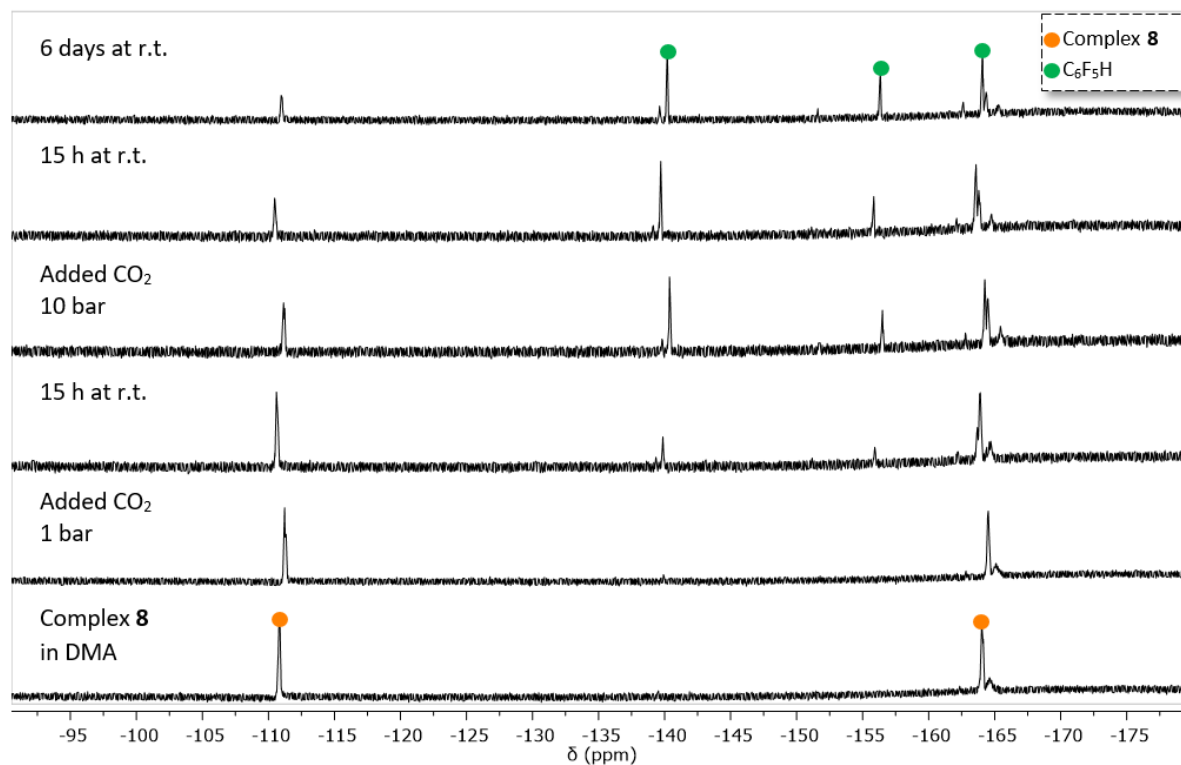


Figure S66. $^{19}F\{^1H\}$ NMR stacked spectra of thermal evolution of complex **8** in DMA with 10 bar of CO_2 .

b. Carboxylation of $[(phen^*)Cu(C_6F_5)]$ (**8**) in quinoline

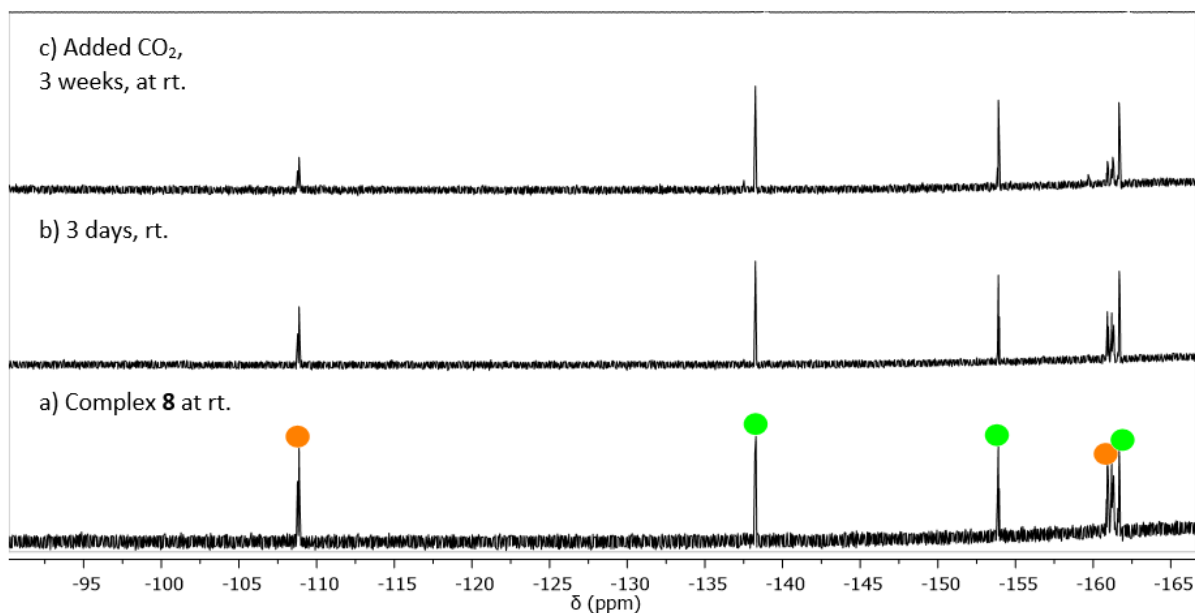


Figure S67. $^{19}F\{^1H\}$ NMR stacked spectra of the thermal evolution of complex **8** in quinoline with 10 bar of CO_2 and evidence for the generation of C_6F_5H . Green circle: C_6F_5H , orange circle: $[(phen^*)Cu(C_6F_5)]$.

c. Carboxylation of $[(phen^*)Cu(C_6F_5)]$ (**8**) in THF- d_8

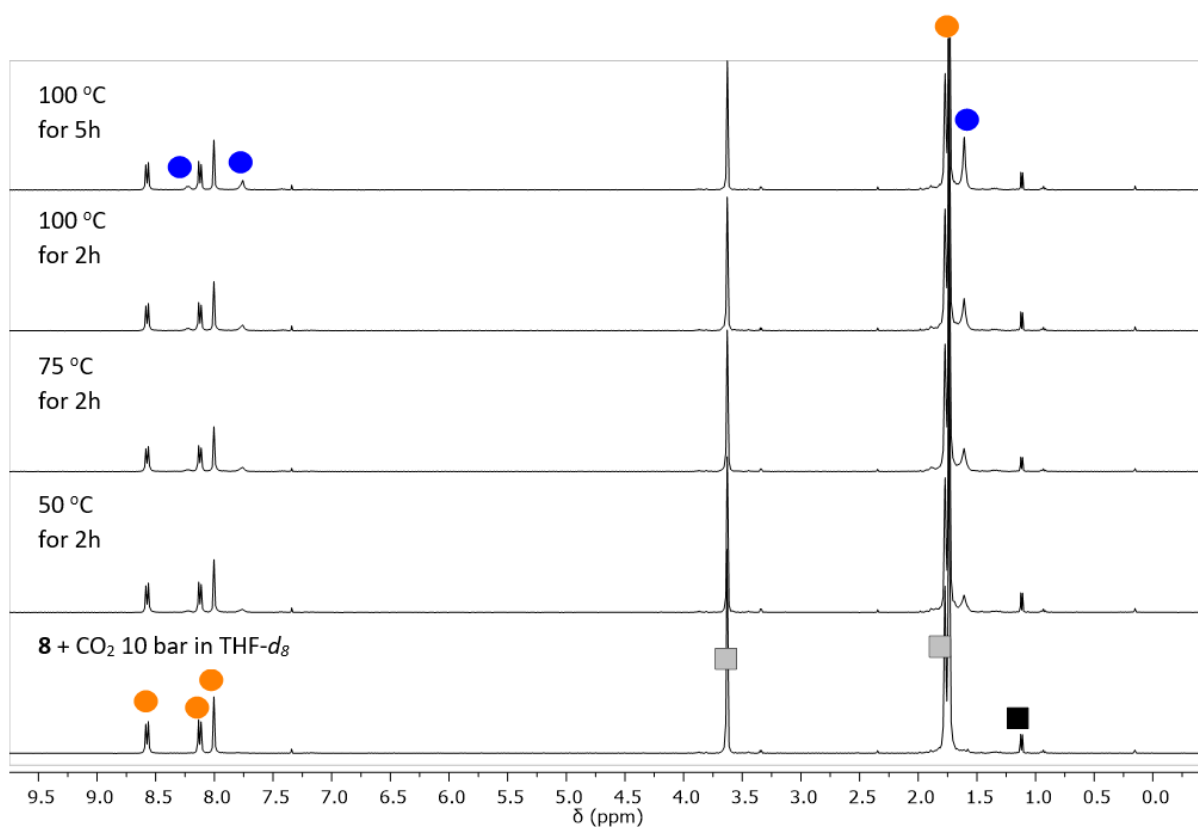


Figure S68. 1H NMR stacked spectra of the thermal evolution of complex **8** in THF- d_8 with 10 bar of CO_2 and the release of C_6F_5H . Orange circle: $[(phen^*)Cu(C_6F_5)]$ (**8**), blue circle: free phen*, gray square: THF- d_8 , black square: impurities.

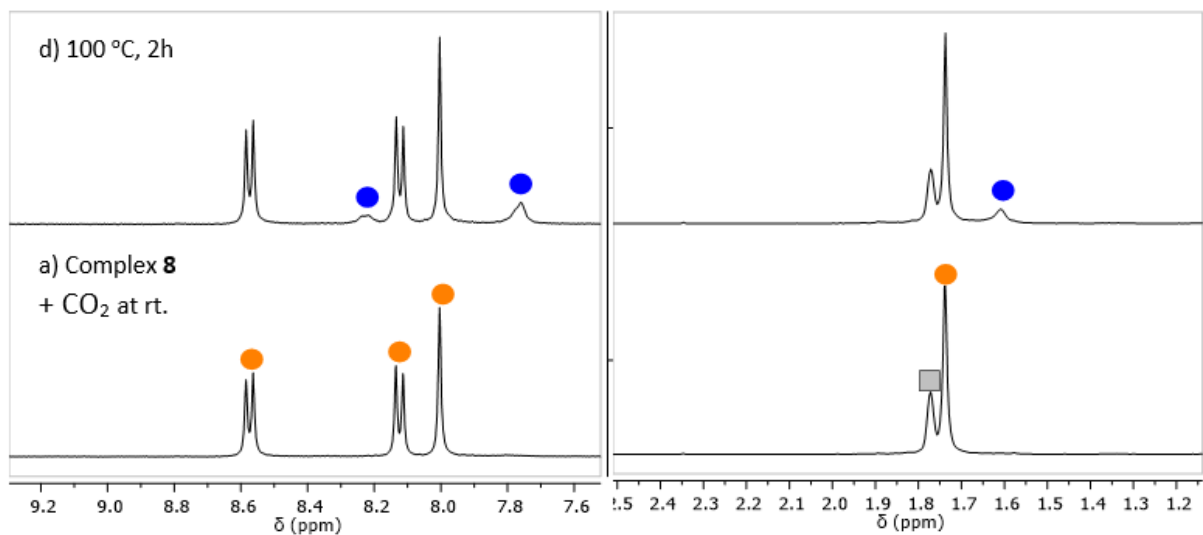


Figure S69. Zoom on 1H NMR stacked spectra of the thermal evolution of complex **8** in THF- d_8 and the release of free phen*. Orange circle: $[(phen^*)Cu(C_6F_5)]$, blue circle: free phen*, gray square: THF- d_8 .

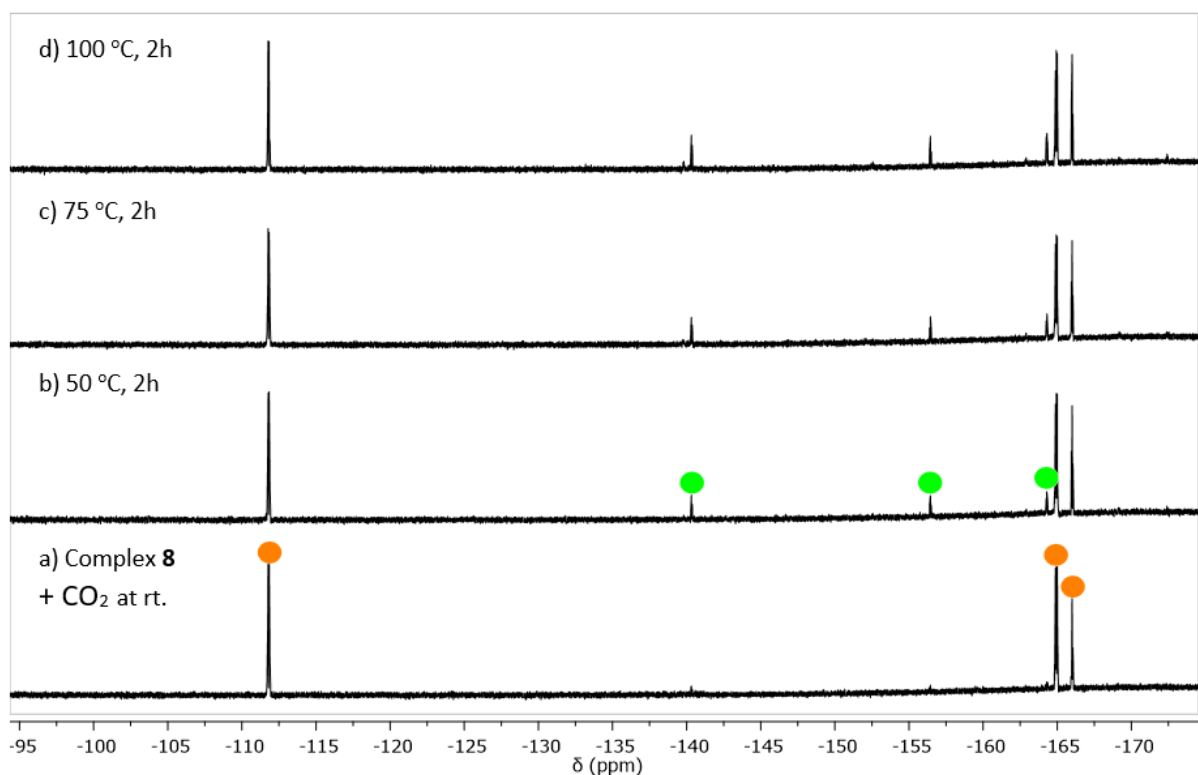


Figure S70. $^{19}\text{F}\{^1\text{H}\}$ NMR stacked spectra of the thermal evolution of complex **8** in THF-d_8 with 10 bar of CO_2 and the release of $\text{C}_6\text{F}_5\text{H}$. Green circle: $\text{C}_6\text{F}_5\text{H}$, orange circle: $[(\text{phen}^*)\text{Cu}(\text{C}_6\text{F}_5)]$.

II. 5. 2. Carboxylation of $[(\text{phen}^*)\text{Cu}(\text{C}_6\text{H}_4\text{-o-NO}_2)]$ (**9**)

In a NMR tube (Young or New Era depending on the pressure of CO_2), complex **9** was dissolved in the tested solvent (C_6D_6 or Toluene- d_8 , or DMA) to result a clear dark-red solution and remained undissolved solid (complex **9** is partially soluble in those tested solvents). The mixture then was added CO_2 (10 bar) or $^{13}\text{CO}_2$ (4 bar). For all the experiment, no immediate change of solution color is noted after the addition of CO_2 gas. The resulted mixture was then heated at indicated time and temperature. The reaction was followed by ^1H NMR and $^{13}\text{C}\{^1\text{H}\}$ NMR.

a. Carboxylation of $[(phen^*)Cu(C_6H_4-o-NO_2)]$ (**9**) in $C_6H_6-d_6$

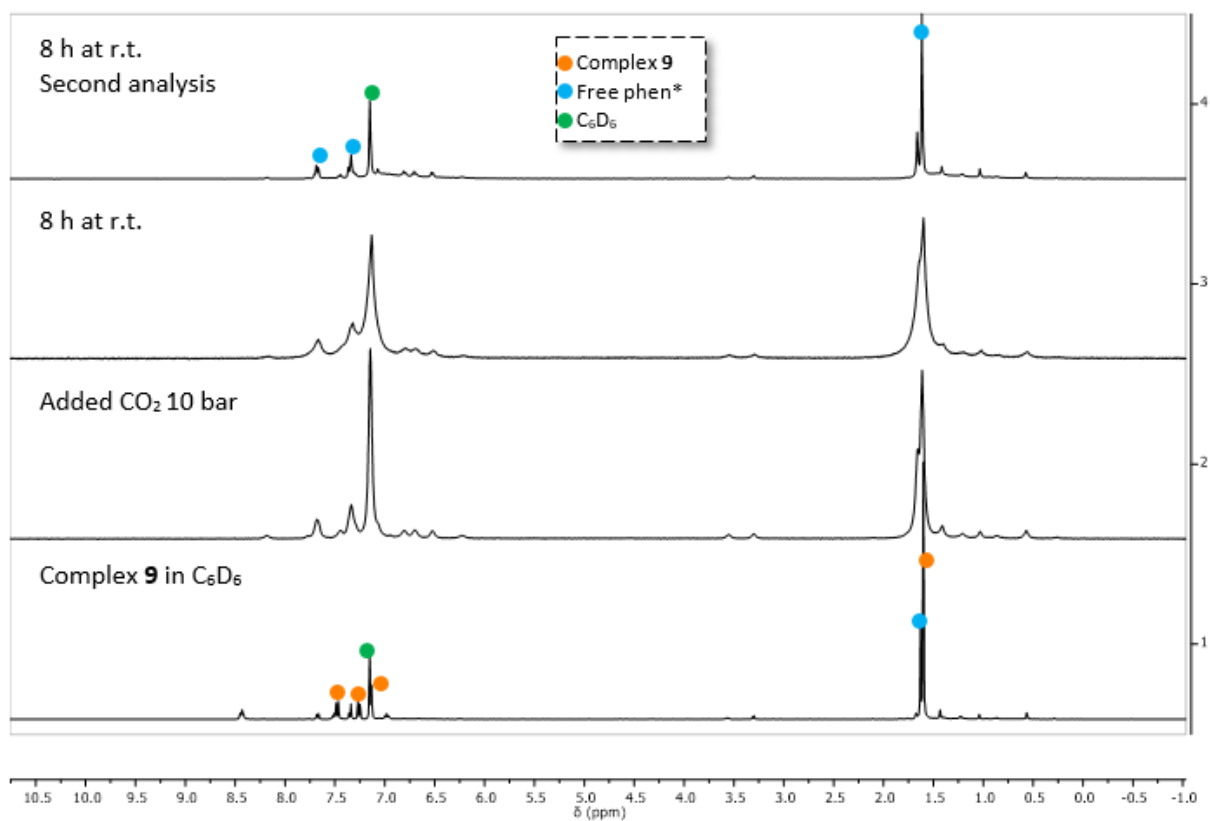


Figure S71. 1H NMR stacked spectra of the thermal evolution of complex **9** in $C_6H_6-d_6$ with 10 bar of CO_2 .

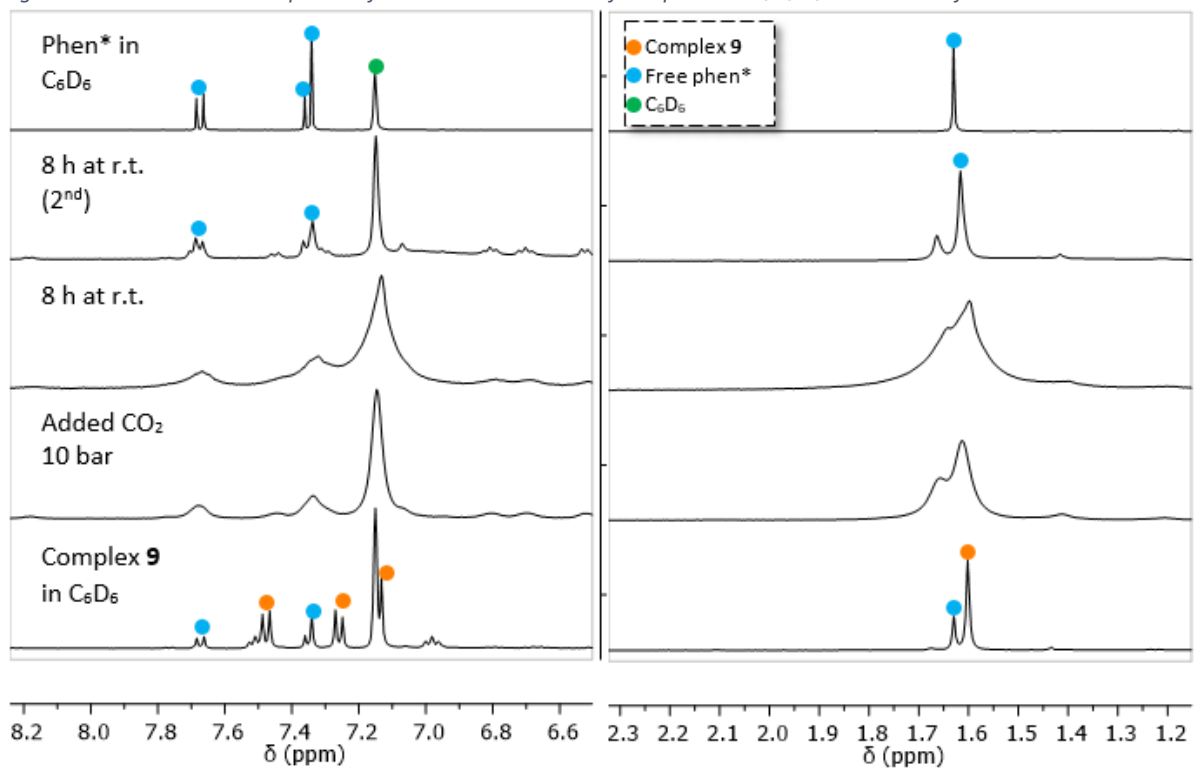


Figure S72. Zoom of 1H NMR stacked spectra of the thermal evolution of complex **9** in $C_6H_6-d_6$ with 10 bar of CO_2 .

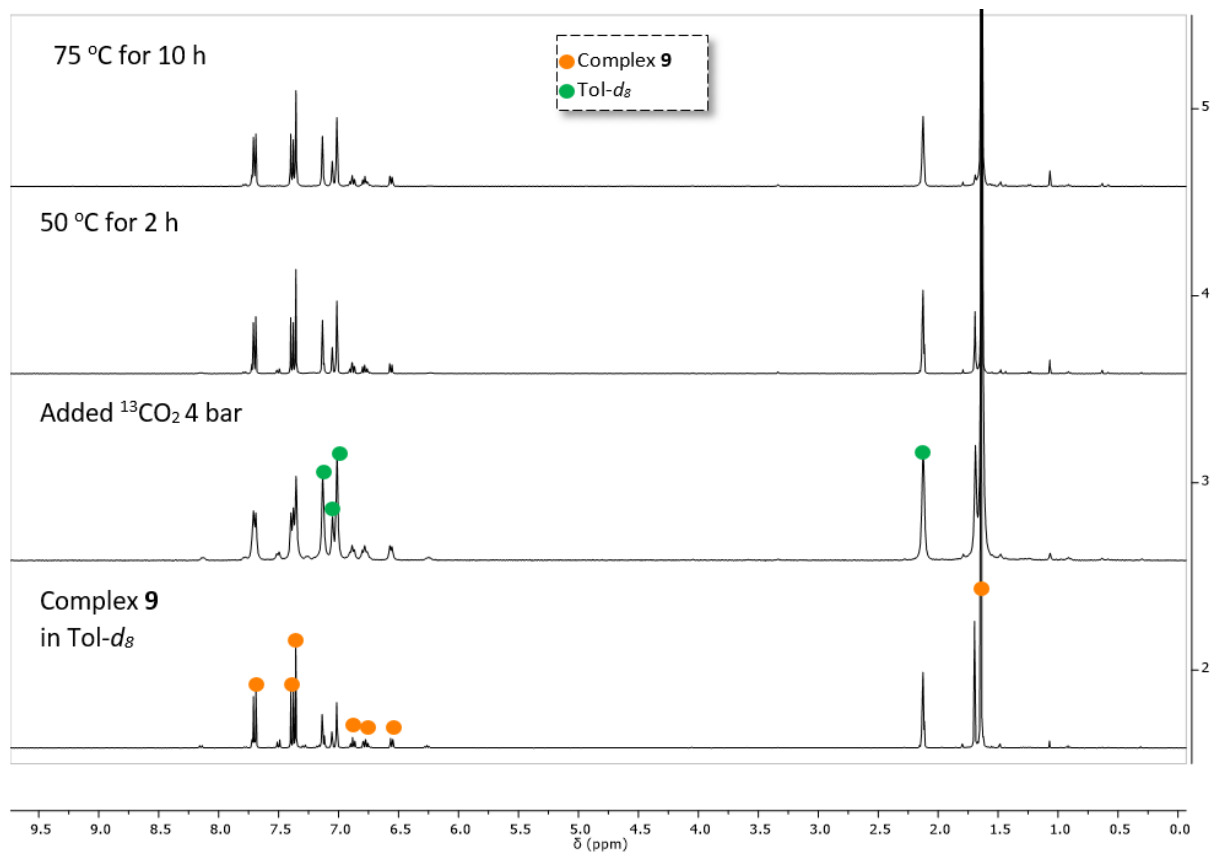
b. Carboxylation of $[(phen^*)Cu(o-NO_2-C_6H_4)]$ (**9**) in Tol- d_8 

Figure S73. 1H NMR stacked spectra of the thermal evolution of complex **9** in Tol- d_8 with 4 bar of $^{13}CO_2$.

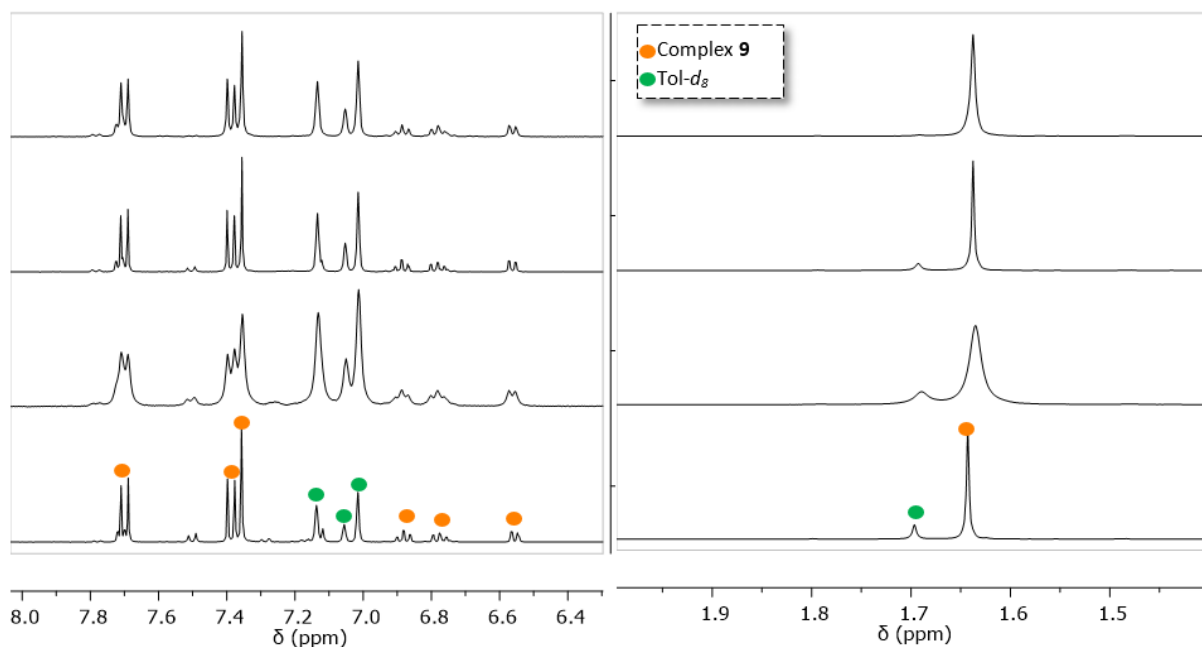


Figure S74. Zoom on 1H NMR stacked spectra of the thermal evolution of complex **9** in Tol- d_8 with 4 bar of $^{13}CO_2$.

Note: Carboxylation of complex **9** in 4 bar of $^{13}CO_2$ in DMA cannot be followed by 1H NMR since the signal of DMA solvent are too high. ^{13}C NMR gave as well only signals of DMA solvent and $^{13}CO_2$.

Decomposition of complex **9** is observed by the change of solution color from clear dark-red to clear orange with black solid after heating at 50 °C for 4h and subsequent heating at 75 °C for 10 h.

II. 5. 3. Carboxylation of $[(\text{phen}^*)\text{Cu}(\text{CF}_3)]$ (**11**) in DMA

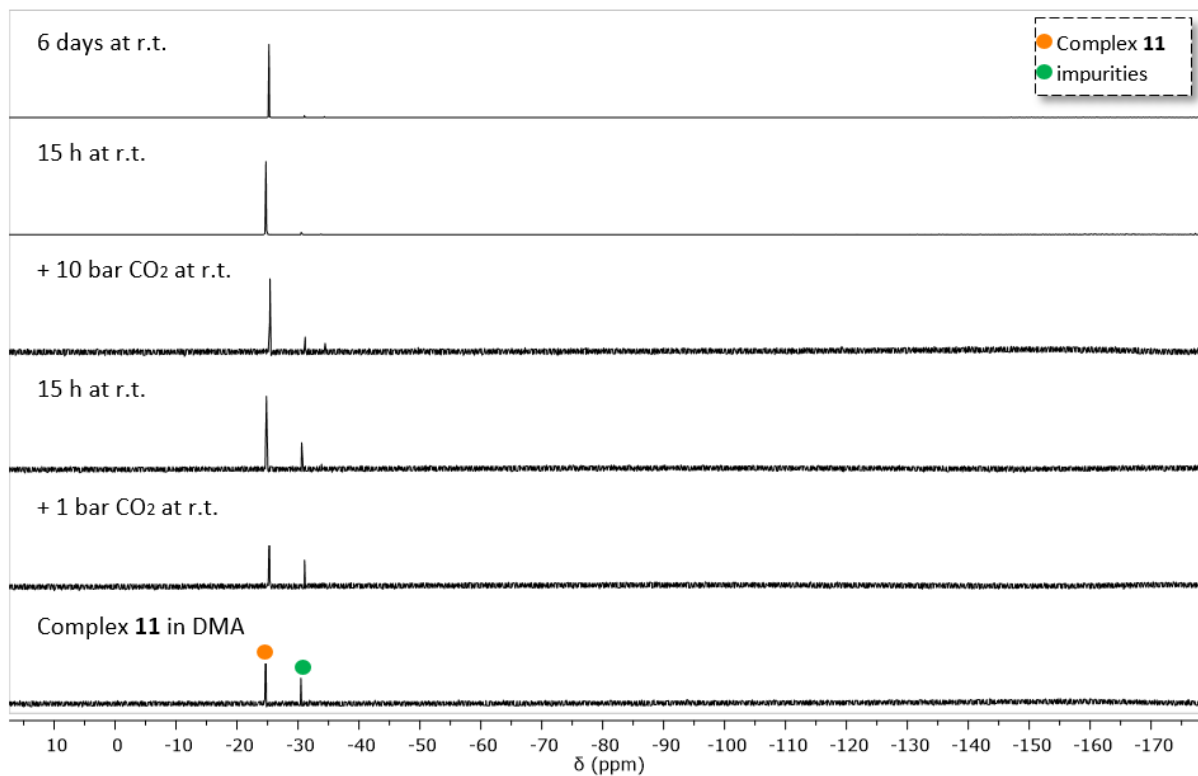


Figure S75. $^{19}\text{F}\{^1\text{H}\}$ NMR stacked spectra of the thermal evolution of complex **11** in DMA with 10 bar of CO_2 .

II. 5. 4. Carboxylation of [(phen*)Cu(CF₃)] (**11**) in THF-*d*₈

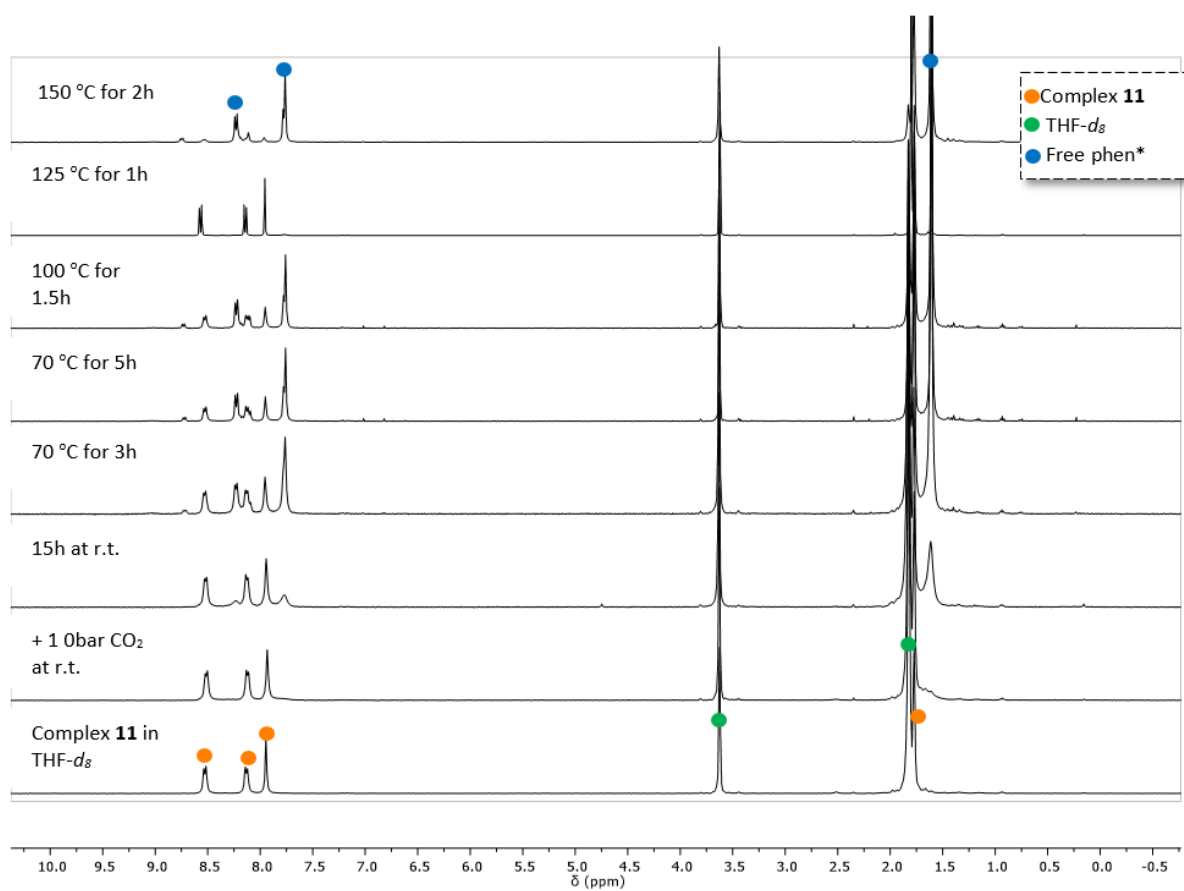


Figure S76. ¹H NMR stacked spectra of the thermal evolution of complex **11** in THF-*d*₈ with 10 bar of CO₂.

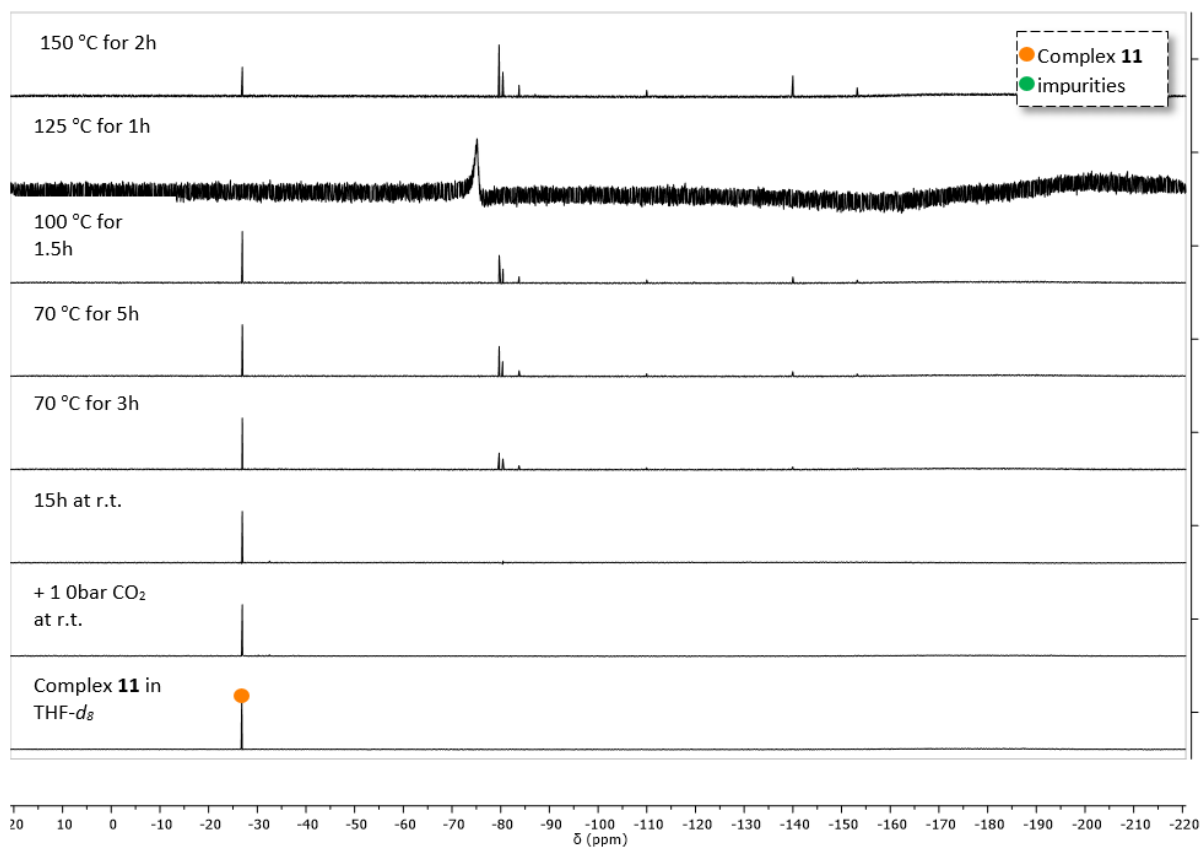


Figure S77. $^{19}\text{F}\{^1\text{H}\}$ NMR stacked spectra of the thermal evolution of complex **11** in $\text{THF-}d_8$ with 10 bar of CO_2 .

Note: Similar in the case using THF as solvent, free ligand and formation of impurities are observed using $\text{C}_6\text{H}_6-*d*_6$ as solvent.

III. Experimental part of Chapter 3

III. 1. Synthesis of [(phen*)Cu(κ^1 -O₂CH)] (**12**) (Formula : C₂₁H₂₅CuN₂O₂, M= 400.99 g/mol)

To a light yellow solution of **12** (180.7 mg, 0.62 mmol) in THF (20 mL) was added 1 equiv. Cu(O^tBu) (84.5 mg, 0.62 mmol). The resulted clear light brown mixture was stirred at room temperature for *ca* 1 h. Then, formic acid (27.6 μ L, 0.62 mmol) was added to result an immediate change of solution color from light brown to clear red. The mixture was stirred for another hour at room temperature. The solvent was then evaporated off under vacuum to afford dark-orange solid, which was washed with pentane (10 mL x 3) and dried under vacuum overnight to yield pure **12** as a dark-orange solid (220.9 mg, 89 %). Compound **12** always retained traces of acid that could not be eliminated by prolonged drying (15 h) under vacuum.

Orange crystals of [(phen*)Cu(κ^1 -O₂CH)_{0.8}l_{0.2}].(THF)_{0.5} (**12'**) were obtained by slow diffusion of pentane to a THF solution containing 10 mg Cu(O^tBu), phen* (1 equiv.) and formic acid (1 equiv.). The iodine atom presence in the crystal likely results from residual KI impurity contained in starting [Cu(O^tBu)], the latter being synthesized from treatment of CuI with KO^tBu. Elemental analysis for the dried crystals C₂₀H₂₄CuN₂(HCO₂)_{0.8}l_{0.2}, (M = 417.37 g/mol), found (theoretical) %: C, 59.43 (59.86); H, 6.02 (5.99); N, 6.92 (6.71).

¹H NMR 400 MHz, THF-*d*₈, δ /ppm): 11.55 (s, HCO₂H), 8.38 (d, *J* = 8.5 Hz, 2H), 8.17 (s, *W*_{1/2} = 16 Hz, 1H, CuO₂CH + HCO₂H), 7.93 (d, *J* = 8.5 Hz, 2H), 7.82 (s, 2H), 1.76 (s, ^tBu, 18H).

¹³C{¹H} NMR (101 MHz, THF-*d*₈, δ /ppm): 168.86, 144.20, 137.58, 127.08, 125.45, 120.95, 120.91, 38.32, 30.03. (carbon of CO₂H cannot be seen)

IR data (ν cm⁻¹) : 2962 (w), 2783 (w), 2696 (w), 1620 (s, CO₂), 1612 (m), 1583 (w), 1550 (m), 1496 (s), 1477 (w), 1415 (w), 1392 (w), 1363 (m), 1327 (s), 1209 (w), 1136 (s), 923 (w), 860 (s), 754 (s), 650 (w), 615 (m).

Elemental analysis for C₂₁H₂₅CuN₂O₂, (M= 400.99 g/mol), found (theoretical) %: C, 62.43 (62.90); H, 6.02 (6.28); N, 6.92 (6.99).

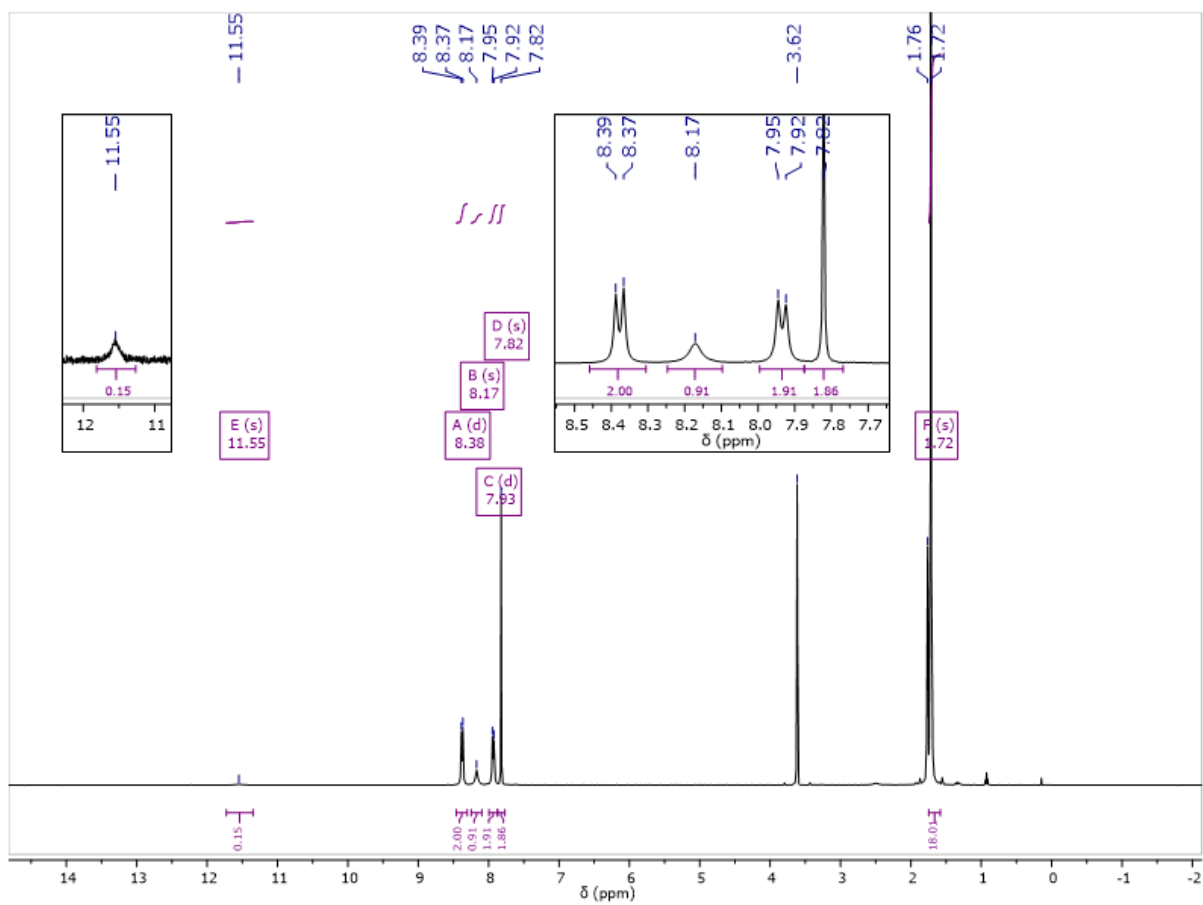


Figure S78: ^1H NMR spectrum of **12** in $\text{THF-}d_8$.

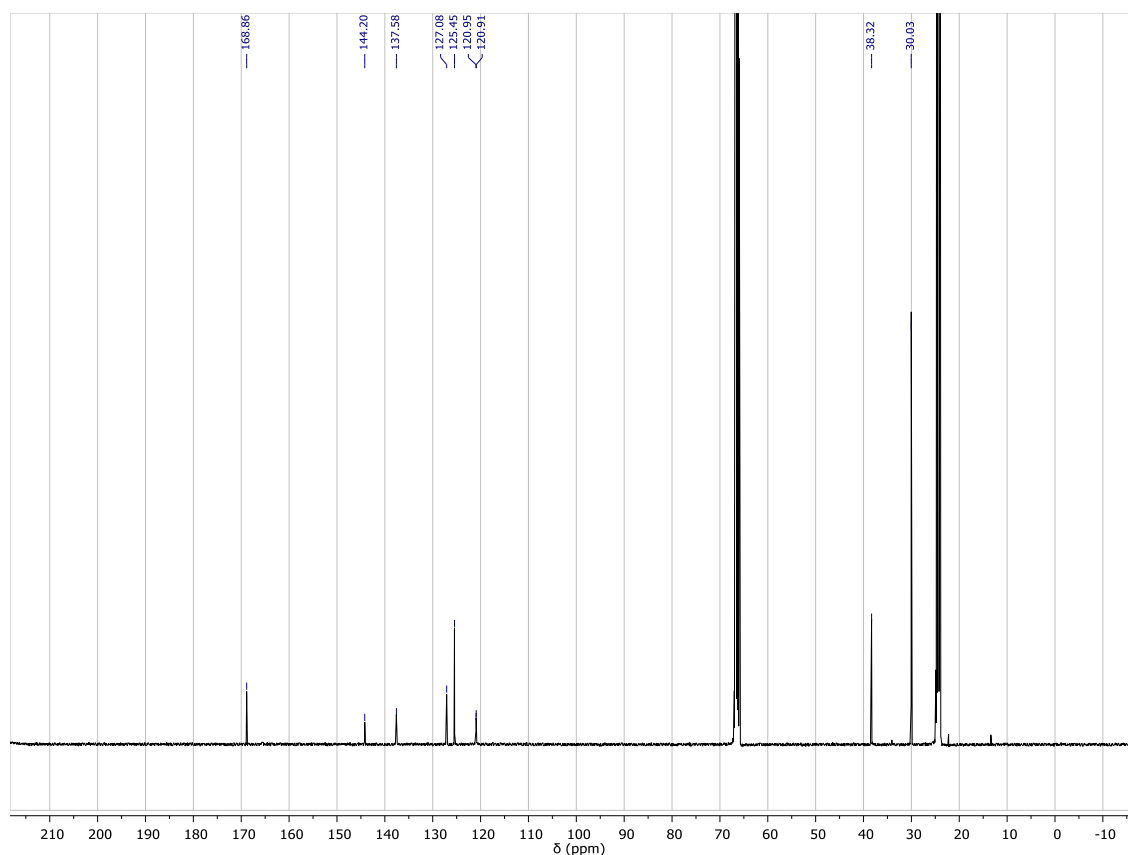


Figure S79: $^{13}\text{C}\{^1\text{H}\}$ NMR spectrum of **12** in $\text{THF-}d_8$.

III. 2. $[(\text{phen}^*)\text{Cu}(\text{O}_2\text{CH})]$ in $\text{THF-}d_8$ at low temperatures.

10 mg of the orange solid of the complex $[(\text{phen}^*)\text{Cu}(\text{O}_2\text{CH})]\cdot(\text{HCO}_2\text{H})_{0.3}$, prepared in-situ in an NMR tube, was solubilized in 0.5 mL $\text{THF-}d_8$. At 298 K, traces of HCOOH (ca. 30 % compared to **12**) can be detected with the acidic proton of FA at 12.28 ppm (Figure S80). The clear orange-red solution was then analyzed by ^1H NMR at different temperatures from 25 °C (298 K) to –63 °C (210 K) (Figure S81 and zoom in Figure S82).

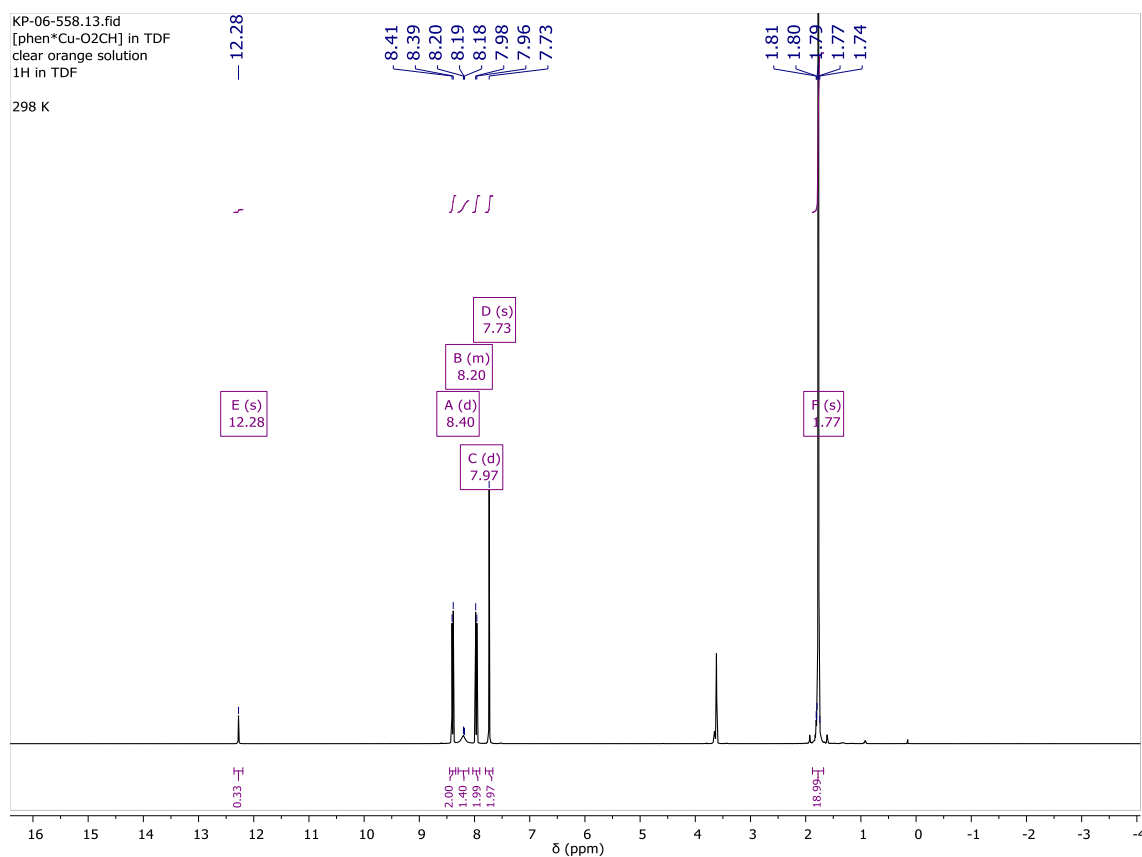


Figure S80. ^1H NMR spectrum of **12** in THF-d_3 at 298 K.

In the spectrum of *Figure S81* and *Figure S82*, the ^1H NMR signal of the *formate* groups (of **12** and the acid) appears as a broad singlet at $\delta = 8.20$ at 298 K. By decreasing the temperature, this singlet becomes finer and moves to higher δ values. At -60°C only a singlet for the formates is visible so that we cannot distinguish the H related to the ligand and the acid. This shows that the two HCO_2 moieties are in rapid equilibrium at -60°C .

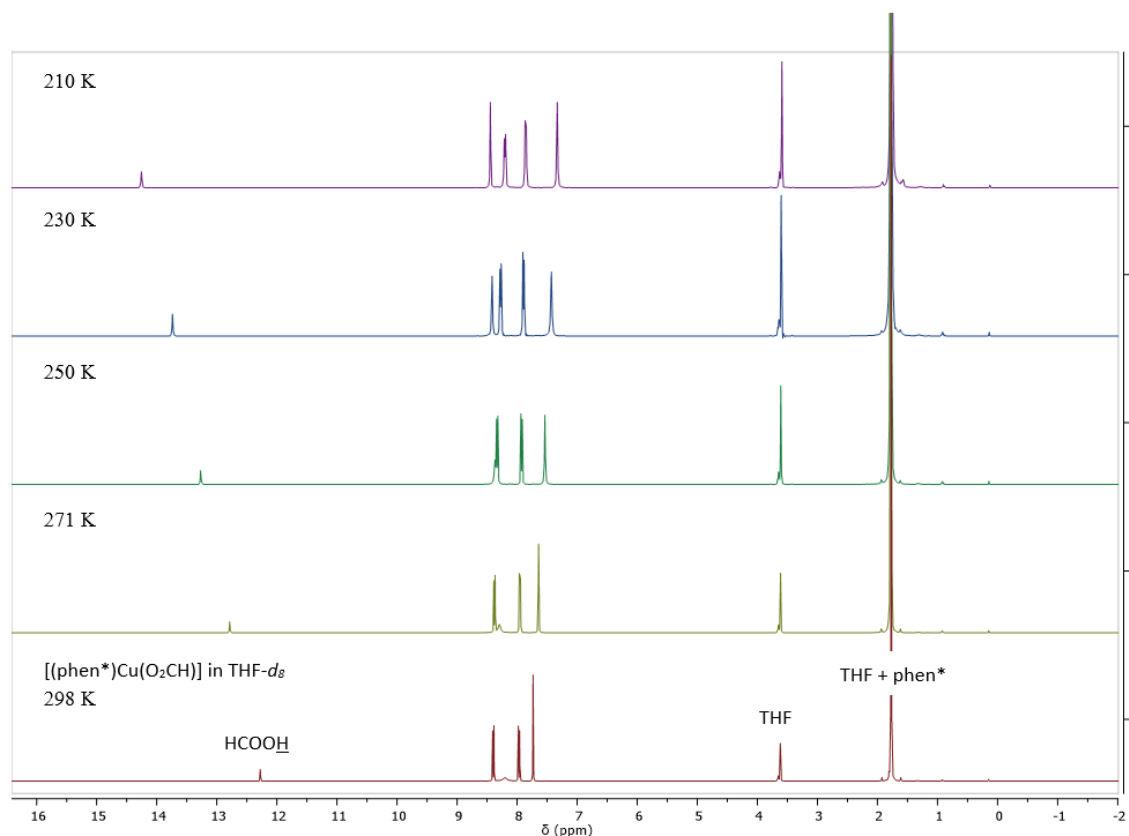


Figure S81. ^1H NMR spectrum in $\text{THF-}d_8$ of the thermal evolution of **12** from 298 K to 210 K.

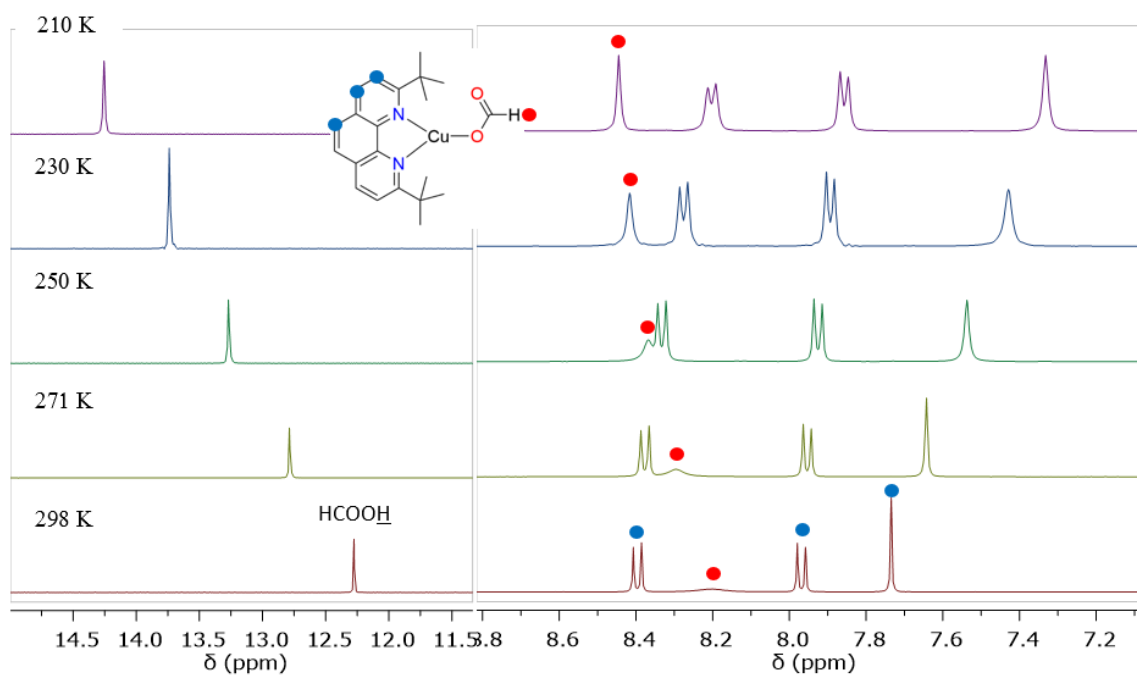


Figure S82. Zoom on Figure S81.

III. 2. 1. Solution of $[(\text{phen}^*)\text{Cu}(\text{O}_2\text{CH})]$ in $\text{THF-}d_8$ at 210 K ($-63\text{ }^\circ\text{C}$)

^1H NMR (400 MHz, $\text{THF-}d_8$, δ/ppm): 14.26 (s, 0.39H, 39 % compared to **12**), 8.44 (s, $W_{1/2} = 4\text{ Hz}$, 1H, O_2CH), 8.20 (d, $J = 8.3\text{ Hz}$, 2H), 7.86 (d, $J = 8.3\text{ Hz}$, 2H), 7.33 (s, 2H), 1.77 (s, 18H, ^tBu).

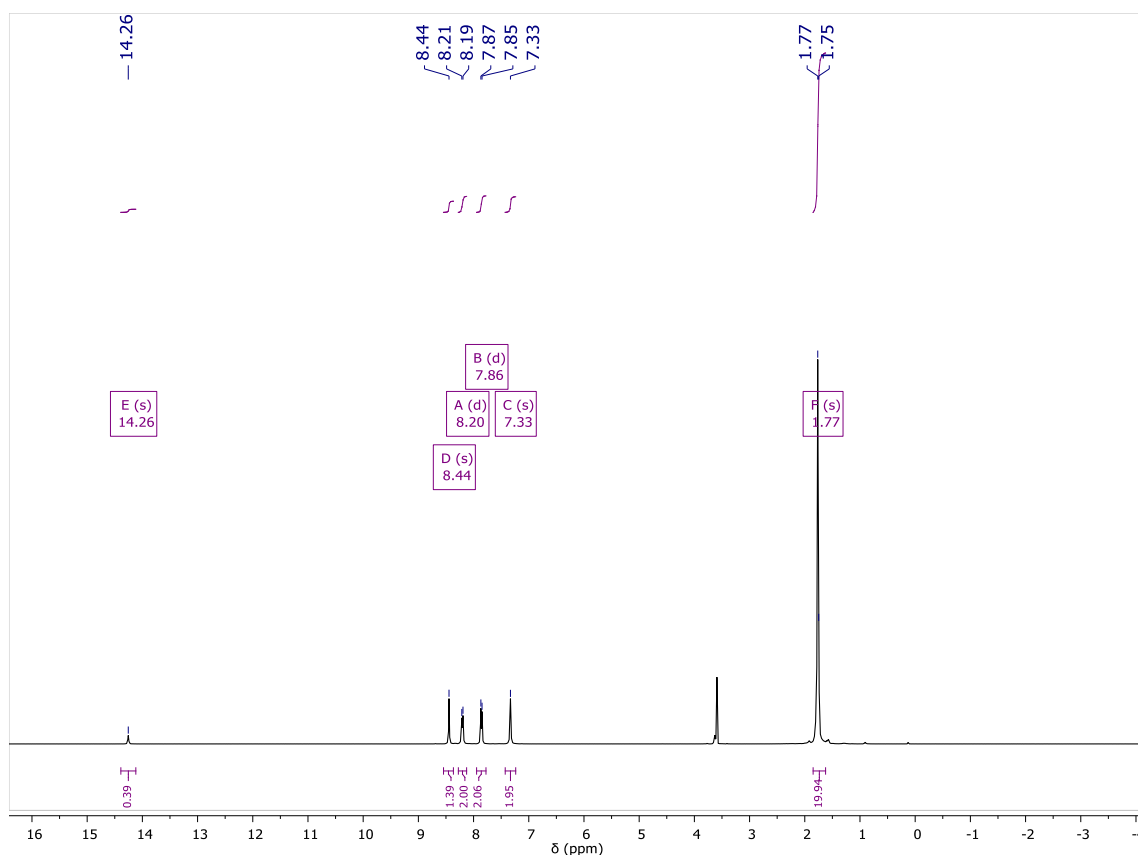


Figure S83. ^1H NMR spectrum of **12** in $\text{THF-}d_8$ at 210 K.

III. 3. Thermal decomposition of $[(\text{phen}^*)\text{Cu}(\text{O}_2\text{CH})]$ (**12**)

An dark-orange solution of **12** (5 mg, 0.012 mmol) in $\text{THF-}d_8$ (0,5 mL) was heated at 50 °C for 5 h. The evolution of **12** was monitored by ^1H NMR after 3 and 5 h of reaction. The reaction mixture was then heated at 60 °C and the ^1H NMR spectra recorded after 4 h and 7 h. After 7 h at 60 °C, complex **12** completely degraded into free ligand with formation of a dark-red deposit (see Figure S84 below).

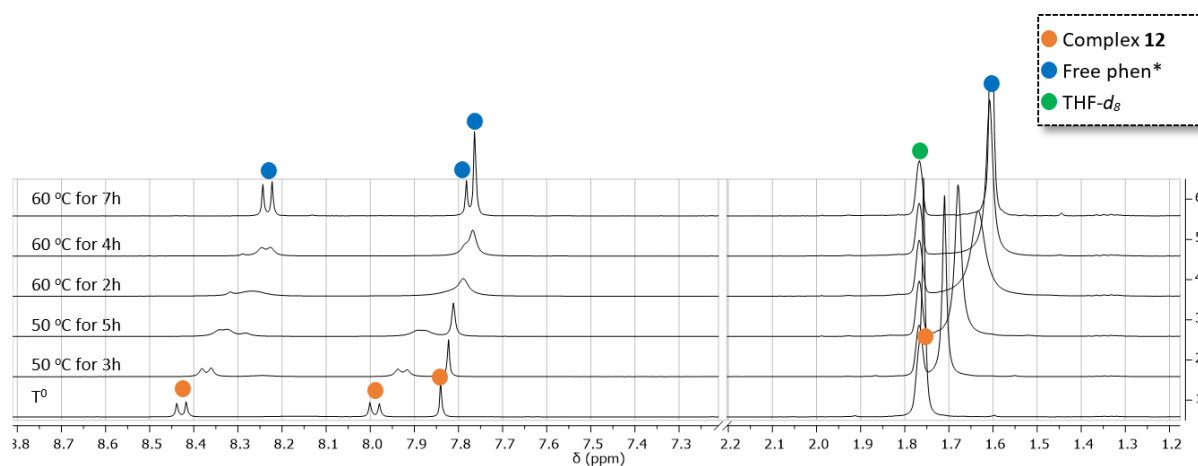


Figure S84: ^1H NMR spectra of the thermal evolution of **12** in $\text{THF-}d_8$.

III. 4. Attempts to isolate/detect copper hydride

III. 4. 1. Reaction of Cu(O^tBu) + Phen* with dihydrogen:

In an NMR tube, Cu(O^tBu) (5 mg, $3.7 \cdot 10^{-2}$ mol) and phen* (10,7 mg, 1 equiv.) was solubilized in THF-*d*₈ (~ 0,5 mL). The clear light brown solution (and black solid resulting from partial decomposition of Cu(O^tBu)) was pressurized with 1 bar H₂ : no change of color can be observed. The tube was rotated for 1 h at r.t. without change. The reaction was heated at 60 °C for another hour giving a light yellow solution and black solid indicating degradation of the complex into Cu(0).

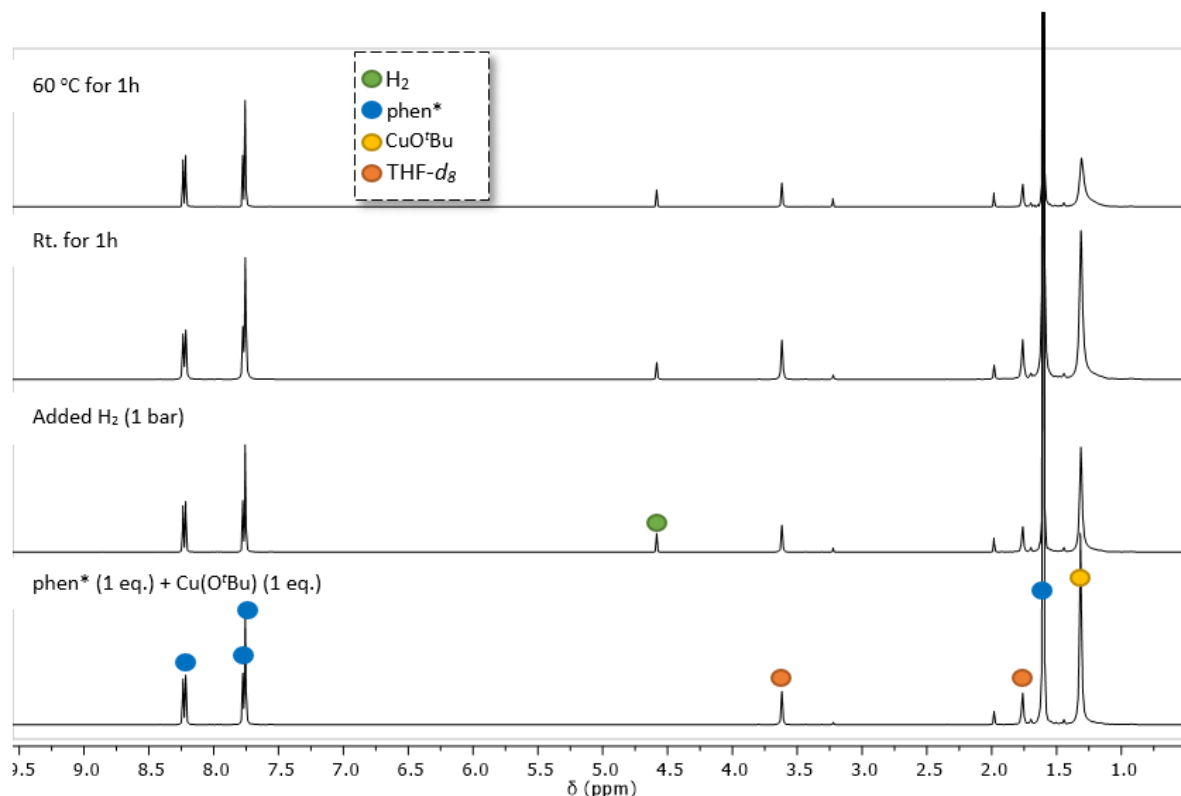


Figure S85. ¹H NMR spectra of the evolution of the mixture Cu(O^tBu) + Phen* under dihydrogen in THF-*d*₈.

III. 4. 2. Reaction of Cu(O^tBu) + Phen* with HBpin:

In an NMR tube, Cu(O^tBu) (5 mg, $3.7 \cdot 10^{-2}$ moles) and phen* (10,7 mg, 1 equiv.) were solubilized in ~0,5 mL C₆D₆. The clear light brown solution was separated from the black solid (partial decomposition of unstable Cu(O^tBu) by pipetting. Pinacolborane (BpinH, 5.7 μL, 1 equiv.) was added into this clear solution: the mixture turned immediately pale yellow (free phen*) with formation of abundant black solid while the release of gas (H₂). At the end, the unreacted HBpin is detected by ¹H NMR.

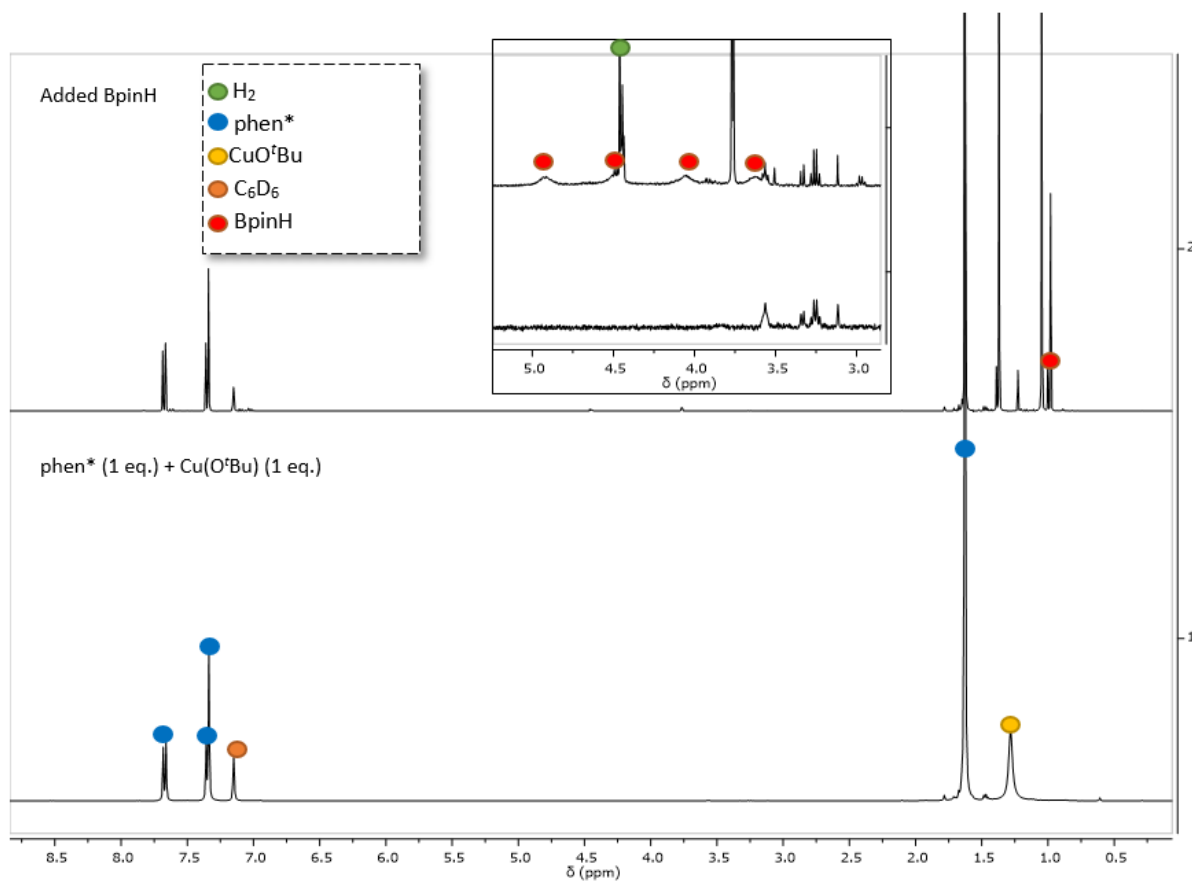


Figure S86. ^1H NMR spectra of the evolution of the mixture $\text{Cu}(\text{O}^t\text{Bu}) + \text{Phen}^*$ with pinacolborane in THF-d_8 .

III. 4. 3. Reaction of Phen^* with Stryker reagent $[\text{Cu}(\text{PPh}_3)\text{H}]_6$:

In a NMR tube, to the brown suspension of the Stryker reagent $[\text{Cu}(\text{PPh}_3)\text{H}]_6$ (5 mg, $2.8 \mu\text{mol}$) in C_6D_6 (0,5 mL) was added phen^* (5.0 mg, $17 \mu\text{mol}$, 1 equiv./Cu) giving a dark orange solution (containing solid deposit). The NMR showed no reaction between free phen^* and the hexamer. After 10 min at 100°C , the solution is pale yellow (free phen^* and PPh_3) with abundant dark deposit.

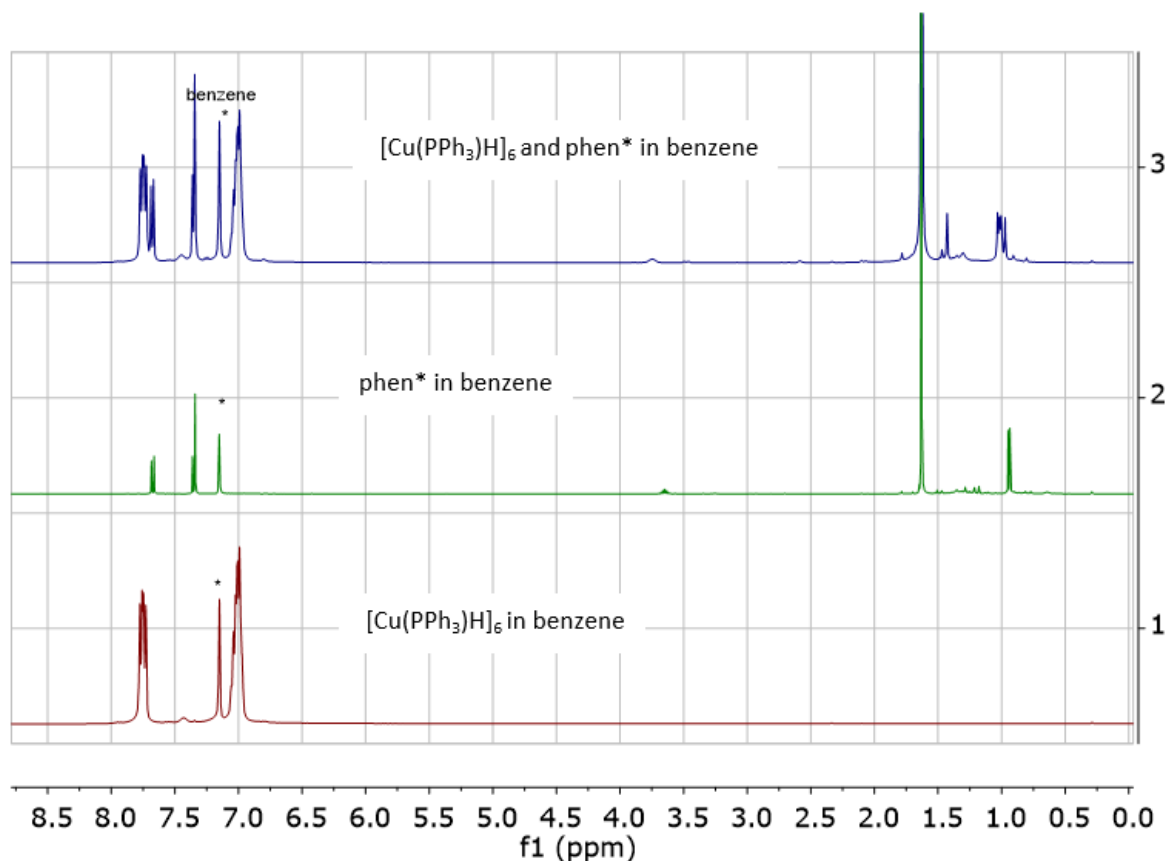


Figure S87. ^1H NMR spectra of $[\text{Cu}(\text{PPh}_3)\text{H}]_6$, phen* and the mixture $[\text{Cu}(\text{PPh}_3)\text{H}]_6 + \text{phen}^*$ in benzene- d_6

III. 4. 4. Reaction of $[(\text{phen}^*)\text{CuI}]$ with hydride reagents:

In a NMR tube, to the yellow suspension of $[(\text{phen}^*)\text{CuI}]$ (5 mg, 10.4 μmol) in THF (~ 0.5 mL) was added 10.4 μL (1 equiv.) of a THF solution of the superhydride KBHET_3 ($C = 1\text{M}$ in THF) (≈ 1.5 mg, 62 μmol). A black solid deposited immediately from the pale yellow solution.

In a NMR tube, to the yellow suspension of $[(\text{phen}^*)\text{CuI}]$ (5 mg, 10.4 μmol) in THF (~ 0.5 mL) was weighted NaH (≈ 1.5 mg, 62 μmol) and the ether 18-crown-6 (2.7 mg, 10.4 μmol). The pale yellow suspension was placed in a ultra-sonic bath for 1 h and we obtained a colorless solution containing a black deposit.

III. 4. 5. Thermal reaction of **12** in presence of $\text{EtN}=\text{C}=\text{O}$:

Into a dark-orange suspension of **12** (8 mg, 0.02 mmol) in THF- d_8 (0.5 mL) was syringed EtNCO (3.1 μL , 0.04 mmol). No change of the color solution and no shift of the ^1H NMR signals of **12** could be detected. The mixture was then warmed at 50 $^\circ\text{C}$ for 4 h and resulted in a dark-yellow solution with deposit of a dark-red solid (Figure S88).

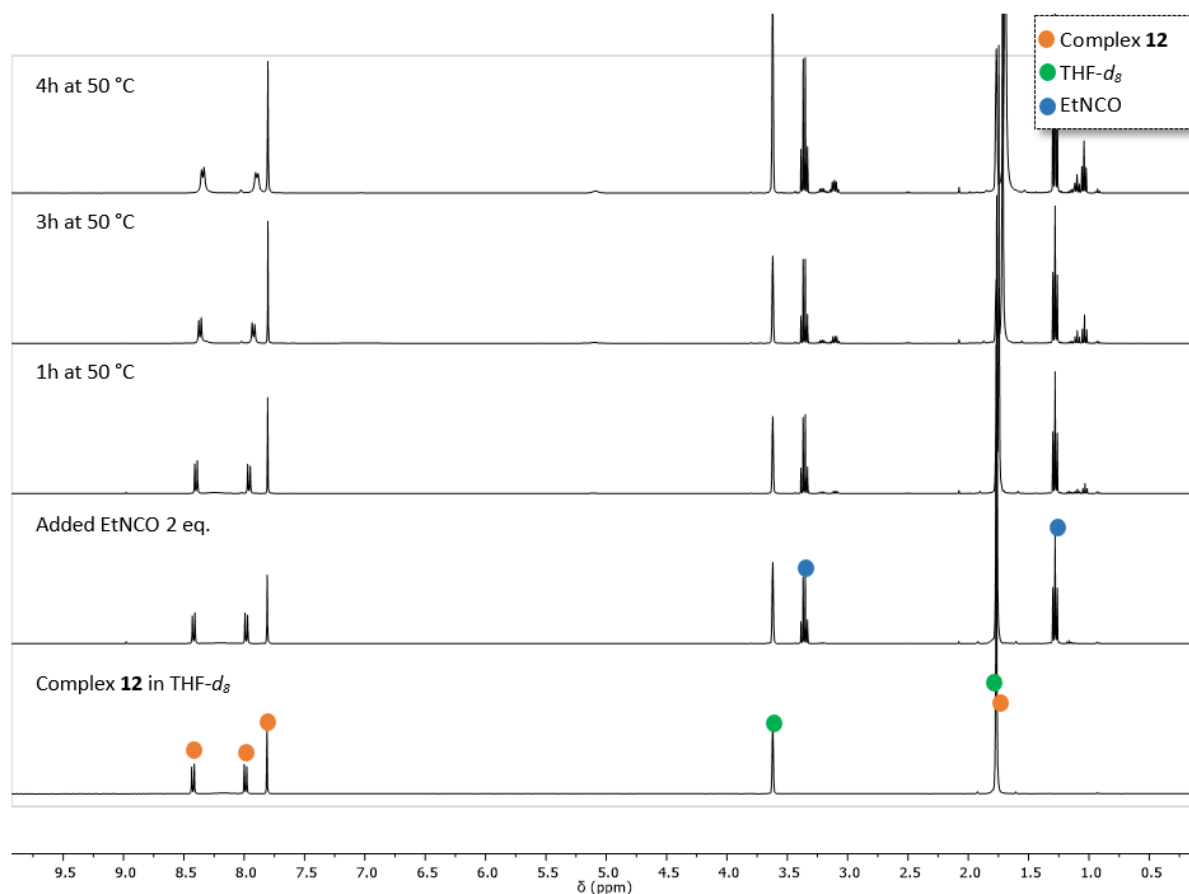


Figure S88: ^1H NMR spectrum in $\text{THF-}d_8$ of the thermal evolution of **12** in presence of $\text{EtN}=\text{C}=\text{O}$.

III. 4. 6. Thermal behavior of **12** in presence of BET_3 :

To a dark-orange suspension of **12** (5 mg, 0.012 mmol) in ~ 0.5 mL $\text{THF-}d_8$ was added BET_3 (1 M in hexane, 12.5 μL , 0.012 mmol, 1 equiv.). The solution immediately turned yellow-green and remained dark-orange solid. After heating at 60 $^\circ\text{C}$ for 2 h, the solution turned green along with the formation of dark solid.

III. 4. 7. Synthesis of $[\{(\text{phen}^*)\text{Cu}\}_2(\mu\text{-O}_2\text{CH})][(\text{HCO}_2\text{-}\kappa^1)\text{B}(\text{C}_6\text{F}_5)_3]$ (**13**) by reaction of **12** with $\text{B}(\text{C}_6\text{F}_5)_3$:

In a NMR tube, to the dark-orange suspension of **12** (7 mg, 0.017 mmol, 1 equiv.) in $\text{THF-}d_8$ (~ 0.5 mL) was added $\text{B}(\text{C}_6\text{F}_5)_3$ (4.5 mg, $8.5 \cdot 10^{-3}$ mmol, 0.5 equiv.). The solution slowly turned to yellow-green solution with some remain of dark-orange solid of **12**. The mixture was left rotating overnight at room temperature (*ca* 15 h) affording a yellow solution containing and small amount of orange solid. Orange crystals of **13** were grown by slow diffusion of pentane to a green solution of **12** (6.5 mg, 0.016 mmol) and $\text{B}(\text{C}_6\text{F}_5)_3$ (8.3 mg, 0.016 mmol, 1 equiv.) in THF.

^1H NMR (400 MHz, $\text{THF-}d_8$, δ/ppm) 8.60 (d, $J = 8.6$ Hz, 4H, phen*), 8.43 (s, 1H, $[\{\text{Cu}\}_2(\mu\text{-O}_2\text{CH})]$), 8.19 (s, 1H, $[(\text{HCO}_2\text{-}\kappa^1)\text{B}(\text{C}_6\text{F}_5)_3]$), 8.10 (d, $J = 8.6$ Hz, 4H, phen*), 8.01 (s, 4H, phen*), 1.65 (s, 36H, ^tBu). The attribution of the formate signals is related to that of $[\text{HNET}_3][(\text{HCO}_2\text{-}\kappa^1)\text{B}(\text{C}_6\text{F}_5)_3]$ (see below) where the HCO_2B singlet is found at 8.18 ppm

$^{19}\text{F}\{^1\text{H}\}$ NMR (377 MHz, $\text{THF-}d_8$, δ/ppm) : -133.85 to -134.23 (m), -163.51 (s), -167.92 (d, $J = 6.6$ Hz).

$^{11}\text{B}\{^1\text{H}\}$ NMR (128 MHz, $\text{THF-}d_8$) : -4.41 .

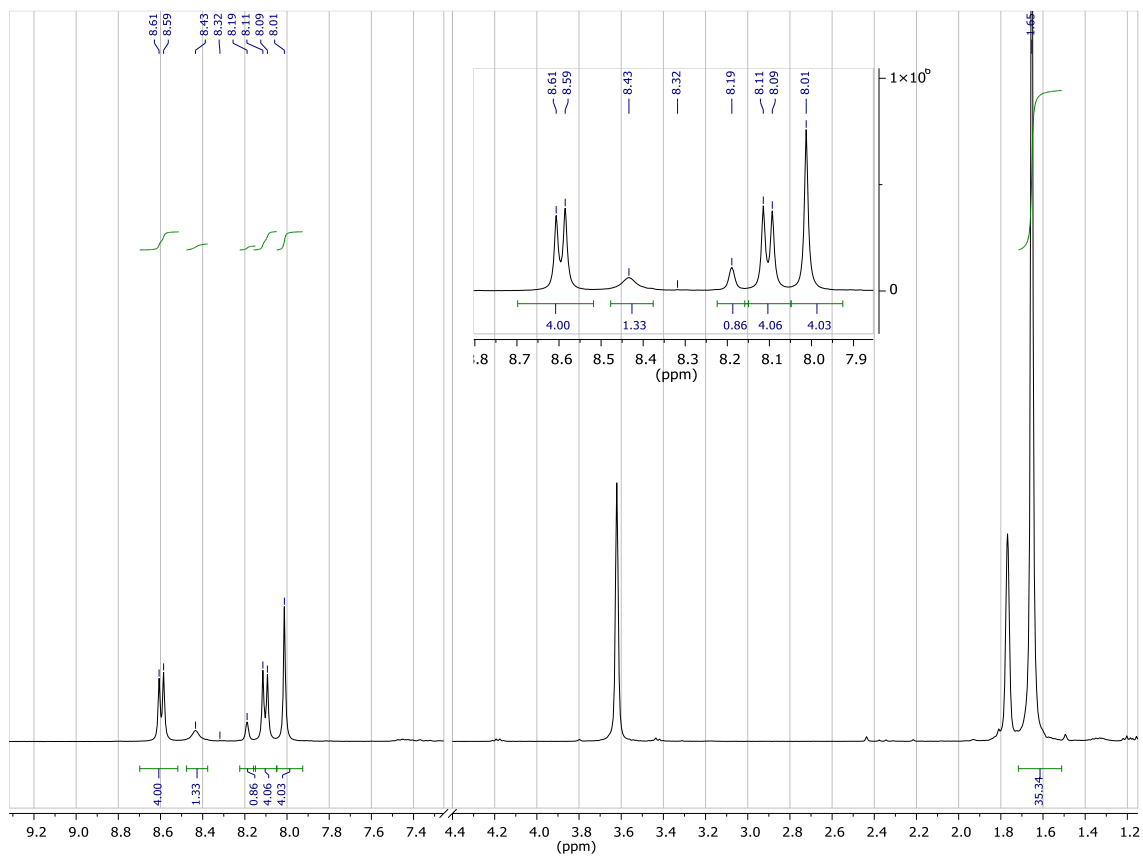


Figure S89: ^1H NMR spectrum of **13** in $\text{THF-}d_8$.

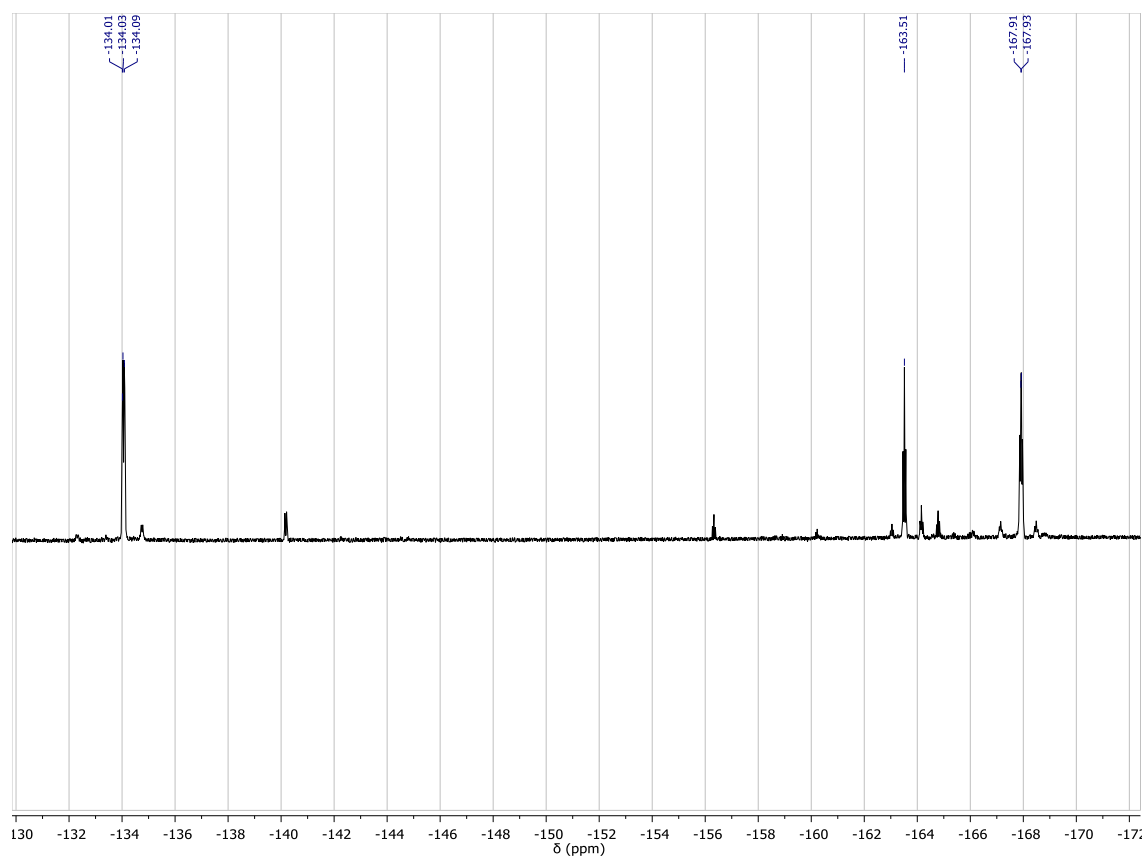


Figure S90: $^{19}\text{F}\{^1\text{H}\}$ NMR spectrum of **13** in THF-d_8 .

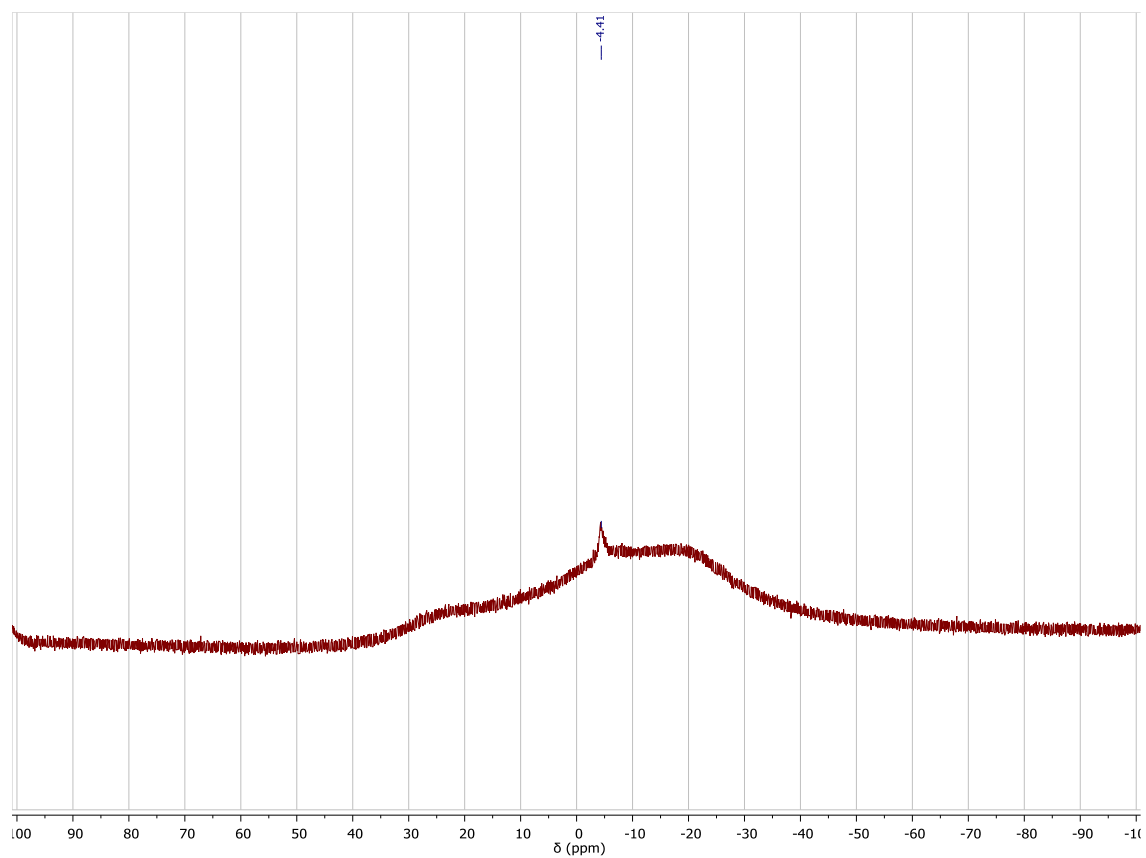


Figure S91: $^{11}\text{B}\{^1\text{H}\}$ NMR spectrum of **13** in THF-d_8 .

III. 4. 8. Synthesis of $[\text{HNEt}_3][(\text{HCO}_2\text{-}\kappa^1)\text{B}(\text{C}_6\text{F}_5)_3]$:

In a NMR tube, $\text{B}(\text{C}_6\text{F}_5)_3$ (10 mg, 19.5 μmoles) was dissolved in 0.5 mL C_6D_6 and HCO_2H (ca 0.8 μL , 21 μmoles) was syringed in it. Addition of NEt_3 (8 μL , 57 μmoles) caused white fumes. The clear and colorless solution is sonicated in an ultrasonic bath for 30 min and the solution is evaporated off under vacuum for 15 h. The residue was dissolved in $\text{THF-}d_8$. The NMR spectra evidenced the formation of the boron formate compound $[\text{HNEt}_3][(\text{HCO}_2)\text{B}(\text{C}_6\text{F}_5)_3]$.

^1H NMR 400 MHz, benzene- d_6 , δ/ppm : 9.02 (s, NEt_3H), 8.18 (s, 1H, HCO_2B), 3.19 (q, $J = 8$ Hz, 6H), 1.29 (t, $J = 8$ Hz, 9H);

^{19}F NMR (377 MHz, $\text{THF-}d_8$, δ/ppm) : -134. (dd), -162.2 (t), -167.3 (split t, $J = 6.6$ Hz).

^{11}B NMR (128 MHz, $\text{THF-}d_8$) : -3.62.

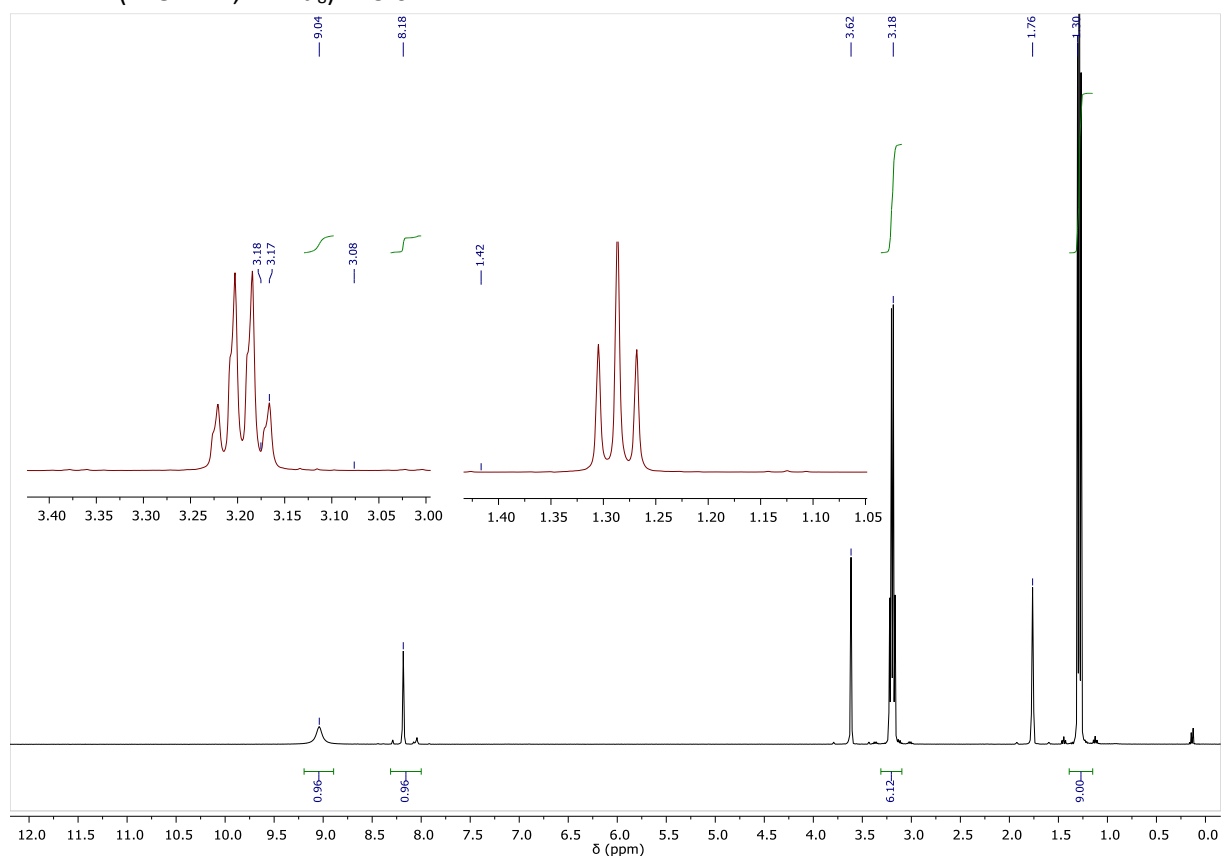


Figure S92. ^1H NMR of $[\text{HNEt}_3][(\text{HCO}_2)\text{B}(\text{C}_6\text{F}_5)_3]$ in $\text{THF-}d_8$.

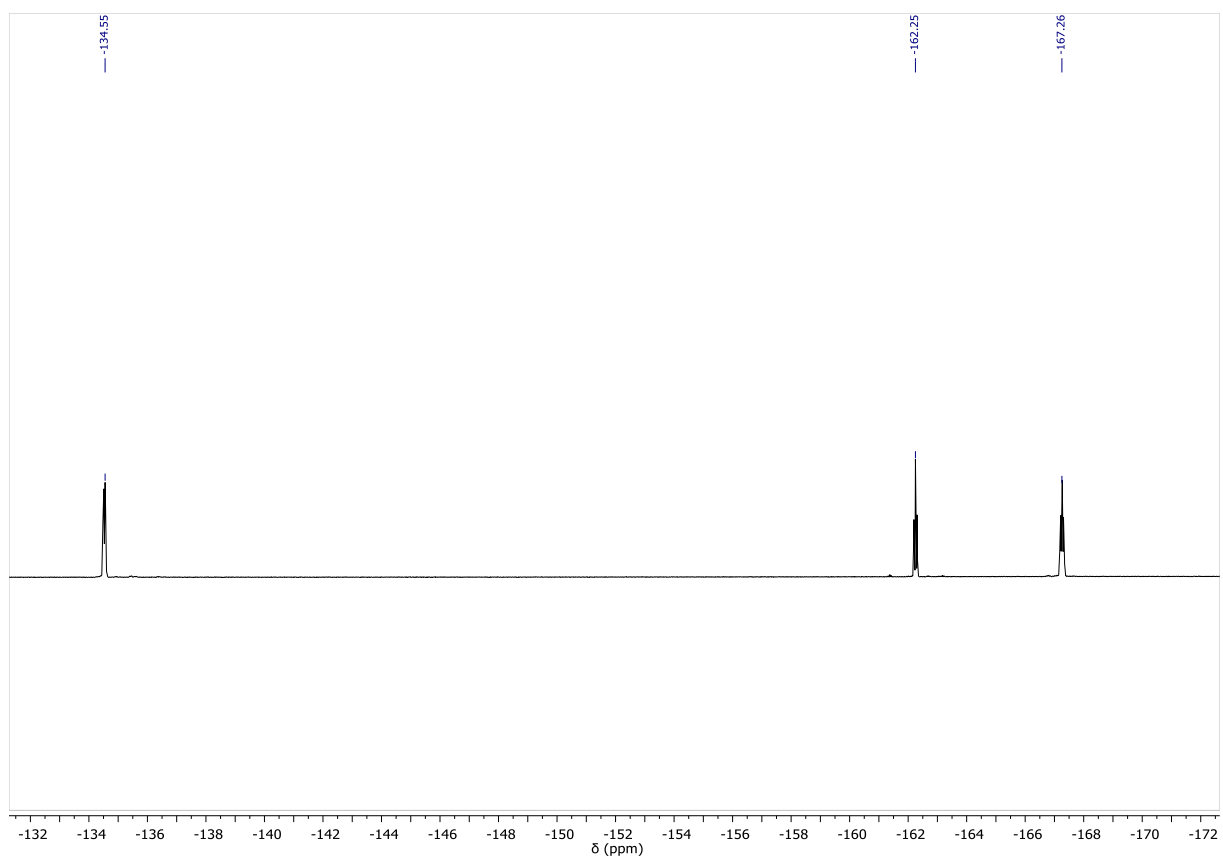


Figure S93. ^{19}F NMR of $[\text{HNEt}_3][(\text{HCO}_2)\text{B}(\text{C}_6\text{F}_5)_3]$ in THF-d_8 .

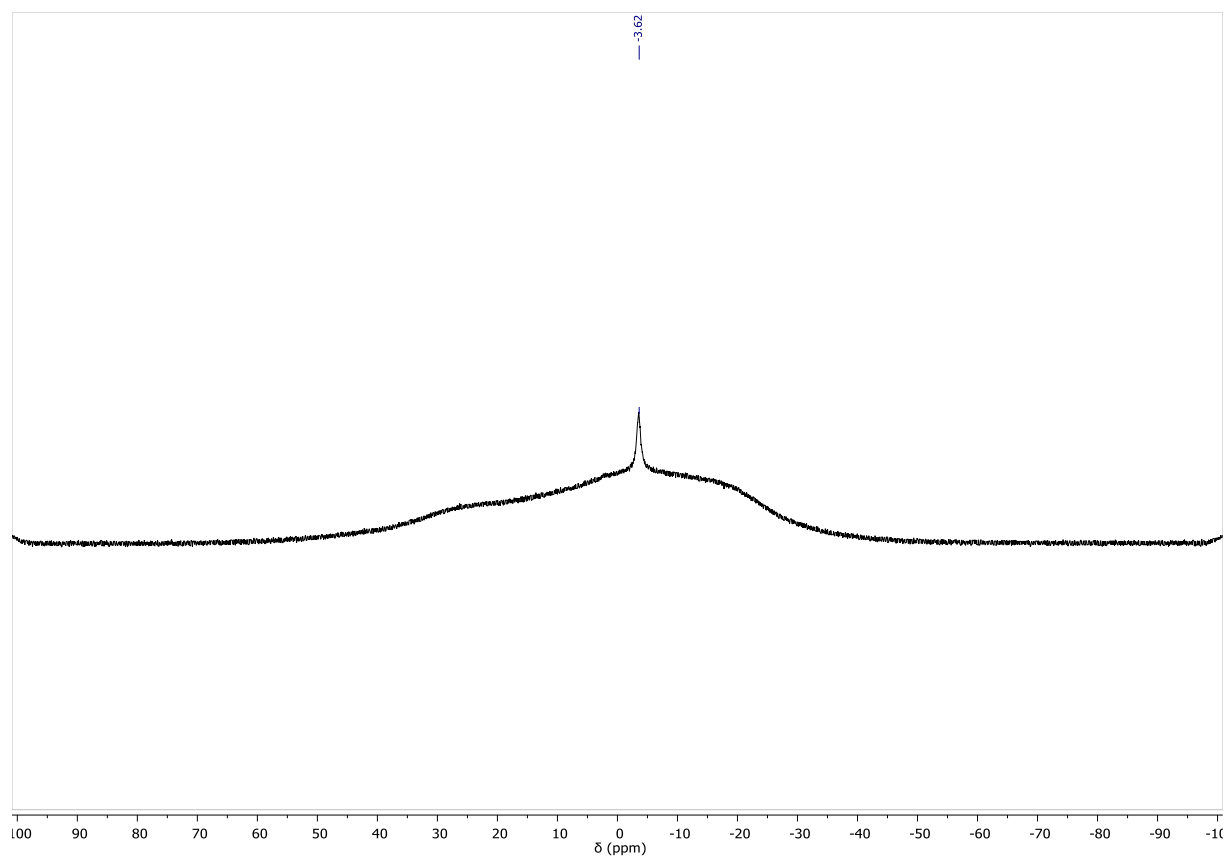


Figure S94. $^{11}\text{B}\{^1\text{H}\}$ NMR of $[\text{HNEt}_3][(\text{HCO}_2)\text{B}(\text{C}_6\text{F}_5)_3]$ in THF-d_8 .

III. 4. 9. Thermal behavior of **12** in presence of with phenylacetylene:

Phenylacetylene (3 μ L, 0.025 mmol) was added into a dark-orange suspension of complex **12** (10 mg, 0.025 mmol, 1 equiv.) in THF- d_8 (~ 0,5 mL). The resulted mixture turned slowly within 5 min at room temperature to yellow-green and remained dark-orange solid (starting material). The reaction was then heated at 80 °C overnight (~ 18 h) and afforded a clear green solution containing a mixture of orange and green solids. ^1H NMR spectra of the final solution showed only the presence of free ligand indicating decomposition of the copper(I) complex.

III. 4. 10. Stoichiometric reaction of **12** with $^{13}\text{CO}_2$

In a New Era NMR tube, complex **12** (10 mg, 0.024 mmol) was solubilized in THF- d_8 (~ 0,5 mL) to afford a dark-orange suspension. The solution was degassed three times by free-pump-thaw technique to eliminate the argon and the tube was pressurized with 1 bar of $^{13}\text{CO}_2$. The color of the solution mixture did not change under CO_2 . The tube was then inserted into the heating plate at 60 °C for 1 h and a dark-orange suspension was obtained. The $^{13}\text{C}\{^1\text{H}\}$ NMR spectrum of the mixture showed a new signal at $\delta = 165$ indicating insertion of the labelled $^{13}\text{CO}_2$ gas into **12**. The mixture was continuing to heat at 60 °C for another 4.5 h and an orange-brown solution with a dark-red precipitate was obtained.

^1H NMR (400 MHz, THF- d_8 , δ /ppm): 8.33 (d, $J = 8.5$ Hz, 2H), 7.89 (d, $J = 8.5$ Hz, 2H), 7.79 (s, 2H), 1.69 (s, 18H).

$^{13}\text{C}\{^1\text{H}\}$ NMR (101 MHz, THF- d_8 , δ /ppm): 168.86, 164.65 (s, [(phen*)-Cu-O $_2$ ^{13}CH], **12***), 144.20, 136.46, 126.84, 125.29, 125.27 ($^{13}\text{CO}_2$), 119.80, 38.30, 39.87. (*carbon of CO_2H of **12** cannot be seen*)

^{13}C NMR (no H decoupling) (101 MHz, THF- d_8 , δ /ppm): 164.24 (d, $J = 198.9$ Hz), 124.90 ($^{13}\text{CO}_2$). Other signals cannot be observed due to less scan.

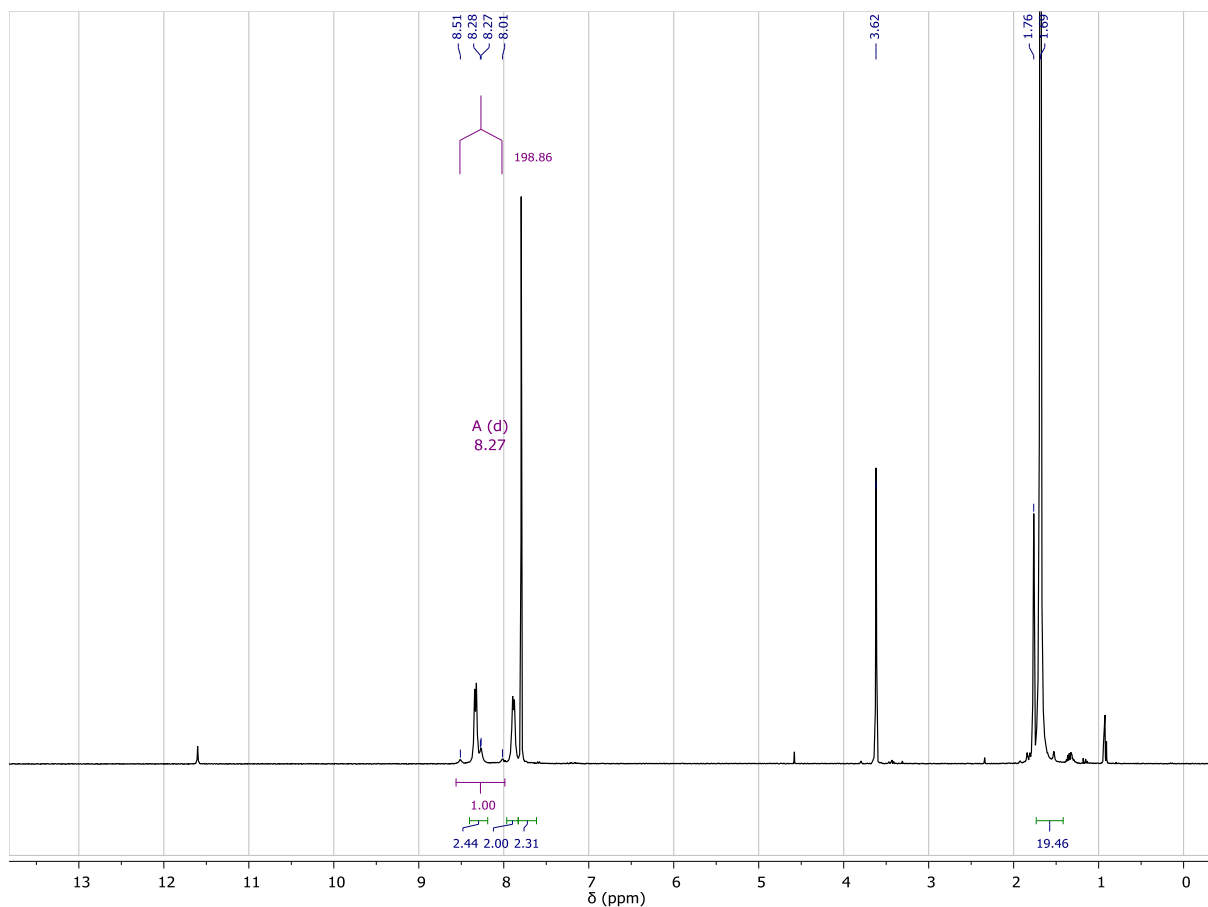


Figure S95: ^1H NMR spectrum of **12** under $^{13}\text{CO}_2$ in THF-d_8 . The peak at $\delta = 11.6$ corresponds to a small amount of formic acid (acid signal) that remains after the synthesis of **12**.

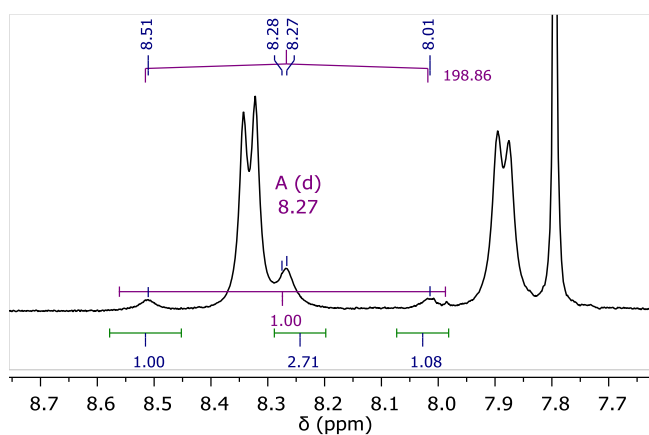


Figure S96: ^1H NMR spectrum of **12** under $^{13}\text{CO}_2$ in THF-d_8 . Enlarged view of the formate CH signals and the triplet due to coupling with the ^{13}C carbon atom.

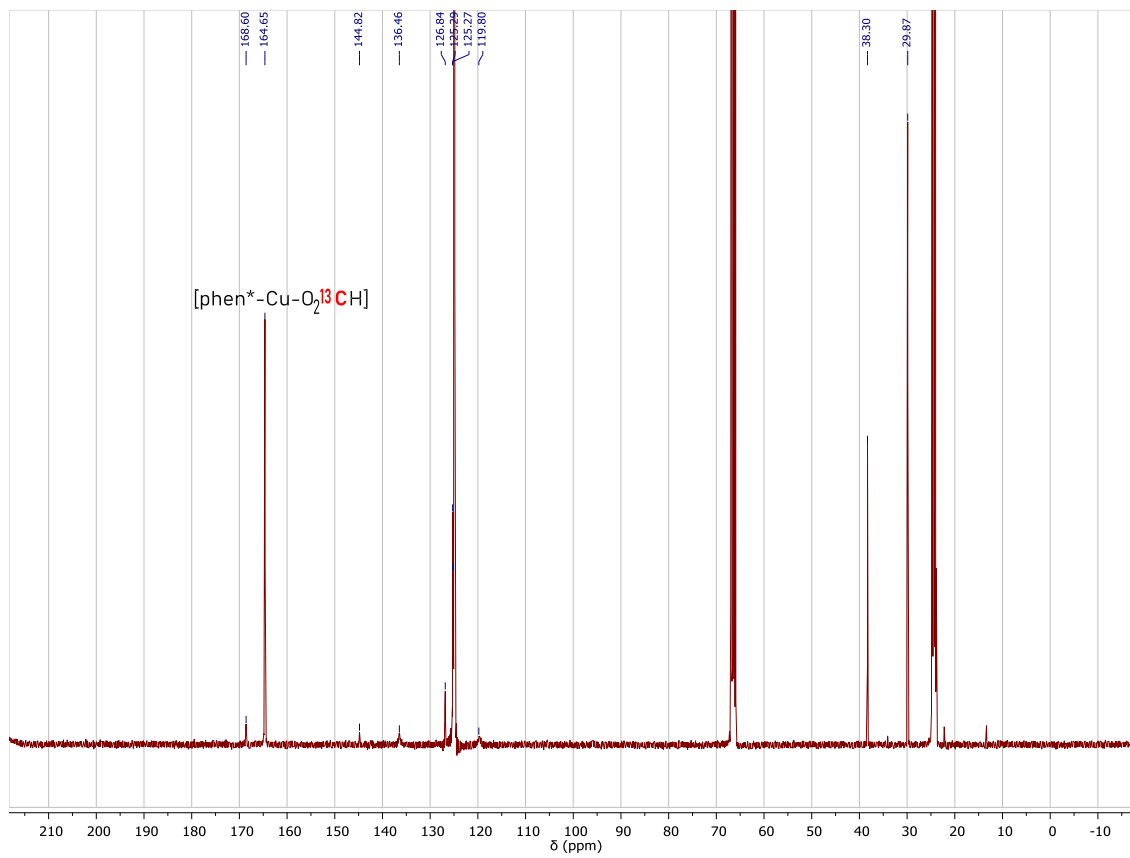


Figure S97: $^{13}\text{C}\{^1\text{H}\}$ NMR of **12** under $^{13}\text{CO}_2$ in THF-d_8 .

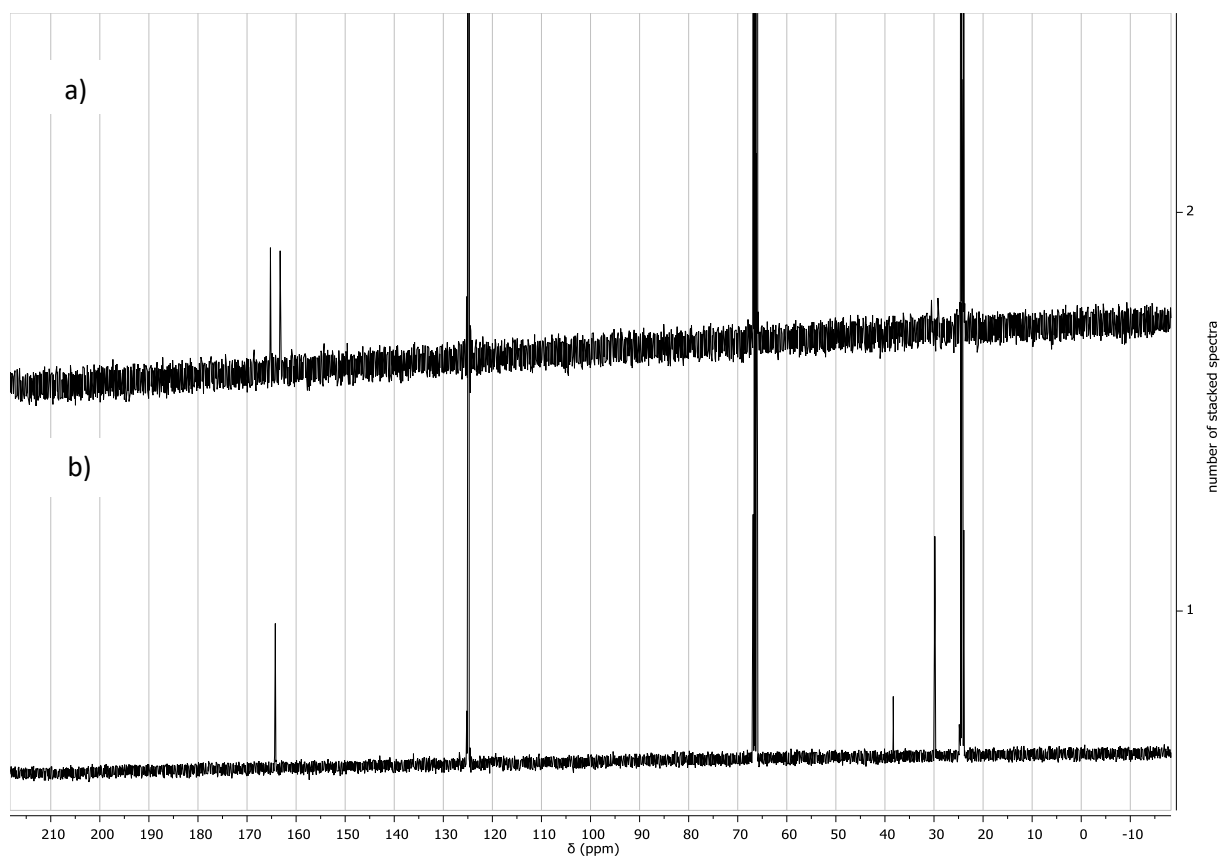


Figure S98: ^{13}C NMR stacked spectra of crude mixture (after 60°C at 4.5 h in THF-d_8 . a) In the ^{13}C NMR spectrum, we observed a doublet signal for the $^{13}\text{CO}_2\text{H}$ signal of **12*** at $\delta = 164.24$ has a coupling constant $J = 198.94$ Hz. b) In the $^{13}\text{C}\{^1\text{H}\}$ NMR spectrum, signal for the $^{13}\text{CO}_2\text{H}$ in **12*** is a singlet at $\delta = 164.24$. (Signals of the ligand in **12** and **12*** are too weak to be detected.)

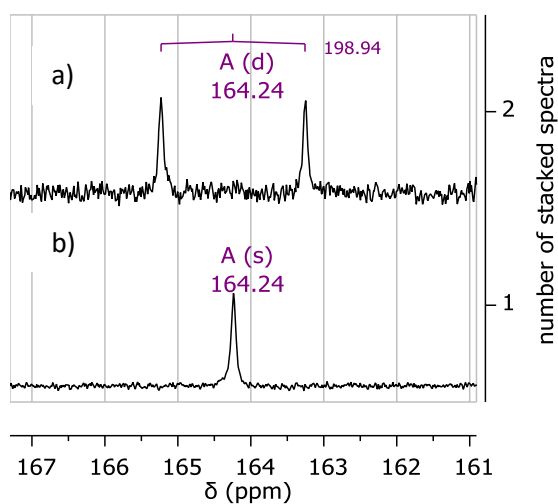


Figure S99: Zoom on the formate signals related to the above ^{13}C NMR spectra in Figure S98

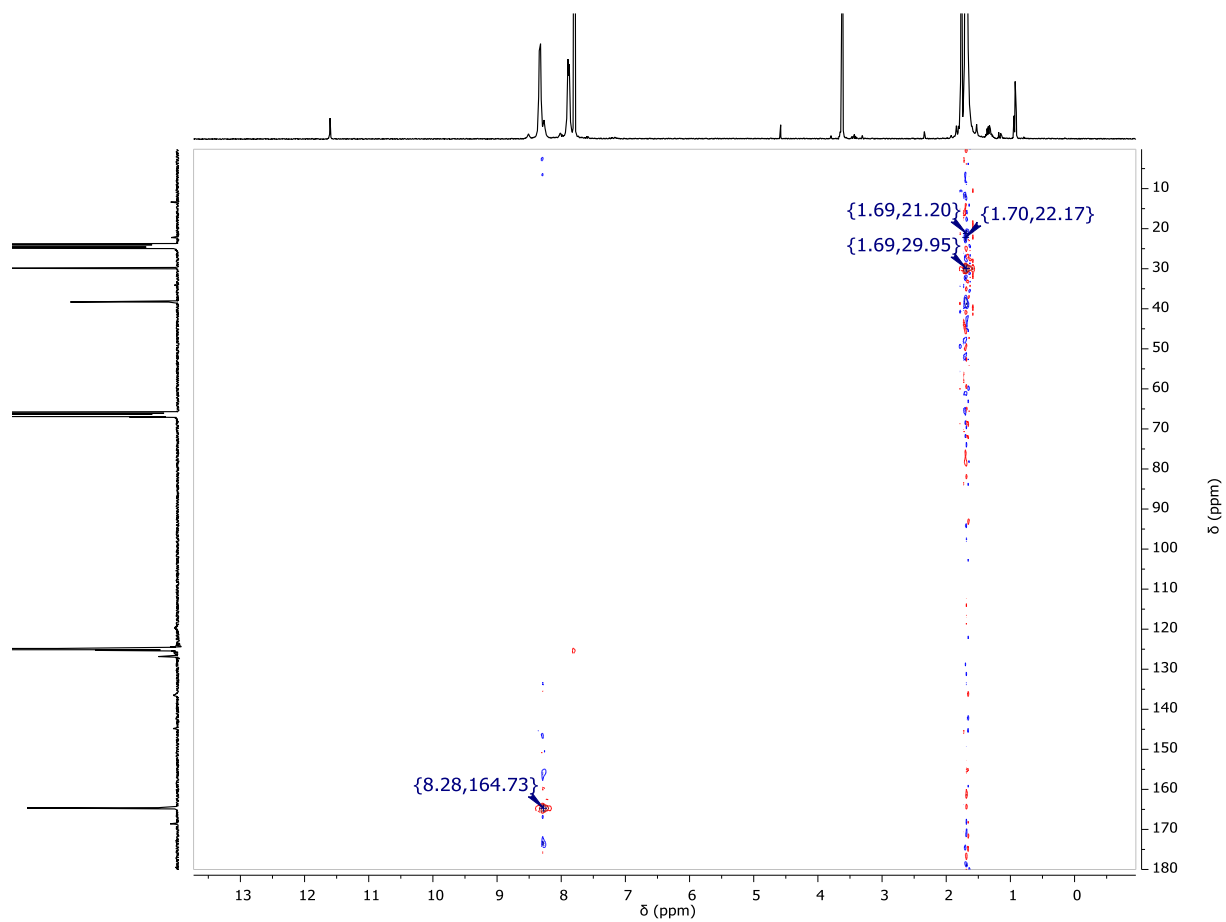


Figure S100 : The ^1H - ^{13}C HSQC spectrum of the crude mixture of **12** under $^{13}\text{CO}_2$ (after 60 °C at 4.5 h) in THF-d_8 evidences a correlation between the $^{13}\text{C}\{^1\text{H}\}$ NMR signal of the formate (at $\delta = 164$) and its H signal in the ^1H NMR spectrum (centered at $\delta = 8.2$).

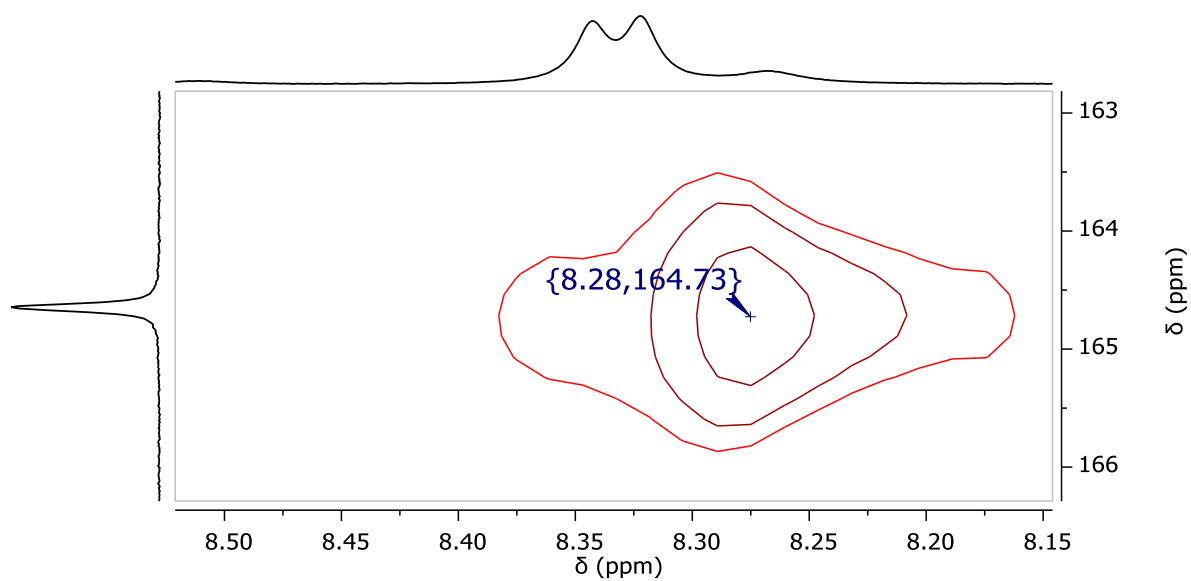


Figure S101: Zoom of the Figure S100.

III. 4. 11. Stoichiometric reaction with CS₂

A dark-orange suspension of **12** (8 mg, 0.02 mmol) in THF-*d*₈ was added CS₂ (3.7 μL, 0.1 mmol, 5 equiv.). The resulted dark-orange mixture was then heated at 50 °C for 2 h to yield a dark-brown solution along with the formation of dark precipitate. ¹³C{¹H} NMR signals of crude reaction mixture showed carbon signal of CS₂ remained untouched.

III. 5. Procedure for the catalytic dehydrogenation of formic acid

III. 5. 1. General catalysis experiment

In solution, the conversion of formic acid was determined by integration of the acid proton of formic acid (HCOOH) versus the internal standard (IS) (aromatic protons of mesitylene, δ = 6.78 in THF-*d*₈) by ¹H NMR. The evolution of H₂ is followed by ¹H NMR (δ = 4.59 in THF-*d*₈). Approximate volumes of H₂ and CO₂ gases are measured by GC analysis.

Turnover number at time *t* (TON) is: $TON = \frac{n_{HCOOH}^i - n_{HCOOH}^t}{n_{cat.}} = \frac{\rho}{x}$

Turnover frequency number (TOF) after *t* hours is: $TOF (h^{-1}) = \frac{TON}{t}$

n_{HCOOH}^i is the initial number of moles of formic acid

n_{HCOOH}^t is the number of moles of formic acid that remains at time *t*

$n^{cat.}$ is the initial number of moles of catalyst

ρ is the measured conversion (%)

x is the molar percentage (mol%) of catalyst introduced for the reaction.

Observation: The addition of formic acid into the suspension of **12** and mesitylene in THF resulted in a shifted to the low-field of the signals of phen* ligand. The formate proton of formic acid (HCOOH) is overlapped with the signals of the ligand and slowly separated during the course of the reaction. The formate proton of **12** ([phen*]Cu(O₂CH)) cannot be detected.

Control experiment: A solution of HCOOH (6 μL, 0.2 mmol) in ~ 5 mL of THF-*d*₈ gave no detectable conversion after 18 h at 100 °C.

III. 5. 2. Representative procedure for the catalytic dehydrogenation

Caution: All the experiments were carried out in a high-pressure New-Era NMR tubes to avoid potential explosion.

To an orange suspension of **12** (*x* mol%) in THF (0.5 mL) was added HCOOH (18 μL, 0.48 mmol) and mesitylene as an internal standard (6.7 μL, 10 mol%). At *t*=0, the ¹H NMR spectrum was first analyzed before the tube was immersed in a heating tube-plate at 100 °C. The reaction was then monitored in time by ¹H NMR to follow the evolution of H₂ (signal at 4.59 ppm in THF-*d*₈) and the disappearance of the acid HCOOH. At the end of the reaction, presence of the free ligand is evidenced in the clear

light yellow solution along with dark-red solid. At the end, the gas phase of the reaction was analyzed by GC for detection of CO₂ and H₂.

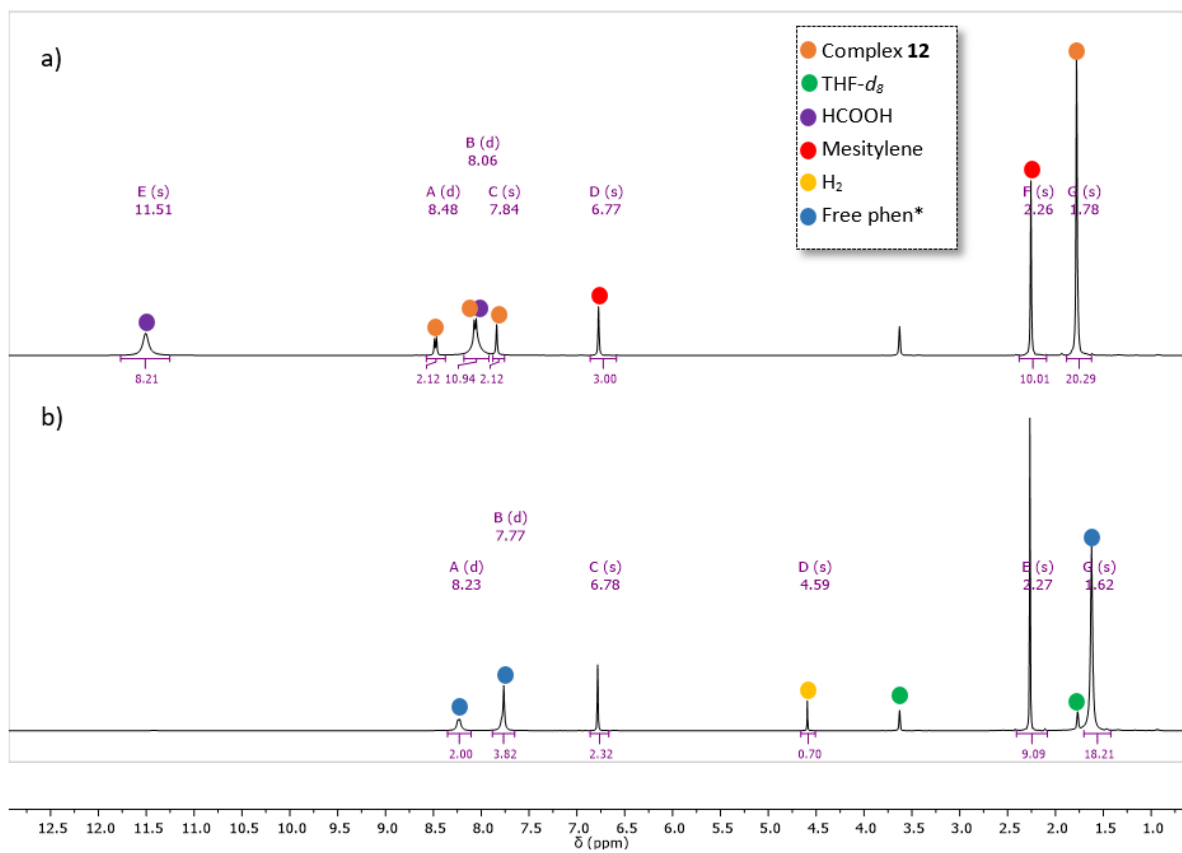


Figure S102: ¹H NMR spectrum obtained in THF-*d*₈ for the catalytic dehydrogenation of formic acid with 10 mol% of **12**. a) Crude reaction mixture before heating at $t = 0$. b) Crude reaction mixture after 150 min at 100 °C (100 % conversion), H₂ gas visible at $\delta = 4.59$.

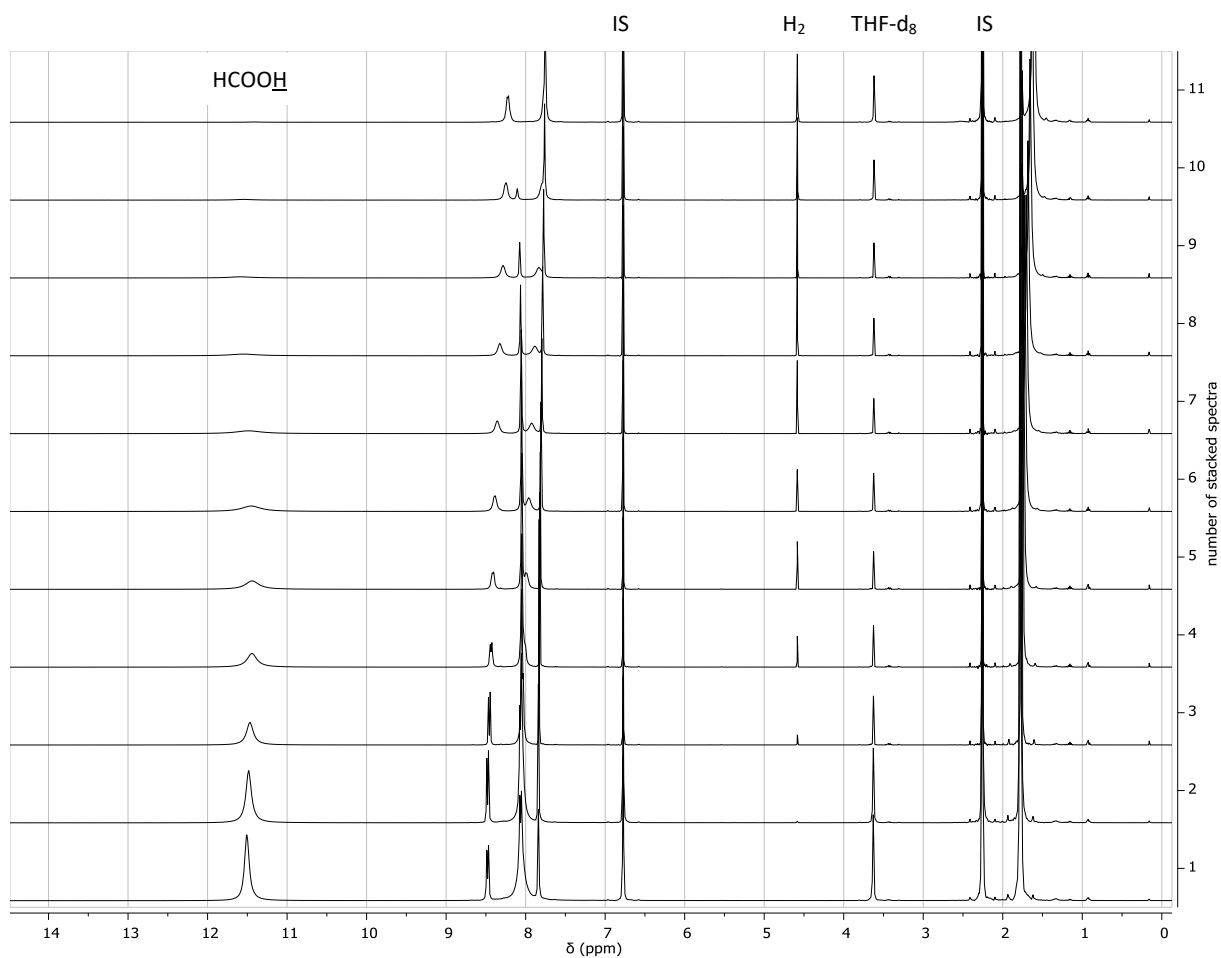


Figure S103: ^1H NMR stacked spectra of a crude mixture containing **12** (10 mol%), mesitylene as internal standard and 1 equiv. formic acid in THF- d_8 at 100 °C. Dehydrogenation of the acid was recorded as a function of time starting from $t = 0$ and the interval between each spectra was 15 min. (IS: internal standard = Mesitylene 10 mol%)

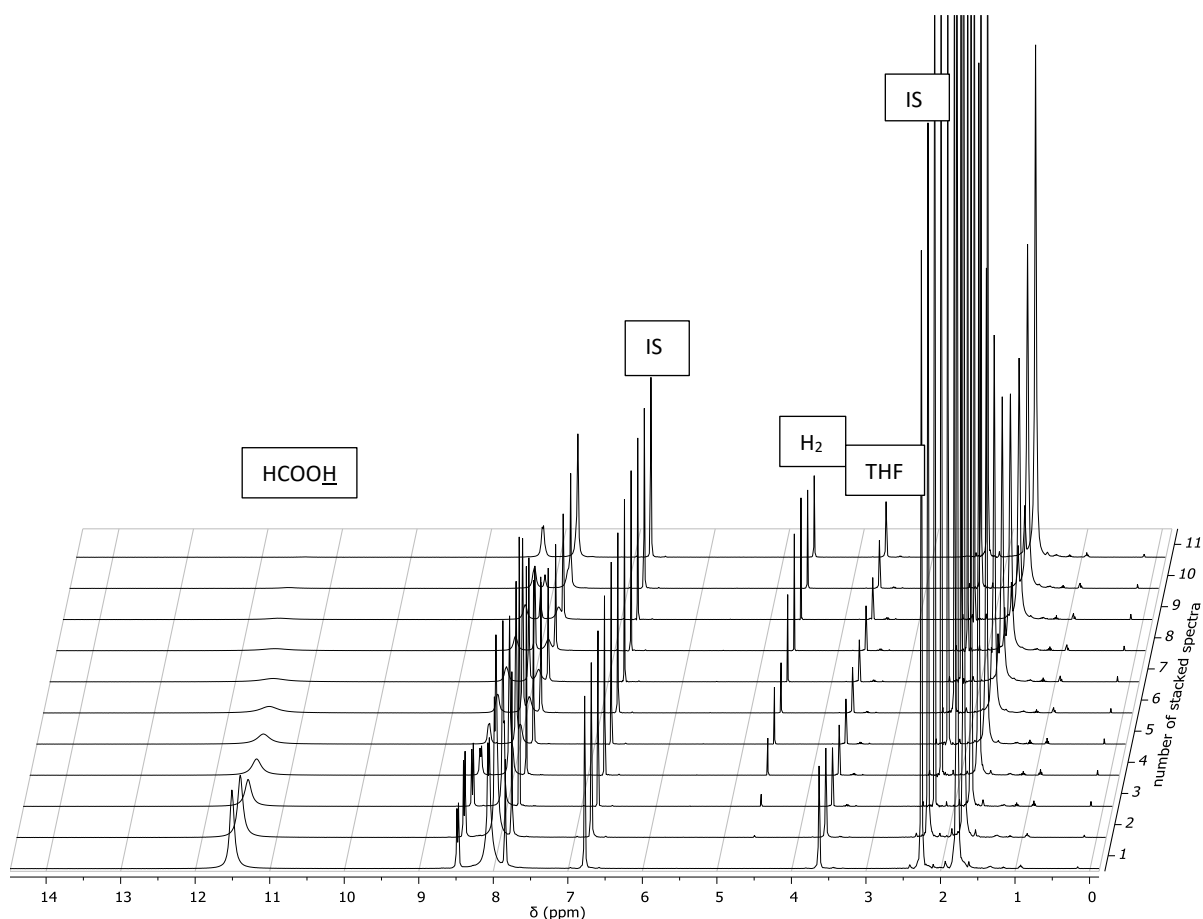


Figure S104: Distinct view of the stacking of the ^1H NMR spectra represented in Figure S103.

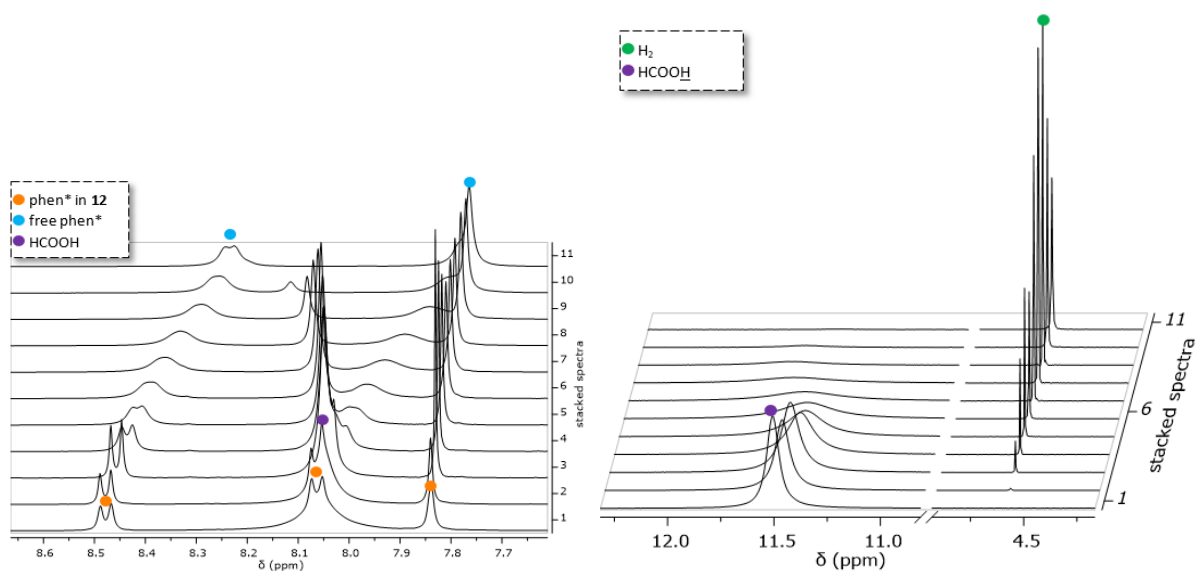


Figure S105: Left: ^1H NMR spectrum showing the aromatic signals of the phen* moiety of **12** (10 mol%) in the formic acid dehydrogenation catalysis. Right: ^1H NMR spectrum showing disappearance of the acidic signal of formic acid and concomitant release of H_2 . Spectra were recorded every 15 min (total reaction time, 2h30).

III. 5. 3. GC analysis for catalytic dehydrogenation of formic acid

Conditions

Column: Carboxen 1010 Plot fused silica capillary (30 m x 0.53 mm x 30 μm); injection temperature: 230 °C; column temperature: 100 °C; flow: 5 mL/min; purge; 2 mL/min; split ratio; 5.0; carrier gas: argon; detector: TCD 230 °C, 30 mA.

Calibration

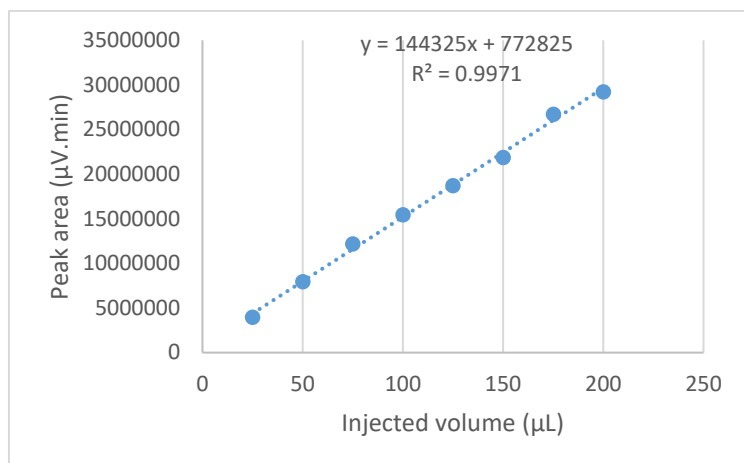


Figure S106 : Calibration curve for H₂

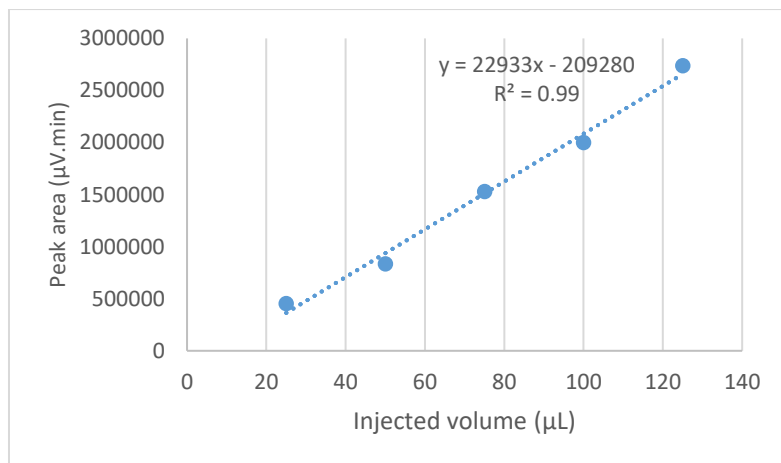


Figure S107 : Calibration curve for CO₂.

Species	Retention time (min)	Response factor (μV.min.μL ⁻¹)
H ₂	2.046	144325x + 772825
CO ₂	6.224	22933x - 209280

Table S1. Retention times and response coefficient for analyzed species.

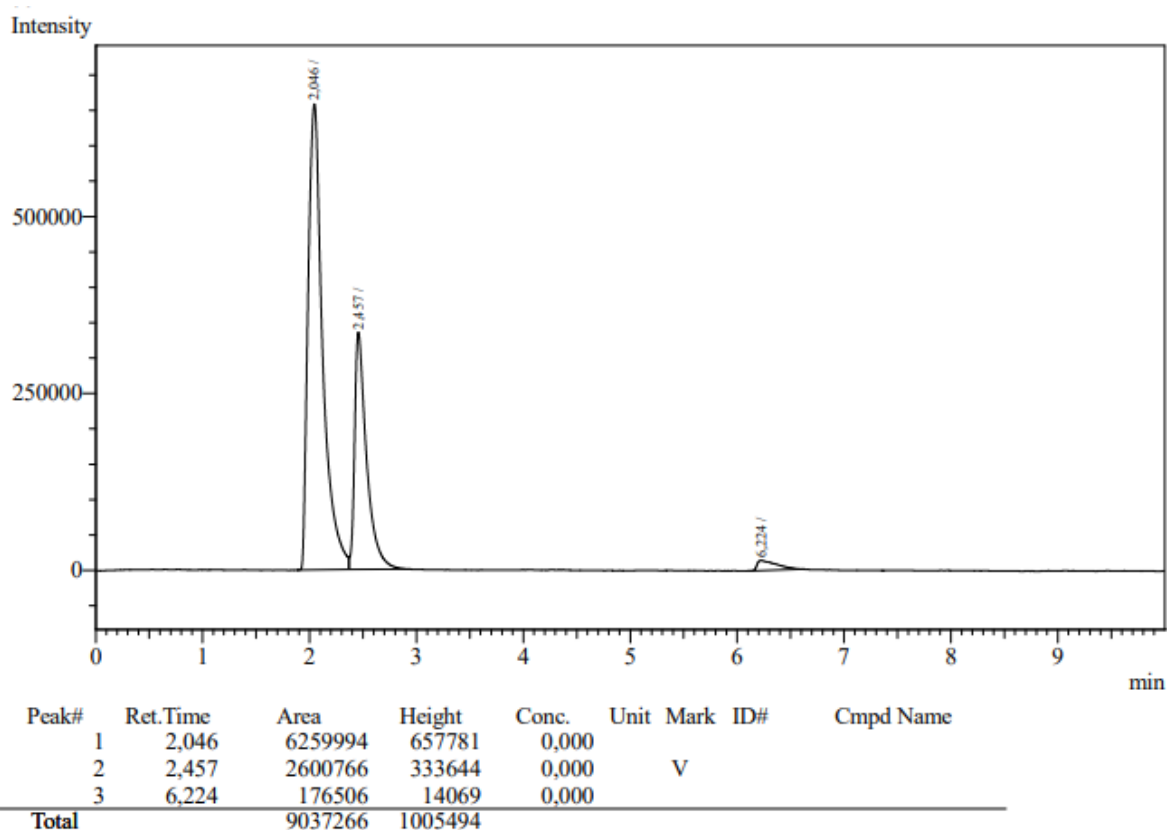


Figure S108 : GC trace after the catalytic dehydrogenation of formic acid (1 equiv.) with 10 mol% of **12**, mesitylene as internal standard in THF- d_8 at 100 °C, 2.5 h.

Ratio of the volumes of H₂ and CO₂ gas was obtained by calculating the area of each gas based on the calibration curves.

$$V_{CO_2} = \frac{176506 + 209282}{22933} = 51 \mu L$$

$$V_{H_2} = \frac{6259994 - 772825}{144325} = 43 \mu L$$

⇒ The ration between H₂ and CO₂ is ~ 1:1.

III. 5. 4. Proof for the decomposition of complex **12** after catalysis

In order to check the capacity of the copper complex at the end of the catalysis (10 mol% of **12** in 0.5 mL of THF and 10 mol% of mesitylene as internal standard) when the free ligand and dark-red deposit were formed, an additional equivalent of formic acid was added into the resulted reaction mixture. The mixture was left reacted at 100 °C for 1.5h. The reaction solution was monitored by ¹H NMR and showed no conversion of the acid.

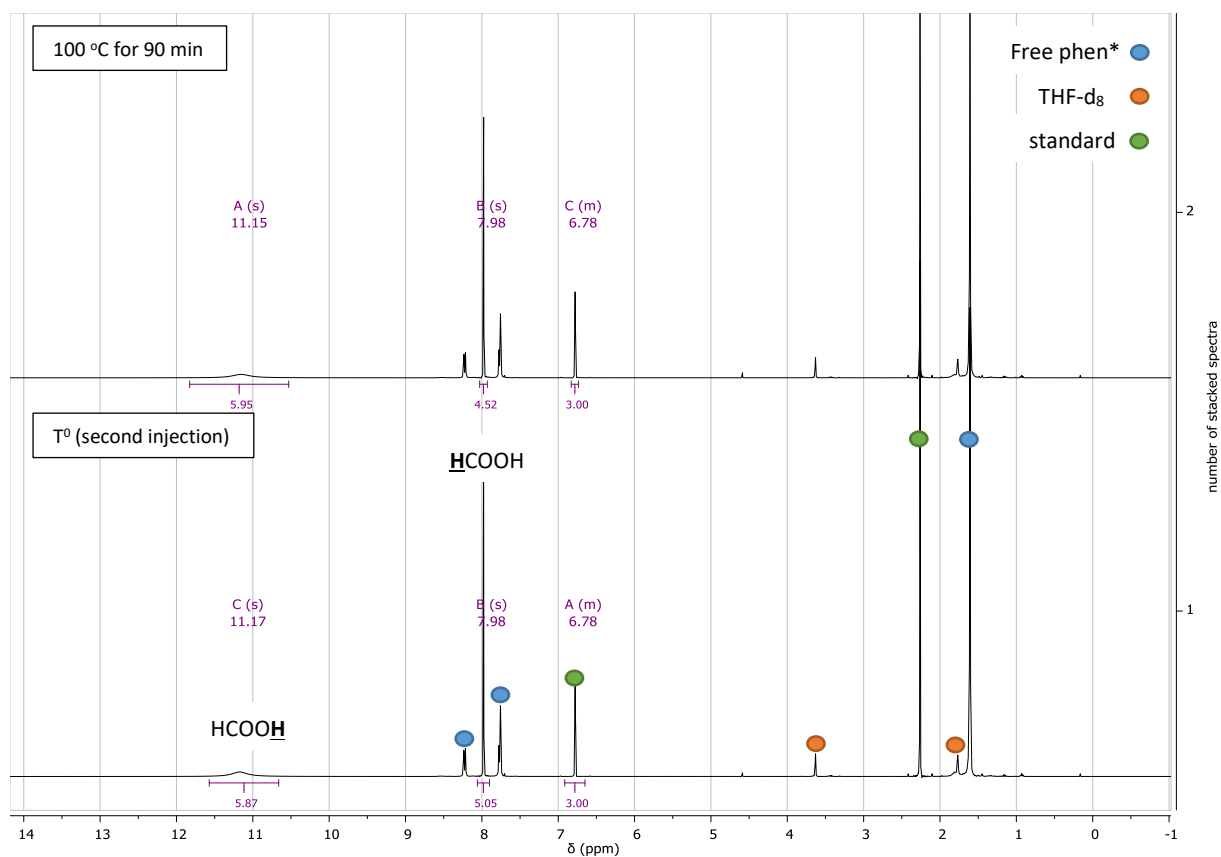


Figure S109 : ¹H NMR spectra for the second injection of formic acid on the catalytic mixture.

VI. Experimental part of Perspectives

VI. 1. Formation of $[\text{Cu}(\mu\text{-O}_2\text{C-C}_6\text{H}_4\{o\text{-NO}_2\})_2(\text{quin})]_2$ (**14**) and $[\text{Cu}(\mu\text{-O}_2\text{C-C}_6\text{H}_4\{o\text{-F}\})_2(\text{quin})]_2$ (**15**)

General procedure: In an Young NMR tube, a light yellow solution of $\text{Cu}(\text{O}^t\text{Bu})$ (6.5 mg, 0.05 mmol) in THF (5 mL) was added 2 equiv. of quinoline (8.6 μL , 0.1 mmol). The resulted light yellow solution was stirred at room temperature for 10 min. Addition of the substituted benzoic acid (0.05 mmol, 1 equiv.) resulted in an immediately change of color (color change from orange to orange-yellow depending on the substituted benzoic acid) and the mixture was stirred at room temperature for another hour. The solvent was evaporated off under vacuum to give an orange-red solid. No yield was obtained.

Orange crystals of **14** and **15** were obtained by solubilizing the solid in THF and added slowly pentane in 1: 10 ratio (THF : pentane).

IV. 1. 1. Data for $[\text{Cu}(\mu\text{-O}_2\text{C-C}_6\text{H}_4\{o\text{-NO}_2\})_2(\text{quin})]_2$ (**14**):

^1H NMR (400 MHz, THF-d_8 , δ/ppm): δ 9.07 (s, 2H), 8.38 (d, $J = 8.5$ Hz, 2H), 8.26 (d, $J = 8.2$ Hz, 2H), 7.95 (d, $J = 7.5$ Hz, 1H), 7.84 (d, $J = 8.2$ Hz, 2H), 7.74 (d, $J = 7.9$ Hz, 1H), 7.68 (t, $J = 7.4$ Hz, 2H), 7.60 (t, $J = 7.1$ Hz, 1H), 7.56 – 7.48 (m, 3H), 7.48 – 7.26 (m, 2H), 3.29 (s, 1H), 1.25 (s, 18H).

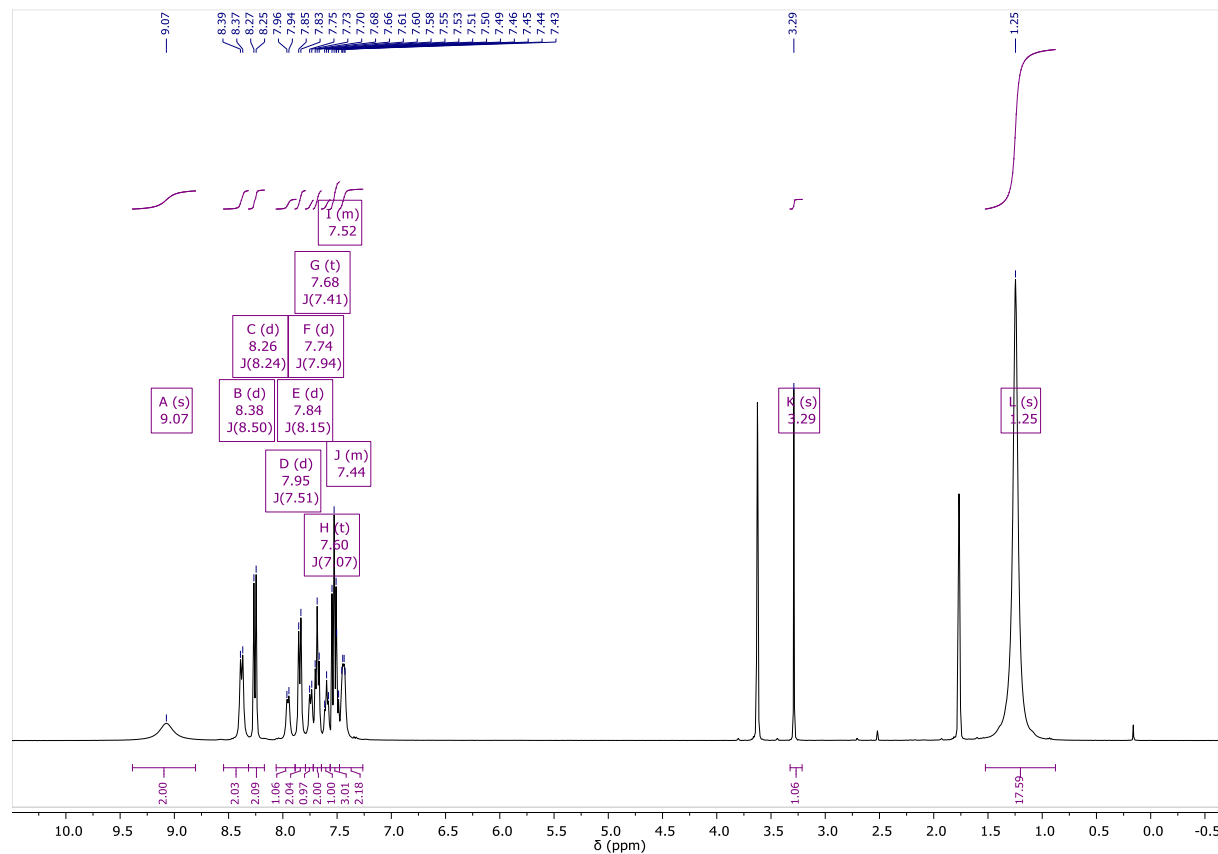


Figure S110. ^1H NMR spectra of $[\text{Cu}(\mu\text{-O}_2\text{C-C}_6\text{H}_4\{o\text{-NO}_2\})_2(\text{quin})]_2$ (**14**) in THF-d_8 .

IV. 1. 2. Data for $[\text{Cu}(\mu\text{-O}_2\text{C-C}_6\text{H}_4\{\text{o-F}\})_2(\text{quin})]_2$ (**15**):

^1H NMR (400 MHz, THF-d_8 , δ/ppm): δ 9.12 (s, 2H), 8.37 (dd, $J = 46.7, 9.1$ Hz, 3H), 8.21 – 7.82 (m, 3H), 7.82 – 7.35 (m, 6H), 7.16 (t, $J = 11.9$ Hz, 1H), 3.32 (d, $J = 6.4$ Hz, 0H), 1.23 (s, 7H).

$^{19}\text{F}\{^1\text{H}\}$ NMR (377 MHz, THF-d_8 , rt, δ/ppm): -111.18 .

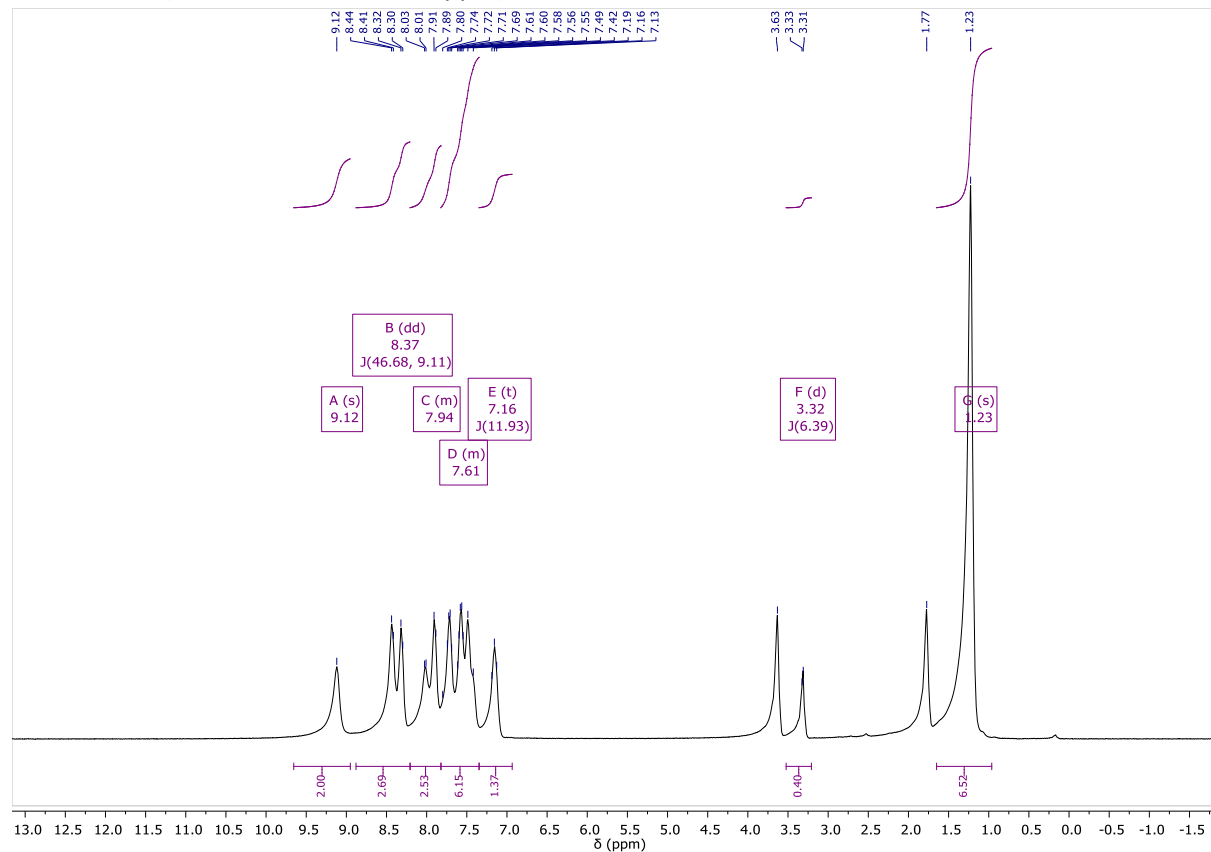


Figure S111. ^1H NMR spectra of $[\text{Cu}(\mu\text{-O}_2\text{C-C}_6\text{H}_4\{\text{o-F}\})_2(\text{quin})]_2$ (**15**) in THF-d_8 .

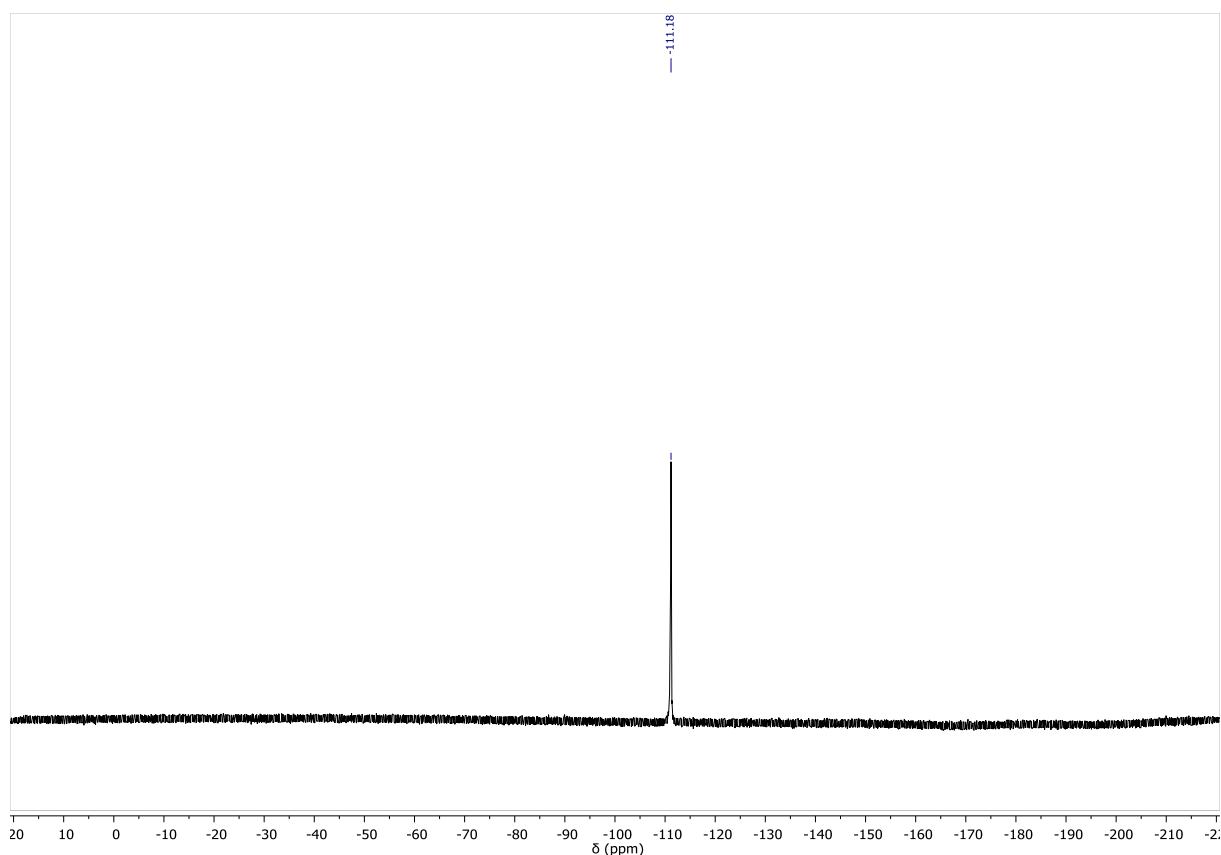


Figure S112. $^{19}\text{F}\{^1\text{H}\}$ NMR spectrum of $[\text{Cu}(\mu\text{-O}_2\text{C-C}_6\text{H}_4\{\text{o-F}\})(\text{quin})]_2$ (**15**) in THF-d_8 .

IV. 2. Synthesis of $[(\text{phen}^*)\text{Cu}(\kappa^1\text{-O}_2\text{SCF}_3)]$ complex (**16**)

The reaction was performed under the absence of light.

In a solution of NaSO_2CF_3 (49.1 mg, 0.31 mmol) in MeCN (10mL) was added AgNO_3 (52.9 mg, 0.31 mmol) to result clear colorless solution and pale orange solid. The mixture was stirred for 3 h at room temperature. The pale orange solid was filtrated by celite to obtain a clear colorless solution. The next addition of CuI (60 mg, 0.31 mmol) into this solution afforded a very light yellow solution and yellow precipitate. A filtration was carried out to remove the yellow solid and obtained a clear light yellow solution. Into this solution, phen* (92 mg, 0.31 mmol) was added, resulting an immediate change of color into clear intense yellow solution. This mixture was kept stirring overnight (15 h) at room temperature to result a clear yellow solution and yellow solid. This suspension was evaporated to dryness to obtain an orange solid. No yield was obtained since the present of side-product $[(\text{phen}^*)\text{Cu-I}]$ cannot be eliminated.

Data of crystal of $[(\text{phen}^*)\text{Cu}(\kappa^1\text{-O}_2\text{SCF}_3)]$ (**16**):

^1H NMR (400 MHz, THF-d_8) δ 8.59 (d, $J = 8.6$ Hz, 2H), 8.16 (d, $J = 8.6$ Hz, 2H), 8.00 (s, 2H), 1.83 (s, 19H).

^{19}F NMR (377 MHz, THF-d_8) δ -87.24.

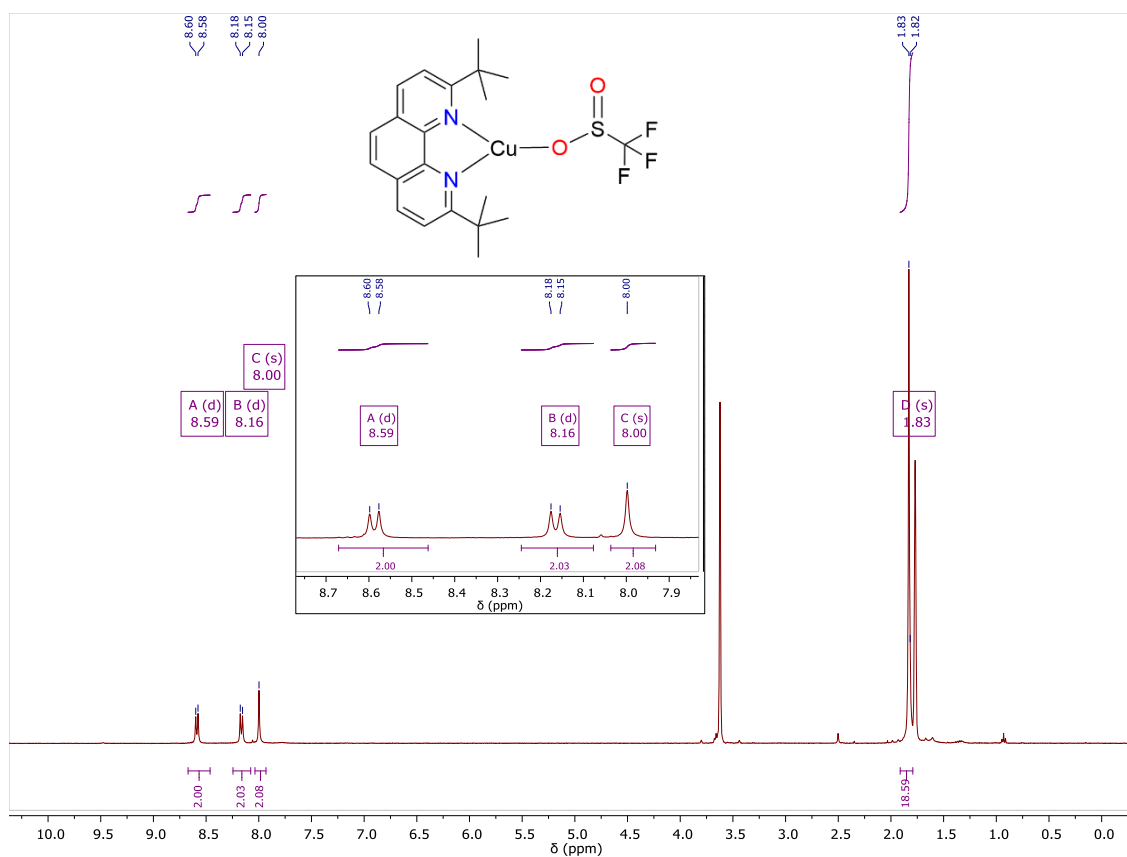


Figure S113. ^1H NMR spectrum of crystal of $[(\text{phen}^*)\text{Cu}-(\kappa^1\text{-O}_2\text{SCF}_3)]$ (**16**) in THF-d_8 .

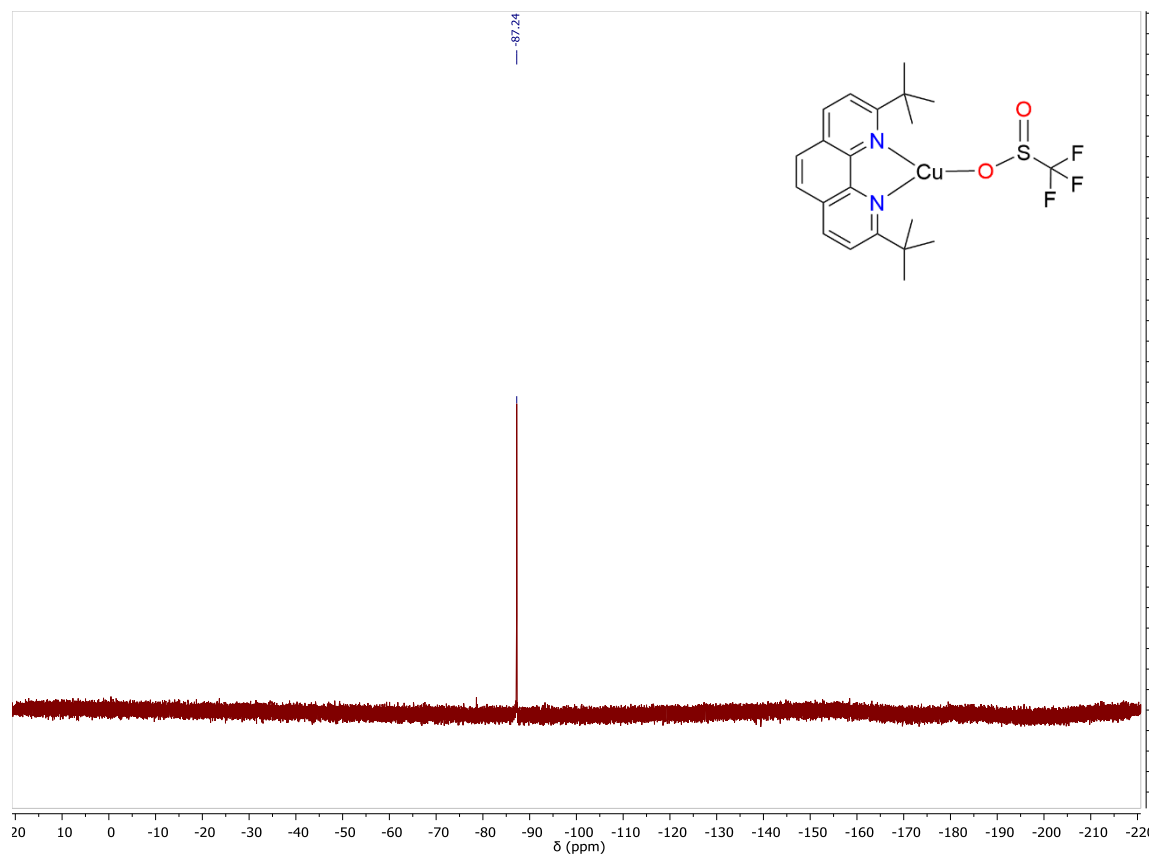


Figure S114. $^{19}\text{F}\{^1\text{H}\}$ NMR spectrum of crystal of $[(\text{phen}^*)\text{Cu}-(\kappa^1\text{-O}_2\text{SCF}_3)]$ (**16**) in THF-d_8 .

IV. 3. SO₂ insertion into [(phen*)Cu-CF₃] (**11**) for the formation of [(phen*-Cu)₂-O₂S-CF₃] (**17**).

[(phen*)Cu-CF₃] (5.3 mg, 0.012 mmol) was diluted in THF (5 mL) to result a clear yellow solution and yellow solid. This mixture was then added SO₂ (1 bar) and the solution color remained with insoluble yellow solid. The reaction was then followed by ¹H and ¹⁹F{¹H} NMR at different temperatures (rt. to 100 °C)(Figure S115 and Figure S116). After reacting at rt. and at 70 °C, the color of the mixture remained yellow. After 2.5 h at 100 °C, the mixture turned to light orange along with small amount of orange solid. At the end of the reaction, this solution was concentrated and recrystallized in THF:pentane (1:10) to obtained an orange crystal of [(phen*-Cu)₂-O₂S-CF₃] (**17**).

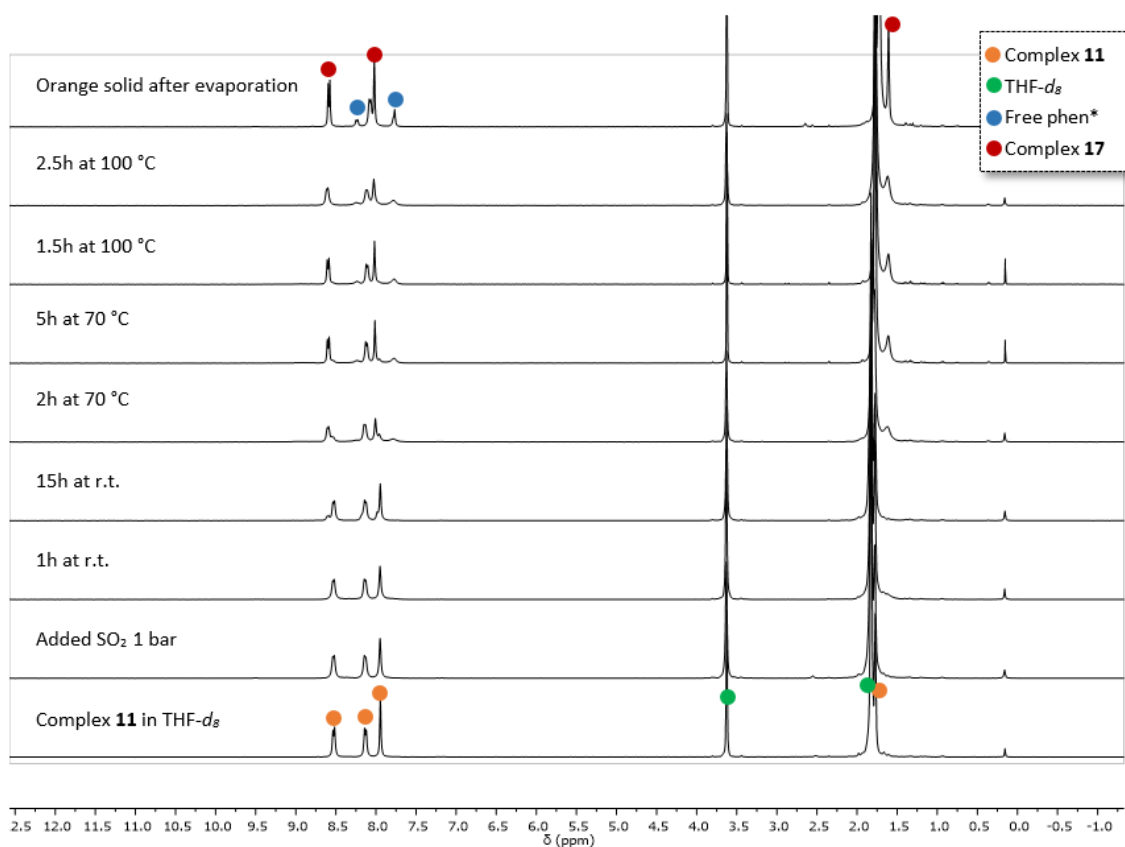


Figure S115. ¹H NMR spectra for the thermal evolution of [(phen*)Cu-CF₃] (**11**) in the presence of SO₂ (1 bar) in THF-d₈.

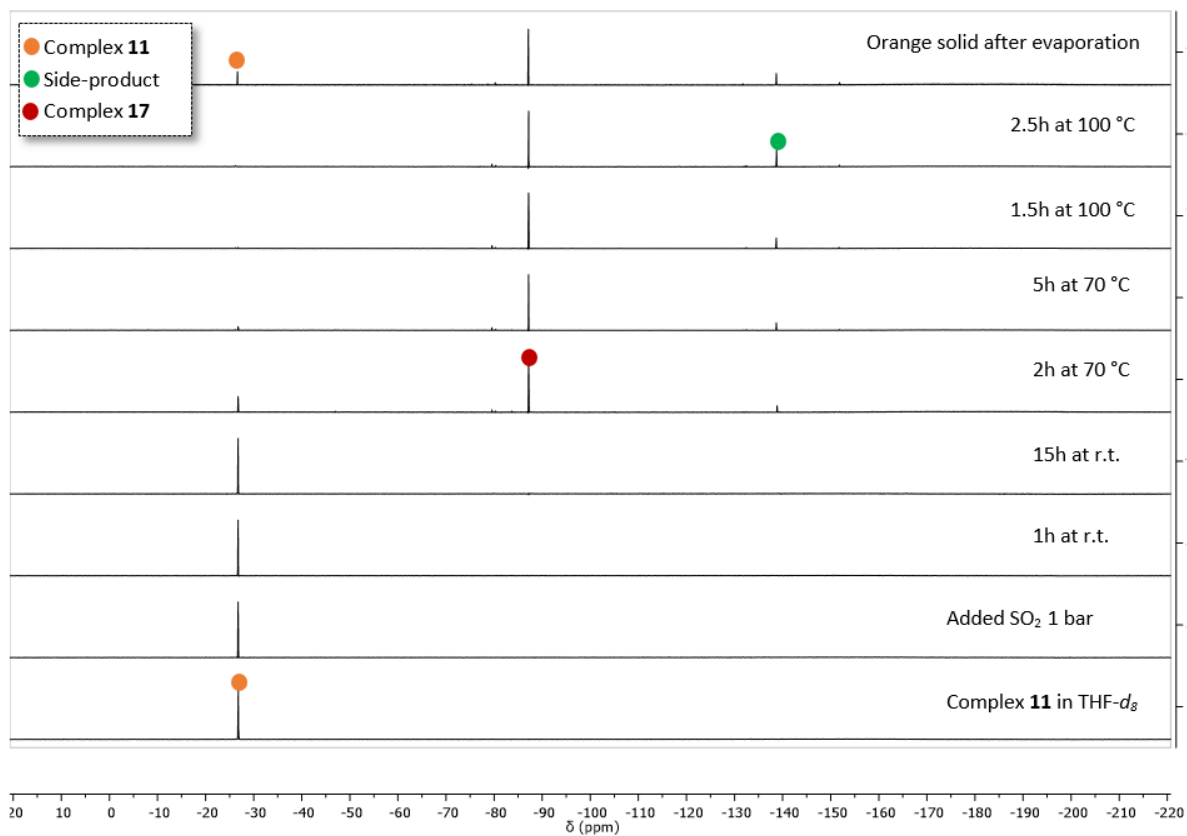


Figure S116. $^{19}\text{F}\{^1\text{H}\}$ NMR spectra for the thermal evolution of $[(\text{phen}^*)\text{Cu-CF}_3]$ (**11**) in the presence of SO_2 (1 bar) in THF-d_8 .

V. Computational details

All the density functional theory calculations were carried out by using the Gaussian16 suite of codes.¹¹ The hybrid functional RM061¹² was used with Grimme's D3 empirical dispersion. The def2tzvp/W06 sets were used for all atoms.^{13–15} All the geometries were fully optimized without any symmetry or geometry constrains. Harmonic vibrational analyses were performed to confirm and characterize the structures as minima. Free energies were calculated within the harmonic approximation for vibrational frequencies. Solvent effects were accounted by application of the implicit solvent model SMD (solvent = quinoline or tetrahydrofuran)¹⁶ through single point calculations on the gas-phase optimized geometry.

All relative energies (corrected for ZPE contributions) and Gibbs free energies (T= 298 K, P = 1 atm) are reported below in Hartree.

VI. Crystallography

The data were collected at 100(2) K on a Bruker D8 Quest diffractometer equipped with an Incoatec microfocus source ($I_{\mu\text{S}}$ 3.0 Mo, $\lambda = 0.71073 \text{ \AA}$) and a PHOTON III area detector, and operated through the APEX3 software.¹⁷ The crystals were mounted on Mitegen micromounts with a protective coating of Paratone-N oil (Hampton Research). The data were processed with SAINT¹⁸ and empirical absorption corrections (multi-scan) were made with SADABS.^{19,20} All structures were solved by intrinsic phasing with SHELXT,²¹ and refined by full-matrix least-squares on F^2 with SHELXL,²² using the ShelXle interface.²³ All non-hydrogen atoms were refined with anisotropic displacement parameters. The hydrogen atom bound to fluorine in **10**·benzene was found on a residual electron density map and was fully refined with no restraint. All other hydrogen atoms were introduced at calculated positions and were treated as riding atoms with an isotropic displacement parameter equal to 1.2 times that of the parent atom (1.5 for CH₃). In **2**·0.5toluene, the aromatic ring of the carboxylate ligand is disordered over two positions which were refined with restraints and with occupancy parameters constrained to sum to unity; the toluene solvent molecule is also disordered over two positions related by symmetry and it was refined as an idealized hexagon, with restraints on displacement parameters. In **5**·THF, one carbon atom of the THF molecule is disordered over two positions which have been refined with occupancy parameters constrained to sum to unity and restraints on bond lengths and displacement parameters. The molecular plots were drawn with ORTEP-3,^{24,25} and the packings with VESTA.²⁶ Crystal data and refinement details are given in *Table S2* to *Table S4* below.

Table S2. Crystal Data and Structure Refinement Details (ligand 1 and complexes 2–6)

	1	2·0.5toluene	3	4	5·THF	6·THF
chemical formula	C ₂₀ H ₂₄ N ₂	C _{30.5} H ₃₂ CuFN ₂ O ₂	C ₂₇ H ₂₈ CuFN ₂ O ₂	C ₂₇ H ₂₄ CuF ₅ N ₂ O ₂	C ₃₁ H ₃₆ CuN ₃ O ₃	C ₃₁ H ₃₆ CuN ₃ O ₃
<i>M</i> (g mol ⁻¹)	292.41	541.12	495.05	567.02	594.17	594.17
cryst syst	trigonal	monoclinic	monoclinic	monoclinic	monoclinic	monoclinic
space group	<i>P</i> -3	<i>P</i> 2 ₁ / <i>c</i>	<i>P</i> 2 ₁ / <i>n</i>	<i>P</i> 2 ₁ / <i>n</i>	<i>P</i> 2 ₁ / <i>c</i>	<i>P</i> 2 ₁ / <i>c</i>
<i>a</i> (Å)	18.7877(6)	11.1230(3)	14.8656(8)	12.8499(4)	14.2807(5)	14.1420(5)
<i>b</i> (Å)	18.7877(6)	11.3976(3)	10.2308(6)	11.2397(3)	12.8242(4)	10.1855(3)
<i>c</i> (Å)	8.5746(3)	20.7849(6)	15.6484(7)	17.4640(5)	15.2113(5)	20.4344(5)
<i>α</i> (deg)	90	90	90	90	90	90
<i>β</i> (deg)	90	102.6668(12)	95.288(2)	104.1912(14)	94.1310(15)	106.1627(12)
<i>γ</i> (deg)	120	90	90	90	90	90
<i>V</i> (Å ³)	2621.15(19)	2570.88(12)	2369.8(2)	2445.34(12)	2778.54(16)	2827.10(15)
<i>Z</i>	6	4	4	4	4	4
reflns colld	62106	75584	69117	99261	97167	71365
indep reflns	3316	4877	4486	4646	8480	5367
obsd reflns [<i>I</i> > 2σ(<i>I</i>)]	3039	4438	4166	3986	7859	4746
<i>R</i> _{int}	0.037	0.039	0.073	0.074	0.035	0.052
params refined	205	419	304	340	377	367
<i>R</i> ₁	0.039	0.033	0.026	0.030	0.030	0.029
<i>wR</i> ₂	0.103	0.093	0.073	0.075	0.080	0.076
Δρ _{min} (e Å ⁻³)	-0.19	-0.52	-0.28	-0.35	-0.48	-0.30
Δρ _{max} (e Å ⁻³)	0.26	0.89	0.35	0.28	0.97	0.34

Table S3. Crystal Data and Structure Refinement Details (complexes 7–11)

	7	8	8'	9	10-benzene	11
chemical formula	C ₂₂ H ₂₄ CuF ₃ N ₂ O ₂	C ₂₆ H ₂₄ CuF ₅ N ₂	C ₁₈ H ₈ CuF ₅ N ₂	C ₂₆ H ₂₈ CuN ₃ O ₂	C ₂₆ H ₃₁ CuF ₂ N ₂	C ₂₁ H ₂₄ CuF ₃ N ₂
<i>M</i> (g mol ⁻¹)	468.97	523.01	410.80	478.05	473.07	424.96
cryst syst	triclinic	triclinic	triclinic	monoclinic	monoclinic	orthorhombic
space group	<i>P</i> $\bar{1}$	<i>P</i> $\bar{1}$	<i>P</i> $\bar{1}$	<i>P</i> 2 ₁ / <i>c</i>	<i>P</i> 2 ₁	<i>Pbca</i>
<i>a</i> (Å)	9.1224(3)	9.3813(3)	6.6077(2)	10.8845(4)	10.0888(4)	9.7948(2)
<i>b</i> (Å)	11.1006(3)	11.1107(4)	13.4948(4)	10.5224(2)	11.0364(4)	19.6573(5)
<i>c</i> (Å)	11.2129(3)	11.8463(4)	17.9310(5)	19.6864(6)	10.2508(5)	20.0545(5)
α (deg)	105.5320(11)	78.2488(14)	109.2263(10)	90	90	90
β (deg)	92.3043(12)	78.6035(14)	91.4095(11)	97.2182(13)	93.6179(18)	90
γ (deg)	104.6160(11)	68.4307(13)	97.6535(10)	90	90	90
<i>V</i> (Å ³)	1051.50(5)	1113.98(7)	1492.26(8)	2236.84(12)	1139.09(8)	3861.28(16)
<i>Z</i>	2	2	4	4	2	8
reflns colld	26300	45617	21822	64452	88106	80367
indep reflns	5409	4229	5647	4248	5871	4980
obsd reflns [<i>I</i> > 2 σ (<i>I</i>)]	4966	3996	4962	3873	5619	4578
<i>R</i> _{int}	0.027	0.057	0.030	0.055	0.061	0.063
params refined	277	313	469	295	291	250
<i>R</i> ₁	0.027	0.028	0.027	0.027	0.026	0.027
<i>wR</i> ₂	0.069	0.068	0.068	0.069	0.060	0.074
$\Delta\rho_{\min}$ (e Å ⁻³)	-0.40	-0.31	-0.30	-0.32	-0.28	-0.39
$\Delta\rho_{\max}$ (e Å ⁻³)	0.43	0.79	0.38	0.40	0.31	0.48

Table S4. Crystal Data and Structure Refinement Details (complexes 12'–17)

	12'	13	14	15	16	17
chemical formula	C _{20.8} H _{24.8} CuI _{0.2} N ₂ O _{1.6}	C ₆₀ H ₅₀ BCu ₂ F ₁₅ N ₄ O ₄	C ₃₂ H ₂₂ Cu ₂ N ₄ O ₈	C ₃₂ H ₂₂ Cu ₂ F ₂ N ₂ O ₄	C ₂₁ H ₂₄ CuF ₃ N ₂ O ₂ S	C ₄₁ H ₄₉ Cu ₂ F ₃ N ₄ O ₆ S ₂
<i>M</i> (g mol ⁻¹)	417.34	1313.93	717.61	663.59	489.02	942.06
cryst syst	orthorhombic	triclinic	monoclinic	monoclinic	monoclinic	triclinic
space group	<i>Pbca</i>	<i>P</i> $\bar{1}$	<i>C2/c</i>	<i>C2/c</i>	<i>P2₁/c</i>	<i>P</i> $\bar{1}$
<i>a</i> (Å)	19.7759(10)	10.2198(3)	12.8387(3)	19.8807(7)	20.9358(6)	11.6637(5)
<i>b</i> (Å)	9.6843(4)	16.5685(6)	10.0229(3)	9.9167(3)	10.1785(3)	12.7685(5)
<i>c</i> (Å)	20.0969(10)	17.8348(5)	22.8680(8)	13.5208(5)	20.8529(6)	15.5631(7)
α (deg)	90	90.3768(12)	90	90	90	74.7403(17)
β (deg)	90	104.3897(11)	102.8895(13)	95.8245(16)	104.0988(13)	88.1366(18)
γ (deg)	90	107.8564(13)	90	90	90	75.8969(16)
<i>V</i> (Å ³)	3848.9(3)	2773.01(15)	2868.53(15)	2651.88(16)	4309.8(2)	2167.43(16)
<i>Z</i>	8	2	4	4	8	2
reflns colld	57102	85638	28427	37722	140836	79654
indep reflns	3640	10556	2540	2518	8192	8229
obsd reflns [<i>I</i> > 2 σ (<i>I</i>)]	3349	9325	2482	2371	7188	7116
<i>R</i> _{int}	0.072	0.056	0.042	0.050	0.055	0.051
params refined	250	787	208	190	554	636
<i>R</i> ₁	0.048	0.030	0.056	0.023	0.043	0.034
<i>wR</i> ₂	0.104	0.076	0.133	0.057	0.111	0.090
$\Delta\rho_{\min}$ (e Å ⁻³)	-0.61	-0.37	-0.46	-0.24	-1.12	-0.49
$\Delta\rho_{\max}$ (e Å ⁻³)	0.45	0.61	1.57	0.41	1.77	0.85

VI. References

- (1) Cairncross, A.; Sheppard, W. A. Fluorinated Organocopper Compounds. *J. Am. Chem. Soc.* **1968**, *90* (8), 2186–2187. <https://doi.org/10.1021/ja01010a050>.
- (2) Jäkke, F. Pentafluorophenyl Copper: Aggregation and Complexation Phenomena, Photoluminescence Properties, and Applications as Reagent in Organometallic Synthesis. *Dalton Trans.* **2007**, No. 27, 2851–2858. <https://doi.org/10.1039/B704372D>.
- (3) Tsuda, T.; Yazawa, T.; Watanabe, K.; Fujii, T.; Saegusa, T. Preparation of Thermally Stable and Soluble Mesitylcopper(I) and Its Application in Organic Synthesis. *J. Org. Chem.* **1981**, *46* (1), 192–194. <https://doi.org/10.1021/jo00314a048>.
- (4) Baur, A.; Bustin, K. A.; Aguilera, E.; Petersen, J. L.; Hoover, J. M. Copper and Silver Benzoate and Aryl Complexes and Their Implications for Oxidative Decarboxylative Coupling Reactions. *Org. Chem. Front.* **2017**, *4* (4), 519–524. <https://doi.org/10.1039/C6QO00678G>.
- (5) Pallenberg, A. J.; Koenig, K. S.; Barnhart, D. M. Synthesis and Characterization of Some Copper(I) Phenanthroline Complexes. *Inorg. Chem.* **1995**, *34* (11), 2833–2840. <https://doi.org/10.1021/ic00115a009>.
- (6) Wang, T.; Chen, F.; Qin, J.; He, Y.-M.; Fan, Q.-H. Asymmetric Ruthenium-Catalyzed Hydrogenation of 2- and 2,9-Substituted 1,10-Phenanthrolines. *Angew. Chem. Int. Ed.* **2013**, *52*, 7172–7176.
- (7) Dietrick-Buchecker, C. O.; Marnot, P. A.; Sauvage, J. P. Direct Synthesis of Disubstituted Aromatic Polyimine Chelates. *Tetrahedron Letters* **1982**, *23* (50), 5291–5294. [https://doi.org/10.1016/S0040-4039\(00\)85821-9](https://doi.org/10.1016/S0040-4039(00)85821-9).
- (8) Tsuda, T.; Hashimoto, T.; Saegusa, T. Cuprous Tert-Butoxide. New and Useful Metalation Reagent. *J. Am. Chem. Soc.* **1972**, *94* (2), 658–659. <https://doi.org/10.1021/ja00757a069>.
- (9) Do, H.-Q.; Khan, R. M. K.; Daugulis, O. A General Method for Copper-Catalyzed Arylation of Arene C–H Bonds. *J. Am. Chem. Soc.* **2008**, *130* (45), 15185–15192. <https://doi.org/10.1021/ja805688p>.
- (10) Liu, Y.; Chen, C.; Li, H.; Huang, K.-W.; Tan, J.; Weng, Z. Efficient S_N2 Fluorination of Primary and Secondary Alkyl Bromides by Copper(I) Fluoride Complexes. *Organometallics* **2013**, *32* (21), 6587–6592. <https://doi.org/10.1021/om4008967>.
- (11) Gaussian 16 Rev C.01, M. J. Frisch, G. W. Trucks, H. B. Schlegel, G. E. Scuseria, M. A. Robb, J. R. Cheeseman, G. Scalmani, V. Barone, G. A. Petersson, H. Nakatsuji, X. Li, M. Caricato, A. V. Marenich, J. Bloino, B. G. Janesko, R. Gomperts, B. Mennucci, H. P. Hratchian, J. V. Ortiz, A. F. Izmaylov, J. L. Sonnenberg, D. Williams-Young, F. Ding, F. Lipparini, F. Egidi, J. Goings, B. Peng, A. Petrone, T. Henderson, D. Ranasinghe, V. G. Zakrzewski, J. Gao, N. Rega, G. Zheng, W. Liang, M. Hada, M. Ehara, K. Toyota, R. Fukuda, J. Hasegawa, M. Ishida, T. Nakajima, Y. Honda, O. Kitao, H. Nakai, T. Vreven, K. Throssell, J. A. Montgomery, Jr., J. E. Peralta, F. Ogliaro, M. J. Bearpark, J. J. Heyd, E. N. Brothers, K. N. Kudin, V. N. Staroverov, T. A. Keith, R. Kobayashi, J. Normand, K. Raghavachari, A. P. Rendell, J. C. Burant, S. S. Iyengar, J. Tomasi, M. Cossi, J. M. Millam, M. Klene, C. Adamo, R. Cammi, J. W. Ochterski, R. L. Martin, K. Morokuma, O. Farkas, J. B. Foresman, and D. J. Fox, Gaussian, Inc., Wallingford CT, 2016.

- (12) Zhao, Y.; Truhlar, D. G. A New Local Density Functional for Main-Group Thermochemistry, Transition Metal Bonding, Thermochemical Kinetics, and Noncovalent Interactions. *The Journal of Chemical Physics* **2006**, *125* (19), 194101. <https://doi.org/10.1063/1.2370993>.
- (13) Weigend, F. Accurate Coulomb-Fitting Basis Sets for H to Rn. *Phys. Chem. Chem. Phys.* **2006**, *8* (9), 1057. <https://doi.org/10.1039/b515623h>.
- (14) Weigend, F.; Ahlrichs, R. Balanced Basis Sets of Split Valence, Triple Zeta Valence and Quadruple Zeta Valence Quality for H to Rn: Design and Assessment of Accuracy. *Phys. Chem. Chem. Phys.* **2005**, *7* (18), 3297. <https://doi.org/10.1039/b508541a>.
- (15) Rappoport, D.; Furche, F. Property-Optimized Gaussian Basis Sets for Molecular Response Calculations. *The Journal of Chemical Physics* **2010**, *133* (13), 134105. <https://doi.org/10.1063/1.3484283>.
- (16) Marenich, A. V.; Cramer, C. J.; Truhlar, D. G. Universal Solvation Model Based on Solute Electron Density and on a Continuum Model of the Solvent Defined by the Bulk Dielectric Constant and Atomic Surface Tensions. *J. Phys. Chem. B* **2009**, *113* (18), 6378–6396. <https://doi.org/10.1021/jp810292n>.
- (17) *APEX3 Crystallography Software Suite, Ver. 2019.1-0; Bruker AXS: Madison, WI, 2019.*
- (18) *SAINT, Ver. 8.40A; Bruker Nano: Madison, WI, 2019.*
- (19) *SADABS, Bruker/Siemens Area Detector Absorption and Other Corrections, Ver. 2016/2; Bruker AXS: Madison, WI, 2016.*
- (20) Krause, L.; Herbst-Irmer, R.; Sheldrick, G. M.; Stalke, D. Comparison of Silver and Molybdenum Microfocus X-Ray Sources for Single-Crystal Structure Determination. *J. Appl. Crystallogr.* **2015**, *48*, 3–10.
- (21) Sheldrick, G. M. SHELXT – Integrated Space-Group and Crystal-Structure Determination. *Acta Crystallogr., Sect. A* **2015**, *71*, 3–8.
- (22) Sheldrick, G. M. Crystal Structure Refinement with SHELXL. *Acta Crystallogr., Sect. C* **2015**, *71*, 3–8.
- (23) Hübschle, C. B.; Sheldrick, G. M.; Dittrich, B. ShelXle: A Qt Graphical User Interface for SHELXL. *J. Appl. Crystallogr.* **2011**, *44*, 1281–1284.
- (24) Burnett, M. N.; Johnson, C. K. ORTEPIII, Report ORNL-6895; Oak Ridge National Laboratory: TN, 1996.
- (25) Farrugia, L. J. WinGX and ORTEP for Windows: An Update. *J. Appl. Crystallogr.* **2012**, *45*, 849–854.
- (26) Momma, K.; Izumi, F. VESTA 3 for Three-Dimensional Visualization of Crystal, Volumetric and Morphology Data. *J. Appl. Crystallogr.* **2011**, *44* (6), 1272–1276. <https://doi.org/10.1107/S0021889811038970>.